Technische Universität München
TUM School of Natural Sciences

Heavier Tetrylenes as Single-Centre Ambiphile Ligands for Cooperative Bond Activation in First-Row Transition Metal Complexes

Philip Maximilian Keil

Vollständiger Abdruck der von der TUM School of Natural Sciences der Technischen Universität München zur Erlangung eines

Doktors der Naturwissenschaften (Dr. rer. nat.)

genehmigten Dissertation.

Vorsitz: Prof. Dr. Tom Nilges

Prüfer*innen der Dissertation:

1. TUM Junior Fellow Dr. Terrance J. Hadlington
2. Prof. Dr. Shigeyoshi Inoue
3. Prof. Dr. Lutz Greb

Die Dissertation wurde am 02.10.2023 bei der Technischen Universität München eingereicht und durch die TUM School of Natural Sciences am 03.11.2023 angenommen.

Diese vorliegende Arbeit wurde im Zeitraum von Februar 2020 bis September 2023 am Lehrstuhl für Anorganische Chemie mit Schwerpunkt Neue Materialien unter der Betreuung von Herrn Dr. Terrance Hadlington angefertigt.

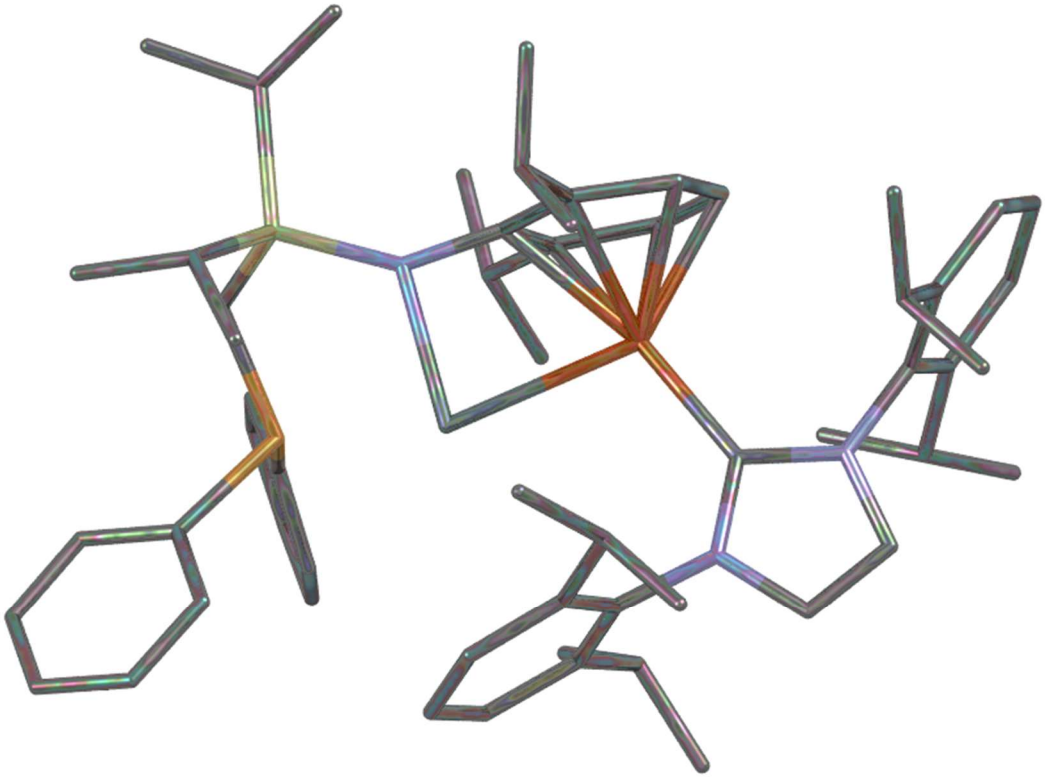

“Study hard what interests you most, in the most undisciplined, irreverent, and original manner possible”

Richard P. Feynman

Danksagung

First of all, I would like to thank my supervisor **Dr. Terrance Hadlington** for his continuous support and guidance. You gave me a chance as your first PhD student, especially as I had never worked in main group chemistry before joining your group, and you have amazed me with your knowledge and enthusiasm over the last three and a half years, while always being there when I had questions or problems. It has been a pleasure to work side by side with you in the lab, gaining all the valuable practical and scientific skills you have taught me. It has been amazing to have such a friendly, approachable, and motivated mentor and to see the Hadlington group grow from just two to seven now, while maintaining such a great atmosphere.

I also want to thank **Prof. Shigeyoshi Inoue** and **Prof. Lutz Greb** for agreeing to evaluate my thesis.

Ich möchte **Prof. Dr. Thomas Fässler** danken, dass er mich und Terry, durch die Arbeitsgruppenseminare und soziale Events wie z.B. Grillabende, in die Fässler Arbeitsgruppe integriert hat. Ebenfalls danke für die Hilfe bei jeglichen administrativen und Laborbezogenen Problemen die in der Zeit aufgekommen sind.

Danke auch an **Maria**, **Viktor**, **Wilhelm** und **Irina** aus der Fässler Arbeitsgruppe. Ihr wart immer hilfsbereit und habt mir bei allen möglichen Problemen und Messungen geholfen. Vor allem **Manuela** möchte ich speziell danken. Du hast mir immer zuverlässig und schnell bei allen administrativen Fragen geholfen und die Zusammenarbeit mit dir war durch deine fröhliche und natürliche Art eine Freude.

Ich will hier auch dem **Fonds der chemischen Industrie** für die finanzielle Unterstützung durch ein Liebig-Doktoranden Stipendium über die ersten drei Jahre meiner Promotion danken.

Verschiedensten Menschen an der TU München möchte ich für diverse Messungen danken: **Maximilian** und **Patrick** (LIFDI/MS), **Lukas** und **Kerstin** (UV/vis und CV), **Sarah** (UV/vis), **Kevin** und **Raphael** (NMR), **Kerstin** (GPC), **Oksana** und **Peter** (EPR), **Ullrike**, **Bircan** und **Petra** (Elementaranalyse), **Kathi** (IR und Gasversorgung). Danke euch allen, ihr wart immer hilfsbereit und habt mir meine Arbeit ungemein erleichtert, vor allem da ich anfangs noch überhaupt nicht wusste, wo irgendwas an der Universität ist.

I would like to thank **Tibor Szilvási**, **Ademola Soyemi** und **Sophia Ezendu**, from the University of Alabama, Tuscaloosa, who have reliably provided countless DFT calculations for my projects.

Ich möchte ebenfalls **Prof. Dr. Christian Limberg** und **Killian Weisser** von der Humboldt Universität zu Berlin für ihre Hilfe durch ^{57}Fe Mössbauer Messungen und wissenschaftlichen Fachwissen zu Eisen-Chemie danken.

Außerdem möchte ich unzähligen Forschungspraktikanten (**Richard**, **Lena**, **Kristoff**, **Julian**, **Tim**, **Alexander**, **Tommy**) für ihr Vertrauen und ihr Engagement im Labor in bedanken.

Toni und **Emeric** möchte ich hier hervorheben, die ich ebenfalls als Forschungspraktikanten betreut habe und danach zur Masterarbeit bzw. Doktorarbeit wiedergekommen sind. Die Atmosphäre mit euch im Labor und auch bei Gruppenausflügen war immer sehr angenehm.

Lisa und **John** von TU München möchte ich ebenfalls danken. Ich habe mit euch einige Konferenzen, mit vielen witzige Momenten und schönen Abenden erlebt, die mir lange im Gedächtnis bleiben werden.

Danke der gesamten Fässler Arbeitsgruppe und vor allem **Christoph**, **Alexander**, **Christian**, **Manuel**, **Kevin**, **Nicole**, **Yasmin**, **Leo**, **Tassilo** und **Jan**. Ihr wart immer bei Fragen oder abendlichem Grillen/Bier trinken für mich da. Ich hatte eine sehr angenehme Doktorandenzeit mit euch und habe mich immer als Teil der Arbeitsgruppe gefühlt.

Vor allem **Till**, **Lisa**, **Annika**, **Malte** und **Samuel** möchte ich hier erwähnen. Ich habe euch in den letzten zwei Jahren als Freunde in der Arbeitsgruppe gefunden. Die Atomsphäre mit euch im Labor und privat weiß ich sehr zu schätzen und hoffe, dass wir auch nach meinem Abschluss weiter Kontakt halten werden. Danke für die großartige Zeit.

Ein großer Dank gilt der Neufahrn Gang (**Sebi**, **Lukas**, **Fabi**, **Pati**, **Margit**, **Philip**, **Karina**, **Stefan**, **Meli**, **Syl**) die mich vor allem zu meiner Anfangszeit, wo ich wegen Corona nur wenig soziale Kontakte hatte, emotional und auch an der Universität sehr unterstützt haben und wo ich Freunde fürs Leben gefunden habe.

Ebenfalls all meinen Studienfreunden aus meiner Ulmer Zeit, im speziellen **Markus**, **Dennis**, **Mini**, **Marvin**, **Kamil**, **Kevin** und **Perly** will ich danken. Ich denke immer gerne an unsere gemeinsame Zeit zurück und bin froh darüber, dass wir Kontakt gehalten haben und uns immer noch ein paar Mal pro Jahr wiedersehen.

Ein großes Dankeschön an alle meine **Freunde** aus München, die zu zahlreich wären, um sie hier einzeln zu nennen. Ihr nehmt mich immer wieder mit offenen Armen nach längerer Abstinenz auf, als wäre nie was gewesen, und das alljährliche Skifahren ist immer ein absolutes Highlight. Im speziellen will ich hier **Johannnes** nennen den ich seit meiner Kindergartenzeit kenne und der mich immer unterstützt.

Danke an **Cornelie**, **Uwe**, **Christoph**, **Vanessa** und **Caius**, die mich vor knapp 9 Jahren mit offenen Armen als Partner von Alex empfangen haben und uns in allen Dingen ungemein unterstützt haben. Ihr wart immer für uns, sei es für Umzug, Hochzeit oder Katzenbetreuung, um nur ein paar Dinge zu nennen.

An dieser Stelle möchte ich auch meinen verstorbenen Großeltern **Inge** und **Karl-August** aus Augsburg danken. Ihr habt mich immer unterstützt und mein Interesse an der Wissenschaft geweckt.

Danke an meine beiden Tanten **Dorothee** und **Helene**, die mich zwar nicht so oft zu Gesicht bekommen aber immer ein offenes Ohr haben.

Auch ein großes Danke an meine Schwester **Leonie**, mit der ich immer Nonsens machen und loslassen kann. Ich kann mit dir über alles reden und das schätze ich ungemein.

Mama und **Papa** ihr habt mich seitdem ich denken immer in allem unterstützt und nie daran gezweifelt, dass ich irgendwie meinen Weg gehe. Ihr habt mich einfach das machen lassen, worauf ich Lust hatte. Danke für Alles!

Ein besonderer Dank gilt meinen Katzen **Cleo** und **Freya**. Ihr wart immer in schlechten und guten Zeiten für Kuscheleinheiten da und habt mir so sehr geholfen. Ihr seid mir sehr ans Herzen gewachsen und für mich mittlerweile unverzichtbar.

Zum Abschluss will ich mich bei der für mich wichtigsten Person **Alexandra** bedanken. Du hast mich in den letzten 9 Jahren beim allem unterstützt und meine Macken und schlechten Launen über dich ergehen lassen. Ich hätte niemals gedacht, dass ich jemanden wie dich finde und dann auch noch mein Leben mit dir verbringen darf. Ich bin unbeschreiblich froh dich zu haben.

Table of Contents

Complete List of Publications

First author publications

1) P. M. Keil, T. Szilvási, T. J. Hadlington, *Chem. Sci.* **2021**, *12*, 5582-5590.

2) P. M. Keil, T. J. Hadlington, *Angew. Chem. Int. Ed.* **2022**, *61*, e202114143.

3) P. M. Keil, T. J. Hadlington, *Chem. Commun.* **2022**, *58*, 3011-3014.

4) P. M. Keil, T. J. Hadlington, *Z. Anorg. Allg. Chem.* **2022**, *648*, e202200141.

5) P. M. Keil, A. Soyemi, K. Weisser, T. Szilvási, C. Limberg, T. J. Hadlington, *Angew. Chem. Int. Ed.* **2023**, *62*, e202218141.

Publications beyond the scope of this thesis

6) A. Schulz, T. L. Kalkuhl, P. M. Keil, T. J. Hadlington, *Angew. Chem. Int. Ed.* **2023**, *62*, e202305996.

Abstract

Hydroamination of unsaturated substrates with ammonia remains one of the holy grails of chemical catalysis. Transition metals (TM) have not been able to catalyse this challenging conversion, due to ammonia being a strong sigma donor ligand. Metal-ligand cooperativity (MLC) is an intriguing concept to potentially achieve hydroamination, where a non-innocent ligand actively participates in bond activation and catalysis. Heavier tetrylenes are such non-innocent ligands, which can remain Lewis acidic in the coordination sphere of a TM. This thesis aims to develop bidentate heavier tetrylene first-row TM complexes to achieve MLC behaviour with catalytically relevant substrates such as ammonia for potential utilisation in catalysis.

In **Chapter 3** we introduced the novel bidentate, monoanionic ligand scaffold ^{PhR}Dipp (^{PhR}Dipp = [{$Ph_2PCH_2Si(R)_2$}(Dipp)N]$^-$; R = *i*Pr, Ph; Dipp = 2,6-*i*$Pr_2C_6H_3$) and synthesised the corresponding (chloro)germylene ligands ^{PhR}DippGeCl. These were used to isolate the (chloro)germylene-nickel(0) complexes [{^{PhR}DippGe(Cl)}·$Ni(PPh_3)_2$]. These showed the ability to reversibly activate ammonia at the ligand binding centre *via* a *σ*-bond metathesis reaction, eliminating ammonium chloride. The corresponding cationic tetryliumylidene-nickel(0) complexes [(^{PhR}DippE)·$Ni(PPh_3)_2$][BAr^F_4] (E = Ge, Sn; [BAr^F_4]$^-$ = [{3,5-$(CF_3)_2C_6H_3$}$_4$B]$^-$), were developed in **Chapter 4**, where the tetrylene ligand centres exhibited remarkably high Lewis acidity, enabling ammonia adduct formation and fluoride abstraction from $[SbF_6]^-$ at the tetrel element. Additionally, efficient and selective catalytic hydrosilylation of alkene and alkynes with phenylsilane was achieved with these tetryliumylidene complexes. The Lewis acidic character of the tetrylene ligands discussed in Chapter 3 and 4 can be traced back to bent ^{PhR}Dipp-E-Ni angles, resulting in minimised *π*-back-donation from the Ni^0 centre to the tetrel element. The importance of the bidentate ligand scaffold for this bent angle was demonstrated in **Chapter 5**, by synthesising the corresponding monodentate (chloro)tetrylenes ^{SiiP}DippECl (^{SiiP}Dipp = [(*i*Pr_3Si(Dipp)N]$^-$) and isolating the tetryliumylidene-nickel(0) complexes [^{SiiP}DippE·$Ni(PPh_3)_3$][BAr^F_4]. These unique species show a linear ^{SiiP}Dipp-E-Ni angle, and thus pronounced *π*-back-donation from the Ni^0 centre to the tetrel elements resulting in a donor-acceptor triple bond, quenching tetryl-centred Lewis acidity.

In **Chapter 6** selective synthetic routes to the free cationic tetrylenes, [^{PhiP}DippE]$^+$, were achieved. This generally allows for easier implementation of the cationic ligand scaffold in generating TM complexes. While the cationic germylene [^{PhiP}DippGe]$^+$ could be generated *via* chloride abstraction from (chloro)germylene ^{PhiP}DippGeCl, the cationic stannylene [^{PhiP}DippSn]$^+$ could only be accessed *via* hydride abstraction from the respective (hydrido)stannylene, ^{PhiP}DippSnH, as a novel synthetic pathway to such cationic tetrylenes.

To achieve a more reactive TM centre, cationic tetrylene (*i.e.* $[^{PhiP}DippE]^{+}$) complexes of low-valent [Fe(IPr)] (IPr = [{HC(Dipp)N}$_2$C:]) were developed in **Chapter 7**. The cationic germylene $[^{PhiP}DippGe]^{+}$ resulted in a diamagnetic low-spin iron(0) complex, $[\{^{PhiP}Ge(IPr)\}\cdot Fe][BAr^F_4]$. This complex activates ammonia giving the 'parent' (amido)germylene complex $[\{^{PhiP}DippGe(NH_2)\}\cdot Fe\{IPr(H)\}][BAr^F_4]$, with proton transfer to the carbene ligand, which maintains η^6-arene interaction with the Fe^0 centre. In contrast, the paramagnetic high-spin iron(0) complex $[(^{PhiP}DippSn)\cdot Fe(IPr)][BAr^F_4]$ was obtained with the cationic stannylene ligand, $[^{PhiP}DippSn]^{+}$. This highly strained system proved to be highly reactive, reversibly activating H_2 across the Fe-Sn bond in forming the bridged dihydride-complex $[^{PhiP}DippSn(\mu\text{-}H_2)Fe(IPr)][BAr^F_4]$. To potentially achieve rare Fe^{-I} complexes, the cationic tetrylene-iron(0) complexes were reduced, which led to the successful isolation of the unprecedented Sn^{II}-Fe^{-I} complex $[^{PhiP}DippSn(IPr)Fe]$, which stands as the only reported example of a covalently bound iron(-I) ferrato species.

Chapter 8 discusses efforts towards the modification of the $^{PhiP}DippGeCl$ ligand, exchanging the chloride for different residues, which controls the electronic properties of the tetrel element in the germylene-nickel(0) complexes $[\{^{PhiP}DippGe(R)\}\cdot Ni(IPr)]$. This enables the modulation of reversible cooperative H_2 activation at the Ge-Ni interface, with the electronic nature of the differing ligands aligning with the kinetic profiles of the H_2 activation profile. This demonstrates the ease with which the developed ligands can be modified, and the profound effect this has on the fine-tuned reactive capacity of subsequent TM complexes. The project is prepared as a manuscript ready for submission.

As a whole, these projects are promising results towards developing and understanding the controlled MLC behavior of heavier tetrylenes in the coordination sphere of a TM. Insights are gained on how to manipulate and promote Lewis acidity and reactivity of the tetrel element in first-row TM complexes *via* ligand design. This thesis also demonstrates the use of these complexes in sustainable catalyses, which we ultimately aim to take towards the hydroamination with ammonia.

Kurzzusammenfassung

Die Hydroaminierung von ungesättigten Substraten mit Ammoniak ist nach wie vor einer der heiligen Grale der chemischen Katalyse. Übergangsmetalle (TM) waren bisher nicht in der Lage, diese anspruchsvolle Umwandlung zu katalysieren, da Ammoniak ein starker Sigma-Donor-Ligand ist. Metall-Ligand-Kooperativität (MLC) ist ein faszinierendes Konzept, mit dem eine Hydroaminierung erreicht werden kann, bei der ein nicht-unschuldiger Ligand aktiv an der Bindungsaktivierung und Katalyse beteiligt ist. Schwere Tetrylene sind solche nicht-unschuldigen Liganden, die in der Koordinationssphäre eines TMs Lewis-sauer bleiben können. Ziel dieser Arbeit ist es, zweizähnige schwere Tetrylen-TM-Komplexe der ersten Reihe zu entwickeln, um ein MLC-Verhalten mit katalytisch relevanten Substraten wie Ammoniak für eine mögliche Nutzung in der Katalyse zu erreichen.

In **Kapitel 3** stellten wir das neue zweizähnige, monoanionische Ligandengerüst ^{PhR}Dipp (^{PhR}Dipp = [{$Ph_2PCH_2Si(R)_2$}(Dipp)N]$^-$; R = *i*Pr, Ph; Dipp = 2,6-*i*$Pr_2C_6H_3$) vor und synthetisierten die entsprechenden (Chlor)germylen-Liganden ^{PhR}DippGeCl. Diese wurden zur Isolierung der (Chloro)germylen-Nickel(0)-Komplexe [{^{PhR}DippGe(Cl)}·Ni(PPh_3)$_2$] verwendet. Diese zeigten die Fähigkeit, Ammoniak am Bindungszentrum des Liganden über eine *σ*-Bindungsmetathesenreaktion reversibel zu aktivieren und Ammoniumchlorid zu eliminieren. Die entsprechenden kationischen Tetryliumyliden-Nickel(0)-Komplexe [(^{PhR}DippE)·Ni(PPh_3)$_2$][BAr^F_4] (E = Ge, Sn; [BAr^F_4]$^-$ = [{3,5-$(CF_3)_2C_6H_3$}$_4$B]$^-$) wurden in **Kapitel 4** entwickelt, wobei die Tetrylen-Ligandenzentren einen bemerkenswert hohe Lewis-Sauren Charakter aufwiesen, die die Bildung von Ammoniak-Addukten und die Abstraktion von Fluorid aus [SbF_6]$^-$ am Tetrel-Element ermöglichte. Außerdem wurde mit diesen Tetryliumylidenkomplexen eine effiziente und selektive katalytische Hydrosilylierung von Alkenen und Alkinen mit Phenylsilan erreicht. Der in Kapitel 4 und 5 erörterte Lewis-saure Charakter der Tetrylen-Liganden lässt sich auf die gekrümmten ^{PhR}Dipp-E-Ni-Winkel zurückführen, was zu einer minimierten *π*-Rückdonierung vom Ni^0-Zentrum zum Tetrel-Element führt.

Die Bedeutung des zweizähnigen Ligandengerüsts für diesen gekrümmten Winkel wurde in **Kapitel 5** durch die Synthese der entsprechenden einzähnigen (Chlor)tetrylenen ^{SiiP}DippECl (^{SiiP}Dipp = [($i$$Pr_3$Si(Dipp)N]$^-$) und die Isolierung der Tetryliumyliden-Nickel(0)-Komplexe [^{SiiP}DippE·Ni(PPh_3)$_3$][BAr^F_4] nachgewiesen. Diese einzigartigen Spezies zeigen einen linearen ^{SiiP}Dipp-E-Ni-Winkel und damit eine ausgeprägte *π*-Rückdonierung vom Ni^0-Zentrum zu den Tetrel-Elementen, was zu einer Donor-Akzeptor-Dreifachbindung führt und die tetrylzentrierte Lewis-Säure Eigenschaft abschwächt.

In **Kapitel 6** wurden selektive Synthesewege zu den freien kationischen Tetrylenen, [^{PhiP}DippE]$^+$, gefunden. Dies ermöglicht im Allgemeinen eine einfachere Implementierung des kationischen Ligandengerüsts bei der Herstellung von TM-Komplexen. Während das kationische Germylen [^{PhiP}DippGe]$^+$ durch Chloridabstraktion vom (Chloro)germylen ^{PhiP}DippGeCl erzeugt werden konnte, war das kationische Stannylen [^{PhiP}DippSn]$^+$ nur durch Hydridabstraktion vom entsprechenden (Hydrido)stannylen, ^{PhiP}DippSnH, als neuartiger Syntheseweg zu solchen kationischen Tetrylenen, zugänglich.

Um ein reaktiveres TM-Zentrum zu erhalten, wurden in **Kapitel 7** kationische Tetrylenkomplexe ([^{PhiP}DippE]$^+$) mit [Fe(IPr)] (IPr = [{HC(Dipp)N}$_2$C:]) entwickelt. Das kationische Germylen [^{PhiP}DippGe]$^+$ führte zu einem diamagnetischen „low-spin“ Eisen(0)-Komplex, [{^{PhiP}DippGe(IPr)}·Fe][BAr$^F{}_4$]. Dieser Komplex aktiviert Ammoniak und ergibt den (Amido-)Germylenkomplex [{^{PhiP}DippGe(NH$_2$)}·Fe{IPr(H)}][BAr$^F{}_4$] mit Protonenübertragung auf den Carben-Liganden, der die η^6-Aren-Wechselwirkung mit dem Fe^0-Zentrum aufrechterhält. Im Gegensatz dazu wurde der paramagnetische „high-spin“ Eisen(0)-Komplex [(^{PhiP}DippSn)·Fe(IPr)][BAr$^F{}_4$] mit dem kationischen Stannylen-Liganden [^{PhiP}DippSn]$^+$ erhalten. Dieses hochgradig gespannte System erwies sich als äußerst reaktiv und aktivierte reversibel H_2 über die Fe-Sn-Bindung unter Bildung des verbrückten Dihydrid-Komplexes [^{PhiP}DippSn(μ-H_2)Fe(IPr)][BAr$^F{}_4$]. Um potenziell seltene Fe^{-I}-Komplexe zu erhalten, wurden die kationischen Tetrylen-Eisen(0)-Komplexe reduziert, was zur erfolgreichen Isolierung des noch nie dagewesenen Sn^{II}-Fe^{-I}-Komplexes [^{PhiP}DippSn(IPr)Fe] führte, der als bisher einziges Beispiel für eine kovalent gebundene Eisen(-I)-Ferrato-Spezies gilt.

In **Kapitel 8** werden die Bemühungen um eine Modifizierung des ^{PhiP}DippGeCl-Liganden erörtert, bei der das Chlorid gegen verschiedene Reste ausgetauscht wird, wodurch die elektronischen Eigenschaften des Tetrelelements in den Germylen-Nickel(0)-Komplexen [{^{PhiP}DippGe(R)}·Ni(IPr)] gesteuert werden. Dies ermöglicht die Modulation der reversiblen kooperativen H_2-Aktivierung an der Ge-Ni-Grenzfläche, wobei die elektronische Natur der unterschiedlichen Liganden mit den kinetischen Profilen des H_2-Aktivierungsprofils übereinstimmt. Dies zeigt, wie einfach die entwickelten Liganden modifiziert werden können und welch tiefgreifende Auswirkungen dies auf die fein abgestimmte Reaktionsfähigkeit der nachfolgenden TM-Komplexe hat. Das Projekt ist als ein einreichungsreifes Manuskript vorbereitet.

Insgesamt sind diese Projekte vielversprechende Ergebnisse für die Entwicklung und das Verständnis des kontrollierten MLC-Verhaltens von schwereren Tetrylenen in der Koordinationssphäre eines TMs. Es werden Erkenntnisse darüber gewonnen, wie die Lewis-Säure und die Reaktivität des Tetrel-Elements in TM-Komplexen der ersten Reihe durch

Ligandendesign manipuliert und gefördert werden können. In dieser Arbeit wird auch die Verwendung dieser Komplexe in nachhaltigen Katalysatoren demonstriert, was wir letztendlich für die Hydroaminierung mit Ammoniak erreichen wollen.

List of Abbreviations

°C	Degree celsius
ΔE_p	Frontier orbital separation of carbenes
ΔE_{ST}	Singlet-triplet splitting energy
ΔG_R	Free enthalpy of a reaction at a given temperature
ΔH_R	Enthalpy of a reaction
ΔS_R	Entropy of a reaction
AA	Ammonia Affinity
Ad	Adamantane
Ar	Aryl
Ar'	4-Me-2,6-{C(H)Ph_2}$_2C_6H_2$
Ar"	2,4,6-*t*$Bu_3C_6H_2$
Ar°	2,6-{2,4,6-$(Me)_3C_6H_2$}$_2C_6H_3$
Ar*	2,6-$(Dipp)_2C_6H_3$
Ar^	*p*-CF_3Ph
Ar:	Ph,*p*-FPh or *p*-OMePh
Atm	Atmospheric pressure
$[BAr^F_4]^-$	$[\{3,5\text{-}(CF_3)_2C_6H_3\}_4B]^-$
CAAC	Cyclic (alkyl)(amino)carbene
cat.	Catalytic
calc.	Calculated
cm	Centimetre
COD	1,5-Cyclooctadiene
[Cp]	$[C_5H_5]^-$
[Cp*]	$[C_5Me_5]^-$
CV	Cyclic Voltammetry
Cy	Cyclohexyl
d	Distance
DFT	Density Functional Theory
Dipp	2,6-*i*$Pr_2C_6H_3$
DMAP	4-Me_2NPyr
DME	1,2-Dimethoxyethane
e.g.	Example given
EPR	Electron paramagnetic resonance
Et	Ethyl
FIA	Fluoride Ion Affinity

GPC	Gel Permeation Chromatography
h	Hour
HOMO	Highest Occupied Molecular Orbital
HIA	Hydride Ion Affinity
Hz	Hertz
i.e.	that is (latin *id est*)
*i*Pr	*iso*-propyl
IPr	[{HC(Dipp)N}$_2$C:]
IR	Infrared
J	Joule
k	Kilo
K	Kelvin
Keq	Equilibirum constant
K-Selectride	K[{CH(CH$_3$)CH$_2$CH$_3$}$_3$BH
KIE	Kinetic Isotope Effect
L	(SiMe$_3$)(Dipp)N
LFSE	Ligand Field Stabilization Energy
^{PhR}Dipp	[{Ph$_2$PCH$_2$Si(R)$_2$}(Dipp)N]$^-$
^{PhiP}Dipp	[{Ph$_2$PCH$_2$Si(*i*Pr)$_2$}(Dipp)N]$^-$
LUMO	Lowest Unoccupied Molecular Orbital
MBO	Mayer Bond Order
Me	Methyl
mg	Milligram
min	Minute
mm	Millimeter
mL	Millilitre
MLC	Metal-Ligand Cooperativity
*n*Bu	*n*Butyl
NBO	Natural Bond Orbital
NHC	N-Heterocyclic Carbene
NHC^{iPr}	[{(Me)CN(*i*Pr)}$_2$C:]
nm	Nanometer
NMR	Nuclear Magnetic Resonance
NPA	Natural Population Analysis
PDI	Polydispersityindex
PEP	Tridentate phosphine-functionalized tetrylene
Ph	Phenyl

Pn	Pnictides
ppm	Parts per million
Pyr	Pyridin
Pyrm	Pyrromethane
R	Residue
$R^{\#}$	Ph or Cy
$R^{:}$	Me, Et or *i*Pr
R*	Me or C_4H_9
R’	Me or C_3H_5
$R°_2$	$(NtBu)_2SiMe_2$
^{RR}Ar	$[\{(R_2PCH_2Si(R)_2)(Ar)\}N]^-$
S	Solvent
s	Second
^{SiiP}Dipp	$[(iPr_3Si)(Dipp)N]^-$
SQUID	Superconducting quantum interference device
T	Temperature
Tbb	$2,6\text{-}(Trip)_2C_6H_3$
*t*Bu	*tert*-Butyl
THF	Tetrahydrofuran
TM	Transition Metal
TMEDA	Tetramethylethylendiamine
tmvs	$SiMe_3C_2H_3$
Trip	$2,4,6\text{-}iPr_3C_6H_2$
Tsi	$C(SiMe_3)_3$
UV	ultraviolet
V	Volt
vis	Visible
viz.	Namely (latin *videlicet*)
VT	Variable Temperature
WA	Water Affinity
WBI	Wiberg Bond Index
WCA	Weakly-coordinating anion
XRD	X-Ray Diffraction
μ_B	Bohr Magneton

Chapter 1

Introduction and State of the Art

Climate change is presently a great challenge for humanity. Due to human anthropogenic carbon dioxide expulsion and the resulting greenhouse effect on the planet, the mean surface temperature has already risen by an average of ~1.06 °C, comparing the year 2022 to the preindustrial period (1880-1900).[1] A temperature increase above 1.5 °C would likely lead to dire consequences, such as mass extinction of species, frequent natural disasters, and inhabitability of large regions.[2] It is estimated that we as humanity must change our way of living and convert our energy consumption from fossil fuels to renewable energy sources within the next 10 to 20 years to avoid these catastrophic effects.[3] An important part of this process is the transformation of the chemical industry by lowering energy consumption, limiting waste production, and using abundant reagents for a sustainable future.[4] Catalysis plays a significant role in this transformation, since it lowers the amount of energy needed for chemical conversion, hence reducing the amount of energy needed for a reaction and potentially also avoiding unnecessary waste along the way.[5] Homogenous catalytic systems bring together a catalyst and reactants in one phase. The catalyst can be tailored through selection of the central reactive atom and ligand scaffold, while the catalyst and the catalytic process can be studied in much detail *via* numerous methods, allowing for rational design of this class of catalyst.[6] Transition metals (TM) have historically been used as central atoms in homogenous catalysts, due their incompletely filled *d*-orbitals enabling them to both donate and accept electrons.[7] More recently low-valent main group elements have also shown that they can act as TM mimics, also possessing the ability to perform catalysis.[8-11] A major challenge concerning homogeneous catalysis lies in avoiding rare, precious metals such as Pd or Pt, which are better exchanged for much more abundant first-row TMs or main group elements. A further important aspect is the discovery of new classes of efficient catalytic reactions, which includes the hydroamination of unsaturated organic substrates like alkenes with ammonia (Figure 1.1).

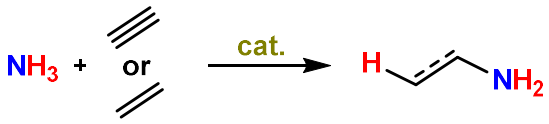

- primary Amines important for industry
- 100% Atom efficient reaction
- Avoiding energy/waster extensive alternatives

Problem: Traditional TM catalysis not applicable
→ Exploring new type of catalysts

Figure 1.1 Hydroamination of alkenes and alkynes with ammonia.

This challenge is considered to be one of the holy grails of modern catalysis.[12-13] The resulting amines are essential building-blocks for chemical and medicinal products in industry. Most current industrial processes to synthesise amines involve energy and waste extensive procedures, highlighting the importance of developing efficient hydroamination catalyses which utilise ammonia, which would be a 100% atom efficient process.[14] Heterogeneous systems (*i.e.* zeolites, alkali-metal amides) are known to achieve hydroamination of unsaturated C-C bonds with ammonia, but require extremely forcing conditions and only lead to rather low conversions.[15-19] TMs have not shown the ability to achieve this type of catalysis since ammonia is an excellent sigma donor ligand. Very few examples of TM-mediated ammonia activation are known, none of which show further catalytic application.[20-23] An intriguing concept which might overcome this problem is metal-ligand cooperativity (MLC), where both the TM and the ligand play a role in activating a substrate.[24] Such systems employ a non-innocent ligand, which can still participate in reactions whilst being bound to a TM.[25] The first cooperative activations of ammonia involving a TM were discovered by the groups of Millstein and Piers, where it was shown that, if a fitting ligand is employed, activation of ammonia can occur at the ligand-metal interface (Scheme 1.1, (a) and (b)).[26-28]

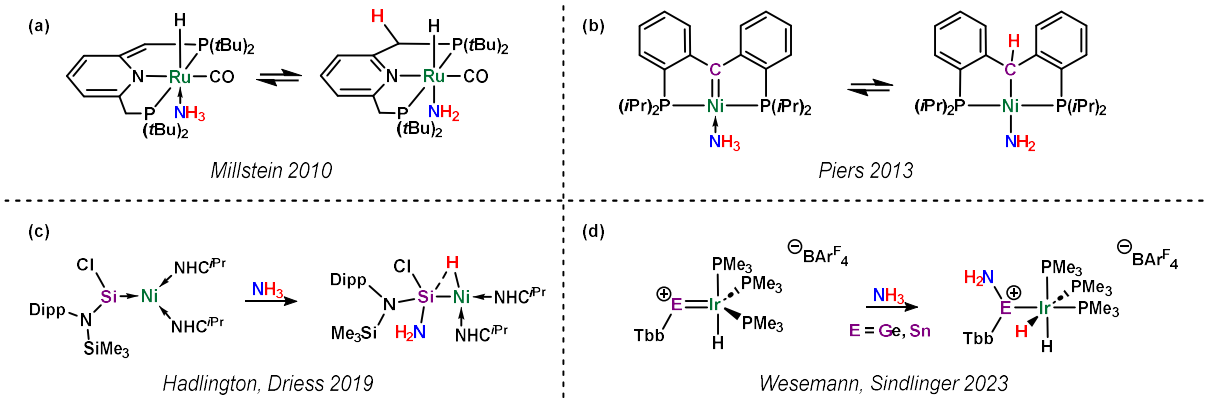

Scheme 1.1 Examples (a)-(d) for cooperative activation of ammonia *via* MLC.

In these examples the activation resulted in a terminal TM-amide without further reactivity, which would be needed for catalytic ability. Switching the reactivity of the non-innocent ligand from Lewis basic to Lewis acidic may lead to a TM-hydride upon N-H bond activation. Given the importance of TM-hydrides in catalysis, this may therefore open the door towards further chemistry and potential catalytic applications.[29] Heavier tetrylenes have emerged as such Lewis acidic non-innocent ligands.[30] They are group 14 elements in the oxidation state +II possessing a lone pair of electrons which can be used for TM coordination, and a vacant *p*-orbital making them Lewis acidic.[31] These ligands have demonstrated the ability to cooperatively activate ammonia *via* the described mechanism (Scheme 1.1, (c) and (d)), with the first such example reported by Hadlington and Driess in 2019.[32-33] Further investigations

into these and related systems are needed to evaluate their potential application for catalytic hydroamination. Activation and utilisation of other catalytically relevant substrates with these heavier tetrylene-TM systems is also of interest since this could provide valuable insights into cooperative activation or catalysis. The gained knowledge could then be used to design systems potentially replacing precious metal catalysts in current relevant catalytic applications. In this regard ligand design becomes paramount to control the electronic character of both the main group element and the transition metal to achieve MLC.

Transition Metal Complexes

Transition metals have historically been the most powerful tool for catalysis, particularly in homogenous systems.[5] They possess partially filled *d*-orbitals, giving them the ability to donate and accept electrons, so enabling the interaction of these orbitals with various different types of ligands and substrates. These *d*-orbitals are classified as five different orbitals, each with a differing spatial orientation and probability surface (Figure 1.2).[34]

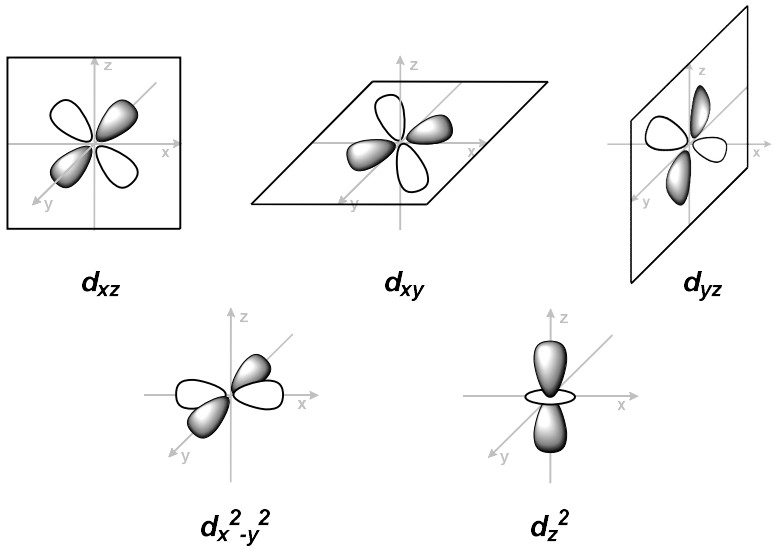

Figure 1.2 Probability surface and orientation of the five different *d*-orbitals.

Ligand field theory is the most common way to describe TM complexes based on these orbitals, leading to the prediction of important properties such as magnetism, reactivity, absorption behaviour, and preferred coordination geometry.[35] This is built on molecular orbital theory, where the *d*-orbitals and higher lying *s*- and *p*-orbitals are combined with the ligand orbitals, examining the interaction between the TM-ion and the ligands. In the naked TM-ion, the *d*-orbitals are of degenerate energy. In the presence of ligands, the energy of the *d*-orbitals is affected to different degrees depending on the geometry of the ligands relative to the five *d*-orbitals at the TM centre. As an example, $[Co(NH_3)_6]^{3+}$ has an octahedral geometry, with the ammonia ligands centred along the *x*, *y* and *z*-axes. This leads to the d_{z^2} and the $d_{x^2-y^2}$ orbitals

being raised relatively high in energy due to the direct interaction with the ligands (Figure 1.3). The energy of the other three *d*-orbitals (*i.e.* d_{xy}, d_{xz} and d_{yz}) changes by a relatively small amount, since the orbitals lie in between the axes and only minimal interaction with the ligands is observed. These two resulting energy levels are separated by the "*d*-orbital splitting energy"

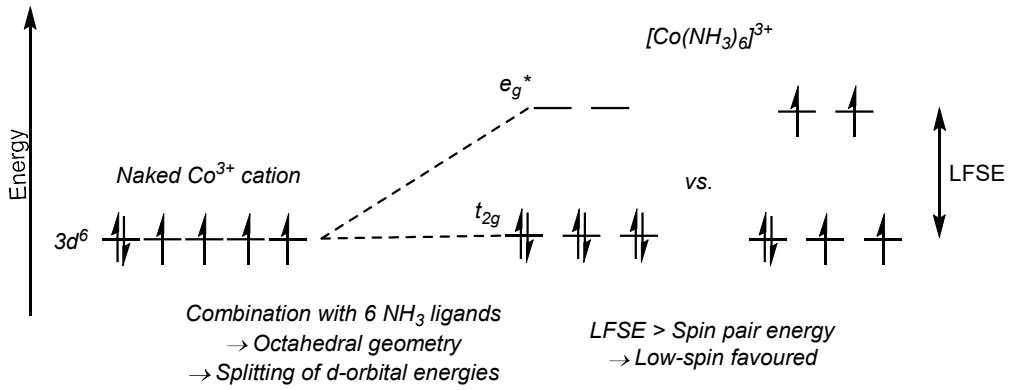

Figure 1.3 Octahedral ligand field splitting in $[Co(NH_3)_6]^{3+}$ favoring the low-spin state.

or the Ligand Field Stabilisation Energy (LFSE). Other geometries (*e.g.* tetrahedral or square-planar) will give different *d*-orbital splitting patterns due to altered interaction of the ligands with the *d*-orbitals. A highly unsymmetrical ligand field can even lead to the splitting of all five *d*-orbitals. The electronic configuration and reactivity are critically impacted by the LFSE. If the LFSE is smaller than the spin pair electron energy, a paramagnetic high-spin complex with multiple unpaired electrons is formed, while a bigger LFSE leads to the low-spin complex having the maximum amount of electron pairs. Naturally, the LFSE also impacts the reactivity of the complex since it can represent the HOMO-LUMO gap (HOMO = Highest occupied molecular orbital; LUMO = Lowest unoccupied molecular orbital) of the molecule.

The two predominantly observed interactions of TMs with ligands are *σ*-donation and *π*-back-donation. While the *σ*-bond is typically the donation of an electron pair of the ligand to one of the empty *d*-orbitals of the TM, *π*-back-bonding occurs from a filled *d*-orbital of the TM to an empty orbital of the ligand. When we look at carbon monoxide as a ligand, both of these

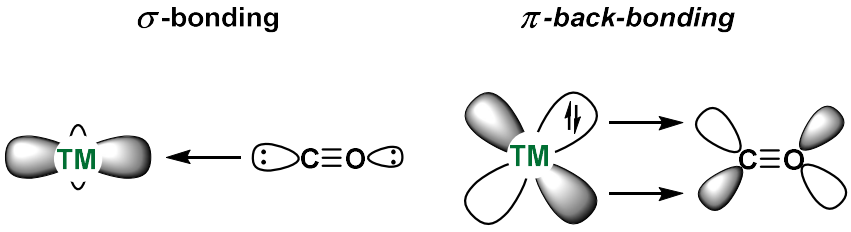

Figure 1.4 σ-bonding (right) and π-back-bonding (left) between a TM centre and carbon monoxide.

interactions can be observed (Figure 1.4). While the *π*-back-bonding leads to a more stable TM-CO bond, this also influences the carbon monoxide itself, weakening the bond between

carbon and oxygen, given that the π^*-acceptor orbital is of anti-bonding character, which can be observed using IR spectroscopy.

Due to the often small energy separation of their frontier orbitals, TM complexes exhibit a vast number of different reactivities allowing for catalytic applications. A reaction common to many catalytic cycles is oxidative addition, which can be followed by a variety of different reactions such as insertion, β-hydride elimination, or transmetallation. The catalytic cycle is often closed by reductive elimination of the product and regeneration of the active catalyst. The ability of the TM to easily interchange between oxidation states and different geometries is key for their excellent catalytic applicability. Taking the active species of Wilkinson's catalyst ([Rh(Cl)(PPh_3)$_2$S] (**I**; S = solvent) as an example, the first step involves oxidative addition of H_2 at the Rh^I centre, which is initiated by overlap of the frontier orbitals (Scheme 1.2). Following the insertion of an alkene into the Rh^{III}-H bond, reductive elimination of the corresponding alkane leads to regeneration of **I**.[36-40] This showcases a typical catalytic cycle for single-site hydrogenation of an alkene.

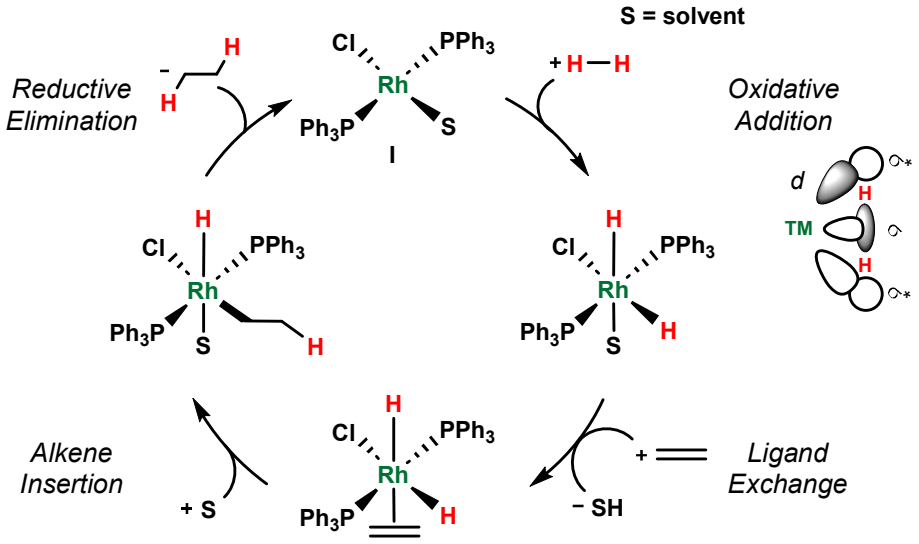

Scheme 1.2 Catalytic cycle of the hydrogenation of ethylene with **I** and frontier orbital interaction between H_2 and a TM centre.

One might assume that the corresponding catalysis using ammonia in place of H_2 can be accessed. Even though primary and secondary amines have been successfully used for TM catalysed hydroamination of alkenes and alkynes, the efficient utilisation of ammonia as a substrate thus far remains elusive, due to the fact that ammonia is an excellent sigma donor ligand, leading to inert Werner-type complexes.[20, 41-42] There have been very few reports on TM complexes which hold the ability to activate ammonia, most prominently by the group of Hartwig. Here, iridium(I) complexes [{(C_2H_4P*t*Bu_2)$_2$C(H)}Ir(C_2H_3R')] (R' = Me (**II**), C_3H_5 (**III**)) demonstrated the reversible oxidative addition of ammonia, but without further catalytic

application (Scheme 1.3).[21-23] Therefore different strategies to achieve this long standing goal need to be explored.

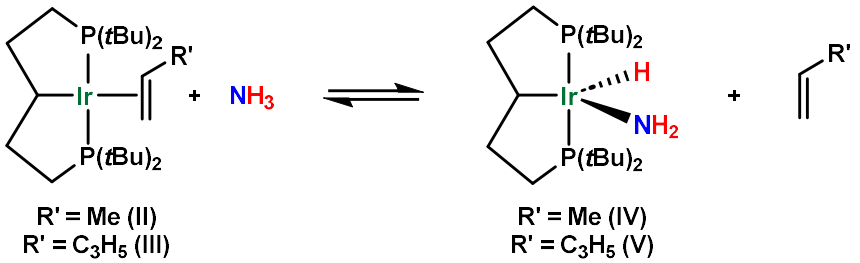

Scheme 1.3 Reversible oxidative activation of ammonia with iridium(I) complexes **II** and **III**

Low-valent Group 14 Element(II) Species

Low-valent main group element compounds have been of growing importance in the last two decades due to their potential to behave like TMs.[8, 43] They typically have a small energy separation between the frontier orbitals, similarly to TMs, enabling the activation of substrates such as H_2 or ammonia.[44-46] These compounds are therefore broadly explored as replacements for TMs as abundant and non-toxic catalysts. A big part of these developments are low-valent

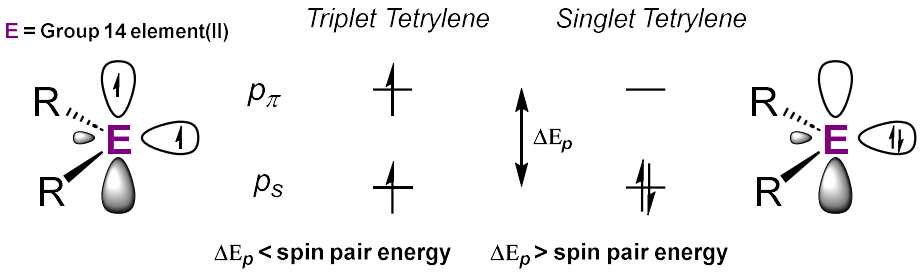

Figure 1.5 Electronic configuration of tetrylenes comparing the triplet state to the singlet state.

group 14 elements in the oxidation state +II, so called tetrylenes. These species have an electron sextet with two non-bonding electrons being present, while the two residues are generally bent resulting in a sp^2-p type hybridisation.[47] This results in a essentially unchanged p_π-orbital and a stabilised p-orbital with s-character (p_s-orbtial), with the frontier orbital separation (ΔE_p) dictating electronic state and reactivity of the tetrylene. In the triplet state the two electrons are unpaired and located in the p_π-orbital and the p_s -orbital, making it a biradicaloid. The singlet state is present if ΔE_p is bigger than the spin pairing energy, with both electrons located in the p_s-orbital leading to a nucleophilic lone pair of electrons and an electrophilic vacant p_π-orbital, making the carbene ambiphilic (Figure 1.5). This already shows certain similarities to the Ligand Field Theory for TMs, where the size of the LFSE dictates if a complex adapts a high-spin or a low-spin state. The energy difference between the triplet and

singlet state is called the singlet-triplet splitting energy (ΔE_{ST}). When calculating these for the parent tetrylenes (*i.e.* [H_2E:]) a trend can be seen. While [H_2C:] occupies the triplet ground state with a singlet-triplet energy difference of -14.0 kcal/mol, the heavier elements (E = Si, Ge, Sn, Pb) all have a positive ΔE_{ST} meaning that these elements favour the singlet state. ΔE_{ST} increases from Si to Pb, in line with an increasing ΔE_p (*i.e.* the HOMO-LUMO gap for singlet tetrylenes), leading to a decrease in reactivity.[48] By choosing the fitting ligands for these tetrylenes the energy of the frontier orbitals can be modified, which is essential for stabilising these reactive species. Introduction of elements such as nitrogen, where the neighbouring element can π-donate into the p_π-orbital, leads to stabilisation of the species by increasing the energy of the p_π-orbital. The bite angle between the two residues also plays an important role since it has a direct impact on the energy of the orbitals and the ΔE_{ST}. A shrinking angle, which can be enforced by geometric constraints, will lead to a bigger ΔE_{ST}.[49] Furthermore the steric demand of the ligand is also of great importance, since this provides kinetic stabilisation, preventing oligomerisation.

The first carbenes were isolated as TM complexes as early as 1964.[50] Still, the isolation of stable 'free' carbenes eluded chemists until the discovery of (silyl)(phosphino)carbene [$(Me_3Si)\{(iPr_2N)_2P\}C$:] (**VI**) in 1988.[51-53] The discovery of the first N-heterocyclic carbene (NHC) [$\{(H)CN(Ad)\}_2C$:] (**VII**; Ad = adamantane) by the group of Arduengo shortly after, in 1991, demonstrated that carbenes can be designed to be highly stable species, and can even be prepared relatively easily on a large scale (Scheme 1.4).[54] This is due to the stabilisation from

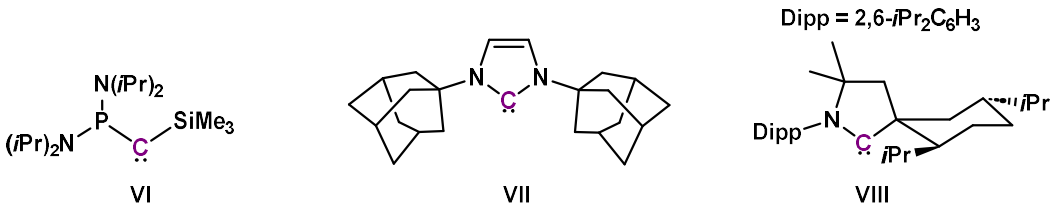

VI VII VIII

Scheme 1.4 First examples of a stable (silyl)(phosphino)carbene **VI**, NHC **VII** and CAAC **VIII**.

the two neighbouring nitrogen atoms, while the cyclic structure enforces a minimal bite angle further stabilising the carbene. This led to the development of a plethora of different NHCs, which have been very widely used as ligands in TM complexes, and are additionally commonly used to stabilise highly reactive main group species.[55-56] Closely related are the cyclic (alkyl)(amino)carbenes (CAACs; *e.g.* **VIII**), which were discovered by the group of Bertrand in 2005 (Scheme 1.4).[57] These carbenes possess an adjacent nitrogen and carbon atom, while still maintaining a cyclic structure. This leads to a higher Lewis acidity due to reduced π-donation into the vacant p_π-orbital, whilst also increasing the nucleophilicity due to the σ-donating effect of the carbon.[58] This goes to show that modifications can have a big impact

on these species, completely changing the electronic nature and reactivity of the tetrylene.

Closely related to carbenes, the heavier tetrylenes have also been extensively studied due their differing properties. They generally have a greater HOMO-LUMO gap, making them more accessible, while reduced bond energies should favour reversible binding, which is an important characteristic for catalytic applications. Additionally, kinetic stabilisation by utilising bulky substituents is critical since oligomerisation - forming dimers, oligomers, or even small clusters - becomes more likely with increasing atomic size.[31] For Pb, the inert pair effect is observed, since a lower ability to form hybrid orbitals leads to a $(ns)^2(np)^2$ hybridisation, resulting in an almost inert lone pair with high *s*-character, an effect which increases on descending group 14.[14, 59] This also increases the Lewis acidity of the compounds, since stabilisation *via* π-donation is less effective.

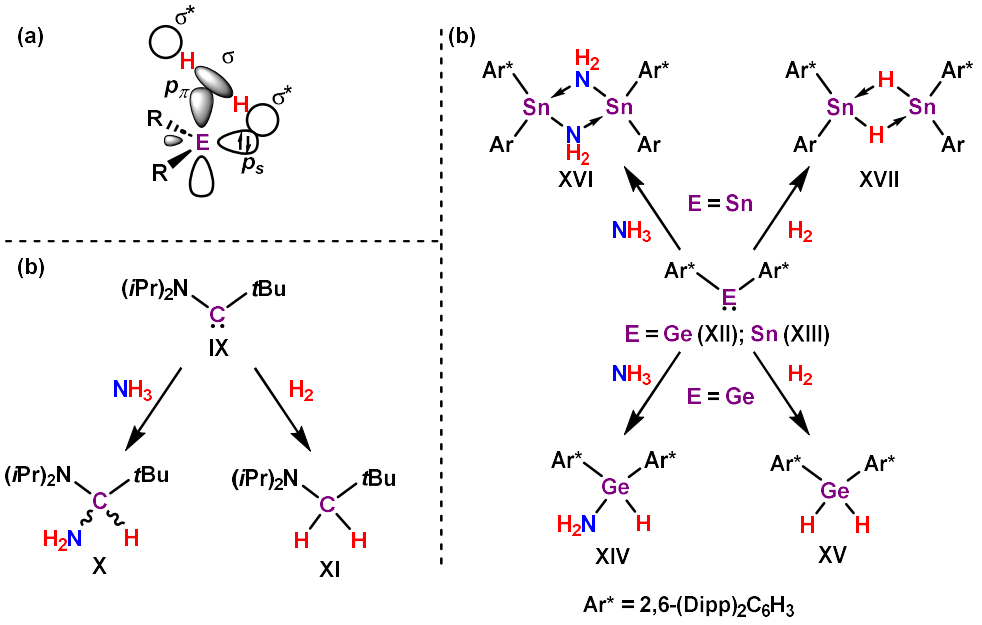

Figure 1.6 (a): Frontier orbital interaction between tetrylenes and H_2; (b): Activation of ammonia and H_2 by carbene **IX**; (c): Activation of ammonia and H_2 by germylene **XII** and stannylene **XIII**.

Due to the highly reactive nature of tetrylenes, small molecule activation *via* oxidative addition can be realised. This reactive capacity defines the TM-like behaviour of these compounds. In 2007 it was shown by the group of Betrand, that the acyclic (alkyl)(amino)carbene [(*t*Bu)(*i*Pr$_2$N)C:] (**IX**) is able to activate H_2 and ammonia under ambient conditions *via* oxidative addition at the carbon centre (Figure 1.6(b)).[45] The same type of oxidative activation with H_2 and ammonia was later reported with bis(aryl)germylene [Ar*$_2$Ge:] (**XII**; Ar* = 2,6-(Dipp)$_2$C$_6$H$_3$; Dipp = 2,6-*i*PrC$_6$H$_3$), whilst the related stannylene, [Ar*$_2$Sn:] (**XIII**), resulted in arene elimination under the same reaction conditions (Figure 1.6(c)).[46] The suggested process for the activation of H_2 *via* orbital overlap, which was supported by DFT calculations, was reminiscent of the H_2 activation with a TM centre (Figure 1.6(a)). Although this form of ammonia activation can be

seen as a first step towards catalytic hydroamination, the resulting products are very stable, since the tetrel element is in the oxidation state +IV and reductive elimination back to +II, as an essential step to achieve catalytic turnover, is highly unfavourable.

The Lewis acidity of heavier tetrylenes can be further enhanced by removing one residue from the tetrel element resulting in cationic compounds with two vacant *p*-orbitals, so called tetryliumylidenes (Figure 1.7(a)).[60] The usage of inert weakly-coordinating anions (WCAs) is crucial to realise this, to avoid coordination of the anion at the tetrel element.[61] The first tetryliumylidene complexes were isolated by utilising Cp* (Cp* = $[C_5Me_5]^-$) as a ligand giving $[ECp^*][B(C_6F_5)_4]$ (E = Ge (**XVIII**), Sn (**XIX**), Si (**XX**)) (Figure 1.7(b)).[62-63] The highly reactive nature of such species is underpinned by the fact that no real naked (*i.e.* one-coordinate) tetryliumylidenes have been isolated to date. Examples of so-called quasi one-coordinate plumbylene (*viz.* $[\{2,6\text{-}(Trip)_2C_6H_3\}Pb]^+$, **XXI**; Trip = 2,4,6-*i*$Pr_3C_6H_2$), germylene (*viz.* $[\{(Me_3Si)(Ar')N\}Ge]^+$, **XXII**; Ar' = 4-Me-2,6-$\{C(H)Ph_2\}_2C_6H_2$), and stannylene (*viz.* $[\{(Me_3Si)(Ar')N\}Sn]^+$, **XXIII**) cations, stabilised using highly bulky ligand systems, are known (Figure 1.7(c) and (d)). In these examples, weak arene stabilisation from the aromatic solvent or the ligand to the tetrel element is observed.[64-65] Otherwise, successful isolation has been reported *via* intermolecular stabilisation from arene[66], carbene[67-70] or carbodiphosphorane[71] donors, while other strategies use intramolecular stabilisation by *N*-Donors[72-75] or phosphines[76-77].

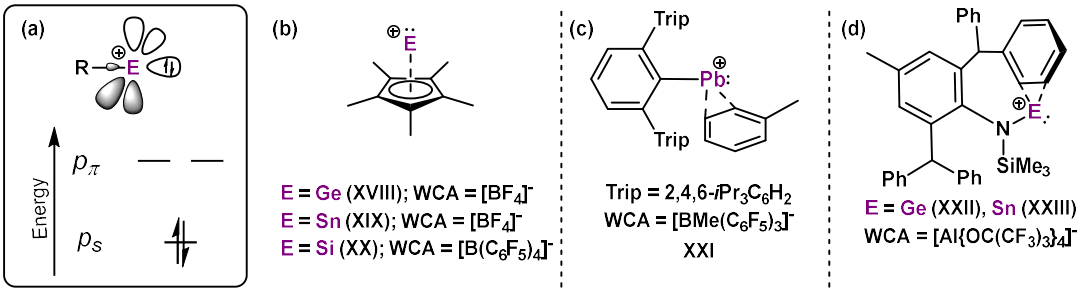

Figure 1.7 (a): Frontier orbitals of tetryliumylidenes; (b)-(d): Selected examples of tetryliumylidenes (**XVIII**-**XXIII**).

Metal-Ligand Cooperativity

Established TM catalysis has relied on ligands which alter the reactivity of the TM *via* electronic or steric influence but do not directly participate in the chemical bond activation, making them spectator ligands. Metal-ligand cooperativity (MLC) has emerged as an important concept for TM complexes to achieve small molecule activation or catalytic conversions by using non-innocent ligands.[78] These ligands remain reactive while being bound to a TM, which can lead to synergistic bond activation. The goal is to either improve working catalytic systems, or indeed to discover new catalytic pathways for challenging chemical conversions. Different

strategies can be employed to allow for cooperative activation. This can involve the ligand acting as a Lewis base or Lewis acid leading to synergistic activation (Figure 1.8(a) and (b)).

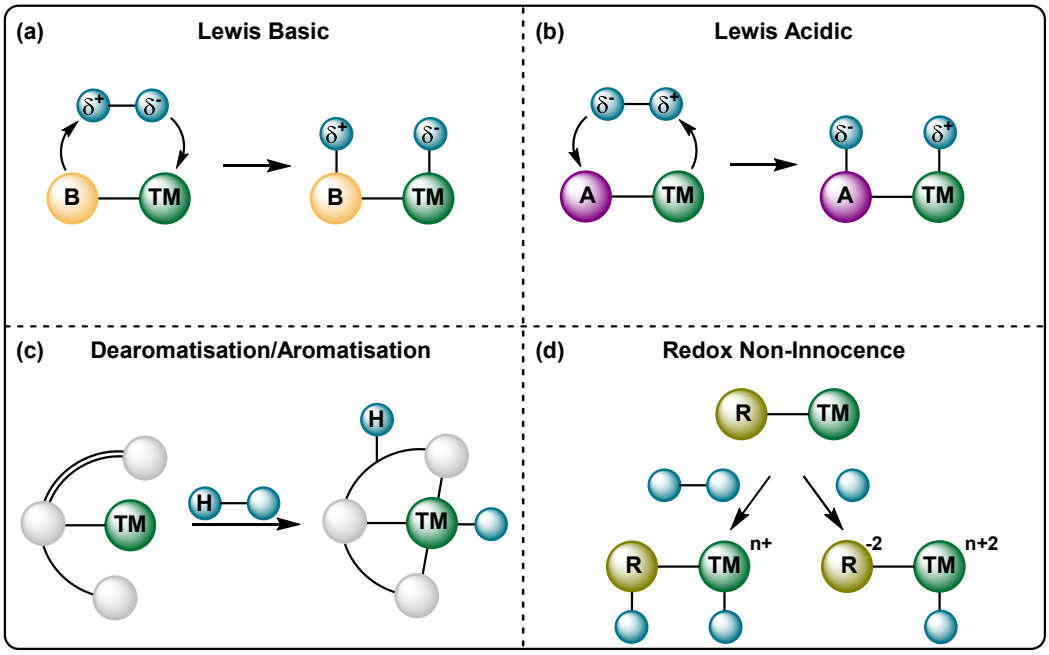

Figure 1.8 Different strategies to achieve MLC: (a) Ligand acting as Lewis base; (b) Ligand acting as Lewis acid; (c) Ligand aromatising upon protonation/activation; (d) Ligand acting redox non-innocent.

Another strategy is the dearomatisation of a ligand backbone by a base, which can lead to aromatisation of the backbone *via* substrate activation and protonation (Figure 1.8(c)).[79-80] Furthermore, redox non-innocent ligands can also be employed, either acting as electron reservoirs or directly participating in bond activation as a radical source (Figure 1.8(d)).

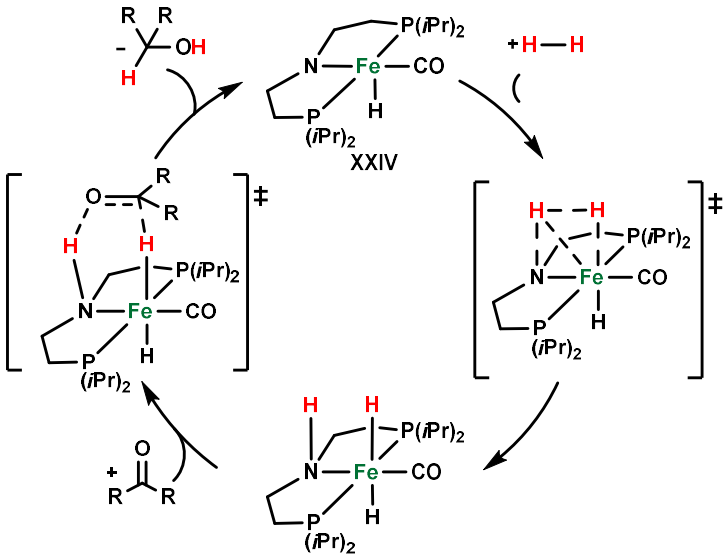

Scheme 1.5 Catalytic cycle for the hydrogenation of ketones *via* MLC mechanism in a Fe^{II} complex using a Lewis basic ligand with **XXIV** as catalytically active species.

The most prominent strategy thus far has been ligands acting as a Lewis base. Morris employed this concept using a tridentate ligand scaffold in a series of Fe complexes (*i.e.* **XXIV**), which exhibited excellent activity and selectivity for the hydrogenation of ketones, which had previously only been viable for complexes incorporating precious metals such as Rh, Ru, or Ir.[81-84] Key insights into the mechanism showed that the active species is the (amido)iron(II)-hydride **XXIV**, and that the catalysis is highly dependent on the synergistic nature of the complex (Scheme 1.5).[85] This showcases that MLC can lead to effective catalytic systems, which can even utilise abundant first-row TM centres.

Cooperative activation of ammonia with a non-innocent Lewis basic ligand has been demonstrated by the groups of Piers, in 2013, and Roesler, in 2015, with the Ni^0 complexes **XXV** and **XXVII** (Figure 1.9(a) and (b)). In these examples, a nucleophilic carbene ligand accepts a proton from nickel-bound ammonia, resulting in a nickel(II)-amide fragment and the

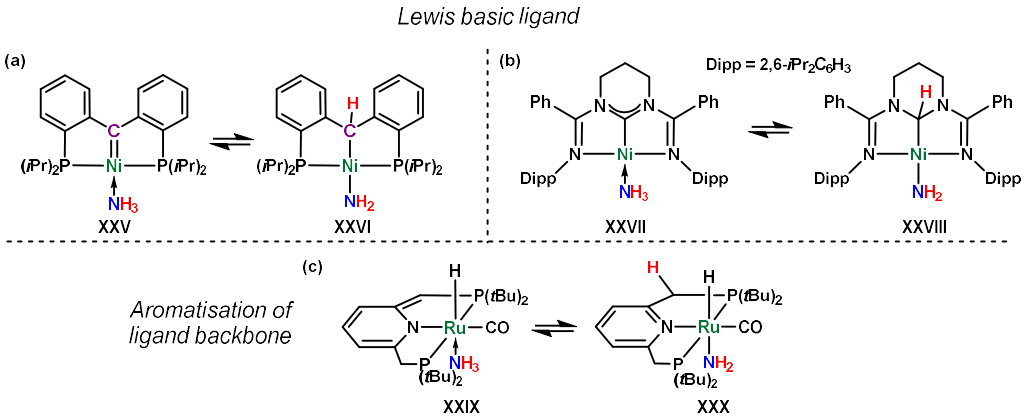

Figure 1.9 (a) and (b): Cooperative ammonia activation with a Lewis basic ligand (**XXV** and **XXVII**); (c): Cooperative ammonia activation *via* aromatisation of the ligand backbone (**XXIX**).

activation products **XXVI** and **XXVIII**.[27-28] The group of Millstein was also reported on the cooperative activation of ammonia in 2010 in the Ru^{II} complex **XXIX**, where the ligand also acts as a hydrogen acceptor leading to aromatisation of the backbone, in forming the ruthenium(II)-amide complex **XXX** (Figure 1.9(c)).[26] Remarkably, all three transformations were shown to be reversible, an important aspect for possible catalytic applications. Although catalysis was not demonstrated in this regard, these are promising examples for the activation of ammonia in a TM complex, aided by a MLC mechanism.

Heavier Tetrylenes as monodentate Ligands

As described above, tetrylene compounds are single-centre ambiphiles, being both Lewis basic and Lewis acidic at the tetryl element. They possess a lone electron pair with high *s*-character, which makes them nucleophilic and allows for coordination to a TM. Additionally,

they have a vacant *p*-orbital leading to Lewis acidic properties, which can be retained once coordinated to a TM. Heavier tetrylenes are reluctant to *sp*-hybridise on descending group 14. This results in a lone pair with higher *s*-character, and an increased electrophilicity and amphiphilicity when compared to carbenes. This makes heavier tetrylenes intriguing candidates for non-innocent ligands and MLC activation. The Lewis acidity of the tetrel element in TM complexes highly depends on the degree of *π*-back-donation from the TM centre. A high

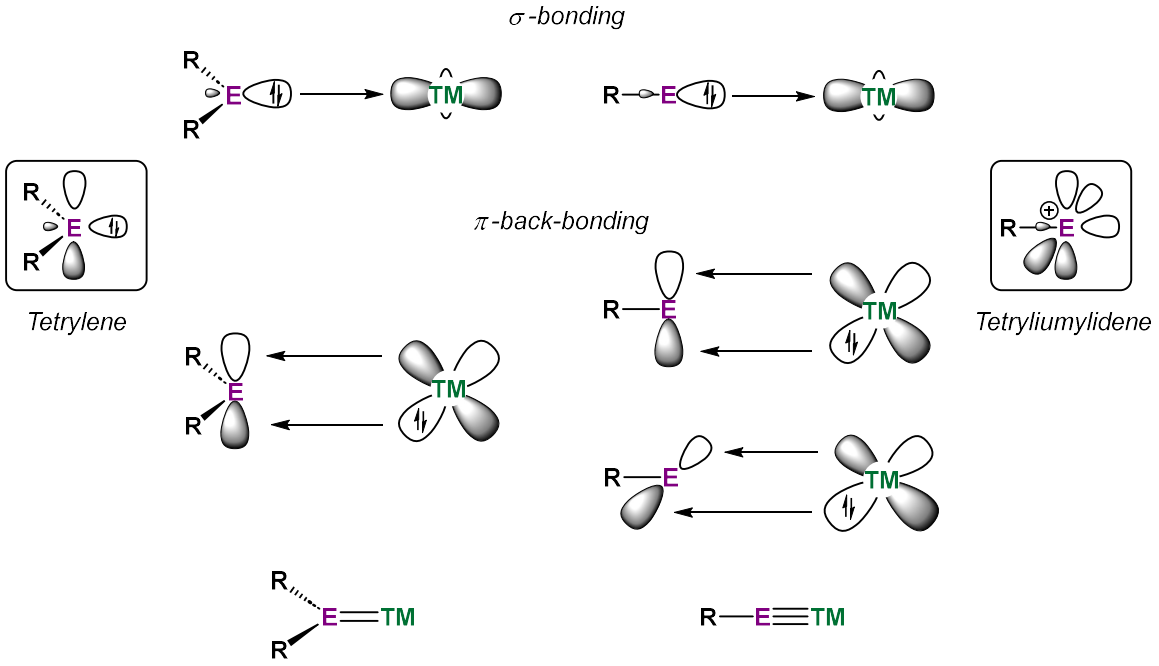

Figure 1.10 Possible frontier orbital interactions of a tetrylene (left) and tetryliumylidene (right) with a TM centre.

degree of back-donation can lead to a formal double bond when two residues are present at the tetrel element and orbital overlap is geometrically allowed/favoured. The same holds true for tetryliumylidenes with one residue, which can result in triple bonds to a TM centre (Figure 1.10). Such back-donation quenches the Lewis acidity of the ligand binding centre and can limit the reactivity. To facilitate cooperative bond activation, ligand design is crucial. Sufficient thermodynamic and/or kinetic stabilisation needs to be in place in order stabilise such reactive species. However, too much stabilisation can hamper reactivity, by quenching the Lewis acidity (thermodynamic) or sterically blocking reactive sites (kinetic), rendering the heavier tetrylene a spectator ligand. Especially cyclic amidinate-stabilised silylenes have been successfully used in catalysis, but generally only act as spectator ligands, due to the high coordination number at silicon in these ligands, minimising Lewis acidity and reactivity.[86-88] A fine balance between stability and sufficient reactivity is therefore critical, to retain Lewis acidity of the low-valent ligand centre, and allow for controlled MLC.

Hieber published the first heavier tetrylene-TM complexes in 1957, being stannylene-cobalt(0) complexes $[(R^*)_2Sn{\cdot}\{Co(CO)_{4-x}(PPh_3)_x\}_2]$ (x = 0, 1; R* = Me, C_4H_9) and the stannylene-iron(0) complex $[(C_4H_9)_2Sn{\cdot}\{Fe(CO)_4\}]$, which were not recognised as tetrylene complexes and only characterised concerning their chemical composition.[89] While the bis(dichlorosilylene)platinum(0) complex $[(Cl_2Si)_2Pt(PPh_3)_2]$ (**XXXI**) was described in 1970, the

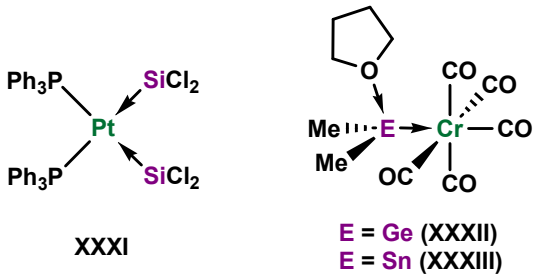

Scheme 1.6 TM complexes **XXXI-XXXIII** marking the beginning of the field of heavier tetrylene TM complexes.

beginning of the field is attributed to Marks, who published germylene and stannylene-chromium(0) complexes $[Me_2(THF)E{\cdot}Cr(CO)_5]$ (E = Ge (**XXXII**), Sn (**XXXIII**)) in 1971 (Scheme 1.6).[30, 90-91] It was shown that the heavier tetrylenes retain their Lewis acidity, in contrast to carbenes, by isolating the THF adducts of the TM bonded tetrylenes.

The first observation of cooperative bond activation with heavier tetrylene-TM complexes was reported by the group of Holl in 1995, utilising the germylene-platinum(0) complex $[\{(Me_3Si)_2N\}_2Ge{\cdot}Pt(PEt_3)_2]$ (**XXXIV**), which could reversibly activate H_2 under ambient conditions yielding the (1,2-dihydro)-germylplatinum complex **XXXV** (Scheme 1.7).[92-93] It was

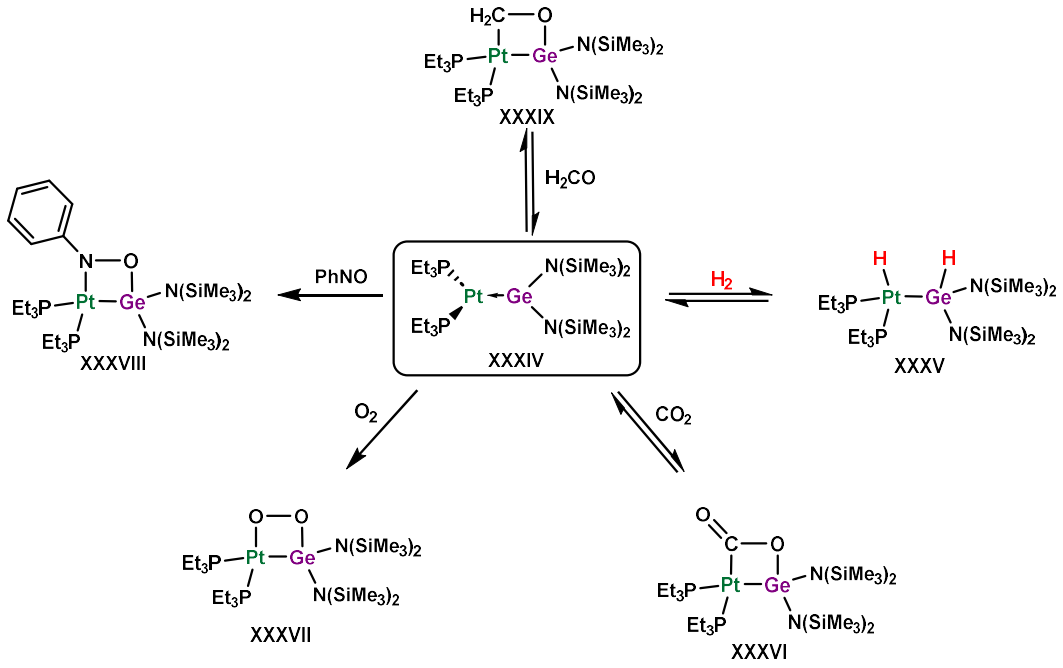

Scheme 1.7 Reactivity of **XXIV** undergoing cooperative activation of various substrates.

shown that the mechanism first involves activation of H_2 at the Pt^0 centre, followed by hydride migration to the germylene. The complex also engaged in cooperative cycloaddition reactions across the Pt-Ge bond with polarised small molecules, such as carbon dioxide, oxygen, nitroso compounds, and formaldehyde, in some cases even reversibly, giving four-membered metallacycles (**XXVI-XXIX**; Scheme 1.7).[92, 94-96] This demonstrated the non-innocent character of heavier tetrylenes in TM complexes, and their ability to act cooperatively in small-molecule activation.

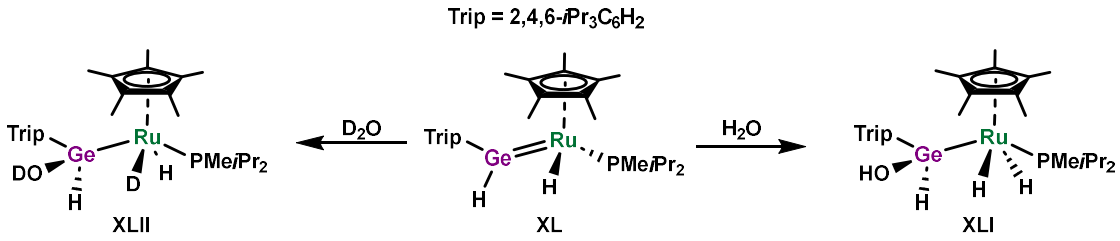

Scheme 1.8 Water activation by Ru^{II} complex **XL** *via* cooperative oxidative addition.

It was later shown that the (hydrido)germylene-ruthenium(II) complex [(Trip)(H)Ge·Ru(H)(Cp*)(PMe*i*Pr$_2$)] (**XL**) can achieve similar bond activation reactions, cleaving H_2O across the Ge-Rh bond to give a Ge-hydroxide (**XLI**) (Scheme 1.8).[97] Through labelling experiments with D_2O, it was shown that the mechanism proceeds *via* oxidative addition across the tetrylene-TM bond without any hydride scrambling. More recently Driess and Hadlington reported on the (chloro)silylene-nickel(0) complex [{(Me$_3$Si)(Dipp)N}(Cl)Si·Ni(NHC^{iPr})$_2$] (**XLIII**; (NHC^{iPr} = [{(Me)CN(*i*Pr)}$_2$C:]), which showed the ability to cooperatively activate a variety of different substrates (Scheme 1.9).[98]

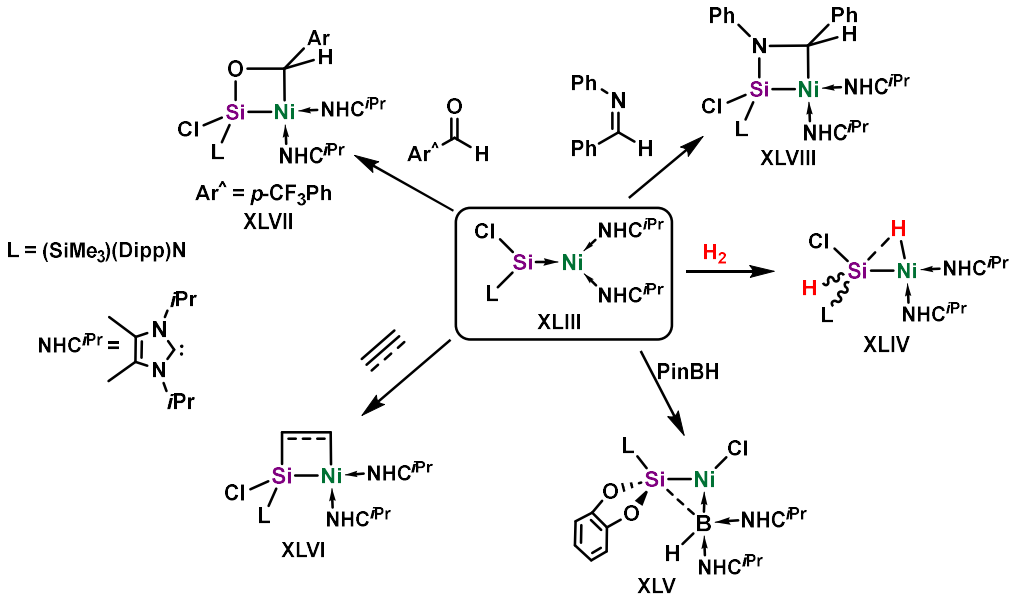

Scheme 1.9 Cooperative reactivities of **XLIII**, activating H_2 *via* oxidative oxidation and unsaturated organic substrates *via* cycloadditon.

H_2 was activated under ambient conditions giving a (1,2-dihydro)-silylnickel complex (**XLIV**), with the Ni-*H* fragment bridging to the silicon centre. As for the above described Ge^{II}-Pt^0 complex **XXXIV**, DFT calculations suggested that the initial activation takes place at the Ni^0 centre, followed by hydride migration to silicon. The reaction with pinacolborane resulted in the activation of the B-O bonds giving a (hydrido)borylene-nickel(II) complex (**XLV**). The intricate cooperative mechanism of this reaction was again eluded using DFT calculations. Additionally, various cooperative cycloaddition reactions were observed with alkenes, alkynes, aldehydes, and imines, resulting in numerous four-membered metallacycles (**XLVI**-**XLVIII**).[99] The same group also reported on the cooperative activation of ammonia with **XLIII**, leading to an {(amido)silyl}nickel(II)-hydride complex (**IL**), with the hydride ligand again having bridging character (Scheme 1.10).[32] The reactivity of the corresponding heavier parent pnictines, PH_3 and AsH_3, resulted in a different mode of activation, in line with their relatively higher acidities when compared with NH_3. In both cases, insertion into the Si-N bond and migration of the chloride to the nickel centre was observed, forming pnictide nickel complexes **L** and **LI** (Scheme 1.10). While these examples showcase the versatility of tetrylene-TM complexes for cooperative bond activation, further reactivity of the activated species would be required for catalytic applications, which were not reported.

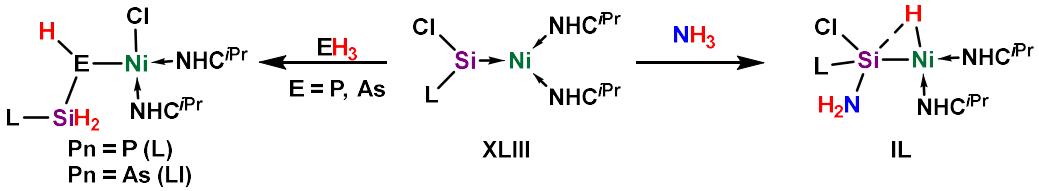

Scheme 1.10 Cooperative oxidation of EH_3 species (E = N, As, P) with **XLIII** leading to differing outcomes.

Another possibility to introduce a vacant *p*-orbital adjacent to a TM centre are metallo-tetrylenes with a formal bond between the tetrel element and TM centre. This results in a lone pair and a vacant *p*-orbital at the tetrylene, which typically lowers the HOMO-LUMO gap, and increases the reactivity of the tetrylene centre.[100-103] The first example of such a species was reported by the group of Jutzi in 1994, being the ferrio-germylene [Ar"Ge·Fe(Cp*)(CO)$_2$] (**LII**, Ar" = 2,4,6-*t*Bu$_3$C$_6$H$_2$) (Scheme 1.11(a)).[104] A number of metallo-tetrylenes have since been published. Due to the high reactivity of the tetrylene centre, however, oxidative addition usually occurs directly at this reactive site, suggesting that they are not ideal for cooperative small molecule activation.[100, 102] Metallo-tetrylenes have a bent angle at the tetrylene centre forming a single bond between TM and tetrel element due to poor orbital overlap between the vacant *p*-orbtial of the tetrylene and filled *d*-orbtials of the TM. Key tautomers of these species are tetrylidyne complexes, which have a near linear angle between the TM, the tetrel element, and the ligand, leading to an ideal orbital overlap. This causes a

high degree of *π*-back-donation and results in a short tetrel-TM bond, which can be best described as a triple bond (Figure 1.10). The first example was reported by the group of Power in 1996, who reported the germylidyne-molybdenum(II) complex [(Tbb)Ge·Mo(Cp)(CO)$_2$] (**LIII;** Tbb = 2,6-(Trip)$_2$C$_6$H$_3$; Cp = $C_5H_5^-$) with a very short Ge-Mo bond length of 2.271(1) Å, and a near liner Mo-Ge-C angle of 172.2(2)° (Scheme 1.11(b)).[105] In a subsequent study, the group

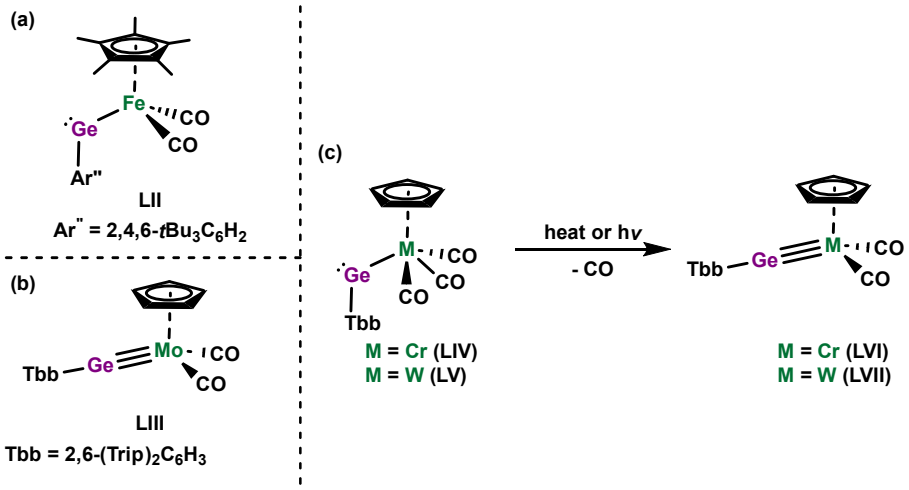

Scheme 1.11 (a): First reported metallo-tetrylene **LII**; (b): First reported tetrylidyne TM complex **LIII**; (c): Transformation of metallo-tetrylenes **LIV** and **LV** to tetrylidyne TM complexes **LVI** and **LVII** *via* CO dissociation.

could also show that metallo-tetrylene and tetrylidyne complexes are interchangeable structural isomers. It was demonstrated that the chromium(II) and tungsten(II)-germylenes [{2,6-(Trip)$_2$C$_6$H$_3$}Ge·M(Cp)(CO)$_3$] (M = Cr (**LIV**), W (**LV**)) are formed when three rather than two CO ligands are bound to the TM (Scheme 1.11(c)).[106] Subjecting **LIV** or **LV** to heat or UV light led to the loss of a CO ligand and generated the corresponding germylidyne-TM complexes [{2,6-(Trip)$_2$C$_6$H$_3$}Ge·M(Cp)(CO)$_2$] (M = Cr (**LVI**), W (**LVII**)). Due to the increased back-donation from the TM in these tetrylidyne complexes, Lewis acidity at the tetrel element is quenched. However, the tetrylidyne-TM bond is still polarised and can achieve cooperative activation of substrates, as demonstrated with germylidyne-tungsten(II) complex [{(Tsi)$_3$C}Ge·W(Cp*)(CO)$_2$] (**LVIII**, Tsi = C(SiMe$_3$)$_3$), where MLC was shown for the activation of alcohols and aldehydes (Scheme 1.12).[107] The reaction with alcohols proceeds in a 1:1 stoichiometry, leading to (alkoxy)germylene-complex **LIX**. In contrast, two equivalents of formaldehyde were shown to react with **LVIII**, resulting in intramolecularly base-stabilised (alkoxy)germylene-complex **LX**. The authors proposed that the reaction is initiated by coordination of the oxygen of the aldehyde to the germanium centre, followed by [2+2] cycloaddition across the Ge-W bond. This leads to C-H activation of the aldehyde proton at the W^{II} centre. Coordination of a second aldehyde at the Ge centre and subsequent hydrogermylation results in **LX**. Pioneered by the groups of Fillipou and Tilley, a number of cationic tetrylene-TM complexes have also been reported, which should exhibit a higher Lewis

acidity at the tetrel element due to the cationic charge.[100,103,108-113] Nevertheless, in most of these systems the cationic charge resides on the TM or the ligand backbone (*e.g.* for NHC-stabilised systems), mitigating this effect. However, some very recent examples have shown that the cationic charge can reside on the tetrel element if a linear angle between the residue, tetrel element, and TM centre can be avoided.

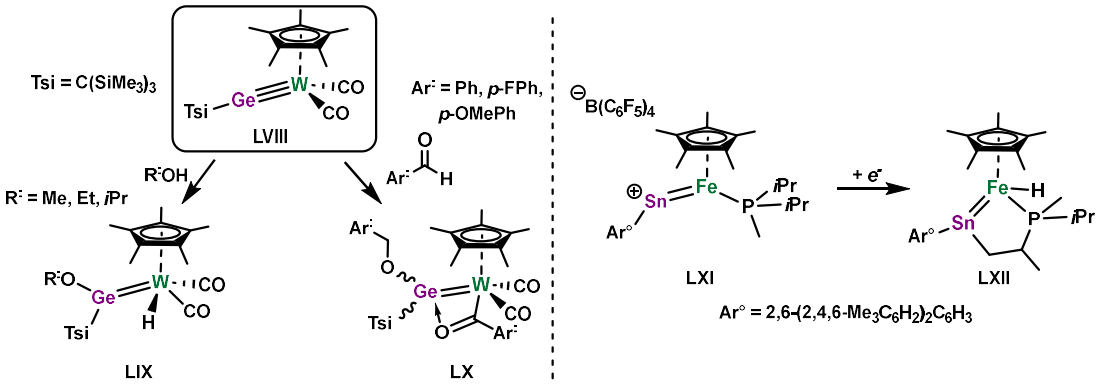

Scheme 1.12 Left: Cooperative activation of aldehydes by **LVIII**; Right: Reduction of cationic **LXI** leading to cooperative C-H activation.

The group of Tilley reported on the cationic stannylidyne-iron(I) complex $[Ar°Sn{\cdot}Fe(Cp^*)(PMe\textit{i}Pr_2)]^+$ (**LXI**; Ar° = 2,6-(2,4,6-$Me_3C_6H_2)_2C_6H_3$), exhibiting a slightly bent Fe-Sn-C angle of 169.85(9)°, resulting in minimised *π*-back-bonding and therefore increased Sn-centred Lewis acidity, with the cationic charge residing on the tetrel element (Scheme 1.12).[114] Further reduction of **LXI** resulted in C-H activation of an *iso*-propyl group of the phosphine ligand bound to the Fe^{I} centre, across the Sn-Fe bond, giving a five-membered metallacycle (**LXII**). In 2023, Wesemann and Sindlinger reported on cationic tetrylidyne-iridium(I) complexes $[(Tbb)E{\cdot}Ir(PMe_3)_3H]^+$ (E = Ge (**LXIII**), Sn (**LXIV**)), which were also able to activate a wide range of substrates including ammonia, hydrazine, water, hydrochloride, and H_2 under ambient conditions *via* MLC, resulting in iridium(III)-dihydride complexes (**LXV**, **LXVI**) (Scheme 1.13).[33] In all cases the nucleophile binds at the tetrel element, underlining its Lewis acidic character. Interestingly, **LXIII** and **LXIV** exhibit a pronounced non-linear Ir-E-C angle of below 160° causing a double bond. The concomitant increased Lewis acidity can explain the observed amplified reactivity and is a good example of the potential importance in minimising *π*-back-donation through ligand design.

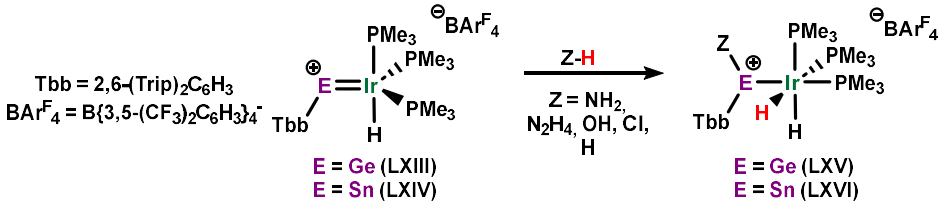

Scheme 1.13 Bent cationic iridium(I) complexes **LXV** and **LXVI** exhibiting oxidative addition reactivity across the Ir-E bond (E = Ge, Sn).

Phosphine-stabilised Tetrylenes as multidentate Ligands

A different approach to establish a Lewis acidic tetrylenes in TM complexes is the usage of multidentate ligand systems. Phosphine-stabilised tetrylenes are ideal candidates for this due to the fact that a TM can insert into the tetrel-phosphine bond.[115-116] These multidentate ligands have additional advantages. They should be easier to handle due to the phosphine stabilisation of the tetrylene prior to complexation. Further, the multidentate scaffold can enforce a bent geometry between the tetrylene and TM, minimising *π*-back-donation from the TM, hence retaining Lewis acidity at the tetrel element.

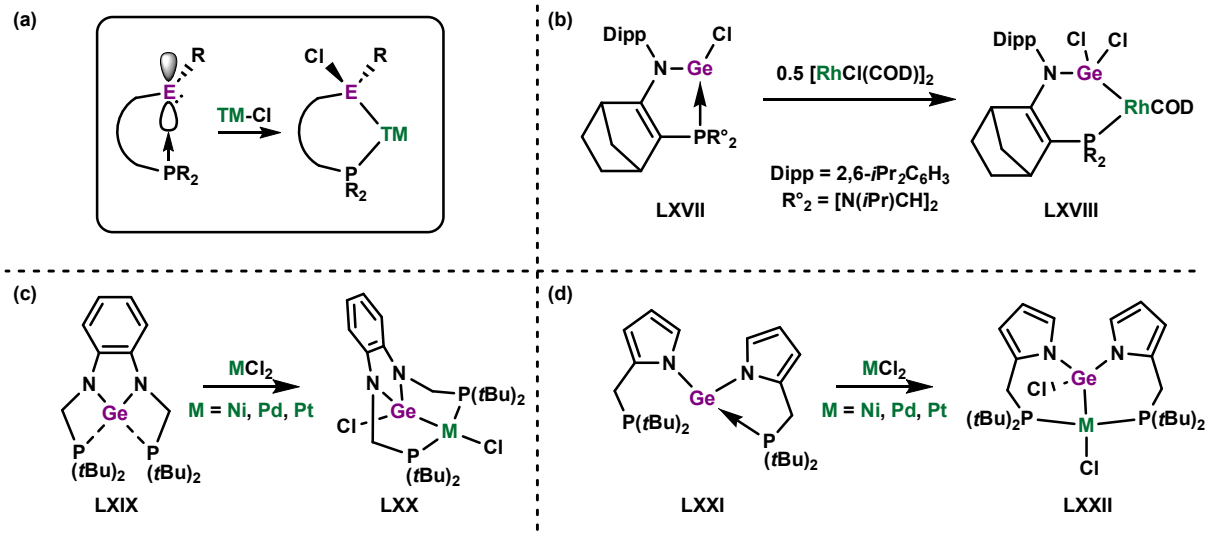

Figure 1.11 (a): Generally observed insertion chemistry of phosphine-stabilised tetrylenes with a TM-chloride; (b)-(d): Selected examples of phosphine-stabilised tetrylenes **LXVII**, **LXIX**, **LXXI** in multidentate ligand scaffolds inserting into a TM-Cl bond.

There have been a number of examples of bidentate and tridentate systems with phosphine-stabilised tetrylenes showing that the reaction of the corresponding phosphine-stabilised tetrylene with a TM-chloride results in the insertion of the tetrel element into the M-Cl bond (Figure 1.11(a)).[115,117-127] Selected examples of phosphine-stabilised tetrylenes (*viz*. **LXVII**, **LXIX**, **LXXI**) with different ligand scaffolds leading to M-Cl insertion are shown in Figure 1.11. Apart from chloride substitution at the tetrel element, no further chemistry has been reported with this class of compounds, which is not surprising due to the coordinatively saturated tetrel element, quenching the Lewis acidity. This gives some evidence that low-valent, sufficiently Lewis acidic tetrel elements are better suited as ligands in TM complexes when aiming to achieve MLC.

The first example of a TM complex accessed *via* insertion into a phosphine-stabilised tetrylene was published by the group of Wesemann, who reported on stannylene-nickel(0) and palladium(0) complexes featuring [(Tbb)Sn{*o*-($PR^{\#}_2$)C_6H_4}] ($R^{\#}$ = Ph (**LXIII**), Cy (**LXIV**)) as a

ligand (Figure 1.12).[128] Following insertion of the TM into the Sn-P bond, genuine stannylene complexes were observed (*viz*. **LXV**,**LXVI**, **LXIX** and **LXX**, Figure 1.12), with one metal-bound ligand (Ni, COD = 1,5-cyclooctadien; Pd, PCy_3) remaining. Sn-Pd bond lengths in **LXIX** and

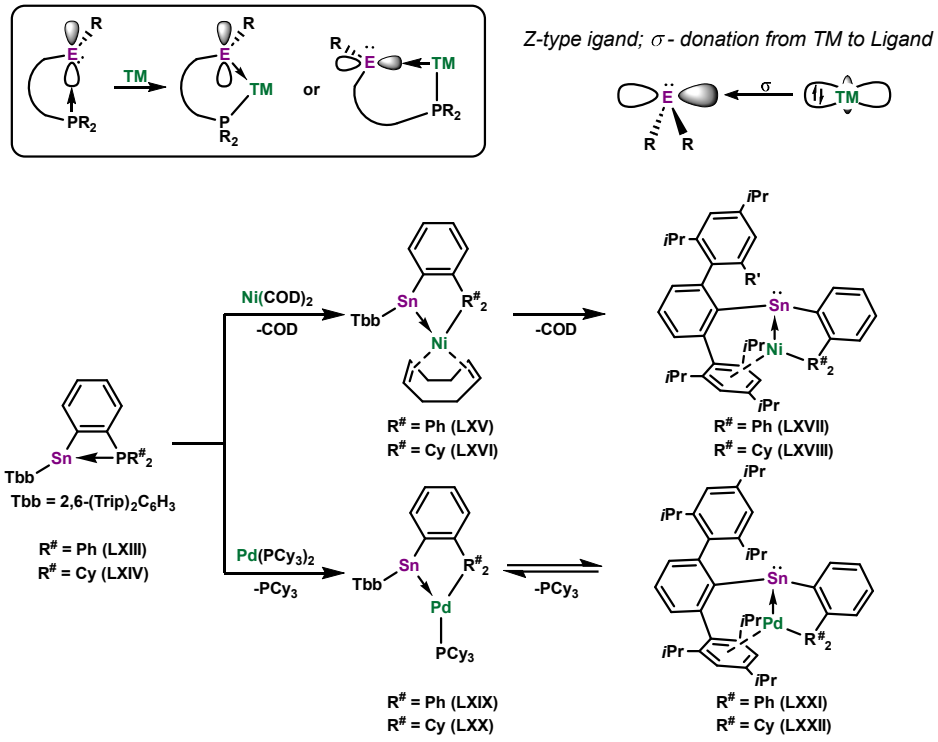

Figure 1.12 Top: Insertion of a TM into P-tetrel bond leading to *σ*-coordination from tetrel element to TM or *σ*-coordination from TM to the tetrel element making it a so-called Z-type ligand; Bottom: Phosphine-stabilised stannylenes **LXIII** and **LXIV** in Ni^0 and Pd^0 complexes showcasing the two different type of possible coordination modes.

LXX (**LXIX** 2.571(1) Å; **LXX** 2.591(1) Å) suggested the main interaction to be the *σ*-donation of the stannylene to the Pd centre, which are in the same range as other related stannylene-palladium(0) complexes in the literature ([{$(SiMe_3N)Sn\}_3$·Pd] 2.540(1) Å, [{$(SiMe_3N)Sn\}_2$·Pd{$P(iPr)_2CH_3\}_2$] 2.481(2) Å).[129-130] Over time these complexes rearrange by loss of a ligand at the TM, giving the tetrylene as a Z-type ligand, with an aryl group of the ligand scaffold binding to the TM in an η^6-fashion (*viz*. **LXVII**,**LXVIII**, **LXXI** and **LXXII**, Figure 1.12). While this was irreversible for the Ni^0 complexes with COD as ligand, the Pd^0 complexes showed reversible behaviour with PCy_3 as a ligand. This Z-type coordination means that *σ*-donation of the TM to the tetrel element is present, which leads to a nucleophilic tetrel element, since Lewis acidity is quenched by *σ*-donation of the TM and the lone pair of electrons is located at the tetrel element. This was indicated by trigonal pyramidal geometry of the tin atoms and confirmed by DFT calculations.

Tridentate phosphine-functionalised diamino tetrylene (PEP; E = Ge, Sn) ligands were also reported to act as Z-type ligands in the Pd^0 complexes [{$Me_2C(pyrmPiPr_2)_2E\}$·Pd]

(E = Ge (**LXXIII**), and Sn (**LXXIV**); pyrm = pyrromethane), resulting in a T-shaped geometry of the Pd^0 centre (Scheme 1.14).[122,131] The group of Goicoechea reported on a closely related tripodal PSnP ligand, which formed the classical L-type stannylene-platinum(0) complex [{(NCH_2)-*o*-$(PPh_2)C_6H_4$}$_2$Sn·Pt] (**LXXV**) (Scheme 1.14).[132] No further reactivity of this complex was reported, which may be due to a quenched Lewis acidity of the stannylene centre through *π*-donation from two neighbouring nitrogen centres. The Ni^0 complex [{(*o*-(P*i*Pr$_2$)C_6H_4)Ge}·Ni(NHC$^{i\text{Pr}}$)] (**LXXVI**) bearing a PGeP ligand was reported by the group of Tobita, which exhibits a Ge-Ni double bond due to pronounced *π*-back-donation from Ni to Ge, permitted by the pyramidal geometry around the Ni^0 centre (Scheme 1.14).[133] DFT analyses

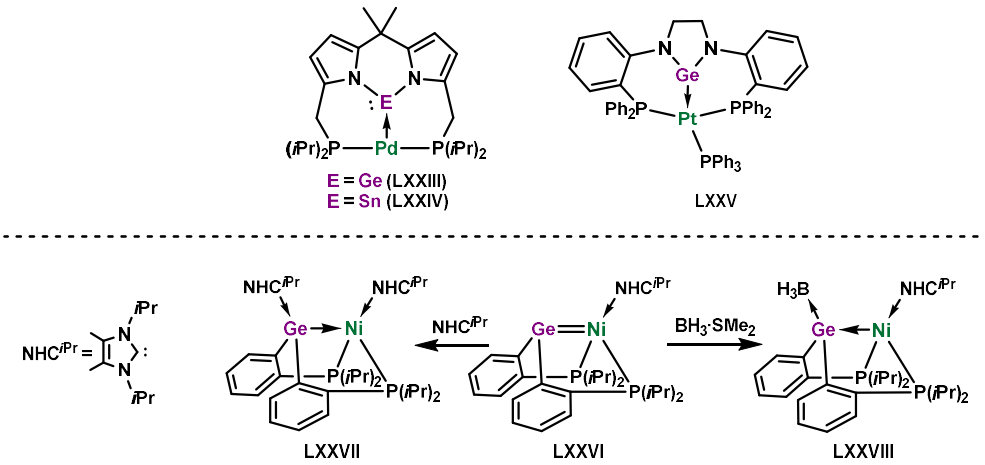

Scheme 1.14 Selected examples of TM complexes with phosphine-stabilised tetrylenes resulting in Z-type coordination of the tetrylene (**LXXIII**, **LXXIV**), low-valent coordinated stannylene (**LXXV**) and ambiphilic germylene (**LXXVI**).

and experimental investigations showed that the germylene in this system behaves as an ambiphile as both the HOMO and LUMO, representing a lone pair of electrons and a vacant *p*-orbital, were calculated to largely reside on the germylene. This was corroborated by the experimentally observed coordination of Lewis basic NHC$^{i\text{Pr}}$ (*viz.* **LXXVII**) and Lewis acidic BH_3 at the Ge centre (*viz.* **LXXVIII**).

Very recently the group of Kato reported on a phosphine-stabilised silylene, which acts as a Z-type ligand in the (chloro)silylene-nickel(0) complex [{$PR°_2(C_5H_8)C_2$(Dipp)N(Cl)Si}·Ni(NHC$^{i\text{Pr}}$)] (**LXXIX**; R°$_2$ = (N*t*Bu)$_2$SiMe$_2$), adopting a T-shaped geometry at the Ni centre (Scheme 1.15).[134] DFT calculations showed that the HOMO resides on the silylene, representing a lone-pair of electrons, while the LUMO is located on the Ni^0 centre, which was experimentally shown to be able to bind a nucleophile, specifically *iso*-propyl isocyanide (**LXXIV**). Extensive MLC-type reaction chemistry was also reported, which exemplifies the nucleophilic nature of the tetrylene and Lewis acidic nature of the Ni centre. Methyl triflate was shown to oxidatively add across the Si-Ni bond under ambient conditions resulting in a Ni-triflate (**LXXXV**). The same type of

reaction was observed for H_2, which was shown to proceed *via* Ni-centred activation (*viz.* **LXXX**), as per examples described previously. The complex further rearranged within six days

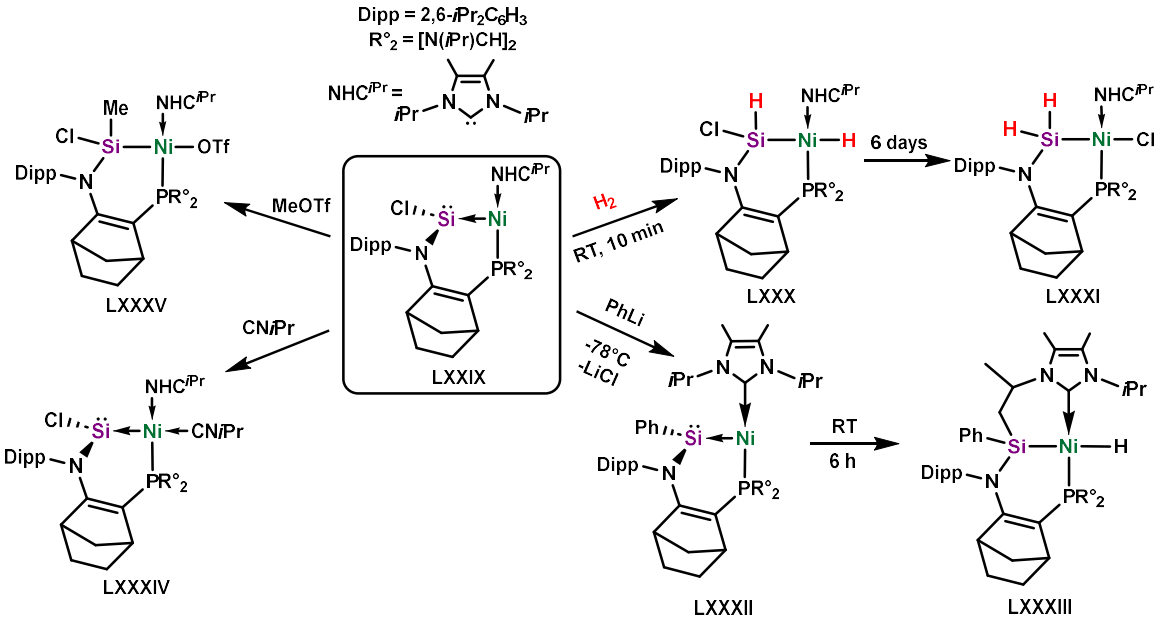

Scheme 1.15 (Chloro)silylene-nickel(0) complex **LXXIX** engaging in cooperative activation of different substrates, showcasing the nucleophilic nature of the silylene and electrophilic nature of the Ni centre.

giving a (dihydro)silyl-nickel(II) complex (**LXXXI**), with the chloride migrating to the nickel centre. In an attempt to increase reactivity by exchange of the *π*-donating chloride substituent at the silylene, the complex was reacted with PhLi at -78°C resulting in a novel (phenyl)silylene-nickel(0) complex (**LXXXII**). However, this complex proved to be highly reactive at ambient temperature, leading to C-H activation of an *iso*-propyl group of the Ni-bound NHC (viz. **LXXXIII**) (Scheme 1.15).

Shortly after this work was reported, a stable species with increased Lewis acidity was reported by the same group, being the corresponding cationic silyliumylidene-nickel(0) complex $[(PR°_2(C_5H_8)C_2(Dipp)NSi\}\cdot Ni(NHC^{iPr})]^+$ (**LXXXVI**). This was synthesised by chloride abstraction from the (chloro)silylene-nickel(0) complex **LXXIX** using $Na[BAr^F_4]$ ($[BAr^F_4]^-$ = $[\{3,5\text{-}(CF_3)_2C_6H_3\}_4B]^-$; Scheme 1.16).[135] The cationic silylene ligand in **LXXXVI** maintains a Z-type character. DFT calculations indicated the expected ambiphilic nature of the Si^{II} centre with both the HOMO and the LUMO, as well as the cationic charge, being largely located on the silyliumylidene. The amphiphilicity was also observed experimentally, resembling classical silylene reactivity, where the activation of methyl triflate and H_2 resulted in the oxidative addition product at silicon (*viz.* **LXXXVII**, **XC**), while the strong Lewis base DMAP (DMAP = 4-NMe_2Pyr) formed an adduct at the silyliumylidene centre (*viz.* **LXXXIX**). Again, it was shown that the H_2 activation was initiated by activation at the Ni^0 centre, followed by hydride migration

to silylene. In addition to these reactions, the cycloaddition of 2,3-dimethylbutadiene could be achieved, leading to a Ni-stabilised cyclic silylium ion (**LXXXVIII**). DFT analysis revealed that the first step of this reaction proceeds *via* a Si-Ni cooperative [2+2] cycloaddition process.

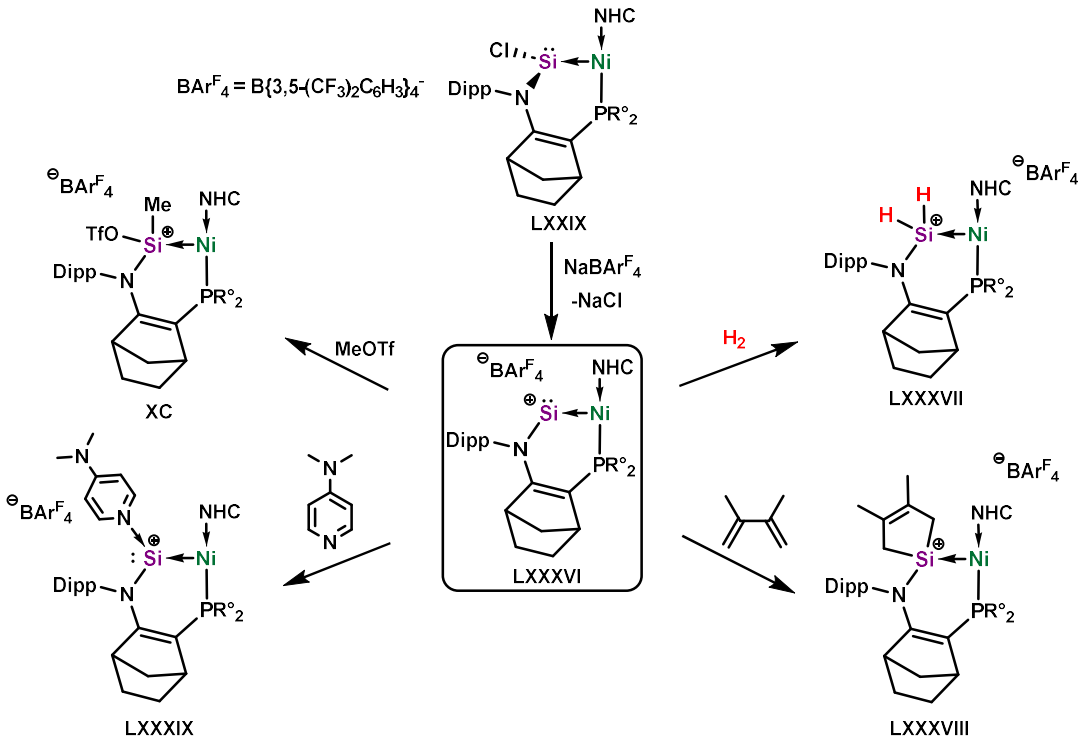

Scheme 1.16 Synthesis and reactivity of the cationic silyliumylidene-nickel(0) complex **LXXXVI** resulting in silicon centred oxidative addition products.

Summary

In conclusion, the development of Lewis acidic heavier tetrylene ligands is of great interest since this can enable challenging cooperative bond activation in TM complexes, which might ultimately lead to the discovery of new catalytic applications. In particular, ammonia activation is an intriguing example, where cooperative N-H bond scission can result in TM-hydride species which are known to be reactive towards insertion chemistry, opening the opportunity for further chemistry such as catalytic hydroamination. To retain the Lewis acidity of the tetrel element, geometric constraint to minimise back-donation from the TM to the tetrel element *via* a multidentate ligand scaffold has proven to be promising strategy. To ultimately achieve cooperative catalysis with these systems, a deeper understanding of how ligand design affects the reactivity of tetrylene-TM complexes is needed.

References

1 NOAA National Centers for Environmental Information, Monthly Global Climate Report for Annual 2022, **2023**.
2 *Climate Change 2022 – Impacts, Adaptation and Vulnerability: Working Group II Contribution to the Sixth Assessment Report of the Intergovernmental Panel on Climate Change*, Intergovernmental Panel on Climate Change, Cambridge, **2023**.
3 *Climate Change 2022 - Mitigation of Climate Change: Working Group III Contribution to the Sixth Assessment Report of the Intergovernmental Panel on Climate Change*, Intergovernmental Panel on Climate Change, Cambridge, **2023**.
4 J. Colberg, K. Kuok Hii, S. G. Koenig, *Org. Process Res. Dev.* **2022**, *26*, 2176–2178.
5 D. Steinborn, *Grundlagen der metallorganischen Komplexkatalyse*, 2nd ed., Vieweg + Teubner Wiesbaden, Wiesbaden, **2010**.
6 B. Cornils, W. A. Herrmann, *J. Catal.* **2003**, *216*, 23–31.
7 P. W. N. M. v. Leeuwen, *Homogeneous catalysis understanding the art*, Kluwer Acad. Publ. Dordrecht, Dordrecht, **2004**.
8 P. P. Power, *Nature* **2010**, *463*, 171–177.
9 T. J. Hadlington, *On the Catalytic Efficacy of Low-Oxidation State Group 14 Complexes*, Springer **2017**.
10 J. M. Gil-Negrete, E. Hevia, *Chem. Sci.* **2021**, *12*, 1982–1992.
11 Q. Wu, B. Huang, Y. Dai, T. Heine, Y. Ma, *NPJ 2D Mater. Appl.* **2022**, *6*, 52.
12 J. I. Van Der Vlugt, *Chem. Soc. Rev.* **2010**, *39*, 2302–2322.
13 L. Huang, M. Arndt, K. Gooßen, H. Heydt, L. J. Gooßen, *Chem. Rev.* **2015**, *115*, 2596–2697.
14 R. B. King, *Encyclopedia of inorganic chemistry*, 2nd ed., Wiley Chichester, West Sussex, England, Chichester, West Sussex, England, **2006**.
15 M. Lequitte, F. Figueras, C. Moreau, S. Hub, *J. Catal.* **1996**, *163*, 255–261.
16 W. F. Hoelderich, *Catal. Today* **2000**, *62*, 115–130.
17 J. Seayad, A. Tillack, C. G. Hartung, M. Beller, *Adv. Synth. Catal.* **2002**, *344*, 795–813.
18 V. Lavallo, G. D. Frey, B. Donnadieu, M. Soleilhavoup, G. Bertrand, *Angew. Chem. Int. Ed.* **2008**, *47*, 5224–5228.
19 C. R. Ho, L. A. Bettinson, J. Choi, M. Head-Gordon, A. T. Bell, *ACS Catal.* **2019**, *9*, 7012–7022.
20 A. Werner, *Z. Anorg. Chem.* **1893**, *3*, 267–330.
21 A. L. Casalnuovo, J. C. Calabrese, D. Milstein, *Inorg. Chem.* **1987**, *26*, 971–973.
22 J. Zhao, A. S. Goldman, J. F. Hartwig, *Science* **2005**, *307*, 1080–1082.
23 C. C. Almquist, N. Removski, T. Rajeshkumar, B. S. Gelfand, L. Maron, W. E. Piers, *Angew. Chem. Int. Ed.* **2022**, *61*, e202203576.
24 J. R. Khusnutdinova, D. Milstein, *Angew. Chem. Int. Ed.* **2015**, *54*, 12236–12273.
25 L. A. Berben, B. De Bruin, A. F. Heyduk, *Chem. Commun.* **2015**, *51*, 1553–1554.
26 E. Khaskin, M. A. Iron, L. J. W. Shimon, J. Zhang, D. Milstein, *J. Am. Chem. Soc.* **2010**, *132*, 8542–8543.
27 D. V. Gutsulyak, W. E. Piers, J. Borau-Garcia, M. Parvez, *J. Am. Chem. Soc.* **2013**, *135*, 11776–11779.
28 R. M. Brown, J. Borau Garcia, J. Valjus, C. J. Roberts, H. M. Tuononen, M. Parvez, R. Roesler, *Angew. Chem. Int. Ed.* **2015**, *54*, 6274–6277.
29 R. H. Crabtree, *The Organometallic Chemistry of the Transition Metals*, 5th ed., John Wiley & Sons Hoboken, Hoboken, **2011**.
30 R. J. Somerville, J. Campos, *Eur. J. Inorg. Chem.* **2021**, *2021*, 3488–3498.
31 Y. Mizuhata, T. Sasamori, N. Tokitoh, *Chem. Rev.* **2009**, *109*, 3479–3511.
32 T. J. Hadlington, T. Szilvasi, M. Driess, *J. Am. Chem. Soc.* **2019**, *141*, 3304–3314.
33 M. Auer, J. Bolten, K. Eichele, H. Schubert, C. P. Sindlinger, L. Wesemann, *Chem. Sci.* **2023**, *14*, 514–524.

34 R. Krishnamurthy, W. B. Schaap, *J. Chem. Educ.* **1969**, *46*, 799–810.
35 J. S. Griffith, L. E. Orgel, *Q. Rev. Chem. Soc.* **1957**, *11*, 381–393.
36 J. A. Osborn, G. Wilkinson, J. F. Young, *Chem. Commun. (London)* **1965**, 17–17.
37 J. F. Young, J. A. Osborn, F. H. Jardine, G. Wilkinson, *Chem. Commun. (London)* **1965**, 131–132.
38 J. Halpern, *Inorg. Chim. Acta* **1981**, *50*, 11–19.
39 J. M. Brown, P. L. Evans, A. R. Lucy, *J. Chem. Soc., Perkin Trans. 2* **1987**, 1589–1596.
40 S. B. Duckett, C. L. Newell, R. Eisenberg, *J. Am. Chem. Soc.* **1994**, *116*, 10548–10556.
41 R. Severin, S. Doye, *Chem. Soc. Rev.* **2007**, *36*, 1407–1420.
42 T. E. Müller, K. C. Hultzsch, M. Yus, F. Foubelo, M. Tada, *Chem. Rev.* **2008**, *108*, 3795–3892.
43 C. Weetman, S. Inoue, *ChemCatChem* **2018**, *10*, 4213–4228.
44 C. Weetman, in *Encyclopedia of Inorganic and Bioinorganic Chemistry*, **2021**, pp. 1–27.
45 G. D. Frey, V. Lavallo, B. Donnadieu, W. W. Schoeller, G. Bertrand, *Science* **2007**, *316*, 439–441.
46 Y. Peng, J.-D. Guo, B. D. Ellis, Z. Zhu, J. C. Fettinger, S. Nagase, P. P. Power, *J. Am. Chem. Soc.* **2009**, *131*, 16272–16282.
47 D. Bourissou, O. Guerret, F. P. Gabbaï, G. Bertrand, *Chem. Rev.* **2000**, *100*, 39–92.
48 G. Trinquier, *J. Am. Chem. Soc.* **1990**, *112*, 2130–2137.
49 A. Nemirowski, P. R. Schreiner, *J. Org. Chem.* **2007**, *72*, 9533–9540.
50 E. O. Fischer, A. Maasböl, *Angew. Chem. Int. Ed.* **1964**, *76*, 645–645.
51 A. Igau, H. Grutzmacher, A. Baceiredo, G. Bertrand, *J. Am. Chem. Soc.* **1988**, *110*, 6463–6466.
52 G. Rouschias, B. L. Shaw, *J. Chem. Soc. A* **1971**, 2097–2104.
53 R. R. Schrock, P. R. Sharp, *J. Am. Chem. Soc.* **1978**, *100*, 2389–2399.
54 A. J. Arduengo III, R. L. Harlow, M. Kline, *J. Am. Chem. Soc.* **1991**, *113*, 361–363.
55 G. C. Fortman, S. P. Nolan, *Chem. Soc. Rev.* **2011**, *40*, 5151–5169.
56 V. Nesterov, D. Reiter, P. Bag, P. Frisch, R. Holzner, A. Porzelt, S. Inoue, *Chem. Rev.* **2018**, *118*, 9678–9842.
57 V. Lavallo, Y. Canac, C. Präsang, B. Donnadieu, G. Bertrand, *Angew. Chem. Int. Ed.* **2005**, *44*, 5705–5709.
58 M. Melaimi, R. Jazzar, M. Soleilhavoup, G. Bertrand, *Angew. Chem. Int. Ed.* **2017**, *56*, 10046–10068.
59 T. Fueno, *Transition state : a theoretical approach*, CRC Press Boca Boca Raton, Florida, **2019**.
60 V. S. V. S. N. Swamy, S. Pal, S. Khan, S. S. Sen, *Dalton Trans.* **2015**, *44*, 12903–12923.
61 I. M. Riddlestone, A. Kraft, J. Schaefer, I. Krossing, *Angew. Chem. Int. Ed.* **2018**, *57*, 13982–14024.
62 P. Jutzi, F. Kohl, P. Hofmann, C. Krüger, Y.-H. Tsay, *Chem. Ber.* **1980**, *113*, 757–769.
63 P. Jutzi, A. Mix, B. Rummel, W. W. Schoeller, B. Neumann, H.-G. Stammler, *Science* **2004**, *305*, 849–851.
64 S. Hino, M. Brynda, A. D. Phillips, P. P. Power, *Angew. Chem. Int. Ed.* **2004**, *43*, 2655–2658.
65 J. Li, C. Schenk, F. Winter, H. Scherer, N. Trapp, A. Higelin, S. Keller, R. Pöttgen, I. Krossing, C. Jones, *Angew. Chem. Int. Ed.* **2012**, *51*, 9557–9561.
66 T. Probst, O. Steigelmann, J. Riede, H. Schmiclbaur, *Angew. Chem. Int. Ed.* **1990**, *29*, 1397–1398.
67 P. A. Rupar, V. N. Staroverov, P. J. Ragogna, K. M. Baines, *J. Am. Chem. Soc.* **2007**, *129*, 15138–15139.
68 A. Rit, R. Tirfoin, S. Aldridge, *Angew. Chem. Int. Ed.* **2016**, *55*, 378–382.
69 S. L. Powley, S. Inoue, *Chem. Rec.* **2019**, *19*, 2179–2188.
70 R. S. P. Turbervill, J. M. Goicoechea, *Aust. J. Chem.* **2013**, *66*, 1131–1137.
71 S. Khan, G. Gopakumar, W. Thiel, M. Alcarazo, *Angew. Chem. Int. Ed.* **2013**, *52*, 5644–5647.
72 H. V. R. Dias, Z. Wang, *J. Am. Chem. Soc.* **1997**, *119*, 4650–4655.

73 M. Stender, A. D. Phillips, P. P. Power, *Inorg. Chem.* **2001**, *40*, 5314–5315.
74 M. Driess, S. Yao, M. Brym, C. van Wüllen, *Angew. Chem. Int. Ed.* **2006**, *45*, 6730–6733.
75 D. C. H. Do, A. V. Protchenko, M. Á. Fuentes, J. Hicks, P. Vasko, S. Aldridge, *Chem. Commun.* **2020**, *56*, 4684–4687.
76 X. Zhou, P. Vasko, J. Hicks, M. Á. Fuentes, A. Heilmann, E. L. Kolychev, S. Aldridge, *Dalton Trans.* **2020**, *49*, 9495–9504.
77 R. Nougué, S. Takahashi, A. Dajnak, E. Maerten, A. Baceiredo, N. Saffon-Merceron, V. Branchadell, T. Kato, *Chem. Eur. J.* **2022**, *28*, e202202037.
78 M. R. Elsby, R. T. Baker, *Chem. Soc. Rev.* **2020**, *49*, 8933–8987.
79 H. Grützmacher, *Angew. Chem. Int. Ed.* **2008**, *47*, 1814–1818.
80 C. Gunanathan, D. Milstein, *Acc. Chem. Res.* **2011**, *44*, 588–602.
81 Y. Li, S. Yu, X. Wu, J. Xiao, W. Shen, Z. Dong, J. Gao, *J. Am. Chem. Soc.* **2014**, *136*, 4031–4039.
82 J. F. Sonnenberg, A. J. Lough, R. H. Morris, *Organometallics* **2014**, *33*, 6452–6465.
83 A. Zirakzadeh, K. Kirchner, A. Roller, B. Stöger, M. Widhalm, R. H. Morris, *Organometallics* **2016**, *35*, 3781–3787.
84 S. A. M. Smith, P. O. Lagaditis, A. Lüpke, A. J. Lough, R. H. Morris, *Chem. Eur. J.* **2017**, *23*, 7212–7216.
85 J. F. Sonnenberg, K. Y. Wan, P. E. Sues, R. H. Morris, *ACS Catal.* **2016**, *7*, 316–326.
86 B. Blom, M. Stoelzel, M. Driess, *Chem. Eur. J.* **2013**, *19*, 40–62.
87 Y. Wang, A. Kostenko, S. Yao, M. Driess, *J. Am. Chem. Soc.* **2017**, *139*, 13499–13506.
88 Y. P. Zhou, M. Driess, *Angew. Chem. Int. Ed.* **2019**, *58*, 3715–3728.
89 W. Hieber, R. Breu, *Chem. Ber.* **1957**, *90*, 1270–1274.
90 G. Schmid, H. J. Balk, *Chem. Ber.* **1970**, *103*, 2240–2244.
91 T. J. Marks, *J. Am. Chem. Soc.* **1971**, *93*, 7090–7091.
92 K. E. Litz, K. Henderson, R. W. Gourley, M. M. B. Holl, *Organometallics* **1995**, *14*, 5008–5010.
93 M. J. S. Gynane, D. H. Harris, M. F. Lappert, P. P. Power, P. Rivière, M. Rivière-Baudet, *J. Chem. Soc., Dalton Trans.* **1977**, 2004–2009.
94 K. E. Litz, M. M. Banaszak Holl, J. W. Kampf, G. B. Carpenter, *Inorg. Chem.* **1998**, *37*, 6461–6469.
95 K. E. Litz, J. W. Kampf, M. M. Banaszak Holl, *J. Am. Chem. Soc.* **1998**, *120*, 7484–7492.
96 K. E. Litz, J. E. Bender, R. D. Sweeder, M. M. Banaszak Holl, J. W. Kampf, *Organometallics* **2000**, *19*, 1186–1189.
97 P. G. Hayes, R. Waterman, P. B. Glaser, T. D. Tilley, *Organometallics* **2009**, *28*, 5082–5089.
98 T. J. Hadlington, T. Szilvasi, M. Driess, *Angew. Chem. Int. Ed.* **2017**, *56*, 7470–7474.
99 T. J. Hadlington, A. Kostenko, M. Driess, *Chem. Eur. J.* **2020**, *26*, 1958–1962.
100 A. C. Filippou, B. Baars, O. Chernov, Y. N. Lebedev, G. Schnakenburg, *Angew. Chem. Int. Ed.* **2014**, *53*, 565–570.
101 P. Wilfling, K. Schittelkopf, M. Flock, R. H. Herber, P. P. Power, R. C. Fischer, *Organometallics* **2015**, *34*, 2222–2232.
102 K. Inomata, T. Watanabe, Y. Miyazaki, H. Tobita, *J. Am. Chem. Soc.* **2015**, *137*, 11935–11937.
103 Y. N. Lebedev, U. Das, G. Schnakenburg, A. C. Filippou, *Organometallics* **2017**, *36*, 1530–1540.
104 P. Jutzi, C. Leue, *Organometallics* **1994**, *13*, 2898–2899.
105 R. S. Simons, P. P. Power, *J. Am. Chem. Soc.* **1996**, *118*, 11966–11967.
106 L. Pu, B. Twamley, S. T. Haubrich, M. M. Olmstead, B. V. Mork, R. S. Simons, P. P. Power, *J. Am. Chem. Soc.* **2000**, *122*, 650–656.
107 T. Fukuda, H. Hashimoto, H. Tobita, *Chem. Commun.* **2013**, *49*, 4232–4234.
108 B. V. Mork, T. D. Tilley, *Angew. Chem. Int. Ed.* **2003**, *115*, 371–374.
109 A. C. Filippou, A. I. Philippopoulos, G. Schnakenburg, *Organometallics* **2003**, *22*, 3339–3341.

110 P. G. Hayes, Z. Xu, C. Beddie, J. M. Keith, M. B. Hall, T. D. Tilley, *J. Am. Chem. Soc.* **2013**, *135*, 11780–11783.
111 A. C. Filippou, P. Ghana, U. Chakraborty, G. Schnakenburg, *J. Am. Chem. Soc.* **2013**, *135*, 11525–11528.
112 L. R. Maurer, J. Rump, A. C. Filippou, *Inorganics* **2023**, *11*, 129–159.
113 T. Watanabe, Y. Miyazaki, K. Inomata, H. Tobita, H. Hashimoto, *Organometallics* **2023**, *42*, 846–858.
114 R. C. Handford, M. A. Nesbit, P. W. Smith, R. D. Britt, T. D. Tilley, *J. Am. Chem. Soc.* **2022**, *144*, 358–367.
115 J. M. García, E. Ocando-Mavárez, T. Kato, D. S. Coll, A. Briceño, N. Saffon-Merceron, A. Baceiredo, *Inorg. Chem.* **2012**, *51*, 8187–8193.
116 J. A. Cabeza, P. García-Álvarez, D. Polo, *Eur. J. Inorg. Chem.* **2016**, *2016*, 10–22.
117 L. Álvarez-Rodríguez, J. Brugos, J. A. Cabeza, P. García-Álvarez, E. Pérez-Carreño, D. Polo, *Chem. Commun.* **2017**, *53*, 893–896.
118 L. Álvarez-Rodríguez, J. Brugos, J. A. Cabeza, P. García-Álvarez, E. Pérez-Carreño, *Chem. Eur. J.* **2017**, *23*, 15107–15115.
119 J. Brugos, J. A. Cabeza, P. García-Álvarez, E. Pérez-Carreño, D. Polo, *Dalton Trans.* **2018**, *47*, 4534–4544.
120 J. Brugos, J. A. Cabeza, P. García-Álvarez, E. Pérez-Carreño, *Organometallics* **2018**, *37*, 1507–1514.
121 J. A. Cabeza, I. Fernández, J. M. Fernández-Colinas, P. García-Álvarez, C. J. Laglera-Gándara, *Chem. Eur. J.* **2019**, *25*, 12423–12430.
122 J. A. Cabeza, I. Fernández, P. García-Álvarez, R. García-Soriano, C. J. Laglera-Gándara, R. Toral, *Dalton Trans.* **2021**, *50*, 16122–16132.
123 A. Arauzo, J. A. Cabeza, I. Fernández, P. García-Álvarez, I. García-Rubio, C. J. Laglera-Gándara, *Chem. Eur. J.* **2021**, *27*, 4985–4992.
124 J. A. Cabeza, J. M. Fernández-Colinas, J. García-Álvarez, P. García-Álvarez, C. J. Laglera-Gándara, M. Ramos-Martín, *Chem. Eur. J.* **2022**, *28*, e202200847.
125 J. A. Cabeza, P. García-Álvarez, C. J. Laglera-Gándara, E. Pérez-Carreño, *Eur. J. Inorg. Chem.* **2021**, *2021*, 1897–1902.
126 S. Takahashi, E. Bellan, A. Baceiredo, N. Saffon-Merceron, S. Massou, N. Nakata, D. Hashizume, V. Branchadell, T. Kato, *Angew. Chem. Int. Ed.* **2019**, *131*, 10416–10420.
127 K. M. Krebs, S. Freitag, J. J. Maudrich, H. Schubert, P. Sirsch, L. Wesemann, *Dalton Trans.* **2018**, *47*, 83–95.
128 K. M. Krebs, S. Freitag, H. Schubert, B. Gerke, R. Pottgen, L. Wesemann, *Chem. Eur. J.* **2015**, *21*, 4628–4638.
129 P. B. Hitchcock, M. F. Lappert, M. C. Misra, *J. Chem. Soc., Chem. Commun.* **1985**, 863–864.
130 J. Krause, K.-J. Haack, K.-R. Pörschke, B. Gabor, R. Goddard, C. Pluta, K. Seevogel, *J. Am. Chem. Soc.* **1996**, *118*, 804–821.
131 J. A. Cabeza, P. García-Álvarez, C. J. Laglera-Gándara, E. Pérez-Carreño, *Chem. Commun.* **2020**, *56*, 14095–14097.
132 S. Bestgen, N. H. Rees, J. M. Goicoechea, *Organometallics* **2018**, *37*, 4147–4155.
133 T. Watanabe, Y. Kasai, H. Tobita, *Chem. Eur. J.* **2019**, *25*, 13491–13495.
134 M. Frutos, N. Parvin, A. Baceiredo, D. Madec, N. Saffon-Merceron, V. Branchadell, T. Kato, *Angew. Chem. Int. Ed.* **2022**, *61*, e202201932.
135 S. Takahashi, M. Frutos, A. Baceiredo, D. Madec, N. Saffon-Merceron, V. Branchadell, T. Kato, *Angew. Chem. Int. Ed.* **2022**, *61*, e202208202.

Chapter 2

Motivation and Scope of this Work

Heavier tetrylenes are an intriguing ligand class for cooperative bond activation in conjunction with a TM centre. The ambiphilic tetrylene can retain its Lewis acidity when coordinated to a TM centre allowing for MLC behaviour (*viz.* Chapter 1). Through the work described in this thesis, we wanted to develop easily accessible and modifiable heavier tetrylene ligands and combine them with cheap and abundant first-row TM centres to achieve cooperative activation of challenging substrates, towards catalytic applications.

A promising approach to implement low-coordinate tetrylenes in TM systems are bidentate phosphine-stabilised tetrylene ligands, which have several advantages compared to their monodentate terminal counterparts. Besides their higher stability introduction of a TM centre typically results in insertion of the TM into the tetrel-phosphorus bond, leading to low-coordinate and Lewis acidic tetryl centres (Figure 2.1).[1-2] The primary goal in developing tetrylenes with a bidentate ligand structure is their potential ability to enforce geometric constraints at the tetryl-transition metal bond, which would lead to non-ideal orbital overlap between the tetrylene and TM centre. This should result in reduced π-back-donation from the

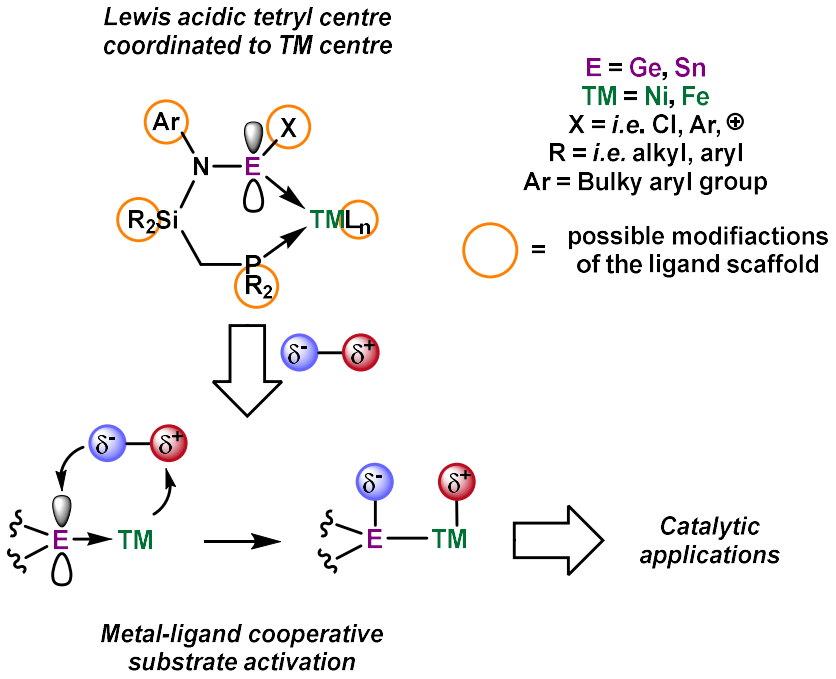

Figure 2.1 General structure of planned phosphine-stabilised heavier tetrylene-TM complexes and targeted metal-ligand cooperative substrate activation, possibly leading to desired catalytic applications.

TM centre to the tetrel element, enhancing the Lewis acidity of the tetrel element, and so potentially elevating reactivity. To achieve this, our goal is to develop the novel ligand scaffold

^{RR}Ar (^{RR}Ar = [{($R_2PCH_2Si(R)_2$)(Ar)}N]$^-$; R = *i.e.* alkyl,aryl group; Ar = Bulky aryl group; Figure 2.1). The here employed (silyl)amido moiety is reminiscent of 'classic' amide ligands, featuring a bulky aryl group at the nitrogen, and alkyl or aryl residues at the silicon, systems which have been successfully used in the past to isolate countless low-coordinate acyclic group 14 element(II) species.[3-7] This includes the acyclic NHC-stabilised (chloro)silylene, [[{(Me_3Si)(Dipp)N}Si(Cl)]·NHC], which has also been introduced to Ni^0 complexes,[8] where a rich cooperative activation chemistry has been reported.[9-10] The adjacent nitrogen centre electronically stabilises the tetrylene *via* π-donation into its vacant *p*-orbital, while the bulky groups at both the nitrogen and silicon provide steric protection. Additionally, the silyl group also has an electron-donating influence, further stabilising the system.[11] To introduce phosphine stabilisation we planned to insert an (alkyl)phosphine unit at the silicon to a obtain robust [Si-CH_2-PR_2] scaffold. The implementation of a CH_2-bridge is necessary since Si-P bonds are known to be quite reactive, which would lead to undesirable instability.[12-13] The envisioned geometric constraint to limit π-back-donation from the TM centre to the tetrel element should also be enforced with this bidentate structure. As tetrel elements, we opted to use germanium and tin since the low-valent precursors $GeCl_2$·dioxane and SnX_2 (X = Cl, Br) are readily available, which is not the case for silicon. Furthermore, compared to silicon, reversibility of potential substrate activations is more likely, due to the generally reduced bond energies of heavier elements. Lead was not considered due to higher toxicity and generally lower stability of Pb^{II}, since aggregation is favoured.[14]

In addition to the above described aspects, the structure of the ligand scaffold also addresses synthetic accessibility and modifiability. The starting materials for the planned synthesis are all commercially available or can be made 'in-house' with ease.[15-18] Given that the designed synthetic route only involves deprotonation or salt metathesis reactions, ligand synthesis is also designed to be highly straightforward. The modular nature of the ligands also means that starting materials can be easily exchanged, varying the residues at the phosphorus, silicon or nitrogen, giving ready access to a broad family of ligand systems. The resulting phosphine-stabilised tetrylene chlorides ^{RR}ArECl (E = Ge, Sn), could also be further modified at the tetrel element *via* substitution of the chloride, introducing different residues such as aryl groups or a cationic charge, directly influencing the electronic nature/Lewis acidity of the tetrel element.[19-20] Once obtained, these ligands will be combined with low-cost, abundant first-row TM species, such as nickel or iron. TM centres which are low-valent and low-coordinate will be preferentially targeted, to obtain both a reactive TM centre and tetrel element. This aims to maximise the possibility for desired dual-centred reactivity at the tetrylene-TM interface. The resulting tetrylene-TM complexes would then be investigated concerning their electronic nature *via* structural and theoretical methods, while also probing their reactivity and cooperative

behaviour experimentally by reacting them with catalytically relevant substrates such as ammonia and H_2. Furthermore, we also wanted to screen these complexes for different catalytic conversions to elucidate if these phosphine-stabilised tetrylenes enable catalysis in TM complexes.

In summary in this thesis, we plan to develop the described ligand scaffold, ^{RR}Ar, for phosphine-stabilised heavier tetrylene ligands, which we want to combine with abundant TM^0 centres. Due to the potential non-innocent character of the tetrel elements in the resulting complexes, we hope to achieve MLC activation. This might enable challenging catalytic transformation, which have not been realised yet, such as hydroamination of alkene with ammonia. Additionally, replacing precious metal catalyst in established catalytic transformations is also of interest, since the here described tetrylene-TM complexes are made of cheap and accessible starting materials.

References

1 J. M. García, E. Ocando-Mavárez, T. Kato, D. S. Coll, A. Briceño, N. Saffon-Merceron, A. Baceiredo, *Inorg. Chem.* **2012**, *51*, 8187–8193.
2 S. Freitag, J. Henning, H. Schubert, L. Wesemann, *Angew. Chem. Int. Ed.* **2013**, *125*, 5750–5754.
3 J. Li, A. Stasch, C. Schenk, C. Jones, *Dalton Trans.* **2011**, *40*, 10448–10456.
4 D. Dange, J. Li, C. Schenk, H. Schnöckel, C. Jones, *Inorg. Chem.* **2012**, *51*, 13050–13059.
5 J. Li, C. Schenk, C. Goedecke, G. Frenking, C. Jones, *J. Am. Chem. Soc.* **2011**, *133*, 18622–18625.
6 J. Li, C. Schenk, F. Winter, H. Scherer, N. Trapp, A. Higelin, S. Keller, R. Pöttgen, I. Krossing, C. Jones, *Angew. Chem. Int. Ed.* **2012**, *51*, 9557–9561.
7 T. J. Hadlington, J. Li, C. Jones, *Can. J. Chem.* **2014**, *92*, 427–433.
8 T. J. Hadlington, T. Szilvasi, M. Driess, *Angew. Chem. Int. Ed.* **2017**, *56*, 7470–7474.
9 T. J. Hadlington, T. Szilvasi, M. Driess, *J. Am. Chem. Soc.* **2019**, *141*, 3304–3314.
10 T. J. Hadlington, A. Kostenko, M. Driess, *Chem. Eur. J.* **2020**, *26*, 1958–1962.
11 P. G. Gassman, P. A. Deck, C. H. Winter, D. A. Dobbs, D. H. Cao, *Organometallics* **1992**, *11*, 959–960.
12 A. G. Baboul, H. B. Schlegel, *J. Am. Chem. Soc.* **1996**, *118*, 8444–8451.
13 C. Zybill, *Inorg. Chim. Acta* **1992**, *202*, 119–120.
14 Y. Mizuhata, T. Sasamori, N. Tokitoh, *Chem. Rev.* **2009**, *8*, 3479–3511.
15 N. E. Schore, L. S. Benner, B. E. LaBelle, *Inorg. Chem.* **1981**, *20*, 3200–3208.
16 F. Eisenträger, A. Göthlich, I. Gruber, H. Heiss, C. A. Kiener, C. Krüger, J. Ulrich Notheis, F. Rominger, G. Scherhag, M. Schultz, B. F. Straub, M. A. O. Volland, P. Hofmann, *New J. Chem.* **2003**, *27*, 540–550.
17 J. T. Patton, M. M. Bokota, K. A. Abboud, *Organometallics* **2002**, *21*, 2145–2148.
18 I. C. Cai, M. I. Lipschutz, T. D. Tilley, *Chem. Commun.* **2014**, *50*, 13062–13065.
19 M. Frutos, N. Parvin, A. Baceiredo, D. Madec, N. Saffon-Merceron, V. Branchadell, T. Kato, *Angew. Chem. Int. Ed.* **2022**, *61*, e202201932.
20 S. Takahashi, M. Frutos, A. Baceiredo, D. Madec, N. Saffon-Merceron, V. Branchadell, T. Kato, *Angew. Chem. Int. Ed.* **2022**, *61*, e202208202.

Chapter 3

Reversible metathesis of ammonia in an acyclic Germylene-Ni^0 complex

P. M. Keil, T. Szilvási, T. J. Hadlington, *Chem. Sci.*, **2021**, *12*, 5582–5590.

This work was done in collaboration with Prof. Tibor Szilvási from the University of Tuscaloosa, who performed all DFT calculations concerning this project.

Synopsis

In this initial project, we were able to successfully establish our ligand scaffold, ^{PhR}Dipp (^{PhR}Dipp = [{$Ph_2PCH_2Si(R)_2$}(Dipp)N]$^-$; R = Ph, *i*Pr; Dipp = 2,6-*i*$Pr_2C_6H_3$). The synthetic route first generates Ph_2PMe by the reaction of Ph_2PCl with MeLi, which can be deprotonated at the Me moiety using *n*-BuLi/TMEDA (TMEDA = N,N,N′,N′-Tetramethylethylendiamin), resulting in [Ph_2PCH_2Li·TMEDA].[1] Carefully reacting one equivalent of [Ph_2PCH_2Li·TMEDA] with R_2SiCl_2 overnight at low temperature, to avoid overreaction with two equivalents of [Ph_2PCH_2Li·TMEDA], results in the formation of $Ph_2PCH_2Si(R)_2Cl$. This can then be further reacted with DippN(H)Li to access the protonated ligand backbone, ^{PhR}DippH, which is subsequently deprotonated with KH, yielding ^{PhR}DippK as a solid.[2] This straightforward synthesis can be performed in a one-pot route starting from [Ph_2PCH_2Li·TMEDA], isolating up to 25 g of ^{PhR}DippK in one synthetic batch. It was later shown within the group that this route could also be used for different combinations of residues at the P, Si, and N, as well as introduction of two phosphine moieties, exemplifying the modifiability of this ligand system.[3]

Using these developed ^{PhR}DippK ligands, we were able to prepare the phosphine-stabilised (chloro)germylene compounds, ^{PhR}DippGeCl, which we could use to obtain the corresponding (chloro)germylene-nickel(0) complexes [{^{PhR}DippGe(Cl)}·$Ni(PPh_3)_2$] in an *in-situ* reduction with $NiCl_2$·DME (DME = 1,2-Dimethoxyethan), two equivalents of PPh_3, and an excess of Zn. In the context of sustainability this method is quite interesting, due to the cheap starting materials and mild reducing agent employed, though it should be noted that this synthetic route was later optimised using $Ni(COD)_2$ (COD = 1,5-cyclooctadiene). This gives increased yields of up to 85%, compared to the here described 52%, whilst $Ni(COD)_2$ can also be generated from low-cost and easily accessible starting materials.[4] The synthesis of the corresponding (chloro)stannylene ligands, ^{PhR}DippSnCl, was also successful (see Chapter 4). However,

obtaining corresponding Ni^0 complexes was not possible in our hands due to their instability, most likely stemming from the activation of the Sn-Cl moiety at Ni^0, leading to Ni-Cl species.

The obtained (chloro)germylene-nickel(0) complexes [{^{PhR}DippGe(Cl)}·Ni(PPh$_3$)$_2$] contain the desired low-coordinate tetrel elements, meaning that their Lewis acidity should be retained, and the *p*-orbital should be accessible. Lewis acidic character of the tetrylene could be experimentally shown, as tetrel centred *σ*-bond metathesis reactions with water and ammonia could be observed, giving access to the corresponding (amido)germylenes [{^{PhR}DippGe(NH$_2$)}·Ni(PPh$_3$)$_2$] and (hydroxy)germylenes [{^{PhR}DippGe(OH)}·Ni(PPh$_3$)$_2$]. Particularly, the occurrence of [{^{PhR}DippGe(OH)}·Ni(PPh$_3$)$_2$] was problematic, which formed as a by-product when minor amounts of water was present in reagents. This was the case for the synthesis of both [{^{PhR}DippGe(Cl)}·Ni(PPh$_3$)$_2$] and [{^{PhR}DippGe(NH$_2$)}·Ni(PPh$_3$)$_2$]. If present, it could not be removed *via* washing, due to similar solubility of these species, or by fractioned crystallisation, since [{^{PhR}DippGe(OH)}·Ni(PPh$_3$)$_2$] co-crystallised with the other species.

In conclusion, were able to show that our developed ligand scaffold can be introduced into TM^0 complexes, even retaining the Lewis acidic character of the tetrylene centre. This opens the door for further development, such as modifications at the tetrylene centre to potentially increase Lewis acidity, and therefore the reactivity of these ligands. Further, the chloride ligand may be extracted or exchanged, to eliminate the possibility of undesired side reactions involving this moiety (see Chapters 4 and 8). Cooperative behaviour with the Ni^0 complexes described in this project could not be achieved, which may be due to the formally 18-electron Ni^0 centre, which is electronically saturated. This point is addressed in Chapters 7 and 8.

Manuscript

The following sections are reproduced and formatted from the following article: P. M. Keil, T. Szilvási, T. J. Hadlington, *Chem. Sci.*, **2021**, *12*, 5582–5590*. Experimental spectra (NMR, LIFDI/MS, UV vis and IR) and further details concerning DFT calculations can be retrieved online (*https://doi.org/10.1039/D1SC00450F).

Abstract

Carbenes, a class of low-valent group 14 ligand, have shifted the paradigm in our understanding of the effects of supporting ligands in transition-metal reactivity and catalysis. We now seek to move towards utilizing the heavier group 14 elements in effective ligands systems, which can potentially surpass carbon in their ability to operate *via* ‘non-innocent’ bond

activation processes. Herein we describe our initial results towards the development of scalable acyclic chelating germylene ligands (*viz*. **1a/b**), and their utilization in the stabilization of Ni^0 complexes (*viz.* **4a/b**), which can readily and reversibly undergo metathesis with ammonia with no net change of oxidation state at the Ge^{II} and Ni^0 centres, through ammonia bonding at the germylene ligand as opposed to the Ni^0 centre. The DFT-derived metathesis mechanism, which surprisingly insights the need for three molecules of ammonia to achieve N-H bond activation, supports reversible ammonia binding at Ge^{II}, as well as the observed reversibility in the overall reaction.

Introduction

Beginning with the inception of transition metal (TM) carbene complexes by E. O. Fischer,[5] research involving the synthesis and utility of metal carbene complexes has long stood as a pillar of modern organometallic chemistry.[6] This has borne numerous classes of carbene complex, a vast number of which have catalytic implications, from highly reactive alkylidene complexes capable of double-bond metathesis,[7] to those involving N-heterocyclic carbene (NHC) spectator ligands.[8] Whilst considerable efforts have also been given to the study of the heavier tetrylenes in TM complexes, this field has largely focused on synthetic access, and less so on reactivity and utilisation in broader synthetic protocols.[9] The heavier tetrylenes have the capacity to act as 'single centre ambiphiles', this effect amplified on decending group 14 due to reduced *sp*-mixing,[10] with a *σ*-donating lone electron pair and a Lewis acidic vacant *p*-orbital. Although heavier tetrylenes have been employed as ligands in catalysis,[9(c),11] and notably so amidinato silylenes,[11] these, like NHCs, are typically spectator ligands due to common examples being N-heterocyclic in nature. Chelating ligands employing an acyclic, low-coordinate germylene have seen some attention in the literature, and are typically doubly substituted by a ligand bearing a phosphine arm; a number of examples of such systems havebeen reported by Cabeza and co-workers,[12,13] which have been combined with first-row TM halides so as to access TM^{II} complexes, often with tetrylene insertion into TM-X bonds (X = halide).[14] Related (carbonyl-free) first-row TM^0 complexes bearing acyclic, two-coordinate germylene ligands are rare,[15] and should allow for metal-ligand cooperativity (MLC) due to their amphiphilic nature imparting them the potential to remain Lewis acidic when bound to a metal centre. MLC, whereby a metal-bound ligand plays an active role in bond activation,[16] is a powerful concept in catalysis,[17,18] and has allowed for the facile activation of bonds which are otherwise challenging to cleave, a prime example being the N-H bonds in ammonia.[19] In a key demonstration of this process, the phosphino-carbene Ni^0 complex **A** can readily bind ammonia at Ni in the displacement of its Ph_3P ligand, with the nucleophilic carbene ligand accepting a proton in N-H bond cleavage (Figure 3.1).[19(c)]

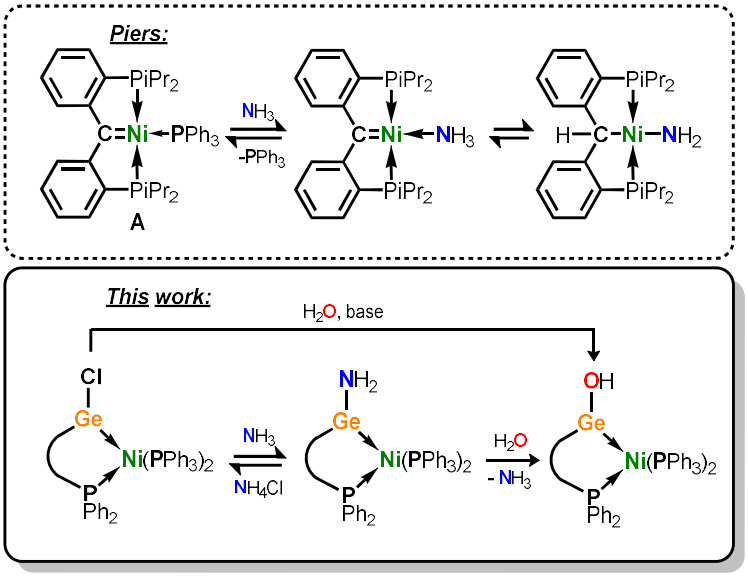

Figure 3.1 The nucleophilic role of a carbene ligand in reversible ammonia activation (*Piers*), and the electrophilic role of a germylene ligand in reversible ammonia activation (*this work*).

Given the potentially Lewis acidic nature of heavier tetrylenes, we envisage that such ligands can reverse the polarity of this MLC process, and act as *electrophilic* binding sites in TM complexes. This would open a new avenue in the dual-centre activation of small molecules, and indeed in catalysis.

In order to investigate the capacity of a tetrylene to remain electrophilic in the coordination sphere of a TM, and perhaps more importantly to be more electrophilic than the TM, we sought to develop a chelating ligand incorporating an acyclic, low-coordinate heavier tetrylene. To this end, we have developed novel phosphine-functionalised amine pro-ligands, ^{PhPh}DippNH and ^{PhiP}DippNH (^{PhPh}DippNH = $Ph_2PCH_2Si(Ph)_2N(H)Dipp$; ^{PhiP}DippNH = $Ph_2PCH_2Si(^iPr)_2N(H)Dipp$; Dipp = 2,6-$^iPr_2$-$C_6H_3$), which can be used to generate phosphine-functionalised (amido)(chloro)germylenes which satisfy the targeted acylic, low-coordinate ligand characteristics when combined with a low-valent TM centre (Figure 3.1). Herein we report the synthesis of these compounds, specifically as their Ni^0 complexes, in which the single centre ambiphile ligand centre (*i.e.* Ge^{II}) maintains its Lewis acidity, and is capable of binding and activating NH_3 and H_2O, in the former case reversibly.

Results and discussion

The phosphine-functionalised germylene ligands feature a novel ancillary ligand scaffold, namely a phosphine-functionalised amide. The amine *pro*-ligands are readily accessed through an initial *in-situ* synthesis of phosphine-functionalised chlorosilanes, $(Ph_2PCH_2)(R)_2SiCl$ (R = Ph, ^iPr),[20] which can then be reacted with the lithium anilide, DippN(H)Li, with loss of LiCl. Although the formed *pro*-ligands, ^{PhiP}DippNH and ^{PhPh}DippNH,

were not isolated in their pure forms, ^{1}H and ^{31}P NMR analyses of crude reaction mixtures suggest they are formed near quantitatively.[21] These crude products are readily deprotonated with a suspension of KH in THF, yielding the potassium amides ^{PhiP}DippNK and ^{PhPh}DippNK in good isolated yields of ~70-75% after work up, based on the Ph_2PCH_2Li·TMEDA starting material.

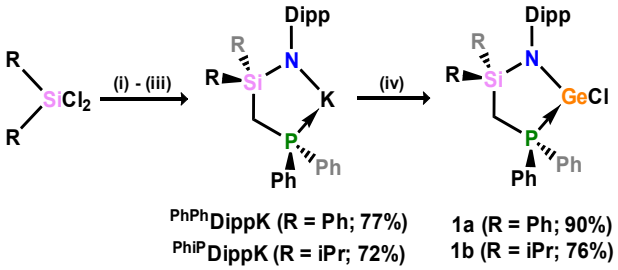

Scheme 3.1 The synthesis of phosphine-functionalised amine *pro*-ligands, their deprotonation, and subsequent synthesis of chloro-germylene complexes. (i) Ph_2PCH_2Li·TMEDA, hexane; (ii) DippN(H)Li, THF; (iii) KH, THF; (iv) $GeCl_2$·dioxane, THF (yields in parentheses). Dipp = 2,6-iPr_2-C_6H_3.

Ge^{II} chloride complexes ^{PhPh}DippNGeCl and ^{PhiP}DippNGeCl (**1a** and **1b**, respectively) are generated through combination of these potassium amides with $GeCl_2$·dioxane in either THF or toluene, yielding the desired germylene ligands in high yields. Both **1a** and **1b** show somewhat complex ^{1}H NMR spectra, when compared with potassium amides ^{PhiP}DippNK and ^{PhPh}DippNK, due to the asymmetric coordination at their Ge^{II} centres. Nevertheless, the presence of a single peak in the respective ^{31}P{^{1}H} NMR spectra confirms the presence of a single ligand environment in these compounds. A single crystal X-ray diffraction analysis of the two germylenes confirms their monomeric nature (*viz.* Figure 3.2), and shows that the Ph_2P moiety of the amide ligands binds the Ge^{II} centre in both species (**1a**: d_{PGe} = 2.4547(9) Å; **1b**:

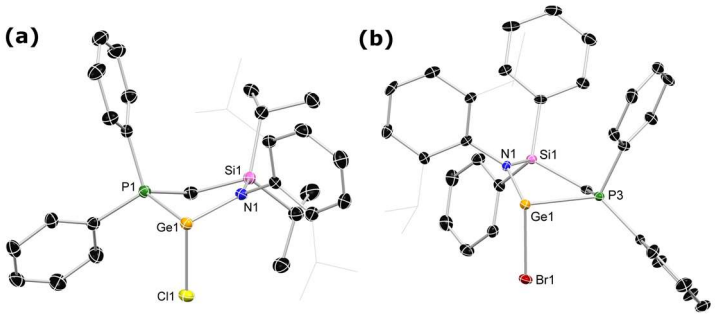

Figure 3.2 The molecular structures of *(a)* **1b** and *(b)* **3a**, with thermal ellipsoids at 40% probability. Hydrogen atoms omitted for clarity. Selected bond distances (Å) and angles (°) for **1b**: Ge1-Cl1 2.355(1); Ge1-P1 2.472(1); Ge1-N1 1.925(3); N1-Ge1-Cl1- 100.69(1); Cl1-Ge1-P1 85.98(4); N1-Ge1-P1 85.85(1). For **3a**: Ge1-Br1 2.512(1); Ge1-P3 2.455(2); Ge1-N1 1.913(4); N1-Ge1-Br1 103.00(1); Br1-Ge1-P3 84.74(4); N1-Ge1-P3 84.98(1).

d_{PGe} = 2.458(1) Å). Complexes **1a**/**b** bear some similarity to complexes reported by Wesemann, incorporating bulky aryl ligands at Ge^{II},[22] and Baceiredo, who also developed Ge^{II} chloride

species bearing phosphine-functionalised amide ligands.[23] In these cases, Ge-P distances are similar to those in **1a**/**b**.

With (amido)(chloro)germylene ligands **1a**/**b** in hand, we began our investigations into the complexation chemistry of these *pro*-chelating ligands towards nickel dihalides. We found that both complexes do not readily react with $NiCl_2$, even after heating, despite a dark red colouration of reaction solutions. However, reactions with an excess of $NiBr_2$·DME in toluene with a small amount of THF led to dark red-brown reaction mixtures, from which dimeric complex **2** could be isolated as large red-brown crystals after filtration (Scheme 3.2). X-ray structural analysis of these crystals (Scheme 3.2, *inset*) revealed that Ni inserts into the Ge-P bond of **1a**, forming a chelating ligand motif incorporating P and Ge as we had hoped.

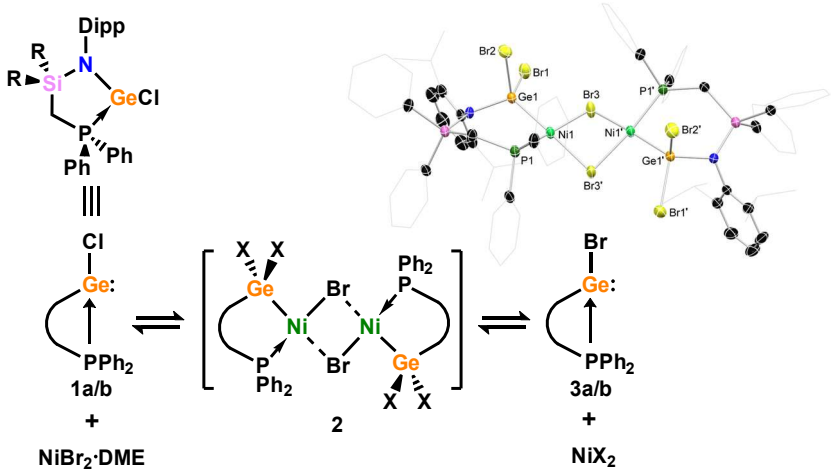

Scheme 3.2 The reaction of chloro-germylenes **1a**/**b** with $NiBr_2$·DME, leading to reversible complexation and Cl/Br exchange at Ge^{II}. *Inset*: the molecular structure of dimeric germyl-nickel complex **2**.

Formal oxidative addition of one Ni-Br bond at Ge^{II} is also observed, akin to previous examples reported by Cabeza and co-workers.[14] Each Ni^{II} centre sits in a square planar geometry, bound by two bridging Br ligands, Ge, and P. Compound **2** represents a surprisingly uncommon example of a germyl-nickel complex, and is unstable in solution in the absence of an excess of $NiBr_2$. This was clear in an attempt to obtain NMR spectroscopic data for **2**, where the only observable species is the bromo germylene ^{PhPh}DippGeBr **3a**, presumably through elimination of the nickel dihalide.[24] Reassessing the reaction of chloro germylene **1a** with $NiBr_2$·DME, we found that addition of a single equivalent leads to a ~50:50 mixture of **1** and **3**, *i.e.* partial Cl/Br exchange. From such a reaction mixture the formation of one or two single crystals of the germyl-nickel mixed halide complex **2'**, the acetonitrile-coordinated monomeric form of **2**, allowed for structural analysis of this 'intermediate'. Addition of 6 equivs. of $NiBr_2$·DME allows for full conversion to bromo germylene **3**,[25] whilst a vast excess (~10 equivs.) of $NiBr_2$·DME affects the crystallisation of small amounts of germyl-nickel bromide complex **2**. We presume that the presence of an excess of $NiBr_2$·DME is required to maintain the stability of **2**, as in all

cases NMR analyses showed only the free chloro/bromo-germylene ligands. Taken as a whole, this demonstrates that $NiBr_2$ can act as a facile halide exchange reagent for the synthesis of bromo germylenes, which are challenging to access *via* conventional routes due to the lack of readily available $GeBr_2$ reagents.[26]

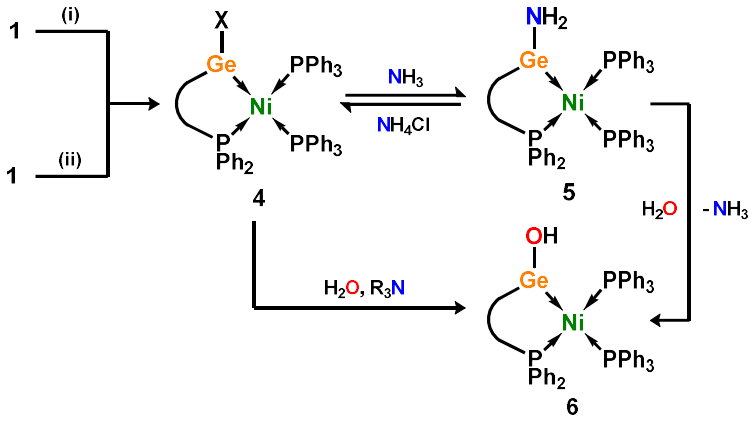

Scheme 3.3 Synthesis of halo-germylene Ni^0 complexes **4** and subsequent reactions with NH_3 and H_2O. (i) 1.1 NiX_2·DME, 2 Ph_3P, 6 Zn, THF, 2 h (X = Br); ~24 h (X = Cl); X = Cl and/or Br; (ii) 1 $Ni(cod)_2$, 2 Ph_3P, toluene, 1 h; X = Cl.

Although the isolation of useful quantities of nickel complex **2** was not possible, the observation that it exists within the reaction mixture seemed a promising start. We found that *in-situ* reduction of this reaction mixture, in the presence of Ph_3P, gave facile access to chelating phosphino-germylene complexes of Ni^0. Room temperature addition of THF to a mixture of **1a**/**b**, $NiBr_2$·DME, Ph_3P, and an excess of Zn powder allowed for the clean formation of Ni^0 complexes **4a**/**b** after 2 h, albeit as a mixture of the chloro- and bromo-germylene ligated species. Employing $NiCl_2$·DME in place of $NiBr_2$·DME led to considerably extended reaction times, but gave clean access to the chloro-germylene species (Scheme 3.3). The pure chloro-germylene analogue can also be accessed through combination of **1**, $Ni(COD)_2$, and PPh_3 in the stoichiometric ratio 1:1:2. Satisfyingly, $^{31}P\{^1H\}$ NMR analysis of crude reaction mixtures in all cases suggest the formation of these novel Ni^0 complexes as the sole products, with the crystalline compounds isolated in good yields from diethyl ether extracts of the crude reaction mixtures. A single crystal X-ray structural analysis of dark red-brown crystals of **4b** reveal a central Ni^0, bound by two Ph_3P ligands, and one chelating phosphino-germylene ligand (Figure 3.4(a)). Notably, the chloride moiety in the germylene ligand remains intact. The three-coordinate Ge^{II} centre holds a trigonal planar geometry, and has a relatively short Ge-Ni contact when compared with previously reported examples, indicative of some back-bonding from Ni to Ge (*vide supra*). The Ni^0 centre holds a tetrahedral geometry, with the three Ni-P distances being as expected when compared with reported phosphine-coordinated Ni^0 complexes. Complex **4a** is essentially isostructural to **4b**.[27] The UV/vis spectra of these species

show two clear absorption bands (**4a**: λ_{max} = 484 nm (ε = 1370 Lcm^{-1}mol^{-1}) and 362 nm (6735 Lcm^{-1}mol^{-1}); **4b**: 473 nm (1685 Lcm^{-1}mol^{-1}) and 362 nm (9160 Lcm^{-1}mol^{-1})), in-keeping with related absorptions for Ni-based *d-d* transitions.[28] Likely due to hindered rotation brought about by the sterics of the chelating ligand system, resonances relating the ligand are broadened in the ^{1}H NMR spectrum of both Ni^0 species.

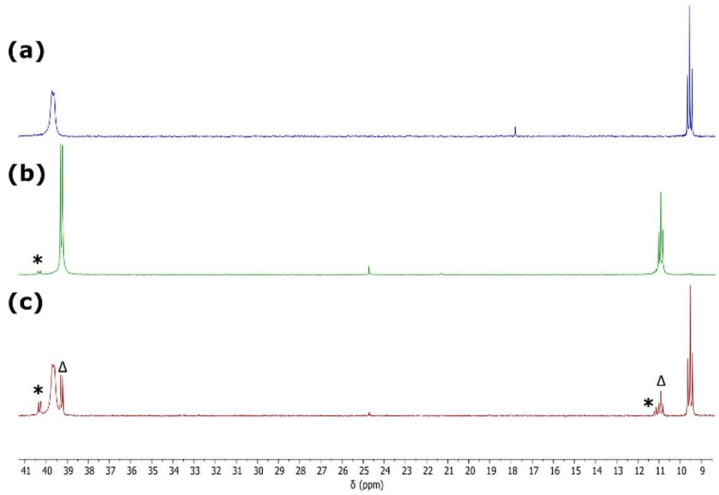

Figure 3.3 The ^{31}P{^{1}H} NMR spectrum of *(a)* **4b**, *(b) in-situ* addition of NH_3 to **5b**, and *(c)* **4b** regenerated after sonication and degassing the sample used for spectrum *(b)*. * = small amounts of **6b**; Δ = small amounts of residual **5b**.

The ^{31}P{^{1}H} NMR spectra show one broadened peak for the Ph_3P ligands, centred at δ = 39.8 ppm(**4a** and **4b**), whilst the flanking phosphine arm of the chelating ligand presents as a well resolved triplet centred at δ = 7.1 (**4a**) and 9.6 (**4b**) ppm (Figure 3.3(a)). For the mixed bromide/chloride samples, a second set of peaks relating to the bromide species is observed in the ^{31}P{^{1}H} NMR spectrum, overlapping with the first.[29] Separation of the two compounds proved impossible in our hands, although using the mixture in subsequent chemistry discussed herein did not pose any issues.

Given the ambiphilic nature of tetrylenes, particularly in acyclic derivatives, the design of complexes **4a**/**b** aims to retain a degree of Lewis acidity at Ge^{II}. This forms the central idea of non-innocent single centre ambiphile ligands. This characteristic was probed by Density Functional Theoretical (DFT) analysis of the frontier orbitals in model complex **4'**, employing ^{PhMe}XylN in place of ^{PhiP}DippN/^{PhPh}Dipp (^{PhMe}XylN = ($Ph_2PCH_2SiMe_2$)(Xyl)N). We found that the LUMO of **4'** is located on the Ge centre (Figure 3.4(a)), and mainly constitutes a vacant *p*-orbital which is expected to be Lewis acidic, particularly given the overall NPA charge at Ge of +1.13. Still, Natural Bond Orbital (NBO) analysis of the Ge-Ni bond indicates strong polarisation toward the Ge centre, whilst the HOMO in **4'** shows some degree of π-bonding, pointing towards a donor-acceptor description of the Ge-Ni bond. In line with the Lewis acidity

of the Ge^{II} centre in **4a**/**b**, deep red-brown solutions of these compounds readily react with

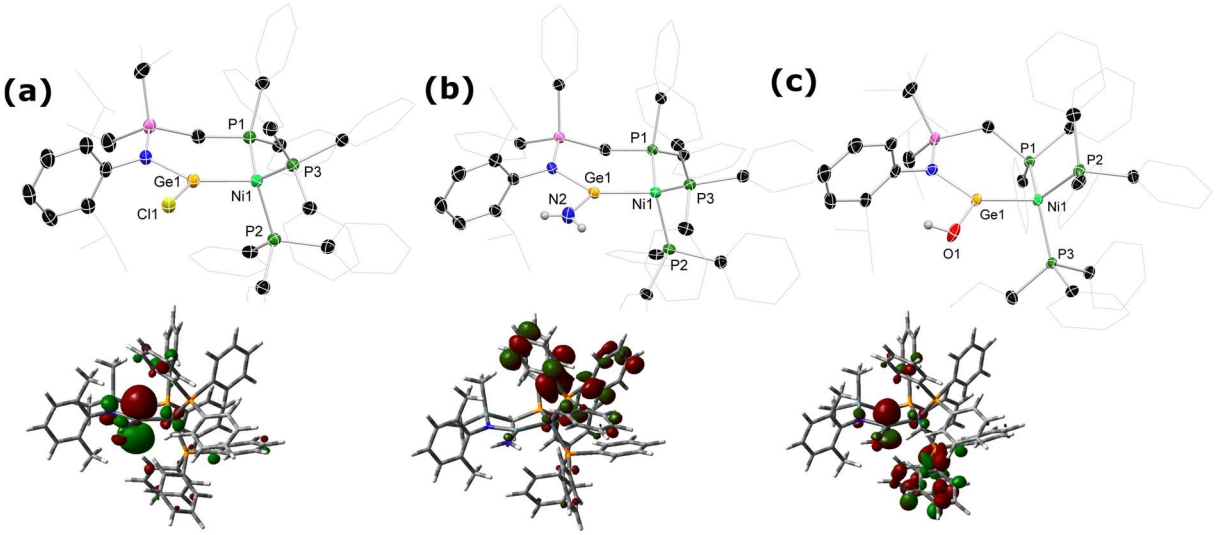

Figure 3.4 Molecular structures of compounds *(a)* **4b**, *(b)* **5a**, and *(c)* **6b**, with thermal ellipsoids at 40% probability. Hydrogen atoms omitted for clarity, aside from those at N2 and O1 in **5a** and **6b**, respectively. The LUMO of each compound is inset below the respective structure. Selected bond distances (Å) and angles (°) for **4b**: Ge1-Ni1 2.1877(7); N1-Ge1 1.869(2); P1-Ni1 2.201(1); P2-Ni1 2.2079(8); P3-Ni1 2.2055(8); N1-Ge1-Cl1 99.57(7); Ni1-Ge1-N1 133.09(7); Ni1-Ge1-Cl1 126.89(3). For **5a**: Ge1-Ni1 2.217(1); N1-Ge1 1.890(2); N2-Ge1 1.819(2); P1-Ni1 2.210(1); P2-Ni1 2.201(1); P3-Ni1 2.1892(9); N1-Ge1-N2 99.07(9); Ni1-Ge1-N1 128.63(6); Ni1-Ge1-N2 132.29(7). For **6b**: Ge1-Ni1 2.2077(7); N1-Ge1 1.885(3); O1-Ge1 1.874(2); P1-Ni1 2.210(1); P2-Ni1 2.202(1); P3-Ni1 2.104(1); N1-Ge1-O1 100.98(1); Ni1-Ge1-O1 128.47(7); Ni1-Ge1-N1 130.49(8).

ammonia at 1 atm pressure to form slightly turbid bright orange reaction mixtures containing ammonia activation products **5a**/**b**. In-situ $^{31}P\{^1H\}$ NMR spectroscopic analysis indicated the formation of a single new product for both systems (Figure 3.3(b)), whilst complimentary ^1H NMR spectra indicated new singlet 2H resonances at δ = 3.13 (**5a**) and 2.96 (**5b**) ppm, which were tentatively assigned to an NH_2 fragment. The IR spectrum of reaction products is in keeping with this, with two weak N-H stretching bands observed at v = 3354 and 3461 (**5a** and **5b**) cm^{-1}. Structural analysis of large orange crystals of the product of the reaction of **4a** with ammonia reveal that the Ge-Cl moiety in this species has in fact undergone a σ-metathesis reaction with one N-H bond of ammonia, yielding the bis(amido)germylene Ni^0 complex **5a** (Scheme 3.3, Figure 3.4(b)).[30]

Presumably, the colourless solid in reaction mixtures is ammonium chloride, through the net loss of HCl in this reaction (*vide supra*). As such, removal of the ammonia atmosphere from reaction mixtures, and sonication of amides **5a**/**b** over the precipitated NH_4Cl with intermittent degassing leads to regeneration of starting materials **4a**/**b** (Figure 3.3), with the loss of ammonia (Scheme 3.3).[31] Such a reversible activation of ammonia is, to the best of our knowledge extremely rare, as is the more general redox-innocent metathesis reaction at a tetrylene centre. Beyond the reaction of **4a/b** with ammonia, these species also readily undergo

a similar metathesis reaction with water in the presence of nitrogen bases to facilitate HCl abstraction (*i.e.* $CyNH_2$), to yield (amido)(hydroxyl)germylene Ni^0 complexes **6a/b** (Scheme 3.3, Figure 3.4(c)). These species can also be accessed by the reaction of amide complexes **5a/b** with water, with concomitant loss of ammonia. The formation of **6a/b** can be clearly observed by ^{1}H NMR and IR spectroscopy, the former containing new 1H resonances pertaining to OH residues (δ = 3.13 (**6a**) and 2.96 (**6b**) ppm), and the latter clear OH stretching bands (v = 3547 (**6a**) and 3541 (**6b**) cm^{-1}). In recent years a flurry of examples of ammonia activation at low-valent group 14 centres have been forthcoming, but lead almost exclusively to oxidative addition reactions, thus yielding E^{IV} compounds (E = C - Sn).[32] That oxidative addition is circumvented in reactions of **4a/b** with both NH_3 and H_2O likely stems from the binding of the Ge lone electron pair to Ni^0. Further, it is surprising that the Ni^0 centre in these complexes remains unchanged, given previous examples of MLC in ammonia activation involving Ph_3P-ligated Ni^0 complexes.[19(c),(d)] Overall, the metathesis reactions of ammonia demonstrated here highlight the targeted high Lewis acidity of the developed acyclic germylene ligands, and are an exciting step towards employing these ligands in complexes which can operate *via* MLC bond activation processes, where a lower coordinate TM centre is utilised.

So as to compare the effects of the differing fragments at Ge^{II} in the described Ni^0 complexes, we performed frontier orbital, NBO, Wiberg Bond Index (WBI), Mayer Bond Order (MBO), and Natural Population analyses on **4'**, **5'**, and **6'**, as model complexes of the real systems, again employing ^{PhMe}XylN in place of ^{PhiP}DippN/^{PhPh}Dipp. We found that **4'**, **5'**, and **6'** all show very similar characteristics in general; the main difference is the interaction of the vacant *p*-orbital on the Ge^{II} centre and the lone pair of the Cl/NH_2/OH moiety. Bond analysis showed the highest bond order for the Ge-NH_2 in **5'** (MBO: 1.10) which is due to the efficient hybridization of the N lone pair and the vacant p-orbital of Ge that are well-described for low-valent germanium compounds.[33] The LUMO of **5'** is the only example in this series which is not represented by a vacant *p*-orbital at Ge (Figure 3.4), most likely due to the described N→Ge donation. Consequently, the Ge-Ni bond order decreases and the Ge-Ni bond length increases (*vide infra*) due to the smaller back donation from the Ni *d*-orbital to the Ge vacant orbital. All systems show some degree of multiple bond character between the Ge^{II} and Ni^0 centres (WBI/MBO for **4'** 1.20/1.13; for **5'**: 1.11/0.98; for **6'**: 1.17/1.07), with predicted Ge-Ni distances (**4'**: 2.161 Å; **5'**: 2.203 Å; **6'**: 2.177 Å) only slightly contracted relative to those observed experimentally (*e.g.* d_{GeNi} for **4b**: 2.1877(7) Å; **5a**: 2.217(1) Å; **6a**: 2.1956(7) Å), possibly due to the increased steric encumbrance in the real complexes. An NBO analysis indicates a large degree of s-character in these bonds, indicative of the greatest contributing factor being Ge→Ni lone-pair donation, but, as already described for **4'**, a high degree of polarisation

towards Ge is also apparent, making a donor-acceptor interaction the best description for the Ge-Ni interaction in these complexes.

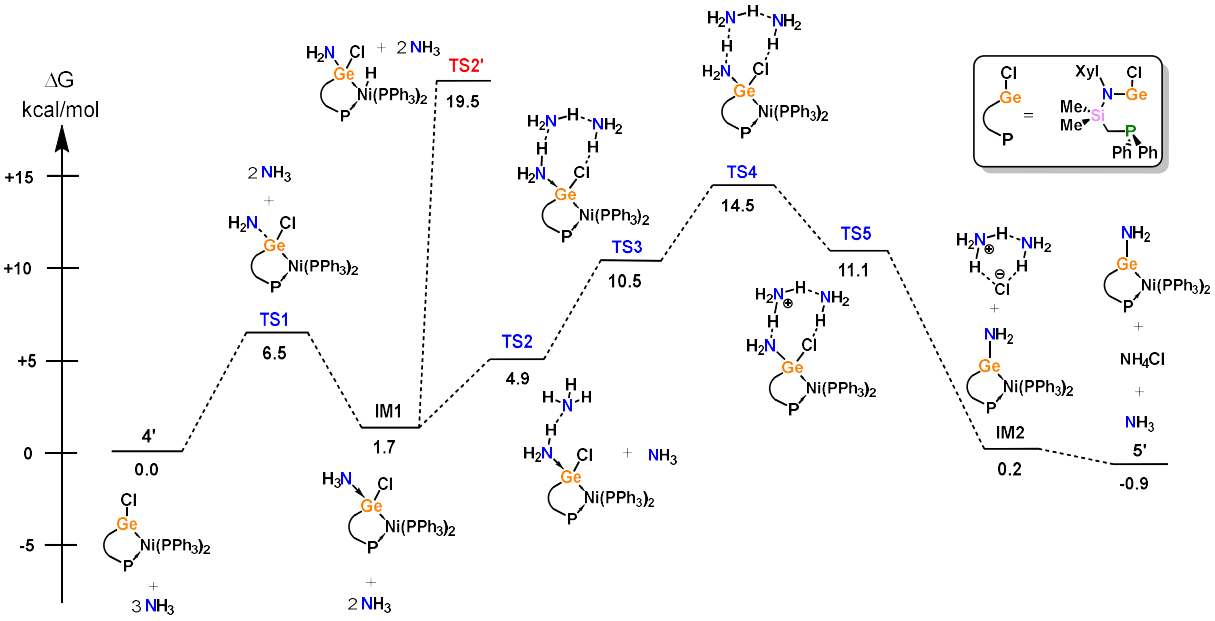

Figure 3.5 DFT-derived mechanism for the σ-metathesis of ammonia in **4'** leading to **5'**

Further, the mechanism for the amination of model complex **4'** was investigated by means of DFT (Figure 3.5), given the reversible nature of this interesting process. The most favourable mechanism begins with binding of NH_3 at Ge^{II}, highlighting the Lewis acidity of this centre. This process is near thermoneutral (**IM1** in Figure 3.5, +1.7 kcal·mol^{-1}), which corroborates reversibility in this key step. Surprisingly, it was found that two further NH_3 molecules are subsequently required to drive the metathesis, which form a H-bond network between the Ge-bound NH_3 and Cl ligands. The most challenging step in the overall process is the ion pair formation (**TS4** in Figure 3.5, +14.5 kcal·mol^{-1}), which is only possible on the potential energy surface (PES) if the H-bond network is present, which stabilises the formation of the NH_4^+ ion. Then, the NH_4^+ and the additional NH_3 molecule facilitate the removal of Cl^-. The overall reaction is very close to thermoneutral (**5'** in Figure 3.5, -0.9 kcal·mol^{-1}), making this process reversible simply by changing the reaction conditions, again corroborating the observed experimental results. Finally, we also considered *(i)* the potential involvement of the Ni centre in NH_3 activation, and *(ii)* oxidative addition of an N-H bond at the Ge centre. Both of these mechanisms can be excluded from the active PES; the Ni-H complex, formed in *(i)*, is relatively unstable (**TS2'** in Figure 3.5, 19.5 kcal·mol^{-1}), whilst the Ge oxidative addition product is not a minimum on the PES (route *(ii)*).

Conclusions

In conclusion, we have developed a chelating phosphino-germylene ligand scaffold, and a facile route to Ni^0 complexes bearing these ligands in a low-cost, one pot synthetic preparation. These ligands, which are centred around an acyclic (amido)(chloro)germylene, remain Lewis acidic when bound to Ni^0. This has been demonstrated by the facile and reversible activation of ammonia, as well as the complimentary irreversible reaction with water, both of which lead to Ge^{II} products through σ-metathesis of the Ge-Cl bond, thus circumventing oxidation at both germanium and nickel. These results form an initial basis for the single centre ambiphile ligand concept, which we are currently expanding to further low-valent main group species, and further first row transition metals, moving towards cooperative bond activation involving both the ligand and the metal centre.

Supporting Information

General experimental considerations

All experiments and manipulations were carried out under a dry oxygen free argon atmosphere using standard Schlenk techniques, or in a MBraun inert atmosphere glovebox containing an atmosphere of high purity argon. THF and diethyl ether were dried by distillation over a sodium/benzophenone mixture and stored over activated 4Å mol sieves. C_6D_6 was dried and stored over a potassium mirror. All other solvents were dried over activated 4Å mol sieves and degassed prior to use. $NiBr_2$·DME,[34] $NiCl_2$·DME,[35] DippN(H)Li,[2(a)] and PPh_2CH_2Li·TMEDA[1(a)] were synthesized according to known literature procedures. All other reagents were used as received. Commercial $CyNH_2$, when used as received, contained enough residual moisture to allow for the synthesis of **6a**. NMR spectra were recorded on a Bruker AV 400 or 500 Spectrometer. The ^1H and $^{13}C\{^1H\}$ NMR spectra were referenced to the residual solvent signals as internal standards. ^{29}Si NMR spectra were externally calibrated with $SiMe_4$. ^{31}P NMR spectra were externally calibrated with H_3PO_4. LIFDI MS spectra were measured at a Waters Micromass LCT TOF mass spectrometer equipped with an LIFDI ion source (LIFDI 700) from Linden CMS GmbH. The samples were dissolved in dry toluene and filtered using a syringe filter under an inert atmosphere. The TOF setup was externally calibrated using polystyrene. ESI-MS was performed on an exactive plus orbitrap spectrometer from Thermo Fischer Scientific. Infrared spectra were measured with the Alpha FT IR from Bruker containing a platinum diamond ATR device. The compounds were measured as solids under inert conditions in a glovebox. For the ammonia activation experiments water free ammonia 5.0 was used.

Experimental procedures

^{PhPh}DippNK. A yellow suspension of PPh_2CH_2Li·TMEDA (6.0 g, 18.6 mmol) in 100 mL hexane was cooled to -78 °C. The mixture was stirred vigorously and Ph_2SiCl_2 (3.9 mL, 18.6 mmol) was added. The mixture was allowed to warm to RT overnight. All volatiles were subsequently removed *in vacuo*, leaving a yellow oil. DippN(H)Li (3.4 g, 18.6 mmol) was added to the residue, and the flask cooled to -78 °C, followed by the addition of 50 mL THF. The mixture was stirred until dissolution of all solids was observed. The cold bath was then removed and the reaction allowed to warm to RT, leading to an orange solution. All volatiles were removed *in vacuo* and the oily residue extracted with 50 mL hexane, and filtered. The solvent was removed *in vacuo* and KH (0.9 g, 28.3 mmol) was added. After addition of 50 mL THF, gas started to evolve, and the mixture was vigorously stirred for a further 16 h. The dark brown suspension was filtered, and all volatiles were removed *in vacuo*. To the resulting oil 50 mL hexane was added, and the mixture treated in an ultrasonic bath causing the precipitation of copious pale brown powder, which was filtered and washed multiple times with hexane, and subsequently dried *in vacuo* to yield ^{PhPh}DippNK as an off-white powder (8.5 g, 14.3 mmol, 77%). Colourless crystals suitable for X-ray diffraction analysis were obtained after two days from a concentrated THF/TMEDA solution layered with hexane stored at -32°C. ^{1}H NMR (THF-d_8, 400 MHz, 298 K): δ = 0.91 (d, 12H, $^3J_{HH}$ = 6.9 Hz, Dipp-Pr^i-C*H*$_3$), 1.97 (d, 2H, $^2J_{HP}$ = 5.4 Hz, Ph_2P-C*H*$_2$), 3.94 (hept, 2H, $^3J_{HH}$ = 6.9 Hz, Dipp-Pr^i-C*H*), 6.24 (t, 1H, $^3J_{HH}$ = 7.4 Hz, Ar-C*H*), 6.74 (d, 2H, $^3J_{HH}$ = 7.4 Hz, Ar-C*H*), 7.00 (m, 6H, Ar-C*H*), 7.10 (m, 6H, Ar-C*H*), 7.27 (m, 4H, Ar-C*H*), 7.48 (m, 4H, Ar-C*H*). ^{13}C{^{1}H} NMR (THF-d_8, 101 MHz, 298 K): δ = 19.7 (d, $^1J_{CP}$ = 29.2 Hz, Ph_2P-*C*H$_2$), 24.9 (Dipp-Pr^i-*C*H$_3$), 28.1 (Dipp-Pr^i-*C*H), 112.6, 123.00, 127.3, 127.5, 128.3, 128.7, 133.4, 133.6, 135.8, 141.4, 143.9, 144.0, 146.7, 146.7 and 156.2 (Ar-*C*). ^{31}P{^{1}H} NMR (THF-d_8, 162 MHz, 298 K): δ = -19.1 (s, CH_2-*P*Ph_2). ^{29}Si{^{1}H} NMR (THF-d_8, 99 MHz, 298 K): δ = - 47.4 (d, $^2J_{SiP}$ = 14.7 Hz, *Si*Ph_2).

^{PhPh}DippGeCl, 1a. A pale brown solution of ^{PhPh}DippNK (7.0 g, 11.7mmol) in 20 mL THF was added dropwise to a stirring solution of $GeCl_2$·dioxane (2.7 g, 11.7 mmol) in 10 mL THF at -78°C, and subsequently allowed to warm to RT, resulting in the formation of an orange solution. All volatiles were removed *in vacuo*, the residue extracted in 20 mL DCM, and filtered. The solvent was removed *in vacuo* and the residue washed with hexane to yield **1a** as an off-white powder (7.0 g, 10.5 mmol, 90 %). Colourless crystals suitable for X-ray diffraction analysis were obtained from a concentrated diethyl ether at RT. ^{1}H NMR (C_6D_6, 400 MHz, 298 K): δ = 0.09 (d, 3H, $^3J_{HH}$ = 6.4 Hz, Dipp-Pr^i-C*H*$_3$), 0.68 (d, 3H, $^3J_{HH}$ = 6.6 Hz, Dipp-Pr^i-C*H*$_3$), 0.86 (d, 3H, $^3J_{HH}$ = 6.5 Hz, Dipp-Pr^i-C*H*$_3$), 1.43 (d, 3H, $^3J_{HH}$ = 6.5 Hz, Dipp-Pr^i-C*H*$_3$), 2.54 (m,

3H, Ph_2P-CH_2/Dipp-Pr^i-C*H*), 4.28 (m, 1H, Dipp-Pr^i-C*H*), 7.02 (m, 14 H, Ar-C*H*), 7.21 (m, 3H, Ar-C*H*), 7.46 (m, 2H, Ar-C*H*), 7.65 (m, 2H, Ar-C*H*), 8.26 (d, 2H, $^3J_{HH}$ = 7.1 Hz, Ar-C*H*). $^{13}C\{^1H\}$ NMR (C_6D_6, 101 MHz, 298 K): δ = 8.1 (Ph_2P-*C*H_2), 21.4, 22.6 and 28.0 (Dipp-Pr^i-*C*H_3), 28.2 and 28.6 (Dipp-Pr^i-*C*H), 28.8 (Dipp-Pr^i-*C*H_3), 123.9, 124.6, 125.6, 129.0, 129.1, 129.6, 129.7, 131.1, 131.5, 132.8, 132.9, 133.3, 133.4, 134.8, 135.4, 137.3, 137.8, 140.8, 140.9, 147.8 and 149.7 (Ar-*C*). $^{31}P\{^1H\}$ NMR (C_6D_6, 162 MHz, 298 K): δ = 4.0 (s, CH_2-*P*Ph_2). $^{29}Si\{^1H\}$ NMR (C_6D_6, 79 MHz, 298 K): δ = - 4.0 (d, $^2J_{SiP}$ = 13.4 Hz, *Si*Ph_2). MS/LIFDI-HRMS found (calcd) m/z: 665.1466 (665.1490) for $[M]^+$.

^{PhPh}DippGeBr, 3a. To a mixture of **1a** (200 mg, 0.30 mmol) and $NiBr_2$·DME (540 mg, 1.8 mmol) was added 5 mL toluene and 1 mL THF, and the resulting mixture stirred for 1 h. All volatiles were removed *in vacuo* and the residue extracted with 5 mL toluene. The solution was concentrated and layered with hexane yielding colourless crystals of **3a** suitable for X-ray diffraction analysis (127 mg, 0.18 mmol, 54%). ^1H NMR (C_6D_6, 400 MHz, 298 K): δ = 0.06 (d, 3H, $^3J_{HH}$ = 6.6 Hz, Dipp-Pr^i-C*H*$_3$), 0.67 (d, 3H, $^3J_{HH}$ = 6.7 Hz, Dipp-Pr^i-C*H*$_3$), 0.93 (d, 3H, $^3J_{HH}$ = 6.6 Hz, Dipp-Pr^i-C*H*$_3$), 1.46 (d, 3H, $^3J_{HH}$ = 6.6 Hz, Dipp-Pr^i-C*H*$_3$), 2.55 (m, 3H, Ph_2P-C*H*$_2$/Dipp-Pr^i-C*H*), 4.26 (hept, 1H, $^3J_{HH}$ = 6.9 Hz, Dipp-Pr^i-C*H*), 6.99 (m, 14 H, Ar-C*H*), 7.21 (m, 3H, Ar-C*H*), 7.46 (m, 2H, Ar-C*H*), 7.60 (m, 2H, Ar-C*H*), 8.30 (d, 2H, $^3J_{HH}$ = 7.3 Hz, Ar-C*H*). $^{13}C\{^1H\}$ NMR (C_6D_6, 101 MHz, 298 K): δ = 8.4 (Ph_2P-*C*H_2), 21.4 and 22.6 (Dipp-Pr^i-*C*H_3), 28.1 and 28.2 (Dipp-Pr^i-*C*H), 28.5 and 29.0 (Dipp-Pr^i-*C*H_3), 123.1, 124.0, 124.8, 125.7, 128.9, 129.0, 129.1, 129.6, 129.8, 131.0, 131.6, 132.7, 132.8, 133.3, 133.4, 134.5, 135.4, 137.6, 140.5, 140.6, 147.8 and 149.9 (Ar-*C*). $^{31}P\{^1H\}$ NMR (C_6D_6, 162 MHz, 298 K): δ = 1.9 (s, CH_2-*P*Ph_2). $^{29}Si\{^1H\}$ NMR (C_6D_6, 99 MHz, 298 K): δ = - 3.9 (d, $^2J_{SiP}$ = 13.9 Hz, *Si*Ph_2); MS/LIFDI-HRMS found (calcd) m/z: 709.1012 (709.0984) for $[M]^+$.

[^{PhPh}DippGe(Cl)]Ni(PPh_3)$_2$, 4a. To a mixture of **1a** (1.60 g, 2.4 mmol), $NiCl_2$·DME (0.53 g, 2.4 mmol), PPh_3 (1.26 g, 4.8 mmol), and Zn (0.94 g, 14.4 mmol) was added 10 mL THF, and the resulting mixture stirred for 24 h at RT resulting in a deep red reaction mixture. All volatiles were removed *in vacuo* and the residue extracted with 20 mL diethyl ether. Dark red crystals of **4a**, which were suitable for X-Ray diffraction analysis, were obtained after storing the solution at RT overnight (1.55g, 1.8 mmol, 52%). ^1H NMR (C_6D_6, 400 MHz, 298 K): δ = 0.49 (d, 6H, $^3J_{HH}$ = 6.6 Hz, Dipp-Pr^i-C*H*$_3$), 1.28 (bs, 6H, Dipp-Pr^i-C*H*$_3$), 3.03 (s, 2H, Ph_2P-C*H*$_2$), 3.72 (hept, 2H, $^3J_{HH}$ = 6.6 Hz, Dipp-Pr^i-C*H*), 6.63 (m, 3 H, Ar-C*H*), 6.94 (m, 36H, Ar-C*H*), 7.32 (d, 5H, $^3J_{HH}$ = 6.2 Hz, Ar-C*H*), 7.52 (s, 9H, Ar-C*H*). $^{13}C\{^1H\}$ NMR (C_6D_6, 101 MHz, 298 K): δ = 20.0 (Ph_2P-*C*H_2), 23.8 and 26.1 (Dipp-Pr^i-*C*H_3), 29.2 (Dipp-Pr^i-*C*H), 124.0, 125.6, 127.2, 128.8,

128.8, 129.1, 132.3, 134.5, 134.6, 135.3, 136.0, 138.6, 138.9, 142.3 and 145.5 (Ar-*C*). $^{31}P\{^1H\}$ NMR (C_6D_6, 81 MHz, 298 K): δ = 7.1 (t, $^2J_{PP}$ = 18.2 Hz, Ph_2*P*-Ni-(PPh_3)$_2$), 39.8 (bs, Ph_2P-Ni-(*P*Ph_3)$_2$). $^{29}Si\{^1H\}$ NMR (C_6D_6, 99 MHz, 298 K): δ = - 13.5 (d, $^2J_{SiP}$ = 5.5 Hz, *Si*Ph_2). MS/LIFDI-HRMS found (calcd) m/z: 985.1705 (985.1755) for $[M\text{-}PPh_3]^+$.

[^{PhPh}DippGe(NH_2)]Ni(PPh_3)$_2$, 5a. Compound **4a** (20 mg, 0.016 mmol) was dissolved in 0.4 mL C_6D_6 in an NMR tube. An excess of ammonia was added to the NMR tube, which was then closed and shaken leading to an immediate colour change from deep red to bright orange, with concomitant formation of a colourless solid (NH_4Cl). The solution was filtered, and volatiles removed *in vacuo* to yield **5a** as an orange powder (15 mg, 0.013 mmol, 83%). Dark orange crystals suitable for X-ray diffraction analysis were obtained by storage of a concentrated toluene solution layered with hexane at -32°C. ^1H NMR (C_6D_6, 400 MHz, 298 K): δ = 0.50 (d, 6H, $^3J_{HH}$ = 6.6 Hz, Dipp-Pr^i-C*H*$_3$), 1.14 (m, 6H, Dipp-Pr^i-C*H*$_3$), 2.97 (s, 2H, Ph_2P-C*H*$_2$), 3.14 (s, 2H, Ge-N*H*$_2$), 3.79 (hept, 2H, $^3J_{HH}$ = 7.3 Hz, Dipp-Pr^i-C*H*), 6.67 (m, 3 H, Ar-C*H*), 6.81 (m, 6H, Ar-C*H*), 7.00 (m, 31H, Ar-C*H*), 7.32 (d, 4H, $^3J_{HH}$ = 6.6 Hz, Ar-C*H*), 7.48 (s, 9H, Ar-C*H*). $^{13}C\{^1H\}$ NMR (C_6D_6, 101 MHz, 298 K): δ = 20.1 (Ph_2P-*C*H$_2$), 23.6 and 26.1 (Dipp-Pr^i-*C*H$_3$), 28.8 (Dipp-Pr^i-*C*H), 124.4, 125.2, 127.1, 131.6, 132.3, 134.3, 134.5, 136.1, 136.3, 140.2, 141.1 and 146.3 (Ar-*C*). $^{31}P\{^1H\}$ NMR (C_6D_6, 81 MHz, 298 K): δ = 9.3 (t, $^2J_{PP}$ = 15.6 Hz, Ph_2*P*-Ni-(PPh_3)$_2$), 39.8 (d, $^2J_{PP}$ = 14.2 Hz, Ph_2P-Ni-(*P*Ph_3)$_2$). $^{29}Si\{^1H\}$ NMR (C_6D_6, 99 MHz, 298 K): δ = - 14.8 (d, $^2J_{SiP}$ = 3.2 Hz, *Si*Ph_2); IR, *v*/cm^{-1} (ATR): 3354 and 3461 (br, w, Ge-NH_2); MS/LIFDI-HRMS found (calcd) m/z: 966.2156 (966.2253) for $[M\text{-}PPh_3]^+$.

[^{PhPh}DippGe(OH)]Ni(PPh_3)$_2$, 6a. 'Wet' cyclohexylaniline (100 mg, 1.00 mmol) was added to a stirring solution of **4a** (200 mg, 0.16 mmol) in 5 mL toluene leading to an immediate colour change from deep red to light red-orange. The mixture was stirred for 30 min. All volatiles were then removed *in vacuo* and the residue extracted with diethyl ether, and filtered. Orange-red crystals of **6a** suitable for X-ray diffraction analysis formed over the course of two hours at ambient temperature (133 mg, 0.11 mmol, 68%). ^1H NMR(C_6D_6, 400 MHz, 298 K): δ = 0.47 (d, 6H, $^3J_{HH}$ = 6.3 Hz, Dipp-Pr^i-C*H*$_3$), 1.10 (m, 6H, Dipp-Pr^i-C*H*$_3$), 2.99 (s, 2H, Ph_2P-C*H*$_2$), 3.77 (hept, 2H, $^3J_{HH}$ = 6.4 Hz, Dipp-Pr^i-C*H*), 4.15 (s, 1H, Ge-O*H*), 6.67 (m, 3 H, Ar-C*H*), 6.83 (m, 6H, Ar-C*H*), 7.01 (m, 30H, Ar-C*H*), 7.34 (d, 4H, $^3J_{HH}$ = 7.0 Hz, Ar-C*H*), 7.54 (s, H, Ar-C*H*). $^{13}C\{^1H\}$ NMR (C_6D_6, 101 MHz, 298 K): δ = 19.4 (Ph_2P-*C*H$_2$), 23.3 and 26.2 (Dipp-Pr^i-*C*H$_3$), 28.9 (Dipp-Pr^i-*C*H), 124.5, 125.7, 127.2, 128.9, 132.3, 134.5, 134.5, 134.6, 135.7, 135.8, 136.0, 138.8, 139.7, 139.9, 140.0 and 146.6 (Ar-*C*). $^{31}P\{^1H\}$ NMR (C_6D_6, 81 MHz, 298 K): δ = 9.0 (t, $^2J_{PP}$ = 15.8 Hz, Ph_2*P*-Ni-(PPh_3)$_2$), 40.6 (d, $^2J_{PP}$ = 15.8 Hz, Ph_2P-Ni-(*P*Ph_3)$_2$). $^{29}Si\{^1H\}$ NMR

(C_6D_6, 99 MHz, 298 K): δ = - 14.4 (d, $^2J_{SiP}$ = 4.6 Hz, *Si*Ph_2); IR, *v*/cm^{-1} (ATR): 3547 (m, Ge-OH); MS/LIFDI-HRMS found (calcd) m/z: 967.2057 (967.2093) for $[M\text{-}PPh_3]^+$.

Reversibility experiments

Compound **4b** (20 mg, 0.17 mmol) was dissolved in 0.4 mL C_6D_6 in an NMR tube and the tube charged with ammonia, closed and shaken. The ^{31}P NMR spectrum was measured to confirm the sole presence of **5b**. All volatiles were removed *in vacuo* and the mixture was redissolved in 0.4 mL C_6D_6 followed by ultrasonication for 30 min. This cycle was repeated two more times, resulting in restoration of the dark red colouration attributable to dissolved **4b**. ^{1}H and ^{31}P NMR spectroscopic analysis of the crude reaction confirmed a mixture with 78% **4b** and 22% **5b**/**6b** confirming the reversibility of the reaction of **4b** with ammonia.

N. B. Related experiment using **4a** also show reversibility, but considerably greater formation of hydroxide compound **6a**, due to extremely high moisture sensitivity of this compound when compared with **4b**.

X-Ray Crystalographic details

Single crystals of ^{PhiP}DippNH, ^{PhPh}DippNK, **1a**/**b**, **1a**·Et_2O, **2**, **2'**, **3a**/**b**, **4a**/**b**, **4-Br**, **5a**, and **6a**/**b** suitable for X-ray structural analysis were mounted in perfluoroalkyl ether oil on a nylon loop and positioned in a 150 K cold N_2 gas stream. Data collection was performed with a STOE StadiVari diffractometer (MoKα radiation) equipped with a DECTRIS PILATUS 300K detector. Structures were solved by Direct Methods (SHELXS-97)[36] and refined by full-matrix least-squares calculations against F^2 (SHELXL-2018).[37] The positions of the hydrogen atoms were calculated and refined using a riding model, aside from protons on N2 (**5a**) and O1 (**6a**/**b**). All non-hydrogen atoms were treated with anisotropic displacement parameters. Crystal data, details of data collections, and refinements for all structures can be found in their CIF files, which are available free of charge via www.ccdc.cam.ac.uk/data_request/cif, and are summarized in Tables 4.1-4.3. In compounds **2** and **4a'** the electron density of highly disordered co-crystallized solvent molecules (details in respective CIFs) was removed using the PLATON SQUEEZE function.[38]

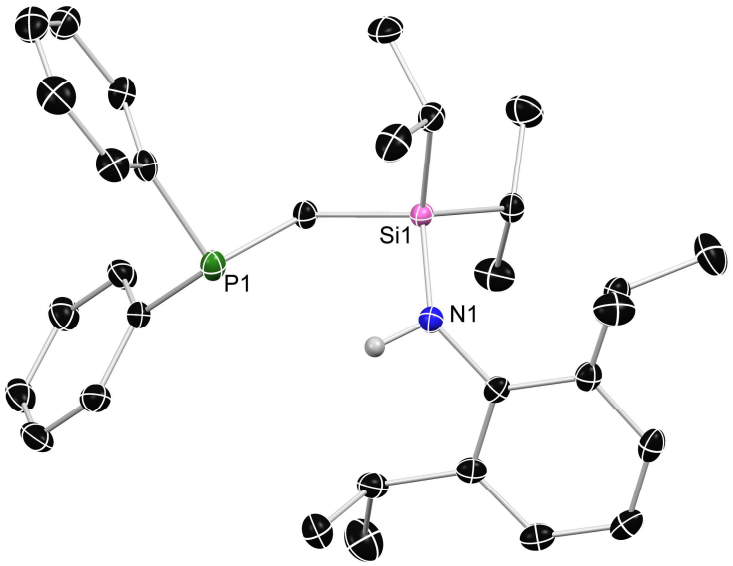

Figure 3.6 Molecular structure of ^{PhiP}DippNH, with thermal ellipsoids at 40% probability. Hydrogen atoms are omitted for clarity, aside from that at N1. Selected bond distances (Å) and angles (°): P1…N1 3.354(2); Si1-N1 1.753(2); Si1-C19 1.894(2); P1-C19 1.868(2); P1-C19-Si1 114.73(1); N1-Si1-C19 105.62(9).

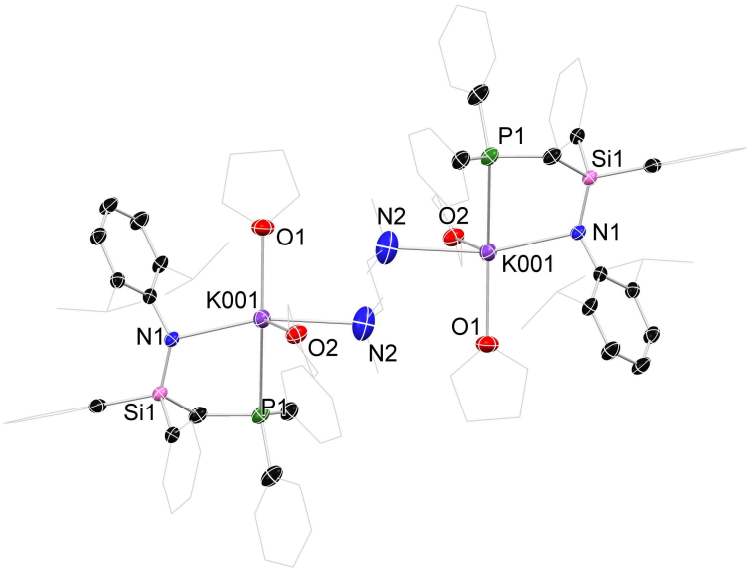

Figure 3.7 Molecular structure of ^{PhPh}DippNK·2(THF)(TMEDA), with thermal ellipsoids at 40% probability. Hydrogen atoms are omitted for clarity. Selected bond distances (Å) and angles (°): N1-K001 2.750(2); N2-K001 2.275(5); P1-K001 3.510(2); N1-K001-P1 69.98(5); P1-K001-N2 81.16(1).

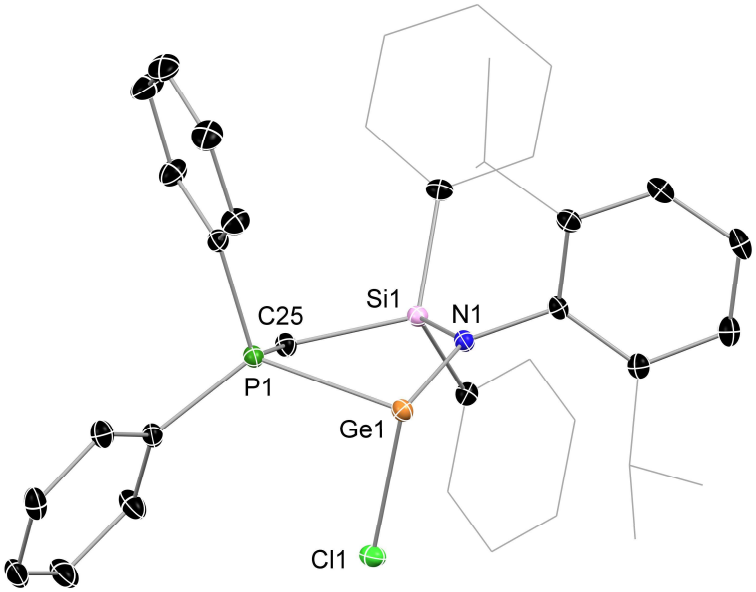

Figure 3.8 Molecular structure of **1a**, with thermal ellipsoids at 40% probability. Hydrogen atoms are omitted for clarity. Selected bond distances (Å) and angles (°): Ge1-Cl1 2.3404(9); Ge1-P1 2.4547(9); Ge1-N1 1.925(2); N1-Ge1-Cl1 101.45(5); Cl1-Ge1-P1 86.08(2); N1-Ge1-P1 85.38(5).

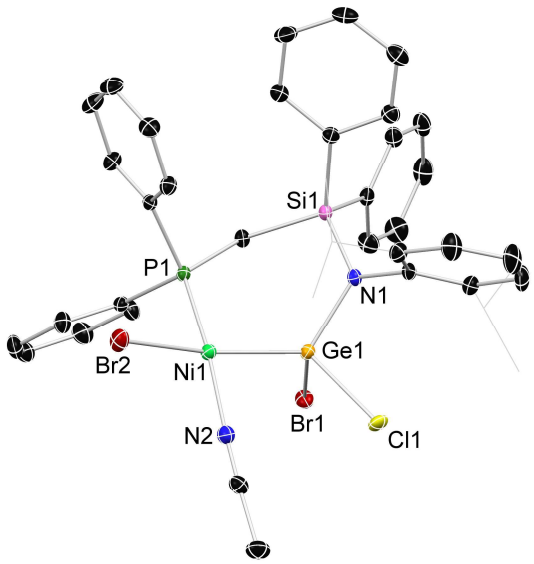

Figure 3.9 Molecular structure of **2'**, with thermal ellipsoids at 40% probability. Hydrogen atoms are omitted for clarity. Selected bond distances (Å) and angles (°): Ni1-N2 1.898(3); N1-Br2 2.3276(6); P1-Ni1 2.175(1); Ni1-Ge1 2.2672(6); N1-Ge1 1.856(3); Ge1-Ni1-P1 88.54(3); N2-Ni1-Ge1 88.59(9); P1-Ni1-Br2 94.86(3); N2-Ni1-Br2 91.75(9).

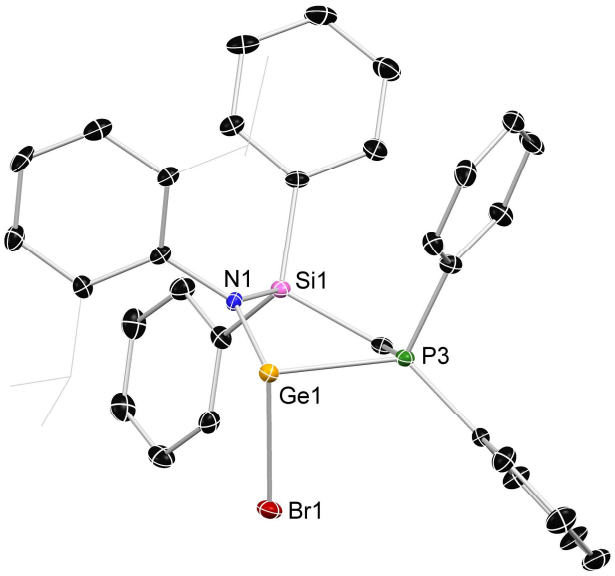

Figure 3.10 Molecular structure of **3b**, with thermal ellipsoids at 40% probability. Hydrogen atoms are omitted for clarity. Selected bond distances (Å) and angles (°): Ge1-Br1 2.468(1); Ge1-P1 2.450(2); Ge1-N1 1.928(6); N1-Ge1-Br1 101.83(2); Br1-Ge1-P1 85.83(4); N1-Ge1-P1 85.92(2).

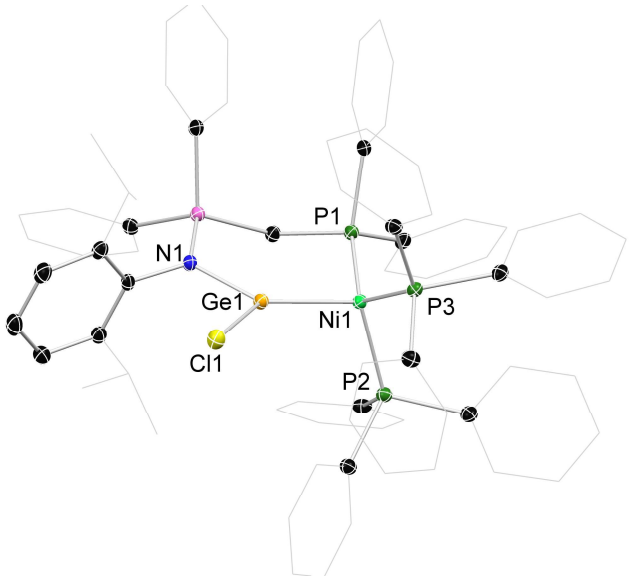

Figure 3.11 Molecular structure of **4a**, with thermal ellipsoids at 40% probability. Hydrogen atoms are omitted for clarity. Selected bond distances (Å) and angles (°): Ge1-Ni1 2.192(1); N1-Ge1 1.869(2); P1-Ni1 2.204(1); P2-Ni1 2.2054(9); P3-Ni1 2.2030(8); N1-Ge1-Cl1 98.62(8); Ni1-Ge1-N1 131.96(6); Ni1-Ge1-Cl1 129.03(6).

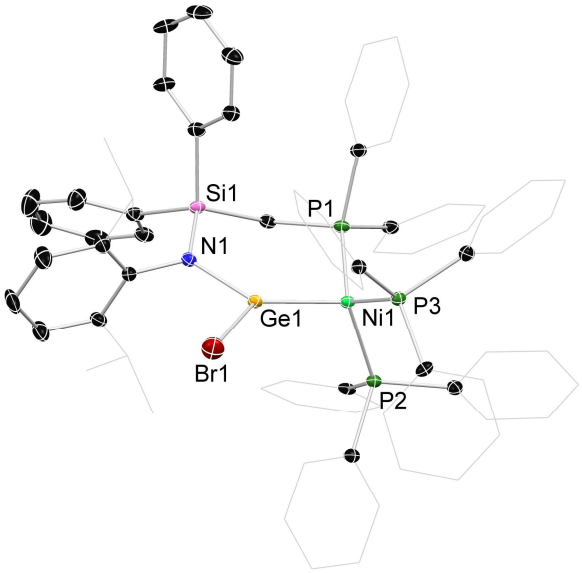

Figure 3.12 Molecular structure of **4-Br**, with thermal ellipsoids at 40% probability. Hydrogen atoms are omitted for clarity. Selected bond distances (Å) and angles (°): Ge1-Ni1 2.1995(7); N1-Ge1 1.876(3); P1-Ni1 2.208(1); P2-Ni1 2.203(1); P3-Ni1 2.215(1); N1-Ge1-Br1 98.86(9); Ni1-Ge1-N1 132.38(9); Ni1-Ge1-Br1 128.46(2).

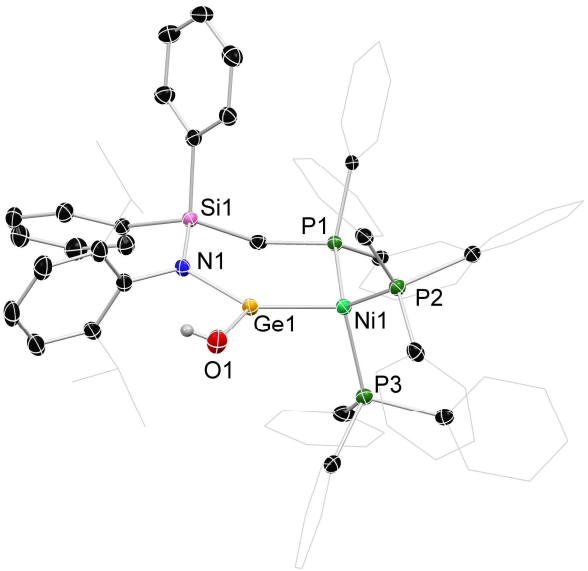

Figure 3.13 Molecular structure of **6a**, with thermal ellipsoids at 40% probability. Hydrogen atoms are omitted for clarity. Selected bond distances (Å) and angles (°): Ge1-Ni1 2.1956(7); N1-Ge1 1.892(3); O1-Ge1 1.780(2); P1-Ni1 2.209(1); P2-Ni1 2.216(1); P3-Ni1 2.196(1); N1-Ge1-O1 100.67(1); Ni1-Ge1-O1 130.08(9); Ni1-Ge1-N1 129.24(8).

Table 3.1 Summary of X-ray crystallographic data for ^{PhiP}DippNH, ^{PhPh}DippNK·2(THF)(TMEDA), and **1a**/**b**.

	^{PhiP}**DippNH**	^{PhPh}**DippNK·2(THF)(TMEDA)**	**1a**	**1a·Et$_2$O**	**1b**
empirical form.	$C_{31}H_{44}NPSi$	$C_{48}H_{63}KN_2O_2PSi$	$C_{37}H_{39}ClGeNPSi$	$C_{41}H_{49}ClGeNOPSi$	$C_{34}H_{46}ClGeNPSi$
formula wt	489.73	798.16	664.79	738.91	635.82
crystal syst.	monoclinic	triclinic	triclinic	triclinic	monoclinic
space group	*C2/c*	*P-1*	*P-1*	*P-1*	*P2$_1$/c*
a (Å)	35.733(7)	11.280(2)	11.000(2)	11.250(2)	15.550(3)
b (Å)	9.740(19)	13.730(3)	12.100(2)	17.780(4)	19.910(4)
c (Å)	17.970(4)	15.610(3)	13.500(3)	20.520(4)	21.820(4)
α (deg.)	90	84.30(3)	96.00(3)	88.30(3)	90
β (δεγ)	107.22(3)	83.70(3)	93.00(3)	75.70(3)	95.60(3)
γ (deg.)	90	72.90(3)	109.00(3)	73.30(3)	90
vol (Å^3)	5974(2)	2291.0(9)	1682.5(7)	3805.8(15)	6723(2)
Z	8	2	2	4	8
ρ(calc) (g.cm^{-3})	1.089	1.157	1.312	1.290	1.256
μ (mm^{-1})	0.150	0.215	1.099	0.981	1.097
F(000)	2128	858	692	1552	2680
T (K)	150(2)	150(2)	150(2)	150(2)	150(2)
reflns collect.	21921	22863	16730	38663	76019
unique reflns	5840	8979	6600	14909	15430
R_{int}	0.0652	0.0469	0.0225	0.0734	0.1118
R1 [$I>2\sigma(I)$]	0.0489	0.0641	0.0318	0.0504	0.0570
*w*R2 (all data)	0.1441	0.1979	0.0855	0.1315	0.1237
CCDC No.	2057308	2057309	2057295	2057296	2057297

Table 3.2 Summary of X-ray crystallographic data for **2**, **2'**, **3a**/**b**, and **4a**.

	2	**2'**	**3a**	**3b**	**4a**
empirical form.	$C_{74}H_{78}Br_6Ge_2N_2$	$C_{41}H_{44}Br_2ClGe$	$C_{43}H_{45}BrGeNP$	$C_{31}H_{43}BrGeNP$	$C_{73}H_{69}Br_{0.19}Cl_{0.8}$
formula wt	1855.56	964.42	787.36	641.22	1256.49
crystal syst.	monoclinic	monoclinic	triclinic	triclinic	triclinic
space group	*C2/c*	*P2$_1$/c*	*P-1*	*P-1*	*P-1*
a (Å)	40.613(8)	20.250(4)	11.330(2)	11.110(2)	12.160(2)
b (Å)	9.870(2)	11.150(2)	13.510(3)	17.260(4)	13.520(3)
c (Å)	23.160(5)	18.550(4)	13.610(3)	18.290(4)	20.800(4)
α (deg.)	90	90	79.10(3)	65.10(3)	75.40(3)
β (δεγ)	101.59(3)	94.50(3)	86.70(3)	88.40(3)	89.00(3)
γ (deg.)	90	90	69.60(3)	85.30(3)	70.90(3)
vol (Å^3)	9094(3)	4175.4(15)	1917.3(8)	3170.5(13)	3119.1(13)
Z	4	4	2	8	2
ρ(calc) (g.cm^{-3})	1.355	1.534	1.364	1.343	1.338
μ (mm^{-1})	3.795	3.248	1.945	2.334	1.080
F(000)	3696	1948	812	1328	1307
T (K)	150(2)	150(2)	150(2)	150(2)	150(2)
reflns collect.	8903	56139	16584	44725	31898
unique reflns	8903	8203	7387	12450	12162
R_{int}	0.0897	0.0421	0.0636	0.0291	0.0301
R1 [$I>2\sigma(I)$]	0.0470	0.0352	0.0513	0.0609	0.0336
*w*R2 (all data)	0.1402	0.0907	0.1598	0.1968	0.0834
CCDC No.	2057298	2057299	2057300	2057301	2057302

Table 3.3 Summary of X-ray crystallographic data for compounds **4-Br**, **4b**, **5a**, and **6a**/**b**.

	4-Br	**4b·Et$_2$O**	**5a**	**6a·Et$_2$O**	**6b·Et$_2$O**
empirical form.	$C_{73}H_{69}BrGeNNi$	$C_{71}H_{83}ClGeNNi$	$C_{73}H_{71}GeN_2NiP$	$C_{77}H_{80}GeNNiO_2$	$C_{71}H_{84}GeNNiO_2$
formula wt	1292.50	1254.13	1228.61	1303.72	1235.69
crystal syst.	triclinic	monoclinic	triclinic	monoclinic	monoclinic
space group	*P-1*	*P2$_1$/c*	*P-1*	*P2$_1$/c*	*P2$_1$/c*
a (Å)	12.680(3)	17.370(4)	12.180(2)	17.680(4)	17.430(4)
b (Å)	15.530(3)	19.770(4)	13.550(3)	19.180(4)	19.840(4)
c (Å)	19.470(4)	19.410(4)	20.860(4)	19.180(4)	19.410(4)
α (deg.)	98.60(3)	90	75.10(3)	90	90
β (δεγ)	92.00(3)	102.70(3)	88.30(3)	108.80(3)	103.40(3)
γ (deg.)	91.30(3)	90	70.40(3)	90	90
vol (Å^3)	3787.1(13)	6502(2)	3128.1(13)	6629(3)	6529(2)
Z	2	4	2	4	4
ρ(calc) (g.cm^{-3})	1.133	1.281	1.304	1.306	1.257
μ (mm^{-1})	1.288	0.928	0.922	0.876	0.885
F(000)	1336	2640	1284	2736	2608
T (K)	150(2)	150(2)	150(2)	150(2)	150(2)
reflns collect.	56477	71318	32911	73271	73734
unique reflns	15676	12767	12253	13006	12827
R_{int}	0.0410	0.0524	0.0395	0.0868	0.0946
R1 [*I*>2σ(*I*)]	0.0531	0.0380	0.0364	0.0426	0.0454
*w*R2 (all data)	0.1658	0.1021	0.0912	0.1056	0.1189
CCDC No.	2057304	2057303	2057305	2057306	2057307

Computational methods and details

DFT calculations were performed at the ωB97X-D3(SMD=benzene)/def2-TZVPP//ωB97X-D3(SMD=benzene)/def2-SVP level of theory.[39] Stationary points on the potential energy surface (PES) were characterized by harmonic vibrational frequency calculations. Transition states, which had one imaginary frequency, were analysed by intrinsic reaction coordinate (IRC) calculations to confirm the corresponding intermediates. Calculations were carried out using the GAUSSIAN 16 program suite.[40]

Table 3.4 NBO analysis of the central GeNi moiety in **4'**.

4'	Occupation	Atom	Polarization	*s*-character	*p*-character	*d*-character
Bond	1.95	Ge	76.43%	88.23%	11.76%	0.01%
		Ni	23.57%	25.89%	72.92%	1.19%

Table 3.5 NBO analysis of the central GeNi moiety in **5'**.

5'	Occupation	Atom	Polarization	*s*-character	*p*-character	*d*-character
Bond	1.93	Ge	74.06%	82.02%	17.97%	0.01%
		Ni	25.94%	26.82%	71.34%	1.84%

Table 3.6 NBO analysis of the central GeNi moiety in **6'**.

6'	Occupation	Atom	Polarization	*s*-character	*p*-character	*d*-character
Bond	1.94	Ge	74.22%	85.75%	14.24%	0.01%
		Ni	25.78%	26.87%	71.56%	1.57%

Table 3.7 Calculated bond lengths [Å], NPA charges of Ge and Ni atoms, Wiberg Bond Index (WBI) and Mayer Bond Order (MBO) in **4'**, **5'**, and **6'**.

	Bond length [Å]		NPA charge		WBI//MBO	
	Ge-Ni	Ge-Cl/Ge-NH_2/Ge-OH	Ge	Ni	Ge-Ni	Ge-Cl/Ge-NH_2/Ge-OH
4'	2.161	2.263/-/-	+1.13	–0.79	1.20//1.13	0.73/-/-//0.82/-/-
5'	2.203	-/1.816/-	+1.34	-0.82	1.11//0.98	-/0.76/-//-/1.10/-/-
6'	2.177	-/-/1.801	+1.40	-0.83	1.17//1.07	-/-/0.61//-/-/0.93

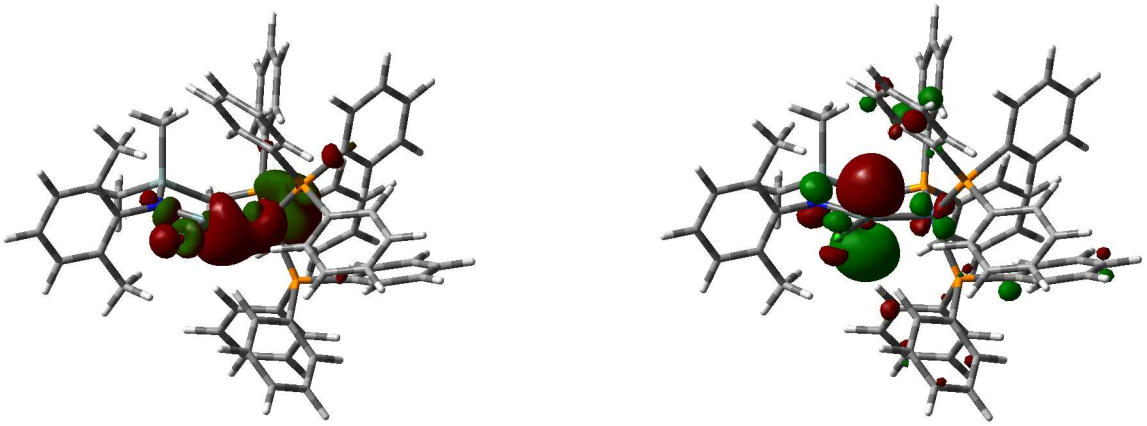

Figure 3.14 HOMO (left, –6.60 eV) and LUMO (right, 0.62 eV) of **4'**.

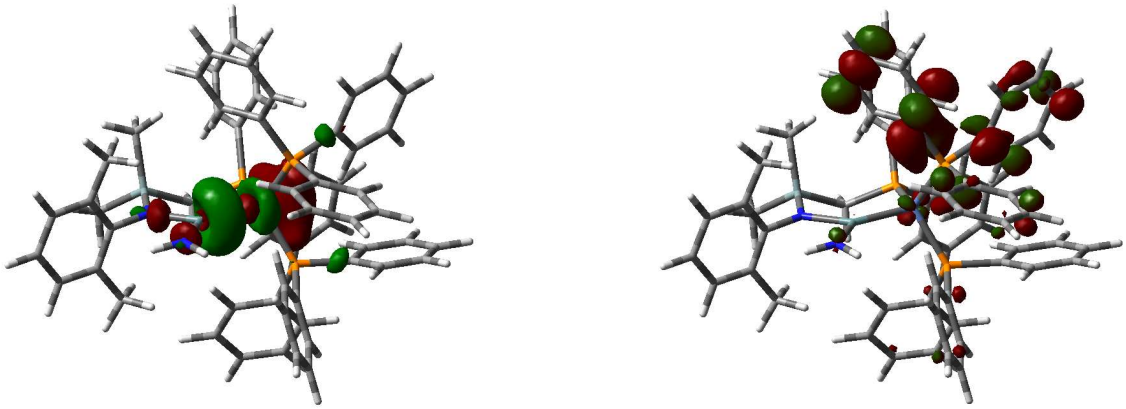

Figure 3.15 HOMO (left, –6.35 eV) and LUMO (right, 0.96 eV) of **5'**.

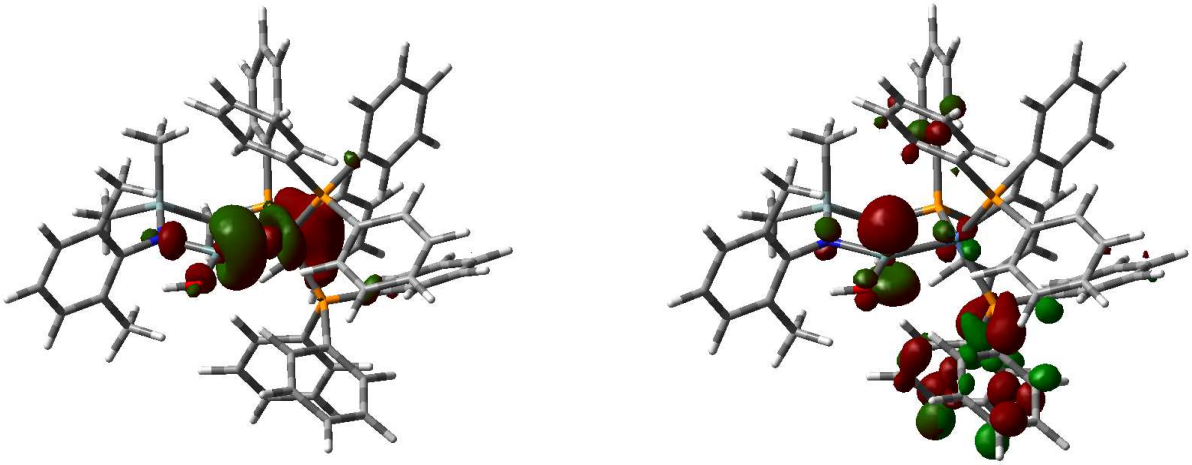

Figure 3.16 HOMO (left, –6.50 eV) and LUMO (right, 0.90 eV) of **6'**.

References

1 (a) N. E. Schore, L. S. Benner, B. E. LaBelle, *Inorg. Chem.* **1981**, *20*, 3200–3208; (b) F. Eisenträger, A. Göthlich, I. Gruber, H. Heiss, C. A. Kiener, C. Krüger, J. Ulrich Notheis, F. Rominger, G. Scherhag, M. Schultz, B. F. Straub, M. A. O. Volland, P. Hofmann, *New J. Chem.* **2003**, *27*, 540–550.

2 (a) J. T. Patton, M. M. Bokota, K. A. Abboud, *Organometallics* **2002**, *21*, 2145–2148. (b) I. C. Cai, M. I. Lipschutz, T. D. Tilley, *Chem. Commun.* **2014**, *50*, 13062–13065.

3 (a) T. J. Hadlington, T. Szilvási, *Nat. Commun.* **2022**, *13*, 461–471; (b) A. Schulz, T. L. Kalkuhl, P. M. Keil, T. J. Hadlington, *Angew. Chem. Int. Ed.* **2023**, *62*, e202305996; (c) *unpublished results*.

4 A. J. Sicard, R. T. Baker, *Org. Process Res. Dev.* **2020**, *24*, 2950–2952.

5 E. O. Fischer, A. Maasböl, *Angew. Chem. Int. Ed.* **1964**, *8*, 580–581.

6 For a broad overview, see the following collections and reviews, and references therein: (a) D. J. Cardin, B. Cetinkaya, M. F. Lappert, *Chem. Rev.* **1972**, *72*, 545–574; (b) A. J. Arduengo, G. Bertrand, *Chem. Rev.* **2009**, *109*, 3209–3210; (c) H. G. Raubenheimer, *Dalton Trans.* **2014**, *43*, 16959–16973; (d) F. Ekkehardt Hahn, *Chem. Rev.* **2018**, *118*, 9455–9456.

7 (a) R. R. Schrock, A. H. Hoveyda, *Angew. Chem. Int. Ed.* **2003**, *42*, 4592–4633; (b) D. Astruc, *Metal-Carbene and -Carbyne Complexes and Multiple Bonds with Transition Metals*. In: Organometallic Chemistry and Catalysis. Springer, Berlin, Heidelberg, 2007.

8 (a) F. Glorius, N-Heterocyclic Carbenes in Transition Metal Catalysis. Springer, Berlin, Heidelberg, 2007; (b) S. Diez-González, N. Marion, S. P. Nolan, *Chem. Rev.* **2009**, *109*, 3612–3676; (c) E. Peris, *Chem. Rev.* **2018**, *118*, 9988−10031.

9 (a) R. Waterman, P. G. Hayes, T. D. Tilley, *Acc. Chem. Res.* **2007**, *40*, 712–719; (b) Judith Baumgartner, Christoph Marschner, *Rev. Inorg. Chem.* **2013**, *34*, 119–152; (c) L. Álvarez-Rodríguez, J. A. Cabeza, P. García-Álvarez, D. Polo, *Coord. Chem. Rev.* **2015**, *300*, 1–28.

10 T. J. Hadlington, M. Driess, C. Jones, *Chem. Soc. Rev.* **2018**, ***47***, 4176–4197.

11 Y.-P. Zhou, M. Driess, *Angew. Chem. Int. Ed.* **2019**, *58,* 3715–3728.

12 (a) L. Álvarez-Rodríguez, J. Brugos, J. A. Cabeza, P. García-Álvarez, E. Pérez-Carreño, D. Polo, *Chem. Commun.*, **2017** *53*, 893–896; (b) L. Álvarez-Rodríguez, J. Brugos, J. A. Cabeza, P. García-Álvarez, E. Pérez-Carreño, *Chem. Eur. J.* **2017**, *23*, 15107–15115; (c) J. Brugos, J. A. Cabeza, P. García-Álvarez, E. Pérez-Carreño, *Organometallics* **2018**, *37*, 1507–1514; (d) J. A. Cabeza, P. García-Álvarez, C. J. Laglera-Gándara, E. Pérez-Carreño, *Chem. Commun.* **2020**, *56*, 14095–14097.

13 A related bis(phosphine) functionalised N-heterocyclic germylene ligand has also been reported by Goicoechea *et al.*, alongside its group 11 halide and Pt^0 complexes: S. Bestgen, N. H. Rees, J. M. Goicoechea, *Organometallics* **2018**, *37*, 4147–4155.

14 (a) J. A. Cabeza, I. Fernández, J. M. Fernández-Colinas, P. García-Álvarez, C. J. Laglera-Gándara, *Chem. Eur. J.* **2019**, *25*, 12423–12430; (b) J. A. Cabeza, I. Fernández, P. García-Álvarez, C. J. Laglera-Gándara, *Dalton Trans.* **2019**, *48*, 13273–13280; (c) A. Arauzo, J. A. Cabeza, I. Fernández, P. García-Álvarez, I. García-Rubio, C. J. Laglera-Gándara, *Chem. Eur. J.* **2021**, *27*, 4985–4992.

15 (a) K. E. Litz, J. E. Bender Iv, J. W. Kampf, M. M. B. Holl, *Angew. Chem. Int. Ed.* **1997**, *36*, 496–498; (b) J. E. Bender IV, A. J. Shusterman, M. M. Banaszak Holl, J. W. Kampf, *Organometallics* **1999**, *18*, 1547–1552; (c) C. Gendy, A. Mansikkamäki, J. Valjus, J. Heidebrecht, P. C.-Y. Hui, G. M. Bernard, H. M. Tuononen, R. E. Wasylishen, V. K. Michaelis, R. Roesler, *Angew. Chem. Int. Ed.* **2019**, *58*, 15–158; (d) T. Watanabe, Y. Kasai, H. Tobita, *Chem. Eur. J.* **2019**, *25*, 13491–13495; (e) Z. Feng, Y. Jiang, H. Ruan, Y. Zhao, G. Tan, L Zhang, X. Wang, *Dalton Trans.* **2019**, *48*, 14975 – 14978; (f) M. Zhong, J. Wei, W.-X. Zhang, Z. Xi, *Organometallics* **2021**, *40*, 310−313.

16 (a) H. Grützmacher, *Angew. Chem. Int. Ed.* **2008**, *47*, 1814; (b) J. R. Khusnutdinova, D. Milstein, *Angew. Chem. Int. Ed.* **2015**, *54*, 12236; (c) M. R. Elsby, R. T. Baker, *Chem. Soc. Rev.* **2020**, *49*, 8933–8987.
17 (a) V. Lyaskovskyy, B. de Bruin, *ACS Catal.* **2012**, *2*, 270; (b) J. van der Vlugt, *Eur. J. Inorg. Chem.* **2012**, 363; (c) S. Schneider, J. Meiners, B. Askevold, *Eur. J. Inorg. Chem.* **2012**, 412.
18 It should be noted that the concept of "Synergistic Catalysis" is perhaps also fitting here, given the generally high reactivity of low-coordinate tetrylenes in their own right. For a review on this concept and its implications, see: U. B. Kim, D. J. Jung, H. J. Jeon, K. Rathwell, S.-gi Lee, *Chem. Rev.* **2020**, *120*, 13382−13433.
19 (a) A. L. Casalnuovo, J. C. Calabrese, and D. Milstein, *Inorg. Chem.* **1987**, *26*, 971–973; (b) E. Khaskin, M. A. Iron, L. J. W. Shimon, J. Zhang, D. Milstein, *J. Am. Chem. Soc.* **2010**, *132*, 8542–8543; (c) D. V. Gutsulyak, W. E. Piers, J. Borau-Garcia, M. Parvez, *J. Am. Chem. Soc.* **2013**, *135*, 11776–11779; (d) R. M. Brown, J. Borau Garcia, J. Valjus, C. J. Roberts, H. M. Tuononen, M. Parvez, R. Roesler, *Angew. Chem. Int. Ed.* **2015**, *54*, 6274–6277.
20 Procedures modified from those previously reported for related compounds were used. See: R. D. Holmes-Smith, R. D. Osei, S. R. Stobart, *J. Chem. Soc., Perkin Trans. 1* **1983**, 861–866.
21 The free ligands typically form oils at ambient temperature, but a few single crystals sometimes deposit from decomposed reaction mixtures of the metalled ligands. See ESI for details.
22 J. Schneider, K. M. Krebs, S. Freitag, K. Eichele, H. Schubert, L. Wesemann, *Chem. Eur. J.* **2016**, *22*, 9812–9826.
23 J. Berthe, J. Manuel Garcia, E. Ocando, T. Kato, N. Saffon-Merceron, A. De Cózar, F. P. Cossío, A. Baceiredo, *J. Am. Chem. Soc.* **2011**, *133*, 15930–15933.
24 The bromo-germylene, PhiPDippGeBr (**3b**), can be accessed using an identical method (see ESI for details).
25 Yields of 50-55 % are obtained after recrystallisation.
26 As an example, $GeBr_2$·dioxane, used as is $GeCl_2$·dioxane, can be synthesised from $GeBr_4$, which is a high-cost starting material.
N. Hayakawa, T. Sugahara, Y. Numata, H. Kawaai, K. Yamatani, S. Nishimura, S. Goda, Y. Suzuki, T. Tanikawa, H. Nakai, D. Hashizume, T. Sasamori, N. Tokitoh, T. Matsuo, *Dalton Trans.* **2018**, *47*, 814–822.
27 Note that single crystals of pure **4a** reproducibly gave poor X-ray diffraction data, not of a publishable standard. However, **4a** co-crystallised with ~19 % of **4-Br** gave data of a publishable standard. See ESI for details.
28 C. A. Tolman, W. C. Seidel, D. H. Gerlach, *J. Am. Chem. Soc.* **1972**, *94*, 2669–2676.
29 Attempts to synthesise pure samples of the bromo-germylene Ni^0 complex, **4-Br**, are outlined in the ESI.
30 Despite attempts to recrystallise the corresponding amide complex **5b** from a range of solvents, only very fine needles could be isolated which diffracted too poorly to attain meaningful X-ray data.
31 As ascertained by ^{1}H and ^{31}P NMR spectroscopic analysis. Due to the extremely high sensitivity of **5a**/**b** towards moisture, the degassing cycles led to the formation of small amounts of hydroxide complexes **6a**/**b**.
32 For some recent examples, see: (a) T. J. Hadlington, J. A. B. Abdalla, R. Tirfoin, S. Aldridge, C. Jones, *Chem Commun.* **2016**, *52*, 1717–1720; (b) A. V. Protchenko, J. I. Bates, L. M. A. Saleh, M. P. Blake, A. D. Schwarz, E. L. Kolychev, A. L. Thompson, C. Jones, P. Mountford, S. Aldridge, *J. Am. Chem. Soc.* **2016**, *138*, 4555–4564; (c) D. C. H. Do, A. V. Protchenko, M. Á. Fuentes, J. Hicks, P. Vasko, S. Aldridge, *Chem. Commun.* **2020**, *56*, 4684–4687.

33 Z. Benedek, and T. Szilvási, *Organometallics* **2017**, *36*, 1591–1600.
34 H. Bauer, J. Weismann, D. Saurenz, C. Färber, M. Schär, W. Gidt, I. Schädlich, G. Wolmershäuser, Y. Sun, S. Harder, H. Sitzmann, *J. Organomet. Chem.* **2016**, *809*, 63–73.
35 A. Boudier, P.-A. R. Breuil, L. Magna, H. Olivier-Bourbigou, P. Braunstein, *J. Organomet. Chem.* **2012**, *718*, 31–37.
36 G. M. Sheldrick, SHELXL-97, Program for Crystal Strucutre Refinement, Göttingen, 1997.
37 G. Sheldrick, *Acta Crystallogr., Sect. C: Struct. Chem.* **2015**, *71*, 3–8.
38 A. Spek, Acta Crystallogr., Sec. D: Struct. Biol. **2009**, *65*, 148–155.
39 (a) F. Weigend, R. Ahlrichs, *Phys. Chem. Chem. Phys.* **2005**, *7*, 3297–3305; (b) J.-D. Chai, M. Head-Gordon, *Phys. Chem. Chem. Phys.* **2008**, *10*, 6615–6620; (c) S. Grimme, J. Antony, S. Ehrlich, H. Krieg, *J. Chem. Phys*. **2010**, *132*, 154104; (d) A. V. Marenich, C. J. Cramer, D. G. Truhlar, *J. Phys. Chem. B* **2009**, *113*, 6378–6396.
40 Gaussian 16, Revision A. 03, M. J. Frisch, G. W. Trucks, H. B. Schlegel, G. E. Scuseria, M. A. Robb, J. R. Cheeseman, G. Scalmani, V. Barone, G. A. Petersson, H. Nakatsuji, X. Li, M. Caricato, A. V. Marenich, J. Bloino, B. G. Janesko, R. Gomperts, B. Mennucci, H. P. Hratchian, J. V. Ortiz, A. F. Izmaylov, J. L. Sonnenberg, D. Williams-Young, F. Ding, F. Lipparini, F. Egidi, J. Goings, B. Peng, A. Petrone, T. Henderson, D. Ranasinghe, V. G. Zakrzewski, J. Gao, N. Rega, G. Zheng, W. Liang, M. Hada, M. Ehara, K. Toyota, R. Fukuda, J. Hasegawa, M. Ishida, T. Nakajima, Y. Honda, O. Kitao, H. Nakai, T. Vreven, K. Throssell, J. A. Montgomery, Jr., J. E. Peralta, F. Ogliaro, M. J. Bearpark, J. J. Heyd, E. N. Brothers, K. N. Kudin, V. N. Staroverov, T. A. Keith, R. Kobayashi, J. Normand, K. Raghavachari, A. P. Rendell, J. C. Burant, S. S. Iyengar, J. Tomasi, M. Cossi, J. M. Millam, M. Klene, C. Adamo, R. Cammi, J. W. Ochterski, R. L. Martin, K. Morokuma, O. Farkas, J. B. Foresman, and D. J. Fox, Gaussian, Inc., Wallingford CT, **2016**.

Chapter 4

Geometrically Constrained Cationic Low-Coordinate Tetrylenes: Highly Lewis Acidic σ-Donor Ligands in Catalytic Systems

P. M. Keil, T. J. Hadlington, *Angew. Chem. Int. Ed.* **2022**, *61*, e202114143

All DFT calculations concerning this project were conducted by Dr. Terrance J. Hadlington.

Synopsis

Following the isolation of the (chloro)germylene-nickel(0) complexes [{^{PhR}DippGe(Cl)}·Ni(PPh_3)$_2$] (^{PhR}Dipp = [{$Ph_2PCH_2Si(R)_2$} (Dipp)N]$^-$; R = Ph, *i*Pr; Dipp = 2,6-*i*$Pr_2C_6H_3$) described in Chapter 3, we aimed to modify these by converting them into the cationic germyliumylidene complexes, potentially further increasing their Lewis acidity and reactivity. By abstracting the chloride and introducing the weakly-coordinating anion [BAr^F_4]$^-$ ([BAr^F_4]$^-$ = [{3,5-$(CF_3)_2C_6H_3$}$_4$B]$^-$) we were able to obtain the cationic germyliumylidene-nickel(0) complexes [(^{PhR}DippGe)·Ni(PPh_3)$_2$]$^+$. In a one-pot route from ^{PhiP}DippSnCl, we were also able to obtain the corresponding cationic stannylidene-nickel(0) complex [(^{PhiP}DippSn)·Ni(PPh_3)$_2$]$^+$. The same ligand scaffold did not lead to stable (chloro)stannylene-nickel(0) complexes, as described in Chapter 3. It should be noted that the complexes with *iso*-propyl groups as residues at the backbone silyl moiety are apparently much more stable/easier to handle compared to the complexes with phenyl residues, resulting in more selective reactions, less decomposition, as well as a higher crystallinity. Therefore, only the *iso*-propyl ligand system, ^{PhiP}Dipp , was utilised for the stannylene complex, and was also the focus in subsequent projects described in Chapters 6, 7 and 8.

X-ray diffraction analysis revealed a bent N-E-Ni angle of the cationic tetryliumylidene-nickel(0) complexes, [(^{PhR}DippE)·Ni(PPh_3)$_2$]$^+$ (E = Ge, Sn), which is apparently enforced by the ligand scaffold, leading to non-ideal orbital overlap, and thus minimised *π*-back-donation from the TM centre to the tetryliumylidene. Furthermore, the cationic charge was calculated to be largely localised at the tetrel element. These are the key points for the here reported tetryliumylidene systems, since previously discussed tetryliumylidene-TM systems usually exhibit a near linear Ligand-E-TM angle, which leads to good orbital overlap and pronounced *π*-back-donation, and charge localisation either at the TM centre or ligand backbone.[1] The here reported systems exhibit remarkably high Lewis acidity at Ge/Sn, pertaining towards Lewis super acidity, as suggested by experimental and theoretical investigations. This is due to the reduced

π-back-donation, which does not quench the Lewis acidity, resulting in two vacant *p*-orbitals being accessible at the tetryl element, affirmed by frontier orbital analysis. Coordination of DMAP (4-Me_2NPyr) and reversible coordination of ammonia at the germanium centre in $[(^{PhR}DippGe)\cdot Ni(PPh_3)_2]^+$ experimentally confirmed the accessibility of these *p*-orbitals. The ammonia coordination was analysed using NMR spectroscopy and theoretical investigation, as crystallisation of the adduct was not possible due to the reversible nature of the coordination. Generally, crystallisation of the here discussed cationic tetryliumylidene compounds posed problems, since the presence of the $[BAr^F_4]^-$ counter anion led to oils when crystallisation was attempted. Crystalline material only ensued when the present compound was of high purity.

Even though these complexes exhibit such a high Lewis acidity, stability is remarkably high, showing no sign of decomposition when heated at 60 °C in solution for an extended period of time, or in the presence of reactive substrates such as $PhSiH_3$. Additionally, we could also show that our ligands are active catalysts for the hydrosilylation of alkenes and alkynes with $PhSiH_3$.

In conclusion, herein we successfully advanced our (chloro)germylene-nickel(0) complexes from Chapter 3 to the tetryliumylidene-nickel(0) complexes $[(^{PhR}DippE)\cdot Ni(PPh_3)_2]^+$, amplifying Lewis acidity of the tetrylene centres. The developed ligand scaffold is key for the observed high ligand-centred Lewis acidity as it enforces a bent N-E-Ni angle, minimising Ni→E *π*-back-donation. In contrast to the complexes in Chapter 3, ammonia is not activated at the tetrel element, but rather displays reversible coordination. Still, MLC could not be observed, which hints that the reactivity of the electronically saturated Ni^0 centre needs to be enhanced, which is addressed in Chapters 7 and 8.

It should be noted, that a related project has recently been published in our group, employing the described cationic germylene and stannylene ligands, and derivatives thereof, to access tetryliumylidene-nickel(0) complexes $[(^{RR}DippE)\cdot Ni(IPr)]$ (IPr = [{HC(Dipp)N}$_2$C:]) with IPr as an ancillary ligand.[2] In this case, the tetryliumylidene ligand switches to a Z-type ligand with *σ*-donation from the Ni^0 centre to the tetrel element allowing for catalytic hydrogenation of alkenes. Even though MLC could, again, not be observed for these complexes, further usage of these ligands for catalytic applications could be shown here.

Manuscript

The following sections are reproduced and formatted from the following article: P. M. Keil, T. J. Hadlington, *Angew. Chem. Int. Ed.* **2022**, *61*, e202114143; *Angew. Chem.* **2022**, *134*, e202114143. *Experimental spectra (NMR, LIFDI/MS, UV/vis and IR) and further details concerning DFT calculations can be retrieved online (*https://doi.org/10.1002/anie.202114143).

Abstract

A novel non-innocent ligand class, namely cationic single-centre ambiphiles, is reported in the phosphine-functionalised cationic tetrylene Ni^0 complexes, $[^{PhR}DippENi(PPh_3)_3]^+$ (**4a/b** (Ge) and **5** (Sn); $^{PhR}Dipp$ = {$[Ph_2PCH_2SiR_2](Dipp)N$}$^-$; R = Ph, ^{i}Pr; Dipp = 2,6-$^i Pr_2C_6H_3$). The inherent electronic nature of low-coordinate tetryliumylidenes, combined with the geometrically constrained [N-E-Ni] bending angle enforced by the chelating phosphine arm in these complexes, leads to strongly electrophilic E^{II} centres which readily bind nucleophiles, reversibly in the case of NH_3. Further, the Ge^{II} centre in **4a/b** readily abstracts the fluoride ion from $[SbF_6]^-$ to form the fluoro-germylene complex $^{PhR}DippGe(F)Ni(PPh_3)_3$ **9**, despite this Ge^{II} centre simultaneously being a *σ*-donating ligand towards Ni^0. Alongside the observed catalytic ability of **4** and **5** in the hydrosilylation of alkynes and alkenes, this forms an exciting introduction to a multi-talented ligand class in cationic single-centre ambiphiles.

Introduction

Singlet tetrylenes are by their nature single-centre ambiphiles, and can thus act as both *σ*-donor ligands and simultaneously accept electron density at the tetryl element centre.[3] Classical Fischer carbenes demonstrate this character through forming often reactive double-bonds with a transition metal,[4] due to the high *π*-acceptor character of the vacant *p*-orbital at carbon. On the contrary, electronically saturated N-heterocyclic carbenes, stabilized by considerable N→C donation, act as strong *σ*-donors but poor electron acceptors, and hence behave as innocent spectator ligands.[5] Heavier tetrylenes, due to an increased HOMO-LUMO separation, have a lessened propensity to partake in multiple bonding;[6] nevertheless a number of multiply bonded heavier tetrylene-transition metal complexes are now known,[3(b),7] the seminal examples of which were reported by the group of Power, and were accessed through the expedient salt metathesis of halo-tetrylenes with anionic metal fragments.[8] Similar complexes have been accessed recently by the same group through the metathesis of E-E and Mo-Mo triple bonds (E = Ge, Sn, Pb), akin to alkyne metathesis.[9] In search for a ligand class which can behave both as a Lewis base (*i.e.* a *σ*-donor) and a Lewis

acid (*i.e.* an electron acceptor), we sought to further amplify the Lewis acidity of heavier tetrylene ligands through generating tetryliumylidene species, which are cationic and hence have a second vacant *p*-orbital when compared with their neutral counterparts. Given their high electrophilic character, they could thus form a novel ligand class, that is highly Lewis acidic *σ*-donor ligands.

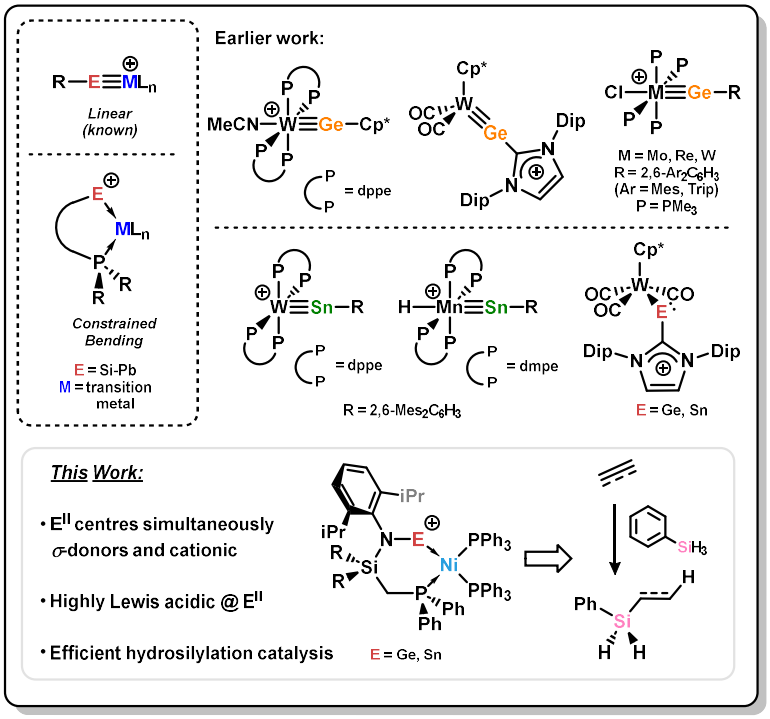

Figure 4.1 Known examples of cationic TM complexes bearing tetrylene E^{II} fragments (E = Ge, Sn), and the concept of 'constrained bending' leading to a cationic E^{II} centre.

Cationic transition metal complexes bearing two-coordinate Ge^{II} ligands, a number of which have been reported by Fillippou (Figure 4.1),[1] typically demonstrate linear L-Ge-M geometries in line with considerable M→Ge back donation, and hence a high degree of multiple bond character pertaining to triple bonds.[10] This, in turn, significantly reduces the Lewis acidity of the Ge centre. In these systems the favourable formation of a triple bond will lead to the cationic charge residing largely on the TM centre or ancillary ligand, sequestering the Lewis acidity of the Ge centre. Whilst less explored, the bonding situation is similar for Sn. In rare cases for both Ge and Sn, multiple bonding is not favoured, and instead a metallotetrylene is formed (Figure 4.1), [10c] again lacking Lewis acidity at the tetryl centre due to the presence of a lone electron pair. It is surprising that the further reactivity of the described species has not yet been forthcoming, although there is a growing interest in the development of mixed-element systems for synergistic bond activation processes.[11]

To circumvent sequestration of reactivity at the tetryl centre, we sought novel *chelating* tetryliumylidene ligands with a geometrically constrained, sub-180° L-E-M angle (Figure 4.1), reducing M→E back-bonding and lending a high degree of Lewis acidity to the E centre. This should allow for strong electrophilic reactivity at this centre, hence opening a new vista in ligand design. Herein we describe such a chelating ligand system bearing E^{II} centres which act simultaneously as *σ*-donors and strong Lewis acids. The Lewis acidic nature of the E^{II} centres has been demonstrated through the binding of nucleophilic substrates such as ammonia, as well as fluoride abstraction from $[SbF_6]^-$. These novel systems have also been employed in the catalytic hydrosilylation of alkenes and alkynes, thus introducing a new ligand class for key transition metal catalysed processes.

Results and Discussion

We recently reported the chloro-germylene Ni^0 complexes **3a** and **3b** (Scheme 4.1), which are accessible in gram-scale from phosphine-chelated chloro-germylenes, ^{PhPh}DippGeCl and ^{PhiP}DippGeCl (^{PhPh}Dipp = {[$Ph_2PCH_2Si(Ph)_2$](Dipp)N}$^-$; ^{PhiP}Dipp = {[$Ph_2PCH_2Si(^iPr)_2$](Dipp)N}$^-$; Dipp = 2,6-$^iPr_2C_6H_3$).[12] Addition of $NaBAr^F_4$ (Ar^F = 3,5-$(CF_3)_2C_6H_2$) to red-brown fluorobenzene solutions of **3a/b** led to an immediate colour change to deep purple. For both species, *in-situ* $^{31}P\{^1H\}$ NMR analysis indicated the formation of a single new compound, with a considerable increase in the $^2J_{PP}$ coupling of the two *P*-environments relative to **3** (*e.g.* for **3a**: $^2J_{PP}$ = 18.2 Hz; for **4a**: $^2J_{PP}$ = 51.5 Hz), concomitant with a shift towards coalescence of these signals.

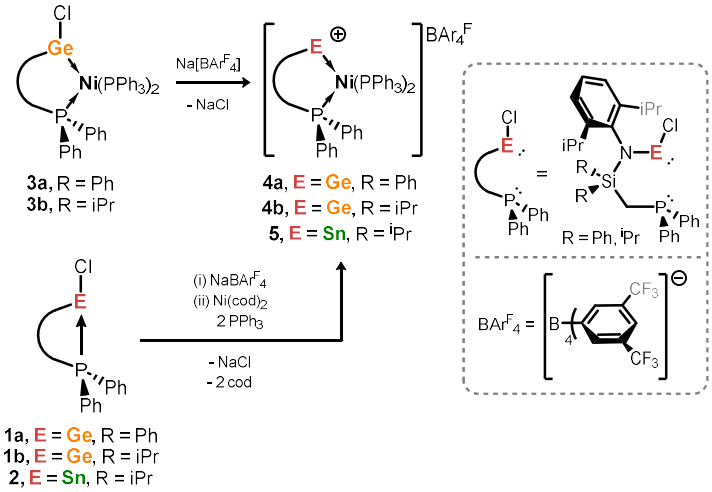

Scheme 4.1 Synthesis of cationic complexes **4** and **5** through chloride abstraction from isolated Ni^0 complexes **3**, or a 'one-pot' pot method utilising chloro-germylenes (**1**) or -stannylene (**2**).

Following work-up, deep purple-orange crystals of cationic species **4a/b** could be isolated, the ^1H and $^{31}P\{^1H\}$ NMR spectra of which match those for crude reaction mixtures. UV/vis analyses of toluene solutions of **4b** show a blue-shift of the main absorbance from 362 nm (*ε* =

9160 $L \cdot mol^{-1} \cdot cm^{-1}$) in **3b** to 346 nm ($\varepsilon$ = 9870 $L \cdot mol^{-1} \cdot cm^{-1}$) in **4b**, as well as a red shift and broadening of a second significant absorbance (486 nm, ε = 2310 $L \cdot mol^{-1} \cdot cm^{-1}$). A TD-DFT analysis suggests that the major absorptions leading to the intense colour of **4b** are centred at 455 and 435 nm, and arise from HOMO→LUMO transitions which are essentially metal-to-ligand charge transfer processes. The molecular structures of both **4a** and **4b** (Figure 4.2) reveal cationic single-centre ambiphile ligated Ni^0 complexes, containing two-coordinate Ge^{II} centres bound to Ni^0.[13] In **4b**, the Ni^0 centre pertains towards a trigonal-pyramidal geometry, the trigonal 'base' formed by the three phosphine ligands (sum of [P-Ni-P] angles = 350.43°), capped by the germyliumylidene arm. The Ni-Ge-N angle of 132.96(1)° deviates considerably from linearity due to the chelation through the phosphine arm of the ligand scaffold, leading to considerable charge localization on Ge (*vide infra*), in stark contrast to previously reported cationic tetrylidyne transition-metal complexes, which contain multiply-bonded, linear L-Ge-M interactions, and hence bear considerable charge at M.[7] Reflecting this, the Ge-Ni distance in cationic **4b** (d_{Ge-Ni} = 2.1908(9) Å) is essentially unchanged when compared to that in neutral **3b** (d_{Ge-Ni} = 2.1877(7) Å), indicating a negligible increase in Ni→Ge back-bonding in forming the cationic complex. The frontier orbitals of cationic model complex **[4']$^+$** (Figure 4.2; **[4']$^+$** = $[^{PhMe}XylGe{\cdot}Ni(PPh_3)_2]^+$; ^{PhMe}Xyl = $[(Ph_2PCH_2SiMe_2)(Xyl)N]^-$; Xyl = 2,6-$Me_2C_6H_3$) calculated using DFT (Density Functional Theory) methods suggest that both the LUMO and LUMO+1 are high *p*-character orbitals localized at Ge (Figure 4.2 (b) and (c)), whilst the MBO (Mayer Bond Order) for the Ge-Ni interaction of 1.11 is similar to that for the related neutral model chloro-germylene complex **3'** (MBO = 1.13) and further related germylene complexes described herein.[14]

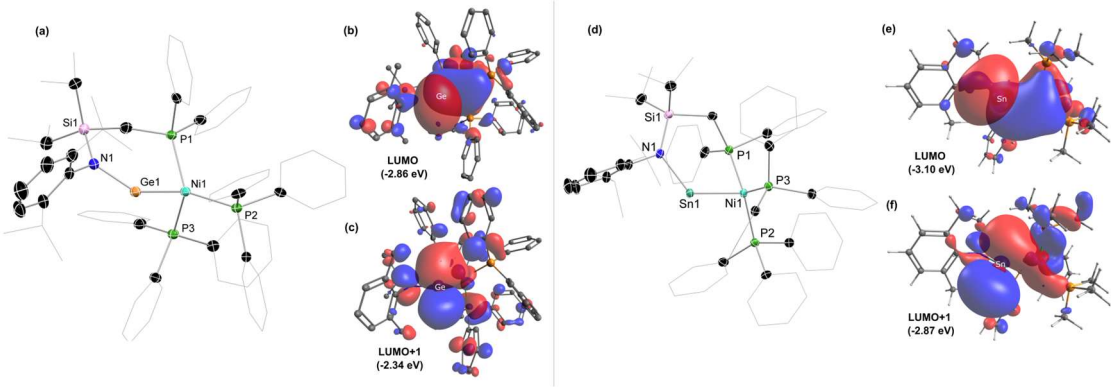

Figure 4.2 (a) The molecular structure of cationic part of **4b**, with hydrogen atoms omitted and thermal ellipsoids at 30% probability. (b) The LUMO and (c) LUMO+1 of **[2']$^+$**. (d) The molecular structure of cationic part of **5**, with hydrogen atoms omitted and thermal ellipsoids at 30% probability. (e) The LUMO and (f) the LUMO+1 of **[5'']$^+$**. Selected distances (Å) and angles (°) for **4b**: Ni1-Ge1 2.1908(9); Ge1-N1 1.851(3); Ni1-Ge1-N1 133.0(1); P1-Ni1-P2 123.42(4); P1-Ni1-P3 117.28(4); P2-Ni1-P3 109.73(4). Selected distances (Å) and angles (°) for **5**: Ni1-Sn1 2.2.4024(9); Sn1-N1 2.068(5); Ni1-Sn1-N1 124.3(1); P1-Ni1-P2 125.51(6); P1-Ni1-P3 118.42(6); P2-Ni1-P3 111.48(6).

An NBO analysis suggests that the largest contributions to the Ge-Ni interaction are Ge→Ni donation, with energies of 52.98 kcal·mol^{-1} and 95.45 kcal·mol^{-1}. Three back-donation interactions can also be found, amounting to 64.55 kcal·mol^{-1}. This reiterates the notion that the Ge-Ni bonding interactions in **4a/b** are dominated by *σ*-donation, but also indicates that the chelate effect in these complexes does not entirely prevent Ni→Ge back-donation. We also note that, unlike a number of low-coordinate cationic main group species reported previously,[15] no arene contacts between flanking ligands in **4a/b** and the Ge^{II} in these species are apparent in their solid state structures,[16] but N→Ge donation does aid in stabilizing the Ge^{II} centre in these complexes (*viz.* HOMO-21, Figure S111 in ESI).[17]

As cationic complexes **4a/b** are diamagnetic, and so formally d^{10} at Ni, they are best described as bearing a cationic one-coordinate germylene in the coordination sphere of neutral Ni^{0}, and as such represent a novel ligand binding motif when compared with any previously reported species.[7d,18] We were thus curious as to whether the related Sn^{II} complex could be accessed, given that such complexes for this element are also unknown. Sn^{II} derivatives of **3a/b** proved unstable, and could not be isolated. However, the one-pot reaction between first the chloro-stannylene **2** and $NaBAr^{F}_{4}$, with subsequent addition of $Ni(cod)_2$ and 2 equivs. PPh_3 led to deep purple reaction mixtures, similar to dissolved **4a/b**. $^{31}P\{^{1}H\}$ NMR spectroscopic analysis of crude reaction mixtures suggested remarkably clean conversion to a single product, with a shift and splitting pattern mirroring that for **4b**. Filtration, removal of volatiles, and addition of small amounts of pentane led to a large crop of dark purple crystals, an X-ray diffraction analysis of which revealed the formation of the cationic stannylene Ni^{0} complex **5** (Figure 4.2 (d)). The high yield (78 %) and expedient nature of this reaction led us to synthesise Ge^{II} complex **4b** in a similar manner, giving access to this species in 80 % yield.

Due to the larger radius of Sn, the Sn-Ni distance in **5** (d_{SnNi} = 2.4024(9) Å) is elongated relative to the Ge-Ni interaction in **4b** ($d_{Ge\text{-}Ni}$ = 2.1908(9) Å). The internal N-Sn-Ni angle of 124.3(1)° is slightly contracted compared to the Ni-Ge-N angle in **4b** most likely due to reduced *sp*-mixing in the Sn derivative, as in known more broadly for the heavier tetrylenes.[19] The Ni^{0} centre in **5**, is coordinated in a near trigonal planar fashion by its three phosphine ligands (sum of [P-Ni-P] angles = 355.41 °), and is capped by the Sn^{II} ligand centre to form a distorted trigonal-pyramidal geometry at nickel. The ^{119}Sn NMR spectrum of **5** presents a broad peak at δ = 1342 ppm, and so reveals no $^{2}J_{SnP}$ coupling information. As for **4b**, a computational NBO analysis of model complex **[5']$^{+}$** is indicative of both Sn→Ni donation (32.59 kcal·mol^{-1}) and back donation from Ni (43.75 kcal·mol^{-1}), both of these interactions being weaker than for the comparable Ge system and leading to a decreased MBO of 0.79 for this interaction. Both the LUMO and LUMO+1 represent vacant orbitals at Sn^{II} (Figure 4.2, (e) and (f)), again in keeping

with the Ge derivative, suggesting this centre too should bear a considerable degree of Lewis acidity.

Metrical and electronic parameters in **4a/b** and **5** suggested to us that the electrophilicity at the Ge^{II}/Sn^{II} centres should be high when compared with related multiply-bonded or metallotetrylene species. The first evidence for this was given by the coordination of DMAP to the Ge^{II} centre in **4b**, leading to brown-purple reaction mixtures, from which deep blue-purple X-ray quality crystals could be isolated. The molecular structure of **4b·DMAP** (Figure 4.3) confirms binding at Ge^{II}, with coordination in the N-Ge-Ni plane forming a trigonal-planar Ge centre (sum of angles = 359.45 °).

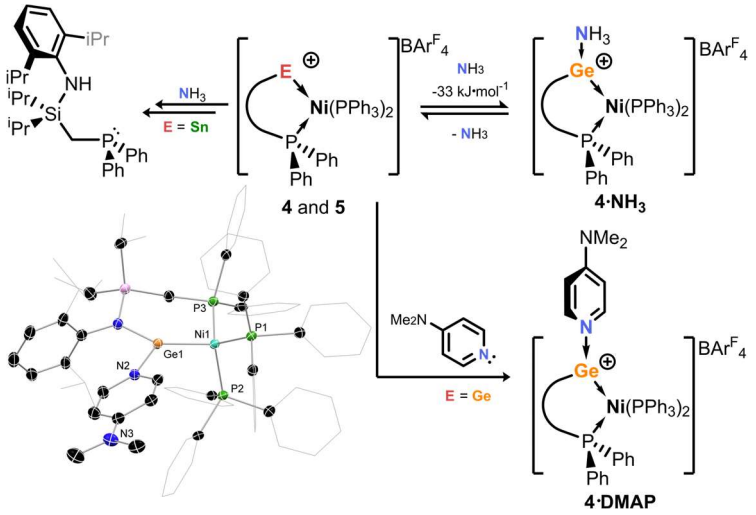

Figure 4.3 Reactivity of cationic **4** and **5** towards NH_3 and DMAP; *Below*: The molecular structure of **4a·DMAP**, with hydrogen atoms eliminated and thermal ellipsoids at 30% probability. Selected distances (Å) and angles (°) for **4a·DMAP**: Ge1-Ni1 2.228(1); Ge1-N1 1.871(3); Ge1-N2 2.114(4); P1-Ni1 2.259(1); P2-Ni1 2.217(1); P3-Ni1 2.258(2); N1-Ge1-N2 101.0(1); Ni1-Ge1-N1 133.5(1); Ni1-Ge-1-N2 124.97(9).

Relative to **4b**, only a small increase in the Ni-Ge distance is observed ($d_{Ge\text{-}Ni}$ = 2.228(1) Å). Adduct **4b·DMAP** is unstable in solution, giving complex $^{31}P\{^1H\}$ NMR spectra upon dissolution of pure crystalline material at ambient temperature. Dissolving samples at -80 °C in D_8-THF, however, allows for the observation of $^{31}P\{^1H\}$ NMR spectra which contain three signals pertaining to the three phosphine ligands, presumably separated due to 'freezing out' of ligand exchange/rotation processes. Slow warming leads to initial broadening of the signals, up to -20°C, followed by the appearance of a number of new resonances due to complex decomposition. Addition of an excess of NH_3 to solutions of **4a** led to the clean formation of a single new species as ascertained by $^{31}P\{^1H\}$ NMR spectroscopy, in the formation of orange solutions. The $^{31}P\{^1H\}$ NMR spectra of these samples show a considerably reduced $^2J_{PP}$ coupling value akin to those in chloro-germylene Ni^0 complex **3a**, *i.e.* with a three-coordinate Ge^{II} centre. Addition of between 0.5 and 3 equivalents of NH_3 leads to the gradual formation

of the same species, whilst removal of volatiles *in vacuo*, followed by redissolving the residue regenerates the starting material, **4a** (Figure 4.4(a)).

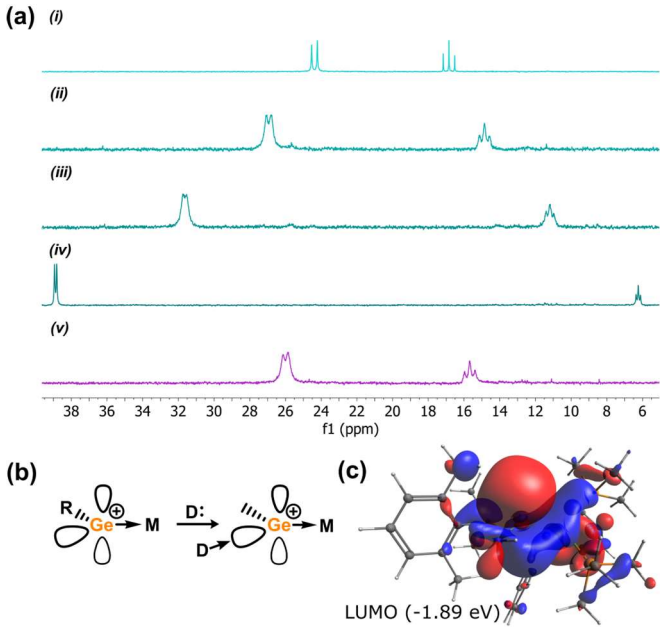

Figure 4.4 (a) $^{31}P\{^{1}H\}$ NMR spectra of *(i)* compound **4a**, *(ii)* **4a** + 0.5 equiv. NH_3, *(iii)* **4a** + 1 equiv. NH_3, *(iv)* **4a** + 3 equiv. NH_3, and *(v)* removal of all volatiles followed by redissolving in C_6H_5F (all other spectra also as C_6H_5F solutions). (b) A schematic representation of the LUMO and LUMO+1 in **4a/b**, and the formation of an in-plane donor-accpetor complex (R = anionic ligand; M = transition metal, D = Lewis basic donor); (c) the LUMO of NH_3 adduct of **[4'']$^+$**.

Resonances for solutions treated with 0.5 and 1 equivalent of NH_3 show signal broadening, which we hypothesise is due to a rapid equilibrium between **4a** and the ammonia adduct, **4a·NH$_3$**. Attempts to crystallise this adduct were unsuccessful, leading only to the isolation of **4a**.[20] Nevertheless, the above observations, alongside the favourable DFT-derived binding energy of NH_3 to the Ge^{II} centre in **[4']$^+$** (ΔG = -33 kJ·mol^{-1}), give strong evidence for a reversible ammonia binding process. We also note that the DFT-optimized geometry of **[4']$^+$·NH$_3$** shows in-plane binding, akin to that observed structurally for **4a·DMAP**, with one remaining vacant *p*-orbital at Ge^{II} (Figure 4.4(b) and (c)).[21]

To further investigate the reversibility in ammonia binding, the previously reported amido-germylene Ni^0 complex **6b** (Scheme 4.2) was reacted with the oxonium salt, $HBAr^F_4$ ($HBAr^F_4$ =$[(Et_2O)_2H][BAr^F_4]$), in order to protonate the NH_2 group in the loss of NH_3. This reaction proceeds remarkably cleanly, forming deep purple solutions with ^1H and $^{31}P\{^1H\}$ NMR spectra matching samples of **4b**. The facility of this reaction was further extended, in addition of $HBAr^F_4$ to the hydroxy-germylene Ni^0 complex **7b**, as well as to the unprecedented hydrido-germylene Ni^0 complexes **8a** and **8b**, synthesized through salt-metathesis of chloro-germylene complexes **3a/b** with Li[^{s}Bu$_3$BH] (Scheme 4.2, Figure 4.5).

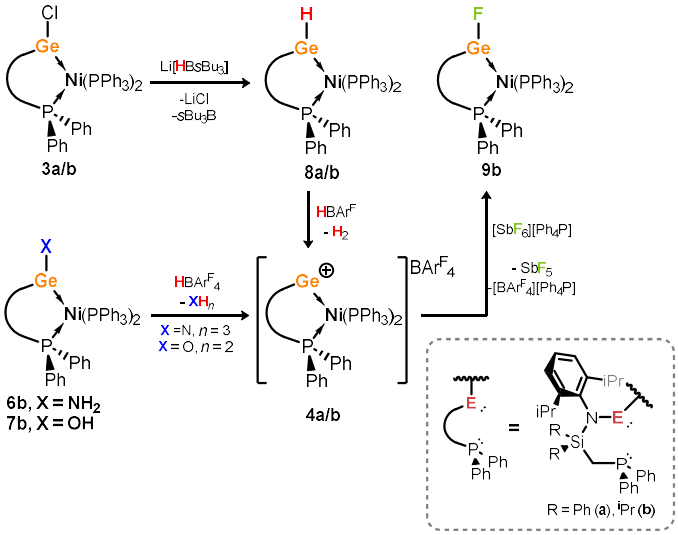

Scheme 4.2 Synthesis of hydrido-germylene complexes **8a/b**, conversion of complexes **6b**, **7b**, and **8a/b** to cationic **4a/b** in loss of NH_3, H_2O, and H_2, respectively, and fluoride abstraction from $[SbF_6]^-$ by **4a/b**.

The former presumably leads to initial formation of the adduct **4b·OH₂**, which eliminates H_2O to form the free cation **4b**. The related reaction is considerably clearer for the hydride complexes **8a** and **8b**. The ^{1}H NMR spectra for these species show considerably down-field shifted Ge-*H* resonances when compared with known Ge^{II} hydride species, indeed more so than any Ge^{II} hydride reported to date,[22] indicative of the electron deficient nature of the Ge^{II} centres in **8a** and **8b**.[23] This clear down-field shift, alongside their characteristic doublet-of-triplets splitting pattern (*e.g.* for **8b**: δ = 11.17 ppm, $^3J_{HP}$ = 37.7, 6.5 Hz) makes the disappearance of these signals quite clear. Addition of $HBAr^F_4$ to C_6D_6 solutions of **8a** and **8b** eliminates H_2, observable in the ^{1}H NMR spectra of reaction mixtures as a singlet at δ = 4.47 ppm, with concomitant disappearance of the distinct Ge-*H* resonances. As a whole, this set of experiments firstly demonstrates the reversible binding of NH_3 (and H_2O) to cations **4a** and **4b**, whilst also giving a range of synthetic routes to these novel cationic complexes which we are currently exploring in related main-group systems.

We also sought to employ chemical probes to access the Lewis acidity of **4a/b** and **5** (*e.g.* Guttmann-Beckett,[24] Childs,[25] and nitrile-binding methods).[26] In all cases, extreme signal broadening or divergent chemical reactivity was observed, a common issue with such methods in more complex chemical systems.[27] Given that the benchmark for Lewis superacidity is the FIA (FIA = Fluoride Ion Affinity) of SbF_5,[28] it so follows that F^- abstraction from the $[SbF_6]^-$ anion indicates a high degree of Lewis acidity, pertaining to Lewis superacidity. It was thus very promising to find that cation **4b** reacts with $[SbF_6][PPh_4]$ in the formation of neutral fluoro-germylene Ni^0 complex **9b**, SbF_5, and $[BAr^F_4][PPh_4]$ (Scheme 4.2).[29] The molecular structure of **9b** is isostructural to chloride derivative **3b** in the solid state (Figure 4.5), showing

a doublet in its ^{19}F NMR spectrum. The $^{31}P\{^{1}H\}$ NMR spectrum of this compound indicates that only the chelating P-arm couples with the Ge-*F* centre, presenting as a doublet of triplets ($^{2}J_{PP}$ = 16 Hz; $^{3}J_{PF}$ = 108 Hz), and a doublet for the two Ph_3P ligands. The instability of the stannylene Ni^0 complex ^{PhiP}DippSnCl·Ni(PPh_3)$_2$ negates the isolation of a fluoro-stannylene complex through reaction of **5** with [SbF_6][PPh_4], although this reaction does produce SbF_5 and [$BAr^F{}_4$][PPh_4], suggesting fluoride abstraction does indeed occur.

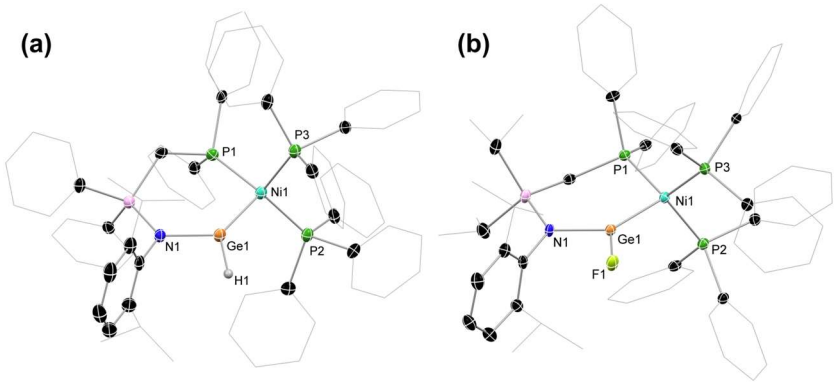

Figure 4.5 Molecular structures of (a) **8a** and (b) **9b**, with hydrogen atoms (aside from the H1 in **8a**) omitted, and thermal ellipsoids at 30% probability. Selected distances (Å) and angles (°) for **8a**: Ge1-Ni1 2.228(2); Ge1-H1 1.64(6); Ge1-N1 1.881(7); N1-Ge1-Ni1 127.7(2); P1-Ni1-Ge1 100.22(6). For **9b**: Ni1-Ge1 2.1758(8); Ge1-N1 1.852(3); Ge1-F1 1.798(2); Ni1-Ge1-N1 133.03(9); F1-Ge1-N1 97.7(1); Ni1-Ge1-F1 129.18(7); P1-Ni1-Ge1 98.33(3).

The calculated FIA and HIA (HIA = Hydride Ion Affinity) values have become a standard measure of the hard and soft Lewis acidity of a system, respectively,[28,30] whilst more recently the AA (Ammonia Affinity) and WA (Water Affinity) have been employed to take account for steric effects.[31] This set of affinities thus gives a multidimensional view of the Lewis acidity of electrophiles accounting for hard and soft Lewis acidity (*i.e.* FIA and HIA), as well as steric effects (*i.e.* AA and WA). These values were calculated for the Ge^{II} systems **[4']$^+$** and **[4'']$^+$** (**[4'']$^+$** = [^{PhMe}XylGe·Ni(PMe_3)$_2$]$^+$), and for the Sn^{II} system **[5'']$^+$**, at the ωB97XD/def2SVP (Ni, Ge, Sn: def2TZVPP) level of theory in the gas phase.[32] Reference values were also calculated for SbF_5 and BCF (BCF = $B(C_6F_5)_3$) at the same level of theory due to the experimentally observed reaction between [SbF_6]$^-$ and **4b**, and BCF being a common reference point for Lewis acidity, which were found to correlate well with literature values obtained with more intensive computational methods (Table 4.1). Values were additionally calculated for the known [Mes_3Si]$^+$ system, as an established cationic strong Lewis acid.[33] Both the FIA (636 kJ·mol^{-1}) and HIA (639 kJ·mol^{-1}) values for **[4'']$^+$** are greater than those for SbF_5 (FIA: 495 kJ·mol^{-1}; HIA: 571 kJ·mol^{-1}) and BCF (FIA: 457 kJ·mol^{-1}; HIA: 493 kJ·mol^{-1}), corroborating the experimental

observation that **4b** abstracts F^- from $[SbF_6]^-$, and further supporting the notion of a high degree of Lewis acidic character in this complex.

Table 4.1 DFT-derived ion Fluoride and Hydride ion affinities (FIA and HIA, respectively) and Ammonia and Water affinities (AA and WA, respectively).[a]

Lewis Acid (LA)	FIA	HIA	AA[b]	WA[b]
[4']$^+$	639	643	33	11
[4'']$^+$	636	639	24	17
[5'']$^+$	618	622	16	11
$B(C_6F_5)_3$	457 (448)[c]	493 (484)[d]	100 (122)[d]	39 (54)[d]
SbF_5	495 (496)[c]	571 (535)[d]	143 (163)[d]	84 (99)[d]
$[Mes_3Si]^+$	841	859	50	57

[a] at the ωB97XD/def2-SVP(Ni,Ge,Sn: def2-TZVPP) level; [b] AA and WA values are calculated as Free Energies; [c] values in parentheses are taken from ref *30c*; [d] values in parentheses are taken from ref *31*.

Similarly high FIA and HIA values are observed for the model Sn^{II} complex **[5'']$^+$** (FIA: 618 kJ·mol^{-1}; HIA: 622 kJ·mol^{-1}). The favourable AA (24 kJ·mol^{-1}) and WA (17 kJ·mol^{-1}) values for **[4'']$^+$** are in keeping with the observed binding of NH_3 to the Ge^{II} centre in **4a**. Still, comparing to the well-established cationic Lewis acid $[Mes_3Si]^+$, which has considerably higher FIA, HIA, AA and WA values (Table 4.1), it is clear that potential Lewis acidity in **4a/b** and **5** is quenched to some degree, most likely through the aforementioned N→E donation. The inclusion of more sterically demanding Ph groups at the R_3P ligands in **[4']$^+$** in fact improves the AA value (33 kJ·mol^{-1}), which we postulate is due to increased dispersion interactions. Notably, however, these AA and WA values are considerably lower than those for SbF_5, BCF, and $[Mes_3Si]^+$, and perhaps reflect the considerable steric congestion in **4b** relative to those classic Lewis acids. Still, this collection of calculated values, alongside the experimental observations of DMAP and ammonia binding, and fluoride abstraction, give strong evidence that **4b** can behave as a universal Lewis acid, aiding in defining a new ligand class in the chelating cationic single-centre ambiphiles.

To probe the tetrylene-like reactive character in **4a/b** and **5** we sought to observe oxidative chemistry at their E^{II} centres, reactivity which has been observed for low-coordinate tetrylene systems in the past.[34] Ethylene and diphenylacetylene, which may be expected to undergo [2+1] cycloaddition processes, showed no reaction. Silanes and boranes, which may undergo oxidative cleavage, also showed no reaction.[35]

Table 4.2 The hydrosilylation of alkynes catalyzed by **4b** or **5**.[a]

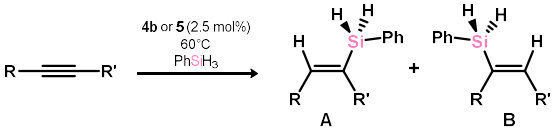

Catalyst	R, R'	Time	Conversion, %
4b	Ph, Ph	18 h	99
4b	Ph, Me	3 h	98 (1:1.3)
4b	$SiMe_3$, Me	72 h	74 (1:0)
4b	^{n}Pr, ^{n}Pr	72 h	64
5	Ph, Ph	4 h	98
5	Ph, Me	5 h	93 (1:1.4)
5	$SiMe_3$, Me	72 h	86 (1:0)
5	^{n}Pr, ^{n}Pr	77 h	77
- [c]	Ph, Me	24	0

[a] Conducted in 0.4 mL C_6D_6 in gas-tight NMR tubes, with 1.0 equiv. of alkyne; [b] Determined by relative integration of Si-*H* signals in ^{1}H NMR spectra of reaction mixtures, and based upon consumption of $PhSiH_3$ starting material; [c] Carried out in the absence of catalyst.

These observations give further evidence of the formal donor nature of the E^{II} centres in these complexes. Remarkably, however, cationic complexes **4b** and **5** proved to be active catalysts for the hydrosilylation of alkynes and alkenes. Given the importance of hydrosilylation in both an academic and industrial setting,[36] alongside the need for the development of systems utilizing benign and abundant elements,[37] this is an exciting finding. In an initial test, a mixture of 1 mol% **4b**, PhCCPh, and $PhSiH_3$ led to selective formation of *trans*-(Ph)(H)C=C(SiH_2Ph)(Ph), with 68% conversion at 60°C after 16 h. Increasing catalyst loading to 2.5 mol% led to full conversion after 18 h. Screening a number of alkynes under similar conditions (Table 4.2) demonstrates this protocol can be extended, allowing hydrosilylation of even the bulky $Me_3SiCCMe$. In all cases, the only species observable in the $^{31}P\{^1H\}$ NMR spectra was **4b**, suggesting that this is the catalyst resting state. Sn^{II} complex **5** also proved to be an active catalyst for alkyne hydrosilylation, generally showing an improved activity relative to **4b** as exemplified by the described reaction of PhCCPh being complete in 4 h, comparing to 18 h for similar conditions using **4b**. The scope of the reaction was then extended to alkenes. This was initially optimized for 1-hexene, which surprisingly seemed to proceed much more rapidly than for alkynes under similar conditions (Table 4.3). Addition of $PhSiH_3$ to 1-hexene in the presence of 2.5 mol% **4b** gave 90% consumption of $PhSiH_3$ in forming the *anti*-Markonikov 1-silylhexane after 12 h at ambient temperature, and 4 h at 60 °C.

Table 4.3 Optimisation of 1-hexene hydrosilylation using complex **4b**.[a]

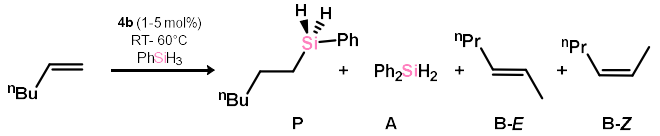

Catalyst loading (mol%)	Temp. (°C)[b]	Time (h)	Conversion (%)[c]	Ratio P:A [d]	Ratio P:B [e]
1	RT	4	75	209:1	3.8:1
1	RT	48	94	72:1	4.5:1
2.5	RT	4	80	203:1	5.9:1
2.5	RT	12	90	98:1	6.5:1
5	RT	4	76	126:1	4.2:1
5	RT	12	91	65:1	4.8:1
1	60	4	88	35:1	4.7:1
2.5	60	4	90	34:1	5.0:1
5	60	4	91	23:1	5.5:1
5	60	90	99[f]	-	- (2.7:1) [g]
- [h]	60	24	0	-	-
2.5 [i]	RT	12	17	-	-
2.5 [j]	RT	0.5	65	-	5.5:1
		12	80	-	5.5:1

[a] Conducted in 0.4 mL C_6D_6 in gas-tight NMR tubes; [b] RT defined as 22 °C; [c] Determined by relative integration of Si-*H* signals in ^{1}H NMR spectra of reaction mixtures, and based upon ratio of $PhSiH_3$ to **P**; [d] Determined by integration of Si-*H* peaks for **P** and **A** in ^{1}H NMR spectra of crude reaction mixtures; [e] Determined by integration of the Si-*H* peak for **P** and alkenyl C-*H* peaks for **B** in ^{1}H NMR spectra of crude reaction mixtures; [f] Conducted in the absence of $PhSiH_3$, showing full isomerisation to **B**; [g] Ratio in parentheses refers to the *cis*:*trans* ratio for the formed 2-hexene; [h] Carried out in the absence of catalyst; [i] $Ni(cod)_2/PPh_3$ (1:4) was employed as the catalyst; [j] Complex **3b** used as the catalyst. N.B. Catalytic activity is not hampered by the addition of 0.1 mL Hg.

As a side reaction, up to 17% of the 1-hexene substrate undergoes isomerization to a mixture of *cis*- and *trans*-2-hexene, with this process being more prominent at lower catalyst loadings. In the absence of $PhSiH_3$, full isomerization of 1-hexene to 2-hexene is achieved (5 mol%, 60 °C, 80 h), a promising observation for the future scope of this catalytic system. The undesirable catalyzed redistribution of $PhSiH_3$ to Ph_2SiH_2 (and presumably SiH_4) is also observed, exacerbated at higher temperatures and catalyst loadings. To assess the importance of the cationic single-centre ambiphile ligand in the catalytic activity of **4b**, $Ni(cod)_2/PPh_3$ (1:4 mixture) was employed as a catalyst, showing a low conversation of 17% at 2.5 mol% loading after 12 h, suggesting that the Ge^{II} centre indeed imparts activity in our system. Utilising the neutral chloro-germylene complex **3b** as a catalyst in fact led to an

extremely high initial activity, reaching 65% after 30 min at ambient temperature. This catalyst proved highly unstable, however, and had largely decomposed after this short time, as shown by ^{31}P NMR spectroscopy, with little further conversion after 12 h. These observations are somewhat surprising; whilst they indicate the benefits of the presence of the germylene/germyliumylidene species for catalytic turnover, the increased activity and instability in the neutral system certainly warrants further investigation in future studies.

Table 4.4 Hydrosilylation of terminal alkenes with complexes **4b** and **5**.[a]

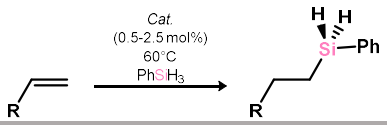

Catalyst	Catalyst loading, mol%	R	Time	Conversion (%)[b]
4b	2.5	H	1 h	99 [c]
4b	2.5	H	24 h	97 [d]
4b	0.5	$CyCH_2$	4 h	69
4b	1	$CyCH_2$	1 h	92
4b	2.5	$CyCH_2$	20 min	99
4b	0.5	$SiMe_3$	4h	62
4b	1	$SiMe_3$	1 h	85
4b	2.5	$SiMe_3$	20 min	90
4b	2.5	*p*-$CF_3C_6H_4CH_2$	17 h	75
4b	2.5	$PhCH_2$	72 h	65
4b	2.5	^{t}Bu	72 h	44
4b	2.5 [e]	^{n}Pr	24 h	16
5	2.5	^{n}Pr	48 h	71
5	2.5	H	1 h	99
5	2.5	$CyCH_2$	48 h	59
5	2.5	$SiMe_3$	20 h	86
5	2.5	*p*-$CF_3C_6H_4CH_2$	24 h	79
5	2.5	$PhCH_2$	72 h	43
5	2.5	^{t}Bu	72 h	20

[a] Conducted in 0.4 mL C_6D_6 in gas-tight NMR tubes, with 1.3 equiv. of alkene;[b] Determined by relative integration of Si-*H* signals in ^{1}H NMR spectra of reaction mixtures, and based upon consumption of $PhSiH_3$ starting material; [c] The only product formed under these conditions is $PhEt_2SiH$; [d] The reaction was carried out at RT; [e] The reaction was carried out in the presence of 250 mol% PPh_3.

Extending this protocol to a range of alkenes showed selective conversion to the *anti*-Markovnikov 1-silylalkanes (Table 4.4). In the majority of cases mono-insertion products are favoured (*i.e.* yielding $PhRSiH_2$); for ethylene, double-insertion leading to the formation of $PhEt_2SiH$ is prominent when the reaction is conducted at 60 °C, and is complete after just 1 h. Conducting the same reaction at room temperature leads to selective formation of the mono-insertion product, $PhEtSiH_2$. The related Sn^{II} system, **5**, was also screened as a catalyst in the hydrosilylation of alkenes (Table 4.4). In contrast to the increased reaction rates for the Sn^{II} system in alkyne hydrosilylation, alkene hydrosilylation is considerably slower, whilst the competing isomerization reaction for 1-hexene is seemingly more pronounced. The hydrosilylation of ethylene with **5** is selective for the formation of the mono-insertion product at 60 °C, in contrast to the Ge^{II} system. In light of these differences, we are presently developing further ligand systems, to conduct an in-depth mechanistic study to determine any involvement of the developed cationic ligands in the catalytic regime. Finally, whilst the activities reported here are rather modest when compared with reported Ni hydrosilylation catalysts,[15] we note that this is the first demonstration of the utility of our novel ligand class in catalysis, opening the door for future developments.

Conclusions

We have developed a chelating ligand system based upon reactive low-coordinate cationic E^{II} centres (E = Ge, Sn), which, due to the electronic ground state of singlet tetrylenes, act as *σ*-donor ligands whilst remaining highly electrophilic. This unique ligand system has been employed in the formation of Ni^0 complexes **4a/b** and **5**, in which the binding of Lewis bases, namely 4-*N,N*-dimethylamino pyridine and ammonia, can readily occur at the E^{II} centre. Formation of the described cationic complexes is also possible through protonation of amido-, hydroxy-, and hydrido-germylene Ni^0 complexes **6-8**, in the loss of NH_3, H_2O, and H_2, respectively. Remarkably, the E^{II} centres in these Ni^0 complexes even pertain towards Lewis superacidity, capable of abstracting the fluoride ion from $[SbF_6]^-$ in the formation of fluoride-germylene complex **9**. The capacity for these complexes to affect catalysis has also been demonstrated; the hydrosilylation of alkenes and alkynes, as well as the isomerization of 1-hexene to 2-hexene, is reported. As a whole, this collection of results thus demonstrates the utility of single-centred ambiphilicity in readily accessible low-valent main group ligands, the further reactivity of which we are presently fervently pursuing, towards defining multi-centred synergistic bond activation processes and catalysis.

Supporting Information

General experimental considerations

All experiments and manipulations were carried out under dry oxygen free argon atmosphere using standard Schlenk techniques or in an MBraun inert atmosphere glovebox containing an atmosphere of high purity argon. THF and diethyl ether were dried by distillation over a sodium/benzophenone mixture and stored over activated 4Å mol sieves. C_6D_6 was dried, degassed and stored over a potassium mirror. All other solvents were dried over activated 4Å mol sieves and vigorously degassed prior to use. ^{PhiP}DippK, ^{PhPh}DippGeCl (**1a**), ^{PhiP}DippGeCl (**1b**), ^{PhPh}DippGe(Cl)Ni(PPh$_3$)$_2$ (**3a**), ^{PhiP}Dipp(Cl)Ni(PPh$_3$)$_2$ (**3b**), ^{PhiP}DippGe(NH$_2$)Ni(PPh$_3$)$_2$ (**6**), ^{PhiP}DippGe(OH)Ni(PPh$_3$)$_2$ (**7**), (^{PhPh}Dipp = {[Ph$_2$PCH$_2$Si(Ph)$_2$](Dipp)N}$^-$; ^{PhiP}Dipp = {[Ph$_2$PCH$_2$Si(^{i}Pr)$_2$](Dipp)N}$^-$; Dipp = 2,6-^{i}Pr$_2$C$_6$H$_3$),[12] Na[BAr$^F_4$] (Ar^F = 3,5-CF$_3$-C$_6$H$_3$),[38] H[BAr$^F_4$]·2Et$_2$O,[39] SnMe$_3$F,[40] and Ni(cod)$_2$ [41] were synthesized according to known literature procedures. All other reagents were used as received. For the ethylene experiments, ethylene 2.5 was used. NMR spectra were recorded on a Bruker AV 400 Spectrometer. The ^{1}H and ^{13}C{^{1}H} NMR spectra were referenced to the residual solvent signals as internal standards. ^{29}Si{^{1}H} NMR spectra were externally calibrated with SiMe$_4$. ^{31}P{^{1}H} NMR spectra were externally calibrated with H$_3$PO$_4$. ^{11}B{^{1}H} NMR spectra were externally calibrated with BF$_3$·Et$_2$O. ^{19}F NMR spectra were externally calibrated with CCl$_3$F. ^{119}Sn NMR spectra were externally calibrated with Me$_4$Sn. Liquid Injection Field Desorption Ionization Mass Spectrometry (LIFDI-MS) was measured directly from an inert atmosphere glovebox with a Thermo Fisher Scientific Exactive Plus Orbitrap equipped with an ion source from Linden CMS.[42] Infrared spectra were measured with the Alpha FT-IR from Bruker containing a platinum diamond ATR device. The compounds were measured as solids under inert conditions in the glovebox. Absorption spectra (UV/vis) were recorded on an Agilent Cary 60 UV/vis spectrophotometer. For the ammonia experiments, water free ammonia 5.0 was used. Elemental analyses (C, H, N) were performed with a combustion analyzer (elementar vario EL, Bruker).

Experimental procedures

[^{iPPh}DippSnCl], 2. SnCl$_2$ (0.9 g, 4.7 mmol) was dissolved in THF (10 mL) and cooled to -78 °C. At this temperature, a solution of ^{PhiP}DippK (2.5 g, 4.7 mmol) in THF (20 mL) was slowly added, the reaction mixture stirred at low temperature for 1h, and subsequently allowed to warm to room temperature, leading to an orange solution. After stirring for a further 2 h, all volatiles are removed *in vacuo*, the pale orange residue extracted in toluene (20 mL), and filtered. Removal of all volatiles and washing the pale yellow residue with hexane (2 x 10 mL) affords a

free-flowing powder suitable for the further use (2.4 g, 3.7 mmol, 79%). X-ray quality crystals of **2** were grown from a benzene solution at RT.

^{1}H NMR (C_6D_6, 400 MHz, 298 K): δ = = 0.60 (d, 3H, $^{3}J_{HH}$ = 7.4 Hz, Si-Pr^{i}-C*H*$_3$),0.74 (hept, 1 H, $^{3}J_{HH}$ = 7.6 Hz, Si-Pr^{i}-C*H*), 0.86 (d, 6H, $^{3}J_{HH}$ = 6.8 Hz, Dipp-Pr^{i}-C*H*$_3$), 1.04 (d, 3H, $^{3}J_{HH}$ = 7.5 Hz, Si-Pr^{i}-C*H*$_3$), 1.19 (m, 4H, Si-Pr^{i}-C*H*$_3$, Si-Pr^{i}-C*H*), 1.42 (d, 3H, $^{3}J_{HH}$ = 6.8 Hz, Dipp-Pr^{i}-C*H*$_3$), 1.44 (d, 3H, $^{3}J_{HH}$ = 6.8 Hz, Dipp-Pr^{i}-C*H*$_3$), 1.60 (m, 3H, Si-Pr^{i}-C*H*$_3$), 1.98 (m, 1H, Ph_2P-C*H*$_2$), 2.23 (m, 1H, Ph_2P-C*H*$_2$), 2.82 (hept, 1H, $^{3}J_{HH}$ = 6.7 Hz, Dipp-Pr^{i}-C*H*), 4.29 (hept, 1H, $^{3}J_{HH}$ = 6.6 Hz, Dipp-Pr^{i}-C*H*), 7.03 (m, 9 H, Ar-C*H*), 7.34 (m, 2H, Ar-C*H*), 7.66 (m, 2H, Ar-C*H*).

^{13}C{^{1}H} NMR (C_6D_6, 101 MHz, 298 K): δ = = 6.4 (d, Ph_2P-*C*H$_2$), 16.0 (d, Si-Pr^{i}-*C*H), 16.6 (d, Si-Pr^{i}-*C*H), 18.1 (Si-Pr^{i}-*C*H$_3$), 20.1, 20.2 and 21.0 (Si-Pr^{i}-*C*H$_3$), 23.0 and 23.1 (Dipp-Pr^{i}-*C*H$_3$), 27.4 and 27.7 (Dipp-Pr^{i}-*C*H), 28.8 and 29.1 (Dipp-Pr^{i}-*C*H$_3$), 123.9, 124.0, 124.2, 129.0, 129.1, 129.2, 129.3, 130.7, 131.5, 132.5, 132.6, 133.5, 133.6, 143.9, 144.0, 146.3, 148.5 (C_{Ar}).

^{31}P{^{1}H} NMR (C_6D_6, 162 MHz, 298 K): δ = 1.3 (s, *P*Ph_2), Sn-satellites (d, $^{1}J_{P,Sn}$ = 723 Hz) and (d, $^{1}J_{P,Sn}$ = 726 Hz).

^{29}Si{^{1}H} NMR (C_6D_6, 99 MHz, 298 K): δ = 11.4 (d, $^{2}J_{SiP}$ = 7.2 Hz, *Si*Pr$^{i}_2$).
^{119}Sn NMR (C_6D_6, 149 MHz, 298 K): δ = -72.3 (d, $^{1}J_{Sn,P}$ = 1482 Hz, N-*Sn*-P).

MS/LIFDI-HRMS found (calcd.) m/z: 608.1894 (608.1924) for $[M\text{-}Cl]^+$.

Anal. calcd. for $C_{31}H_{43}ClNPSiSn$: C, 57.91%; H, 6.74%; N, 2.18%; found: C, 53.9%; H, 6.8%; N, 2.3%. Repeated element analysis gave variable but consistently low values for C, possibly due to Si-carbide formation.

[^{PhPh}DippGeNi^{0}(PPh$_3$)$_2$][BAr$^{F}_4$], 4a.

Method (a): A solid mixture of **3a** (1.00 g, 0.80 mmol) and Na[BAr$^{F}_4$] (0.71 g, 0.80 mmol) were dissolved in fluorobenzene (20 mL) at ambient temperature, and stirred for 5 min. The deep purple solution was filtered and all volatiles were removed *in vacuo*, yielding a dark purple amorphous powder of pure **4a** (1.35 g, 0.65 mmol, 81%), which was found to be analytically pure. Addition of *n*-pentane (~5 mL) to the solid led to a dark purple oil below a pale red-purple solution. Crystals which were suitable for X-Ray diffraction analysis were obtained after storing the flask overnight at RT.

^{1}H NMR (C_6D_6, 400 MHz, 298 K): δ = 0.41 (d, 6H, $^{3}J_{HH}$ = 6.6 Hz, Dipp-Pr^{i}-C*H*$_3$), 0.67 (d, 6H, $^{3}J_{HH}$ = 6.6 Hz, Dipp-Pr^{i}-C*H*$_3$), 2.56 (d, 2H, $^{2}J_{HP}$ = 12.9 Hz, C*H*$_2$-PPh_2), 3.27 (hept, 2H,

$^{3}J_{HH}$ = 6.7 Hz, Dipp-Pr^{i}-C*H*), 6.66 (m, 8H, Ar-C*H*), 6.94 (m, 45H, Ar-C*H*), 7.68 (s, 4H, Ar_{BArF}-H_{para}), 8.46 (s, 8H, Ar_{BArF}-H_{ortho}).

$^{13}C\{^{1}H\}$ NMR (C_6D_6, 101 MHz, 298 K): δ = 15.4 (Ph_2P-CH_2), 22.1 (Dipp-Pr^{i}-CH_3), 28.1 (Dipp-Pr^{i}-CH_3), 29.1 (Dipp-Pr^{i}-*C*H), 118.1, 121.3, 124.0, 125.0, 126.7, 128.7, 128.8, 128.9, 128.9, 128.9, 129.0, 129.4, 129.8, 130.1, 130.5, 130.9, 131.0, 131.8, 132.5, 132.6, 133.3, 133.8, 133.8, 133.9, 135.4, 135.5, 146.8, 162.1, 162.6, 163.1, 163.6 (Ar-*C*).

$^{31}P\{^{1}H\}$ NMR (C_6D_6, 162 MHz, 298 K): δ = 16.9 (t, $^{2}J_{PP}$ = 51.5 Hz, Ni-*P*Ph_2), 24.4 (d, $^{2}J_{PP}$ = 51.6 Hz, Ni-*P*Ph_3).

$^{29}Si\{^{1}H\}$ NMR (C_6D_6, 99 MHz, 298 K): δ = -10.4 (d, $^{1}J_{SiC}$ = 6.0 Hz, CH_2-*Si*Ph_2).

$^{11}B\{^{1}H\}$ NMR (C_6D_6, 128 MHz, 298 K): δ = -5.8 (s, B_{BArF}).

^{19}F NMR (C_6D_6, 128 MHz, 298 K): δ = -62.1 (s, Ar_{BArF}-CF_3).

λ_{max}, nm (*ε*, $Lmol^{-1}cm^{-1}$): 342 (7790).

MS/LIFDI-HRMS found (calcd.) m/z: 950.1994 (950.2061) for $[M\text{-}PPh_3]^+$.

Anal. calcd. for $C_{105}H_{81}BF_{24}GeNNiP_3Si$: C, 60.75%; H, 3.93%; N, 0.67%; found: C, 56.89%; H, 3.48%; N, 0.75%. Repeated element analysis gave variable but consistently low values for C, possibly due to Si-carbide/Ni-carbide formation.

In-situ generation of 4a. Compound **8a** (15 mg, 0.012 mmol) and $H[BAr^F_4]\cdot 2Et_2O$ (13 mg, 0.012 mmol) were added to an an NMR tube, and fluorobenzene (0.4 mL) and C_6D_6 (0.1 mL) were added. Gas evolution was observed and the colour of the solution changed from dark red to dark purple. The sole presence of **4a** was confirmed by $^{31}P\{^{1}H\}$ NMR spectroscopy, and the formation of H_2 was confirmed by ^{1}H NMR spectroscopy.

[^{PhiP}DippGeNi^{0}(PPh_3)$_2$][BAr^F_4], 4b.

Method (a): The procedure for the synthesis of **4a** was followed using **3b** (400 mg, 0.34 mmol) and $Na[BAr^F_4]$ (300 mg, 0.34 mmol). Compound **4b** was isolated as a dark purple amorphous powder (582 mg, 0.29 mmol, 85%). Crystals were obtained by the addition of pentane (5 mL) to this solid, leading to a dark purple oil below a pale red solution. Crystals which were suitable for X-Ray diffraction analysis were obtained after storing the flask overnight at RT.

Method (b): A solid mixture of **1b** (500 mg, 0.84 mmol), $Na[BAr^F_4]$ (742 mg, 0.84 mmol), $Ni(cod)_2$ (231 mg, 0.84 mmol) and PPh_3 (439 mg, 1.68 mmol) were dissolved in toluene

(20 mL) at ambient temperature and stirred for 5 min. The deep purple solution was filtered and all volatiles were removed *in vacuo*. Pentane (5 mL) was added to the flask leading to a dark purple oil below a pale red-pruple solution. The flask was stored at RT overnight yielding dark purple-red crystals of **4b** (1.35 g, 0.67 mmol, 80%).

^{1}H NMR (C_6D_6, 400 MHz, 298 K): δ = 0.41 (s, 2H, Si-Pr^{i}-C*H*), 0.52 (d, 6H, $^{3}J_{HH}$ = 7.1 Hz, Si-Pr^{i}-C*H*$_3$), 0.57 (d, 6H, $^{3}J_{HH}$ = 7.1 Hz, Si-Pr^{i}-C*H*$_3$), 0.65 (d, 6H, $^{3}J_{HH}$ = 6.6 Hz, Dipp-Pr^{i}-C*H*$_3$), 1.11 (d, 6H, $^{3}J_{HH}$ = 6.6 Hz, Dipp-Pr^{i}-C*H*$_3$), 1.55 (d, 2H, $^{2}J_{HP}$ = 11.4 Hz, C*H*$_2$-PPh$_2$), 3.03 (hept, 2H, $^{3}J_{HH}$ = 7.4 Hz, Dipp-Pr^{i}-C*H*), 6.80 (m, 12H, Ar-C*H*), 6.94 (m, 27H, Ar-C*H*), 7.08 (m, 27H, Ar-C*H*), 7.69 (s, 4H, Ar$_{BArF}$-*H*$_{para}$), 8.46 (s, 8H, Ar$_{BArF}$-*H*$_{ortho}$).

^{13}C{^{1}H} NMR (C_6D_6, 101 MHz, 298 K): δ = 16.7 (Ph$_2$P-*C*H$_2$), 18.1 (Si-Pr^{i}-*C*H), 20.1 and 20.6 (Si-Pr^{i}-*C*H$_3$), 21.3 (Dipp-Pr^{i}-*C*H$_3$), 28.5 (Dipp-Pr^{i}-*C*H), 29.6 (Dipp-Pr^{i}-*C*H$_3$), 118.1, 121.3, 124.0, 124.5, 126.7, 128.7, 128.8, 128.9, 129.4, 129.8, 129.8, 130.1, 130.1, 130.7, 131.6, 133.1, 133.2, 133.5, 133.7, 133.8, 134.2, 135.5, 147.0, 162.1, 162.6, 163.1, 163.6 (Ar-*C*).

^{31}P{^{1}H} NMR (C_6D_6, 162 MHz, 298 K): δ = 22.1 (m).

^{29}Si{^{1}H} NMR (C_6D_6, 99 MHz, 298 K): δ = 4.7 (s, CH$_2$-*Si*Pr$^{i}_2$).

^{11}B{^{1}H} NMR (C_6D_6, 128 MHz, 298 K): δ = -5.8 (s, *B*$_{BArF}$).

^{19}F NMR (C_6D_6, 128 MHz, 298 K): δ = -62.1 (s, Ar$_{BArF}$-C*F*$_3$).

λ$_{max}$, nm (*ε*, Lmol^{-1}cm^{-1}): 486 (2310), 346 (9870).

MS/LIFDI-HRMS found (calcd.) m/z: 882.2296 (882.2374) for [M-PPh$_3$]$^{+}$.

Anal. calcd. for $C_{99}H_{85}BF_{24}GeNNiP_3Si$: C, 59.22%; H, 4.27%; N, 0.70%; found: C, 58.52%; H, 4.55%; N, 0.76%.

N.B. Repeated element analysis gave variable but consistently low values for C, possibly due to Si-carbide/Ni-carbide formation.[43]

In-situ generation of 4b. Compound **8b** (15 mg, 0.012 mmol) and H[BAr$^{F}_4$]·2Et$_2$O (13 mg, 0.012 mmol) were added to an NMR tube, and fluorobenzene (0.4 mL) and C_6D_6 (0.1 mL) were added. Rapid gas evolution was observed, concomitant with a colour change from dark red to dark purple. The sole presence of **4b** was confirmed by ^{31}P{^{1}H} NMR spectroscopy, whilst H_2 could be observed in the ^{1}H NMR spectrum.

Similar reactions were conducted for **6b** (15 mg, 0.012 mmol) and **7b** (15 mg, 0.012 mmol). In these cases H_2O and NH_3 could not be observed in the ^{1}H NMR spectra, but **4b** was the sole product as confirmed by $^{31}P\{^1H\}$ NMR spectroscopy.

N.B. It is interesting to observe here that this complex in in fact quite stable in the presence of the eliminated water, although we hypothesise that this may be due to adsorption of the moisture to the thoroughly dried walls of the NMR tube.

[^{PhiP}DippSnNi^0(PPh$_3$)$_2$][BAr$^F_4$], 5. A solid mixture of **2** (500 mg, 0.78 mmol) and Na[BAr$^F_4$] (690 mg, 0.78 mmol) was dissolved in toluene (20mL) at ambient temperature and stirred for 5 min. After removing all volatiles in vacuo Ni(COD)$_2$ (214 mg, 0.78 mmol) and PPh_3 (408 mg, 1.56 mmol) were added to the residue and the mixture was dissolved in toluene (20 mL) at ambient temperature and stirred for 5 min. The deep purple solution was filtered, and all volatiles were removed in *vacuo*. Pentane (5 mL) was added to the flask leading to a dark purple oil below a pale orange solution. The flask was stored at RT overnight yielding dark purple-red crystals of **5** (1.25 g, 0.61 mmol, 78%), which were suitable for X-Ray diffraction analysis.

^{1}H NMR (C_6D_6, 400 MHz, 298 K): δ = 0.41 (s, 2H, Si-Pr^i-C*H*), 0.60 (m, 18H, Si-Pr^i-C*H*$_3$), 1.13 (d, 6H, $^3J_{HH}$ = 6.5 Hz, Dipp-Pr^i-C*H*$_3$), 1.72 (d, 2H, $^2J_{HP}$ = 11.6 Hz, C*H*$_2$-PPh$_2$), 3.09 (s, Dipp-Pr^i-C*H*), 6.82 (t, 11H, $^3J_{HH}$ = 7.3 Hz, Ar-C*H*), 6.99 (m, 32H, Ar-C*H*), 7.69 (s, 4H, Ar$_{BArF}$-*H*$_{para}$), 8.46 (s, 8H, Ar$_{BArF}$-*H*$_{ortho}$).

^{13}C{^{1}H} NMR (C_6D_6, 101 MHz, 298 K): δ = 17.5 (Ph$_2$P-*C*H$_2$), 19.0 (Si-Pr^i-*C*H), 20.3, 20.9, 21.7 (Si-Pr^i-*C*H$_3$, Dipp-Pri-*C*H$_3$), 27.8 (Dipp-Pr^i-*C*H), 29.6 (Dipp-Pr^i-*C*H$_3$), 118.2, 121.3, 124.0, 124.5, 126.7, 128.7, 128.8, 129.0, 129.0, 129.4, 129.8, 130.2, 130.8, 131.6, 133.3, 133.7, 133.7, 135.5, 137.7, 146.4, 162.1, 162.6, 163.1, 163.6 (Ar-*C*).

^{31}P{^{1}H} NMR (C_6D_6, 162 MHz, 298 K): δ = 17.9 (m).

^{29}Si{^{1}H} NMR (C_6D_6, 99 MHz, 298 K): δ = 2.8 (s, CH$_2$-*Si*Pr$^i_2$).

^{11}B{^{1}H} NMR (C_6D_6, 128 MHz, 298 K): δ = -5.8 (s, *B*$_{BArF}$).

^{19}F NMR (C_6D_6, 128 MHz, 298 K): δ = -62.0 (s, Ar$_{BArF}$-C*F*$_3$).

^{119}Sn NMR (C_6D_6, 149 MHz, 298K): δ = 1342.0 (s, N-*Sn*-Ni).

λ$_{max}$, nm (*ε*, Lmol^{-1}cm^{-1}): 447 (4450), 386 (10650).

MS/LIFDI-HRMS found (calcd.) m/z: 928.2099 (928.2189) for [M-PPh$_3$]+.

Anal. calcd. for $C_{99}H_{85}BF_{24}SnNNiP_3Si$: C, 57.89%; H, 4.17%; N, 0.68%; found: C, 56.67%; H, 4.20%; N, 0.77%.

N.B. Repeated element analysis gave variable but consistently low values for C, possibly due to Si-carbide/Ni-carbide formation.

[^{PhPh}DippGe(DMAP)Ni^{0}(PPh$_3$)$_2$][BAr$^{F}_4$], 4a·DMAP. Compound **4a** (300 mg, 0.15 mmol) and DMAP (18 mg, 0.15 mmol) were dissolved in fluorobenzene (10 mL), leading to a dark brown-purple solution. All volatiles were removed *in vacuo* and pentane (2 mL) was added to the oily residue, leading to a dark oil beneath a near colourless solution. The flask was stored at RT overnight yielding dark blue-purple crystals of **4a·DMAP** (285 mg, 0.11 mmol, 71%) which were suitable for X-Ray diffraction analysis.

^{31}P{^{1}H} NMR (C_6D_6, 162 MHz, 233 K): δ = 5.8 (t, $^{2}J_{PP}$ = 15.5 Hz, Ni-*P*Ph$_2$), 36.9 and 46.8 (s, Ni-*P*Ph$_3$).

MS/LIFDI-HRMS found (calcd.) m/z: 882.2297 (882.2374) for [M-PPh$_3$-DMAP]$^+$.

Anal. calcd. for $C_{106}H_{95}BF_{24}GeN_3NiP_3Si$: C, 59.77%; H, 4.50%; N, 1.97%; found: C, 55.42%; H, 4.04%; N, 1.98%.

N.B. Dissolution of crystals of **4a·DMAP** led to rapid decomposition at ambient temperature, and ^{1}H NMR spectra collected at low temperature were too broadened, presumably due to hindered rotation or rapid exchange processes, for meaningful data to be extracted.

N.B. Repeated element analyses gave variable but consistently low values for C, possibly due to Ni-carbide formation, which was previously reported for Ni^{0} complexes.

^{PhPh}DippGeHNi^{0}(PPh$_3$)$_2$, 8a. 3a (985 mg, 0.79 mmol) was dissolved in toluene (20 mL) and cooled to -78°C. A solution of DIBAL (1M in THF, 1.97 mL, 1.97 mmol) was then slowly added, and the mixture was allowed to warm to RT, over which time a colour change from dark red to dark brown was observed. The reaction mixture was filtered, and all volatiles were removed *in vacuo*. The residue was extracted in pentane (15 mL), filtered, and stored at RT overnight to obtain dark red crystals. The supernatant solution was removed by filtration, the resulting crystalline solid washed with pentane (2 x 5 mL), and dried *in vacuo* to yield **8a** (487 mg, 0.40 mmol, 51%) as a dark brown crystalline powder. Crystals which were suitable for X-Ray diffraction analysis were obtained from a concentrated ether solution at RT. We note that single crystals of **8a** are brown-blue dichroic when observed under a microscope.

^{1}H NMR(C_6D_6, 400 MHz, 298 K): δ = 0.56 (d, 6H, $^{3}J_{HH}$ = 6.7 Hz, Dipp-Pr^{i}-C*H$_3$*), 0.93 (m, 6H, Dipp-Pr^{i}-C*H$_3$*), 3.02 (d, 2H, C*H$_2$*-PPh$_2$), 3.87 (hept, 2H, $^{3}J_{HH}$ = 6.6 Hz, Dipp-Pr^{i}-C*H*), 6.66 (t,

4 H, Ar-C*H*), 6.84 (q, 3H, Ar-C*H*), 6.98 (m, 29H, Ar-C*H*), 7.37 (d, 2H, $^{3}J_{HH}$ = 7.0 Hz, Ar-C*H*), 7.49 (s, 10H, Ar-C*H*), 11.23 (dt, 1H, $^{3}J_{HP}$ = 37.9, 6.8, Ni-Ge-*H*) .

^{13}C{^{1}H} NMR (C_6D_6, 101 MHz, 298 K): δ = 19.8 (Ph_2P-*C*H_2), 22.7 (Dipp-Pr^{i}-*C*H_3), 26.5 (Dipp-Pr^{i}-*C*H_3), 29.0 (Dipp-Pr^{i}-*C*H), 123.8, 124.9, 127.1, 127.6, 127.7, 128.9, 132.2, 134.2, 134.3, 135.8, 236.1, 149.4, 139.7, 144.5, 149.3 (Ar-*C*).

^{31}P{^{1}H} NMR (C_6D_6, 162 MHz, 298 K): δ = 8.3 (t, $^{2}J_{PP}$ = 15.4 Hz, Ni-*P*Ph_2), 43.3 (d, $^{2}J_{PP}$ = 15.1 Hz, Ni-*P*Ph_3).

^{29}Si{^{1}H} NMR (C_6D_6, 79 MHz, 298 K): δ = - 13.8 (d, $^{1}J_{SiC}$ = 2.0 Hz, *Si*Ph_2).

MS/LIFDI-HRMS found (calcd.) m/z: 951.2156 (951.2139) for $[M\text{-}PPh_3]^+$.

IR, *v*/cm^{-1} (ATR): 1819 (s, m, Ge-H).

Anal. calcd. for $C_{73}H_{70}GeNNiP_3Si$: C, 72.24%; H, 5.81%; N, 1.15%; found: C, 67.39%; H, 5.58%; N, 1.25%. N.B. Repeated element analysis gave variable but consistently low values for C, possibly due to Si-carbide/Ni-carbide formation.

^{PhiP}DippGeHNi^{0}(PPh_3)$_2$, 8b.

Method (a): The reaction was carried out as for **8a**, but using **3b** (200 mg, 0.17 mmol), and DIBAL (1M in THF, 0.42 mL, 0.42 mmol) The crude reaction mixture was filtered, all volatiles removed *in vacuo*, the residue redissolved in pentane (20 mL) and concentrated to 10 mL. The solution was stored at 4°C for four days yielding dark red-blue crystals of **8b** (70 mg, 0.06 mmol, 36%) which were suitable for X-Ray diffraction analysis.

Method (b): 3b (200 mg, 0.17 mmol) was dissolved in toluene (10 mL), and cooled to -78 °C. A solution of Li[HB^{s}Bu$_3$] (1M in THF, 0.43 mL, 0.43 mmol) was slowly added, and the reaction mixture allowed to warm to ambient temperature overnight. All volatiles were subsequently removed from the reaction mixture, the residue extracted in Et_2O (20 mL), and filtered. Concentration to ~7 mL, followed by storage a 4 °C for several days led to the formation of a crop dark red-blue crystals, which were ascertained to be analytically pure (90 mg, 46%).

^{1}H NMR (C_6D_6, 400 MHz, 298 K): δ = 0.71 (d, 2H, $^{3}J_{HH}$ = 7.2 Hz, Si-Pr^{i}-C*H*$_3$), 0.88 (d, 6H, $^{3}J_{HH}$ = 7.3 Hz, Si-Pr^{i}-C*H*$_3$), 0.98 (d, 6H, $^{3}J_{HH}$ = 6.3 Hz, Dipp-Pr^{i}-C*H*$_3$), 1.32 (hept, 2H, $^{3}J_{HH}$ = 7.2 Hz, Si-Pr^{i}-C*H*), 1.43 (d, 6H, $^{3}J_{HH}$ = 6.6 Hz, Dipp-Pr^{i}-C*H*$_3$), 2.32 (d, 2H, $^{2}J_{HP}$ = 8.7 Hz, C*H*$_2$-PPh_2), 3.99 (hept, 2H, $^{3}J_{HH}$ = 6.7 Hz, Dipp-Pr^{i}-C*H*), 6.87 (m, 4H, Ar-C*H*), 6.96 (m, 23H, Ar-C*H*), 7.26 (m, 4H, Ar-C*H*), 7.41 (m, 12H, Ar-C*H*), 11.17 (dt, 1H, $^{3}J_{HP}$ = 37.7, 6.5, Ni-Ge-*H*).

$^{13}C\{^1H\}$ NMR (C_6D_6, 101 MHz, 298 K): δ = 14.9 (Si-Pr^i-*C*H), 18.4 and 18.7 (Si-Pr^i-*C*H_3), 19.1 (Ph_2P-*C*H_2), 23.3 and 26.7 (Dipp-Pr^i-*C*H_3), 28.4 (Dipp-Pr^i-*C*H), 123.9, 124.8, 127.7, 127.7, 127.7, 133.2, 133.3, 134.1, 134.2, 134.3, 139.7, 139.8, 139.9, 140.1, 140.1, 144.3, 145.0, 145.1, 150.1 (Ar-*C*).

$^{31}P\{^1H\}$ NMR (C_6D_6, 162 MHz, 298 K): δ = 9.9 (t, $^2J_{PP}$ = 15.7 Hz, Ni-*P*Ph_2), 42.6 (d, $^2J_{PP}$ = 15.7 Hz, Ni-*P*Ph_3).

$^{29}Si\{^1H\}$ NMR (C_6D_6, 99 MHz, 298 K): δ = 7.1 (s, CH_2-*Si*Pr$^i_2$).

MS/LIFDI-HRMS found (calcd.) m/z: 883.2426 (883.2452) for $[M\text{-}PPh_3]^+$.

IR, *v*/cm^{-1} (ATR): 1809 (s, m, Ge-H).

Anal. calcd. for $C_{67}H_{74}GeNNiP_3Si$: C, 70.24%; H, 6.51%; N, 1.22%; found: C, 63.44%; H, 6.82%; N, 1.12%. N.B. Repeated element analysis gave variable but consistently low values for C, possibly due to Si-carbide/Ni-carbide formation.

^{PhiP}Ge(F)Ni^0(PPh$_3$)$_2$, 9b. To a solid mixture of **3b** (300 mg, 0.25 mmol) and $SnMe_3F$ (70 mg, 0.38 mmol) was added THF (30 mL), and the suspension stirred for 24 h at ambient temperature leading to a dark orange solution over a white solid. All volatiles were subsequently removed from the reaction mixture *in vacuo*, and the residue extracted in Et_2O (20 mL) and filtered. Concentration to ~10 mL and storage of the solution at RT led to the formation of dark orange crystals of 9b (187 mg, 0.16 mmol, 63%) which were suitable for X-Ray diffraction analysis.

^1H NMR (C_6D_6, 400 MHz, 298 K): δ = 0.65 (d, H, $^3J_{HH}$ = 7.3 Hz, Si-Pr^i-C*H*$_3$), 0.84 (d, 6H, $^3J_{HH}$ = 7.5 Hz, Si-Pr^i-C*H*$_3$), 1.18 (d, 6H, $^3J_{HH}$ = 6.7 Hz, Dipp-Pr^i-C*H*$_3$), 1.30 (hept, 2H, $^3J_{HH}$ = 7.4 Hz , Si-Pr^i-C*H*), 1.43 (d, 6H, $^3J_{HH}$ = 6.7 Hz, Dipp-Pr^i-C*H*$_3$), 2.28 (d, 2H, $^2J_{HP}$ = 9.0 Hz, C*H*$_2$-PPh_2), 3.94 (hept, 2H, $^3J_{HH}$ = 5.6 Hz, Dipp-Pr^i-C*H*), 6.85 (t, 4H, Ar-C*H*), 6.97 (m, 21H, Ar-C*H*), 7.19 (m, 6H, Ar-C*H*), 7.43 (m, 12H, Ar-C*H*).

$^{13}C\{^1H\}$ NMR (C_6D_6, 101 MHz, 298 K): δ = 14.4 and 14.4 (Si-Pr^i-*C*H), 18.3 and 18.5 (Si-Pr^i-*C*H_3), 18.7 (Ph_2P-*C*H_2), 23.6 and 26.7 (Dipp-Pr^i-*C*H_3), 28.9 (Dipp-Pr^i-*C*H), 123.8, 125.1, 128.5, 133.2, 133.3, 134.3, 134.5, 139.3, 139.3, 139.4, 139.5, 139.6, 139.7, 140.9, 141.0, 144.2, 144.4, 145.4 (Ar-*C*).

$^{31}P\{^1H\}$ NMR (C_6D_6, 162 MHz, 298 K): δ = 11.4 (dt, $^3J_{PF}$ = 108.3 Hz, $^2J_{PP}$ = 15.7 Hz, Ni-*P*Ph_2), 40.7 (d, $^2J_{PP}$ = 15.7 Hz, Ni-*P*Ph_3).

^{29}Si{^{1}H} NMR (C_6D_6, 99 MHz, 298 K): δ = 6.4 (s, CH_2-*Si*Pr^i_2).

^{19}F NMR (C_6D_6, 128 MHz, 298 K): δ = -37.8 (d, $^3J_{FP}$ = 108.4 Hz, Ge-*F*).

MS/LIFDI-HRMS found (calcd.) m/z: 901.2317 (901.2385) for $[M\text{-}PPh_3]^+$.

Reactions of 4a with Ammonia: Compound **4a** (50 mg, 0.024 mmol) was dissolved in 0.4 mL PhF and 0.1 mL C_6D_6 in an air-tight NMR tube. A dried Schlenk was purged with ammonia using a needle-adapter directly from the cylinder, and a specific volume (0.55 mL, 0.012mmol) was added *via* syringe to the NMR tube, the NMR tube quickly closed and shaken. $^{31}P\{^1H\}$ NMR spectra were collected within 10 min of the addition. This process was repeated to attain samples with roughly 0.5, 1.0, 3.0 and 6.0 equiv. of ammonia. During this process, the colour of the solution gradually changed from dark purple, first to dark brown and then to orange. To show reversibility all volatiles were removed *in vacuo* and the residue was redissolved in 0.4 mL PhF and 0.1 mL C_6D_6. The colour of the solution clearly reverted to dark purple, and $^{31}P\{^1H\}$ NMR spectra showed almost complete regeneration of **4a**. The described sequence of experiments was carried out in triplicate. The spectrum of amido-germylene complex **5a** is included to show that this species is not directly formed.

Catalytic experiments

General Method for Catalytic Hydrosilylation

4b or **5** (1.0, 2.5 or 5.0 mol%) was dissolved in C_6D_6 in a gas tight NMR tube (0.4 mL), and substrate (0.39 mmol) and phenylsilane (0.30 mmol) subsequently added *via* micro-pipette. The resulting solution was heated at 60 ºC. The reactions were monitored via ^{1}H NMR spectroscopy with their progress evidenced by the consumption of the PhSi*H*$_3$ resonances alongside the emergence of the respective PhSi*H*$_2$ resonances in reaction products. The yield was determined by comparing integrals of the PhSi*H*$_2$ resonances of the product to the integrals of the PhSi*H*$_3$ and Ph_2Si*H*$_2$ resonances.

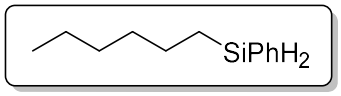

(*n*-hexyl)phenylsilane

The catalysis was done via the general method. The yield was determined to be 90% (**4b**, 4h) and 71%(**5**, 48h). The ^{1}H NMR spectroscopic data in C_6D_6 matched those found in the literature.[44]

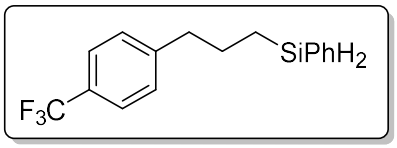

(3-(4-(Trifluoromethyl)phenyl)propyl)phenylsilane

The catalysis was done via the general method. The yield was determined to be 75% (**4b**, 17h) and 79%(**5**, 24h).

^{1}H NMR (C_6D_6, 400 MHz, 298 K): δ = 0.69 (m, 2H, Si-CH_2-CH_2), 1.50 (m, 2H, Si-CH_2-CH_2), 2.29 (t, 2H, $^{3}J_{HH}$ = 7.6 Hz, CH_2-CH_2-Ph-CF_3), 4.42 (t, 2H, $^{3}J_{HH}$ = 3.6 Hz, SiPhH_2), 6.75 (d, $^{3}J_{HH}$ = 8.0 Hz, *H*-C_{PhCF3}), 7.15 (m, 2H, *H*-C_{SiPh}) 7.31 (d, $^{3}J_{HH}$ = 8.0 Hz, *H*-C_{PhCF3}), 7.44 (m, 2H, *H*-C_{SiPh}). ^{13}C{^{1}H} NMR (C_6D_6, 101 MHz, 298 K): δ = 9.9, 26.9, 28.8 (C_{Alkyl}), 125.4 (q, $^{1}J_{CF}$ = 3.8 Hz, Ph-CF_3), 126.3, 128.4, 130.1, 132.3, 135.5 (C_{Aryl}). ^{29}Si{^{1}H} NMR (C_6D_6, 99 MHz, 298 K): δ = -31.2 (s, *Si*PhH_2). ^{19}F NMR (C_6D_6, 128 MHz, 298 K): δ = -62.0 (s, Ph-CF_3).

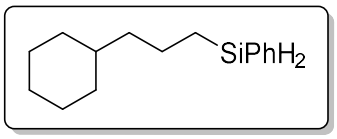

(3-Cyclohexylpropyl)phenylsilane

The catalysis was done via the general method. The yield of **3** was determined to be 99% (**4b**, 20min) and 59%(**5**, 48h). The ^{1}H NMR spectroscopic data in $CDCl_3$ matched those found in the literature.[45]

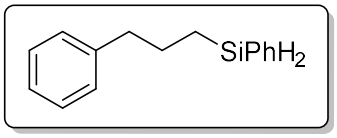

(3-Phenylpropyl)phenylsilane

The catalysis was done via the general method. The yield of **4** was determined to be 65% (**4b**, 72h) and 43%(**5**, 72h). The ^{1}H NMR spectroscopic data in C_6D_6 matched those found in the literature.[44]

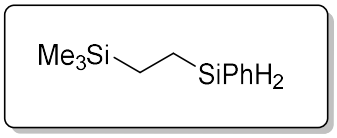

(1-Trimethylsilylethyl)phenylsilane

The catalysis was done via the general method. The yield of **5** was determined to be 90% (**4b**, 20min) and 86%(**5**, 20h). The ^{1}H NMR spectroscopic data in C_6D_6 matched those found in the literature.[46]

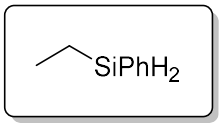

Ethylphenylsilane

(a) **4b** (2.5%) was dissolved in C_6D_6 in a NMR tube (0.4 mL) following the addition of phenylsilane (0.20 mmol). The NMR tube was charged with ethylene and shaken for 30s. The resulting solution was kept RT. The yield was determined to be 97% after 24h.

(b) **5** (2.5%) was dissolved in C_6D_6 in a NMR tube (0.4 mL) following the addition of phenylsilane (0.10 mmol). The NMR tube was charged with ethylene and shaken for 30s. The resulting solution was heated at 60 ºC. The yield of was determined to be 99% after 1h.

The ^{1}H NMR spectroscopic data in C_6D_6 matched those found in the literature.[47]

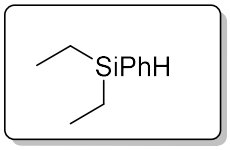

Diethylphenylsilane

4b (2.5%) was dissolved in C_6D_6 in a NMR tube (0.4 mL) following the addition of phenylsilane (0.10 mmol). The NMR tube was charged with ethylene and shaken for 30s. The resulting solution was heated at 60 ºC. The yield was determined to be 99% after 2h. The ^{1}H NMR spectroscopic data in $CDCl_3$ matched those found in the literature.[48]

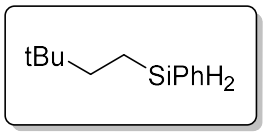

(3,3-Dimethylbutyl)phenylsilan

The catalysis was done via the general method. The yield was determined to be 44% (**4b**, 72h) and 29%(**5**, 72h). The ^{1}H NMR spectroscopic data in C_6D_6 matched those found in the literature.[44]

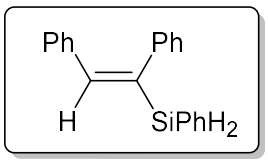

(E)-(1,2-diphenylvinyl)(phenyl)silane

The catalysis was done via the general method. The yield was determined to be 99% (**4b**, 18h) and 98%(**5**, 4h). The ^{1}H NMR spectroscopic data in C_6D_6 matched those found in the literature.[44]

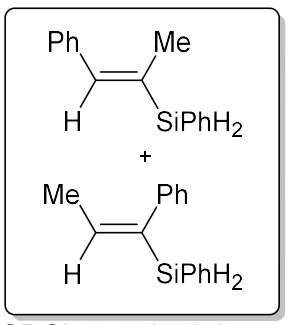

(*E*)-phenyl(1-phenylprop-1-en-2-yl)silane (A)

(*E*)-phenyl(1-phenylprop-1-en-1-yl)silane (B)

The catalysis was done via the general method. The yield of the two isomers (**A** and **B**) were determined to be 98% (**4b**, 3h, 0.77:1 (**A**:**B**)) and 93%(**5**, 5h, 0.70:1 (**A**:**B**)). The ^{1}H NMR spectroscopic data in $CDCl_3$ matched those found in the literature.[49]

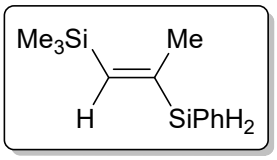

(*E*)-1-(Trimethylsilyl)-2-(phenylsilyl)-1-propene

The catalysis was done via the general method. The yield was determined to be 74% (**4b**, 72h) and 86%(**5**, 72h). The ^{1}H NMR spectroscopic data in $CDCl_3$ matched those found in the literature.[50]

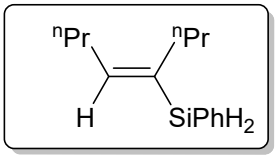

(E)-oct-4-en-4-yl(phenyl)silane

The catalysis was done via the general method. The yield was determined to be 64% (**4b**, 72h) and 77%(**5**, 72h). The ^{1}H NMR spectroscopic data in $CDCl_3$ matched those found in the literature.[51]

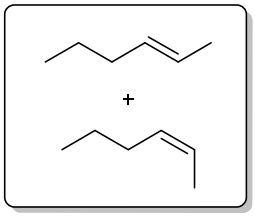

2-hexene

4b (5.0%) was dissolved in C_6D_6 in an NMR tube (0.4 mL) and the resulting solution was heated at 60 ºC. The yield of **13** was determined to be 99% after 80h.[52]

Catalytic Hydrosilylation in the presence of Mercury

4b (2.5 mol%) was dissolved in 1.0 mL C_6D_6 in a Schlenk flask following the addition of 50 µL Mercury. The mixture was stirred for 5 min following the addition of 1-hexene (1.38 mmol) and phenylsilane (0.60 mmol). The resulting solution was stirred for 18h at RT. ^{1}H NMR spectroscopy confirmed catalytic hydrosilylation, with a yield of 95% 1-($PhSiH_2$)-hexane.

Catalytic Hydrosilylation with PPh_3

4b (2.5 mol%) and PPh_3 (250 mol%) were dissolved in in C_6D_6 (0.4 mL) in a gas tight NMR tube, and 1-hexene (0.39 mmol) and phenylsilane (0.30 mmol) added. The resulting solution was kept at RT for 24h. The reaction was monitored via ^{1}H NMR spectroscopy showing only a conversion of 16% after this time.

X-ray crystallographic details

Single crystals of **2**, **4a**, **4b**, **4a·DMAP**, **5**, **8a**, **8b**, and **9b** suitable for X-ray structural analysis were mounted in perfluoroalkyl ether oil on a nylon loop and positioned in a 150 K cold N_2 gas stream. Data collection was performed with a STOE StadiVari diffractometer (MoKα radiation) equipped with a DECTRIS PILATUS 300K detector. Structures were solved by Direct Methods (SHELXS-97)[53] and refined by full-matrix least-squares calculations against F^2 (SHELXL-2018).[54] The positions of the hydrogen atoms were calculated and refined using a riding model, aside from hydride ligands in **8a** and **8b**. All non-hydrogen atoms were treated with anisotropic displacement parameters. Crystal data, details of data collections, and refinements for all structures can be found in their CIF files, which are available free of charge via www.ccdc.cam.ac.uk/data_request/cif, and are summarized in Table 4.5 and 5.6. In compound **4a** the electron density of highly disordered co-crystallized solvent molecules was removed using the PLATON SQUEEZE function.[55]

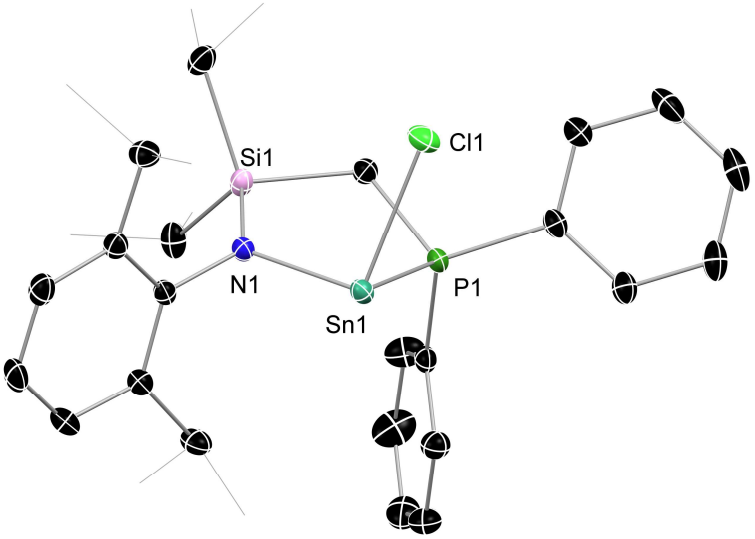

Figure 4.6 Molecular structure of **2**, with thermal ellipsoids at 30% probability. Selected bond distances (Å) and angles (°) for **3**: N1-Sn1 2.122(2); P1-Sn1 2.657(1); Cl1-Sn1 2.487(1); N1-Sn1-P1 82.37(5); Cl1-Sn1-N1 99.30(5); Cl1-Sn1-P1 84.82(2).

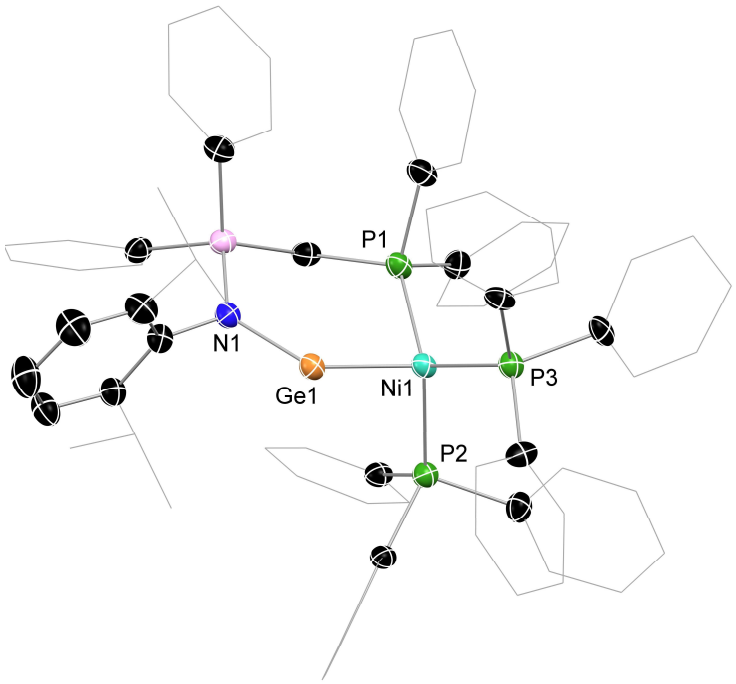

Figure 4.7 Molecular structure of the cationic part of **4a**, with thermal ellipsoids at 30% probability. Selected bond distances (Å) and angles (°) for **4a**: Ni1-Ge1 2.202(1); Ge1-N1 1.847(4); P1-Ni1 2.208(1); P2-Ni1 2.275(1) P3-Ni1 2.296(1); Ni1-Ge1-N1 130.6(1); Ge1-Ni1-P1 91.94(4); Ge1-Ni1-P2 101.59(4); Ge1-Ni1-P3 110.22(4); P1-Ni1-P2 115.56(5); P1-Ni1-P3 122.10(5); P2-Ni1-P3 111.24(4).

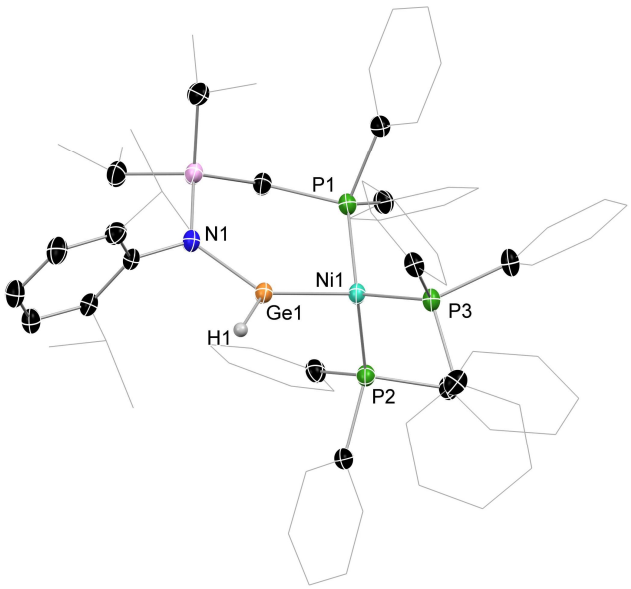

Figure 4.8 Molecular structure of **8b**, with thermal ellipsoids at 30% probability. Selected bond distances (Å) and angles (°) for **8b**: Ge1-Ni1 2.209(1); Ge1-H1 1.425(5); Ge1-N1 1.876(4); Ni1-P1 2.211(1); Ni1-P2 2.197(1); Ni1-P3 2.206(1), N1-Ge1-Ni1 129.2(1); P1-Ni1-Ge1 100.15(4); P1-Ni1-P2 107.86(5); P1-Ni1-P3 119.84(5); P2-Ni1-P3 110.33(5).

Table 4.5 Crystallographic details for **2**, **4a**, **4b**, and **5**.

	2	**4a**	**4b·(C_6H_6)(C_5H_{12})**	**5·(C_6H_6)(C_5H_{12})**
empirical form.	$C_{31}H_{43}ClNPSiSn$	$C_{105}H_{81}BF_{24}GeNNiP_3Si$	$C_{110}H_{103}BF_{24}GeNNiP_3Si$	$C_{110}H_{103}BF_{24}NNiP_3SiSn$
formula wt	642.86	2075.81	2158.04	2204.14
crystal syst.	triclinic	triclinic	monoclinic	monoclinic
space group	*P-1*	*P-1*	*P2₁/c*	*P2₁/c*
a (Å)	11.080(2)	17.740(4)	13.470(3)	13.390(3)
b (Å)	17.460(4)	18.760(4)	28.510(6)	28.590(6)
c (Å)	18.340(4)	20.840(4)	27.730(6)	27.710(6)
α (deg.)	65.00(3)	85.30(3)	90	90
β (δεγ)	88.50(3)	67.70(3)	83.70(3)	91.40(3)
γ (deg.)	86.10(3)	72.50(3)	90	90
vol ($Å^3$)	3208.1(13)	6116(3)	10646(4)	10605(4)
Z	4	2	4	4
ρ(calc) ($g.cm^{-3}$)	1.331	1.127	1.346	1.381
μ (mm^{-1})	0.986	0.524	0.604	0.559
F(000)	1328	2116	4440	4512
T (K)	150(2)	150(2)	150(2)	150(2)
reflns collect.	46712	63494	146868	149058
unique reflns	12596	23947	23172	20822
R_{int}	0.0212	0.0608	0.0711	0.0555
R1 [$I>2\sigma(I)$]	0.0235	0.0649	0.0661	0.0531
*w*R2 (all data)	0.0615	0.1814	0.2053	0.1576
CCDC No.	2114015	2099955	2099956	2114016

Table 4.6 Crystallographic details for **4a·DMAP**, **7a**, **7b**, and **8**.

	[4a·DMAP]·(C_5H_{12})$_{0.5}$	**8a·(Et_2O)**	**8b·(C_5H_{12})$_2$**	**9b·(Et_2O)**
empirical form.	$C_{108.5}H_{98}BF_{24}GeN_3NiP_3Si$	$C_{77}H_{80}GeNNiOP_3Si$	$C_{77}H_{98}GeNNiP_3Si$	$C_{71}H_{83}FGeNNiOP_3Si$
formula wt	2163.00	1287.72	1289.86	1237.68
crystal syst.	triclinic	monoclinic	monoclinic	monoclinic
space group	*P-1*	*P2$_1$/c*	*C2/c*	*P2$_1$/c*
a (Å)	14.600(3)	17.730(4)	42.110(8)	17.230(3)
b (Å)	17.200(3)	19.100(4)	20.050(4)	19.820(4)
c (Å)	23.451(5)	20.690(4)	19.320(4)	19.350(4)
α (deg.)	98.55(3)	90	90	90
β (δεγ)	107.93(3)	109.40(3)	109.30(3)	104.40(3)
γ (deg.)	96.60(3)	90	90	90
vol (Å^3)	5459(2)	6609(3)	15395(6)	6400(2)
Z	2	4	8	4
ρ(calc) (g.cm^{-3})	1.316	1.294	1.113	1.284
μ (mm^{-1})	0.590	0.876	0.751	0.904
F(000)	2220	2704	5488	2608
T (K)	150(2)	150(2)	150(2)	150(2)
reflns collect.	110172	88464	126458	45192
unique reflns	25047	12982	17652	12557
R_{int}	0.0897	0.2014	0.0946	0.0805
R1 [$I>2\sigma(I)$]	0.0624	0.0725	0.0596	0.0532
*w*R2 (all data)	0.1801	0.2090	0.2106	0.1095
CCDC No.	2099957	2099958	2099959	2099960

Computational methods and details

Computational experiments were performed using the Gaussian 16 program.[56] Geometry optimization was carried out at the ωB97XD level with the def2-TZVPP basis set for Ni and Ge, and the def2-SVP basis set for all other atoms.[57] Stationary points were confirmed as true minima by vibrational frequency analysis (no negative eigenvalues). Bond indices (Wiberg Bond Index, Mayer Bond Order) and NPA charges were determined using the NBO 6.0 program implemented in Gaussian 09, using optimized geometries from above.[58] Dative interactions were determined through analysis of the NBO output, and visualized in ChemCraft through combination of the associated MOs.

Table 4.7 The DFT derived E-Ni bond distances, and NPA derived Natural Charges (Ge, Sn, Ni), MBO, and WBI values. The Schematic represents the reduced structures used in calculations throughout.

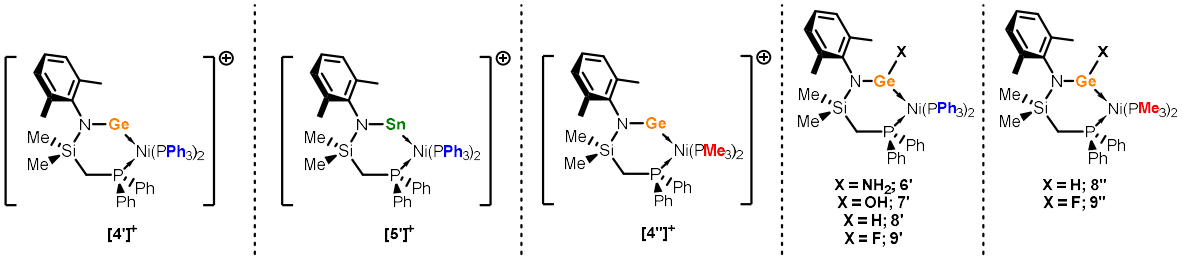

Compound	d(Ge/Sn-Ni), Å	NPA charge		MBO(Ge-Ni)/WBI(Ge-Ni)
		Ge/Sn	Ni	
[4']$^+$	2.183	+0.86	-0.02	1.11/0.58
[5']$^+$	2.404	+1.15	-0.07	0.77/0.46
6'	2.213	+1.05	-0.06	1.07/0.43
7'	2.204	+1.10	-0.06	1.06/0.44
8'	2.205	+0.61	-0.02	1.19/0.50
9'	2.198	+1.12	-0.06	1.15/0.46

*NBO visualization of Ge-Ni donor-acceptor bonds in **[4']$^+$**:*

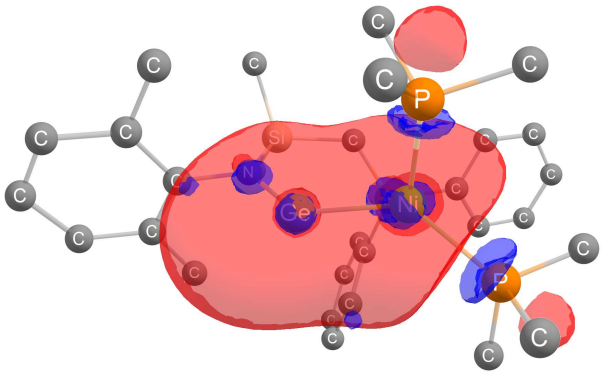

Figure 4.9 Ge→Ni (MO77 to MO176, 52.98 kcalmol^{-1}).

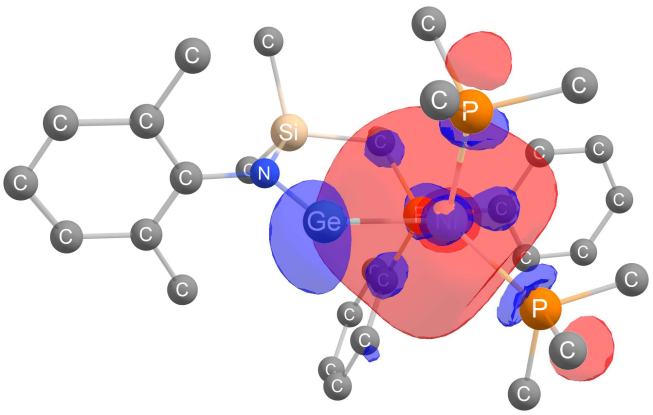

Figure 4.10 Ge→Ni (MO105 to MO176, 95.45 kcalmol^{-1}).

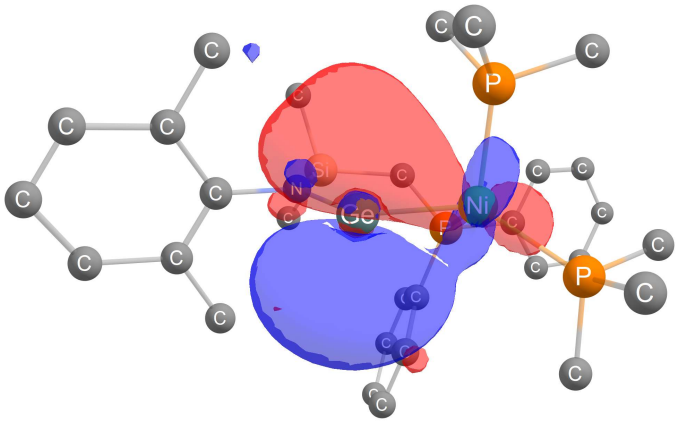

Figure 4.11 Ni→Ge (MO82 to MO174, 12.23 kcalmol^{-1}).

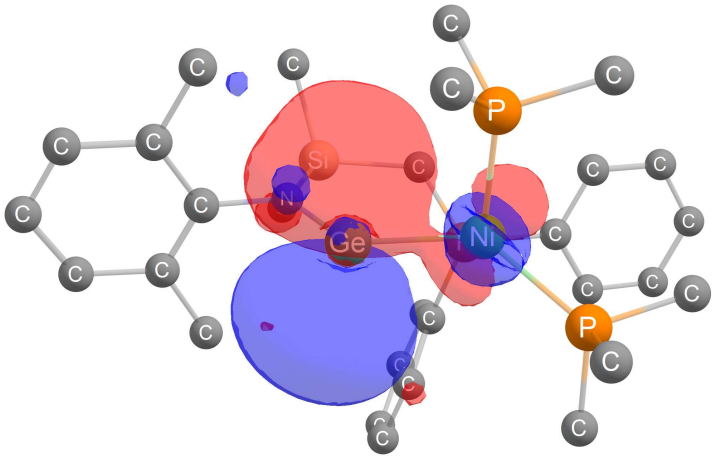

Figure 4.12 Ni→Ge (MO81 to MO174, 12.23 kcalmol^{-1}).

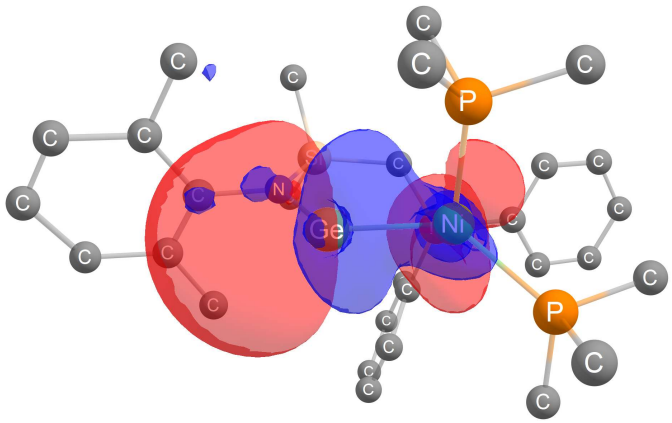

Figure 4.13. Ni→Ge (MO81 to MO197, 44.29 kcalmol^{-1}).

*NBO visualization of Sn-Ni donor-acceptor bonds in **[5']⁺**:*

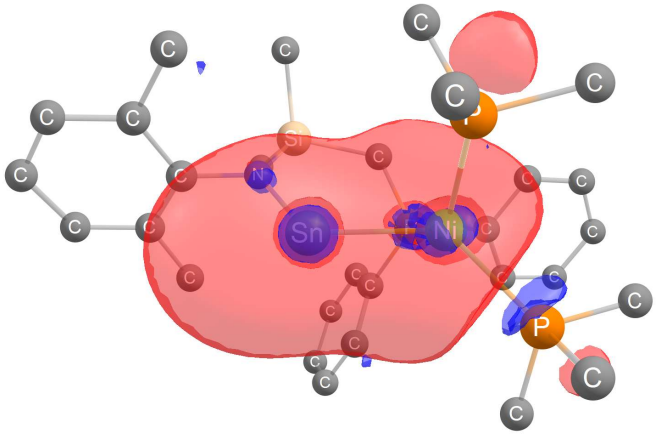

Figure 4.14 Sn→Ni (MO73 to MO172, 32.59 kcalmol^{-1}).

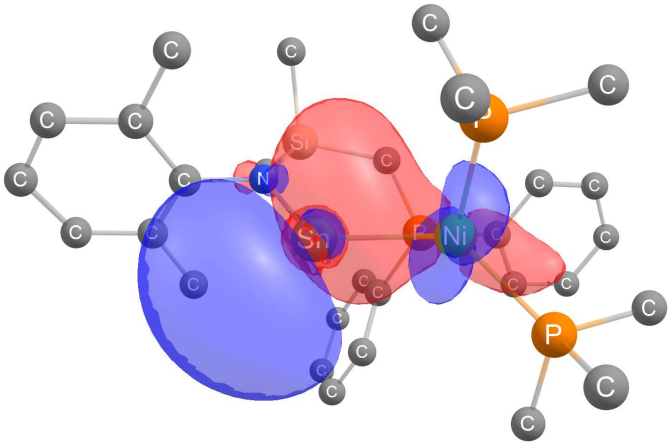

Figure 4.15 Ni→Sn (MO78 to MO169, 43.75 kcalmol^{-1}).

Selected frontier orbitals for the optimized structures of ***[2']⁺, 5'****, and* ***6'*** *are given below, pertaining to vacant orbitals at Ge, or bonding interactions between the Ge and Ni centres:*

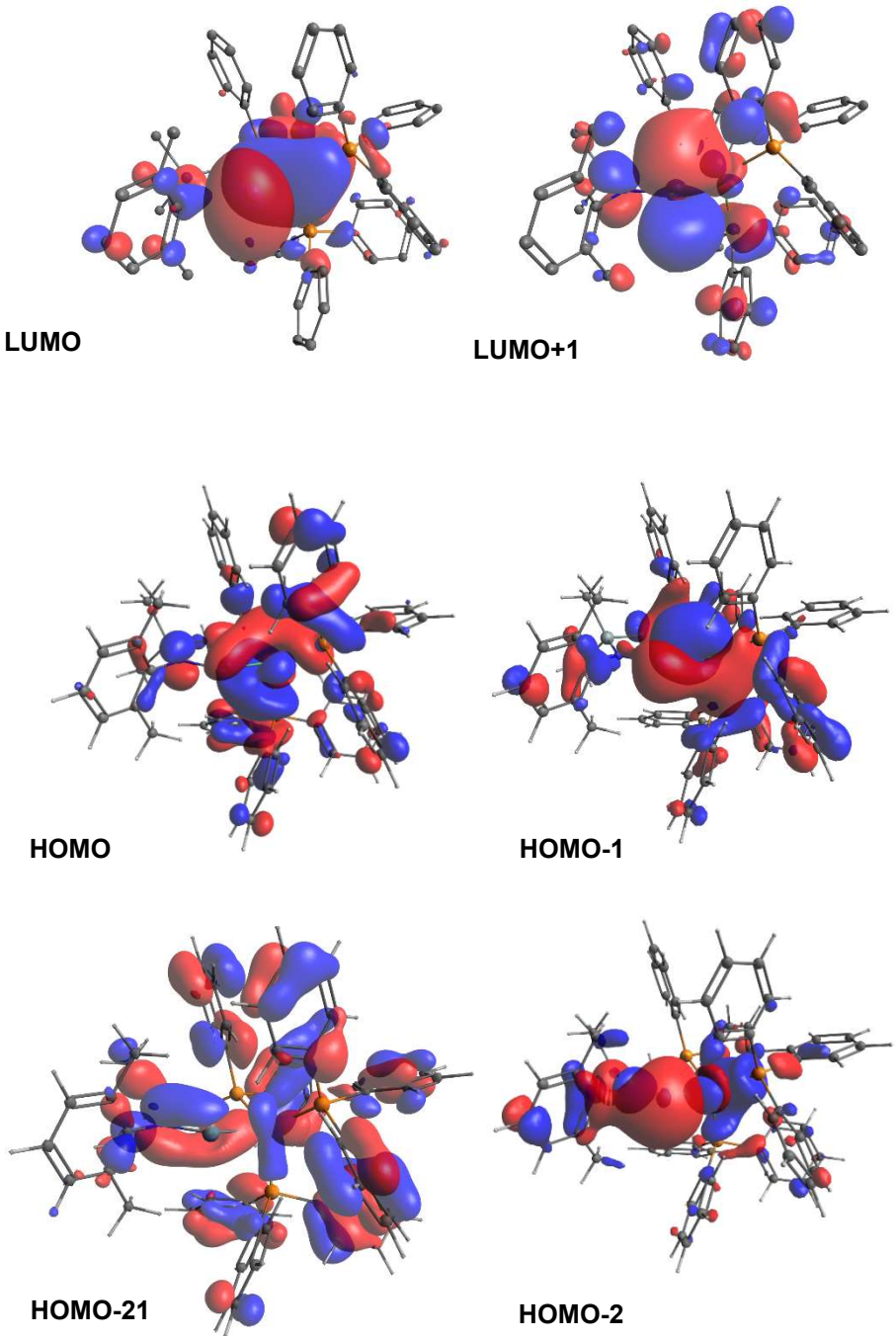

Figure 4.16 Selected frontier orbitals for **[2']⁺**.

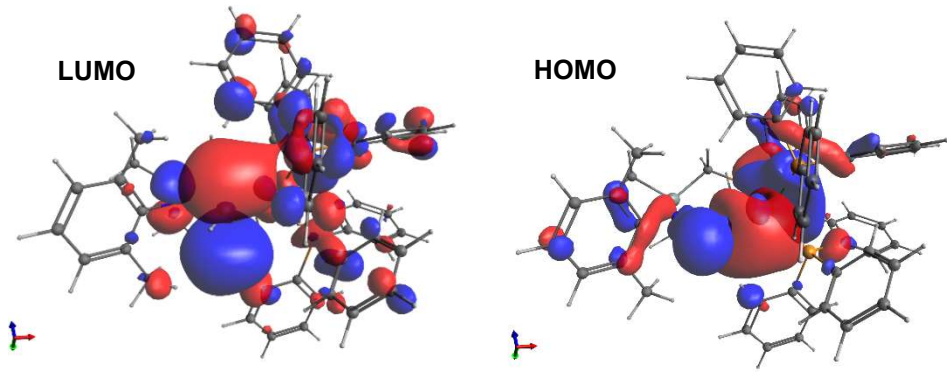

Figure 4.17 Selected frontier orbitals for **5'**.

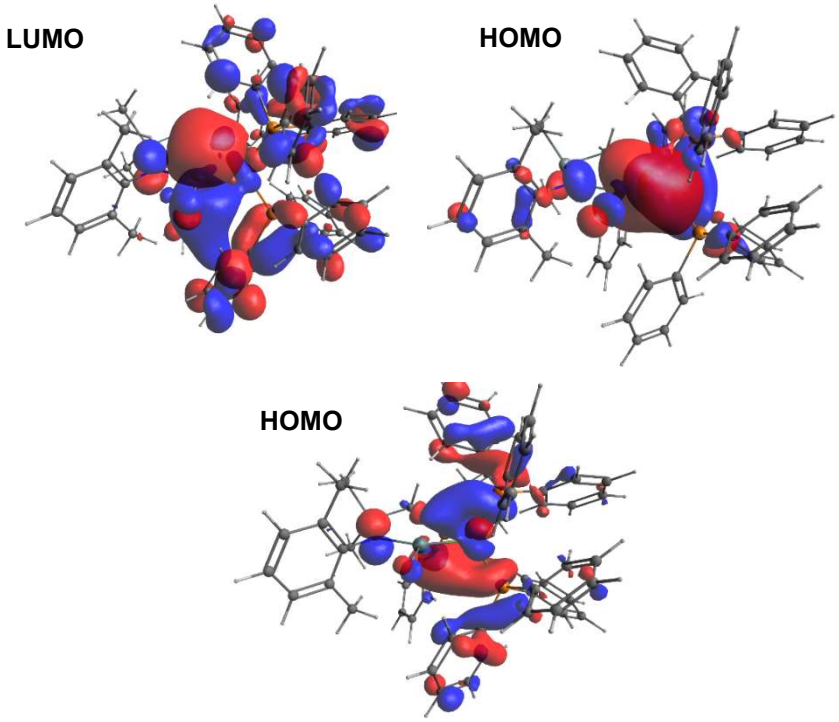

Figure 4.18 Selected frontier orbitals for **6'**.

*TD-DFT description of excited states **2** and **3**:*

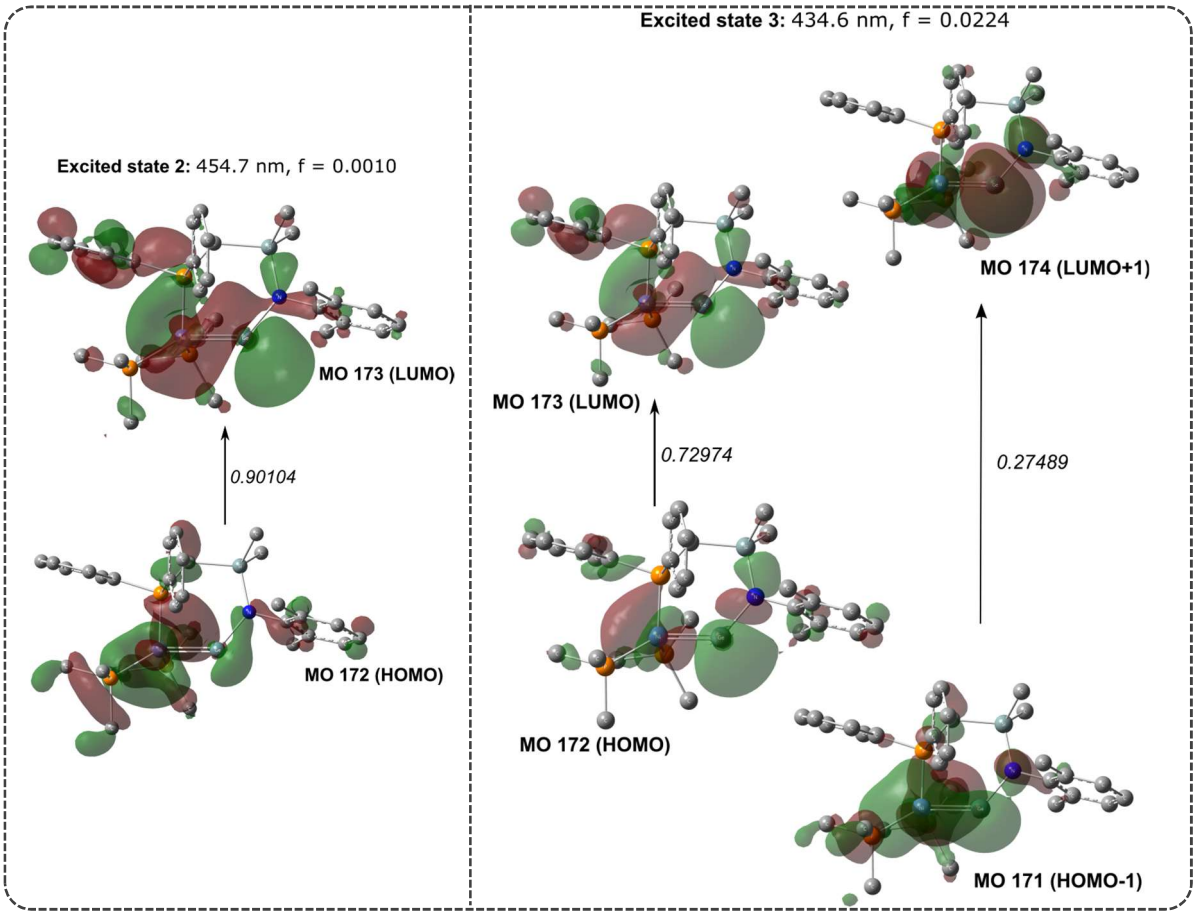

Figure 4.19 Visualization of the electronic transitions leading to abortions in the visible region of the UV/vis spectrum of **4b**.

FIA, HIA, AA, and WA calculations

Fluoride and Hydride ion affinities (FIA and HIA, respectively) were determined employing the procedure recently established by Krossing and Greb.[30(b,c)59] As such, gas phase FIA and HIA values were isodesmically anchored; the Me_3SiF/Me_3Si^+ reference system was utilised for the calculation of absolute FIA values (FIA(Me_3Si^+) = 952.5 kJ·mol^{-1}),[30(b)] and HIA values were referenced to the related Me_3SiH/Me_3Si^+ system (HIA(Me_3Si^+) = 959 kJ·mol^{-1}).[30(c)] Geometry optimisations were performed at the ωB97XD level with the def2-TZVPP basis set for Ni and Ge, and the def2-SVP basis set for all other atoms. Stationary points were confirmed as true minima by vibrational frequency analysis (no negative eigenvalues). Using these values, the enthalpies for Eq. 1 were determined and subtracted from the reference values for the Me_3SiX/Me_3Si^+ (X = F, H) given in Eq. 2, giving the gas phase FIA and HIA enthalpy values.

For the ammonia and water affinities (AA and WA, respectively), the method recently described by Greb was employed. Specifically, non-isodesmic methods were used through calculating the direct free energy of association of NH_3 or H_2O with **[4']$^+$**, **[4'']$^+$**, and **[5']$^+$** in the gas phase, as per Eq. 3, again with geometry optimisation conducted at the ωB97XD level with the def2-TZVPP basis set for Ni and Ge, and the def2-SVP basis set for all other atoms.

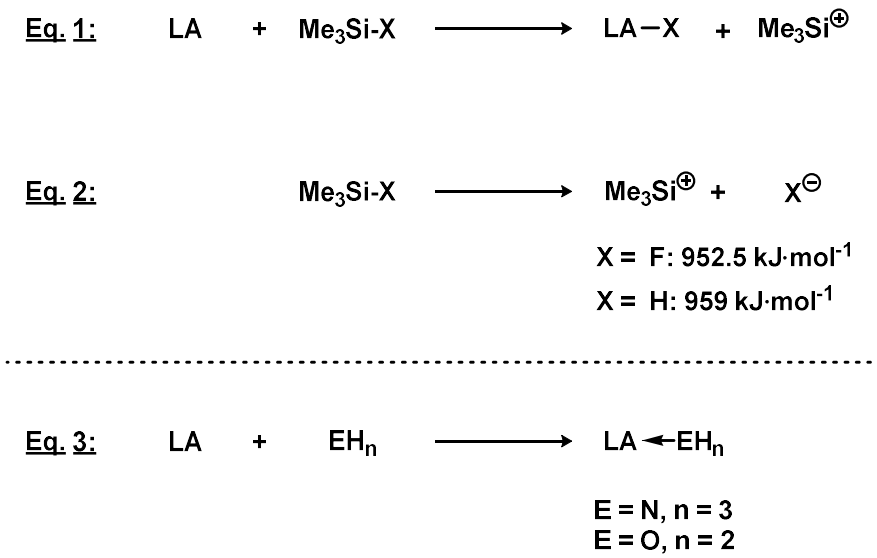

References

1 (a) A. C. Filippou, A. I. Philippopoulos, P. Portius, G. Schnakenburg, *Organometallics* **2004**, *23*, 4503-4512; (b) A. C. Filippou, A. Barandov, G. Schnakenburg, B. Lewall, M. van Gastel, A. Marchanka, *Angew. Chem. Int. Ed.* **2012**, *51*, 789–793; (c) A. C. Filippou, U. Chakraborty, G. Schnakenburg, *Chem. Eur. J.* **2013**, *19*, 5676–5686; (d) Y. N. Lebedev, U. Das, G. Schnakenburg, A. C. Filippou, *Organometallics* **2017**, *36*, 1530−1540.

2 A. Schulz, T. L. Kalkuhl, P. M. Keil, T. J. Hadlington, *Angew. Chem. Int. Ed.* **2023**, *62*, e202305996.

3 (a) Y. Mizuhata, T. Sasamori, N. Tokitoh, *Chem. Rev.* **2009**, *109*, 3479–3511; (b) G. Frenking, R. Tonner, S. Klein, N. Takagi, T. Shimizu, A. Krapp, K. K. Pandey, P. Parameswaran, *Chem. Soc. Rev.* **2014**, *43*, 5106–5139; (c) J.Baumgartner, C. Marschner, *Rev. Inorg. Chem.* **2014**, *34*, 119–152.

4 (a) K. H. Dötz, Ed., *Metal carbenes in organic synthesis*; Springer, Berlin, 2004; (b) K. H. Dötz, J. Stendel, Jr., *Chem. Rev*. **2009**, *109*, 3227–3274.

5 (a) M. N. Hopkinson, C. Richter, M. Schedler, F. Glorius, *Nature* **2004**, *510*, 485–496; (b) F. Glorious, Ed., *N-Heterocyclic Carbenes in Transition Metal Catalysis*, Springer, Berlin, 2007; (c) V. Nesterov, D. Reiter, P. Bag, P. Frisch, R. Holzner, A. Porzelt, S. Inoue, *Chem. Rev.* **2018**, *118*, 9678−9842.

6 P. Jutzi, *Angew. Chem. Internat. Edit.* **1975**, *14*, 232–245.

7 For key examples of multiply-bonded germylene-TM complexes, see: W.-W. du Mont, L. Lange, S. Pohl, and W. Saak, *Organometallics* **1990**, *9*, 1395–1399; (b) P. G. Hayes, R. Waterman, P. B. Glaser, T. D. Tilley, *Organometallics* **2009**, *28*, 5082–

5089; (c) M. C. Lipke, F. Neumeyer, T. D. Tilley, *J. Am. Chem. Soc.* **2014**, *136*, 6092−6102; (d) A. C. Filippou, D. Hoffmann, G. Schnakenburg, *Chem. Sci.* **2017**, *8*, 6290–6299.

8 L. Pu, B. Twamley, S. T. Haubrich, M. M. Olmstead, B. V. Mork, R. S. Simons, P. P. Power, *J. Am. Chem. Soc.* **2000**, *122*, 650–656.

9 J. D. Queen, A. C. Phung, C. A. Caputo, J. C. Fettinger, P. P. Power, *J. Am. Chem. Soc.* **2020**, *142*, 2233−2237.

10 Related neutral complexes are known for germanium, formally tetrylidyne complexes, as are a handful of related singly-bonded complexes which are better described as metallo-tetrylenes. For examples of the former, see refs [6], [7], and:
(a) A. C. Filippou, A. I. Philippopoulos, P. Portius, D. U. Neumann, *Angew. Chem. Int. Ed.* **2000**, *39*, 2778–2781; (b) A. C. Filippou, K. W. Stumpf, O. Chernov, G. Schnakenburg, *Organometallics* **2012**, *31*, 748–755.
For examples of the latter, see ref [6] and:
(c) R. S. Simons, P. P. Power, *J. Am. Chem. Soc.* **1996**, *118*, 11966–11967; (d) H. Lei, J.-D. Guo, J. C. Fettinger, S. Nagase, P. P. Power, *Organometallics* **2011**, *30*, 6316–6322; (e) J. Hicks, T. J. Hadlington, C. Schenk, J. Li, C. Jones, *Organometallics* **2013**, *32*, 323–329.

11 R. J. Somerville, J. Campos, *Eur. J. Inorg. Chem.* **2021**, 3488–3498.

12 P. M. Keil, T. Szilvasi, T. J. Hadlington, *Chem. Sci.* **2021**, *12*, 5582–5590.

13 CCDC deposition numbers for novel compounds: 2114015 (**2**), 2099955 (**4a**), 2099956 (**4b**), 2114016 (**5**), 2099957 (**4a·DMAP**), 2099958 (**8a**), 2099959 (**8b**), and 2099960 (**9b**).

14 Value for the MBO of **1'** taken from ref. [9].

15 (a) S. Hino, M. Brynda, A. D. Philips, P. P. Power, *Angew. Chem. Int. Ed.* **2004**, *43*, 2655–2658; (b) Li, C. Schenk, F. Winter, H. Scherer, N. Trapp, A. Higelin, S. Keller, R. Pöttgen, I. Krossing, C. Jones, *Angew. Chem. Int. Ed.* **2012**, *51*, 9557–9561.

16 Close contacts are considered to be those with a distance less than the sum of the van der Waals radii of the two elements.

17 (a) J. Li, C. Schenk, C. Goedecke, G. Frenking, and C. Jones, *J. Am. Chem. Soc.* **2011**, *133*, 18622–18625; (b) T. J. Hadlington, B. Schwarze, E. I. Izgorodina, and C. Jones, *Chem. Commun.* **2015**, *51*, 6854–6857; (c) D. L. Kays, *Chem. Soc. Rev.* **2016**, *45*, 1004–1018.

18 To the best of our knowledge, the only reported examples of related species, that is cationic complexes in which a non-linear L-E-M interaction is observed, can be found in the following. However, these are better described as metallotetrylenes, without significant charge localization at the E centre (E = Ge, Sn).
(a) A. C. Filippou, B. Baars, O. Chernov, Y. N. Lebedev, G. Schnakenburg, *Angew. Chem. Int. Ed.* **2014**, *53*, 565–570; (b) K. Inomata, T. Watanabe, H. Tobita, *J. Am. Chem. Soc.* **2014**, *136*, 14341–14344.

19 (a) R. C. Fischer, P. P. Power *Chem. Rev.* **2010**, *110*, 3877–3923; (b) P. P. Power, *Nature* **2010**, *463*, 171–177.

20 Similar results were obtained when using **4b**.

21 We note that attempts to extend this reaction to the SnII system **5** led only to the formation of protonated ligand, PhiPDippH.

22 M. M. D. Roy, A. A. Omaña, A. S. S. Wilson, M. S. Hill, S. Aldridge, E. Rivard, *Chem. Rev.* **2021**, *121*, 12784–12965.

23 T. J. Hadlington, M. Driess, C. Jones, *Chem. Soc. Rev.* **2018**, *47*, 4176–4197.

24 U. Mayer, V. Gutmann and W. Gerger, *Monatsh. Chem.* **1975**, *106*, 1235–1257.

25 R. F. Childs, D. L. Mulholland, A. Nixon, *Can. J. Chem.* **1982**, *60*, 809 – 812.

26 S. Künzler, S. Rathjen, A. Merk, M. Schmidtmann, T. Müller, *Chem. Eur. J.* **2019**, *25*, 15123–15130.

27 (a) J. Pahl, S. Brand, H. Elsen, S. Harder, *Chem. Commun.* **2018**, *54*, 8685–8688; (b) M. Schorpp, I. Krossing, *Chem. Sci.* **2020**, *11*, 2068–2076.
28 L. O. Müller, D. Himmel, J. Stauffer, G. Steinfeld, J. Slattery, G. Santiso-Quiñones, V. Brecht, I. Krossing, *Angew. Chem. Int. Ed.* **2008**, *47*, 7659–7663.
29 Fluoride complex **6** can also be independently synthesized through reaction of Me3SnF with chloride complex **3b**.
30 (a) I. A. Koppel, P. Burk, I. Koppel, I. Leito, T. Sonoda, M. Mishima, *J. Am. Chem. Soc.* **2000**, *122*, 5114–5124; (b) L. Greb, *Chem. Eur. J.* **2018**, *24*, 17881–17896; (c) P. Erdmann, J. Leitner, J. Schwarz, L. Greb, *ChemPhysChem* **2020**, *21*, 987–994 (d) A. Hermannsdorfer, M. Driess, *Angew. Chem. Int. Ed.* **2021**, *60*, 13656–13660.
31 P. Erdmann, L. Greb, *ChemPhysChem* **2021**, *22*, 935–943.
32 Details given in ESI.
33 H. Großekappenberg, M. Reißmann, M. Schmidtmann, T. Müller, *Organometallics* **2015**, *34*, 4952−4958.
34 (a) F. Lips, J. C. Fettinger, A. Mansikkamäki, H. M. Tuononen, Philip P. Power, *J. Am. Chem. Soc.* **2014**, *136*, 634–637; (b) A. V. Protchenko, J. I. Bates, L. M. A. Saleh, M. P. Blake, A. D. Schwarz, E. L. Kolychev, A. L. Thompson, C. Jones, P. Mountford, and S. Aldridge, *J. Am. Chem. Soc.* **2016**, *138*, 4555–4564; (c) C. Shan, S. Yao, M. Driess, *Chem. Soc. Rev.* **2020**, *49*, 6733–6754.
35 K. Inomata, T. Watanabe, Y. Miyazaki, H. Tobita, *J. Am. Chem. Soc*. **2015**, *137*, 11935–11937.
36 J. V. Obligacion, Paul J. Chirik, *Nat. Rev. Chem.* **2018**, *2*, 15–34.
37 (a) M. Bogdan, Ed., *Hydrosilylation: A Comprehensive Review on Recent Advances*; Springer, Netherlands, 2009; (b) Y. Nakajima, S. Shimada, *RSC Adv.* **2015**, *5*, 20603–20616.
38 A. J. Martínez-Martínez, A. S. Weller, *Dalton Trans.*, **2019**, *48*, 3351–3354.
39 F. K. Scharnagl, M. F. Hertrich, G. Neitzel, R. Jackstell, M. Beller, *Adv. Synth. Catal.,* **2019***, 361,* 374–379.
40 M. R. Elsby, S. A. Johnson, *J. Am. Chem. Soc.*, **2005**, *127*, 21, 7857–7870.
41 A. J. Sicard, R. T. Baker, *Org. Process Res. Dev.* **2020**, *24*, 2950−2952.
42 M. Muhr, P. Heiß, M. Schütz, R. Bühler, C. Gemel, M. H. Linden, H. B. Linden, R. A. Fischer, *Dalton Trans.*, **2021**, *50*, 9031–9036.
43 M. R. Elsby, S. A. Johnson, *J. Am. Chem. Soc.*, **2017**, *139*, 27, 9401–9407.
44 L. Garcia, C. Dinoi, M. F. Mahon, L. Maron, M. S. Hill, *Chem. Sci.*, **2019**,*10*, 8108–8118.
45 E. Shirakawa, D. Ikeda, S. Masui, M. Yoshida, T. Hayashi, *J. Am. Chem. Soc.* **2012**, *134*, 1, 272–279.
46 P. Fu, *J. Mol. Catal. A Chem.*, **2006**, *243*, 2, 253–257.
47 P. Bissinger, M. Paul, J. Riede, H. Schmidbaur, *Chem. Ber.* **1993**, *126*, 2579–2584.
48 H. R. Wiltse, A. N. Johnson, R. J. Durand W. Brennessel, R. M. Chin, *Organometallics* **2016**, *35*, 8, 1079–1085.
49 M. Hu, P. He, T. Qiao, W. Sun, W. Li, J. Lian, J. Li, S. Zhu, *J. Am. Chem. Soc.* **2020**, *142*, 39, 16894–16902.
50 T. Takahashi, F. Bao, G. Gao, M. Ogasawara, *Org. Lett.* **2003**, *5*, 19, 3479–3481.
51 S.Zhang, J. J. Ibrahim, Y. Yang, *Org. Lett.* **2018**, *20*, 19, 6265–6269.
52 C. Zarate, H. Yang, M. J. Bezdek, D. Hesk, P. J. Chirik, *J. Am. Chem. Soc.* **2019**, *141*, 12, 5034–5044.
53 G. M. Sheldrick, SHELXL-97, Program for Crystal Strucutre Refinement, Göttingen, **1997**.
54 G. Sheldrick, *Acta Crystallogr., Sect. C: Struct. Chem.*, **2015**, *71*, 3–8.
55 A. Spek, *Acta Crystallogr., Sec. D: Struct. Biol.*, **2009**, *65*, 148–155.
56 M. J. Frisch, G. W. Trucks, H. B. Schlegel, G. E. Scuseria, M. A. Robb, J. R. Cheeseman, G. Scalmani, V. Barone, G. A. Petersson, H. Nakatsuji et al., Gaussian 16 Rev. C.01, Wallingford, CT, **2016**.

57 a) A. D. Becke, *J. Chem. Phys*., **1997**, *107*, 8554–8560; (b) F. Weigend, R. Ahlrichs, *Phys. Chem. Chem. Phys.*, **2005**, *7*, 3297–3305; (c) J.-D. Chai, M. Head-Gordon, *Phys. Chem. Chem. Phys.*, **2008**, *10*, 6615–6620; (d) S. Grimme, J. Antony, S. Ehrlich, H. Krieg, *J. Chem. Phys*., **2010**, *132*, 154104.
58 Glendening, E. D., Badenhoop, J, K.; Reed, A. E.; Carpenter, J. E.; Bohmann, J. A.; Morales, C. M.; Landis, C. R.; Weinhold, F. Theoretical Chemistry Institute, University of Wisconsin, Madison, **2013**.
59 (a) L. O. Müller, D. Himmel, J. Stauffer, G. Steinfeld, J. Slattery, G. Santiso-Quiñones, V. Brecht, I. Krossing, *Angew. Chem. Int. Ed.* **2008**, *47*, 7659–7663.

Chapter 5

Accessing cationic tetrylene-nickel(0) systems featuring donor-acceptor E-Ni triple bonds (E = Ge, Sn)

P. M. Keil, T. J. Hadlington, *Chem. Commun.*, **2022**, *58*, 3011-3014.

All DFT calculations concerning this project were conducted by Dr. Terrance J. Hadlington.

Synopsis

In Chapter 4 it was demonstrated that our bidentate ligand scaffold ^{PhR}Dipp (^{PhR}Dipp = [{$Ph_2PCH_2Si(R)_2$}(Dipp)N]$^-$ R = Ph, *i*Pr; Dipp = 2,6-*i*$Pr_2C_6H_3$) leads to a bent N-E-Ni (E = Ge, Sn) in the cationic tetryliumylidene-nickel(0) complexes [(^{PhR}DippE)·Ni(PPh_3)$_2$]$^+$. This minimises *π*-back-donation from the Ni^0 centre to the tetrel element and leads to highly Lewis acidic tetrel element centres. We wanted to further explore if this bent angle is a result of the forced geometry by the bidentate ligand structure, or due to a different effect. Therefore, we synthesised the analogous ligand system ^{SiiP}Dipp (^{SiiP}Dipp = [(*i*Pr_3Si)(Dipp)N]$^-$), which lacks a chelating phosphine arm, and successfully obtained the corresponding (chloro)-germylene and -stannylene ligands, ^{SiiP}DippGeCl and [^{SiiP}DippSnCl]$_2$. These were converted in a one-pot reaction to the cationic tetryliumylidene-nickel(0) complexes [^{SiiP}DippE·Ni(PPh_3)$_3$]$^+$, with [BAr^F_4]$^-$ ([BAr^F_4]$^-$ = [{3,5-$(CF_3)_2C_6H_3$}$_4$B]$^-$) as counter anion.

In contrast to the tetryliumylidene-nickel(0) complexes [(^{PhR}DippE)·Ni(PPh_3)$_2$]$^+$ from Chapter 4, the crystal structures of [^{SiiP}DippE·Ni(PPh_3)$_3$]$^+$ revealed near linear N-E-Ni angles and considerably contracted E-Ni bonds. DFT analysis showed that the HOMO and HOMO+1 are dominated by the backdonation from the Ni^0 centre to the tetrel element, while the donation from the tetrel element to the Ni centre can be observed in the HOMO+2. Therefore, the bonding in these complexes could be best described as a donor-acceptor triple bond between the tetrel and TM centres. We could therefore conclude that the bidentate ligand scaffold ^{PhR}Dipp with a phosphine arm is essential to enforce a bent N-E-Ni angle, minimising *π*-back-donation from the TM centre and thereby greatly enhancing the Lewis acidity of the tetrel element.

Furthermore, [^{SiiP}DippE·Ni(PPh_3)$_3$]$^+$ proved to be rather unstable, decomposing at elevated temperatures in PhF and even at ambient temperature in THF, while only giving intractable

reaction mixtures when attempting substrate activation with them. Therefore, the bidentate ligand scaffold also increases the stability of the resulting TM complexes, allowing for interaction with ammonia and controlled catalytic application as described in Chapter 3 and 4.

It should be noted that very recently, after this project was published, the group of Fillipou reported on similar cationic group 10 ylidene complexes and investigated their electronic nature and bonding situation in more depth, also including our reported structures in the process.[1]

Manuscript

The following sections are reproduced and formatted from the following article: P. M. Keil, T. J. Hadlington, Chem. Commun., **2022**, 58, 3011-3014. *Experimental spectra (NMR, LIFDI/MS, and UV/vis) and further details concerning DFT calculations can be retrieved online* (https://doi.org/10.1039/D2CC00422D).

Abstract

We describe facile synthetic methods for accessing linear cationic tetrylene nickel(0) complexes $[^{SiiP}DippE{\cdot}Ni(PPh_3)_3]^+$ (E = Ge (4) and Sn (5); $^{SiiP}Dipp$ = $[(iPr_3Si)(Dipp)N]^-$), which feature donor-acceptor E-Ni triple bonds. These species are readily accessed in a one-pot protocol, combining the bulky halo-tetrylenes $^{SiiP}DippECl$ (E = Ge (1) and Sn (2)), $Ni(cod)_2$, PPh_3, and $Na[BAr^F{}_4]$. Given the diamagnetic nature of 4 and 5, they each contain a formal zero-valent Ni centre, making the E-M triple bonds in these complexes unique compared to previously reported metal tetrylidyne complexes, which typically feature covalent/ionic bonding. In-depth computational analyses of these species further support triple bond character in their E-Ni interactions.

Introduction

Multiple bonding between carbon and transition metals stands as an historic cornerstone of organometallic chemistry, forming the basis for now ubiquitous catalytic transformations such as alkene and alkyne metathesis.[2] The past two decades have seen this interest migrate to the heavier group 14 elements, Si-Pb: where once it was thought multiple bonds involving these elements were not viable (*viz*. the double bond rule), we now know that this is not the case,[3] with an ever-growing number of multiply-bonded species involving these heavier tetryl elements.[4] In 1996, the first compound featuring an E-M triple bond (E = Si-Pb, M = transition

metal) was reported by the group of Power, in the molybdenum-germylyne complex **A**,[5] followed soon after by analogous chromium- and tungsten-germylyne complexes **B** and **C** (Figure 5.1).[6] All of these species feature short Ge-M bonding interactions, and were synthesised through salt metathesis of bulky ArGeCl (Ar = 2,6-$Mes_2C_6H_3$, $Trip_2C_6H_3$; Mes = 2,4,6-$Me_3C_6H_2$; Trip = 2,4,6-$^iPr_3C_6H_2$) with the anionic metal salts (*viz*. $CpM(CO)_3$; M = Cr, Mo, W). The same year, Fillippou reported a related tungsten-germylyne complex (**D**, Figure 5.1),[7] which formed upon oxidative addition of Cp*GeX to the tungsten(0) precursor, $(dppe)_2(N_2)_2W$ (Cp* = C_5Me_5; X = Cl, Br; dppe = $Ph_2PC_2H_4PPh_2$). Since these early examples, numerous compounds featuring triple bonds between a transition metal and Si,[8] Ge,[5,6,7,8(d),9] Sn,[8(d),10] and Pb [11] have been forthcoming. Notably, however, these almost exclusively feature heavier, non-zero valent transition metals, and have formal bonds between the two elements centres. In addition to neutral complexes **A-D** and related species, cationic complexes are also known, all of which bear their cationic charge at the transition metal (*viz*. **E**, Figure 5.1 [10(b)]) or at an ancillary carbene ligand (*viz*. **F**, Figure 5.1 [9(k)]). This is important, as this indicates a formal (*i.e.* covalent/ionic) bond between E and M, borne out by known singly-bonded tautomeric forms which are all best described as metallo-tetrylenes (*viz*. Figure 5.1).[12] E-M complexes featuring exclusively donor-acceptor E-M triple bonds, to the best of our knowledge, are not yet known.

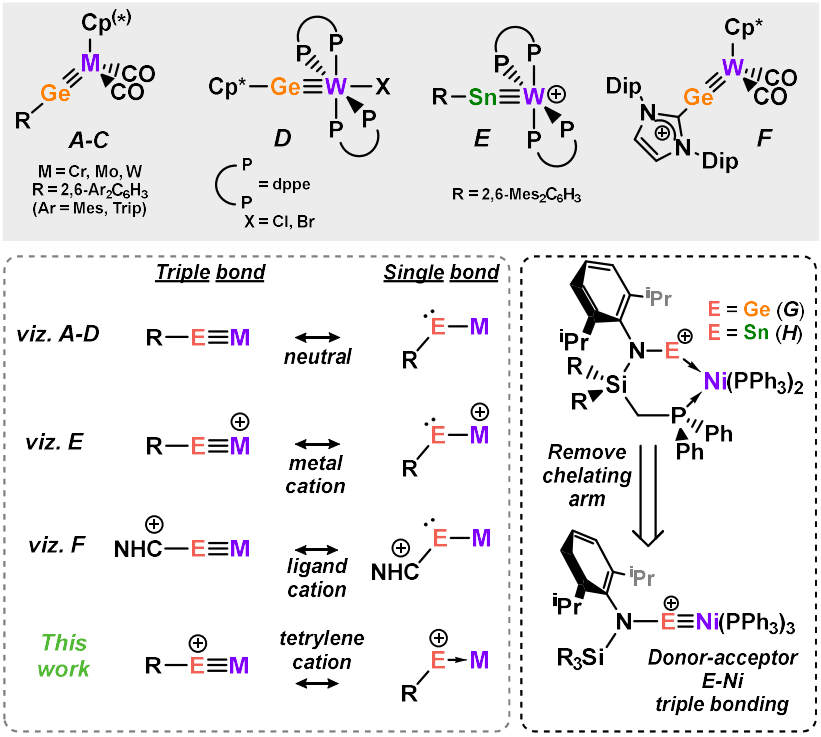

Figure 5.1 Known and possible triple-bonding modes for group 14-transition metal species, and related 'bent' derivatives featuring E-M single bonds (E = C-Pb, M = transition metal).

We recently reported a straight-forward synthetic route to non-linear cationic tetrylene-nickel(0) complexes (*viz*. **G** and **H**, Figure 5.1) in which the cationic charge resides on the group 14 element centre, rendering these centres highly Lewis acidic.[13] In these systems, a chelating phosphine arm prevents a linear L-E-Ni geometry, and thus hinders the formation of a multiple bond between E and M. This ligand design feature lends the E centre a considerably amplified reactivity relative to known triply-bonded systems. Curious as to the true importance of the chelating arm in these systems in forming reactive systems **G** and **H**, we sought to develop closely related systems utilising the monodentate bulky amide ^{SiiP}Dipp (^{SiiP}Dipp = [Dipp(^{i}Pr$_3$Si)N]$^-$).[14] Herein we report on the resulting cationic tetrylene nickel(0) complexes, [^{SiiP}DippE·Ni(PPh$_3$)$_3$]$^+$ (E = Ge (**4**) and Sn (**5**)), which feature linear L-E-Ni bonding interactions which are best described as *donor-acceptor* E-M triple bonds. This gives clear evidence that the chelating phosphine arms in **G** and **H** do indeed lead to a reduced bond order in those compounds, thus amplifying their reactivity. Further insights into these unique bonding interactions are given through computational DFT analyses.

Results and Discussion

The (amido)(chloro)tetrylenes, ^{SiiP}DippECl (E = Ge (**1**), Sn (**2**)) were accessed by reacting the known potassium amide (^{i}Pr$_3$Si)DippNK with GeCl$_2$·dioxane or SnCl$_2$ in a 1:1 ratio, respectively, forming the desired products in good yield after recrystallisation from pentane (Scheme 5.1). X-ray diffraction analysis of **1** confirmed the monomeric form of this species, in keeping with, previously reported examples of Ge^{II} chloride species bearing bulky amido ligands.[15] On the contrary, **2** forms a chloride-bridged dimeric structure, which is also common for such Sn^{II} species given the larger radius of this element.[16,17]

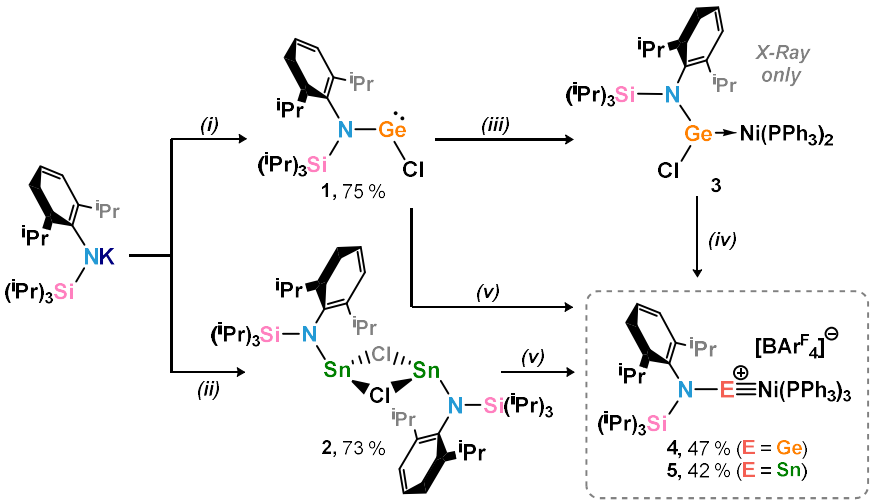

Scheme 5.1 Synthetic access E^{II} chloride complexes **1** and **2**, and subsequent synthesis of triply-bonded E^{II}-Ni^0 complexes **4** and **5**. (i) GeCl$_2$·dioxane, THF, -78 °C; (ii) SnCl$_2$, THF, -78 °C; (iii) Ni(cod)$_2$, 2 PPh$_3$, toluene, -78 °C; (iv) Na[BAr$^F_4$], toluene, RT; (v) Ni(cod)$_2$, 3 PPh$_3$, Na[BAr$^F_4$], toluene, -78 °C.

With these tetrylenes in hand we set out to synthesize the desired Ni^0 complexes. We first sought to isolate species bearing the (amido)(chloro)tetrylenes, from which one could abstract the chloride ligand by addition of $Na[BAr^F{}_4]$ (Ar^F = 3,5-$(CF_3)_2C_6H_2$), which has proved successful in previous investigations.[11(b)] Dropwise addition of toluene solutions containing a mixture of 3 equivs. PPh3 and 1 equiv. **1**, to a cooled toluene solution of $Ni(cod)_2$ resulted in deep red solutions. Warming these solutions followed by work-up led to eventual precipitation of fine grey/black powder, which auto ignites on exposure to air, thought to be a mixture of nickel and germanium powders. Repeating this reaction, with carefully work-up of reaction mixtures did allow for the isolation of a few crystals of the 16-electron Ni^0 complex **3**, this species being too unstable to attain further analytical data.[18] It is interesting to note that even in the presence of 3 equiv. of PPh_3 this compound selectively forms, possibly due to the steric pressure of the ^{SiiP}Dipp ligand. Attempting to isolate the same compound utilizing **2** was not possible in our hands, in line with our failed earlier attempts to isolate the closely related chloro-stannylene complex employing our phosphine-functionalised chelating ligands.[19]

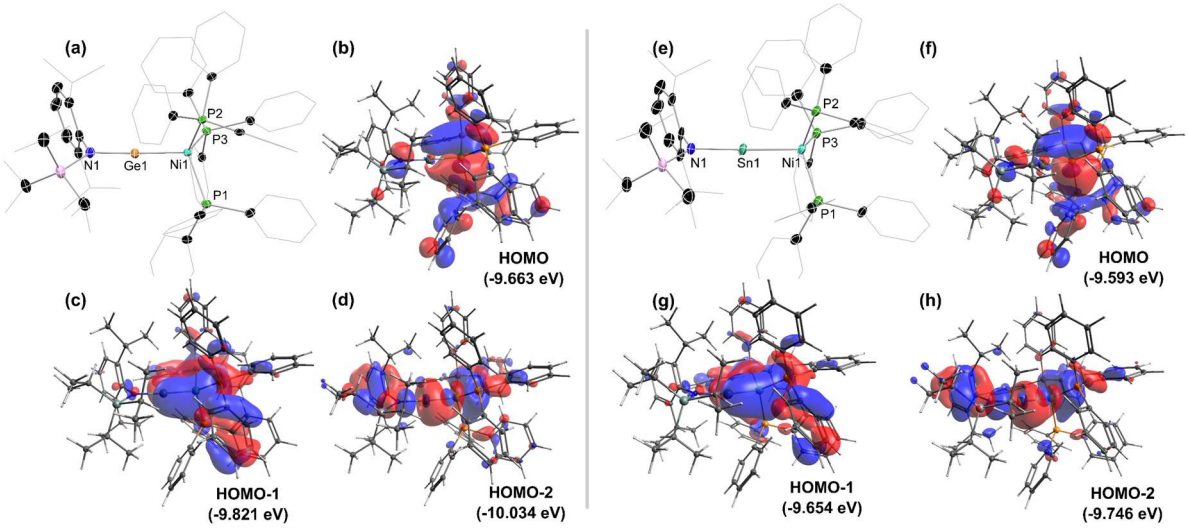

Figure 5.2 ***(a)*** The molecular structure of the cationic part of **4**, with thermal ellipsoids at 30% probability, hydrogen atoms omitted, and peripheral substituents in wire-frame for clarity; ***(b)*** the calculated HOMO of **4**; ***(c)*** the calculated HOMO-1 of **4**; ***(d)*** the calculated HOMO-2 of **4**; ***(e)*** The molecular structure of the cationic part of **5**, with thermal ellipsoids at 30% probability, hydrogen atoms omitted, and peripheral substituents in wire-frame for clarity; ***(f)*** the calculated HOMO of **5**; ***(g)*** the calculated HOMO-1 of **5**; ***(h)*** the calculated HOMO-2 of **5**. Selected bond lengths (Å) and angles (°) for **4**: Ge1-Ni1 2.1596(7); Ge1-N1 1.853(2); Ni1-P1 2.311(1); Ni-P2 2.289(1); Ni1-P3 2.307(1); N1-Ge1-Ni1 175.9(9); P1-Ni1-P2 105.9(4); P2-Ni-P3 110.7(4); P1-Ni-P3 115.50(4). For **5**: Sn1-Ni1 2.355(1); Sn1-N1 2.066(6); Ni1-P12.296(3); Ni-P2 2.267(3); Ni1-P3 2.281(3); N1-Sn1-Ni1 173.6(2); P1-Ni1-P2 108.0(1); P2-Ni-P3 112.9(1); P1-Ni-P3 118.6(1).

To circumvent the formation of unstable **3**, we instead attempted to generate the cationic complexes *in-situ*, using a similar approach to that used previously in accessing **G** and **H**.[13] That is, mixtures of **1** or **2**, PPh_3, and $Ni(cod)_2$ with additional $NaBAr^F{}_4$ directly form the target

cationic complexes [^{SiiP}DippE·Ni(PPh_3)$_3$][BAr^F_4] (E = Ge (**4**), E = Sn (**5**)), which were isolated as deep red-purple (**4**) or deep blue-purple (**5**) crystals (Scheme 5.1). Compound **4** was found to be stable in solution at RT, in stark contrast to **3**. Still, dissolution of pure **4** gave $^{31}P\{^1H\}$ NMR spectra with one major, slightly broadened singlet (δ =37.2 ppm), and one small sharp singlet (δ = 36.6 ppm; Fig S11 in ESI)). We hypothesized that this may be due to dynamic loss of one PPh_3 ligand in solution, generating a 16 electron Ni^0 complex akin to **3**. Addition of two further equivs. of PPh_3 to dissolved **4** led to complete disappearance of the peak at 36.6 ppm, and retention of the peak centred at 37.2 ppm, somewhat confirming this hypothesis. ^1H NMR spectroscopic data of these mixtures are also in keeping with the presence of a single compound, which we assign as 18-electron complex **4**. Attaining NMR spectroscopic data for Sn^{II} complex **5** proved more challenging, as this species decomposes in solution at ambient temperature, with dark blue-black solutions of pure **5** becoming red over time, concomitant with appearance of numerous broad peaks in ^1H NMR spectra for these solutions. Solutions of **5** maintained below 0°C hampered decomposition, allowing us to attain clear NMR spectroscopic data. Compound **5** appears as one species in its ^1H and $^{31}P\{^1H\}$ NMR spectra recorded at -20 °C, showing no dynamic behavior of the PPh_3 ligands. The ^{119}Sn NMR spectrum reveals a highly broadened peak at 885 ppm, in keeping with reported Sn-M triply bonded complexes.[20] The UV/vis spectra for **4** and **5** show one broad absorption band (**4**: λ_{max} = 423 nm (9384 $Lcm^{-1}mol^{-1}$); **5**: 450 nm (5520 $Lcm^{-1}mol^{-1}$)), beginning at 600 nm for **4** and 780 nm at **5**, in line with the deep blue-black colour of **5** in solution.

An X-ray crystallographic analysis of these complexes reveals two coordinate E^{II} centres bound to Ni^0, with near linear N-E-Ni bonding interactions (**4**: 175.90°, **5**: 173.65°; Figure 5.2, Table 5.1). The geometry at Ni for both structures is best described as distorted tetrahedral, with all P-Ni-P and E-Ni-P angles being close to 109.5°. The Ge1-Ni1 bond distance in **4** (d = 2.1596(7) Å) is shorter than all reported Ge-Ni distances, to the best of our knowledge, with reported Ge-Ni bonds in germylene-nickel complexes ranging from 2.179 to 2.337 Å.[21] This bond distance in **4** is also notably contracted when compared to that in our related chelating complex, **G**, which indicates that multiple-bonding is indeed perturbed in the latter due to the geometrically enforced N-Ge-Ni binding angle of 133.0(1)°. The bond distance in **4** of 2.1596(7) Å is also only slightly greater than the sum of predicted values for the triple bond radii of Ni (*viz*. 1.01 Å) and Ge (*viz*. 1.14 Å; ∑ = 2.15 Å),[22] giving further evidence for the ascribed bond order.

Similar metrical parameters are observed for the related Sn^{II} system, **5** (Table 5.1). The Sn1-Ni1 distance in **5** (d = 2.355(1) Å) is shorter than all reported Sn-Ni distances bar one, the only shorter example being in the icosahedral $[Ni_{11}(SnR)_2(CO)_{18}]^{2-}$ clusters (R = ^{n}Bu, Me), which feature interstitial Ni atoms.[23] The observed bond order is also in line with the sum of predicted

values for triply bonded Ni (*viz*. 1.01 Å) and Sn (*viz*. 1.33 Å; ∑ = 2.34 Å).[22] Our previously reported complex **H**, which also has a geometrically constrained N-Sn-Ni binding angle, has a Sn-Ni bond distance (d = 2.4024(9) Å) elongated relative to that in linear **5** and again highlighting the effect of the chelating arm in **H**.[13] The linear E-Ni bonding interactions in **4** and **5**, combined with their short E-Ni bonds, lead us to believe these represent triply-bonded compounds. These in fact represent complexes bearing donor-acceptor E-Ni triple bonds (E = C-Pb), given the diamagnetic Ni^0 centres in these species. That is, they feature a strong dative E→Ni interaction, and two Ni→E back-bonding interactions. In this, these species also represent the first reported triply-bonded E-Ni complexes. The bonding nature in **4** and **5** is further borne out through DFT analyses of their electronic structure. The first three Kohn-Sham HOMOs (Highest Occupied Molecular Orbitals) of both species represent E-Ni bonding interactions. The HOMO and HOMO-1 are essentially of π-symmetry, involving Ni→E electron donation to the two vacant *p*-orbitals on E (Figure 5.2, (b), (c), (f), and (g)), whilst the HOMO-2 signifies E→Ni σ-donation (Figure 5.2, (d) and (h)). NBO-derived (Natural Bond Order) second order perturbation theory analyses do not classify the E-Ni interactions as formal bonds, but as donor-acceptor interactions, in keeping with our assessment of the bonding in **4** and **5**. The Mayer Bond Orders (MBO) for **4** (1.59) and **5** (1.31) would suggest that the triple bonds in these species are weak. Still, when compared with our previously reported chelating systems, these values are considerably increased (Table 5.1), showing the importance of the chelating arm in those systems in directing their high Lewis acidity.

Table 5.1 Selected metrical and calculated parameters for **4**, **5**, **G**, and **H**.

		4	**G** [a]	**5**	**H** [a]
		(E = Ge)		**(E = Sn)**	
$d_{E\text{-}Ni}$ (Å)		2.1596(7)	2.1908(9)	2.355(1)	2.4024(9)
$d_{N\text{-}E}$ (Å)		1.853(2)	1.851(3)	2.066(6)	2.068(5)
$\angle_{N\text{-}E\text{-}Ni}$ (°)		175.90°	133.0(1)°	173.65°	124.3(1)°
MBO [b]		1.59	1.13	1.31	0.79
NPA Charge [b]	**E**	1.01	0.86	1.42	1.15
	Ni	0.05	0.03	-0.19	-0.07

[a] Values taken from *ref. 19*; [b] Calculated for the optimised structures, at the ωB97XD/def2-SVP(Ni,Ge,Sn:def2-TZVPP) level.

Due to the increased back bonding from the Ni^0 centres in **4** and **5**, these species should have a significantly reduced Lewis acidity when compared with the bent systems **G** and **H**; **G**, shows the capacity to both abstract the fluoride ion from $[SbF_6]^-$ and bind ammonia at the low-coordinate Ge^{II} centre, due to its high Lewis acidity.[13] Reactions of **4** and **5** with $[PPh_4][SbF_6]$ and NH_3 in fact do appear to proceed, but in both cases result only in decomposition, forming protonated ligand, ^{DiiP}DippH, even when conducted at low temperature. It is unclear whether reactivity is due to the low-valent E centres here, but we note that the chelating arm in **G** and **H** leads to considerably more stable complexes in further reactivity, which is key in utilising such systems in catalysis.

Conclusions

To summarise, the novel cationic E^{II}-Ni^0 complexes **4** and **5** have been synthesised and fully characterised (E = Ge,Sn), and represent the first triply-bonded group 14-nickel systems. X-ray diffraction analyses reveal near linear N-E-Ni interactions and remarkably short E-Ni bond distances for both compounds. When compared with our previously reported chelating E^{II} systems (*viz*. **G** and **H**), in which E-Ni multiple bonding is strongly perturbed, the present study gives valuable insight into the effects of ligand design in tuning stability and reactivity in potentially cooperative ligand-metal systems. We continue to pursue the implementation of low-valent main group ligands for cooperative bond activation.

Supporting Information

General experimental considerations

All experiments and manipulations were carried out under dry oxygen free argon atmosphere using standard Schlenk techniques or in a MBraun inert atmosphere glovebox containing an atmosphere of high purity argon. THF was dried by distillation over a sodium/benzophenone mixture and stored over activated 4Å mol sieves. C_6D_6 was dried, degassed and stored over a potassium mirror. All other solvents were dried over activated 4Å mol sieves. ^{SiiP}DippK (^{SiiP}DippK = (^{i}Pr$_3$Si)DippNK; Dipp = 2,6-^{i}Pr$_2$-C$_6$H$_3$),[24] Na[BAr$^F_4$] (Ar^F = 3,5-CF$_3$-C$_6$H$_3$),[25] and $Ni(cod)_2$ [26] were synthesized according to known literature procedures. All other reagents were used as received. NMR spectra were recorded on a Bruker AV 400 Spectrometer. The ^{1}H and ^{13}C{^{1}H} NMR spectra were referenced to the residual solvent signals as internal standards. ^{29}Si{^{1}H} NMR spectra were externally calibrated with $SiMe_4$. ^{31}P{^{1}H} NMR spectra were externally calibrated with H_3PO_4. ^{119}Sn{^{1}H} NMR spectra were externally calibrated with $SnMe_4$. Liquid Injection Field Desorption Ionization Mass Spectrometry (LIFDI-MS) was measured directly from an inert atmosphere glovebox with a Thermo Fisher Scientific Exactive Plus Orbitrap equipped with an ion source from Linden CMS.[27] Absorption spectra (UV/vis)

were recorded on an Agilent Cary 60 UV/vis spectrophotometer. For the ammonia experiments ammonia 5.0 was used. Elemental analyses (C, H, N) were performed with a combustion analyzer (elementar vario EL, Bruker).

Experimental procedures

^{SiiP}DippGeCl, 1. A solution of ^{SiiP}DippK (1.60 g, 4.30 mmol) in 20 mL THF was added dropwise to a stirring solution of $GeCl_2$·dioxane (1.00 g, 4.30 mmol) in 10 mL THF at -78°C, and subsequently allowed to warm to RT, resulting in the formation of a pale-yellow solution. All volatiles were removed *in vacuo* and the residue extracted in 20 mL of pentane. The solution was concentrated and stored at -30°C for 16h to yield colorless crystals suitable for X-ray diffraction analysis (1.42 g, 3.22 mmol, 75%).

^{1}H NMR (C_6D_6, 400 MHz, 298 K): δ = 0.99 (d, 18H, $^{3}J_{HH}$ = 7.5 Hz, Si-Pr^{i}-C*H*$_3$), 1.25 (m, 15H, Dipp-Pr^{i}-C*H*$_3$, Si-Pr^{i}-C*H*), 3.14 (hept, 2H, $^{2}J_{HP}$ = 6.9 Hz, Dipp-Pr^{i}-C*H*), 7.12 (m, 3H, Ar-C*H*). **^{13}C{^{1}H} NMR** (C_6D_6, 101 MHz, 298 K): δ = 13.1 (Si-Pr^{i}-*C*H), 18.8 (Si-Pr^{i}-*C*H$_3$), 24.0 (Dipp-Pr^{i}-*C*H$_3$), 26.4 (Dipp-Pr^{i}-*C*H$_3$), 28.2 (Dipp-Pr^{i}-*C*H), 124.3, 125.9, 142.4, 143.2 (Ar-*C*).

^{29}Si{^{1}H} NMR (C_6D_6, 99 MHz, 298 K): δ = 12.8 (s, *Si*-Pr^{i}).

MS/LIFDI-HRMS found (calcd.) m/z: 406.1996 (406.1980) for $[M\text{-}Cl]^+$.

[^{SiiP}DippSnCl]$_2$, 2. The procedure for the synthesis of **1** was followed using **^{SiiP}DippK** (4.00 g, 10.76 mmol) and $SnCl_2$ (2.04 g, 10.76 mmol). Compound **2** was isolated as colorless crystals suitable for X-ray diffraction analysis from a concentrated pentane solution stored at -32°C after 16h (3.80 mg, 7.81 mmol, 73%).

N.B. On one occasion, a low yield of crystalline **2·KCl** was obtained *via* this procedure, which is formally the KCl adduct of **2**. No further data was obtained for this compound.

^{1}H NMR (C_6D_6, 400 MHz, 298 K): δ = 1.11 (d, 36H, $^{3}J_{HH}$ = 7.5 Hz, Si-Pr^{i}-C*H*$_3$), 1.28 (m, 30H, Dipp-Pr^{i}-C*H*$_3$, Si-Pr^{i}-C*H*), 3.51 (hept, 4H, $^{2}J_{HP}$ = 6.8 Hz, Dipp-Pr^{i}-C*H*), 7.10 (m, 6H, Ar-C*H*). **^{13}C{^{1}H} NMR** (C_6D_6, 101 MHz, 298 K): δ = 14.3 (Si-Pr^{i}-*C*H), 19.4 (Si-Pr^{i}-*C*H$_3$), 24.2 (Dipp-Pr^{i}-*C*H$_3$), 27.6 (Dipp-Pr^{i}-*C*H), 27.9 (Dipp-Pr^{i}-*C*H$_3$), 124.1, 125.2, 142.7, 145.9 (Ar-*C*).

^{29}Si{^{1}H} NMR (C_6D_6, 99 MHz, 298 K): δ = 9.0 (s, *Si*-Pr^{i}).

^{119}Sn NMR (C_6D_6, 149 MHz, 298K): δ = 232 (s, N-*Sn*-Cl).

MS/LIFDI-HRMS found (calcd.) m/z: 452.1787 (452.1790) for $[M\text{-}iPr_3SiNDippSnCl\text{-}Cl]^+$.

Anal. calcd. for $C_{21}H_{38}ClNSiSn$: C, 51.82%; H, 7.87%; N, 2.88%; found: C, 50.81%; H, 7.44%; N, 2.92%. Repeated element analysis gave variable but consistently low values for C, possibly due to Si-carbide formation.

[(^{SiiP}Dipp)(Cl)Ge·Ni^0(PPh$_3$)$_2$], 3. A toluene solution of **1** (300 mg, 0.68 mmol) and PPh_3 (535 mg, 2.04 mmol) was added dropwise to a toluene solution of $Ni(cod)_2$ (187 mg, 0.68 mmol) at -40°C and stirred for 30 min. The mixture was filtrated, layered with pentane, and stored at -32°C. After 24 h a few orange crystals of **3** were isolated suitable for X-ray diffraction analysis. No further data on **3** could be collected due to insufficient quantity and instability of the compound.

[^{SiiP}DippGe·Ni^0(PPh$_3$)$_3$][BAr$^F_4$], 4. Compound **1** (272 mg, 0.62 mmol), $Ni(cod)_2$ (170 mg, 0.62 mmol), PPh_3 (485 mg, 1.85 mmol) and Na[BAr^F_4] (547 mg, 0.62 mmol) were mixed together in a Schlenk flask and cooled to -78°C. 10 mL of toluene was slowly added to the flask and the resulting reaction mixture was slowly warmed to RT overnight, leading to a dark purple precipitate within a dark red solution. All volatiles were removed *in vacuo* and the residue was extracted with fluorobenzene. The deep purple solution was concentrated to approximately 2 mL and 5 mL of pentane were slowly added to the flask while constantly shaking the flask. The resulting solution was stored at -32°C overnight yielding a crop of dark purple crystals. The remaining solution was removed, and the crystals subsequently washed with toluene and pentane and dried *in vacuo* yielding **4** (614 mg, 0.29 mmol, 47%) as a purple crystalline powder. Deep red-purple crystals which were suitable for X-Ray diffraction analysis were obtained from a concentrated fluorobenzene solution layered with pentane at RT after 24h.

N. B. Dissolving the pure compound in THF-d_8 resulted in two species being present in the NMR spectra, which we hypothesise is due to reversible dissociation of one PPh_3 ligand from Ni^0. Even though two species were present, the integrals of the aromatic and the aliphatic in the ^{1}H NMR matched for 3 equivs. of PPh_3 being present. Addition of 2 equivs. of PPh_3 to the NMR tube led to the formation of one species. The spectra with added PPh_3 are described here; both sets of spectra are shown later in the Supporting Information.

^{1}H NMR (THF-d_8, 400 MHz, 298 K): δ = 0.80 (m, 24 H, Si-Pr^i-C*H*$_3$/Dipp-Pr^i-C*H*$_3$), 0.98 (hept, 3 H, $^3J_{HH}$ = 7.5 Hz, Si-Pr^i-C*H*), 1.20 (d, 6 H, $^3J_{HH}$ = 6.7 Hz, Dipp-Pr^i-C*H*$_3$), 3.23 (hept, 2H, $^3J_{HH}$ = 6.7 Hz, Dipp-Pr^i-C*H*), 7.26 (m, 108 H, Ar-C*H*), 7.60 (s, 4H, Ar$_{BArF}$-*H*$_{para}$), 7.83 (s, 8H, Ar$_{BArF}$-*H*$_{ortho}$).

$^{13}C\{^1H\}$ NMR (THF-d_8, 101 MHz, 298 K): δ = 15.0 (Si-Pr^i-*C*H), 18.8 (Si-Pr^i-*C*H$_3$), 23.6 (Dipp-Pr^i-*C*H$_3$), 28.6 (Dipp-Pr^i-*C*H$_3$), 29.0 (Dipp-Pr^i-*C*H), 118.3, 121.5, 124.3, 126.1, 126.9, 128.9, 129.0, 129.4, 129.5, 129.6, 129.9, 130.2, 130.6, 131.4, 131.7, 133.3, 134.9, 135.7, 140.7, 148.2, 162.2, 162.7, 163.1, 163.6 (Ar-*C*).

$^{31}P\{^1H\}$ NMR (THF-d_8, 162 MHz, 298 K): δ = 37.2 (s, Ni-*P*Ph$_3$).

$^{29}Si\{^1H\}$ NMR (THF-d_8, 79 MHz, 298 K): δ = 17.3 (s, Pr$^i_3$-*Si*).

λ_{max}, nm (*ε*, Lmol^{-1}cm^{-1}): 323 (9384).

MS/LIFDI-HRMS found (calcd.) m/z: 988.3169 (988.3162) for [M-PPh$_3$]$^+$.

Anal. calcd. for $C_{107}H_{95}BF_{24}GeNNiP_3Si$: C, 60.79%; H, 4.53%; N, 0.66%; found: C, 60.31%; H, 4.54%; N, 0.75%. Repeated element analysis gave variable but consistently low values for C, possibly due to Si-carbide/Ni-carbide formation

[^{SiiP}DippSn·Ni^0(PPh$_3$)$_3$][BAr$^F_4$], 5. Compound **2** (300 mg, 0.62 mmol), Ni(cod)$_2$ (170 mg, 0.62 mmol), PPh$_3$ (485 mg, 1.85 mmol) and Na[BAr$^F_4$] (546 mg, 0.62 mmol) were mixed together in a Schlenk flasked and cooled to -78°C. 10 mL of toluene was slowly added to the flask and the resulting reaction mixture was slowly warmed to RT overnight leading to a dark blue precipitate within a light yellow solution. All volatiles were removed *in vacuo* and the residue was exctracted with fluorobenzene. The deep black solution was concentrated to approximately 2 mL and 5 mL of pentane were slowly added to the flask while constantly shaking the flask. The resulting solution was stored at -32°C overnight yielding a crop of dark blue crystals. The remaining solution was removed, and the crystals subsequently washed with toluene and pentane and dried *in vacuo* yielding **5** (595 mg, 0.28 mmol, 45%) as a blue crystalline powder. Dark blue-purple crystals which were suitable for X-Ray diffraction analysis were obtained from a concentrated fluorobenzene solution layered with pentane at RT after 24h.

^1H NMR (THF-d_8, 400 MHz, 233 K): δ = 0.83 (m, 24 H, Si-Pr^i-C*H*$_3$/Dipp-Pr^i-C*H*$_3$), 1.19 (d, 6 H, $^3J_{HH}$ = 6.5 Hz, Dipp-Pr^i-C*H*$_3$), 1.29 (m, 3 H, Si-Pr^i-C*H*), , 3.26 (hept, 2H, $^3J_{HH}$ = 6.3 Hz, Dipp-Pr^i-C*H*), 6.85 (m, 17 H, Ar-C*H*), 7.07 (t, 17 H, $^3J_{HH}$ = 7.5 Hz, Ar-C*H*), 7.18 (m, 2 H, Ar-C*H*), 7.41 (m, 12 H, Ar-C*H*), 7.65 (s, 4H, Ar$_{BArF}$-*H*$_{para}$), 7.85 (s, 8H, Ar$_{BArF}$-*H*$_{ortho}$).

$^{13}C\{^1H\}$ NMR (THF-d_8, 101 MHz, 233 K): δ = 15.5 (Si-Pr^i-*C*H), 18.8 (Si-Pr^i-*C*H$_3$), 23.6 (Dipp-Pr^i-*C*H$_3$), 28.5 (Dipp-Pr^i-*C*H$_3$), 28.8 (Dipp-Pr^i-*C*H), 115.9, 116.1, 118.3, 121.4, 124.1, 126.2, 126.4, 126.8, 128.3, 129.0, 129.6, 129.7, 129.8, 129.9, 130.2, 131.1, 131.2, 131.5, 134.4, 135.5, 135.9, 147.8, 162.2, 162.7, 163.2, 163.7 (Ar-*C*).

$^{31}P\{^{1}H\}$ NMR (THF-d_8, 162 MHz, 233 K): δ = 40.1 (s, Ni-*P*Ph_3).

^{119}Sn NMR (THF-d_8, 149 MHz, 233K): δ = 886 (s, N-*Sn*-Ni).

λ_{max}, nm (*ε*, $Lmol^{-1}cm^{-1}$): 350 (5520).

MS/LIFDI-HRMS found (calcd.) m/z: 726.2233 (726.2211) for $[M\text{-}2PPh_3\text{-}CH\text{-}C_3H_7+10H]^+$.

Anal. calcd. for $C_{107}H_{95}BF_{24}SnNNiP_3Si$: C, 59.50%; H, 4.43%; N, 0.65%; found: C, 57.67%; H, 4.20%; N, 0.74%. Repeated element analysis gave variable but consistently low values for C, possibly due to Si-carbide/Ni-carbide formation

N. B. It was not possible to obtain a $^{29}Si\{^{1}H]$ NMR spectrum of **5** due to the instability of this compound in THF-d_8.

Experiments with $[SbF_6][PPh_4]$:

4 (30 mg, 0.014 mmol) was mixed with $[PPh_4][SbF_6]$ (8 mg, 0.024 mmol) in a NMR tube. The solids were mixed with 0.4 mL PhF and 0.1 mL C_6D_6 and sonicated for 5 min in an ultrasonic water bath. After 12 h the mixture changed color from blue to brown. ^{1}H and $^{31}P\{^{1}H\}$ NMR showed that **4** had been completely consumed. A mixture of many different products had formed including the protonated ligand ^{SiiP}DippH.

5 (30 mg, 0.014 mmol) was mixed with $[PPh_4][SbF_6]$ (8 mg, 0.024 mmol) in a NMR tube. The solids were mixed with 0.4 mL PhF and 0.1 mL C_6D_6 and ultrasonicated for 5 min. After 12 h the mixture changed colour from blue to brown. ^{1}H and $^{31}P\{^{1}H\}$ NMR showed that **5** had completely been consumed. A mixture of many different products had formed including the protonated ligand ^{SiiP}DippH.

Ammonia experiments:

4 (30 mg, 0.014 mmol) was dissolved in 0.4 mL PhF and 0.1 mL C_6D_6 in a NMR tube. The NMR tube was filled with ammonia and then quickly closed and shaken. After 2 h the colour the reactions had changed from purple to brown. ^{1}H and $^{31}P\{^{1}H\}$ showed that **4** had completely been consumed. A mixture of many different products had formed including the protonated ligand ^{SiiP}DippH. Conducting at low-temperature had a similar outcome.

5 (30 mg, 0.014 mmol) was dissolved in 0.4 mL PhF and 0.1 mL C_6D_6 in a NMR tube. The NMR tube was filled with ammonia and then quickly closed and shaken. After 2 h the colour the reactions had changed from blue to brown. ^{1}H and $^{31}P\{^{1}H\}$ NMR showed that **5** had

completely been consumed. A mixture of many different products had formed including the protonated ligand ^{SiiP}DippH. Conducting at low-temperature had a similar outcome.

X-ray crystallographic details

Single crystals of **1**, **2**, **2**·KCl, **3**, **4**, and **5** suitable for X-ray structural analysis were mounted in perfluoroalkyl ether oil on a nylon loop and positioned in a 150 K cold N_2 gas stream. Data collection was performed with a STOE StadiVari diffractometer (MoKα radiation) equipped with a DECTRIS PILATUS 300K detector. Structures were solved by Direct Methods (SHELXS-97)[28] and refined by full-matrix least-squares calculations against F^2 (SHELXL-2018).[29] The positions of the hydrogen atoms were calculated and refined using a riding model. All non-hydrogen atoms were treated with anisotropic displacement parameters. Crystal data, details of data collections, and refinements for all structures can be found in their CIF files, which are available free of charge via www.ccdc.cam.ac.uk/data_request/cif, and are summarized in Table 5.2. Details for **3** are not given due to the unpublishable quality of the collected X-ray data. The structure for this compound is given in Figure 5.6, as proof of connectivity.

Table 5.2 Summary of X-ray crystallographic data for 1, 2, 2·KCl, 4, and 5.

	1	**2**	**2**·KCl	**4**·0.55(C_6H_5F),	**5**·C_6H_6
empiric	$C_{21}H_{38}ClGe$	$C_{42}H_{76}Cl_2N_2Si_2$	$C_{42}H_{76}Cl_3KN_2Si_2$	$C_{112.5}H_{103.2}BF_{24.6}GeNNi$	$C_{113}H_{101}BF_{24}NNiP_3$
formula	440.65	973.50	1048.05	2199.14	2238.15
crystal	monoclinic	triclinic	triclinic	triclinic	triclinic
space	*P2₁/n*	*P-1*	*P-1*	*P-1*	*P-1*
a (Å)	15.832(3)	9.148(2)	11.130(2)	13.186(3)	13.245(3)
b (Å)	9.619(2)	9.655(2)	14.968(3)	18.874(5)	18.891(4)
c (Å)	16.603(3)	15.011(3)	16.561(3)	22.343(6)	22.423(5)
α (deg.)	90	101.80(3)	72.19(3)	94.774(10)	94.60(3)
β (δεγ)	112.86(3)	96.15(3)	77.40(3)	103.543(11)	103.40(3)
γ (deg.)	90	109.26(3)	79.94(3)	92.404(12)	91.59(3)
vol ($Å^3$)	2329.9(9)	1203.1(5)	2546.1(10)	5376(2)	5434.2(2)
Z	4	1	2	2	2
ρ(calc)	1.257	1.343	1.367	1.359	1.368
μ (mm-	1.486	1.227	1.296	0.600	0.546
F(000)	936	504	1080	2261	2288
T (K)	150(2)	150(2)	150(2)	150(2)	150(2)
reflns	13412	16820	27458	48303	71208
unique	4014	4727	9943	21106	21204
R_{int}	0.0907	0.0131	0.0438	0.0346	0.1473
R1	0.0519	0.0167	0.0347	0.0590	0.0957
*w*R2	0.1094	0.0439	0.0631	0.1733	0.2688
CCDC	2143456	2143457	2143458	2143459	2143460

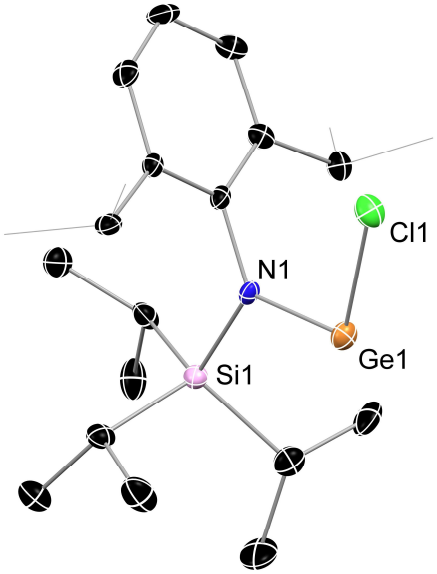

Figure 5.3 Molecular structure of ^{SiiP}DippGeCl, with thermal ellipsoids at 30% probability, hydrogen atoms omitted, and peripheral substituents in wire-frame for clarity. Selected bond lengths (Å) and angles (°): Ge1-N1 1.843(5); Ge1-Cl1 2.226(1); N1-Ge1-Cl1 100.1(1)

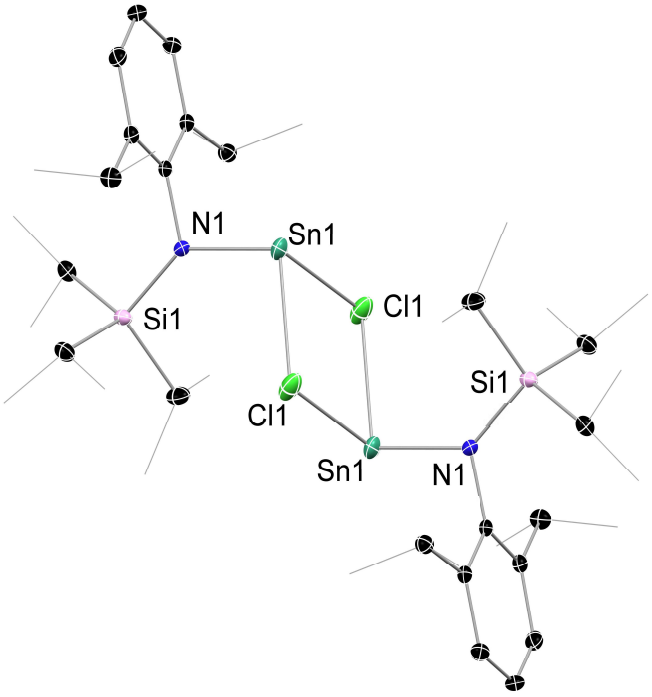

Figure 5.4 Molecular structure of [^{SiiP}DippSnCl]$_2$, with thermal ellipsoids at 30% probability, hydrogen atoms omitted, and peripheral substituents in wire-frame for clarity. The prime label (‘) indicates atoms at the equivalent position, (2-x, 1-y, 2-z). Selected bond lengths (Å) and angles (°): Sn1-N1 2.083(1); Sn1-Cl1 2.620(1); Sn1-Cl1’ 2.7290(9); Sn1···Sn1’ 4.081(2); N1-Sn1-Cl1 102.88(4); N1-Sn1-Cl1’ 103.19(4); N1-Sn1-Sn1’ 107.20(3).

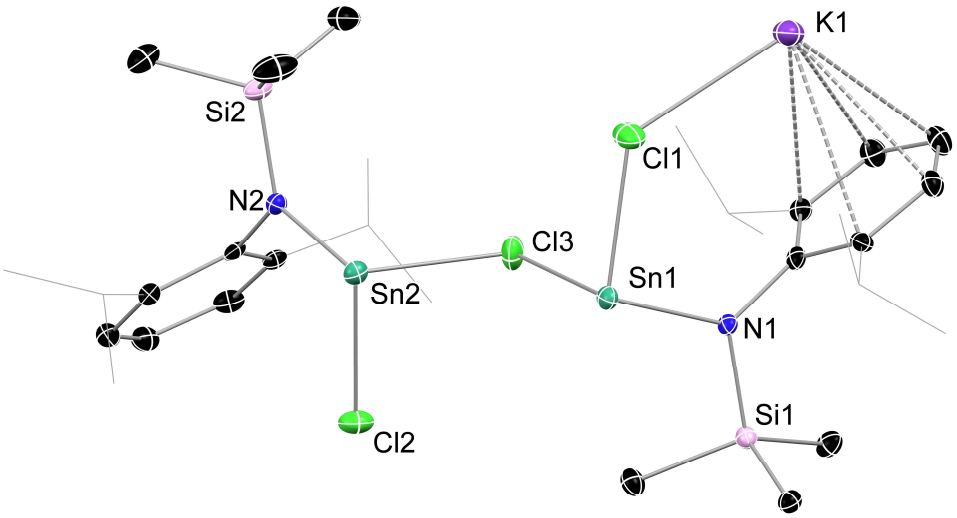

Figure 5.5 Molecular structure of [^{SiiP}DippSnCl]$_2$·KCl, with thermal ellipsoids at 30% probability, hydrogen atoms omitted, and peripheral substituents in wire-frame for clarity. Selected bond lengths (Å) and angles (°): N1-Sn1 2.116(3); Cl1-Sn1 2.470(1); Cl3-Sn1 2.664(1); N2-Sn2 2.125(3); Cl2-Sn2 2.475(1); Cl3-Sn2 2.631(1); Cl1-K1 2.948(2); Sn1···Sn2 3.929(1); Sn1-Cl3-Sn2 95.81(4) N1-Sn-Cl1 98.75(8); N1-Sn1-Cl3 96.22(8); N2-Sn2-Cl2 98.66(8); N2-Sn2-Cl3 98.91(8); Sn1-Cl3-Sn2 95.81(4).

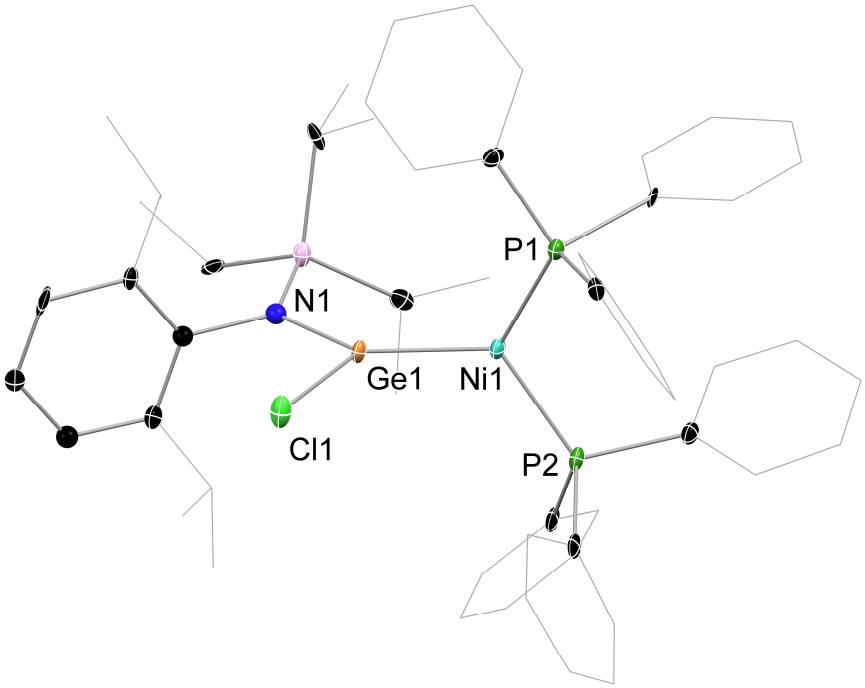

Figure 5.6 Molecular structure of **3**, with thermal ellipsoids at 30% probability, hydrogen atoms omitted, and peripheral substituents in wire-frame for clarity. Metrical parameters are not discussed due to the low quality of the collected data.

Computational methods and details

Computational experiments were performed using the Gaussian 16 program.[30] Geometry optimization was carried out at the ωB97XD level with the def2-TZVPP basis set for Ni, Ge, and Sn, and the def2-SVP basis set for all other atoms.[31] Stationary points were confirmed as true minima by vibrational frequency analysis (no negative eigenvalues). Bond indices (Wiberg Bond Index, Mayer Bond Order) and NPA charges were determined using the NBO 6.0 program implemented in Gaussian 09, using optimized geometries from above.[32] Dative interactions were determined through the NBO-derived second order perturbation theory analysis, and visualized in ChemCraft through combination of the associated MOs.

Table 5.3 Summary of NBO parameters for donor-acceptor orbitals in **4**.

		Orbital number	Occupancy	Composition (%)		
				s	*p*	*d*
Lone pairs	**Ge**	120	1.824	92.11	0.09	0.00
	Ni	121	1.970	0.00	0.02	99.98
	Ni	122	1.969	0.00	0.01	99.98
	Ni	123	1.966	0.04	0.02	99.93
	Ni	124	1.850	0.01	0.02	99.97
	Ni	125	1.766	0.00	0.02	99.98
Vacant orbitals	**Ge**	330	0.431	0.00	99.83	0.05
	Ge	331	0.400	0.17	99.53	0.22
	Ni	333	0.395	99.89	0.04	0.06

Table 5.4 Summary of NBO parameters for donor-acceptor orbitals in **5**.

		Orbital number	Occupancy	Composition (%)		
				s	*p*	*d*
Lone pairs	**Sn**	115	1.779	98.33	1.63	0.03
	Ni	116	1.973	0.21	0.11	99.68
	Ni	117	1.967	0.00	0.01	99.99
	Ni	118	1.964	0.01	0.02	99.97
	Ni	119	1.897	0.03	0.08	99.89
	Ni	120	1.843	0.09	0.17	99.75
Vacant orbitals	**Sn**	325	0.270	0.01	99.79	0.00
	Sn	326	0.251	0.02	99.73	0.18
	Ni	328	0.474	98.53	1.03	0.44

*NBO visualization of major contributions to the Ge-Ni donor-acceptor bonds in **4***

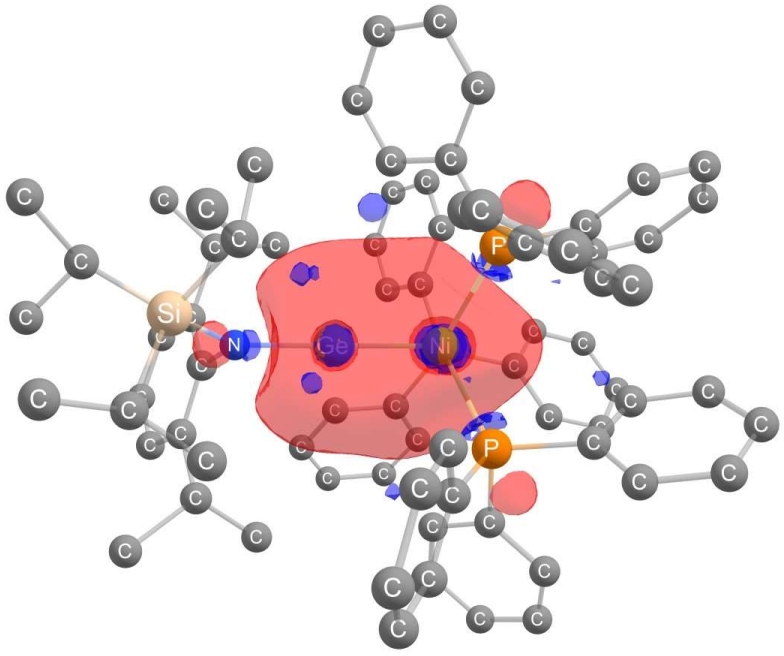

Figure 5.7 Ge→Ni donor interaction (MO120 to MO333, 92.40 kcalmol^{-1}).

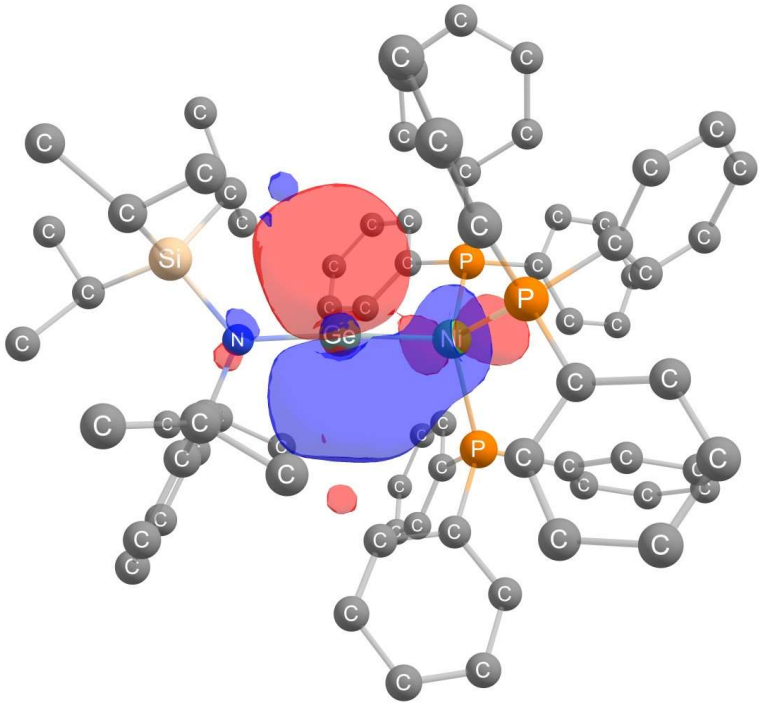

Figure 5.8 Ge→Ni donor interaction (MO124 to MO330, 18.98 kcalmol^{-1}).

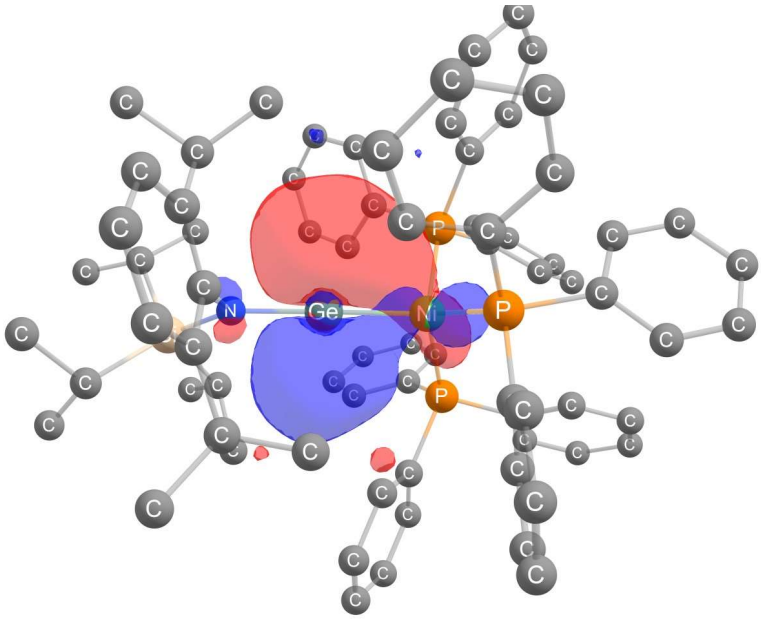

Figure 5.9 Ge→Ni donor interaction (MO125 to MO331, 28.00 kcalmol^{-1}).

*NBO visualization of major contributions to the Sn-Ni donor-acceptor bonds in **5***

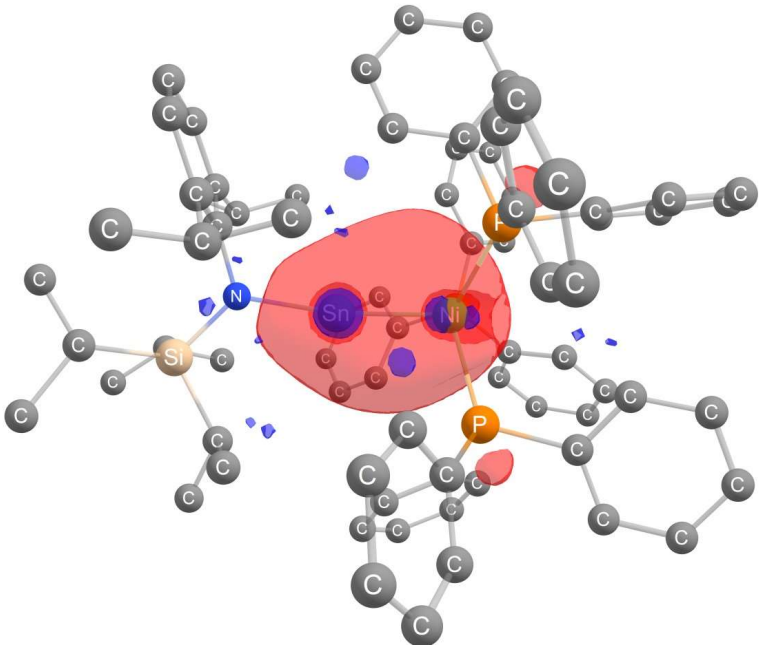

Figure 5.10 Ge→Ni donor interaction (MO115 to MO328, 141.27 kcalmol^{-1}).

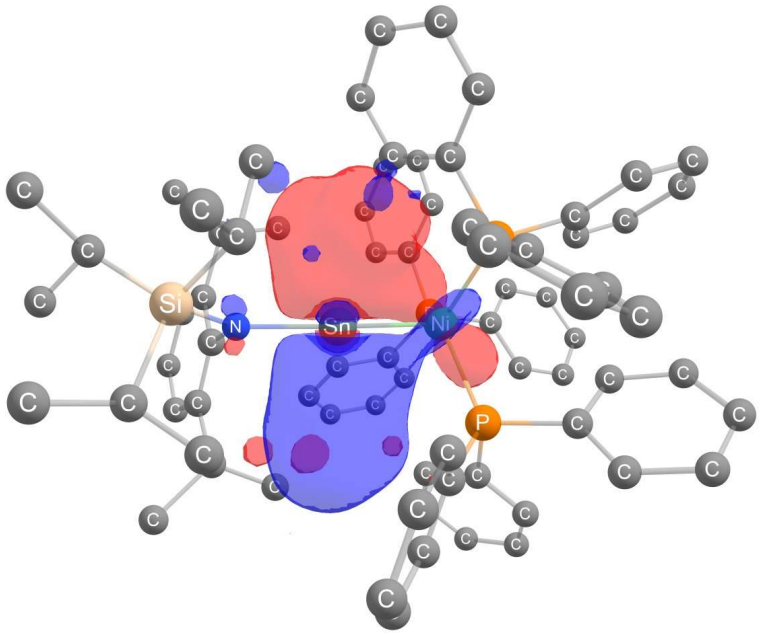

Figure 5.11 Ge→Ni donor interaction (MO119 to MO325, 6.24 kcalmol^{-1}).

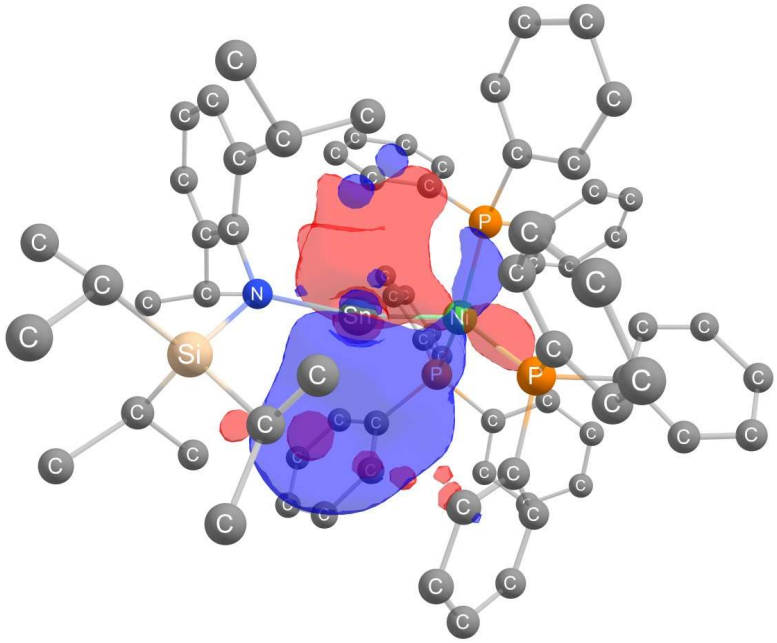

Figure 5.12 Ge→Ni donor interaction (MO120 to MO326, 10.80 kcalmol^{-1}.

References

1 L. R. Maurer, J. Rump, A. C. Filippou, *Inorganics* **2023**, *11*, 129–159.

2 (a) R. R. Schrock, *Science* **1983**, *219*, 13–18; (b) R. R. Schrock, *J. Chem. Soc., Dalton Trans.* **2001**, 2541–2550; (c) R. R. Schrock, *Angew. Chem. Int. Ed.* **2006**, *45*, 3748–3759; (d) R. R. Schrock, C. Czekelius, *Adv. Synth. Catal.* **2007**, *349*, 55–77; (e) R. H. Grubbs, A. G. Wenzel, D. J. O'Leary, E. Khosravi, Eds., *Handbook of Metathesis*, Wiley VCH, 2015.

3 (a) R. S. Mulliken, *J. Am. Chem. Soc.* **1950**, *72*, 4493–4503; (b) R. S. Mulliken, *J. Am. Chem. Soc.* **1955**, *77*, 884–887; (c) B. Hoogenboom, *J. Chem. Educ.* **1998**, *75*, 596–603.

4 (a) P. P. Power, *Chem. Rev.* **1999**, *99*, 3463–3504; (b) R. C. Fischer, P. P. Power, *Chem. Rev.* **2010**, *110*, 3877–3923; (c) P. P. Power, *Organometallics* **2020**, *39*, 4127–4138.

5 R. S. Simons, P. P. Power, *J. Am. Chem. Soc.* **1996**, *118*, 47, 11966–11967.

6 L. Pu, B. Twamley, S. T. Haubrich, M. M. Olmstead, B. V. Mork, R. S. Simons, Philip P. Power, *J. Am. Chem. Soc.* **2000**, *122*, 650–656.

7 A. C. Filippou, A. I. Philippopoulos, P. Portius, D. U. Neumann, *Angew. Chem. Int. Ed.* **2000**, *39*, 2778–2781.

8 (a) A. C. Filippou, O. Chernov, K. W. Stumpf, G. Schnakenburg, *Angew. Chem. Int. Ed.* **2010**, *49*, 3296–3300; (b) A. C. Filippou, B. Baars, O. Chernov, Y. N. Lebedev, G. Schnakenburg, *Angew. Chem. Int. Ed.* **2014**, *53*, 565–570; (c) T. Fukuda, T. Yoshimoto, H. Hashimoto, H. Tobita, *Organometallics* **2016**, *35*, 921–924; (d) A. C. Filippou, D. Hoffmann, G. Schnakenburg, *Chem. Sci.* **2017**, *8*, 6290–6299; (e) P. Ghana, M. I. Arz, G. Schnakenburg, M. Straßmann, A. C. Filippou, *Organometallics* **2018**, *37*, 772−780; (f) P. Ghana, M. I. Arz, U. Chakraborty, G. Schnakenburg, A. C. Filippou, *J. Am. Chem. Soc.* **2018**, *140*, 7187−7198.

9 (a) A. C. Filippou, P. Portius, A. I. Philippopoulos, *Organometallics* **2002**, *21*, 653–661; (b) A. C. Filippou, A. I. Philippopoulos, P. Portius, G. Schnakenburg, *Organometallics* **2004**, *23*, 4503–4512; (c) A. C. Filippou, G. Schnakenburg, A. I. Philippopoulos, N. Weidemann, *Angew. Chem. Int. Ed.* **2005**, *44*, 5979–5985; (d) A. C. Filippou, N. Weidemann, A. I. Philippopoulos, G. Schnakenburg, *Angew. Chem. Int. Ed.* **2006**, *45*, 5987–5991; (e) A. C. Filippou, A. Barandov, G. Schnakenburg, B. Lewall, M. van Gastel, A. Marchanka, *Angew. Chem. Int. Ed.* **2012**, *51*, 789 –793; (f) A. C. Filippou, K. W. Stumpf, O. Chernov, G. Schnakenburg, *Organometallics* **2012**, *31*, 748–755; (g) H. Hashimoto, T. Fukuda, H. Tobita, M. Ray, S. Sakaki, *Angew. Chem. Int. Ed.* **2012**, *51*, 2930–2933; (h) J. Hicks, T, J, Hadlington, C. Schenk, J. Li, C. Jones, *Organometallics* **2013**, *32*, 323–329; (i) A. C. Filippou, U. Chakraborty, G. Schnakenburg, *Chem. Eur. J.* **2013**, *19*, 5676–5686; (j) A. C. Filippou, D. Hoffmann, G. Schnakenburg, *Chem. Sci.* **2017**, *8*, 6290–6299; (k) Y. N. Lebedev, G. Schnakenburg, A. C. Filippou, *Organometallics* **2017**, *36*, 1530–1540; (l) J. D. Queen, A. C. Phung, C. A. Caputo, J. C. Fettinger, P. P. Power, *J. Am. Chem. Soc.* **2020**, *142*, 2233–2237.

10 (a) A. C. Filippou, P. Portius, A. I. Philippopoulos, H. Rohde, *Angew. Chem. Int. Ed.* **2003**, *42*, 445–447; (b) A. C. Filippou, A. I. Philippopoulos, G. Schnakenburg, *Organometallics* **2003**, *22*, 3339–3341; (c) A. C. Filippou, P. Ghana, U. Chakraborty, G. Schnakenburg, *J. Am. Chem. Soc.* **2013**, *135*, 11525–11528.

11 (a) A. C. Filippou, H. Rohde, G. Schnakenburg, *Angew. Chem. Int. Ed.* **2004**, *43*, 2243–2247; (b) A. C. Filippou, N. Weidemann, G. Schnakenburg, H. Rohde, A. I. Philippopoulos, *Angew. Chem. Int. Ed.* **2004**, *43*, 6512–6516; (c) A. C. Filippou, N. Weidemann, G. Schnakenburg, *Angew. Chem. Int. Ed.* **2008**, *47*, 5799–5802.

12 For examples of metallo-tetrylene systems and their conversion to tetrylidyne complexes, see refs. 8(b), 9(h), and 9(k). For further examples of metallotetrylenes, see:
(a) L. Pu, P. P. Power, I. Boltes, R. Herbst-Irmer, *Organometallics* **2000**, *19*, 352–356; (b) B. E. Eichler, A. D. Phillips, S. T. Haubrich, B. V. Mork, P. P. Power, *Organometallics* **2002**, *21*, 5622–5627; (c) H. Lei, J.-D. Guo, J. C. Fettinger, S. Nagase, P. P. Power, *Organometallics* **2011**, *30*, 6316–6322; (d) K. Inomata, T. Watanabe, H. Tobita, *J. Am. Chem. Soc.* **2014**, *136*, 14341–14344.

13 P. M. Keil, T. J. Hadlington, *Angew. Chem. Int. Ed.* **2022**, *61*, e202114143.

14 (a) I. C. Cai, M. I. Lipschutz, T. D. Tilley, *Chem. Commun.* **2014**, *50*, 13062–13065; (b) I. C. Cai, M. S. Ziegler, P. C. Bunting, A. Nicolay, D. S. Levine, V. Kalendra, P. W. Smith, K. V. Lakshmi, T. D. Tilley, *Organometallics* **2019**, *38*, 1648–1663.

15 J. Li, A. Stasch, C. Schenk, C. Jones, *Dalton Trans.* **2011**, *40*, 10448–10456.

16 We also note that on one occasion the interesting KCl adduct of the chlorostannylene, **2·KCl**, was crystallised in small quantities. We report here the X-ray crystal structure of this compound, but were not able to collect further analytical data.

17 (a) R. W. Chorley, P. B. Hitchcock, B. S. Jolly, M. F. Lappert, G. A. Lawless*, J. Chem. Soc., Chem. Commun*. **1991**, *18*, 1302–1303; (c) T. J. Hadlington, M. Hermann, J. Li, G. Frenking, C. Jones, *Angew. Chem. Int. Ed.* **2013**, *52*, 10199–10203.

18 These thin plates allowed us to ascertain the connectivity in this compound, but are not of a publishable standard.

19 P. M. Keil, T. Szilvási, T. J. Hadlington, *Chem. Sci.*, **2021**, *12*, 5582–5590.

20 We note that metallo-stannylenes are known to have a much lower field ^{119}Sn NMR chemical shift (*viz.* ref. 9(l)). Triply bonded species have shifts in the range δ = 1040 – 340 ppm. See ref. 9.

21 For the longest and shortest Ge-Ni bonds, respectively, see:
(a) D. Gallego, A. Brück, E. Irran, F. Meier, M. Kaupp, M. Driess, J. F. Hartwig, *J. Am. Chem. Soc.* **2013**, *135*, 15617–15626; (b) T. Watanabe, Y. Kasai, H. Tobito, *Chem. Eur. J.* **2019**, *25*, 13491–13495.

22 P. Pyykkç, S. Riedel, Michael Patzschke, *Chem. Eur. J.* **2005**, *11*, 3511–3520.

23 J. P. Zebrowski, R. K. Hayashi, L. F. Dahl, *J. Am. Chem. Soc.* **1993**, *115*, 1142–1144.
24 (a) I. C. Cai, M. I. Lipschutz, T. D. Tilley, *Chem. Commun.* **2014**, *50*, 13062–13065; (b) I. C. Cai, M. S. Ziegler, P. C. Bunting, A. Nicolay, D. S. Levine, V. Kalendra, P. W. Smith, K. V. Lakshmi, T. D. Tilley, *Organometallics* **2019**, *38*, 1648–1663.
25 A. J. Martínez-Martínez, A. S. Weller, *Dalton Trans.* **2019**, *48*, 3351–3354.
26 A. J. Sicard, R. T. Baker, *Org. Process Res. Dev.* **2020**, *24*, 2950–2952.
27 M. Muhr, P. Heiß, M. Schütz, R. Bühler, C. Gemel, M. H. Linden, H. B. Linden, R. A. Fischer, *Dalton Trans.* **2021**, *50*, 9031–9036.
28 G. M. Sheldrick, SHELXL-97, Program for Crystal Strucutre Refinement, Göttingen, 1997.
29 G. Sheldrick, *Acta Crystallogr., Sect. C: Struct. Chem.* **2015**, *71*, 3–8.
30 M. J. Frisch, G. W. Trucks, H. B. Schlegel, G. E. Scuseria, M. A. Robb, J. R. Cheeseman, G. Scalmani, V. Barone, G. A. Petersson, H. Nakatsuji et al., Gaussian 16 Rev. C.01, Wallingford, CT, **2016**.
31 a) A. D. Becke, *J. Chem. Phys*. **1997**, *107*, 8554–8560; (b) F. Weigend, R. Ahlrichs, *Phys. Chem. Chem. Phys.* **2005**, *7*, 3297–3305; (c) J.-D. Chai, M. Head-Gordon, *Phys. Chem. Chem. Phys.* **2008**, *10*, 6615–6620; (d) S. Grimme, J. Antony, S. Ehrlich, H. Krieg, *J. Chem. Phys*. **2010**, *132*, 154104.
32 Glendening, E. D., Badenhoop, J, K.; Reed, A. E.; Carpenter, J. E.; Bohmann, J. A.; Morales, C. M.; Landis, C. R.; Weinhold, F. Theoretical Chemistry Institute, University of Wisconsin, Madison, **2013**.

Chapter 6

Protonation of Hydrido-Tetrylenes: H_2 Elimination vs. Tetrylium Cation Formation

P. M. Keil, T. J. Hadlington, *Z. Anorg. Allg. Chem.* **2022**, *648*, e202200141.

All DFT calculations concerning this project were conducted by Dr. Terrance J. Hadlington.

Synopsis

The work described in Chapter 4, introduced cationic tetryliumylidenes into Ni^0 complexes through their *in-situ* generation directly from the (chloro)tetrylenes, ^{PhiP}DippECl (^{PhR}Dipp = [{$Ph_2PCH_2Si(R)_2$} (Dipp)N]$^-$; E = Ge, Sn). In this project, the aim was to gain access to the free cationic tetrylenes, [^{PhR}DippE]$^+$ (E = Ge, Sn), in order to implement these species in future projects for the synthesis of TM complexes. This avoids the formation of by-products when compared to the described one-pot route.

This proved to be rather straight-forward in the case of germanium, where chloride abstraction with Na[BAr^F_4] ([BAr^F_4]$^-$ = [{3,5-$(CF_3)_2C_6H_3$}$_4$B]$^-$) led to the isolation of [^{PhiP}DippGe]$^+$. However, this was not possible for the generation of [^{PhiP}DippSn]$^+$. Therefore, an alternative synthesis route was chosen, by first generating (hydrido)tetrylenes, ^{PhiP}DippEH, and further reacting these with the oxonium-ion salt, [$H(Et_2O)_2$][BAr^F_4]. For ^{PhiP}DippSnH this led to the release of H_2, forming the desired cationic stannylene, [^{PhiP}DippSn]$^+$. The same route was not amenable to obtain [^{PhiP}DippGe]$^+$, as the reaction of [$H(Et_2O)_2$][BAr^F_4] with ^{PhiP}DippGeH led to the cationic (dihydrido)germyl complex, [^{PhiP}DippGeH_2]$^+$. It should be noted that hydride abstraction employing [CPh_3][BAr^F_4] led to an easier workup, and overall to a better yield of the cationic stannylene, [^{PhiP}DippSn]$^+$. This was not reported as it was discovered after publication.

DFT calculations on 'ligand-reduced' derivatives of described cationic tetrylenes revealed rather large HOMO-LUMO gaps (Ge: 7.28 eV; Sn: 6.87 eV). The calculated LUMOs represent the vacant *p*-orbital at the tetrel element, while the HOMO can be seen as the lone pair at the tetrylene. This means that [^{PhiP}DippE]$^+$ should be ambiphilic. The coordination of DMAP to the cationic germylene, giving [^{PhiP}DippGe(DMAP)]$^+$, showcased the Lewis acidity of these compounds. Furthermore, [^{PhiP}DippGe]$^+$ exhibited reactivity towards ammonia, resulting in the loss of the [DippN] group (as $DippNH_2$), which is exchanged by an [NH] group (from NH_3), giving a dimeric cationic structure through N···Ge coordination.

In conclusion, we could successfully access the cationic tetrylenes $[^{PhiP}DippE]^+$ and (hydrido)tetrylenes $^{PhiP}DippEH$ of the $^{PhiP}Dipp$ ligand scaffold introduced in Chapter 4. The cationic tetrylenes $[^{PhiP}DippE]^+$ were obtained *via* chloride (for Ge with $Na[BAr^F_4]$) and hydride (for Sn with $[H(Et_2O)_2][BAr^F_4]$) abstraction, and further investigated concerning their electronic structure and reactivity. Interestingly, attempted hydride abstraction from $^{PhiP}DippGeH$ resulted in $[^{PhiP}DippGeH_2]^+$, rather than H_2 elimination. The cationic tetrylene ligands, $[^{PhiP}DippE]^+$, should lead to easier access to the corresponding cationic tetrylene-TM complexes, as discussed in Chapter 7.

Manuscript

The following sections are reproduced and formatted from the following article: P. M. Keil, T. J. Hadlington, *Z. Anorg. Allg. Chem.* **2022**, *648*, e202200141. *Experimental spectra (NMR, LIFDI/MS, UV/vis and IR) and further details concerning DFT calculations can be retrieved online* (https://doi.org/10.1002/zaac.202200141).

Abstract

We describe the reactions of amido-E^{II} hydride complexes, $^{PhiP}DippEH$ ($^{PhiP}Dipp$ = $\{[Ph_2PCH_2Si^iPr_2](Dipp)N\}^-$; Dipp = 2,6-$^iPr_2C_6H_3$; E = Ge (**5**), Sn (**6**)), towards the oxonium complex $[(Et_2O)_2H][BAr^F_4]$ (Ar^F = 3,5-CF_3-C_6H_3). For **5**, formation of the dihydro-tetrylium complex (*i.e.* $[^{PhiP}DippGeH_2][BAr^F_4]$, (**7**)) is favoured, in contrast to the same reaction for **6** which selectively leads to H_2 elimination, furnishing the novel tetryliumylidene $[^{PhiP}DippSn][BAr^F_4]$ (**4**). The related cationic Ge^{II} complex (*i.e.* $[^{PhiP}DippGe][BAr^F_4]$ (**3**)) could be accessed *via* the often utilised chloride abstraction route with $Na[BAr^F_4]$. The high Lewis acidity of this species has been demonstrated through the reaction of **3** towards the nitrogen bases, NH_3 and 4-dimethylaminopyridine. In the latter case, a classic donor-acceptor complex is formed. Conversely, for NH_3, the [DippN] fragment of the ligand is intriguingly displaced by [HN], presumably through double proton-transfer in loss of $DippNH_2$.

Introduction

Carbocations have been considered as some of the most reactive carbon species since the discovery of the first carbocation in 1901.[1] The chemistry of the heavier Group 14 cations ER_3^+ (E= Si, Ge or Sn) has been of growing interest in the last two decades, and has proved to display similar reactivity, but a much richer coordination chemistry due to their progressively

larger coordination sphere and more diffuse valence orbtials.[2] Closely related cationic tetrylenes, where E has an oxidation state of +2, are of particular interest, possessing a nucleophilic lone pair of electrons as well as two vacant *p*-orbitals, making them highly Lewis acidic ambiphilic compounds.[3] Their isolation can be achieved by utilising a weakly coordination anion (WCA), so forming highly reactive systems which typically require additional thermodynamic and/or kinetic stabilization. Nevertheless, remarkable examples of quasi one-coordinate amido E^{II} cations (E = Ge, Sn) have been isolated by Jones et al., stabilized by the extremely bulky (aryl)(silyl)amide ligand, L* (L* = {[2,6-$(Ph_2CH)_2$-4-MeC_6H_2](SiMe$_3$)N}$^-$). These species were accessed through chloride abstraction from (amido)(chloro)tetrylene precursors with the metal-aluminate salts, M[Al{$OC(CF_3)_3$}$_4$] (M = Li, Ag), eliminating LiCl or AgCl (Figure 6.1).[4] These are considered to be quasi one-coordinate cations since they bear only weak intramolecular arene stabilization.[5] Other examples of E^{II} cations include the use of cyclopentadienyl,[6] N-donor,[7] carbodiphosphorane,[8] carbene,[9] and phosphine ligands for additional stabilization.[10] Most commonly, these E^{II} cations are formed *via* halide abstraction from halo-tetrylene precursors (Figure 6.1(a)).

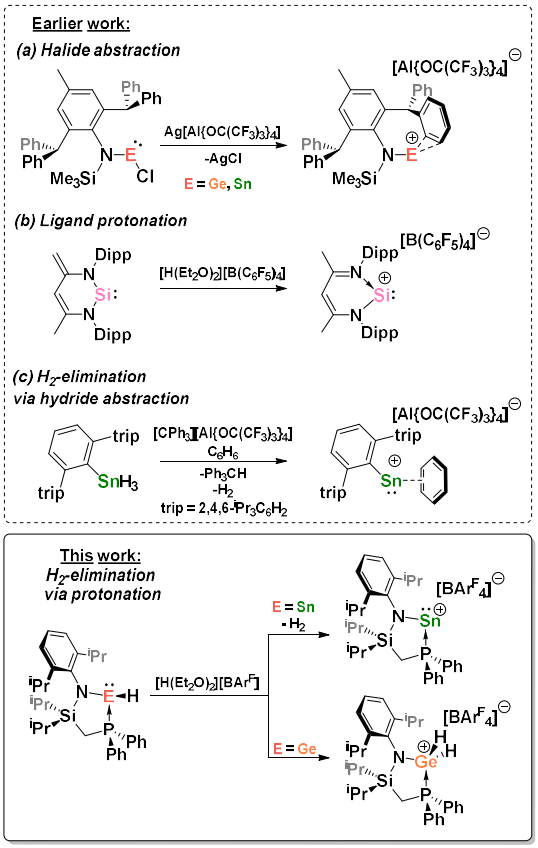

Figure 6.1 Selected known examples of low coordinate E^{II} cationic synthesis and the new synthetic route of H_2-elimination via protonation presented in this work.

Utilising an alternative route, Driess et al. showed that protonation of the unsaturated ligand scaffold of a diamino silylene with [$(Et_2O)_2$H][$B(C_6F_5)_4$] results in Nacnac-stabilized Si^{II} cations

(Figure 6.1(b)).[11] The group of Wesemann have more recently shown that H_2 elimination from aryl tin trihydride species is also a promising method for the generation of Sn^{II} cations (Figure 6.1(c)).[5] The further chemistry of tetryliumylidenes has demonstrated the activation of challenging chemical bonds in ammonia, silanes, boranes, and dihydrogen.[7d,9f,10] It was shown by Inoue et al. that a simple NHC-stabilized Ge^{II} cation is even an effective catalyst for challenging processes such as the hydrosilylation of CO_2, showing the great potential of this compound class.[12]

In our own work, we have recently reported the synthesis of (amido)(chloro)tetrylenes, featuring both mono-dentate and phosphine-functionalised bidentate amide ligands, which were utilized in the synthesis of cationic E^{II}-Ni^0 complexes (E = Ge, Sn).[13] In these cases, the tetrylenes were combined with Na[BAr^F_4] *in situ* in order to obtain cationic Ni^0 complexes. Given that our developed bidentate ligand systems led to Ni^0 complexes having a rich chemistry, such as hydrosilylation catalysis and reversible ammonia binding, we wished to develop synthetic routes to the free E^{II} cations, to investigate their chemistry and make them available as ligands towards TM complexes beyond those which we have already reported. Herein, we describe the successful synthesis of these phosphine stabilized E^{II} cations *via* two routes, including the novel protonation-H_2 elimination route. The further reactivity of the Ge^{II} cation is also described.

Results and Discussion

We first attempted to access the cations *via* simple chloride abstraction from the reported phosphine-stabilized (amido)(chloro)tetrylenes, ^{PhiP}DippGeCl (**1**) and ^{PhiP}DippSnCl (**2**) (^{PhiP}Dipp = {[$Ph_2PCH_2Si^iPr_2$](Dipp)N}$^-$) with Na[BAr^F_4] in DCM (Scheme 6.1). The reaction between **1** and Na[BAr^F_4] immediately became deep yellow after addition of DCM, with concomitant

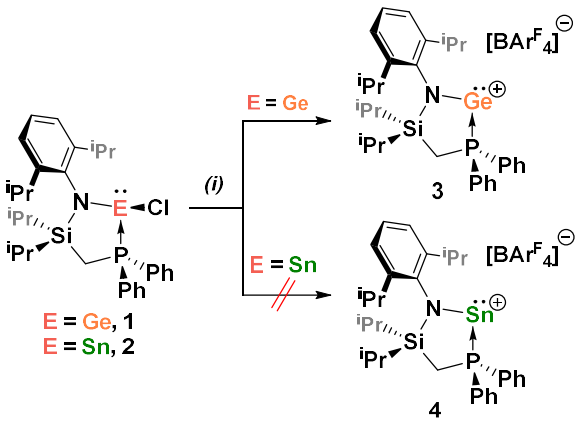

Scheme 6.1 Reaction of **1** with $NaBAr^F_4$ to give **3**, and unsuccessful conversion of **2** to **4**. *(i)* Na[BAr^F_4], DCM, 30 min.

formation of a white precipitate. Workup afforded a yellow powder of cationic complex

[^{PhiP}DippGe][BAr^F_4] (**3**) in good yields of up to 86%. The $^{31}P\{^1H\}$ NMR spectrum of **3** in THF-d_8 shows one singlet at 7.0 ppm, and a considerably more symmetrical ^1H NMR spectrum than the chloro-germylene precursor.[13a] Layering DCM solutions of **3** with pentane led to formation of large yellow crystalline blocks of this species, which confirmed the successful synthesis of **3** through X-ray diffraction analysis (Figure 6.2(a)).

Utilising the same route with **2**, we were not able to access to cationic species [^{PhiP}DippSn][BAr^F_4] (**4**). That is, the reaction of the Sn^{II} analogue **2** with Na[BAr^F_4] in DCM did not result in a color change, although did appear to form a single new species as ascertained from crude ^{31}P NMR spectra. However, from these reactions only an oily residue could be isolated, which provided no crystalline species in our hands. Varying the solvent (*e.g.* to PhF or Et_2O) did not improve this. Nevertheless, as integrations in ^1H NMR spectra of these oily residues did not match the potential Sn^{II} cation, we concluded that **4** did not form in this reaction.[14]

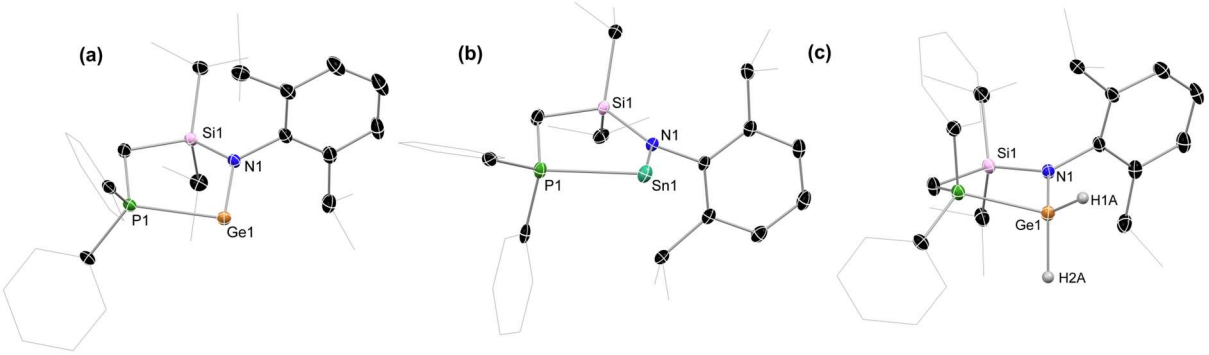

Figure 6.2 The molecular structures of (a) **3**, (b) **4**, and (c) **7**, with thermal ellipsoids at 25% probability. [BAr^F_4] anions and hydrogen atoms omitted for clarity, aside from hydrogen atoms of the GeH_2 moiety in **7**. Selected bond distances (Å) and angles (°) for **3**: Ge1-P1 2.461(1); Ge1-N1 1.822(3); N1-Ge1-P1 86.71(8) (1); For **5**: Sn1-P1 2.668(1); Sn1-N1 2.060(3); N1-Sn1-P1 81.22(8); for **7**: Ge1-P1 2.336(1); Ge1-N1 1.829(2); N1-Ge1-P1 92.60(8).

We have recently shown that the related hydrido, amido, and hydroxy Ge^{II}-Ni^0 complexes can be reacted with [$(Et_2O)_2H$][BAr^F_4] in the elimination of dihydrogen, ammonia, and water, respectively, to yield cationic Ge^{II}-Ni^0 complexes.[13b] Wesemann et al. have also shown that hydride abstraction from aryl tin trihydrides leads to dihydrogen elimination, resulting in the corresponding stannylene cations.[5] Therefore, we were curious as to whether the synthesis of the cationic tetrylenes (*viz.* **3** and **4**) could be possible *via* the analogous hydrido-tetrylenes, ^{PhiP}DippEH (E = Ge (**5**) and Sn (**6**)), which would then be protonated with [$(Et_2O)_2H$][BAr^F_4], in the loss of H_2. Hydride complexes **5** and **6** were readily accessed through reaction of **1** and **2** with K[HB^SBu_3] at -78°C (Scheme 6.2). The Ge^{II} derivative **5** is particularly straight forward to isolate, after simply filtering the reaction mixture, removing all volatiles, and washing with pentane. The Ge-*H* signal can be seen in the ^1H NMR spectrum of **5**, at 7.45 ppm, as a doublet through coupling to the phosphine moiety. It is also clearly visible in the IR spectrum as an

intense stretching band at 1758 cm^{-1}. For the Sn^{II} system, some decomposition can be seen upon warming crude reaction mixtures to ambient temperatures, indicated by dark brown reaction mixtures. Nevertheless, extracting these reaction mixtures with a combination of toluene and pentane precipitates the dark impurities, giving a colourless filtrate from which **6** crystallizes after storage at -32°C overnight. The ^{1}H NMR spectrum of **6** reveals a very low-field shift for the Sn-*H* moiety, as a doublet at 12.09 ppm, shifted lower than all bar one reported Sn^{II} hydride systems.[15] One set of Sn-satellites can also clearly be observed as doublets, with a $^{1}J_{SnH}$ coupling of 27.7 Hz, presumably with both ^{117}Sn and ^{119}Sn satellites overlapping. Clear $^{1}J_{SnP}$ satellites are observed are observed in the $^{31}P\{^{1}H\}$ NMR spectrum of this species (δ = -1.1 ppm; $^{1}J_{117SnP}$ = 1184 Hz; $^{1}J_{119SnP}$ = 1240 Hz). The IR spectrum of **6** has a sharp signal at 1619 cm^{-1} which can be attributed to the Sn-H stretching frequency.[15b] The X-ray crystal structures of **5** and **6** indicate three-coordinate E^{II} centres, with *pseudo*-tetrahedral geometry due to the presence of stereoactive lone pairs of electrons at these centres. Remaining metrical parameters are in keeping with our previously reported halo-tetrylenes bearing the same phosphine-functionalised amide ligands.[13a]

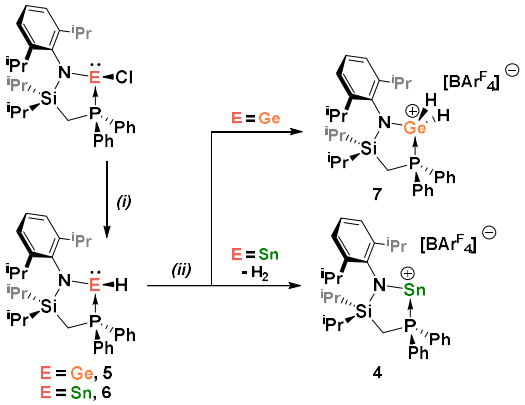

Scheme 6.2 Conversion of the tetrylene chlorides **1** and **2** to the tetrylenes hydrides **5** and **6** with K-Selectride followed by protonation to get the cationic complexes **7** and **4**. *(i)* K-Selectride, toluene, -78°C; *(ii)* $[(Et_2O)_2H][BAr^F_4]$, PhF, -40°C.

With these hydride complexes in hand, we attempted the synthesis of the cationic tetrylenes **3** and **4** by addition of fluorobenzene solutions of $[(Et_2O)_2H][BAr^F_4]$ to fluorobenzene solutions of **5** or **6** at -40°C (Scheme 6.2). For the Ge^{II} complex **5** no color change or gas evolution could be observed, but crude $^{31}P\{^{1}H\}$ NMR spectra clearly suggested formation of one new species, with a singlet resonance at δ = -0.8 ppm. After addition of pentane and storing the mixture at ambient temperature for three days, large colourless crystals could be isolated, revealing that the amido-germylium dihydride complex **7** had formed (Figure 6.2(c)). The ^{1}H NMR spectrum of **7** reveals a distinct shift of the Ge-*H* resonance, observed at δ = 7.45 ppm in **5**, now appearing as a doublet at δ = 6.37 ppm with a considerably larger $^{2}J_{PH}$ coupling of 35.1 Hz, and integrating to 2H. This is in keeping with the structure as determined by X-ray

crystallography, featuring a cationic GeH_2 moiety, which apparently does not eliminate H_2 to form **3**. The formally Ge^{IV} centre in **5** contains a tetrahedral, four coordinate cationic germanium centre, which electronically bears resemblance to the related (carbene)(boryl)germylium dihydride reported by Aldridge et al.,[16] as well as the terphenyl-ligated germylium complex recently reported by Wesemann et al..[5] The reactivity of the latter compound, which features a lower coordinate Ge centre, is seemingly amplified relative to **5**, represented by its C-H and arene activation reactions above 0 °C. Indeed, closely related E^{IV} cations (E = Si-Pb) are also known to strongly interact with C-C π-systems.[17] This would suggest that the flanking phosphine arm in **5** aids greatly in stabilizing this species. The IR spectrum of **5** confirms the presence of hydride ligands, featuring two Ge-H stretching bands at 1759 and 1611 cm^{-1}. Notably, attempts to thermally drive elimination of H_2 were unsuccessful, only resulting in decomposition.

In contrast to these findings, the reaction of the related Sn^{II} system, **6**, with $[(Et_2O)_2H][BAr^F{}_4]$ resulted in an immediate colour change to yellow, concomitant with gas evolution. Addition of pentane and storage at 4 °C led to formation of yellow crystals of **4** in a moderate yield. X-ray diffraction analysis of these crystals confirmed the formation of the Sn^{II} cation **4** (Figure 6.2(b)), presumably in a similar H_2 reductive elimination to known neutral and cationic Sn^{IV} poly-hydrides.[5,18] The $^{31}P\{^1H\}$ NMR spectrum of **4** in THF-d_8 contains a single singlet signal at δ = 16.5 ppm, with distinct ^{117}Sn and ^{119}Sn satellites ($^1J_{117Sn}$ = 1552 Hz; $^1J_{119SnP}$ = 1630 Hz). A doublet at δ = 31.6 ppm can be observed in the ^{119}Sn NMR, with a $^1J_{119SnP}$ coupling matching that observed in the $^{31}P\{^1H\}$ NMR spectrum.

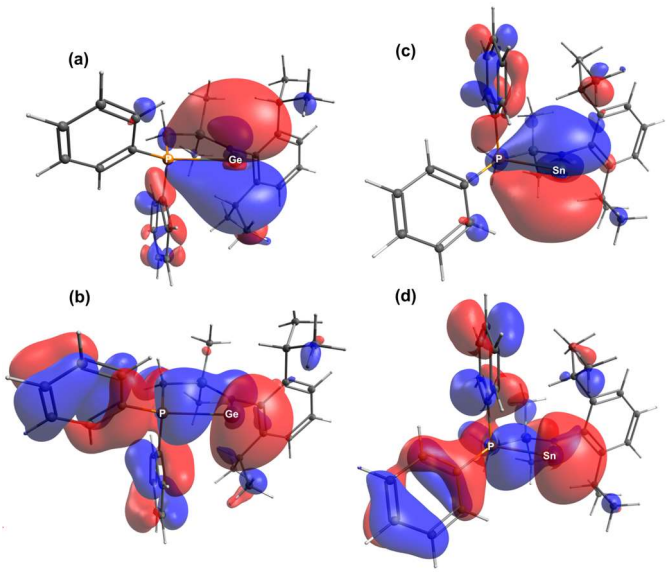

Figure 6.2 (a) The calculated LUMO of **3**; (b) the calculated HOMO-2 of **3**; (c) the calculated LUMO of **4**; (d) the calculated HOMO-2 of **4**.

The crystal structures of **3** and **4** show that the tetrel element centres are two-coordinate, bound by the amido ligand's N- and P-centres. A considerable contraction of the Ge-N and Sn-N bond distances (d_{GeN} = 1.822(3) Å, d_{SnN} = 2.060(3) Å) of roughly 0.1 Å and 0.06 Å, compared to the corresponding chloro-tetrylenes (d_{GeN} = 1.925(3) Å, d_{SnN} = 2.122(3) Å), can be observed.[13a,b] This can be attributed to the enhancement of the Lewis acidity leading to stronger electron donation of the N-centre to the vacant *p*-orbitals of the tetrel element centres. Interestingly, the Ge-P and Sn-P distances (d_{GeP} = 2.461(1) Å, d_{SnP} = 2.668(1) Å) are slightly elongated compared to the distances in the corresponding chloro-tetrylenes (d_{GeP} = 2.472(1) Å, d_{SnP} = 2.657(1) Å), despite the now cationic E^{II} centres, most likely caused by the increased $N \rightarrow E^{II}$ donation. The lowest energy conformation and the related frontier orbitals of the full molecules of **3** and **4** were calculated using Density Functional Theory (DFT).[19] For both systems, a large HOMO-LUMO gap was found (**3**: 7.28 eV; **4**: 6.87 eV), which would typically indicate that these species are not reactive towards relatively inter small molecules such as H_2.[20] Nevertheless, the Lewis acidity of these compounds it borne out by the LUMOs, which represent vacant *p*-orbitals localized at the E^{II} centres (Figure 6.3(a) and (c)). Lone electron pairs localized at the same centres can be found at the HOMO-2 level (Figure 6.3, (b) and (d)).

Following the successful isolation of the cations **3** and **4** *via* different routes, they were briefly screened in their reactivity in small molecule activation (Scheme 6.3), given that two-coordinate neutral tetrylenes, with which **3** and **4** are isoelectronic, are known to react with H_2,[21] NH_3,[22] CO_2,[23] and even CO.[24] As suggested by their wide HOMO-LUMO separations, neither of these cations showed any reaction towards H_2, despite the stability of the germylium dihydride **7**, which would represent the formal H_2 addition product of **3**. Reactions with CO, CO_2, and N_2O also did not proceed. The reaction of this Ge^{II} cation with DMAP, however, did

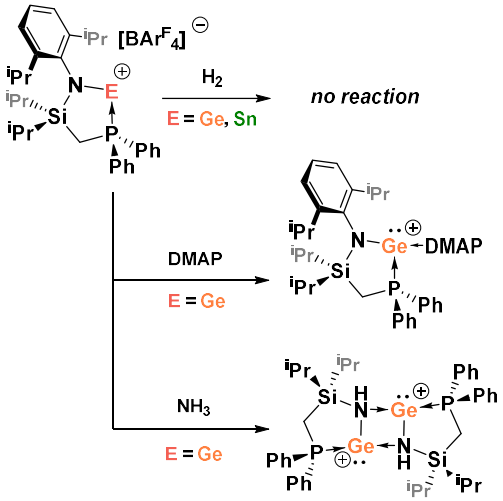

Scheme 6.3 Reaction of **3** with DMAP and ammonia giving the DMAP adduct **8** and the dimeric activation product **9**.

proceed, leading to discoloration of the reaction solution. Following work-up, colorless crystals could be isolated, which were found to be the three-coordinate Ge^{II} cation **8** through single-crystal X-ray diffraction analysis. Compound **8** is essentially isostructural with hydride complex **5**, with a *pseudo*-tetrahedral Ge^{II} centre. That is, DMAP coordination reduces the $^{Dipp}N\rightarrow Ge$ donation, leading to an elongation of this bond (d_{NGe} = 1.916(3) Å). A concomitant contraction of the P-Ge bond is also seen (d_{PGe} = 2.487(1) Å).

Reaction of **3** towards the protic N-base, ammonia, gave quite different results. Whilst our previously reported Ni^0 complex, $[^{PhiP}DippGe]^+\cdot[Ni(PPh_3)_2]$, reversibly binds ammonia at the Ge^{II} centre,[13b] addition of ammonia to solutions of **3** irreversibly leads to colorless solutions after carefully agitating the solution for 5 min. Remarkably, an X-ray diffraction analysis of crystals isolated from such reactions revealed the unexpected product **9** formed through complete elimination of the [NDipp] fragment of the ligand, now replaced by an [NH] unit (Figure 6.4(b)).

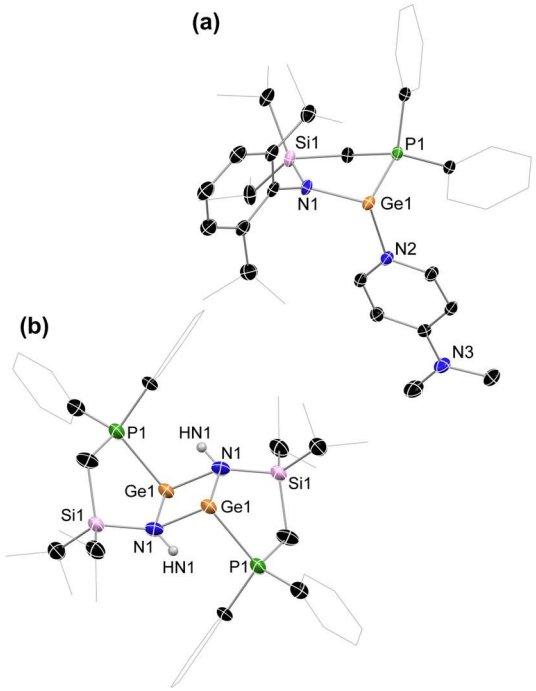

Figure 6.4 The molecular structures of the cation parts in (a) **8**, and (b) **9**, with thermal ellipsoids at 25% probability, and hydrogen atoms omitted for clarity. Selected bond distances (Å) and angle (°) for **8**: Ge1-P1 2.487(1); Ge1-N1 1.916(3); Ge1-N2 2.096(3); N1-Ge1-P1 86.99(8); For **9**: Ge1-P1 2.472(3); Ge1-N1 2.021(1); Ge1-N1' 2.053(9); Ge1···Ge1' 3.064(2); N1-N1' 2.686(1); P1-Ge1-N1 86.2(3); P1-Ge1-N1' 90.3(3); Ge1-N1-Ge1' 97.5(4); N1-Ge1-N1' 82.5(3); P1-Ge1-Ge1' 87.63(8).

Due to the reduced steric bulk, the cationic complex **9** forms a dimeric structure where the [NH] functionalities bridge the two cationic Ge^{II} centres, which has a crystallographic plane of symmetry cutting the central $[Ge_2N_2]$ ring. A degree of delocalization in this central unit can be assumed, given the two very similar Ge-N bond lengths of 2.021(1) and 2.053(9) Å. The P-Ge

bond distances are in keeping with those observed in DMAP adduct **8** (d_{PGe} = 2.472(3) Å), as one might expect given the similar coordination nature at Ge^{II} in these compounds. The N-*H* unit in **9** can be seen as a doublet in the ^{1}H NMR spectrum of this species, at δ = 5.01 ppm, coupling to the two chelating phosphine arms in a symmetrical manner, giving further evidence for a delocalized bonding model in the central [Ge_2N_2] ring system. The loss of the characteristic Dipp signals, *e.g.* those of the isopropyl C*H* and CH_3 groups, is in keeping with the observed solid-state structure whereby the DippNH_2 fragment has been entirely eliminated. A similar phosphine stabilized amido Ge^{II} cation reported by Aldridge et al. also insights reactive non-innocence of the neighboring N-Dipp unit, the ammonia adding across the Ge-N bond resulting in a $GeNH_2$ unit and a cationic nitrogen atom.[10]

Conclusions

As a whole, we have shown that the cations **3** and **4** can be synthesized from their chloro-tetrylenes **1** and **2**. This can either be done by chloride abstraction in the case of Ge^{II} to isolate **3** or by H_2 elimination *via* protonation of the Sn^{II} hydride **6** to get **4**. When the protonation was attempted with the Ge^{II} hydride **5**, H_2 elimination was not observed, resulting in the cationic Ge^{IV} dihydride **7**. The reactivity and Lewis acidity of the cationic tetrylenes **3** and **4** was analyzed by reacting **3** with DMAP and ammonia. Whilst the reaction with DMAP results in the expected DMAP adduct **8**, ammonia is cooperatively activated in an unusual manner leading to the elimination of DippNH_2 in exchange for an [NH] fragment, forming novel cationic tetrylene **9**. For future research, the cationic tetrylenes **3** and **4** can be employed as ligands directly, avoiding *in situ* generation, allowing for more controlled synthesis of transition metal complexes, in contrast to our previously utilized 'uncontrolled' one pot synthesis of Ni^0 complexes.

Supporting Information

General experimental considerations

All experiments and manipulations were carried out under dry oxygen free argon atmosphere using standard Schlenk techniques or in a MBraun inert atmosphere glovebox containing an atmosphere of high purity argon. C_6D_6 was dried, degassed and stored over a potassium mirror. All other solvents were dried over activated 4Å mol sieves. ^{PhiP}DippGeCl,[13a] ^{PhiP}DippSnCl,[13b] Na[BAr^F_4] ([BAr^F_4]$^-$ = [B(3,5-CF_3-C_6H_3)$_4$]),[25] and [$(Et_2O)_2H$][BAr^F_4] [26] were synthesized according to known literature procedures. All other reagents were used as received. NMR spectra were recorded on a Bruker AV 400 Spectrometer. The ^{1}H and ^{13}C{^{1}H} NMR spectra were referenced to the residual solvent signals as internal standards. ^{29}Si{^{1}H} NMR spectra were externally calibrated with $SiMe_4$. ^{31}P{^{1}H} NMR spectra were

externally calibrated with H_3PO_4. $^{119}Sn\{^1H\}$ NMR spectra were externally calibrated with $SnMe_4$. Liquid Injection Field Desorption Ionization Mass Spectrometry (LIFDI-MS) was measured directly from an inert atmosphere glovebox with a Thermo Fisher Scientific Exactive Plus Orbitrap equipped with an ion source from Linden CMS.[27] For the ammonia experiments ammonia 5.0 was used. Elemental analyses (C, H, N) were performed with a combustion analyzer (elementar vario EL, Bruker). Infrared spectra were measured with the Alpha FT IR from Bruker containing a platinum diamond ATR device.

Experimental procedures

[^{PhiP}DippGe][BAr$^F_4$], 3. A solid mixture of **1** (2.50 g, 4.19 mmol) and Na[BAr$^F_4$] (3.71 g, 4.19 mmol) was dissolved in DCM at ambient temperature and stirred for 30 min. The resulting light-yellow suspension was filtered, and all volatiles removed *in vacuo*. The resulting yellow residue was washed with pentane twice and dried *in vacuo* yielding analytically pure **3** (5.12 g, 86%) as a pale yellow powder. Yellow crystals suitable for X-ray diffraction were obtained from a concentrated DCM solution layered with pentane stored for 4 days at ambient temperature.

^{1}H NMR (THF-d_8, 400 MHz, 298 K): δ = 0.81 (d, 6H, $^3J_{HH}$ = 7.3 Hz, Si-Pr^i-C*H*$_3$), 1.06 (m, 8H, Dipp-Pr^i-C*H*$_3$, Si-Pr^i-C*H*), 1.13 (d, 6H, $^3J_{HH}$ = 6.7 Hz, Dipp-Pr^i-C*H*$_3$), 1.24 (d, 6H, $^3J_{HH}$ = 7.3 Hz, Si-Pr^i-C*H*$_3$), 2.54 (d, 2H, $^2J_{HP}$ = 16.1 Hz, C*H*$_2$-PPh$_2$), 3.04 (hept, 2H, $^2J_{HP}$ = 6.5 Hz, Dipp-Pr^i-C*H*), 7.18 (s, 3H, Ar-C*H*), 7.58 (s, 4H, Ar$_{BArF}$-*H*$_{para}$), 7.68 (m, 6H, Ar-C*H*), 7.80 (s, 8H, Ar$_{BArF}$-*H*$_{ortho}$), 7.97 (m, 4H, Ar-C*H*).

^{31}P{^{1}H} NMR (THF-d_8, 162 MHz, 298 K): δ = 7.0 (s, *P*Ph$_2$)

^{13}C{^{1}H} NMR (THF-d_8, 101 MHz, 298 K): δ = 2.3 (*C*H$_2$-PPh$_2$), 17.0 and 17.0 (Si-Pr^i-*C*H), 19.0 and 20.2 (Si-Pr^i-*C*H$_3$), 22.9 and 28.9 (Dipp-Pr^i-*C*H$_3$), 29.2 (Dipp-Pr^i-*C*H), 118.4, 121.6, 124.3, 125.4, 127.0, 127.7, 128.1, 128.5, 129.7, 130.1, 130.3, 130.7, 131.1, 131.2, 133.0, 133.1, 134.1, 134.1, 135.8, 148.0, 162.2, 162.7, 163.2 and 163.7(Ar-*C*).

^{29}Si{^{1}H} NMR (THF-d_8, 99 MHz, 298 K): δ = 24.4 (d, $^2J_{SiP}$ = 10.8 Hz, CH$_2$-*Si*-Pr$^i_2$).

MS/LIFDI-HRMS found (calcd.) m/z: 562.2057 (562.2114) for [M-BAr$^F_4$]$^+$.

Anal. calcd. for $C_{21}H_{38}ClNSiSn$: C, 53.12%; H, 3.89%; N, 0.98%; found: C, 53.07%; H, 3.85%; N, 1.21%.

[^{PhiP}DippSn][BAr$^F_4$], 4. A solution of [(Et$_2$O)$_2$H][BAr$^F_4$] (250 mg, 0.247 mmol) in PhF was added dropwise to a solution of **6** (150 mg, 0.247 mmol) in PhF at -40°C with stirring, resulting in a light yellow solution. This was allowed to warm to ambient temperature, leading to dark brown

suspension which was filtered and concentrated *in vacuo* to ~2 mL. Addition of 10 mL of pentane led to a light yellow solution formation of some dark droplets of oil. The solution was separated from the oil *via* canula transfer, and placed at 4°C overnight yielding light yellow crystals of **4** (130 mg, 36%), which were suitable for X-ray diffraction analysis.

^{1}H NMR (THF-d_8, 400 MHz, 298 K): δ = 0.81 (d, 6H, $^{3}J_{HH}$ = 7.3 Hz, Si-Pr^{i}-C*H*$_3$), 1.04 (m, 8H, Dipp-Pr^{i}-C*H*$_3$, Si-Pr^{i}-C*H*), 1.11 (d, 6H, $^{3}J_{HH}$ = 6.7 Hz, Si-Pr^{i}-C*H*$_3$), 1.23 (d, 6H, $^{3}J_{HH}$ = 7.4 Hz, Dipp-Pr^{i}-C*H*$_3$), 2.50 (d, 2H, $^{2}J_{HP}$ = 15.2 Hz, C*H*$_2$-PPh$_2$), 3.18 (hept, 2H, $^{2}J_{HP}$ = 6.8 Hz, Dipp-Pr^{i}-C*H*), 7.13 (m, 3H, Ar-C*H*), 7.58 (s, 4H, Ar$_{BArF}$-*H*$_{para}$), 7.65 (m, 6H, Ar-C*H*), 7.80 (s, 8H, Ar$_{BArF}$-*H*$_{ortho}$), 7.91 (m, 4H, Ar-C*H*).

^{31}P{^{1}H} NMR (THF-d_8, 162 MHz, 298 K): δ = 16.5 (s, *P*Ph$_2$, $^{1}J_{117SnP}$ = 1552 Hz, $^{1}J_{119SnP}$ = 1630 Hz).

^{13}C{^{1}H} NMR (THF-d_8, 101 MHz, 298 K): δ = 4.3 (*C*H$_2$-PPh$_2$), 17.2 and 17.2 (Si-Pr^{i}-*C*H), 18.9 and 20.1 (Si-Pr^{i}-*C*H$_3$), 23.3 and 28.6 (Dipp-Pr^{i}-*C*H$_3$), 29.2 (Dipp-Pr^{i}-*C*H), 118.4, 121.6, 124.3, 125.3, 126.4, 127.0, 129.3, 129.7, 130.0, 130.4, 130.6, 131.0, 131.1, 133.2, 133.3, 133.6, 133.7, 135.7, 141.1, 141.2, 147.3, 162.2, 162.7, 163.2 and 163.7(Ar-*C*).

^{29}Si{^{1}H} NMR (THF-d_8, 99 MHz, 298 K): δ = 18.6 (d, $^{2}J_{SiP}$ = 6.9 Hz, CH$_2$-*Si*-Pr$^{i}_2$).

^{119}Sn NMR (THF-d_8, 149 MHz, 233K): δ = 31.6 (d, $^{1}J_{SnP}$ = 1630 Hz, *Sn*-PPh$_2$).

MS/LIFDI-HRMS found (calcd.) m/z: 608.1860 (608.1924) for [M-BAr$^{F}_4$]$^{+}$.

Anal. calcd. for $C_{21}H_{38}ClNSiSn$: C, 51.45%; H, 3.77%; N, 0.95%; found: C, 52.27%; H, 3.86%; N, 1.08%.

^{PhiP}DippGeH, 5. A solution of **1** (1.28 g, 2.14 mmol) in toluene was cooled to -78°C, and a solution of K-Selectride (1M in THF, 2.14 mL, 2.14 mmol) slowly added. The mixture was subsequently allowed to warm to ambient temperature. The light orange mixture was filtered, and all volatiles were removed *in vacuo*. The oily residue was extracted in pentane, filtered, and concentrated to ~20 mL. The solution was placed at -32°C overnight leading to a crop of light yellow crystals. The solution was decanted with a canula, the crystals washed with pentane (1 x 5 mL), and dried *in vacuo* to afford **5** (0.53 g, 44%) as a light yellow crystalline solid. Crystals suitable for X-ray diffraction analysis were obtained from a concentrated pentane solution at ambient temperature after 1 day.

^{1}H NMR (C_6D_6, 400 MHz, 298 K): δ = 0.74 (d, 3H, $^{3}J_{HH}$ = 7.1 Hz, Si-Pr^{i}-C*H*$_3$), 0.89 (d, 3H, $^{3}J_{HH}$ = 6.7 Hz, Dipp-Pr^{i}-C*H*$_3$), 1.00 (d, 3H, $^{3}J_{HH}$ = 6.9 Hz, Dipp-Pr^{i}-C*H*$_3$), 1.07 (m, 1H, Si-Pr^{i}-C*H*), 1.16 (m, 6H, Si-Pr^{i}-C*H*$_3$), 1.36 (d, 3H, $^{3}J_{HH}$ = 7.4 Hz, Si-Pr^{i}-C*H*$_3$), 1.42 (d, 3H, $^{3}J_{HH}$ = 6.8 Hz,

Dipp-Pr^i-C*H*$_3$), 1.46 (d, 3H, $^3J_{HH}$ = 6.8 Hz, Dipp-Pr^i-C*H*$_3$), 1.77 (m, 3H, Si-Pr^i-C*H,* C*H*$_2$-PPh$_2$), 2.87 (hept, 1H, $^3J_{HH}$ = 6.7 Hz, Dipp-Pr^i-C*H*), 4.11 (hept, 1H, $^3J_{HH}$ = 6.9 Hz, Dipp-Pr^i-C*H*), 6.95 (m, 3H, Ar-C*H*), 7.07 (m, 6H, Ar-C*H*), 7.45 (d, 1H, $^2J_{HP}$ = 5.8 Hz, Ge-*H*), 7.50 (m, 2H, Ar-C*H*), 7.65 (m, 2H, Ar-C*H*).

^{31}P{^{1}H} NMR (C_6D_6, 162 MHz, 298 K): δ = 9.2 (s, *P*Ph$_2$)

^{13}C{^{1}H} NMR (C_6D_6, 101 MHz, 298 K): δ = 9.2 (*C*H$_2$-PPh$_2$), 15.9 and 16.1 (Si-Pr^i-*C*H), 18.0, 19.7, 20.4 and 20.7 (Si-Pr^i-*C*H$_3$), 23.0, 23.3, 26.9 and 27.2 (Dipp-Pr^i-*C*H$_3$), 28.0 and 28.6 (Dipp-Pr^i-*C*H), 123.3, 123.9, 124.1, 129.0, 129.0, 129.1, 129.1, 130.6, 130.7, 130.8, 130.9, 132.0, 132.3, 132.5, 132.6, 132.7, 132.8, 134.4, 134.6, 146.3, 146.3, 147.1, 147.2, 148.5 and 148.5 (Ar-*C*).

^{29}Si{^{1}H} NMR (C_6D_6, 99 MHz, 298 K): δ = 10.1(d, $^2J_{SiP}$ = 10.2 Hz, CH$_2$-*Si*-Pr$^i_2$).

MS/LIFDI-HRMS found (calcd.) m/z: 562.2086 (562.2114) for $[M-H]^+$.

Anal. calcd. for $C_{21}H_{38}ClNSiSn$: C, 66.21%; H, 7.89%; N, 2.49%; found: C, 66.20%; H, 8.15%; N, 2.59%.

IR, *ṽ*/cm^{-1} (ATR): 1758 (s, m, Ge-H).

^{PhiP}DippSnH, 6. A solution of **2** (2.51 g, 3.90 mmol) in toluene was cooled to -78°C and a solution of K-Selectride (1M in THF, 3.90 mL, 3.90 mmol) was slowly added. The mixture was subsequently allowed to warm to ambient temperature, during which time the color of the mixture changed from orange to dark brown. The mixture was concentrated, and pentane was added until a dark precipitate had formed. The mixture was filtered and placed at -32°C overnight, leading to a crop of colorless crystals. The solution was removed *via* canula, the crystals washed with pentane (~5 mL) and dried *in vacuo* to yield **6** (1.85 g, 3.04 mmol, 78%) as an off-white crystalline solid. Crystals suitable for X-ray diffraction analysis were obtained from a concentrated pentane solution stored at ambient temperature, after 1 day.

^{1}H NMR (C_6D_6, 400 MHz, 298 K): δ = 0.77 (d, 3H, $^3J_{HH}$ = 7.2 Hz, Si-Pr^i-C*H*$_3$), 0.93 (d, 3H, $^3J_{HH}$ = 6.7 Hz, Dipp-Pr^i-C*H*$_3$), 1.00 (d, 3H, $^3J_{HH}$ = 6.9 Hz, Dipp-Pr^i-C*H*$_3$), 1.06 (m, 1H, Si-Pr^i-C*H*), 1.14 (d, 3H, $^3J_{HH}$ = 7.3 Hz, Si-Pr^i-C*H*$_3$), 1.23 (d, 3H, $^3J_{HH}$ = 7.4 Hz, Si-Pr^i-C*H*$_3$), 1.38 (m, 9H, Dipp-Pr^i-C*H*$_3$), 1.75 (m, 2H, Si-Pr^i-C*H,* C*H*$_2$-PPh$_2$), 2.00 (m, 1H, C*H*$_2$-PPh$_2$), 3.01 (hept, 1H, $^3J_{HH}$ = 6.8 Hz, Dipp-Pr^i-C*H*), 4.19 (hept, 1H, $^3J_{HH}$ = 6.9 Hz, Dipp-Pr^i-C*H*), 6.96 (m, 3H, Ar-C*H*), 7.05 (m, 5H, Ar-C*H*), 7.16 (m, 1H, Ar-C*H*), 7.56 (m, 4H, Ar-C*H*), 12.09 (d, 1H, $^2J_{HP}$ = 4.5 Hz, Sn-*H; S*n-satellites (d, $^1J_{HSn}$ = 14.1 Hz) and (d, $^1J_{HSn}$ = 14.1 Hz)).

$^{31}P\{^1H\}$ NMR (C_6D_6, 162 MHz, 298 K): δ = -1.1 (s, *P*Ph_2, $^1J_{117SnP}$ = 1184 Hz, $^1J_{119SnP}$ = 1240 Hz).

$^{13}C\{^1H\}$ NMR (C_6D_6, 101 MHz, 298 K): δ = 11.4 (*C*H_2-PPh_2), 16.1 and 16.7 (Si-Pr^i-*C*H), 18.2, 19.6, 20.2 and 20.9 (Si-Pr^i-*C*H_3), 23.1, 23.6, 26.9 and 27.0 (Dipp-Pr^i-*C*H_3), 27.7 and 28.3 (Dipp-Pr^i-*C*H), 123.1, 123.3, 124.1, 129.1, 129.1, 129.2, 129.2, 130.6, 130.6, 130.9, 130.9, 131.8, 132.1, 132.8, 132.9, 132.9, 133.0, 134.9, 135.1, 145.4, 145.4, 147.6, 147.7, 148.4 and 148.4 (Ar-*C*).

$^{29}Si\{^1H\}$ NMR (C_6D_6, 99 MHz, 298 K): δ = 7.72 (d, $^2J_{SiP}$ = 9.2 Hz, CH_2-*Si*-Pr$^i_2$).

^{119}Sn NMR (C_6D_6, 149 MHz, 233K): δ = -86.5 (d, $^1J_{SnP}$ = 1240 Hz, *Sn*-PPh_2).

MS/LIFDI-HRMS found (calcd.) m/z: 608.1893 (608.1924) for $[M-H]^+$.

Anal. calcd. for $C_{21}H_{38}ClNSiSn$: C, 61.19%; H, 7.29%; N, 2.30%; found: C, 60.70%; H, 7.01%; N, 2.44%.

IR, *ν*/cm^{-1} (ATR): 1619 (s, m, Sn-H).

[^{PhiP}DippGeH_2][BAr^F_4], 7. A solid mixture of **5** (200 mg, 0.36 mmol) and [$(Et_2O)_2H$][BAr^F_4] (360 mg, 0.36 mmol) was dissolved in PhF at ambient temperature and stirred for 30 min. All volatiles were removed from the solution *in vacuo*, and pentane (10 mL) added. The solution was placed at 4°C overnight yielding colorless crystals of **7** (352 mg, 0.25 mmol, 69%), which were suitable for X-ray diffraction analysis.

^1H NMR (THF-d_8, 400 MHz, 298 K): δ = 0.83 (d, 6H, $^3J_{HH}$ = 7.4 Hz, Si-Pr^i-C*H*$_3$), 1.05 (d, 6H, $^3J_{HH}$ = 6.8 Hz, Dipp-Pr^i-C*H*$_3$), 1.11 (d, 6H, $^3J_{HH}$ = 7.5 Hz, Si-Pr^i-C*H*$_3$), 1.28 (d, 6H, $^3J_{HH}$ = 6.8 Hz, Dipp-Pr^i-C*H*$_3$, Si-Pr^i-C*H*), 2.48 (d, 2H, $^2J_{HP}$ = 16.8 Hz, C*H*$_2$-PPh_2), 3.19 (hept, 2H, $^2J_{HP}$ = 6.8 Hz, Dipp-Pr^i-C*H*), 6.37 (d, 2H, $^2J_{HP}$ = 35.1 Hz, PPh_2-Ge*H*$_2$), 7.18 (s, 3H, Ar-C*H*), 7.58 (s, 4H Ar_{BArF}-*H*$_{para}$), 7.78 (m, 14H, Ar-C*H*/ Ar_{BArF}-*H*$_{ortho}$), 7.96 (m, 4H, Ar-C*H*).

$^{31}P\{^1H\}$ NMR (THF-d_8, 162 MHz, 298 K): δ = -0.8 (s, *P*Ph_2).

$^{13}C\{^1H\}$ NMR (THF-d_8, 101 MHz, 298 K): δ = 5.6 (*C*H_2-PPh_2), 15.7 (Si-Pr^i-*C*H), 17.8 and 19.0k (Si-Pr^i-*C*H_3), 23.9 and 26.9 (Dipp-Pr^i-*C*H_3), 29.3 (Dipp-Pr^i-*C*H), 116.7, 118.4, 121.6, 122.8, 123.5, 124.3, 125.9, 127.1, 127.7, 129.8, 130.1, 130.4, 130.7, 130.9, 131.6, 131.7, 133.9, 134.0, 135.8, 147.8, 162.3, 162.8, 163.2 and 163.7(Ar-*C*).

$^{29}Si\{^1H\}$ NMR (THF-d_8, 99 MHz, 298 K): δ = 15.0 (d, $^2J_{SiP}$ = 2.5 Hz, *Si*-Pr^i).

MS/LIFDI-HRMS found (calcd.) m/z: 562.2106 (562.2114) for $[M-2H-BAr^F_4]^+$.

Anal. calcd. for $C_{21}H_{38}ClNSiSn$: C, 53.04%; H, 4.03%; N, 0.98%; found: C, 53.02%; H, 3.70%; N, 1.04%.

IR, *v*/cm^{-1} (ATR): 1759 (s, w, Ge-H), 1611 (s, w, Ge-H).

[^{PhiP}DippGe·DMAP][BAr$^F_4$], 8. A solid mixture of **3** (200 mg, 0.36 mmol) and DMAP (360 mg, 0.36 mmol) was dissolved in PhF at ambient temperature and stirred for 30 min. All volatiles were removed from the solution *in vacuo*, and pentane added (5 mL). The solution was placed at 4°C overnight yielding colorless crystals of **8** (352 mg, 0.25 mmol, 69%), which were suitable for X-ray diffraction analysis.

^{1}H NMR (THF-d_8, 400 MHz, 298 K): δ = 0.55 (d, 3H, $^3J_{HH}$ = 7.3 Hz, Si-Pr^i-C*H*$_3$), 0.65 (d, 3H, $^3J_{HH}$ = 6.6 Hz, Dipp-Pr^i-C*H*$_3$), 0.75 (m, 1H, Si-Pr^i-C*H*), 0.94 (d, 3H, $^3J_{HH}$ = 6.9 Hz, Dipp-Pr^i-C*H*$_3$), 1.09 (d, 3H, $^3J_{HH}$ = 7.4 Hz, Si-Pr^i-C*H*$_3$), 1.20 (m, 6H, Dipp-Pr^i-C*H*/Si-Pr^i-C*H*$_3$), 1.30 (d, 3H, $^3J_{HH}$ = 6.7 Hz, Dipp-Pr^i-C*H*$_3$), 1.37 (d, 3H, $^3J_{HH}$ = 7.3 Hz, Si-Pr^i-C*H*$_3$), 1.52 (m, 1H, Si-Pr^i-C*H*), 2.06 (m, 1H, C*H*$_2$-PPh$_2$), 2.80 (m, 2H, C*H*$_2$-PPh$_2$/Dipp-Pr^i-C*H*), 3.10 (s, 6H, DMAP-N-C*H*$_3$), 3.68 (m, 1H, Dipp-Pr^i-C*H*), 6.76 (d, $^3J_{HH}$ = 6.6 Hz, Ar$_{DMAP}$-C*H*), 7.10 (s, 3H, Ar-C*H*), 7.32 (m, 4H, Ar-C*H*), 7.43 (m, 1H, Ar-C*H*), 7.58 (s, 4H, Ar$_{BArF}$-*H*$_{para}$), 7.72 (m, 3H, Ar-C*H*), 7.80 (s, 8H, Ar$_{BArF}$-*H*$_{ortho}$), 8.10 (m, 4H, Ar-C*H*).

^{31}P{^{1}H} NMR (THF-d_8, 162 MHz, 298 K): δ = -1.1 (s, *P*Ph$_2$).

^{13}C{^{1}H} NMR (THF-d_8, 101 MHz, 298 K): δ = 4.7 (*C*H$_2$-PPh$_2$), 17.3 and 17.3 (Si-Pr^i-*C*H), 19.2, 20.3, 20.8 and 20.9 (Si-Pr^i-*C*H$_3$), 21.0, 22.3, 27.6, and 29.1 (Dipp-Pr^i-*C*H$_3$), 29.5 and 29.6 (Dipp-Pr^i-*C*H), 39.6 (DMAP-N-*C*H$_3$), 108.6, 116.0, 116.2, 118.4, 121.6, 124.3, 124.4, 125.6, 126.7, 127.1, 129.8, 130.0, 130.3, 130.4, 130.7, 130.8, 130.9, 131.0, 131.1, 132.0, 132.6, 134.2, 134.3, 135.8, 145.4, 147.9, 148.5, 157.5, 162.3, 162.8, 163.2 and 163.7 (Ar-*C*).

^{29}Si{^{1}H} NMR (THF-d_8, 99 MHz, 298 K): δ = 19.0 (d, $^2J_{SiP}$ = 12.3 Hz, CH$_2$-*Si*-Pr$^i_2$).

MS/LIFDI-HRMS found (calcd.) m/z: 684.2890 (680.2958) for [M- BAr$^F_4$]$^+$.

Anal. calcd. for $C_{21}H_{38}ClNSiSn$: C, 54.36%; H, 4.24%; N, 2.72%; found: C, 54.18%; H, 4.04%; N, 2.81%.

[(Ph$_2$PCH$_2$Si^{i}Pr$_2$N(H)Ge]$_2$[BAr$^F_4$]$_2$, 9. A solution of **3** (250 mg, 0.18 mmol) in PhF was cooled to -40°C. Addition of NH_3 (8 mL,0.36 mmol) led to a colorless solution, which was swirled for 5 min at -40°C. Then the mixture was subjected to vacuum to remove excess ammonia. The solution was subsequently allowed to warm to ambient temperature, and the solution

concentrated to ~5 mL *in vacuo*. Pentane (5 mL) was added, and the solution placed at 4°C for 7 days, leading to colorless crystals of **9** (132 mg, 0.11 mmol, 59%), which were suitable for X-ray diffraction analysis.

^{1}H NMR (THF-d_8, 400 MHz, 298 K): δ = 0.97 (m, 14H, Si-Pr^i-C*H*/ Si-Pr^i-C*H*$_3$), 1.99 (d, 2H, $^3J_{HP}$ = 16.5 Hz, C*H*$_2$-PPh$_2$), 5.01 (d, 1H, $^3J_{HP}$ = 35.0 Hz, Ge-N-*H*), 7.09 (m, 2H, Ar-C*H*), 7.34 (m, 1H, Ar-C*H*), 7.59 (m, 8H, Ar-C*H*), 7.79 (m, 11H, Ar-C*H*).

^{31}P{^{1}H} NMR (THF-d_8, 162 MHz, 298 K): δ = 13.5 (s, *P*Ph$_2$).

2.35 (*C*H$_2$-PPh$_2$), 16.2 and 16.2 (Si-Pr^i-*C*H), 18.1 and 18.3 (Si-Pr^i-*C*H$_3$), 116.0, 116.2, 118.4, 121.6, 124.3, 125.1, 125.1, 127.0, 128.6, 129.0, 129.8, 130.1, 130.4, 130.8, 130.9, 131.0, 131.1, 133.4, 133.5, 133.6, 133.6, 135.8, 162.3, 162.7, 163.7, 163.7 and 165.3 (Ar-*C*).

^{29}Si{^{1}H} NMR (THF-d_8, 99 MHz, 298 K): δ = 31.2 (d, $^2J_{SiP}$ = 18.0 Hz, *Si*-Pr^i).

Anal. calcd. for $C_{21}H_{38}ClNSiSn$: C, 48.45%; H, 3.11%; N, 1.11%; found: C, 50.03%; H, 3.14%; N, 1.24%.

N.B. The acquisition of mass spectrometry data was not successful due to repeated strong fragmentation and instability of the compound.

X-ray crystallographic details

Single crystals of **3**-**9** suitable for X-ray structural analysis were mounted in perfluoroalkyl ether oil on a nylon loop and positioned in a 150 K cold N_2 gas stream. Data collection was performed with a STOE StadiVari diffractometer (MoKα radiation) equipped with a DECTRIS PILATUS 300K detector. Structures were solved by Direct Methods (SHELXS-97)[28] and refined by full-matrix least-squares calculations against F^2 (SHELXL-2018).[29] The positions of the hydrogen atoms were calculated and refined using a riding model, aside from Ge-*H* atoms in **7**, which were located and freely refined. All non-hydrogen atoms were treated with anisotropic displacement parameters. Crystal data, details of data collections, and refinements for all structures can be found in their CIF files, which are available free of charge via www.ccdc.cam.ac.uk/data_request/cif, and are summarized in Tables 7.1 and 7.2.

Table 6.1 Summary of X-ray crystallographic data for **3**-**6**.

	3	**4·0.5(Et$_2$O)**	**5**	**6**
empirical form.	$C_{63}H_{55}BF_{24}GeNPSi$	$C_{65}H_{60}BF_{24}NO_{0.5}PSiSn$	$C_{31}H_{44}GeNPSi$	$C_{31}H_{43.95}NPSiSn$
formula wt	1424.54	1507.70	562.32	608.37
crystal syst.	triclinic	triclinic	monoclinic	monoclinic
space group	*P-1*	*P-1*	*P2$_1$/c*	*C2/c*
a (Å)	12.110(2)	12.770(3)	19.510(4)	40.750(8)
b (Å)	14.210(3)	14.400(3)	9.720(19)	10.070(2)
c (Å)	20.860(4)	19.740(4)	17.190(3)	31.350(6)
α (deg.)	83.30(3)	71.60(3)	90	90
β (δεγ)	81.40(3)	78.30(3)	112.00(3)	105.90(3)
γ (deg.)	89.00(3)	83.80(3)	90	90
vol (Å^3)	3525.1(13)	3369.0(14)	3022.5(12)	12372(5)
Z	2	2	4	16
ρ(calc) (g.cm^{-3})	1.342	1.486	1.367	1.307
μ (mm^{-1})	0.574	0.528	1.125	0.935
F(000)	1444	1522	1192	5056
T (K)	150(2)	150(2)	150(2)	150(2)
reflns collect.	35235	52781	39193	106322
unique reflns	10946	13233	5913	12127
R_{int}	0.0333	0.1112	0.0211	0.0960
R1 [$I>2\sigma(I)$]	0.0574	0.0457	0.0354	0.0272
*w*R2 (all data)	0.1700	0.0999	0.0910	0.0394
CCDC No.	2163896	2163892	2163893	2163898

Table 6.2 Summary of X-ray crystallographic data for **7**-**9**.

	7	**8**	**9**
empirical form.	$C_{63}H_{57}BF_{24}GeNPSi$	$C_{75}H_{77}BF_{24}GeN_3PSi$	$C_{102}H_{78}B_2F_{48}Ge_2N_2P_2Si_2$
formula wt	1426.55	1618.85	2528.58
crystal syst.	triclinic	triclinic	triclinic
space group	*P-1*	*P-1*	*P-1*
a (Å)	12.980(3)	13.240(3)	14.240(3)
b (Å)	14.430(3)	14.030(3)	14.750(3)
c (Å)	19.650(4)	22.640(5)	17.350(4)
α (deg.)	70.70(3)	78.60(3)	109.00(3)
β (δεγ)	76.80(3)	76.80(3)	95.70(3)
γ (deg.)	83.20(3)	81.10(3)	113.70(3)
vol ($Å^3$)	3378.2(14)	3987.1(15)	3041.5(13)
Z	2	2	1
ρ(calc) ($g.cm^{-3}$)	1.402	1.348	1.381
μ (mm^{-1})	0.599	1.227	0.656
F(000)	1448	1660	1268
T (K)	150(2)	150(2)	150(2)
reflns collect.	53272	50954	38836
unique reflns	13214	15573	11970
R_{int}	0.0800	0.0704	0.1774
R1 [$I>2\sigma(I)$]	0.0635	0.0543	0.1041
*w*R2 (all data)	0.1749	0.1431	0.3217
CCDC No.	2163894	2163897	2163895

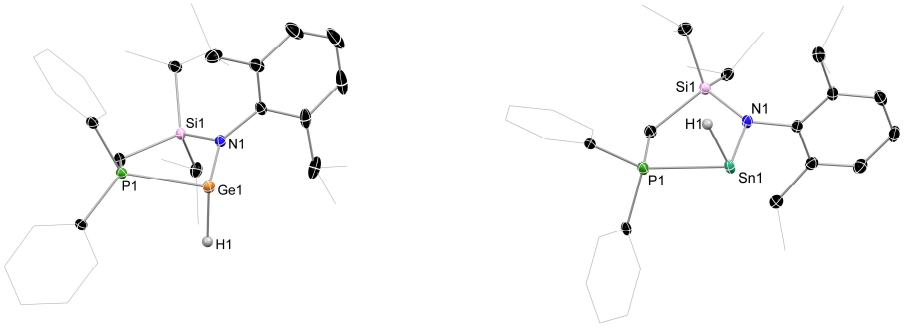

Figure 6.5 The molecular structures of **5** and **6**, with thermal ellipsoids at 25% probability, and hydrogen atoms omitted for clarity, aside from the E-H moieties. Selected bond distances (Å) and angle (°) for **5**: Ge1-P1 2.4482(8); Ge1-N1 1.947(2); N1-Ge1-P1 86.13(6) (1); For **6**: Sn1-P1 2.670(1); Sn1-N1 2.157(2); N1-Sn1-P1 81.65

Computational methods and details

Computational experiments were performed using the Gaussian 16 program.[30] Geometry optimization was carried out at the ωB97XD level with the def2-TZVPP basis set for Ge and Sn, and the def2-SVP basis set for all other atoms.[31] Stationary points were confirmed as true minima by vibrational frequency analysis (no negative eigenvalues).

References

1 (a) J. F. Norris, W. W. Sanders, *Am. Chem. J.* **1901**, *25*, 54–62; (b) J. F. Norris, *Am. Chem. J.* **1901**, *25*, 117–122; (c) F. Kehrmann, F. Wentzel, *Chem. Ber.* **1901**, *34*, 3815–3819.

2 (a) M. Asay, C. Jones, M. Driess, *Chem. Rev.* **2011**, *111*, 354–396; (b); (c) H. Fang, Z. Wang, X. Fu, Coord. *Chem. Rev.* **2017**, *344*, 214–237; H. F. T. Klare, L. Albers, L. Süsse, S. Keess, T. Müller, and M. Oestreich, *Chem. Rev.* **2021**, *121*, 5889–5985.

3 (a) V. S. V. S. N. Swamy, S. Pal, S. Khan, S. S. Sen, *Dalton Trans.* **2015**, *44*,12903–12923; (b) P. Frisch, and S. Inoue, *Dalton Trans.* **2020**, *49*, 6176–6182.

4 J. Li, C. Schenk, F. Winter, H. Scherer, N. Trapp, A. Higelin, S. Keller, R. Pöttgen, I. Krossing, C. Jones, *Angew. Chem., Int. Ed.* **2012**, *51*, 9557–9561.

5 A quasi-one coordinate Sn^{II} cation: F. Diab, F. S. W. Aicher, C. P. Sindlinger, K. Eichele, H. Schubert, L. Wesemann, *Chem. Eur.J.* **2019**, *25*,4426–4434.

6 (a) P. Jutzi, F. Kohl, P. Hoffmann, C. Krüger, Y. Tsay, *Chem. Ber.* **1980**, *113*, 757–769. A related example with neutral arene donor stabilization: (b) T. Probst, O. Steigelmann, J. Riede and H. Schmidbaur, *Angew. Chem., Int. Ed.* **1990**, *29*, 1397–1398.

7 (a) H. V. R. Dias, Z. Wang, *J. Am. Chem. Soc.* **1997**, *119*, 4650–4655; (b) M. Stender, A. D. Phillips, P. P. Power, *Inorg. Chem*. **2001**, *40*, 5314–5315; (c) A. E. Ayers, H. V. R. Dias, *Inorg. Chem.* **2002**, *41*, 12, 3259–3268 (d) F. Cheng, J. M. Dyke, F. Ferrante, A. L. Hector, W. Levason, G. Reid, M. Webster, W. Zhang, *Dalton Trans.* **2010**, *39*, 847–856; (e) Y. Xiong, S. Yao, S. Inoue, A. Berkefeld, M. Driess, *Chem. Commun.* **2012**, *48*, 12198–12200, (f) T. Ochiai, D. Franz, E. Irran, S. Inoue, *Chem. Eur. J.* **2015**, *21*, 6704–670; (f) D. C. H. Do, A. V. Protchenko, M. Á. Fuentes, J. Hicks, P. Vasko, S. Aldrige, *Chem. Commun.* **2020**, *56*, 4684–4687.

8 S. Khan, G. Gopakumar, W. Thiel, M. Alcarazo, *Angew. Chem., Int. Ed.* **2013**, *52*, 5644–5647.

9 (a) P. A. Rupar, V. N. Staroverov, P. J. Ragogna, K. M. Baines, *J. Am. Chem. Soc.* **2007**, *129*, 15138–15139; (b) Y. Xiong, S. Yao, G. Tan, S. Inoue, M. Driess, *J. Am. Chem. Soc.*

2013, *135*, 5004–5007; (c) K. Inomata, T. Watanabe, H. Tobita, J. *Am. Chem. Soc.* **2014**, *136*, 14341–14344; (d) K. Inomata, T. Watanabe, Y. Miyazaki, H. Tobita, *J. Am. Chem. Soc.* **2015**, *137*, 11935–11937; (e) A. Rit, R. Tirfoin, S. Aldridge, *Angew. Chem., Int. Ed.* **2016**, *55*, 378–382; (f) M. Roy, S. Fujimori, M. Ferguson, R. McDonald, N. Tokitoh, E. Rivard, *Chem. – Eur. J.* **2018**, *24*, 14392–14399; (g) R. J. Mangan, A. Rit, C. P. Sindlinger, R. Tirfoin, J. Campos, J. Hicks, K. E. Christensen, H. Niu, S. Aldridge, *Chem. Eur. J.* **2020**, *26*, 306–315.

10 Y. Zhou, P. Vasko, J. Hicks, M. Á. Fuentes, A. Heilmann, E. L. Kolychev, S. Aldrige, *Dalton Trans.* **2020**, *49*, 9495–9504.

11 M. Driess, S. Yao, M. Brym, C. van Wüllen, *Angew. Chem. Int. Ed.* **2006**, *45*, 6730–6733.

12 D. Sarkar, S. Dutta, C. Weetman, E. Schubert, D. Koley, S. Inoue, *Chem. Eur. J.* **2021**, *27*, 13072–13078.

13 (a) P. M. Keil, T. Szilvási, T. J. Hadlington, *Chem. Sci.* **2021**,*12*, 5582–5590; (b) P. M. Keil, T. J. Hadlington, *Angew. Chem. Int. Ed.* **2022**, *61*, e202114143; *Angew. Chem.* **2022**, *134*, e202114143; (c) P. M. Keil, T. J. Hadlington, *Chem. Commun.* **2022**, *58*, 3011–3014.

14 A possible product might be two Sn-atoms being linked by a Cl atom, which would result in a mono cationic complex and fits the ^{1}H NMR.

15 (a) T. J. Hadlington, M. Hermann, J. Li, G. Frenking, C. Jones, *Angew. Chem. Int. Ed.* **2013**, *52*, 10199–10203; (b) T. J. Hadlington, M. Driess, C. Jones, *Chem. Soc. Rev.* **2018**, *47*, 4176–4197.

16 R. J. Mangan, A. Rit, C. P. Sindlinger, R. Tirfoin, J. Campos, J. Hicks, K. E. Christensen, H. Niu, S. Aldridge, *Chem. Eur. J.* **2020**, *26*, 306–315.

17 (a) T. Müller, C. Bauch, M. Ostermeier, M. Bolte, N. Auner, *J. Am. Chem. Soc.* **2003**, *125*, 2158–2168; (b) Y. Yang, R. Panisch, M. Bolte, T. Meller, *Organometallics* **2008**, *27*, 4847–4853.

18 (a) C. P. Sindlinger, L. Wesemann, *Chem. Sci.* **2014**, *5*, 2739–2746; (b) C. P. Sindlinger, A. Stasch, H. F. Bettinger, L. Wesemann, *Chem. Sci.* **2015**, *6*, 4737–4751.

19 Calculated at the ωB97XD/def2-SVP(*Ge, Sn*: def2-TZVPP) level.

20 (a) A. V. Protchenko, J. I. Bates, L. M. A. Saleh, M. P. Blake, A. D. Schwarz, E. L. Kolychev, A. L. Thompson, C. Jones, P. Mountford, S. Aldridge, *J. Am. Chem. Soc.* **2016**, *138*, 4555−4564; (b) M. V. Zabalov, M. A. Syroeshkin, B. N. Mankaev, S. V. Timofeev, M. P. Egorov, S. S. Karlov, *Russ. Chem. Bull. Int. Ed.* **2021**, *70*, 1075–1079.

21 (a) Y. Peng, B. D. Ellis, X. Wang, P. P. Power, *J. Am. Chem. Soc.* **2008**, *130*, 12268–12269; (b) A. V. Protchenko, K. H. Birjkumar, D. Dange, A. D. Schwarz, D. Vidovic, C. Jones, N. Kaltsoyannis, P. Mountford, S. Aldridge, *J. Am. Chem. Soc.* **2012**, *134*, 6500–6503.

22 (a) Y. Peng, J.-D. Guo, B. D. Ellis, Z. Zhu, J. C. Fettinger, S. Nagase, P. P. Power, *J. Am. Chem. Soc.* **2009**, *131*, 16272–16282; (b) T. J. Hadlington, M. Hermann, G. Frenking, C. Jones, *Chem. Sci.* **2015**, *6*, 7249–7257; (c) T. J. Hadlington, J. A. B. Abdalla, R. Tirfoin, S. Aldridge, C. Jones, *Chem. Commun.* **2016**, *52*, 1717–1720.

23 F. Hanusch, L. Groll, S. Inoue, *Chem. Sci.* **2021**, *12*, 2001–2015.

24 (a) Y. Wang, A. Kostenko, T. J. Hadlington, M.-P. Luecke, S. Yao, M. Driess, *J. Am. Chem. Soc.* **2019**, *141*, 626–634; (b) D. Reiter, R. Holzner, A. Porzelt, P. Frisch, S. Inoue, *Nature Chem.* **2020**, *11*, 1131–1135; (c) S. Fujimori, S. Inoue, *J. Am. Chem. Soc.* **2022**, *144*, 2034–2050.

25 A. J. Martínez-Martínez, A. S. Weller, *Dalton Trans.*, **2019**, *48*, 3351–3354.

26 F. K. Scharnagl, M. F. Hertrich, G. Neitzel, R. Jackstell, M. Beller, *Adv. Synth. Catal.* **2019**, *361,* 374–379.

27 M. Muhr, P. Heiß, M. Schütz, R. Bühler, C. Gemel, M. H. Linden, H. B. Linden, R. A. Fischer, *Dalton Trans.* **2021**, *50*, 9031–9036.

28 G. M. Sheldrick, SHELXL-97, Program for Crystal Strucutre Refinement, Göttingen, **1997**.

29 G. Sheldrick, *Acta Crystallogr., Sect. C: Struct. Chem.*, **2015**, *71*, 3–8.

30 M. J. Frisch, G. W. Trucks, H. B. Schlegel, G. E. Scuseria, M. A. Robb, J. R. Cheeseman, G. Scalmani, V. Barone, G. A. Petersson, H. Nakatsuji et al., Gaussian 16 Rev. C.01, Wallingford, CT, **2016**.

31 a) A. D. Becke, *J. Chem. Phys*. **1997**, *107*, 8554–8560; (b) F. Weigend, R. Ahlrichs, *Phys. Chem. Chem. Phys.* **2005**, *7*, 3297–3305; (c) J.-D. Chai, M. Head-Gordon, *Phys. Chem. Chem. Phys.* **2008**, *10*, 6615–6620; (d) S. Grimme, J. Antony, S. Ehrlich, H. Krieg, *J. Chem. Phys*. **2010**, *132*, 154104.

Chapter 7

Cationic Tetrylene-Iron(0) Complexes: Access Points for Cooperative, Reversible Bond Activation and Open-Shell Iron(-I) Ferrato-Tetrylenes

P. M. Keil, A. Soyemi, K. Weisser, T. Szilvási, C. Limberg, T. J. Hadlington, *Angew. Chem. Int. Ed.* **2023**, *62*, e202218141.

This project was done in collaboration with two research groups. DFT calculations were performed by Prof. Tibor Szilvási and Ademola Soyemi from the University of Tuscaloosa. Killian Weiser from the Humboldt-Universität Berlin performed all ^{57}Fe Mössbauer spectroscopy measurements, while Chrisitan Limberg from the Humboldt-Universität Berlin helped with the interpretation of all obtained results in this project.

Synopsis

In Chapters 3 and 4 we introduced the bidentate ligand scaffold ^{PhR}Dipp (^{PhR}Dipp = [{$Ph_2PCH_2Si(R)_2$}(Dipp)N]$^-$; R = Ph, *i*Pr; Dipp = 2,6-*i*$Pr_2C_6H_3$), and synthesised corresponding E^{II}-Ni^0 complexes (E = Ge, Sn). These complexes only demonstrated tetryl centered reactivity, most likely due to the electronically saturated nature of their Ni^0 centres. We were particularly interested in further utilising the cationic tetryliumylidene ligands, [^{PhR}DippE]$^+$, as the tetrel centre exhibited remarkably high Lewis acidity in the Ni^0 complexes [(^{PhR}DippE)·Ni(PPh_3)$_2$]$^+$. Therefore, we aimed to introduce these tetryliumylidene ligands to a potentially more reactive low-valent Fe^0 centre in this project, to possibly achieve metal-ligand cooperative (MLC) behaviour.

As an easily accessible Fe^0 precursor, we utilized [(η^2-tmvs)$_2$Fe(IPr)] (tmvs = $SiMe_3C_2H_3$; IPr = [{HC(Dipp)N}$_2$C:]), since the labile alkene ligands are easily replaced when introducing donor ligands, based on earlier work.[1] This class of precursor, featuring IPr and tmvs ligands, can also be used for the introduction of other first-row TM^0 centres such as Mn, Co and Ni.[2] Reacting the cationic tetrylene ligands [^{PhiP}DippE]$^+$ (see Chapter 6) with this Fe^0 precursor led to different coordination patterns for Ge and Sn, governed by η^6-arene interactions to the Fe^0 centre. The cationic germylene-iron(0) complex [{^{PhiP}DippGe(IPr)}·Fe]$^+$ is a diamagnetic low-spin complex with a closed shell Fe^0 centre. On the other hand, the cationic stannylene-iron(0) complex [(^{PhiP}DippSn)·Fe(IPr)]$^+$ is a paramagnetic high-spin complex with

an open-shell Fe^0 centre. This Sn^{II}-Fe^0 complex is particularly interesting due to the fact that it has a highly strained N-Sn-Fe angle of 81.32(1)°, and the phosphine arm is not coordinated to the Fe^0 centre, leading to a very small HOMO-LUMO gap of 0.89 eV.

The different electronic states of these Fe^0 complexes also translates to differing reactivities. [{^{PhiP}DippGe(IPr)}·Fe]$^+$ was shown to cleanly react with ammonia, *via* N-H cleavage across the Ge-NHC linkage, giving the 'half-parent' (amido)germylene complex [{^{PhiP}DippGe(NH_2)}·Fe·{IPr(H)}]$^+$. Formally, the IPr ligand is protonated, and bears the cationic charge. On the other hand, the related cationic stannylene complex, [(^{PhiP}DippSn)·Fe(IPr)]$^+$, decomposes when reacted with ammonia, but was shown to react with H_2 reversibly and cooperatively, forming a diamagnetic complex with two hydride ligands bridging the Sn and Fe centres, in the Fe^{II} complex [^{PhiP}DippSn(μ-H_2)Fe·(IPr)]$^+$. The bridging hydrides could be observed in the ^{1}H NMR spectrum, at δ -13.63 ppm, with Sn-satellites ($^1J_{HSn}$ = 331 Hz) confirming their bridging character. Obtaining crystals of this compound was challenging, due to the reversibility of the H_2 activation, but giving data good enough to ascertain the connectivity in this complex. DFT calculations of the model complex strengthened our hypothesised presence of two bridging hydrides, while analysis of the mechanism showed that the activation proceeds *via* an Fe-centred H_2 *σ*-complex, followed by Fe-Sn cooperative activation.

Moreover, we attempted to reduce the here obtained Fe^0 complexes, to obtain rare Fe^{-I} complexes. Further chemistry of such complexes is unknown and may enable targeted MLC. The reduction of [{^{PhiP}DippGe(IPr)}·Fe]$^+$ was achieved with $CoCp^*_2$, resulting in a phosphide-iron(I) complex. This presumably occurs *via* the targeted Fe^{-I} compound, which proved highly reactive, leading to oxidative activation of one P-Ph bond of the ligand scaffold. However, the Sn^{II}-Fe^{-I} complex [^{PhiP}Dipp(IPr)SnFe] was stable and isolable. This complex was obtained *via* the *in-situ* reaction of two equivalents of the [(η^2-tmvs)$_2$Fe(IPr)] precursor with [^{PhiP}DippSn]$^+$. This compound now exhibits a related structural configuration as observed in [{^{PhiP}DippGe(IPr)}·Fe]$^+$, with IPr coordinated to the Sn^{II} centre, and one Dipp group of the IPr ligand exhibiting an η^6-arene interaction with the Fe^{-I} centre. However, the Sn^{II} centre is now pyramidalised, indicating the presence of a lone pair of electrons. SQUID magnetometry measurements of this species confirmed its paramagnetic nature, with one unpaired electron observed. Additionally, EPR spectroscopy and DFT analysis strongly suggest that the one unpaired electron in these complexes is localised at the Fe^{-I} centre, allowing for its classification as a Sn^{II}-Fe^{-I} compound, making it the first reported covalently bound Fe^{-I} compound.

In conclusion, we could show that our ligands can be successfully introduced into highly reactive low-valent Fe^0 and elusive Fe^{-I} complexes, with diverse geometries dominated by η^6-arene interactions towards the Fe centre. Compared to the Ni^0 complexes described in Chapters 3 and 4, with electronically saturated Ni^0 centres, the here discussed Fe^0 complexes exhibit increased reactivity. This includes targeted MLC behaviour for $[(^{PhiP}DippSn)\cdot Fe(IPr)]^+$ in the reversible activation of H_2, leading to the bridged dihydride complex $[^{PhiP}DippSn(\mu\text{-}H)_2Fe]^+$. The importance of a low-coordinate TM centre for MLC is further examined in Chapter 8, whilst the here described Sn^{II}-Fe^{-I} complex may further be expanded to other systems, and studied towards reactivity and catalysis.

Manuscript

The following sections are reproduced and formatted from the following article: P. M. Keil, A. Soyemi, K. Weisser, T. Szilvási, C. Limberg, T. J. Hadlington, *Angew. Chem. Int. Ed.* 2023, *62*, e202218141. *Experimental spectra (NMR, LIFDI/MS, UV/vis, CV, EPR and IR), SQUID magnetometry data and further details concerning DFT calculations can be retrieved online* (https://doi.org/10.1002/anie.202218141).

Abstract

The open-shell cationic stannylene-iron(0) complex **4** (**4** = $[^{PhiP}DippSn\cdot Fe\cdot IPr]^+$; $^{PhiP}Dipp$ =[{$Ph_2PCH_2Si(iPr)_2$}(Dipp)N]$^-$; Dipp = 2,6-$^iPr_2C_6H_3$; IPr = $[(Dipp)NC(H)]_2C$:) cooperatively and reversibly cleaves dihydrogen at the Sn-Fe interface under mild conditions (1.5 bar, 298K), in forming bridging hydrido-complex **6**. One-electron reduction of the related Ge^{II}-Fe^0 complex **3** leads to oxidative addition of one C-P linkage of the $^{PhiP}Dipp$ ligand in an intermediary Fe^{-I} complex, leading to Fe^I phosphide species **7**. One-electron reduction reaction of **4** gives access to the iron(-I) ferrato-stannylene, **8**, giving evidence for the transient formation of such a species in the reduction of **3**. The covalently bound tin(II)-iron(-I) compound **8** has been characterised through EPR spectroscopy, SQUID magnetometry, and supporting computational analysis, which strongly indicate a high localization of electron spin density at Fe^{-I} in this unique d^9-iron complex.

Introduction

The seminal discovery of stable carbene complexes by E. O. Fischer marked a turning point in modern organometallic chemistry,[3] our broader interest in the reactive capacity of carbene

ligands blossoming since that time.[4] Extending from earlier concepts, bespoke pincer ligands incorporating nucleophilic carbene centers have the capacity to actively partake in cooperative bond scission processes across the carbene metal linkage,[5] in some cases reversibly.[6] Moving beyond the lightest element of group 14, the heavier tetrylenes also have the capacity to behave in this manner.[7] The past two decades have seen a significant growth in interest regarding the electronic nature of low-valent group 14 species,[8] and their bonding interactions with transition metals.[7,9] Due to the greater stability of lower oxidation states and the decrease in electronegativity on descending group 14, their chemistry also deviates from that for carbon. Notably, the heavier tetrylenes have an amplified ambiphilicity, and are more Lewis acidic due to a lessened electronegativity. This allows such ligands to behave as electrophiles whilst simultaneously being strong σ-donors towards a transition metal,[10] opening up a new vista in non-innocent ligand design (Figure 7.1). Non-innocent ligand systems have been central in accessing challenging bond activation processes with the abundant first-row transition metals, notably so for iron.[11] Two-electron oxidative addition processes, key in classic cross-coupling reactions, are in fact quite uncommon for this abundant element,[12] with key methods which have enabled such processes at iron revolving almost exclusively around ligand design.[13]

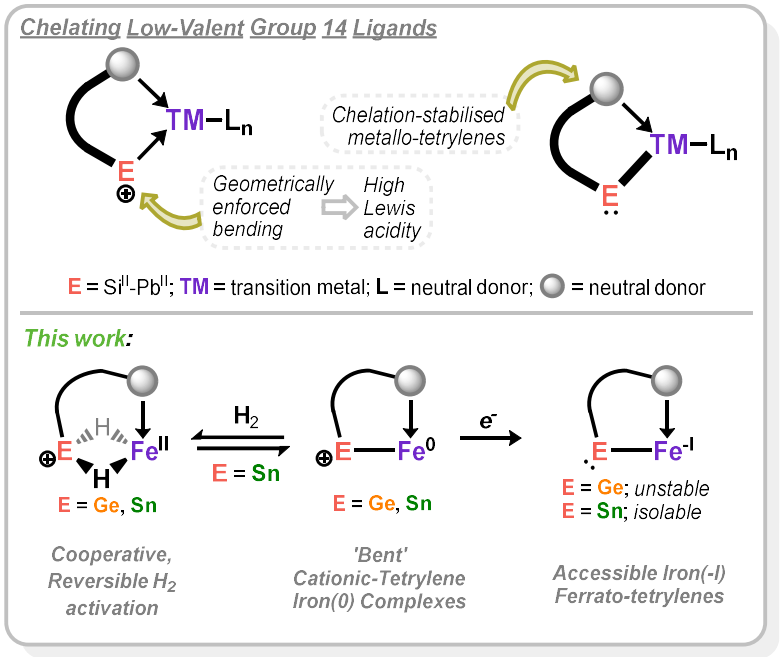

Figure 7.1 *Above:* Concepts in developing chelating low-valent group 14 systems, for geometrically activated ligand Lewis acidity, and stabilisation of otherwise inaccessible low-valent complexes. *Below:* this work involving chelating low-valent group 14 ligands in low-valent iron chemistry.

Utilizing chemically or redox non-innocent organic ligand systems, well-defined oxidative addition of catalytically essential bonds such as C-C, C-X (X = Cl-I),[10] and H-H[14] bonds have been realized. In order to further expand accessibility to such key processes, our own research

looks towards the development of non-innocent ligands based upon heavier low-valent group 14 elements. In this regard, heavier group 14-iron chemistry certainly has precedent. A small number of base-free silylene,[15] germylene,[16] and stannylene [16(a),17] complexes of iron(0) are now known, although it is noted that the vast majority involve the $[Fe(CO)_4]$ fragment or derivatives thereof, rendering reactivity involving the iron centre essentially nil. Closely related ferrato-tetrylenes, have also seen considerable attention, exclusively featuring iron in the oxidation state -2. Here, base-free derivatives bearing two-coordinate group 14 centers are also rare, based largely on the monoanionic $[CpFe(CO)_2]^-$ fragment (Cp = η^5-$[C_5H_5]^-$).[18] One very recent report on unique binding modes in ferrato-stannylene systems featuring the $[Cp^*(^iPr_2MeP)Fe]$ (Cp^* = η^5-$[C_5Me_5]^-$) anionic fragment have been reported by Tilley *et al.*,[19] whilst a Rh^{-I} metallo-stannylene recently reported by Wesemann *et al.* was shown to activate H_2 in the formation of a Rh^I metallo-stannylene,[20] though a mechanistic investigation into the involvement of the Sn^{II} center was not disclosed.

Our own efforts have focused on the development of chelating ligands featuring a tetrylene binding center, which remains highly Lewis acidic even when bound to a transition metal due to chelation-induced geometric constraints (Figure 7.1).[10,21] This aims to exploit the tetrylene centre as an additional reactive site, to allow for tetrylene-transition metal cooperativity in bond activation. We also hypothesised that such a chelating ligand may give access to unique examples of metallo-tetrylenes, due to the strong stabilising nature of the chelate effect. Herein we describe the extension of our reported cationic Ge^{II} and Sn^{II} ligand systems to low-valent iron chemistry, in the facile 'one-pot' synthesis of cationic germylene and stannylene complexes of iron(0). The resulting systems are electronically distinct, the Sn^{II} complex having an open-shell ground state which allows for the facile and reversible activation of dihydrogen, the mechanism for which involves both the Sn^{II} and Fe^0 centers in the critical H-H bond activation step. These complexes are also convenient access points for hitherto unknown open-shell ferrato-tetrylenes featuring Fe^{-I} centers. Whilst the target germanium system is unstable relative to ligand activation, the tin congener can be isolated as a stable, crystalline solid, which represents an open-shell, ferrato-stannylene featuring a Fe^{-I}-Sn^{II} covalent bond.

Results and Discussion

Cationic Tetrylene-Fe^0 Complexes

Two-coordinate-tetrylene complexes of first-row transition metals are, as mentioned, uncommon.[15,16,17] Furthermore, almost all low-valent group 14-iron complexes employ carbonyl ligands at iron, leading to electronic saturation and thus diminished reactivity. Our earlier reports regarding the synthesis of reactive Ni^0 systems bearing our cationic tetrylene

ligands relied upon the use of the commonly employed Ni^0 synthon, $Ni(cod)_2$. Earlier reports on similar chemistry for Fe^0 systems utilized the elegant, but somewhat inaccessible metal-vapor synthesis of bis(η^6-toluene)iron(0), used to generate the thermally labile (η^6-tolulene)(η^2-ethene)iron(0) complex.[17(c),(d)] More recently, a handful of closely related bis-η^2-alkene Fe^0 complexes were reported,[1,2(c)] stabilized by bulky N-heterocyclic carbenes, which we believed may also readily undergo alkene substitution reactions.[22] To this end, the addition of the cationic E^{II} ligand precursors, [^{PhiP}DippE][BAr^F_4] (E = Ge (**1**), Sn (**2**); ^{PhiP}Dipp = {[$Ph_2PCH_2Si(^iPr)_2$](Dipp)N}; Dipp = 2,6-$^iPr_2C_6H_3$; Ar^F = 3,5-$(CF_3)_2C_6H_3$),[23,24] to deep green solutions of IPr·Fe[η^2-(vtms)]$_2$ (IPr = [(Dipp)NC(H)]$_2$C:; vtms = $C_2H_3SiMe_3$) rapidly led to the formation of deep yellow-brown reaction mixtures (Scheme 7.1). *In-situ* $^{31}P\{^1H\}$ NMR spectroscopic analysis already suggested differing outcomes for the two reactions, that for the Ge^{II} system indicative of a single diamagnetic reaction product, and that for the Sn^{II} system being silent, thus indicative of a paramagnetic reaction product. Isolation of crystalline material from the two reaction mixtures (**3**: 80%; **4**: 76%) revealed considerably different structures for the two ligand systems.

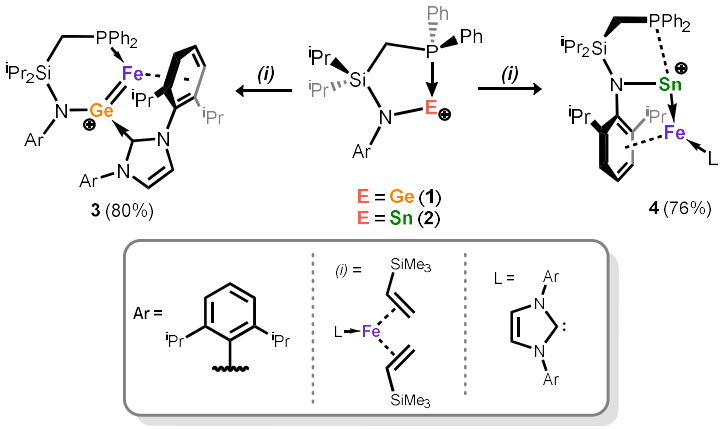

Scheme 7.1 Synthesis of compounds **3** and **4** (isolated yields in parentheses); *(i)*: IPr·Fe[η^2-(vtms)]$_2$, toluene, RT. Only the cationic part is shown in molecular structures. In all cases the counter-anion is [BAr^F_4]$^-$ (Ar^F = 3,5-$CF_3C_6H_3$).

The sole reaction product formed utilising the Ge^{II} ligand system (*viz*. **3**) shows Fe^0 insertion into the Ge-P bond, forming our previously observed chelating ligand motif (Figure 7.2(a)).[25] However, presumably due to the high Lewis acidity of the cationic Ge^{II} centre, the NHC ligand has migrated from iron to germanium, the iron centre now forming an η^6-arene interaction with one Dipp group of this NHC ligand. The Ge-Fe distance in **3** (d_{GeFe} = 2.1978(6) Å) is shorter than all but one reported Ge-Fe interactions, the one shorter example being found in a remarkable (alkyl)(hydrido)germylene iron(II) complex.[16(c)] The Ge^{II} center in **3** has a perfectly planar coordination geometry (sum of angles = 359.8°), representative of a Ge→Fe dative interaction. The DFT derived HOMO (-9.16 eV) shows considerable π-character, which would

suggest a degree of Fe→Ge back-bonding in this interaction and some degree of multiple-bond character. This is further borne out by both the Mayer Bond Order (MBO) and Wiberg Bond Index (WBI) for this bond, at 1.37 and 1.35, respectively, as calculated for model complex **3'** (**3'** = [^{MeMe}XylGe·Fe·^{Ph}NHC]$^{+}$; ^{MeMe}Xyl = {[$Me_2PCH_2SiMe_2$](Xyl)N}$^{-}$; Xyl = 2,6-$Me_2C_6H_3$; ^{Ph}NHC = [(Ph)NC(H)]$_2$C:). The average of the C-C bond distances in the Fe-bound arene (d = 1.419 Å) is slightly greater than the same value for the unbound arene of the NHC ligand (d = 1.390 Å), as is known in related arene complexes of low-valent iron.[26] Considerable broadening of aliphatic signals in the ^{1}H NMR spectrum of **3** indicates a fluxional character in solution, which sharpen when THF-d_8 solutions are heated to 60 °C. Notably, at low temperature (*i.e.* -80 °C) clear signals at δ = 4.5, 5.4, and 6.5 ppm can be seen, pertaining to the Fe-bound Dipp group.[27] The ^{57}Fe Mössbauer spectrum of **3** (δ = 0.472 mm·s^{-1}; ΔE_Q = 1.349 mm·s^{-1}) is in keeping with known Fe^0 arene systems,[26(b)] aiding in confirmation of a low-spin, d^8 Fe^0 complex. This species, to the best of our knowledge, thus represents a unique example of a cationic-tetrylene Fe^0 complex, and the first Ge^{II}-Fe^0 complex absent of carbonyl ligands. The structural and electronic nature of the closely related Sn^{II} system, **4** (Figure 7.2(b)), contrasts that of the described Ge^{II} complex.

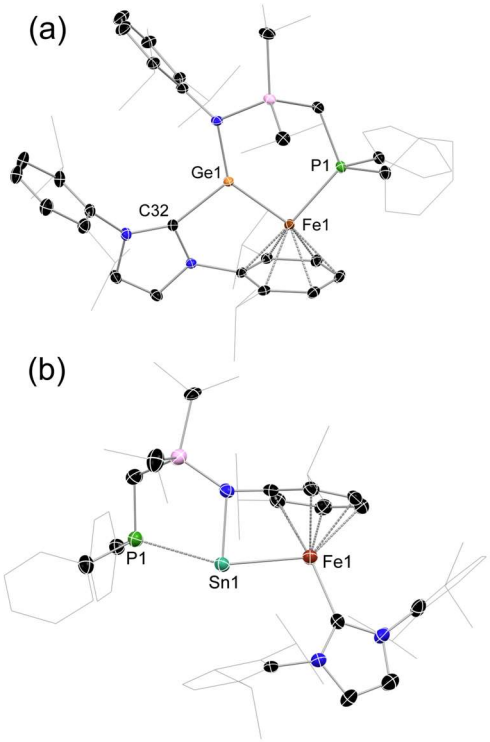

Figure 7.2 Molecular structure of the cationic parts in (a) **3** and (b) **4**, with thermal ellipsoids at 25% probability, and hydrogen atoms omitted for clarity. Selected bond distance (Å) and angles (°) for **3**: Ge1-Fe1 2.1978(6); Ge1-C32 2.049(2); Ge1-N1 1.845(2); P1-Fe1 2.2109(9); N1-Ge1-Fe1 137.75(6); N1-Ge1-C32 119.77(7); Fe1-Ge1-C32 102.28(6); Ge1-Fe1-P1 94.17(3). For **4**: Sn1-Fe1 2.717(1); P1-Sn1 2.998(2); Fe1-C32 2.073(5); Sn1-N1 2-140(3); C1-N1 1.396(7).

The Sn^{II} center indeed binds the Fe^0 center; surprisingly, however, insertion into the Sn-P bond is not observed, but rather the Fe^0 center forms an η^6-arene interaction with the Dipp group of the stannylene ligand, generating a highly strained conformation. This strain presumably leads to a significant weakening of the P-Sn interaction, which is longer than 98% of reported Sn-P single-bonded interactions ($d_{Sn\cdots P}$ = 2.999(2) Å; sum of covalent radii = 2.51 Å). The ligand strain is exemplified by the acute Sn-Fe binding angle ($\angle_{NSnFe}$ =81.32(1)°), and further borne out by the angles at the ^{PhiP}Dipp ligand's N-donor atom: the Sn-N-C^{Dipp} and Si-N-C^{Dipp} angles of 94.81(3)° and 142.61(3)° deviate significantly from the ideal of 120°. Finally, the Sn-Fe bond distance of 2.717(1) Å is longer than all known terminal Sn-Fe bonding interactions. The low-coordinate Sn^{II} center appears to have some degree of stabilization from one aryl group of the NHC ligand bound to Fe^0, with a distance of 3.316 Å between the Sn^{II} center and the center of the arene plane. This is within the sum of the van der Waals radii for tin and carbon (3.97 Å),[28] but considerably longer than such interactions in related low-coordinate tetrylene cations.[29] Electronically, Sn^{II} complex **4** also differs to the Ge^{II} system. Solutions of redissolved crystalline **4** yield highly broadened ^{1}H NMR spectra, indicative of a paramagnetic system. This paramagnetism is rationalized best assuming a high-spin configuration for the d^8 Fe^0 center, with S = 1. Consistent with this, complex **4** is not active when studied by X-band EPR spectroscopy, and shows the expected behavior for an S = 1 system in SQUID magnetometry measurements (Figure 7.3).

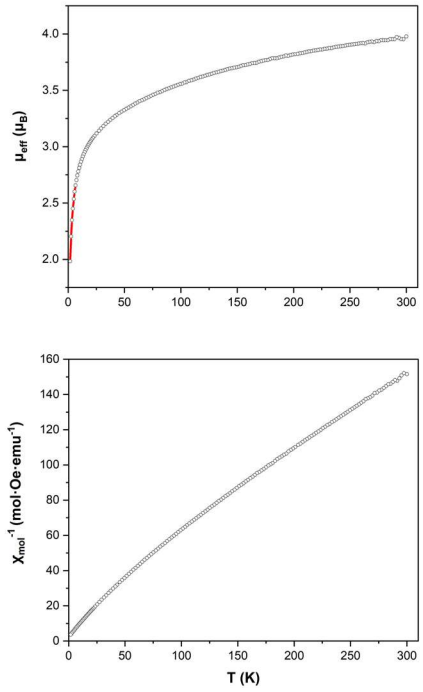

Figure 7.3 Plots of μ_{eff} vs. T (above) and χ_{mol} vs. T (below) for paramagnetic Sn^{II}-Fe^0 complex **4**.

Here, the ambient temperature μ_{eff} value of 3.95 μ_B is higher than would be expected for the spin-only value for two unpaired electrons (*e.g.* 2.83 μ_B), indicative of spin-orbit coupling, which is known for heavier group 14 element first-row transition metal complexes.[30] These SQUID data are also in good agreement with Curie-Weiss paramagnetism, indicative of spin-density located at iron, with no indication of spin-coupling *e.g.* arising from ligand reduction. Density Functional Theory (DFT) calculations on model complex **4'** (**4'** = $[^{MeMe}XylSn{\cdot}Fe{\cdot}^{Xyl}NHC]^+$; ^{Xyl}NHC = [(Xyl)NC(H)]$_2$C:) also suggest a high spin density at iron. Notably. this spin state leads to a very narrow calculated HOMO-LUMO gap in **4'** of 0.89 eV.[31] Alongside the geometrically perturbed Sn-Fe interaction and low-coordination environment at the cationic Sn^{II} center, this provides a promising platform for synergistic bond activation in this complex.

Cooperative bond activation

The differing electronic nature of the described complexes stands as an exciting point of comparison, exemplified by their reactivity. One of our key aims in the development of ambiphilic main group ligands (*e.g.* **1** and **2**) seeks to access systems whereby the ambiphilic ligand has the capacity to bind incoming nucleophiles, with a focus on ammonia.[32] This aims to activate ammonia in the coordination sphere of the transition metals, which is typically a highly challenging reaction.[33] Both complexes **3** and **4** rapidly react with ammonia. Addition of ~1.5 equiv. of ammonia to dissolved **3** led to dissipation of its characteristic deep golden-yellow color, and formation of deep red solutions. *In-situ* ^{1}H and ^{31}P{^{1}H} NMR spectroscopic analysis indicated the clean formation of a single reaction product, with a broad 2H singlet in the ^{1}H NMR spectrum attributable to an NH_2 moiety (δ = 2.26 ppm). In contrast, the same reaction for the Sn^{II} system **4** led instead to a complex mixture of products,[34] highlighting differences in the reactivity of these distinct iron-tetrylene species. Deep red single crystals isolated from the former reaction indicated the activation of ammonia, through binding at Ge^{II}, and proton transfer to the NHC ligand, in the formation of **5** (Figure 7.4), in 93% isolated yield.

This thus indicates that the Ge^{II} center in **4** is indeed of high Lewis acidity, and so capable of binding the incoming nucleophilic NH_3. Compound **5** represents a rare example of a 'half-parent' amido tetrylene-transition metal complex,[35] and the first such example for germanium. Remarkably, the now protonated imidazolium salt remains bound to the Fe^0 center through an η^6-arene interaction. The Ge-Fe distance of 2.219(1) Å is slightly elongated relative to starting material **3**, likely due to increased N→Ge donation, so reducing Fe→Ge back-bonding. As described, the NH_2 ligand at Ge can be observed in the ^{1}H NMR spectrum (δ = 2.26 ppm), as well as in the IR spectrum of the powdered compound (ν = 3434 and 3335 cm^{-1}). Despite the persistent binding of the protonated NHC in **5**, attempts to drive reversibility in this ammonia activation reaction failed, *e.g.* through application of heat and/or vacuum to

dissolved **5**. Still, this reaction demonstrates a unique cooperative ammonia activation mechanism, in which the low-valent group 14 element (*e.g.* Ge^{II}) interestingly maintains its low oxidation state.

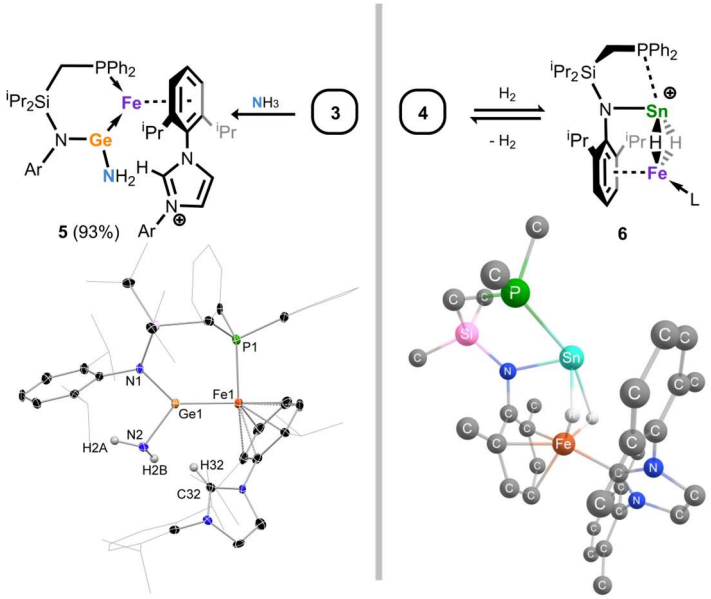

Figure 7.4. *Above*: the reactivity of **3** and **4** towards NH_3 and H_2, respectively, showing reversibility in the latter. *Below*: the molecular structure of the cationic part in NH_3-activation product **5**, with thermal ellipsoids at 25% probability, and the DFT-derived structure of the cationic part in H_2 activation product **6**. Selected bond distance (Å) and angles (°) for **5**: Ge1-Fe1 2.219(1); Ge1-N1 1.853(5); Ge1-N2 1.870(7); Fe1-P1 2.210(3); Ge1···C32 3.520(9); N1-Ge1-N2 98.8(3); Fe1-Ge1-N1 136.2(2); Fe1-Ge1-N2 124.8(2).

We then moved our sights to the activation of H_2, expected to be more challenging given the nonpolar nature of this small molecule. Here, Ge^{II} complex **3** showed no signs of reactivity, even after prolonged heating and increased H_2 pressures (*e.g.* up to 3 bar). Complex **4**, on the other hand, readily reacts with H_2 under 1.5 bar pressure, and at ambient temperature. Charging a gas-tight NMR tube containing a C_6D_6 solution of paramagnetic **4** with H_2 led to the formation of a single new diamagnetic reaction product, showing a singlet in the $^{31}P\{^1H\}$ NMR spectrum at δ = -24.2 ppm. More poignantly, a broad signal is observed in the ^1H NMR spectrum, at δ = -13.63 ppm, integrating to 2H and bearing clear $^{117/119}Sn$ satellites ($^1J_{SnH}$ = 331 Hz). Conducting the same reaction with D_2 gives a ^1H NMR spectrum identical to that described, but absent of the described high-field resonance. The ^2D NMR spectrum of these reaction mixtures reveals a resonance at δ = -13.97 ppm, in keeping with the activation of D_2. Evidence that these oxidative addition reactions may be reversible was found on addition of D_2 to *in-situ* generated **6**, which led to the formation of HD gas. Confirming this, degassing these reaction mixtures leads to quantitative regeneration of the starting material, thus signifying the facile reversible H_2 activation by **4**. This point rendered it highly challenging to attain further analytical data on this complex, and indeed to crystallize pure samples of H_2

activation product **6**. Although crystalline material of this species could be isolated by crystallising under an atmosphere of H_2,[36] high levels of disorder prevented refinement to levels acceptable for publication; nevertheless, this did allow us to ascertain the connectivity in **6**. Furthermore, this data could be utilized for the computationally derived lowest energy conformation of model complex **6'** (**6'** = $[^{MeMe}XylSn(\mu\text{-}H)_2Fe{\cdot}^{Xyl}NHC]^+$; Figure 7.4). Here, it is found that the hydride ligands in this complex symmetrically bridge the Sn and Fe centers, in keeping with the single resonance observed for these ligands in ^1H NMR spectra of reaction mixtures. Indeed, although rare, known examples of stannane-iron complexes featuring bridging hydride ligands have similar shifts and coupling constants in their respective ^1H NMR spectra.[37] At this stage, we were particularly curious as to whether the reversible activation of H_2 in **4** proceeds *via* a cooperative mechanism, that is, involving both Sn and Fe.

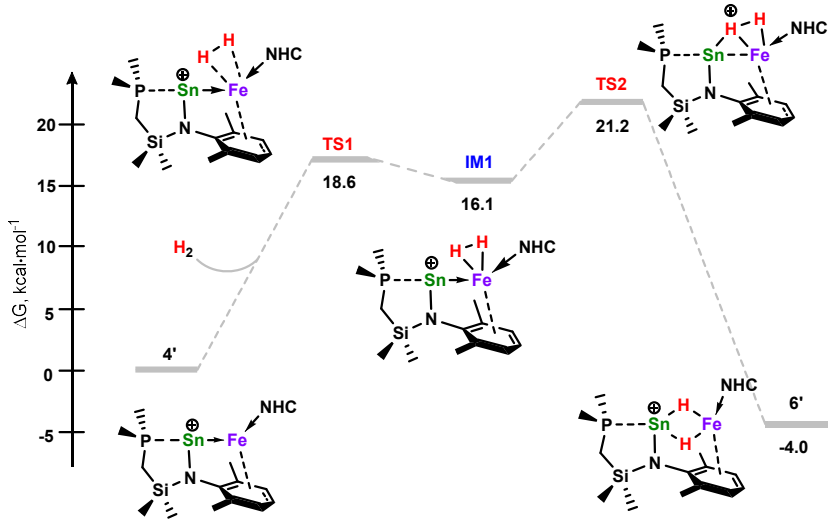

Figure 7.5. The DFT-derived reaction coordinate for the cooperative activation of H_2 by model cationic stannylene-iron(0) complex **4'**, yielding **6'**.

A DFT investigation of the potential energy surface for this reaction mechanism suggests that this is indeed the case (Figure 7.5). Upon initial H_2 addition an intermediary *σ*-bond complex is formed at Fe^0 (IM1, 16.1 kcalmol^{-1}). One H-atom can then form a bridging interaction with the cationic Sn^{II} center (TS2, 21.2 kcalmol^{-1}). This then proceeds by H-H bond scission, so forming bridging hydride complex **6** (-4.0 kcalmol^{-1}). This reaction coordinate therefore incites the involvement of both Sn and Fe centres in the cleavage of H_2, giving insights into the design of heteroelemental systems for the cooperative activation of typically nonlabile bonds. The small exergonic value for the overall reaction (4.0 kcalmol^{-1}) is in keeping with the observed reversibility in this process. An additionally important point here is the oxidation state of iron in the formed hydride complex. Combined X-ray crystallographic studies and DFT calculations indicate a *pseudo*-octahedral iron centre in **6**. This, in addition to the diamagnetic nature of this compound, would indicate a low-spin d^6 Fe^{II} electronic configuration, indicative of a

two-electron oxidative addition at the iron centre in **4** upon H_2 addition.[10-12] This further highlights the utility of the novel cationic tetrylene ligands employed here, in assisting otherwise challenging bond activation processes.

Accessing Open-Shell Ferrato-Tetrylenes

Despite the low-valent nature of both the tetryl and transition elements in complexes **3** and **4**, we hypothesized that their reduction may be possible, given that sub-valent iron systems (*viz*. ferrates) are known.[38] The most common such species are Fe^{-II} complexes, which are stable due to their d^{10} electronic configuration.[38(b)] On the other hand, formal d^9 Fe^{-I} complexes are very rare indeed. This compound class is largely represented by ion-separated alkali metal ferrates, such as Ellis's $[(\eta^4\text{-anth})_2Fe][K(L)_n]$.[38(c)] A number of reduced complexes derived from or relating to this ferrate involving redox active ligands are indeed known, whereby ligand reduction occurs, forming higher valent iron species.[39] Further examples of salt-separated anionic complexes, potentially featuring Fe^{-I} centers have been reported by Peters *et al.*, although the oxidation state at iron is not entirely clear, with potential reduction of employed ligands (*e.g.* borane, dinitrogen, and/or cyclic-alkylaminocarbene).[40] Covalently bound Fe^{-I} species remain elusive. In this regard, one-electron reduction of both **3** and **4** would lead to neutral ferrato-tetrylene complexes, featuring covalently bound, open-shell Fe^{-I} centers (Scheme 7.2).

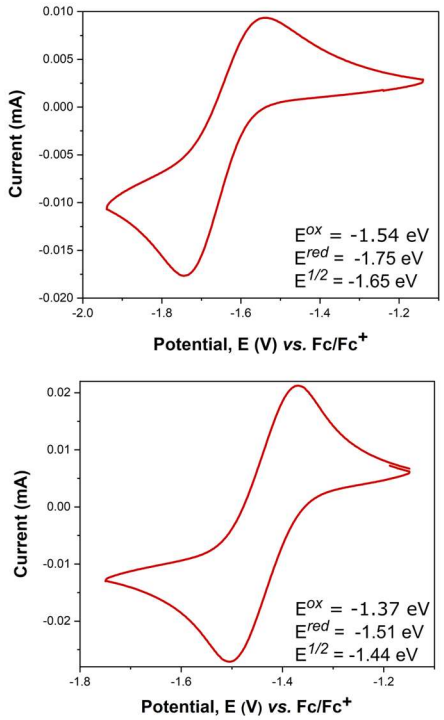

Figure 7.6. Cyclic voltammograms of complexes **3** (above) and **4** (below), in THF/$[N(n\text{-}Bu)_4]PF_6$, at a scan rate of 100 $mV \cdot s^{-1}$.

We first investigated the electrochemistry of complexes **3** and **4**, as THF solutions against the ferrocene reference electrode (Figure 7.6). Both complexes show chemically reversible reduction events (Ge: $E_{1/2}$ = -1.65 V; Sn: $E_{1/2}$ = -1.44 V).[41] Given that these values are roughly within the reduction potential of Cp^*_2Co,[42] we sought the chemical one-electron reduction of both **3** and **4** with this soluble reducing agent. Reduction of the Ge^{II} system led to formation of a deep red solution, with the precipitation of a pale yellow powder presumed to be $[Cp^*_2Co][BAr^F_4]$. Analysis of the reaction mixture by ^1H NMR spectroscopy revealed only highly broadened spectra indicative of paramagnetism in reaction products. Yields of up to 62% of a single reaction product could be isolated as deep red crystals, found to be the ligand activated product **7** (Scheme 7.2, *inset*), formally a phosphido-iron(I) compound.

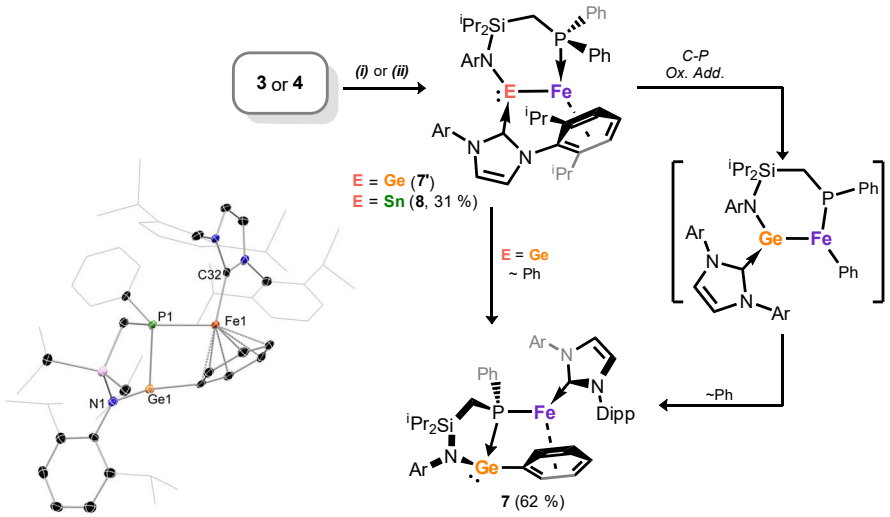

Scheme 7.2 Reduction of complexes **3** and **4**, forming ferrato-stannylene **8**, and ligand-activation product **7** (*inset*: molecular structure of **7**, with thermal ellipsoids at 25% probability); *(i)* Cp^*_2Co, toluene, -40°C – RT (E = Ge); *(ii)* IPr·Fe[η^2-(vtms)]$_2$, toluene, RT (E = Sn). Selected bond lengths (Å) and angles (°) for compound **7**: Ge1-P1 2.393(2); Ge1-N1 1.953(5); Fe1-P1 2.272(2); Fe1-C32 1.956(6); N1-Ge1-P1 92.1(1); P1-Ge1-C26 75.5(2); N1-Ge1-C26 105.8(2); C32-Fe1-P1 100.7(2); P1-Fe1-C26 76.7(2).

We hypothesise that this forms *via* an intermediary ferrato-germylene **7'**, with an Fe^{-I} centre, which oxidatively cleaves one P-Ph bond of the flanking ligand arm. Ph-migration from Fe to Ge generates the final (phenyl-germylene)iron-phosphide product (Scheme 7.2).[43] In such a case, this process would represent a further example of a formal two-electron oxidative addition involving iron, albeit at an Fe^{-I} center. Structurally, complex **7** contains no formal Ge-Fe interaction ($d_{Ge\cdots Fe}$ = 3.432(2) Å); the NHC ligand has now migrated back to the iron(I) center, which also bears an η^6-arene interaction with the phenyl moiety at Ge^{II}.

Extending this chemistry to the Sn^{II} system, we were surprised to find that in fact the tin congener of the target d^9 ferrato-tetrylene is indeed stable. Although reduction with Cp^*_2Co also led to the formation of a yellow precipitate, again presumably $[Cp^*_2Co][BAr^F_4]$, isolation of

meaningful quantities of a pure product proved challenging from these reaction mixtures. However, direct addition of two equivalents of the Fe^0 synthon IPr·Fe[η^2-(vtms)]$_2$ to the cationic stannylene **2** proved to be reducing enough to form the ferrato-stannylene **8** in crystalline yields of up to 31% (Scheme 7.2, Figure 7.7), with isolated yields being hindered by challenges in its separation from oily cationic by-products. The molecular structure of compound **8** is similar to that for the cationic germylene complex **3**, in that the ligand's phosphine arm now chelates the formally Fe^{-I} center, and the NHC is now located on Sn^{II}, with one Dipp fragment forming an η^6-arene interaction with iron. The key difference is the coordination geometry at Sn^{II}, which is now trigonal pyramidal due to the presence of a stereo-active lone pair of electrons (sum of angles = 309.76°). This contrasts with that of the Ge^{II} center in **3**, the planarity of which indicates Ge→Fe electron donation (sum of angles = 359.8°), and thus the absence of a formal bonding interaction. A notable contraction of the Sn-Fe bond distance is observed on moving from cationic **4** to neutral **8**, concomitant with a considerable decrease in the calculated polarization in this bond (Table 7.1).

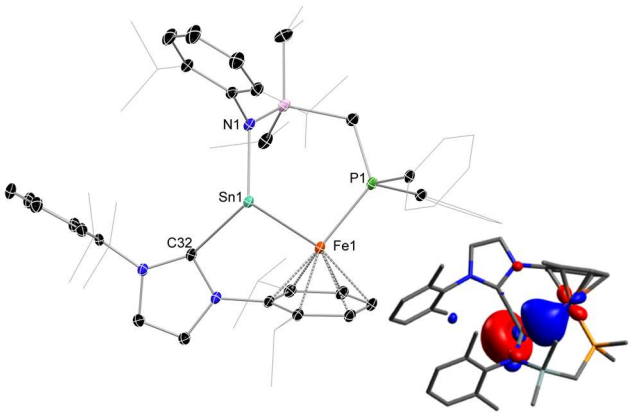

Figure 7.7 The molecular structure of iron(-I) ferrato-stannylene **8**, with ellipsoids at 25% probability, and hydrogen atoms omitted for clarity (*inset:* HOMO-1, representing the Sn-centered lone electron pair). Selected bond lengths (Å) and angles (°) for **8**: Sn1-Fe1 2.6489(9); P1-Fe1 2.238(1); Sn1-N1 2.186(2); Sn1-C32 2.444(3); Sn1-Fe1-P1 96.06(2); Fe1-Sn1-N1 107.59(6); Fe1-Sn1-C32 86.34(6); N1-Sn1-C32 115.44(8).

These observations point towards a formal covalent Sn-Fe bonding interaction in **8**. The absence of any other redox-active ligand bound to the Fe center in this complex would lead to the formal oxidation states of Sn^{II}/Fe^{-I}. The paramagnetic nature of **8**, ascertained by its ^{1}H NMR spectrum (μ_{eff} = 2.38 μ_B using Evans method), indicates that this species is indeed an example of an open-shell metallo-tetrylene. To the best of our knowledge this represents the first example of such a compound, and indeed a unique example of a covalently bound iron(-I) complex.

To gain further insights into the electronic nature of ferrato-stannylene **8**, and to ascertain the location of the free electron in this species, a combination of SQUID magnetometry, and EPR

and Mössbauer spectroscopy were employed, supported by DFT calculations. The EPR spectrum of a frozen glass of **8** in toluene (5 mM) yields a rhombic spectrum (Figure 7.8).[44] Supported by the simulated spectrum, three g-values of 2.0126, 2.0410, and 2.3050 are found, giving a g_{iso} of 2.1195, fitting well for an iron-centered electron.[45] Hyperfine coupling to ^{31}P, ^{117}Sn, and ^{119}Sn is clearly observable, the scales of which also indicate negligible radical character at these centers.[46]

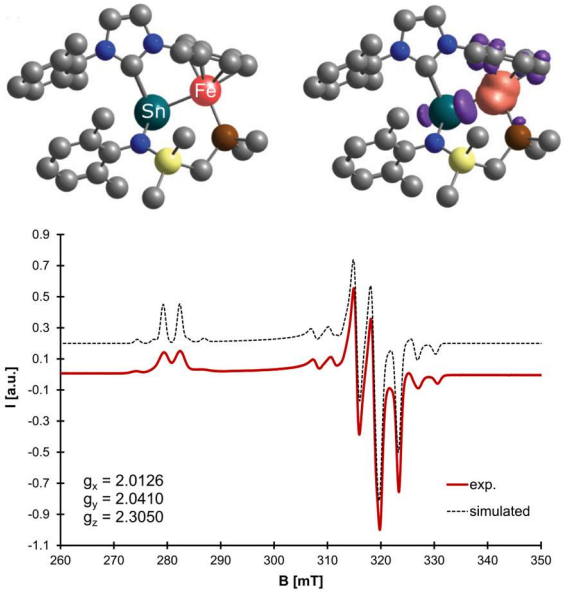

Figure 7.8 *Above*: the DFT optimized structure of **8**, and a spin-density plot of **8**, orange showing areas of positive density, and purple negative. *Below*: the EPR spectrum of **8** as a frozen THF glass at 113 K, overlaid with the simulated spectrum.

Calculated spin-density plots of model complex **8'** also infer a high degree of spin-density at Fe (77.95%; Figure 7.8). The zero-field ^{57}Fe Mössbauer spectrum of **8** exhibits an unsymmetrical quadrupole doublet with an isomer shift of δ = 0.520 mm·s^{-1}, and a large quadrupole splitting of ΔE_q = 1.574 mm·s^{-1}. Although the isomer shift is typically considered a key parameter for the assignment of the oxidation state, the lack of reported Fe^{-I} compounds limits the applicability of this tool in the present case, especially given that isomer shifts have also been found to depend on various other factors (ligand properties, ligation etc.).[47] In this regard, **8** is compared perhaps most reasonably with compound **3** (δ = 0.472 mm·s^{-1}; ΔE_Q = 1.349 mm·s^{-1}), which features a rather similar ligand scaffold around the iron center. Lowering the oxidation state from Fe^0 to Fe^{-I} on going from **3** to **8** would be expected to lead to a shift of the isomer shift into the positive region. The lengthening of the iron-tetryl element bond in **8** compared to that in **3** should also lead to a more positive isomer shift, which is indeed the case. However, even more factors change (replacement of Ge by softer Sn, and transformation of a dative bond into a covalent bond), so that it is advisable not to overinterpret these data.

Table 7.1 Selected metrical, analytical, and calculated parameters for **4** and **8**.

		4	**8**
d_{Sn-Fe}, Å		2.717(1)	2.6489(9)
Mössbauer	Isomer Shift, δ	0.777	0.520
	ΔE_Q, mm·s^{-1}	1.349	1.574
Fe-Sn Bond Polarisation[a]	Fe/Sn	24.23/75.77	58.19/41.81
Spin population, %[b]	Fe/Sn	70.97/11.13	77.95/16.36
NPA charge[a]	Sn/Fe/C	0.59/0.53/0.15	0.65/-0.19/1.02
WBI[a]	Sn-Fe/Fe-C	0.52/0.57	0.78/0.73
MBO[a]	Sn-Fe/Fe-C	0.53/0.77	0.82/0.80

[a] as determined through an NBO analysis of model complexes **4'** and **8'**; [b] as determined through spin-unrestricted DFT computations of model complexes **4'** and **8'**.

The same holds true for the quadrupole splitting that is comparable for both compounds. Looking now at magnetometry data, the inverse of μ_{eff}, derived from SQUID measurements, shows a linear increase with increasing temperature, in keeping with Curie-Weiss magnetism, and again indicative of an iron-centered electron. The SQUID-derived magnetic moment for **8** (μ_{eff}^{298} = 2.33 μ_B) is in keeping with that found in the solution state using the Evans method (2.38 μ_B), and is considerably lower than that observed for cationic complex **4** (3.95 μ_B), as is expected following a one electron reduction. Again, as for **4**, this is greater than the spin-only value expected for an S = ½ system, indicative of spin-orbit coupling in this compound.[30] With these key data in hand, it is clear that **8** bears a single unpaired electron, which is localized at the iron center in this compound, demonstrated primarily through EPR spectroscopy, and supported by DFT studies. Thus, the data discussed here strongly support the formation of a molecular, covalent d^9 Fe^{-I} compound in **8**.

Conclusion

We have presented facile synthetic routes for access to unprecedented cationic-tetrylene complexes of iron(0). Intrinsic differences in the electronic nature of the Ge^{II} and Sn^{II} ligands leads to considerably different electronic states in the formed complexes: the Ge^{II} system forms a low-spin, closed shell ground state, whilst the Sn^{II} complex has a high-spin, open shell ground state. The high reactivity of the latter open shell system is demonstrated through the activation of dihydrogen, a process which is in fact reversible, and proceeds *via* a cooperative mechanism

involving both Sn^{II} and Fe^{0} in the key bond scission step. Further, the described tetrylene iron(0) complexes prove to be ideal synthons for accessing hitherto unknown iron(-I) ferrato tetrylenes. Whilst the germanium system is unstable, undergoing ligand activation presumably through a two-electron oxidative addition process at iron, the Sn^{II}-Fe^{-I} system is a stable, crystalline compound. Thorough analysis of this unique species suggests a high degree of spin density at Fe, and a highly covalent Sn-Fe bonding interaction, opening a new vista in low-valent *d*-block chemistry. Further expansion of this compound class is currently underway in our laboratories, to uncover the reactivity of these unprecedented species, with a focus on two-electron oxidative addition processes which are typically challenging in iron chemistry.

Supporting Information

General experimental considerations

All experiments and manipulations were carried out under dry oxygen free argon atmosphere using standard Schlenk techniques or in a MBraun inert atmosphere glovebox containing an atmosphere of high purity argon. C_6D_6 was dried, degassed and stored over a potassium mirror. All other solvents were dried over activated 4Å mol sieves. [^{PhiP}DippGe][BAr^F_4] (^{PhiP}Dipp = {[$Ph_2PCH_2Si(^iPr)_2$](Dipp)N}$^-$; Dipp = 2,6-$^iPr_2C_6H_3$),[23] ^{PhiP}DippSnCl,[10(b)] Na[BAr^F_4] ([BAr^F_4] = [B(3,5-CF_3-C_6H_3)$_4$]$^-$),[48] IPr·Fe(η^2-vtms)$_2$ (IPr = [(Dipp)NC(H)]$_2$C:; vtms = $C_2H_3SiMe_3$),[1] and $CoCp^*_2$,[49] were synthesized according to known literature procedures. All other reagents were used as received. NMR spectra were recorded on a Bruker AV 400 Spectrometer. The ^{1}H and ^{13}C{^{1}H} NMR spectra were referenced to the residual solvent signals as internal standards. ^{29}Si{^{1}H} NMR spectra were externally calibrated with $SiMe_4$. ^{31}P{^{1}H} NMR spectra were externally calibrated with H_3PO_4. Evans' method was used for solution state magnetic susceptibility measurements, using C_6D_6 or THF-d_8 as the solvent and as the standard in a capillary.[50] Liquid Injection Field Desorption Ionization Mass Spectrometry (LIFDI-MS) was measured directly from an inert atmosphere glovebox with a Thermo Fisher Scientific Exactive Plus Orbitrap equipped with an ion source from Linden CMS.[51] Commercial ammonia and hydrogen gas with a purity of ≥ 99.999% were used in the gas experiments. Elemental analyses (C, H, N) were performed with a combustion analyzer (elementar vario EL, Bruker). Infrared spectra were measured with the Alpha FT IR from Bruker containing a platinum diamond ATR device. Absorption spectra (UV/vis) were recorded on an Agilent Cary 60 UV/vis spectrophotometer.

SQUID/Magnetic susceptibility measurements

Magnetic susceptibility data collected on solid samples were recorded using a MPMS XL 5 (Quantum Design) superconducting quantum interference device (SQUID) magnetometer with

liquid Helium cooling in a temperature range of 1.8–300 K and a magnetic field of 1.0 T. The samples were placed in a calibrated gelatin capsule and fixed in the center of a plastic straw. Data were corrected for underlying diamagnetism using tabulated Pascal's constant and corrected for the magnetism of the gelatin capsule by comparison to a measurement of the capsule without compound.

EPR

EPR measurements were carried out using a JEOL JES-FA 200 spectrometer at X-band frequency (approximately 9.05 GHz, sweep width 325 mT, modulation frequency 100 kHz, modulation amplitude 0.4 mT, microwave power 5.0 mW). The g values were determined using Mn^{2+} (nuclear spin I = 5/2) embedded in MgO as a standard (fourth line g = 1.981). The temperature was monitored with a JEOL DVT4 temperature controller. Sample preparation occurred in an argon-filled glovebox by dissolution of ground single crystals of 8 in toluene. The samples were frozen in liquid nitrogen prior to the measurements. The spectra were plotted using Origin Pro2016G (Origin Lab).

Mössbauer

Zero-field Mössbauer spectra were acquired on a SeeCo MS6 spectrometer comprising the following instruments: a JANIS CCS-850 cryostat, including a CTI-CRYOGENICS closed cycle 10 K refrigerator, and a CTI-CRYOGENICS 8200 helium compressor. The cold head and sample mount were equipped with calibrated DT-670-Cu-1.4L silicon diode temperature probes and heaters. Temperature was controlled by a LAKESHORE 335 temperature controller. Spectra were recorded using an LND-45431 Kr gas proportional counter with beryllium window connected to the SeeCo W204 γ-ray spectrometer that includes a high voltage supply, a 10 bit and 5 µs ADC and two single channel analyzers. Motor control and recording of spectra were taken care of by the W304 resonant γ-ray spectrometer. For the reported spectra a RIVERTEC MCO7.114 source (^{57}Co in Rh matrix) with an activity of about 1 GBq was used. Spectra were recorded in PTFE sample holders with about 30 mg of sample at 13 K and data was accumulated for about 48 hours each. Mössbauer data was processed and simulated using the WMOSS4 program ver. 4F (www.wmoss.org). Isomeric shifts are referenced to alpha-iron at room temperature.

Cyclic Voltammetry

Cyclic Voltammetry was carried out with a BioLogic SP200 potentiostat with EC-Lab software, using 3 mm diameter glassy carbon disk electrodes (PalmSens, Houten Netherlands) as working and counter electrodes. Prior to use, electrodes were polished with 0.05 µm alumina suspensions (CH Instruments Inc., USA). $Ag/AgNO_3$ (10 mM $AgNO_3$ and 0.1 M $[N(n\text{-}Bu)_4]PF_6$

in MeCN) was used as the reference electrode, separated via a Vycor 3535 frit (Advanced Glass & Ceramics, Holden, MA). CV measurements were performed in a five-necked glass cell under an Ar atmosphere. Unless noted otherwise, a scan rate of 100 mV/s was applied. Potentials are reported with reference to an internal standard of ferrocenium/ferrocene.

Experimental procedures

[^{PhiP}DippGe·Fe·IPr][BAr$^{F}_4$], 3. To a solid mixture of [^{PhiP}DippGe][BAr$^{F}_4$] (750 mg, 0.53 mmol) and IPr·Fe(η^2-vtms)$_2$ (340 mg, 0.53 mmol) toluene was added (10 mL) at ambient temperature, and the mixture stirred at this temperature for 30 min, resulting in a dark yellow solution. All volatiles were subsequently removed *in vacuo*, and pentane was added to the oily residue resulting in a dark yellow oil below a colorless pentane phase. The flask was stored at ambient temperature for 24 h yielding dark yellow crystals of **3** (797 mg, 0.42 mmol, 80%), which were suitable for X-ray diffraction analysis.

^{1}H NMR (THF-d$_8$, 400 MHz, 333 K): δ = 0.36 (d, 6H, $^3J_{HH}$ = 7.4 Hz, ^{i}PrC*H*$_3$), 0.62 (d, 6H, $^3J_{HH}$ = 7.4 Hz, ^{i}PrC*H*$_3$), 0.74 (m, 2H, ^{i}PrC*H*), 0.88 (m, 2H, ^{i}PrC*H*), 1.00 (m, 6H, ^{i}PrC*H*$_3$), 1.05 (d, 6H, $^3J_{HH}$ = 6.7 Hz, ^{i}PrC*H*$_3$), 1.27 (m, 18H, ^{i}PrC*H*$_3$), 1.43 (d, 6H, $^3J_{HH}$ = 7.4 Hz, ^{i}PrC*H*$_3$), 1.81 (d, 2H, $^2J_{HP}$ = 13.3 Hz, C*H*$_2$-PPh$_2$), 2.34 (hept, 4H, $^3J_{HH}$ = 7.9 Hz, ^{i}PrC*H*), 5.12 (m, 1H, Fe--Ar$_{Dipp}$-C*H*), 7.04 (m, 3H, Fe--Ar$_{Dipp}$-C*H*, Ar-C*H*), 7.20 (d, 2H, $^3J_{HH}$ = 7.8 Hz, Ar-C*H*), 7.47 (m, 8H, Ar-C*H*), 7.54 (s, 4H, Ar$_{BArF}$-*H$_{para}$*), 7.65 (m, 1H, N-C*H*=CH-N), 7.77 (m, 13H, Ar$_{BArF}$-*H$_{ortho}$*, Ar-C*H*), 8.37 (m, 1H, N-C*H*=CH-N).

^{31}P{^{1}H} NMR (THF-d$_8$, 162 MHz, 333 K): δ = 40.5 (s, *P*Ph$_2$)

^{13}C{^{1}H} NMR (THF-d$_8$, 101 MHz, 333 K): δ = 15.6 (*C*H$_2$-PPh$_2$), 18.1 and 18.2 (^{i}Pr*C*H), 18.8, 19.1, 23.0 and 23.5 (^{i}Pr*C*H$_3$), 23.6 and 24.5 (^{i}Pr*C*H), 26.4 and 26.4 (^{i}Pr*C*H$_3$), 29.7 (^{i}Pr*C*H), 30.1 and 31.0 (^{i}Pr*C*H$_3$), 85.6, 87.1 and 87.1 (Fe--Ar$_{Dipp}$-*C*H), 115.0 (Ar-*C*), 118.1 (Ar$_{BArF}$-*C*H$_{para}$), 121.5, 124.2, 125.8, 125.8, 126.0, 126.6 and 126.9 (Ar-*C*), 127.9 (H*C*=CH), 129.1, 129.2, 129.6, 129.9, 130.2, 130.5 and 132.6 (Ar-*C*), 133.2 (H*C*=CH), 135.1 (Ar-*C*), 135.6 (Ar$_{BArF}$-*C*H$_{ortho}$), 143.7, 145.9, 146.0, 146.1, 162.1, 162.6, 163.1 and 163.6 (Ar-*C*), 172.9 (*C$_{NHC}$*-Ge).

^{29}Si{^{1}H} NMR (THF-d$_8$, 99 MHz, 333 K): δ = -11.7 (d, $^2J_{SiP}$ = 2.2 Hz, CH$_2$-*Si*-Pr$^i_2$).

MS/LIFDI-HRMS found (calcd.) m/z: 1006.4271 (1006.4352) for [M-BAr$^{F}_4$]$^+$.

Anal. calcd. for $C_{90}H_{91}BF_{24}FeGeN_3PSi$: C, 57.84%; H, 4.91%; N, 2.25%; found: C, 55.14%; H, 4.70%; N, 2.39%.

λ$_{max}$, nm (*ε*, Lcm^{-1}mol^{-1}): 726 (2869), 480 (9120), 364 (11185).

^{57}Fe Mössbauer: δ = 0.472 mm·s^{-1}; ΔE_Q = 1.349 mm·s^{-1}.

N.B. NMR spectroscopic data were collected at 60 °C due to an improved separation and sharpness of signals at this temperature, presumably due to hindered rotation of ligand substituents at ambient temperature.

N.B. Repeated element analysis gave variable but consistently low values for C, possibly due to Si-carbide/Fe-carbide formation.

[^{PhiP}DippSn·Fe·IPr][BAr$^F_4$], 4. A solid mixture of ^{PhiP}DippSnCl (349 mg, 0.54 mmol) and Na[BAr$^F_4$] (481 mg, 0.54 mmol) was suspended in fluorobenzene (5 mL) and stirred for 30 min at ambient temperature, resulting in a light-yellow suspension. The mixture was cooled to -40 °C, and IPr·Fe(η^2-vtms)$_2$ (350 mg, 0.54 mmol) was added as a solution in toluene (5 mL), dropwise at -40 °C. The reaction mixture was removed from the cooling bath, allowed to warm to ambient temperature, and stirred for a further 4 h, resulting in a dark brown suspension. The reaction mixture was filtered, and all volatiles removed *in vacuo*. Addition of pentane led to a dark brown oil below a colorless pentane phase. All volatiles were again removed *in vacuo*, followed by the addition of pentane. Storing the flask at ambient temperature for 2 h led to the formation of dark brown crystals of **4** (783 mg, 0.41 mmol, 76%), which were suitable for X-ray diffraction analysis.

^{1}H NMR (THF-d$_8$, 400 MHz, 273 K): -0.56, -0.08, 0.54, 0.91, 1.11, 1.21, 1.30, 1.56, 2.46, 3.76, 6.53, 7.27, 7.57, 7.79, 8.39, 10.91, 11.43.

Magnetic moment (Evans' method; THF-d$_8$, 400 MHz, 298 K): 3.56 μ_B; (SQUID; crystalline solid, 298 K): 3.95 μ_B.

MS/LIFDI-HRMS found (calcd.) m/z: 1052.4094 (1052.4152) for [M-BAr$^F_4$]$^+$.

Anal. calcd. for $C_{90}H_{91}BF_{24}FeSnN_3PSi$: C, 56.44%; H, 4.79%; N, 2.19%; found: C, 53.37%; H, 4.46%; N, 2.16%.

λ_{max}, nm (ε, Lcm^{-1}mol^{-1}): 361 (7520).

^{57}Fe Mössbauer: δ = 0.777 mm·s^{-1}; ΔE_Q = 1.349 mm·s^{-1}.

N.B. Repeated element analysis gave variable but consistently low values for C, possibly due to Si-carbide/Fe-carbide formation.

[^{PhiP}Dipp(NH$_2$)Ge·Fe(η^6-IPrH)][BAr$^F{}_4$], 5. A solution of **3** (350 mg, 0.19 mmol) in toluene (20 mL) was cooled to -40 °C, and gaseous ammonia (20 mL, 0.9 mmol) was slowly added *via* syringe, leading to an immediate colour change from dark yellow to dark red. The mixture was subsequently allowed to warm to ambient temperature. The solution was concentrated *in vacuo* to <1 mL, and pentane (25 mL) was added, yielding a dark red oil below a light-yellow solution. The flask was stored at ambient temperature for 24 h yielding dark red crystals of **5** (328 mg, 0.17 mmol, 93%), which were suitable for X-ray diffraction analysis.

^{1}H NMR (THF-d$_8$, 400 MHz, 298 K): δ = 0.54 (d, 6H, $^3J_{HH}$ = 6.4 Hz, Si-Pr^i-C*H$_3$*), 0.62 (d, 6H, $^3J_{HH}$ = 6.3 Hz, Dipp-Pr^i-C*H$_3$*), 0.81 (m, 8H, Dipp-Pr^i-C*H$_3$*, Si-Pr^i-C*H*), 1.20 (m, 24H, Dipp-Pr^i-C*H$_3$*, Si-Pr^i-C*H$_3$*), 2.23 (m, 6H, Ge-N*H$_2$*, Dipp-Pr^i-C*H*, C*H$_2$*-PPh$_2$), 2.38 (m, 2H, Dipp-Pr^i-C*H*), 2.55 (m, 2H, Dipp-Pr^i-C*H*), 3.95 (m, 1H, Fe-Ar$_{Dipp}$-C*H*), 5.08 (s, 2H, Fe-Ar$_{Dipp}$-C*H*), 6.93 (m, 3H, Ar$_{Dipp}$-CH), 7.46 (m, 8H, Ar-CH), 7.58 (s, 4H, Ar$_{BArF}$-*H$_{para}$*), 7.64 (m, 5H, Ar-C*H*), 7.80 (s, 8H, Ar$_{BArF}$-*H$_{ortho}$*), 8.10 (s, 1H, N-C*H*=CH-N), 8.41 (s, 1H, N-C*H*=CH-N), 9.65 (s, 1H, N-C*H*=N$^+$).

A doublet from Dipp-^{i}Pr-CH$_3$ protons is obscured by the THF-d$_8$ signal at 1.73 ppm and is not reported here.

^{31}P{^{1}H} NMR (THF-d$_8$, 162 MHz, 298 K): δ = 46.89 (s, *P*Ph$_2$)

^{13}C{^{1}H} NMR (THF-d$_8$, 101 MHz, 298 K): δ = 14.0 (Si-Pr^i-*C*H), 14.2 (*C*H$_2$-PPh$_2$), 18.5 (Si-Pr^i-*C*H$_3$) and 19.6 (Si-Pr^i-*C*H$_3$), 24.0, 24.3, 24.7, 25.9, 26.3, 26.7 and 26.8 (Dipp-Pr^i-*C*H$_3$), 27.8, 30.3 and 30.81 (Dipp-Pr^i-*C*H), 78.0, 79.0 and 80.2 (Fe-Ar$_{Dipp}$-*C*H), 118.4 (Ar$_{BArF}$-*C*H$_{para}$), 124.4, 125.4, 125.9, 126.6, 127.1, 127.3, 128.5, 128.6, 128.7, 129.8, 129.9, 130.1, 130.4, 130.7, 131.2, 133.4 and 133.6 (Ar-*C*, H*C*=CH), 135.8 (Ar$_{BArF}$-*C*H$_{para}$), 140.6, 141.0, 146.2, 147.5, 162.3, 162.8, 163.3 and 163.8 (Ar-*C*).

^{29}Si{^{1}H} NMR (THF-d$_8$, 99 MHz, 298 K): δ = 4.68 (d, $^2J_{SiP}$ = 21.8 Hz, CH$_2$-*Si*-Pr$^i{}_2$).

MS/LIFDI-HRMS found (calcd.) m/z: 1024.4387 (1024.4686) for [M-BAr$^F{}_4$+H]$^+$.

Anal. calcd. for $C_{90}H_{94}BF_{24}FeGeN_4PSi$: C, 57.31%; H, 5.02%; N, 2.97%; found: C, 53.89%; H, 4.60%; N, 2.78%.

IR, *v*/cm^{-1} (ATR): 3434 and 3335 (Ge-NH$_2$).

N.B. Repeated element analysis gave variable but consistently low values for C, possibly due to Si-carbide/Fe-carbide formation.

[^{PhiP}DippSn(μ-H)$_2$Fe·IPr][BAr$^F{}_4$], 6. A 50mL flask with a concentrated toluene solution of **4** (75 mg, 0.039 mmol) was subjected to an atmosphere of hydrogen, leading to a colour change from deep brown to red. Pentane was added, and the flask was again subjected to a hydrogen pressure (1.5 bar). Storage of the flask at ambient temperature led to dark crystals of 6 suitable for X-ray diffraction analysis, co-crystallized with starting material **4**, which could not be avoided. This circumvented the acquisition of meaningful analytical data using these samples. As such, NMR spectroscopic data was collected using *in-situ* generation of 6 as follows:

For the acquisition of NMR data through *in situ* generation of **6**, a gas-tight NMR tube containing **4** (20 mg, 0.011 mmol) was cooled to -80 °C and dissolved in THF-d_8. The deep brown mixture was degassed by freezing the solution in liquid nitrogen, placing under a static vacuum, thawing at -80 °C, and re-pressurising with hydrogen gas (1.5 bar), leading to a colour change to red. The NMR sample was maintained at -80 °C, and transferred to an NMR machine precooled to 0 °C to minimize decomposition. NMR spectroscopic data was collected at this temperature. Reversibility was demonstrated by degassing the solution *via* three freeze-pump-thaw cycles, leading to a colour change to deep brown, and NMR spectroscopic data in keeping with those observed for paramagnetic compound **4**.

^{1}H NMR (THF-d_8, 400 MHz, 273 K): δ = -13.63 (s, 2H, Sn-*H*-Fe, $^1J_{SnH}$ = 331Hz), 0.44 (s, 6H, Pr^i-C*H*$_3$), 1.01 (m, 20H, Pr^i-C*H*$_3$, Pr^i-C*H*), 1.13 (d, 12H, $^3J_{HH}$ = 6.6 Hz, Pr^i-C*H*$_3$), 1.45 (d, 12H, $^3J_{HH}$ = 6.7 Hz, Pr^i-C*H*$_3$, Pr^i-C*H*), 1.63 (d, 2H, $^3J_{HH}$ = 11.9 Hz, C*H*$_2$-PPh$_2$), 2.57 (hept, 4H, $^3J_{HH}$ = 6.6 Hz, Dipp-Pr^i-C*H*), 2.92 (s, 2H, Fe-Dipp-Pr^i-C*H*), 4.66 (t, 1H, $^3J_{HH}$ = 6.0 Hz, Fe-Ar-C*H*), 4.81 (s, 1H, Fe-Ar-C*H*), (m, 21H, Ar-C*H*, N-C*H*=CH-N, Ar$_{BArF}$-*H*$_{para}$), 7.80 (s, 10H, Ar-C*H*, N-C*H*=CH-N Ar$_{BArF}$-*H*$_{ortho}$,).

^{31}P{^{1}H} NMR (THF-d_8, 162 MHz, 273 K): δ = -24.2 (s, *P*Ph$_2$).

^{29}Si{^{1}H} NMR (THF-d_8, 99 MHz, 273 K): δ = -20.7 (d, $^2J_{SiP}$ = 10.7 Hz, *Si*-Pr^i).

[^{PhiP}DippSn(μ-D)$_2$Fe·IPr][BAr$^F{}_4$], 6-D. For the acquisition of NMR data through *in situ* generation of **6-D**, the protocol as for the formation of **6** was used, with deuterium gas in place of hydrogen gas. Reversibility was again shown through three freeze-thaw-degas cycles, with subsequent NMR data in keeping with those for **4**.

^{1}H NMR (THF-d_8, 400 MHz, 273 K): δ = 0.43 (s, 6H, Pr^i-C*H*$_3$), 1.01 (m, 32H, Pr^i-C*H*$_3$, Pr^i-C*H*), 1.45 (m, 12H, Pr^i-C*H*$_3$, Pr^i-C*H*), 1.63 (d, 2H, $^3J_{HH}$ = 11.8 Hz, C*H*$_2$-PPh$_2$), 2.57 (m, 4H, Dipp-Pr^i-C*H*), 2.91 (m, 2H, Fe--Dipp-Pr^i-C*H*), 4.68 (m, 1H, Fe--Ar-C*H*), 4.83 (s, 1H, Fe-Ar-C*H*),

7.53 (m, 21H, Ar-C*H*, N-C*H*=CH-N, Ar_{BArF}-H_{para}), 7.80 (s, 10H, Ar-C*H*, N-C*H*=CH-N Ar_{BArF}-H_{ortho},).

^{2}H NMR (50% v/v fluorobenzene/C_6D_6, 400 MHz, 298 K): δ = -13.97 (Sn-*D*-Fe).

^{31}P{^{1}H} NMR (THF-d_8, 162 MHz, 273K): δ = -24.4 (s, *P*Ph_2).

^{29}Si{^{1}H} NMR (THF-d_8, 99 MHz, 273 K): δ = -22.6 (d, $^{2}J_{SiP}$ = 10.7 Hz, *Si*-Pr^{i}).

[PhPCH$_2$Si(^{i}Pr$_2$)N(Dipp)Ge-(η^6-Ph)]Fe·IPr, 7. Compound **3** (250 mg, 0.134 mmol) was dissolved in toluene (15 mL), cooled to -40 °C, and $CoCp^*_2$ (44 mg, 0.134 mmol) added as a solution in toluene (5 mL). The reaction mixture was allowed to warm to ambient temperature, leading to a colour change to dark red and the formation of a light-yellow precipitate. The solution was filtered, and all volatiles were removed *in vacuo*. The residue was taken up in pentane, concentrated and stored at 4°C for 18 h leading to dark red crystals of **7** (83 mg, 0.083 mmol, 62%), which were suitable for X-ray diffraction analysis.

^{1}H NMR (C_6D_6, 400 MHz, 298 K): δ = 0.13, 1.20, 1.30, 1.38, 1.84, 2.04, 2.11, 2.21, 2.48, 2.95, 5.83, 6.46, 7.48, 7.65, 8.09, 8.38, 8.51.

Magnetic moment (Evans' method; C_6D_6, 400 MHz, 298 K): 1.99 μ_B.

MS/LIFDI-HRMS found (calcd.) m/z: 1006.4340 (1006.4342) for $[M]^+$.

Anal. calcd. for $C_{58}H_{79}FeSnN_3PSi$: C, 69.26%; H, 7.92%; N, 4.18%; found: C, 67.79%; H, 7.94%; N, 4.06%.

N.B. Repeated element analysis gave variable but consistently low values for C, possibly due to Si-carbide/Fe-carbide formation.

^{PhiP}DippSnFe·IPr, 8. A solid mixture of ^{PhiP}DippSnCl (1.05 g, 1.64 mmol), Na[BAr^F_4] (1.45 g, 1.64 mmol), and IPr·Fe(η^2-vtms)$_2$ (2.12 g, 3.28 mmol) were dissolved in toluene (5 mL) and stirred for 3 days at ambient temperature, resulting in a deep red reaction mixture. The mixture was concentrated to 1 mL, and pentane (10 mL) was added, leading to a deep pink oil beneath a deep red-orange solution. The pentane layer was decanted, and all volatiles were removed *in vacuo*. Further addition of pentane (10 mL) led to a deep red solution, which was concentrated to ~4 mL, leading to the formation of deep pink oily droplets at the walls of the flask. The pentane solution was again separated from this oil *via* canula transfer, and stored

at 4 °C for 24 h leading to red-pink crystals of **8** (529 mg, 0.31 mmol, 31%), which were suitable for X-ray diffraction analysis.

^{1}H NMR (C_6D_6, 400 MHz, 298 K): δ = -0.52, 0.00, 0.44, 1.03, 1.21, 1.28, 2.11, 2.27, 2.98, 3.61, 4.10, 6.15, 6.63, 7.57, 7.68, 8.35, 10.80, 12.92.

Magnetic moment (Evans' method; C_6D_6, 400 MHz, 298 K): 2.38 μ_B; (SQUID; crystalline solid, 298 K): 2.33 μ_B.

MS/LIFDI-HRMS found (calcd.) m/z: 1052.4213 (1052.4152) for $[M]^+$.

Anal. calcd. for $C_{58}H_{79}FeSnN_3PSi$: C, 66.23%; H, 7.57%; N, 3.99%; found: C, 64.57%; H, 7.34%; N, 3.73%.

λ_{max}, nm (ε, $Lcm^{-1}mol^{-1}$): 360 (7528).

^{57}Fe Mössbauer: δ = 0.520 $mm \cdot s^{-1}$; ΔE_Q = 1.574 $mm \cdot s^{-1}$.

N.B. Repeated element analysis gave variable but consistently low values for C, possibly due to Si-carbide/Fe-carbide formation.

X-ray crystallographic details

Single crystals of complexes **3-8**, $(^{PhiP}DippFeNH_2)_2$, and $[^{PhiP}DippFe{\cdot}IPr][BAr^F{}_4]$ suitable for X-ray structural analysis were mounted in perfluoroalkyl ether oil on a nylon loop and positioned in a 150 K cold N_2 gas stream. Data collection was performed with a STOE StadiVari diffractometer (MoKα radiation) equipped with a DECTRIS PILATUS 300K detector. Structures were solved by Direct Methods (SHELXS-97),[52] or using SHELXT-16,[53] and refined by full-matrix least-squares calculations against F^2 (SHELXL-2018).[54] The positions of the hydrogen atoms were calculated and refined using a riding model, aside from N-*H* fragments in **5** and $(^{PhiP}DippFeNH_2)_2$. All non-hydrogen atoms were treated with anisotropic displacement parameters. Crystal data, details of data collections, and refinements for all structures can be found in their CIF files, which are available free of charge via www.ccdc.cam.ac.uk/data_request/cif, and are summarized in Table 7.2 and 8.3. Details for **6** are not given due to levels of disorder leading to unpublishable data quality for this complex. The structure for this compound is given in Figure 7.10, as proof of connectivity. In compound **4** the electron density of highly disordered co-crystallized solvent molecules was removed using the Platon SQUEEZE function (details in respective CIFs).

Table 7.2 Summary of X-ray crystallographic data for compounds 3-7.

	3	**4**	**5**	**7**
empirical	$C_{90}H_{91}BF_{24}FeGeN_3PSi$	$C_{90}H_{91}BF_{24}FeN_3PSiSn$	$C_{90}H_{94}BF_{24}FeGeN_4PSi$	$C_{58}H_{79}FeGeN_3PSi$
formula wt	1868.96	1915.06	1886.00	1005.74
crystal syst.	monoclinic	triclinic	orthorhombic	monoclinic
space group	*P2₁/n*	*P-1*	*P₂₁₂₁₂₁*	*P2₁/c*
***a* (Å)**	16.028(3)	13.150(3)	14.990(3)	19.130(4)
***b* (Å)**	14.327(3)	16.100(3)	19.640(4)	15.790(3)
***c* (Å)**	38.426(7)	22.910(5)	30.480(6)	18.380(4)
***α* (deg.)**	90	86.50(3)	90	90
***β* (δεγ)**	92.211(8)	75.20(3)	90	95.80(3)
***γ* (deg.)**	90	85.20(3)	90	90
vol (Å³)	8817(3)	4669.1(17)	8973(3)	5523.5(19)
Z	4	2	4	4
ρ(calc)	1.408	1.362	1.396	1.209
μ (mm^{-1})	0.634	0.545	0.624	0.895
***F*(000)**	3840	1956	3880	2140
***T* (K)**	150(2)	150(2)	150(2)	150(2)
reflns	79368	61807	60042	35946
unique	20206	18246	17437	10843
R_{int}	0.0188	0.0640	0.1650	0.1155
R1 [*I*>2σ(*I*)]	0.0413	0.0597	0.0576	0.0868
***w*R2 (all**	0.1113	0.1320	0.1155	0.2215
CCDC No.	2202847	2202848	2202849	2202850

Table 7.3 Summary of X-ray crystallographic data for compounds 8, (^{PhiP}DippFeNH$_2$)$_2$, and [^{PhiP}DippFe·IPr][BAr$^F{}_4$].

	8, 0.5(C_6H_{14})	**(^{PhiP}DippFeNH$_2$)$_2$**	**[^{PhiP}DippFe·IPr][BAr$^F{}_4$], C_6H_6**
empirical form.	$C_{61}H_{86}FeN_3PSiSn$	$C_{62}H_{90}Fe_2N_4P_2Si_2$	$C_{96}H_{97}BF_{24}FeN_3PSi$
formula wt	1094.92	1121.19	1874.48
crystal syst.	triclinic	monoclinic	monoclinic
space group	*P-1*	*P2$_1$/c*	*P2$_1$/c*
***a* (Å)**	10.810(2)	13.880(3)	20.260(4)
***b* (Å)**	12.650(3)	14.910(3)	23.000(5)
***c* (Å)**	23.000(5)	16.090(3)	20.000(4)
***α* (deg.)**	94.30(3)	90	90
***β* (δεγ)**	94.20(3)	111.30(3)	96.40(3)
***γ* (deg.)**	113.40(3)	90	90
vol (Å^3)	2860.1(12)	3102.4(12)	9262(3)
Z	2	2	4
ρ(calc) (g.cm^{-3})	1.271	1.200	1.344
μ (mm^{-1})	0.779	0.597	0.288
F(000)	1156	1200	3880
T (K)	150(2)	150(2)	150(2)
reflns collect.	47273	21862	51336
unique reflns	11244	6082	18014
R_{int}	0.0307	0.0389	0.1393
R1 [I>2σ(I)]	0.0337	0.0451	0.0721
*w*R2 (all data)	0.0771	0.1074	0.1920
CCDC No.	2202851	2202852	2202853

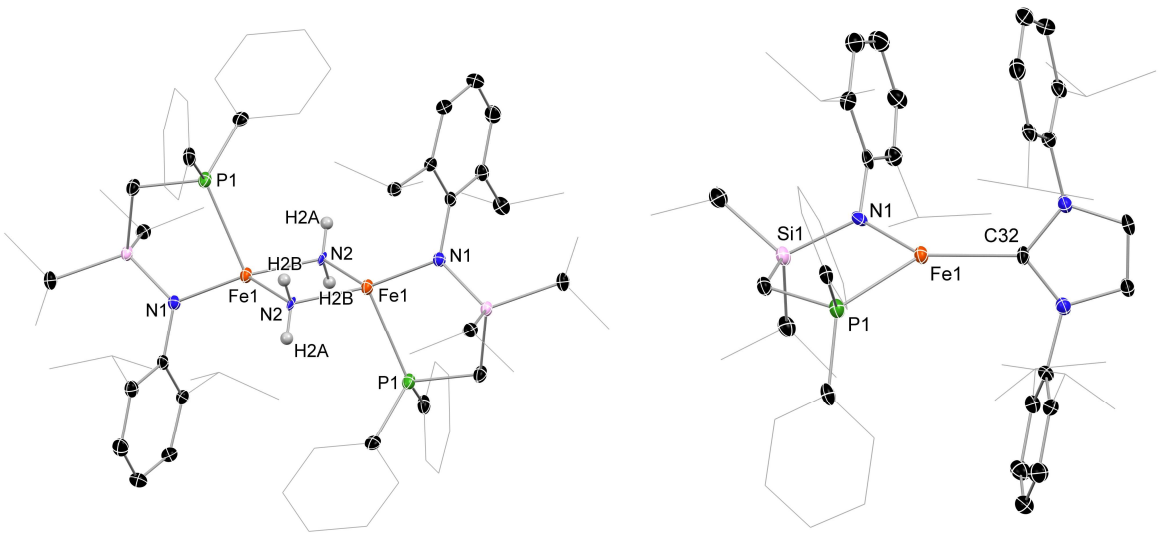

Figure 7.9 The molecular structures of (^{PhiP}DippFeNH$_2$)$_2$ (*left*) and [^{PhiP}DippFe·IPr][BAr$^F{}_4$] (*right*), with thermal ellipsoids at 25% probability, and hydrogens omitted for clarity, aside from those in NH$_2$ moieties.

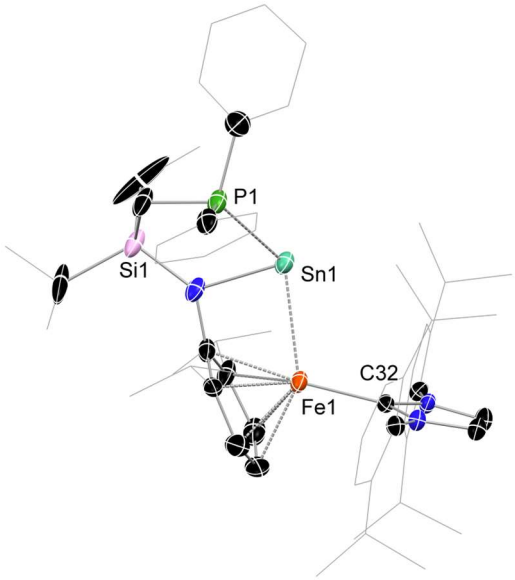

Figure 7.10 The molecular structure of the cationic part in **6**, with thermal ellipsoids at 25% probability. Note that due to significant disorder, in addition to the large atomic mass of Sn, the bridging H atoms of the Sn-(μ-H)$_2$-Fe moiety could not be located in the electron difference map.

Computational methods and details

DFT calculations for the reaction mechanism discovery were performed at the ωB97X-D(SMD=benzene)/def2-TZVPP//ωB97X-D/def2-SVP level of theory.[55] Stationary points on the potential energy surface (PES) were characterized by harmonic vibrational frequency calculations. Transition states, which had one imaginary frequency, were analysed by intrinsic

reaction coordinate (IRC) calculations to confirm the corresponding intermediates. Calculations were carried out using the GAUSSIAN 16 program suite.[56]

Spin-unrestricted density functional theory (DFT) computations of the g-matrix, and hyperfine couplings were performed using the ORCA software package (Version 5.0.2).[57] Geometry optimizations were performed using the ωB97X-D3 [58] functional together with the def2-SVP basis set,[55(b)] and the RIJCOSX density fitting scheme with the def2/J auxiliary basis set.

For the EPR calculations in ORCA, we used the ωB97X-D3 functional with the SARC-ZORA-TZVPP basis set on the Sn atom,[59] ZORA-def2-TZVPP basis set on all other atoms,[55(b)] and RIJCOSX density fitting scheme with the SARC/J auxiliary basis set. In the EPR calculation step, solvent effects have been taken into account by applying the Solvent Model Density (SMD) implicit solvation model.[60] Finally, the EPR spectra of complex **8'** was simulated using the EasySpin software program (Development version 6.0.0-dev.39).[61] The hyperfine couplings of the Sn and P atoms along with the Fe atom were considered in order to simulate the spectra, while a line width of 2 mT, a modulation amplitude of 0.4 mT, and microwave frequency of 9.05 GHz were assumed. To validate our methodology, we calculated the g-values and hyperfine coupling constants for a similar Fe-Sn complex reported by Handford, *et al.*.[19] To achieve better agreement between the computational and experimental EPR spectrum for Handford's system, we defined a constant shift for the g_x (0.001), g_y, (0.04) and g_z (0.04) values. Similarly, for complex **8'**, we applied a constant shift for the g_x (0.01), g_y, (0.04) and g_z (0.13) values to achieve better agreement between computations and experiment. Tight convergence of the electronic iterations was set using the TIGHTSCF keyword in the ORCA input file, while a dense integration grid (ORCA grid 7) was used on the Fe atom. Solvent effects have been considered by applying the Solvent Model Density (SMD) implicit solvation model. To produce the spin density plots, molecular orbitals for the optimized geometries were taken from the gbw file produced by the ORCA geometry optimization. By using the orca_plot utility program, spin densities were plotted with 120 grid points and stored in the cube file format. Finally, the spin densities were visualized using the Chemcraft program.

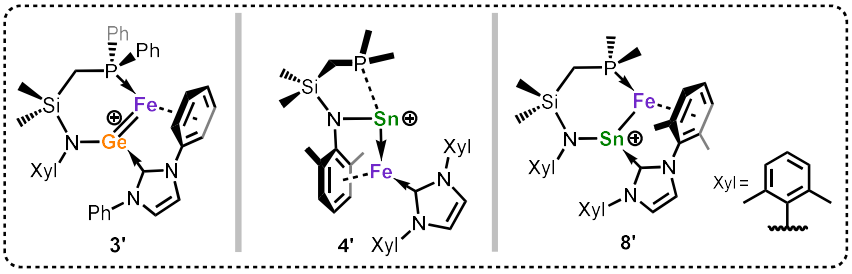

Scheme 7.3 Molecular structures for model complexes **3'**, **4'**, and **8'**.

Table 7.4 NBO analysis of the GeFeP moiety in **3'**.

3'	Occupation	Atom	Polarization	s-character	p-character	d-character
Bond	1.83	Ge	65.08%	48.50%	51.46%	0.04%
		Fe	34.92%	25.26%	47.93%	26.82%
Bond	1.88	Ge	17.07%	29.96%	69.54%	0.50%
		N	82.93%	54.52%	45.46%	0.02%
Bond	1.95	Ge	22.11%	21.50%	78.02%	0.48%
		C	77.89%	42.43%	57.57%	0.00%
Bond	1.92	Fe	29.86%	19.47%	43.83%	36.70%
		P	70.14%	31.92%	68.03%	0.05%
Lone Pair	1.91	Fe	-	0.52%	0.04%	99.45%
Lone Pair	1.72	Fe	-	0.02%	2.73%	97.25%
Empty orbital	0.63	Ge	-	0.70%	99.16%	0.14%
Empty orbital	0.25	Fe	-	1.67%	91.87%	6.46%

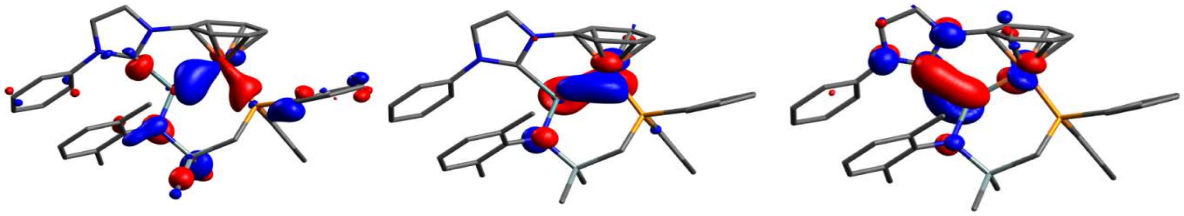

Figure 7.11 HOMO-13 (left, -12.28 eV), HOMO (middle, -9.16 eV), and LUMO (right, -2.18 eV) of 3'.

Table 7.5 Calculated bond lengths [Å], NPA, Wiberg Bond Index (WBI), Mayer Bond Order (MBO), and percent spin population in the SnFeP moiety in 3'.

Property	3'	
Bond length [Å]	Ge-Fe/Fe-P	2.184/2.225
NPA charge	Ge/Fe/P	+1.19/-0.61/+1.17
Wiberg Bond Index	Ge-Fe/Fe-P	1.35/0.85
Mayer Bond Order	Ge-Fe/Fe-P	1.37/0.97

Table 7.6 NBO analysis of the SnFeP moiety in 4'.

Alpha orbitals	Occupation	Atom	Polarization	s-character	p-character	d-character
Lone Pair	0.99	Fe	-	0.01%	0.77%	99.23%
Lone Pair	0.98	Fe	-	1.00%	0.13%	98.87%
Lone Pair	0.96	Fe	-	0.23%	0.17%	99.60%
Lone Pair	0.94	Fe	-	1.38%	0.52%	98.11%
Lone Pair	0.93	Fe	-	1.93%	0.59%	97.48%
Lone Pair	0.96	Sn	-	93.38%	6.61%	0.01%
Lone Pair	0.81	C	-	41.74%	58.25%	0.01%
Empty orbital	0.17	Fe	-	65.27%	30.24%	4.49%
Empty orbital	0.07	Fe	-	8.53%	90.42%	1.03%
Empty orbital	0.05	Fe	-	7.49%	91.33%	1.17%
Empty orbital	0.04	Fe	-	14.28%	84.80%	0.92%
Empty orbital	0.19	Sn	-	3.62%	96.16%	0.22%
Empty orbital	0.12	Sn	-	0.71%	98.92%	0.37%
Empty orbital	0.11	Sn	-	2.68%	96.95%	0.37%
Beta orbitals	**Occupation**	**Atom**	**Polarization**	**s-character**	**p-character**	**d-character**
Bond	0.96	Fe	24.23%	26.72%	39.46%	33.82%
		Sn	75.77%	14.47%	85.47%	0.06%
Lone Pair	0.82	C	-	42.36%	57.64%	0.01%
Lone Pair	0.94	Fe	-	2.21%	0.21%	97.57%
Lone Pair	0.81	Fe	-	0.01%	0.01%	99.98%
Lone Pair	0.97	Sn	-	79.78%	20.20%	0.01%
Empty orbital	0.17	Fe	-	28.33%	21.65%	50.01%
Empty orbital	0.08	Fe	-	0.93%	45.04%	54.02%
Empty orbital	0.07	Fe	-	1.01%	60.88%	38.09%
Empty orbital	0.05	Fe	-	38.31%	57.34%	4.35%
Empty orbital	0.01	Fe	-	1.65%	23.94%	74.39%
Empty orbital	0.00	Fe	-	2.60%	50.78%	46.52%
Empty orbital	0.20	Sn	-	3.97%	95.79%	0.24%
Empty orbital	0.12	Sn	-	2.19%	97.38%	0.43%

Table 7.7 Calculated bond lengths [Å], NPA, Wiberg Bond Index (WBI) and Mayer Bond Order (MBO) in the SnFeP moiety in model complex4'.

Property	**4'**	
Bond length [Å]	Sn-Fe/Fe-C	2.876/2.019
NPA charge	Sn/Fe/C	+0.59/+0.53/+0.15
Wiberg Bond Index	Sn-Fe/Fe-C	0.52/0.57
Mayer Bond Order	Sn-Fe/Fe-C	0.53/0.77

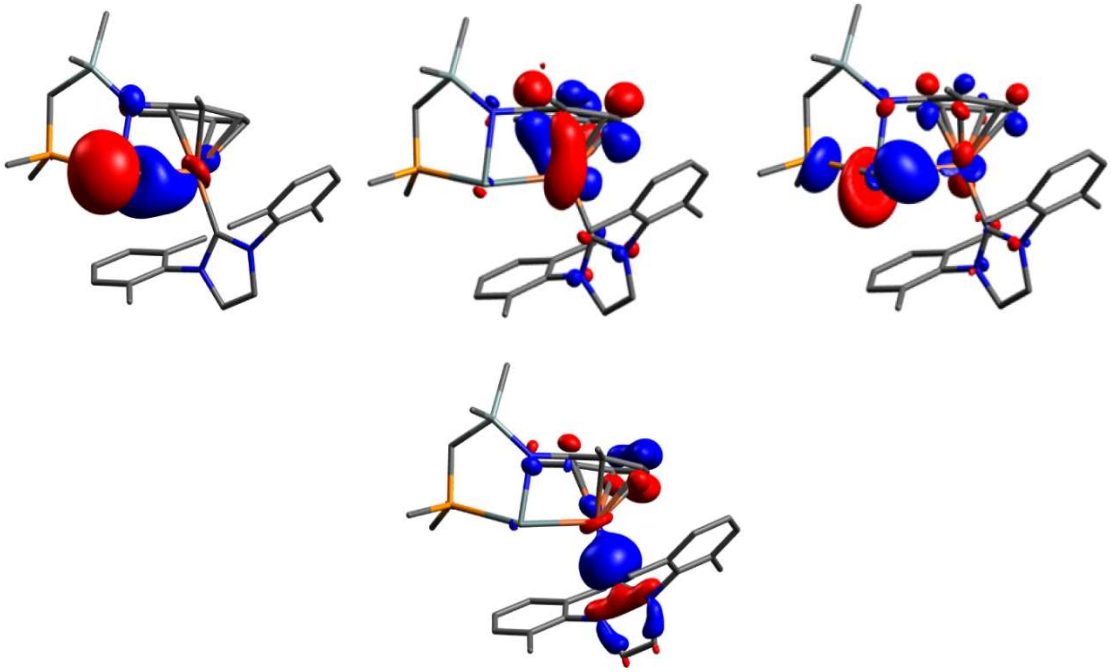

Figure 7.12 HOMO-1 (left, -10.95 eV), HOMO (middle, -10.81 eV), LUMO (right, -9.92 eV), and the isolated NBO-derived bonding interaction between the C-based lone-pair and Fe (bottom right) with an energy of 98.26 kcal mol^{-1} in 4'.

Table 7.8 NBO analysis of the SnFeP moiety in 8'.

Alpha orbitals	Occupation	Atom	Polarization	s-character	p-character	d-character
Bond	0.88	Sn	27.18%	6.21%	93.60%	0.19%
		Fe	72.82%	19.61%	22.89%	57.50%
Bond	0.88	Fe	28.01%	24.86%	39.55%	35.59%
		P	71.99%	33.41%	66.52%	0.07%
Lone Pair	0.95	Sn	-	85.61%	14.39%	0.01%
Lone Pair	0.97	Fe	-	0.03%	1.55%	98.43%
Lone Pair	0.97	Fe	-	0.78%	0.09%	99.13%
Lone Pair	0.88	Fe	-	0.06%	0.09%	99.85%
Lone Pair	0.85	Fe	-	0.16%	0.09%	99.75%
Empty orbital	0.17	Sn	-	7.30%	92.51%	0.19%
Empty orbital	0.13	Sn	-	1.35%	98.38%	0.27%
Empty orbital	0.12	Fe	-	2.32%	89.98%	7.68%
Empty orbital	0.08	Fe	-	0.76%	97.06%	2.17%
Empty orbital	0.07	Fe	-	51.41%	47.97%	0.62%
Beta orbitals	Occupation	Atom	Polarization	s-character	p-character	d-character
Bond	0.94	Sn	58.19%	15.29%	84.63%	0.08%
		Fe	41.81%	21.97%	41.62%	36.41%
Bond	0.98	Fe	23.36%	23.68%	41.97%	34.34%
		P	76.64%	34.30%	65.65%	0.05%
Lone Pair	0.96	Sn	-	76.66%	23.33%	0.01%
Lone Pair	0.95	Fe	-	1.18%	0.05%	98.77%
Empty orbital	0.17	Sn	-	6.93%	92.89%	0.18%
Empty orbital	0.13	Sn	-	1.59%	98.15%	0.26%
Empty orbital	0.15	Fe	-	0.01%	64.66%	35.32%
Empty orbital	0.08	Fe	-	39.84%	42.45%	17.70%
Empty orbital	0.01	Fe	-	0.19%	63.99%	35.78%

Table 7.9 Calculated bond lengths [Å], NPA, Wiberg Bond Index (WBI) and Mayer Bond Order (MBO) in the SnFeP moiety in model complex 8'.

Property	4'		8'	
Bond length [Å]	Sn-Fe/Fe-C	2.876/2.019	Sn-Fe/Fe-P	2.667/2.258
NPA charge	Sn/Fe/C	+0.59/+0.53/+0.15	Sn/Fe/P	+0.65/-0.19/+1.02
Wiberg Bond Index	Sn-Fe/Fe-C	0.52/0.57	Sn-Fe/Fe-P	0.78/0.73
Mayer Bond Order	Sn-Fe/Fe-C	0.53/0.77	Sn-Fe/Fe-P	0.82/0.80

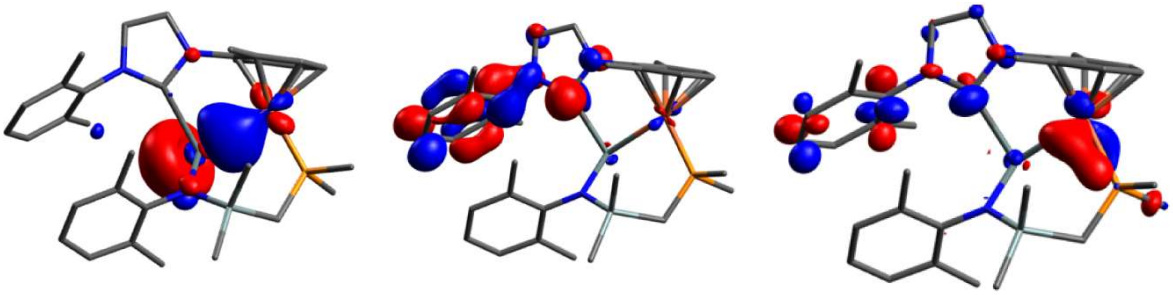

Figure 7.13 HOMO-1 (left, -7.14 eV), HOMO (middle, -5.84 eV), and LUMO (right, 1.30 eV) of 8'.

EPR Parameters

Below are the calculated EPR g-values, using the methods described above.

Table 7.10 DFT-derived g-values for 8'.

	g_x	g_y	g_z
8'	2.0055	2.0573	2.3031

Table 7.11 Experimentally derived g-values, confirmed with modelling using EasySpin, for 8'.

	g_x	g_y	g_z
8'	2.0126	2.0410	2.3050
A_P^{31}(MHz)	98	91	100
$A_{Sn}^{117/119}$(MHz)	412	456	310

Spin Density Plots

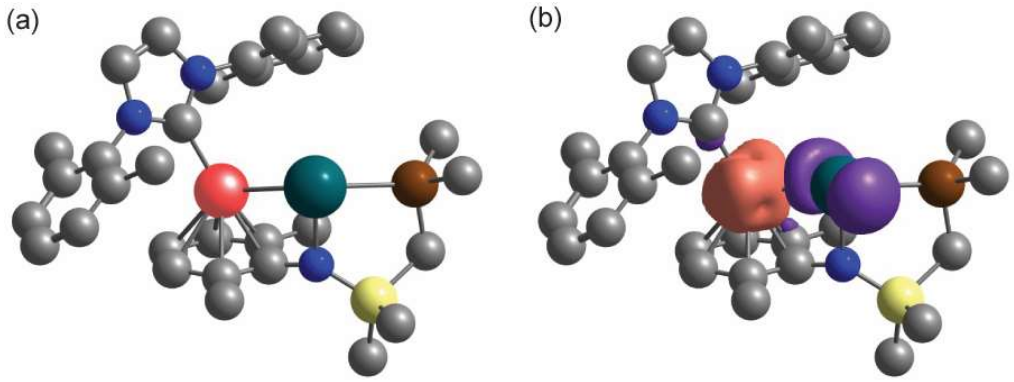

Figure 7.14 a) Optimized geometry of 4' and b) spin density distribution of 4'. Orange regions indicate positive spin density and purple regions indicates negative spin density. Hydrogen atoms are omitted for clarity. Color code: C – gray, Fe – red, N – blue, P – brown, Si - yellow, Sn – teal.

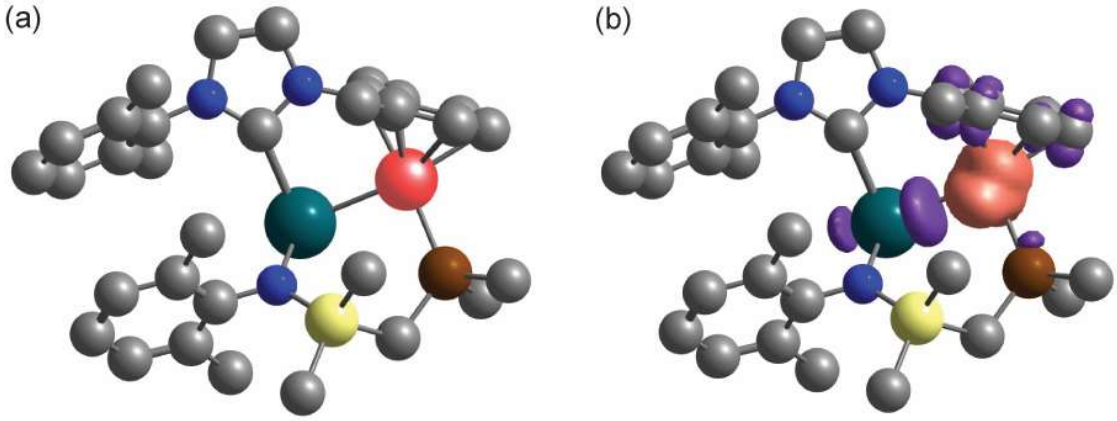

Figure 7.15 a) Optimized geometry of 8' and b) spin density distribution of 8'. Orange regions indicate positive spin density and purple regions indicates negative spin density. Hydrogen atoms are omitted for clarity. Color code: C – gray, Fe – red, N – blue, P – brown, Si - yellow, Sn – teal.

References

1 J. Cheng, J. Liu, X. Leng, T. Lohmiller, A. Schnegg, E. Bill, S. Ye, L. Deng, *Inorg. Chem.* **2019**, *58*, 7634–7644.

2 (a) J. Du, L. Wang, M. Xie, L. Deng, *Angew. Chem. Int. Ed.* **2015**, *54*, 12640–12644; (b) M. R. Elsby, S. A. Johnson, *J. Am. Chem. Soc.* **2017**, *139*, 9401–9407; (c) J. Cheng, Q. Chen, X. Leng, Z. Ouyang, Z. Wang, S. Ye, L. Deng, *Chem* **2018**, *4*, 2844–2860; (d) A. Schulz, T. L. Kalkuhl, P. M. Keil, T. J. Hadlington, *Angew. Chem. Int. Ed.* **2023**, *62*, e202305996.

3 E. O. Fischer, A. Maasbçl, *Angew. Chem. Int. Ed. Engl.* **1964**, *3*, 580–581.

4 (a) D. J. Cardin, D. Çetinkaya, M. F. Lappert, *Chem. Rev.* **1972**, *72*, 545–574; (b) F. Glorious, *N-Heterocyclic Carbenes in Transition Metal Catalysis*; Springer Berlin, Heidelberg, 2007; (c) F. E. Hahn, *Chem. Rev.* **2018**, *118*, 9455−9456; (d) A. Feliciano, J. L. Vázquez, L. J. Benítez-Puebla, I. Velazco-Cabral, D. C. Cruz, F. Delgado, M. A. Vázquez, *Chem. Eur. J.* **2021**, *27*, 8233–8251.

5 K.-S. Feichtner, V. H. Gessner, *Chem. Commun.* **2018**, *54*, 6540–6553.

6 For examples, see:
(a) D. V. Gutsulyak, W. E. Piers, J. Borau-Garcia, M. Parvez, *J. Am. Chem. Soc.* **2013**, *135*, 11776−11779; (b) R. M. Brown, J. Borau-Garcia, J. Valjus, C. J. Roberts, H. M. Tuononen, M. Parvez, R. Roesler, *Angew. Chem. Int. Ed.* **2015**, *54*, 6274–6277.

7 R. J. Somerville, J. Campos, *Eur. J. Inorg. Chem.* **2021**, 3488–3498.

8 (a) R. C. Fischer, P. P. Power, *Chem. Rev.* **2010**, *110*, 3877–3923; (b) P. P. Power, *Nature* **2010**, *463*, 171–177; (c) T. J. Hadlington, M. Driess, C. Jones, *Chem. Soc. Rev.*, **2018**, *47*, 4176–4197.

9 H. Hashimoto, K. Nagata, *Chem. Lett.* **2021**, *50*, 778–787.

10 (a) P. M. Keil, T. Szilvasi, T. J. Hadlington, *Chem. Sci.* **2021**, *12*, 5582–5590; (b) P. M. Keil, T. J. Hadlington, *Angew. Chem.* **2022**, *134*, e202114143.

11 M. Beller, *Chem. Rev.* **2019**, *119*, 2089−2089.

12 See the below, and references therein:
S. M. Rummelt, P. O. Peterson, H. Zhong, P. J. Chirik, *J. Am. Chem. Soc.* **2021**, *143*, 5928−5936.

13 R. Arevalo, P. J. Chirik, *J. Am. Chem. Soc.* **2019**, *141*, 9106−9123.

14 (a) T. Zell, D. Milstein, *Acc. Chem. Res.* **2015**, *48*, 1979−1994; (b) R. P. Yu, J. M. Darmon, S. P. Semproni, Z. R. Turner, P. J. Chirik, *Organometallics* **2017**, *36*, 4341−4343.

15 (a) T. A. Schmedake, M. Haaf, B. J. Paradise, A. J. Millevolte, D. R. Powell, R. West, *J. Organomet. Chem.* **2001**, *636*, 17–25; (b) H. Tobita, A. Matsuda, H. Hashimoto, K. Ueno, H. Ogino, *Angew. Chem. Int. Ed.* **2004**, *43*, 221 –224; (c) H. P. Hickox, Y. Wang, Y. Xie, M. Chen, P. Wei, H. F. Schaefer III, G. H. Robinson, *Angew. Chem. Int. Ed.* **2015**, *54*, 10267–10270; (d) M. M. Hänninen, K. Pal, B. M. Day, T. Pugh, R. A. Layfield, *Dalton Trans.* **2016**, *45*, 11301–11305; (e) (b) P. W. Smith, T. D. Tilley, *J. Am. Chem. Soc.* **2018**, *140*, 3880−3883.

16 (a) P. B. Hitchcock, M. F. Lappert, S. A. Thomas, A. J. Thorne, A. J. Carty, N. J. Taylor, *J. Organomet. Chem.* **1986**, *315*, 27–44; (b) T. Ochiai, D. Franz, X.-N. Wu, S. Inoue, *Dalton Trans.* **2015**, *44*, 10952–10956; (c) T. P. Dhungana, H. Hashimoto, H. Tobita, *Dalton Trans.* **2017**, *46*, 8167–8179.

17 (a) M. Weidenbruch, A. Stilter, K. Peters, H. G. Von Schnering, *Chem. Ber.* **1996**, *129*, 1565–1567; (b) M. Weidenbruch, A. Stilter, W. Saak, K. Peters, H. G. Von Schnering, *J. Organomet. Chem.* **1998**, *560*, 125–129; (c) J. J. Schneider, N. Czap, D. Bläser, R. Boese, *J. Am. Chem. Soc.* **1999**, *121*, 1409–1410; (d) J. J. Schneider, N. Czap, D. Bläser, R. Boese, J. Ensling, P. Gütlich, C. Janiak, *Chem. Eur. J.* **2000**, *6*, 468–474; (e) S. M. Mansell, R. H. Herber, I. Nowik, D. H. Ross, C. A. Russell, D. F. Wass, *Inorg. Chem.* **2011**, *50*, 2252–2263; (f) H. Zhao, J. Li, X. Xiao, M. Kira, Z. Li, T. Müller, *Chem. Eur. J.* **2018**, *24*, 5967–5973.

18 H. Lei, J.-D. Guo, J. C. Fettinger, S. Nagase, P. P. Power, *Organometallics* **2011**, *30*, 6316–6322.

19 R. C. Handford, M. A. Nesbit, P. W. Smith, R. D. Britt, T. D. Tilley, *J. Am. Chem. Soc.* **2022**, *144*, 358–367.

20 M. Widemann, K. Eichele, H. Schubert, S. P. Sindlinger, S. Klenner, R. Pöttgen, L. Wesemann, *Angew. Chem. Int. Ed.* **2021**, *60*, 5882–5889.

21 P. M. Keil, T. J. Hadlington, *Chem. Commun.* **2022**, *58*, 3011–3014.

22 Y. Liu, J. Cheng, L. Deng, *Acc. Chem. Res.* **2020**, *53*, 244−254.

23 P. M. Keil, T. J. Hadlington, *Z. Anorg. Allg. Chem.* **2022**, e202200141.

24 These are stabilized by the $[BAr^F_4]^-$ counter anion (Ar^F = 3,5-$(CF_3)_2C_6H_3$).
25 The Crystallographic Information File for this and all other crystallographically characterised compounds reported here are deposited in the CCDC, with deposition numbers 2202847, 2202848, 2202849, 2202850, 2202851, 2202852, and 2202853. These are accessible at www.ccdc.cam.ac.uk/data_request/cif.
26 (a) B. Blom, G. Tan, S. Enthaler, S. Inoue, J. D. Epping, M. Driess, *J. Am. Chem. Soc.* **2013**, *135*, 18108−18120; (b) M.-P. Luecke, D. Porwal, A. Kostenko, Y.-P. Zhou, S. Yao, M. Keck, C. Limberg, M. Oestreich, M. Driess, *Dalton Trans.* **2017**, *46*, 16412–16418.
27 We note that the remainder of aromatic signals, including those relating to the 'free' Dipp group of the NHC ligand, are found as broad signal in the usual region, between 6.9 and 8.0 ppm.
28 A. Bondi, *J. Phys. Chem.*, **1964**, *68*, 441–451.
29 (a) S. Hino, M. Brynda, A. D. Philips, P. P. Power, *Angew. Chem. Int. Ed.* **2004**, *43*, 2655–2658; (b) J. Li, S. Schenk, F. Winter, H. Scherer, N. Trapp, A. Higelin, S. Keller, R. Pöttgen, I. Krossing, C. Jones, *Angew. Chem. Int. Ed.* **2012**, *51*, 9557–9561.
30 (a) B. N. Figgis, *Nature* **1958**, *182*, 1568–1570; (b) S. C. Coste, T. J. Pearson, D. E. Freedman, *Inorg. Chem.* **2019**, *58*, 11893−11902.
31 Derived through DFT calculations. See supporting information for details.
32 For examples of our earlier endeavours here, see refs. *10* and *21*.
33 (a) J. Zhao, A. S. Goldman, J. F. Hartwig, *Science* **2005**, *307*, 1080–1082; (b) J. I. var der Vlugt, *Chem. Soc. Rev.* **2010**, *39*, 2302–2322.
34 From these mixtures, only very small amounts of the iron(II) amide compound, ^{PhiP}DippFeNH$_2$, could be isolated, formed presumably through a complex ligand redistribution reaction.
35 (a) A. Meltzer, S. Inoue, C. Präsang, M. Driess, *J. Am. Chem. Soc.* **2010**, *132*, 3038–3046; (b) T. J. Hadlington, T. Szilvasi, M. Driess, *J. Am. Chem. Soc.* **2019**, *141*, 3304–3314.
36 Compound **6** isolated in this way always formed as a mixture with **4**, which could not be separated.
37 U. Schubert, S. Gilbert, S. Mock, *Chem. Ber.* **1992**, *125*, 835–837.
38 (a) Y. Wakatsuki, K. Aoki, H. Yamazaki, *J. Am. Chem. Soc.* **1974**, *96*, 5285–5287; (b) R. G. Teller, R. G. Finke, J. P. Collman, H. B. Chin, R. Ban, *J. Am. Chem. Soc.* **1977**, *99*, 1104–1111; (c) W. W. Brennessel, R. E. Jilek, J. E. Ellis, *Angew. Chem. Int. Ed.* **2007**, *46*, 6132–6136.
39 For selected examples, see:
(a) C. Mahon, W. L. Reynolds, *Inorg. Chem.* **1967**, *6*, 1927–1928; (b) P. Le Floch, F. Knoch, F. Kremer, F. Mathey, J. Scholz, W. Scholz, K.-H. Thiele, U. Zenneck, *Eur. J. Inorg. Chem.* **1998**, 119−126; (c) C. Lichtenberg, L. Viciu, M. Adelhardt, J. Sutter, K. Meyer, B. de Bruin, H. Grutzmacher, *Angew. Chem., Int. Ed.* **2015**, *54*, 5766−5771; (d) T. M. Maier, M. Gawron, P. Coburger, M. Bodensteiner, R. Wolf, M. P. van Leest, B. de Bruin, S. Demeshko, *Inorg. Chem.* **2020**, *59*, 16035–16052.
40 (a) M.-E. Moret, J. C. Peters, *Angew. Chem. Int. Ed.* **2011**, *50*, 2063–2067; (b) M. E. Moret, J. C. Peters, *J. Am. Chem. Soc.* **2011**, *133*, 18118–18121; (c) G. Ung, J. C. Peters, *Angew. Chem. Int. Ed.* **2015**, *54*, 532–535.
41 We note that the CV of **3** shows a relatively large peak separation, ΔE_p, which is most likely due to the high concentration of this sample (3 mM). To corroborate this, a 3 mM ferrocene sample was run under identical conditions, also giving a large ΔE_p of 234 mV (see Fig. S59 in ESI).
42 N. G. Connelly, W. E. Geiger, *Chem. Rev.* **1996**, *96*, 877−910.
43 This would suggest that the reduced species has some degree of stability at ambient temperature on the timescale of the CV experiments (*e.g.* minutes). However, due to

challenges in generating and isolating this species through reduction using chemical methods, the Ge^{II}-Fe^{-I} species (*viz*. **7'**) could not be accessed in our hands.
44 Spectrum referenced to a Mn^{2+} standard, see ESI for details.
45 (a) M. J. Therien, W. C. Trogler, *J. Am. Chem. Soc.* **1986**, *108*, 3697–3702; (b) R. Gilbert-Wilson, L. D. Field, S. B. Colbran, M. M. Bhadbhade, *Inorg. Chem.* **2013**, *52*, 3043–3053; (c) M. A. Nesbit, P. H. Oyala, J. C. Peters, *J. Am. Chem. Soc.* **2019**, *141*, 8116–8127.
46 (a) A. G. Davies, D. Griller, B. P. Roberts, *J. Am. Chem. Soc.* **1972**, *94*, 1782−1783; (b) B. Das, A. Makol, S. Kundu, *Dalton Trans.* **2022**, *51*, 12404–12426; (c) A. Sekiguchi, T. Fukawa, V. Ya Lee, M. Nakamoto, *J. Am. Chem. Soc.* **2003**, *125*, 9250−9251; (d) T. Y. Lai, L. Tao, R. D. Britt, P. P. Power, *J. Am. Chem. Soc.* **2019**, *141*, 12527−12530.
47 P. Gütlich, E. Bill, A. X. Trautwein, *Mössbauer Spectroscopy and Transition Metal Chemistry*; Springer-Verlag Berlin Heidelberg, Berlin Heidelberg, **2011**.
48 A. J. Martínez-Martínez, A. S. Weller, *Dalton Trans.*, **2019**, *48*, 3351–3354.
49 U. Koelle, F. Khouzami, *Angew. Chem. Int. Ed. Engl.* **1980**, *19,* 640–641.
50 D. F. Evans, *J. Chem. Soc.* **1959**, 2003–2005.
51 M. Muhr, P. Heiß, M. Schütz, R. Bühler, C. Gemel, M. H. Linden, H. B. Linden, R. A. Fischer, *Dalton Trans.* **2021**, *50*, 9031−9036.
52 G. M. Sheldrick, SHELXL-97, Program for Crystal Strucutre Refinement, Göttingen, **1997**.
53 G. M. Sheldrick, *Acta Cryst.* **2015**, *A71*, 3–8
54 G. M. Sheldrick, *Acta Cryst.* **2015**, C*71*, 3–8.
55 (a) J. D. Chai, M. Head-Gordon, *Phys. Chem. Chem. Phys.* **2008**, *10*, 6615–6620; (b) F. Weigend, R. Ahlrichs, *Phys. Chem. Chem. Phys.* **2008**, *7*, 3297–3305.
56 *Gaussian 16 Rev. C.01*; Wallingford, CT, 2016.
57 (a) F. Neese, *WIREs Comput. Mol. Sci.* **2012**, *2*, 73–78 (b) F. Neese, *WIREs Comput. Mol. Sci.* **2022**, *12*, e1606.
58 Y. S. Lin, G. D. Li, S. P. Mao, J. D. Chai, *J. Chem. Theory Comput.* **2013**, *9*, 263–272.
59 (a) J. D. Rolfes, F. Neese, D. A. Pantazis, *J. Comput. Chem*. **2020**, *41*, 1842–1849; (b) D. A. Pantazis, X. Y. Chen, C. R. Landis, F. J. Neese, *Chem. Theory Comput.* **2008**, *4*, 908–919.
60 A. V. Marenich, C. J. Cramer, D. G. Truhlar, *J. Phys. Chem. B* **2009**, *113*, 6378–6396.
61 S. Stoll, A. Schweiger, *J. Magn. Reason.* **2006**, *178*, 42–55.

Chapter 8

Modulating Cooperative H_2 Activation with Modifiable Non-innocent Tetrylenes in 16-Electron Ni^0 Complexes

Philip M. Keil, Sophia Ezendu, Annika Schulz, Malte Kubisz, Tibor Szilvási,* and Terrance J. Hadlington*

*This project was done in collaboration with Sophia Ezendu and Prof. Tibor Szilvási from the University of Tuscaloosa, who performed all DFT calculations. Within the Hadlington group, Malte Kubisz helped develop the synthetic route for the modified tetrylenes **2a-f**, while Annika Schulz performed all experiments involving the H_2 activation of complex **3**. The here shown results will be submitted to a peer-reviewed journal and might undergo changes in the process of publishing.*

Synopsis

In Chapters 3 and 4, the ligand scaffold ^{PhR}Dipp (^{PhR}Dipp = [{$Ph_2PCH_2Si(R)_2$}(Dipp)N]$^-$; R = Ph, *i*Pr; Dipp = 2,6-*i*$Pr_2C_6H_3$) was introduced and used to isolate (chloro)germylene- and cationic germylene-nickel(0) complexes, which showed tetryl centred reactivity and Lewis acidity. MLC was not observed, partly because of the electronically saturated Ni^0 centre, but also because activation of substrates often led to elimination of the chloride substituent for the (chloro)germylene complexes, or elimination of salts of the $[BAr^F_4]^-$ counter anion ($[BAr^F_4]^-$ = [{3,5-$(CF_3)_2C_6H_3$}$_4$B]$^-$) for the cationic germylene complexes. To prevent these processes, and to have a direct handle on the electronic properties of the tetrel element, we aimed to substitute the chloride moiety in ^{PhiP}DippGeCl with different aryl substituents exhibiting varying electron withdrawing/donating properties. This substitution should increase the Lewis acidity of the germylene centre, since the chloride ligand *π*-donates electrons into the vacant *p*-orbital of the germylene. Additionally, we aimed to combine these germylene ligands with a carbene-stabilised Ni^0 moiety, [Ni(IPr)] (IPr = [{HC(Dipp)N}$_2$C:]), since this type of TM^0 moiety has already led to the successful isolation of low-valent TM complexes, with ^{PhR}Dipp as ligand scaffold, as described in Chapter 7, and a further recently published project from our group;[1] there, the isolation of the low-valent Ni^0 complex, [{^{PhiP}DippGe(Cl)}·Ni(IPr)], was achieved, where the (chloro)germylene acts as an L-type ligand, in contrast to the cationic tetrylenes acting as Z-type ligands in this class of three-coordinate, carbene stabilised Ni^0 complex.

Modifying ^{PhiP}DippGeCl with different arenes was possible by reacting the (chloro)germylene with aryl Grignard or lithium reagents, giving ^{PhiP}DippGe(R) (R = 4-CNC_6H_4, 3,5-$(CF_3)_2C_6H_3$, C_6H_5, 4-MeC_6H_4, 4-$OMeC_6H_4$, 4-$NMe_2C_6H_4$), so introducing arenes with different electronic influences on the tetrylene centre. Akin to the synthesis of [{^{PhiP}DippGe(Cl)}·Ni(IPr)], the (aryl)germylene-nickel(0) complexes [{^{PhiP}DippGe(R)}·Ni(IPr)] could be obtained. The synthesis of these complexes in most cases also yielded [{^{PhiP}DippGe(R)}·Ni(COD)] (COD = 1,5-cyclooctadiene) as a by-product, stemming from the reaction with $Ni(COD)_2$, which remains in the reaction mixture. However, due to differing solubilities of the complexes, [{^{PhiP}DippGe(R)}·Ni(IPr)] could be isolated *via* fractional crystallisation in reasonable yields between 46 and 59%. The [Ni(COD)] complexes are not reported herein since these are currently under investigation for the catalytic hydrosilylation of alkenes within the group. It should be noted that the arene substitution and synthesis of corresponding (aryl)stannylene-nickel(0) complexes, [{^{PhiP}DippSn(R)}·Ni(IPr)], was also successful, employing the (chloro)stannylene ^{PhiP}DippSnCl. These are not included here because they are part of another project from our group.

The aryl residues were shown to have the anticipated varying electronic influence on the complexes, which is well illustrated by UV/vis spectroscopy, where the UV/vis spectra of the (aryl)germylene-nickel(0) complexes each exhibit a characteristic absorption maximum between 652 nm and 799 nm, which correlates to the HOMO-LUMO gap for these complexes, in keeping with values obtained by DFT calculations. The maxima undergo a red shift for an increasing electron withdrawing effect of the residue at the germylene, which in turn means a decreasing HOMO-LUMO gap. The (aryl)germylene-nickel(0) complexes also reversibly activate H_2 across the Ge-Ni bond, giving the (hydridogermyl)nickel-hydride complexes [{^{PhiP}DippGe(R)(H)}Ni(H)·(IPr)]. In all cases, ^{1}H and ^{31}P NMR spectra showed an equilibrium between the initial complex and activation product in solution, where more electron withdrawing aryl groups at the germylene led to the equilibrium favouring the activation product. This equilibrium allowed us to obtain kinetic parameters for the activation reactions using variable temperature ^{1}H NMR spectroscopy. These correlate with the electronic influence of the substituents: the obtained exergonic values for ΔH_R and ΔG_R were largest for the complexes with the strongest electron withdrawing substituents (*i.e.* R = 4-CNC_6H_4, 3,5-$(CF_3)_2C_6H_3$). ΔH_R and ΔG_R also correlate well with calculated DFT parameters (*e.g.* NPA charges of Ge and Ni, Mayer Bond Order of the Ge-Ni bond), showing anticipated linear correlation. Further, the H_2 activation reaction is completely inhibited through introduction of the strongly *π*-donating dimethyl-amino residue at germanium, in the complex [{^{PhiP}DippGe(NMe_2)}·Ni(IPr)].

The germylene-nickel(0) complexes [{^{PhiP}DippGe(R)}·Ni(IPr)] also showed the ability to catalyse the dehydrogenative coupling of $PhSiH_3$, which was shown to result in (poly)phenysilane, as evidenced by GPC analysis. The dehydrogenative coupling is linked to the ability of the complexes to release H_2, which is demonstrated by the fact that [{^{PhiP}DippGe(Ph)(H)}Ni(H)·(IPr)] could be isolated from the reaction of [{^{PhiP}DippGe(Ph)}·Ni(IPr)] with a slight excess of $PhSiH_3$. This gives good evidence that the (hydridogermyl)nickel-hydride complex is an intermediate in the catalytic cycle, and is probably the rate determining step is the H_2 elimination. When comparing the catalytic activity of the complexes, the lowest reaction rate was measured for [^{PhiP}DippGe{3,5-$(CF_3)_2C_6H_3$}·Ni(IPr)] as this species disfavours H_2 elimination the most, since it has the highest ΔG_R value for the H_2 activation. This further supports the notion that H_2 elimination is the rate determining step of the catalysis.

In conclusion, we were able to further develop the (chloro)germylene ligand ^{PhiP}DippGeCl, introduced in Chapter 3, through the substitution of the chloride moiety by different arene residues, directly influencing the electronic nature of the germylene binding centre. Combination with a low-valent Ni^0 centre led to 16-electron Ni^0 species, [{^{PhiP}DippGe(R)}·Ni(IPr)], which demonstrate the desired MLC behaviour, in reversibly activating H_2. We could further show that the complexes catalyse the dehydrogenative coupling of $PhSiH_3$, while linking the catalytic activity of the complexes to the ability of the complexes to release H_2. The investigated influence of ligand modifications on the HOMO-LUMO gap of these Ni^0 complexes, and their catalytically-linked H_2 activation capacity, is promising for future projects, as it demonstrates that simple modifications of the ligand have a pronounced influence on the electronics and reactivity of the ensuing TM complexes. Furthermore, the ligand backbone could also be modified at N, Si, and P positions, perhaps leading to diverse reactivity, such as cooperative ammonia activation or further application in catalysis. The combination with different low-valent TM centres such as Mn, Co, or Fe is also a promising strategy, as discussed in Chapter 7, where Fe^0 centres were employed leading to differing reactivity and coordination patterns in resulting complexes, when compared to their Ni^0 counterparts.[1]

Manuscript

The here shown results will be submitted to a peer-reviewed journal and might undergo changes in the process of publishing. Further DFT calculations are underway and will be added to the Manuscript. Experimental spectra (NMR, LIFDI/MS, UV/vis and IR) and further details concerning DFT calculations will be included in the supporting information of the manuscript and can be retrieved online as soon as it will be accepted for publication.

Introduction

Many industrial processes for fundamental chemical conversions rely on H_2.[2-9] The activation of H_2 is employed in catalytic hydrogenation for the synthesis of important base and fine chemicals[10-11], while H_2 storage *via* binding and controlled release of H_2 has been of growing relevance.[12-15] Historically, the majority of compounds able to activate H_2 are transition metal (TM) complexes[16-17], but in the last two decades metal-free systems such as FLPs[18-19] or low-valent main group compounds[20-23] have been of growing interest. Another strategy for the activation of H_2 has been Metal-Ligand Cooperativity (MLC), where non-innocent ligands are used in TM complexes for the cooperative activation of substrates and catalysis.[24-25] Spearheaded by Morris, the use of Lewis basic ligands has been shown to efficiently perform hydrogenation of different substrates using abundant first-row TM centres such as Fe, Co or Mn, avoiding rare TMs.[26-29] Lewis acidic ligands have not been studied as extensively but have also shown the ability to activate H_2.[30] Heavier tetrylenes can be used as such ligands, which have shown the ability to remain Lewis acidic while coordinating to a TM centre due to their 'single-centre' ambiphilic nature, bearing a lone pair of electrons and a vacant *p*-orbital.[31]

The first study of a heavier tetrylene-TM system concerning MLC behaviour was conducted by the group of Holl in 1995, where the reversible addition of H_2 to a germylene-platinum(0) complex across the Ge-Pt bond was shown (Figure 8.1, **A**).[32] In an acyclic silylene-nickel(0) complex, the same type of activation was shown to result in a TM-hydride, which was bridged to the tetrel element *via* an agostic interaction (Figure 8.1, **B**).[33] These two types of activation were shown to generally proceed *via* H_2 activation at the TM and subsequent hydride migration to the tetryl element..[34-37] Closely related systems also activate H_2 leading to systems bearing two bridging hydride ligands between the tetrylene and TM, first reported by the group of Driess in 2017 with a (bis-silylene)nickel(0) complex, where H_2 activation resulted in a Ni^{II}-dihydride silylene stabilised compound with strong Si-H interactions (Figure 8.1, **C**).[38] We have recently reported a similar type of H_2 activation with a cationic stannylene-iron(0) complex, resulting in

two bridging hydrides between the TM and the stannylene.[39] Modifying such tetrylene-TM systems directly at the tetrylene would allow for the control of the electronic nature of these complexes, which could give a deeper understanding of such systems, and how to achieve efficient catalytic transformations such as hydrogenation. A broad study in this regard has not been carried out, presumably due to challenges regarding modifications directly at the tetrel element.

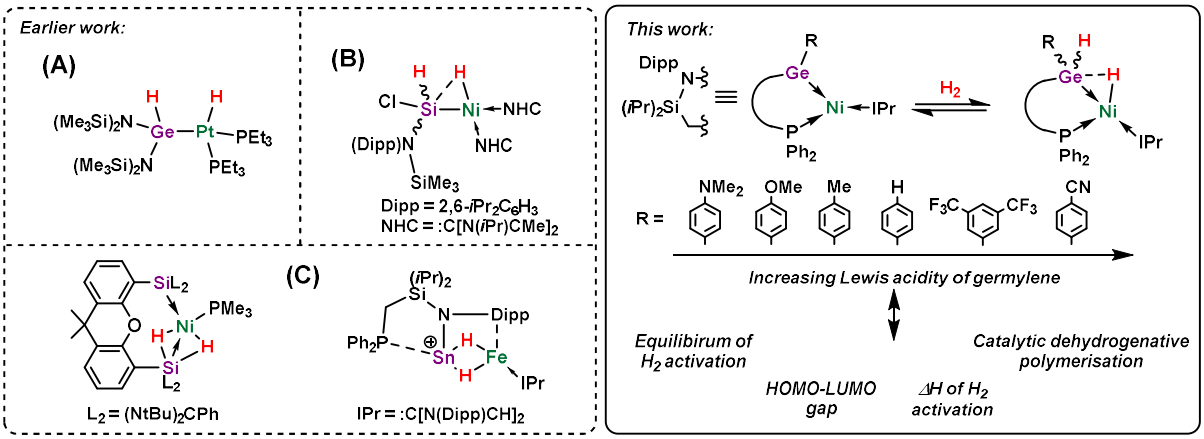

Figure 8.1 Known examples of different types of H_2 activations by tetrylene TM complexes, and the germylene Ni^0 system studied in this work with modifiable germylene residues influencing the electronic character and reactivity of the complex.

Initial studies from our group have used the ^{PhiP}Dipp ligand scaffold (^{PhiP}Dipp = [{$Ph_2PCH_2Si(iPr)_2$}(Dipp)N]$^-$; Dipp = 2,6-iPr_2-C_6H_3), in developing (chloro)tetrylene- or cationic tetrylene-nickel(0) complexes. Though these did not demonstrate cooperative bond activation, they did show the ability to perform hydrogenation and hydrosilylation catalysis, making this scaffold an interesting candidate for further investigation.[40-41] We attributed the lack of MLC behaviour to unreactive 18-electron Ni^0 centres, while the elimination of the chloride or the weakly-coordinating anion either led to Ge-centred metathesis reactions or decomposition of the complexes. In a more recent study, we could show that switching to a low-coordinate Ni^0 centre, stabilised by the bulky N-heterocyclic carbene, IPr (IPr = [(H)CN(Dipp)]$_2$C:), leads to a Z-type coordination of the cationic tetrylene ligands, [^{PhiP}DipE]$^+$, enabling hydrogenation catalysis, while the related (chloro)germylene, ^{PhiP}DipGeCl, behaves as an L-type ligand, leading to a 16-electron Ni^0 complex.[1]

In this work, we present a simple route to the modification of (chloro)germylene ligands, by chloride substitution with aryl residues. The accessed ^{PhiP}DippGe(R) ligands (R = C_6H_5 (**2a**), 3,5-$(CF_3)_2C_6H_3$ (**2b**), 4-CNC_6H_4 (**2c**), 4-MeC_6H_4 (**2d**), 4-$OMeC_6H_4$ (**2e**), 4-$NMe_2C_6H_4$ (**2f**)) were used in the generation of the corresponding Ni^0 complexes, **4a-f** [{^{PhiP}DippGe(R)}·Ni(IPr)], all of which showed the ability to reversibly activate H_2 across the Ge-Ni bond, resulting in an

equilibrium between **4a-f** and **5a-f** (*i.e.* [^{PhiP}DippGe(H)(R)Ni·(H)(IPr)]) in solution (Figure 8.1). The distinct influence of the aryl residues on the electronic nature, and thus the H_2 activation energies, of the corresponding complexes is clearly displayed. Additionally, the direct influence of the H_2 activation equilibria on the activity of these complexes for catalytic dehydrogenative polymerisation of $PhSiH_3$ is investigated.

Results and discussion

Synthesis and characterisation of 16-electron Ni^0 complexes

To modify our developed phosphine functionalised germylene systems, we wanted to substitute the labile chloride ligand in ^{PhiP}DippGeCl with a non-labile, electron withdrawing arene ligand. This should impact the electronic nature on two fronts, since the chloride ligand, contrary to the phenyl group, can *π*-donate electrons into the vacant *p*-orbital of the germylene centre. Addition of a freshly prepared solution of PhMgBr to a colourless toluene solution of **1** at -78 °C led to a yellow suspension upon warming the mixture to ambient temperature (Scheme 8.1). The $^{31}P\{^1H\}$ NMR of the crude reaction mixture indicated the clean formation of a single new species (δ = 3.2 ppm). Obtaining XRD data has not been successful thus far but NMR spectroscopy, mass spectrometry and elemental analysis all strongly indicate that the product of the reaction is indeed the targeted (phenyl)germylene ligand, ^{PhiP}DippGePh (**2a**).

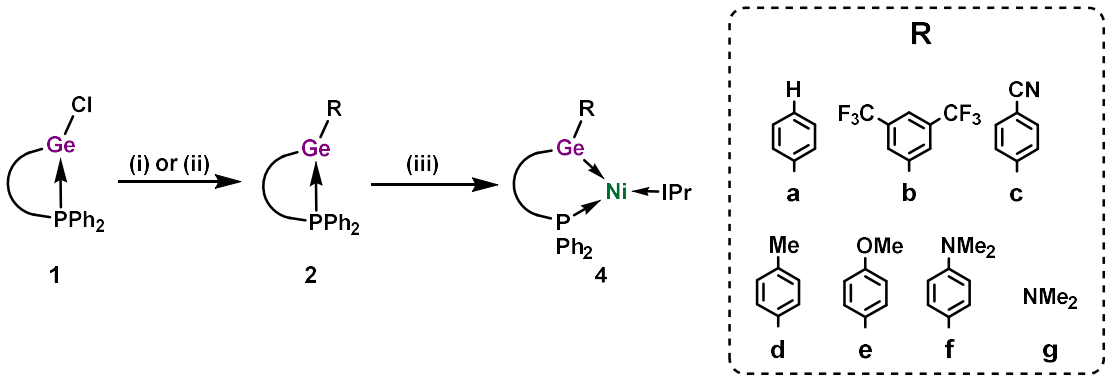

Scheme 8.1 Synthesis of the modified tetrylene ligands **2a-g** and the corresponding Ni^0 complexes **4a-g**. (i) RMgBr, Et_2O/toluene, -78°C → RT (**2a,b**); (ii) RLi, Et_2O/toluene, -78°C → RT (**2c-g**); (iii) $Ni(COD)_2$/IPr, toluene, -78°C → RT, 3 h.

Reminiscent of the synthesis of previously reported [{^{PhiP}DippGe(Cl)}·Ni(IPr)] (**3**), the addition of a toluene solution of **2a** to a toluene solution of $Ni(COD)_2$ and IPr led to a colour change from light orange to deep red, with a concomitant shift in the $^{31}P\{^1H\}$ NMR spectrum from δ = 3.2 ppm to 8.7 ppm (Scheme 8.1).[1] Storage of a concentrated pentane solution of this compound led to the crystallisation of **4a** ([{^{PhiP}DippGe(Ph)}·Ni(IPr)]), confirming the formation of a 16-electron Ni^0 complex. Compound **4a** differs considerably in colour to our previously

reported 16-electron Ni^0 (chloro)germylene complex **3**, the former being deep red in solution (λ_{max} = 752 nm), and the latter deep green (λ_{max} = 652 nm). Nevertheless, single crystal X-ray diffraction analysis showed an analogous solid-state structure for the two species, **4a** bearing a trigonal planar Ni^0 centre (sum of all angles at Ni = 359.9°) and a similar Ge-Ni bond length to that in **3** (**4a**: d_{GeNi} = 2.219(1) Å; **3**: d_{GeNi} = 2.217(1) Å; Figure 8.2). The Ge-Ni bond length is in the range of other reported germylene-nickel(0) complexes reported by our group with related ligand scaffolds, where reduced *π*-back-donation from the TM centre is observed.[40-41] The frontier orbitals of **4a** were calculated using DFT (Density Functional Theory) methods, suggesting that both the HOMO and LUMO are mainly located at the Ge-Ni bond. Therefore, the HOMO and LUMO can best be described as distorted *π*- and *π**-orbitals of the Ge-Ni bond. Both orbitals are delocalised across the NHC and the phenyl group at the germylene centre, although the delocalisation is more pronounced in case of the LUMO. The calculated MBO (Mayer bond order) of the Ge-Ni bond, at 1.12, is comparable to those in our previously reported model germylene-nickel(0) triphenylphosphine complexes ([{^{PhiP}DippGe}·Ni$(PPh_3)_2$]$^+$, MBO = 1.11; [{^{PhiP}DippGe(Cl)}·Ni$(PPh_3)_2$], MBO = 1.13), confirming some degree of *π*-back-donation from the TM centre to the tetrel element.[40-41]

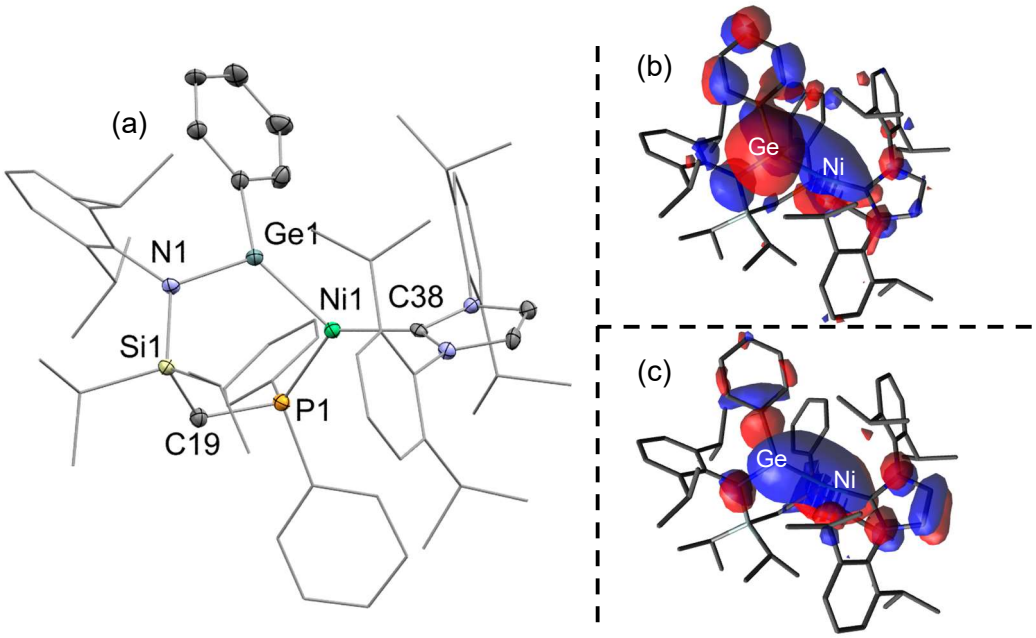

Figure 8.2 (a) The molecular structure of **4a** with hydrogen atoms omitted and thermal ellipsoids at 25% probability. Selected distances and [Å] and angles [°] for **4a**: Ni1-Ge1 2.219(1), Ge1-N1 1.898(8), Ni1-C38 1.929(8),Ge1-Ni1-C38 133.5(2), C38-Ni1-P1 130.1(2), P1-Ni1-Ge1 96.33(7). (b) The calculated LUMO and (c) HOMO of **4a**.

The absorption maxima in the UV/vis spectra of these species relates to the substitution at germylene, thus indicating a correlation of the HOMO-LUMO gap to this substitution. This kind of correlation between substituents and reactivity of heavier group 14 element(II) compounds is well documented in the literature.[21, 42-46] The red shift observed for **4a** relative to **3** would indicate a narrowing of the HOMO-LUMO separation on substituting the Cl for a Ph ligand.

This gives some evidence that an increased Lewis acidity of the germylene centre correlates to a potentially more reactive Ge-Ni bond.[47] The calculated HOMO-LUMO gaps for **3** (1.82 eV) and **4a** (1.62 eV) correlate well with the obtained energy values of λ_{max} for the measured UV/vis maxima (**3**: 1.90 eV; **4a**: 1.65 eV). Since the calculated HOMO and LUMO of **4a** are respectively reminiscent of the π- and π^*-orbitals of the Ge-Ni bond, the HOMO-LUMO gap and the discussed absorption maximum relate to the $\pi \rightarrow \pi^*$-transition in these complexes.

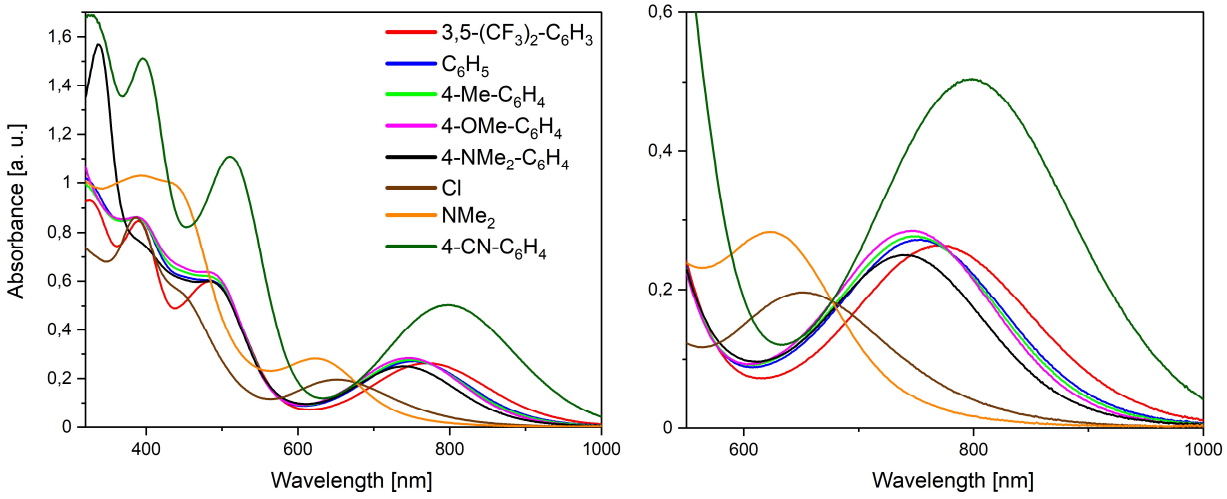

Figure 8.2 Left: UV/vis spectra of a 10^{-4} M toluene solution of **3** and **4a-g** at ambient temperature; Right: Cutout of the UV/vis spectra between 550 and 1000 nm showing the maximum associated with the HOMO-LUMO gap.

To further investigate the correlation between the residue at germanium and the electronic nature of the resulting germylene-nickel(0) complex, we wanted to introduce different residues at the germylene with varying electron donating/withdrawing properties. In this regard, the aryl-substituted germylenes, ^{PhiP}DippGe(R) (R = 3,5-$(CF_3)_2C_6H_3$ (**2b**), 4-CNC_6H_4 (**2c**), 4-MeC_6H_4 (**2d**), 4-$OMeC_6H_4$ (**2e**), 4-$NMe_2C_6H_4$ (**2f**)), as well as the amido derivative ^{PhiP}DippGe(NMe_2) (**2g**), were synthesised. This was achieved in similar manner as for the synthesis of **2a,** either using aryl Grignard or lithium reagents, or $LiNMe_2$ (Scheme 8.1). Fluorine-functionalised aryl-germylene ^{PhiP}DippGe{3,5-$(CF_3)_2C_6H_3$} (**2b**) was isolated as an off-white solid and was coherently used for the isolation of **4b** [^{PhiP}DippGe{3,5-$(CF_3)_2C_6H_3$}·Ni(IPr)]. However, **2c-g** could not be precipitated from a concentrated pentane solution, even after prolonged cold storage, indicating a high solubility. These ligands were characterised by *in-situ* $^{31}P\{^1H\}$ NMR spectroscopy, which indicated the presence of a single new species in all cases. Assuming full conversion, these solutions could successfully be utilised in generating chelating germylene-nickel(0) complexes **4c-g**. Characterisation *via* single crystal X-ray diffraction indicates similar structural features as for **3** and **4a**, with a trigonal planar Ni^0 centres, and Ge-Ni bond lengths between 2.209(1) Å and 2.231(1) Å (Table 8.1). A notable anagostic interaction between one C-*H* fragment of the backbone Si-*i*Pr group and the Ni^0 centre is

observed in all cases, leading to a 'boat' conformation for the central 6-membered ring in **4a**-**g**. The impact of the different residues has a marked effect on the electronic nature of these complexes, as can be observed in the UV/vis spectra of **3** and **4a**-**g**. The absorption maximum undergoes a red-shift with an increased electron-withdrawing effect of the residue (Figure 8.3, Table 8.1).

Table 8.1 Selected structural and spectroscopic parameters of **3** and **4a-g**.

Ni^0-Complex (R)	*d_{GeNi} [Å]*	*$\angle_{NGeNi}$ [°]*	*UV/Vis maximum [nm; eV]*	*Calc. HOMO-LUMO gap [eV]*	*High-field ^1H NMR shift [ppm]*	*$^{31}P\{^1H\}$ NMR shift [ppm]*
3 (Cl)	2.217(1)	120.9(1)	652 ; 1.90	1.82	/	13.5
4a (C_6H_5)	2.219(1)	116.8(2)	752 ; 1.65	1.62	-0.54	8.7
4b (3,5-$(CF_3)_2C_6H_3$)	2.209(1)	116.3(1)	770 ; 1.61	1.55	-0.63	11.1
4c (4-CNC_6H_4)	2.2216(8)	117.1(1)	799 ; 1.55	1.43	-0.66	12.8
4d (4-MeC_6H_4)	2.231(1)	116.6(1)	748 ; 1.66	1.62	-0.48	8.1
4e (4-$OMeC_6H_4$)	2.2203(8)	117.7(1)	747 ; 1.66	1.64	-0.44	7.7
4f (4-$NMe_2C_6H_4$)	2.2176(9)	117.5(1)	741 ; 1.67	1.64	-0.33	6.5
4g (NMe_2)	2.2162(9)	118.16(8)	623 ; 1.99	1.80	0.32	1.5

Fittingly, the strongest electron withdrawing residue, the *para*-cyanophenyl moiety (**4c**), leads to the lowest energy maxima at 799 nm, exhibiting a deep purple colour in solution. On the other extreme, the most pronounced electron donating residue, the $[Me_2N]^-$ moiety (**4g**), results in a deep green solutions and an absorption maximum at 623 nm, equal to the largest HOMO-LUMO gap. The maxima for the other substituents lie in between these two values, in the order Cl > 4-$N(Me)_2C_6H_4$ > 4-$OMeC_6H_4$ > 4-MeC_6H_4 > C_6H_5 > 3,5-$(CF_3)_2C_6H_3$. The same trend can be observed for the calculated HOMO-LUMO gap energies of the complexes, which are slightly smaller than the energies of the absorption maxima in UV/vis spectra (Table 8.1). DFT calculations further show that both the HOMO and LUMO are being stabilised with an

increasing electron withdrawing effect of the residue at the germylene. Since the LUMO is stabilised to a greater extent, a decreasing HOMO-LUMO gap is the consequence.

Further trends relating the electronic influence of the residue at the germylene with the bonding situation between Ge-Ni in **4a**-**g** are borne out through DFT calculations, particularly so the calculated NPA charges (NPA = Natural Population Analysis) of the Ge and Ni centres, and the Mayer Bond Order (MBO) of the Ge-Ni bond. The NPA charges in these structures were calculated to be between -0.512 and -0.586 for Ni, and between +1.116 and +1.313 for Ge, while the calculated Mayer Bond Order (MBO) of the Ge-Ni bonds ranges from 1.107 to 1.230 (Table 8.2). These values increase in accordance with the electron donor strength of the residue at germylene, in the order 3,5-$(CF_3)_2C_6H_3$ < C_6H_5< 4-MeC_6H_4 < 4-$OMeC_6H_4$ < 4-$N(Me)_2C_6H_4$ < NMe_2, with the exception of 4-CNC_6H_4. Here, the MBO is smaller than for 3,5-$(CF_3)_2C_6H_3$, while the values for NPA charges lie in between 3,5-$(CF_3)_2C_6H_3$ and C_6H_5.

Table 8.2 Measured Ge-Ni bond distances and selected DFT-calculated parameters of **3**, **4a**-**g** and

Ni^0 Complex (R)	*d_{GeNi} [Å]*	*Calcd. Ge-Ni Bond Length [Å]*	*NPA charges*		*Mayer Bond Order (MBO)*
			Ni	*Ge*	
3 (Cl)	2.217(1)	2.232	-0.535	1.110	1.074
4a (C_6H_5)	2.219(1)	2.241	-0.534	1.147	1.121
4b (3,5-$(CF_3)_2C_6H_4$)	2.209(1)	2.243	-0.512	1.116	1.107
4c (4-CNC_6H_4)	2.2216(8)	2.240	-0.515	1.129	1.106
4d (4-MeC_6H_4)	2.231(1)	2.242	-0.535	1.150	1.119
4e (4-$OMeC_6H_4$)	2.2203(8)	2.242	-0.539	1.152	1.130
4f (4-$NMe_2C_6H_4$)	2.2176(9)	2.243	-0.546	1.160	1.130
4g (NMe_2)	2.2162(9)	2.252	-0.586	1.313	1.230

The shift of the phosphine signal in the $^{31}P\{^1H\}$ NMR spectra of complexes **4a**-**g** is also dependent on the residue at Ge, again increasing with the electron-withdrawing effect of this ligand (Table 8.1). Here, more electron withdrawing ligands neatly lead to a more de-shielded (*i.e.* low-field shifted) resonance. A similar trend can also be observed in the ^1H NMR spectrum for **4a**-**g** where a methyl group appears with an unusually up-field shift. We believe that this is related to the anagostic interaction observed in the solid-state structures of **4a**-**g** described

above (Table 8.1). This signal undergoes a high-field shift with an increasing electron-withdrawing effect of the ligand at Ge, from δ = 0.32 ppm for the NMe_2 residue, to δ = -0.66 ppm for the 4-CNC_6H_4 residue. The only exception to these NMR spectroscopic trends is for **3**, where no low-field shifted signal is observed, and the signal in the $^{31}P\{^1H\}$ NMR spectrum appears at a higher field (δ = 13.5 ppm).

As a whole, the combined experimental and computational analyses indicate that the residues at Ge have a pronounced influence on the electronics of **4a**-**g**, which should also impact the reactivity of the complexes.

Reversible H_2 activation

With complexes **4a**-**g** in hand, we aimed to investigate the effect of the varying ligand Lewis acidity and HOMO-LUMO gap modulation on their reactive capacity. All aryl-substituted complexes (*i.e.* **4a**-**f**) were found to react with H_2 at just 1 atm of pressure and ambient temperature, leading to a single activation product as ascertained by ^1H and $^{31}P\{^1H\}$ NMR spectroscopy (Figure 8.4(b)).

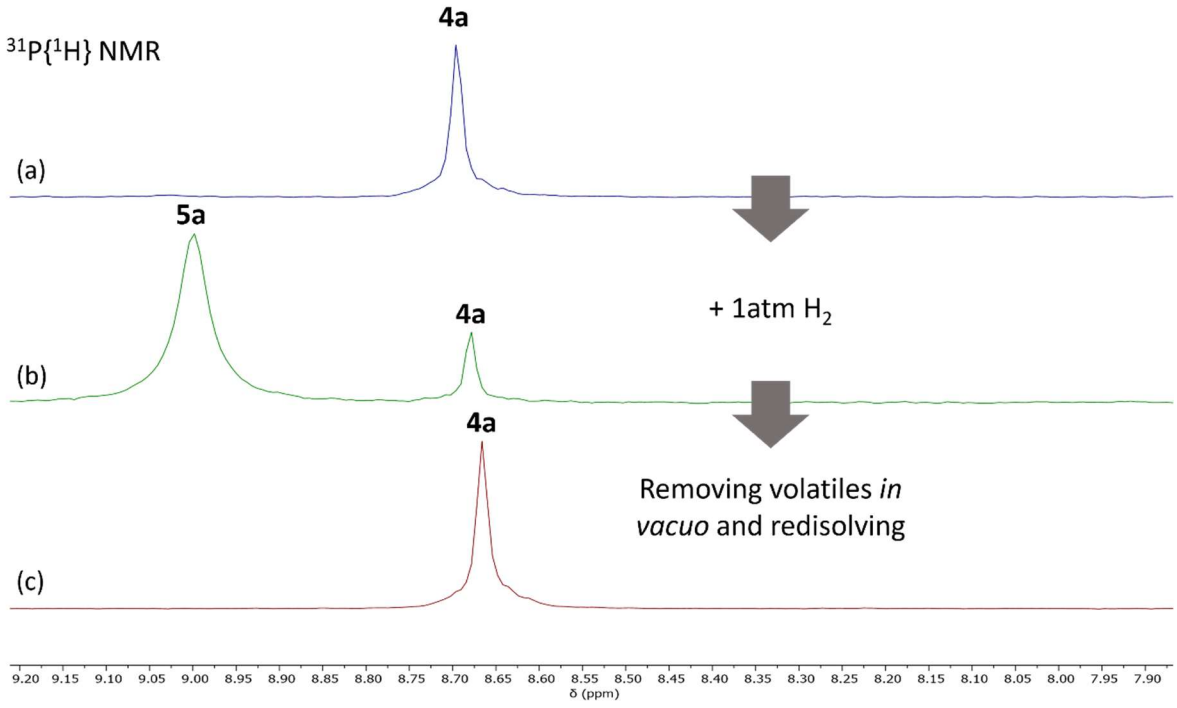

Figure 8.4 (a) $^{31}P\{^1H\}$ NMR spectrum of **4a** at 8.7 ppm in C_6D_6 at ambient temperature; (b) $^{31}P\{^1H\}$ NMR spectra of **4a** under 1 atm H_2 in C_6D_6 at ambient temperature showing **4a** and a new signal at 9.0 ppm, and of the (c) subsequent removal of all volatiles in vacuo and redissolution in C_6D_6 only displaying **4a** again.

All reactions also proved to be reversible, as small but varying amounts of **4a**-**f** were always observed in these NMR spectra, and the full regeneration of those starting materials is

achieved by removing all volatiles *in vacuo*, followed by re-dissolution (Figure 8.4(b) and (c)). Precipitation of analytically pure yellow solids of the H_2 activation products **5a**, and **5c-f** was possible by subjecting an Et_2O or pentane solution of **4a** or **4c-f** to 1.5 bar H_2, and storing the solutions for 24 h at ambient temperature. Structural characterisation, *via* single crystal X-ray diffraction, was achieved for **5a** and **5c**, showing that the reaction with H_2 in these complexes leads to cooperative activation, in forming (hydrido-germyl)nickel-hydride complexes (Scheme 8.2, Figure 8.5).

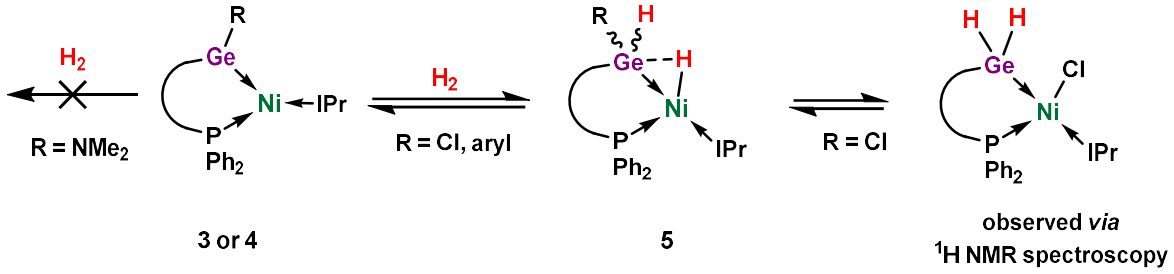

Scheme 8.2 Reversible cooperative activation of H_2 by **3** and **4a-f** across the Ge-Ni bond under ambient conditions and no reaction of **4g** with H_2.

In both cases, the Ni centre is now in a distorted square planar geometry (sum of all angles at Ni: **5a** = 360.46°; **5c** = 360.97°), and the Ge holds a tetrahedral geometry. The Ge-Ni bonds are elongated when compared to those in **4a** and **4c** (d_{GeNi}: **4a** = 2.219(1); **5a** = 2.312(1); **4c** = 2.2216(8); **5c** = 2.323(1) Å), presumably due to absent π-back-donation from Ni to Ge, due to the coordinatively saturated Ge centre. The Ni-hydride exhibits a bridging character to the Ge centre, reminiscent of related H_2 activation reactions in an acyclic silylene-nickel(0) complex (Figure 8.1, **B**).[33]

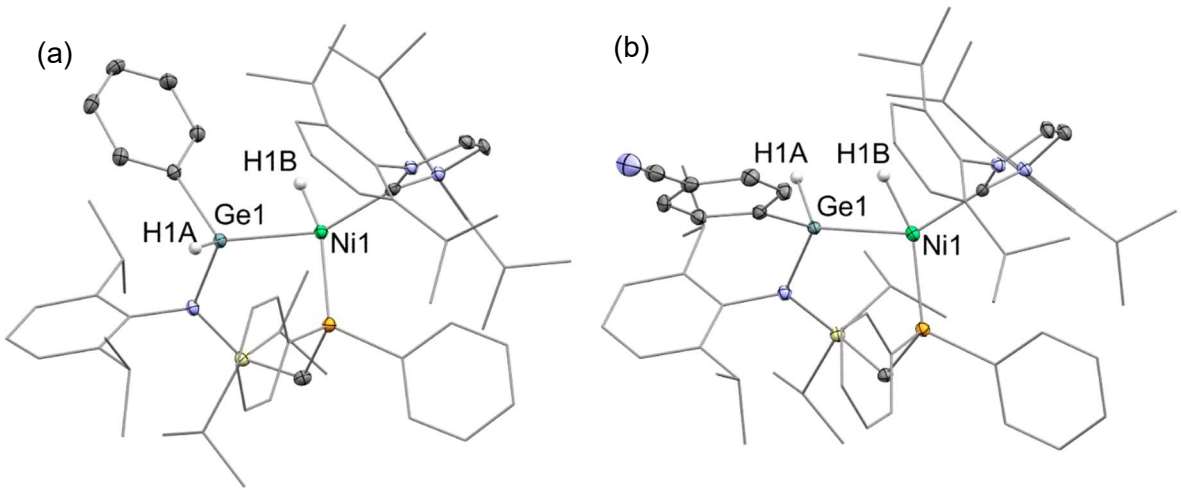

Figure 8.5 The molecular structure of **5a** and **5c** with hydrogen atoms omitted and thermal ellipsoids at 25% probability. Selected distances and [Å] and angles [°] for **5a**: Ni1-Ge1 2.312(1), Ge1-N1 1.931(4), Ni1-C38 1.920(5), Ni1-P1 2.174(1), C38-Ni1-P1 111.3(1), P1-Ni1-Ge1 92.16(4); **5c**: Ni1-Ge1 2.323(1), Ge1-N1 1.923(3), Ni1-C39 1.918(3), Ni1-P1 2.201 (1), C39-Ni1-P1 114.71(9), P1-Ni1-Ge1 100.16(4).

The hydrides can also be observed in the IR spectra of the isolated solids of **5a** and **5c-f**, exhibiting stretching bands between 1934 and 1949 cm^{-1} for the Ge-H moiety, and between 1878 and 1893 cm^{-1} the Ni-H moiety, which can be assigned by comparison to related compounds in the literature.[33, 48] Due to its high solubility, **5b**, bearing the 3,5-$(CF_3)C_6H_3$ group, could not be isolated in the solid state, and was therefore not analysed using IR spectroscopy. However, this species was characterised by *in-situ* NMR spectroscopy. One would expect to also observe signals for the hydride ligands in ^1H NMR spectra of H_2 activation products. At ambient temperature, however, this was not the case. Variable temperature (VT) NMR spectroscopy, in either toluene-d_8 or THF-d_8, allowed for the observation of resonances relating to both the Ge-*H* and Ni-*H* moieties, between -40 and -80 °C, where the Ge-*H* is observed as a broad resonance between δ = 5.22 (**4f**) and 6.03 (**4c**) ppm, while the Ni-*H* could be seen as a broad doublet between δ = -9.76 (**4f**) and -10.83 (**4c**) ppm, both integrating to 1H. The coupling of these two peaks could be shown via 2D-COSY experiments for **5b**. Conducting these measurements at 60°C, a new peak at approximately δ = -2 ppm for all compounds appeared, which integrates to 2H. This speaks for a dynamic exchange between the hydrides at the NMR timescale, as has previously been observed for Si-*H* and Ni-*H* hydrogen atoms in (hydrido)(silyl)nickel complexes.[49] This could further be shown by the generation of H-D gas when adding D_2 to the H_2 activation product **5a**. The activation of D_2 with **4a** leads to the disappearance of the respective hydride peaks otherwise observed in the ^1H NMR spectrum of **5a**, affirming their assignment. For complex **4g**, where the NMe_2 residue quenches the Lewis acidity through π-donation of the nitrogen to germanium, no detectable H_2 activation reaction is observed (Scheme 8.2).

The (chloro)germylene complex **3** also activates H_2, showing the formation of two different sets of new signals in the ^1H and ^{31}P NMR spectra, while **3** could also still be observed, indicating reversibility. This was clearly shown by removing all volatiles from this sample, and redissolving the residue in C_6D_6, leading to full regeneration of **3**. When looking at the *in-situ* ^1H NMR spectrum for the reaction between **3** and H_2, the signals at δ = 5.84 ppm and -11.84 ppm should be pointed out, coupling both to each other and the phosphine moiety of the ligand backbone. These signals are notably in the range for the Ge-*H* and Ni-*H* signals for compounds **5a-f**, indicative of the cooperative activation of H_2 by **3**. Performing the same reaction with D_2 led to the disappearance of these two signals, further showing that they originate from activated H_2. This D_2 addition reaction also led to the disappearance of a broad singlet observed at δ = 4.61 ppm in the corresponding H_2 addition reaction. This hints that the initial activation product undergoes hydride migration to the Ge centre, resulting in a (dihydridogermyl)nickel-chloride complex (Scheme 8.2). This type of hydride and chloride rearrangement has been reported for

a similar (chloro)silylene-nickel(0) species.[34] However, we were as yet unable to obtain structural confirmation of such activation products in this case.

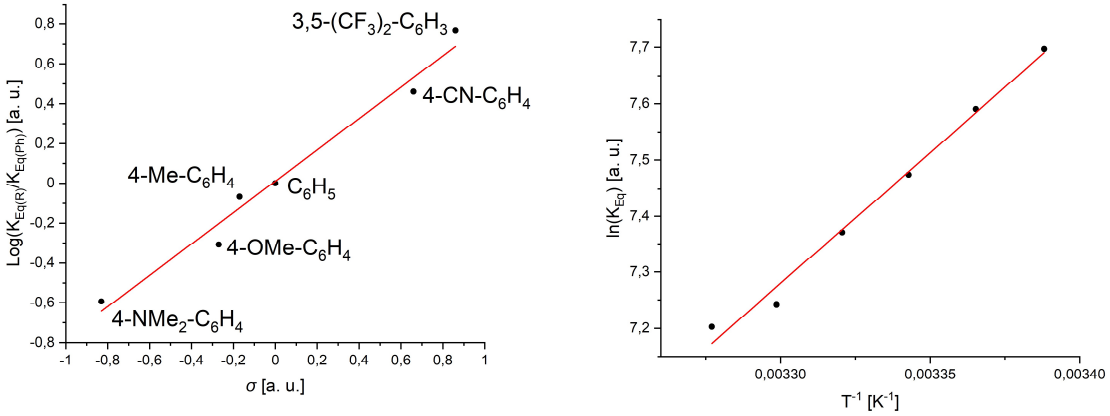

Figure 8.6 Analysis of the equilibrium for the H_2 activation of **4a-f**; Left: Hammet plot for **4a-f** of $Log(K_{eq(R)}/K_{eq(C6H5)})$ vs Hammet parameters σ showing linear correlation (y = 0.788x + 0.010; R^2 = 0.972); Right: Plot for **4a** of $ln(K_{eq})$ vs. T^{-1} from VT ^1H NMR data giving linear regression, which can be analysed to obtain ΔH_R and ΔS_R of the equilibrium (y = 4661.57x - 8.10 R^2 = 0.987).

As mentioned above, the addition of H_2 to solutions of complexes **4a-f** leads to an equilibrium between these starting Ni^0 complexes, and the associated activation products **5a-f**. Complex **4b**, bearing the highly electron withdrawing 3,5-$(CF_3)_2C_6H_3$ group at Ge, led to an almost

Table 8.3 Kinetic parameters for the equilibrium of H_2 activation of **4a-f** obtained via VT ^1H NMR spectroscopy.

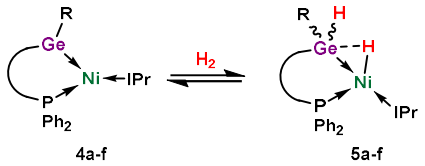

4a-f 5a-f

	K_{eq} at 299.15 K [Lmol^{-1}]	ΔH_R [kJmol^{-1}]	ΔS_R [Jmol^{-1}K^{-1}]	ΔG_{298K} [Jmol^{-1}K^{-1}]
***4a* (C_6H_5)**	1761	-38.76±1.99	-67.37±6.65	-18.68±3.97
***4a* (C_6H_5) + D_2**	2129	-39.90±1.44	-69.60±4.81	-19.16±2.87
***4b* (3,5 $(CF_3)_2$-C_6H_3)**	10307	-42.69±1.52	-66.08±5.06	-23.00±3.03
***4c* (4-CN-C_6H_4)**	5089	-44.39±1.14	-77.59±3.79	-21.27±2.27
***4d* (4-Me-C_6H_4)**	1504	-37.35±0.95	-64.15±3.20	-18.23±1.90
***4e* (4-OMe-C_6H_4)**	867	-34.75±2.23	-59.76±7.42	-16.94±4.44
***4f* (4-NMe_2-C_6H_4)**	449	-33.09±1.20	-59.81±3.99	-15.27±2.39

complete generation of **5b** under 1 atm H_2 at 26°C (K_{eq} = 10307 L/mol). Conversely, complex **4f**, with the strongly electron donating 4-$Me_2NC_6H_4$ group at Ge, results in 75% of **5f** under the same reaction conditions (K_{eq} = 449 L/mol). The other complexes lie between these extremes, the equilibria being in good agreement with the Hammet parameters for the differing R groups. This is clearly depicted by the Hammet plot of $\log(K_{eq(R)}/K_{eq(Ph)})$ *vs.* the respective Hammet parameters, σ (Figure 8.6, Table 8.3).[50] When comparing the K_{eq} values for the activation of D_2 (K_{eq} = 2129 L/mol) and H_2 (K_{eq} = 1761 L/mol) by **4a**, an inverse KIE of 0.83 was calculated, which is expected for equilibria involving the activation of H_2/D_2.[51] Further kinetic data for the H_2 activation could be obtained by VT ^{1}H NMR spectroscopy, between 20 and 32°C, by calculating the corresponding K_{eq} at different temperatures. The resulting plot of $\ln(K_{eq})$ *vs*. T^{-1} gave a linear correlation, from which ΔH_R and ΔS_R of the reaction can be calculated (Table 8.3). The ΔH_R values are in line with the UV/vis-determined HOMO-LUMO gaps for **4a-f**, with **4c** having the highest value, at -44.4 kJmol^{-1}, and **4f** having the lowest value, at -33.1 kJmol^{-1}. Even though **4c** has the highest ΔH_R, this does not result in the biggest K_{eq} at 26°C, which can be explained by the much higher ΔS_R value of -77.6 Jmol^{-1}K^{-1} for this system, leading to a greater influence of the temperature on K_{eq}. All other complexes have ΔS_R values between -67 and -59 Jmol^{-1}K^{-1}. The negative entropy for the reaction is expected since H_2 is bound in the process of activation, while the much higher value for **4c** could be rationalised by the weakly basic cyano group, which may result in dimer formation of the activation product **5c** in solution, further lowering its entropy.

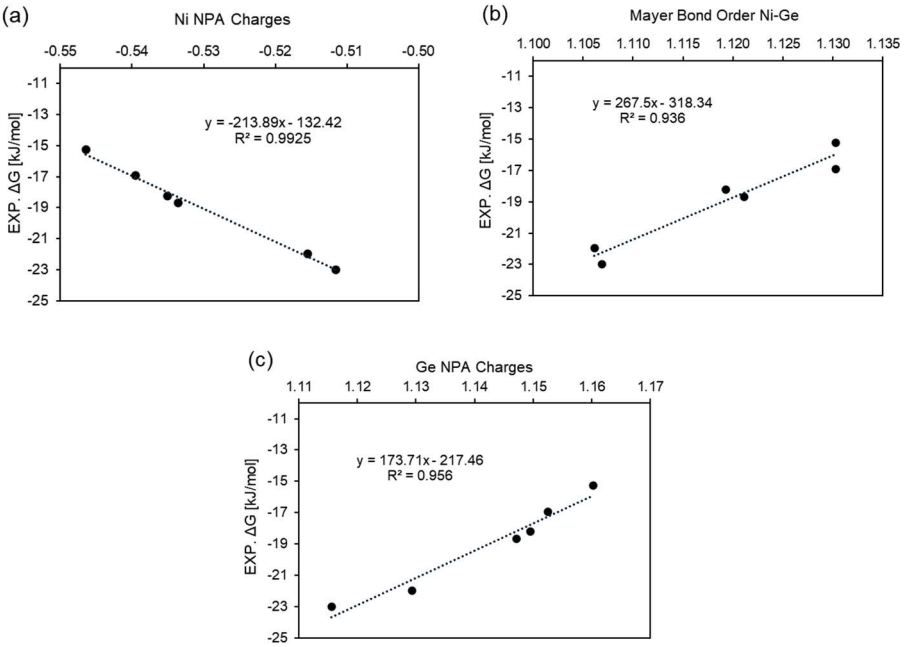

Figure 8.7 Correlation between experimentally measured ΔG_R and calculated a) Ni NPA charges, b) Ni-Ge Mayer Bond Order (MBO), and c) Ge NPA charges for **4a-f**.

Plotting the experimentally obtained ΔH_R and ΔG_R values shown in Table 8.3 against the calculated NPA charges of Ni and Ge, and the MBO of the Ge-Ni bond (Table 8.2), gives a linear correlation. This is in accordance with the electronic influence of the residue at the germylene (Figure 8.7). The ΔH_R and ΔG_R values become more negative with decreasing NPA charges of Ge and Ni and the MBO values. This further illustrates the impact of the residue at germanium on the properties of the Ni^0 complexes **4**, and is in direct correlation with the kinetic parameters of the respective reversible H_2 activation by these well-defined species.

Dehydrogenative coupling of $PhSiH_3$

Following the investigation of the cooperative H_2 activation process for **3** and **4a-g**, we wanted to explore if the complexes are capable of catalysis, and if the catalysis is also impacted by the differing electronic nature of these species. All complexes are active in the catalytic dehydrocoupling of $PhSiH_3$, a reaction which is known for a small number of Ni complexes.[52-53] Initial experiments indicated that H_2 is released when a slight excess of $PhSiH_3$ is added to **4a**. From these reactions, **5a** could be isolated, which indicates that the H_2 elimination is likely the

Table 8.4 Catalytic dehydrogenative coupling with 1 mol% of **3** and **4a-g** and the, via ^1H NMR spectroscopy, quantified amount of $PhSiH_3$ after three hours.

Ni^0 Complex (R)	*Consumption of $PhSiH_3$ after 3 h*
3 (Cl)	*70%*
4a (C_6H_5)	62%
4b (3,5 (CF_3)$_2$-C_6H_3)	48%
4c (4-CN-C_6H_4)	57%
4d (4-Me-C_6H_4)	60%
4e (4-OMe-C_6H_4)	62%
4f (4-NMe_2-C_6H_4)	64%
4g (NMe_2)	65%

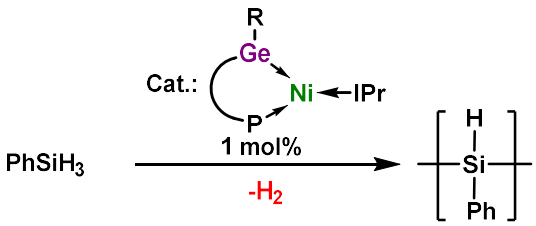

rate limiting step of this coupling process. Making this reaction catalytic, considerable H_2 evolution is observed when $PhSiH_3$ is dehydrocoupled by 2.5 mol% **4a** in C_6D_6 solutions. A similar observation is made when conducting the same reaction with **3** and **4b-g**. Stirring these mixtures and allowing for out-gassing (*i.e.* release of H_2 pressure) leads to the full consumption

of $PhSiH_3$, and formation of poly(phenylsilane) (Table 8.4). The resulting polymer was analysed via GPC analysis, exhibiting a mean molecular weight of 1788 $gmol^{-1}$, with a PDI of 1.6. This means that approximately 17 units of phenylsilane are contained in one polymer. The ^1H NMR spectrum of the polymer in C_6D_6 revealed broad peaks at 7.69 ppm and 7.02 ppm likely stemming from the phenyl group of the polymer. A broad peak of low intensity is observed between 6.0 ppm and 4.8 ppm for the remaining Si-hydrides contained in the polymer, indicating a high degree of branching.[54]

Two different mechanisms can be envisioned for the coupling of two $PhSiH_3$ units, considering that the hydride complexes **5** are likely involved in this process (Figure 8.8). The activation of the Si-H bond in $PhSiH_3$ across Ge-Ni bond in **3** or **4** can either lead to the (hydrido-germyl)nickel-silane complex **6**, or the (silyl-germy)nickel-hydride complex **7**. Since the hydride in $PhSiH_3$ has a partial negative charge and the germyl centre a partial positive charge, one can assume that the catalysis most likely proceeds *via* the (hydrido-germyl)nickel-silane complex **6**. Activation of another $PhSiH_3$ molecule with these complexes can lead in both cases to H_2 or $(H_2PhSi)_2$ elimination, either resulting in the (silyl-germyl)nickel silane species **8**, or the earlier discussed (hydrido-germyl)nickel-hydride species **5**. This would be followed by the concomitant release of H_2 or $(H_2PhSi)_2$ regenerating the catalyst (*i.e.* **3** or **4**). The fact that we isolated the (hydrido-germyl)nickel hydride complex **5a** from a reaction of **4a** with $PhSiH_3$ indicates that the catalysis proceeds *via* this complex, and not the (silyl-germyl)nickel-silane species **8**. This type of mechanism can also be applied to already coupled $PhSiH_3$ fragments, which would then lead to the observed polymers.

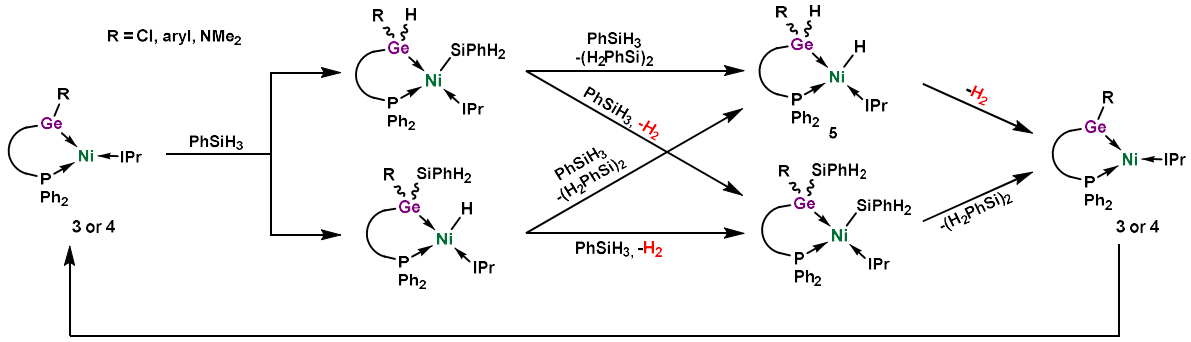

Figure 8.8 Postulated mechanism for the catalytic coupling of two $PhSiH_3$ units with **3** or **4** as catalyst.

To evaluate the performance of the catalysts, the catalyst loading was reduced to 1 mol% to prevent reactions from going to completion, and the consumption of $PhSiH_3$ measured after three hours *via* ^1H NMR spectroscopy (Table 8.4). In-line with the H_2 elimination step being the rate determining step, the lowest catalytic activity was observed for the complexes **4b** (48% $PhSiH_3$-consumption after three hours) and **4c** (57% $PhSiH_3$-consumption after three hours), which both bear the smallest HOMO-LUMO gap. This is logical, given that the systems with a

larger HOMO-LUMO gap favour H_2 liberation, and *vice-versa* for the systems with a smaller HOMO-LUMO gap, as shown through our described kinetic investigations of the H_2 activation reaction. This demonstrates that the residue at the germylene has a pronounced effect on the catalytic performance.

Conclusion

We have developed a synthetic route to modify the bidentate phosphine functionalised (chloro)germylene ligand **1**, in accessing aryl- and amide-functionalised ^{PhiP}DippGe(R) systems (R = C_6H_5 (**2a**), 3,5-$(CF_3)_2$-C_6H_3(**2b**), 4-CN-C_6H_4 (**2c**), 4-Me-C_6H_4 (**2d**), 4-OMe-C_6H_4 (**2e**), 4-NMe_2-C_6H_4 (**2f**), NMe_2 (**2g**)). These ligands were utilised in the synthesis of corresponding 16-electron Ni^0 complexes **4a**-**g**. We were able to show that the electronic influence of the residue on the germylene affects the absorption maxima in the UV/vis spectra of these complexes, which undergo a red-shift with increasing electron-withdrawing effect of the residue. This indicates that the absorption maxima are correlated to the HOMO-LUMO gaps of the complexes, which is supported by DFT calculations. This translates to the reactivity of the complexes with H_2, which are shown to be cooperative and reversible, leading to the (hydrido-germyl)nickel-hydride species **5a**-**f**. Additionally, all such H_2 activation reactions result in an equilibrium with **4a**-**f**. This equilibrium and related kinetic parameters (*i.e.* ΔH_R, ΔS_R, K_{eq}, KIE) could be studied in depth using VT ^{1}H NMR spectroscopic methods. Here we could observe the correlation between the energy of the absorption maxima, DFT-calculated Ge-Ni bond parameters of **4a**-**f,** and the experimentally determined kinetic parameters. Finally, **4a**-**g** were also capable of catalysing the dehydrogenative polymerisation of $PhSiH_3$, which we found to likely be impacted by the H_2 equilibrium between **4a**-**f** and **5a**-**f**: complexes which favour the release of H_2, bearing electron donating residues, exhibited increased catalytic activity, and *vice-versa* for electron withdrawing residues. These are highly promising results regarding the development of non-innocent ligands based upon low-valent *p*-block species, demonstrating that simple modifications of our germylene ligand system, ^{PhiP}DippGe(R), has a pronounced influence on the electronics and reactivity of the ensuing TM complexes.

Supporting Information

General experimental considerations

All experiments and manipulations were carried out under dry oxygen free argon atmosphere using standard Schlenk techniques or in a MBraun inert atmosphere glovebox containing an atmosphere of high purity argon. C_6D_6 was dried, degassed and stored over a potassium mirror. THF and Et_2O were dried over Na/Benzophenon, distilled and stored over 4Å molecular sieves. All other solvents were dried over activated 4Å molecular sieves. **1** ^{PhiP}DippGeCl[40],

4-Me-C_6H_4-Li[55], 4-OMe-C_6H_4-Li[56], 4-NMe_2-C_6H_4-Li[57], **3** [{^{PhiP}DippGe(Cl))}·Ni(IPr)][1], $Ni(COD)_2$[58] and IPr[59] were made using literature known procedures. All other reagents were used as received. NMR spectra were recorded on a Bruker AV 400 Spectrometer. The ^{1}H and ^{13}C{^{1}H} NMR spectra were referenced to the residual solvent signals as internal standards. ^{29}Si{^{1}H} NMR spectra were externally calibrated with $SiMe_4$. ^{31}P{^{1}H} NMR spectra were externally calibrated with H_3PO_4. Liquid Injection Field Desorption Ionization Mass Spectrometry (LIFDI-MS) was measured directly from an inert atmosphere glovebox with a Thermo Fisher Scientific Exactive Plus Orbitrap equipped with an ion source from Linden CMS.[60] Commercial hydrogen gas with a purity of ≥ 99.999% was used in the gas experiments. Elemental analyses (C, H, N) were performed with a combustion analyzer (elementar vario EL, Bruker). Infrared spectra were measured with the Alpha FT IR from Bruker containing a platinum diamond ATR device. Absorption spectra (UV/vis) were recorded on an Agilent Cary 60 UV/vis spectrophotometer.

Experimental procedures

General Method for preparation of 2 ^{PhiP}DippGe(R):

A solution of freshly prepared Grignard- or Lithium-reagent was added dropwise to a solution of **1** ^{PhiP}DippGeCl in toluene at -78°C, while being stirred. The mixture was then allowed to warm to ambient temperature and stirred for 30 min. All volatiles were removed *in vacuo* and the residue was extracted with toluene. All volatiles were removed in vacuo and the residue dissolved in pentane and stored at -32°C overnight. The resulting suspension was filtered and the solid washed with pentane and dried in vacuo, yielding the substituted germylene **2**. If no solid formed after storing the pentane solution at -32°C it was used without further purification in further steps.

^{PhiP}DippGe(C_6H_5), 2a. The germylene was synthesized according to the general method using **1** (2.00 g, 3.4 mmol) and a freshly prepared Et_2O solution of PhMgBr using PhBr (0.68 g, 4.4 mmol), Mg (0.16 g, 6.5 mmol) and a pinch of iodide. An off-white powder of **2a** (1.35 g, 2.1 mmol, 63%) was isolated after precipitation from a pentane solution at -32°C.

^{1}H NMR (C_6D_6, 400 MHz, 298 K): δ = 0.81 (m, 3H, Si-^{i}PrC*H*$_3$), 0.87 (m, 1H, Si-^{i}PrC*H*), 1.04 (m, 9H, Si-^{i}PrC*H*$_3$/Dipp-^{i}PrC*H*$_3$), 1.28 (d, 3H, $^3J_{HH}$ = 7.6 Hz, Si-^{i}PrC*H*$_3$), 1.37 (d, 3H, $^3J_{HH}$ = 6.4 Hz, Dipp-^{i}PrC*H*$_3$), 1.42 (d, 3H, $^3J_{HH}$ = 7.3 Hz, Si-^{i}PrC*H*$_3$), 1.47 (d, 3H, $^3J_{HH}$ = 6.7 Hz, Dipp-^{i}PrC*H*$_3$), 1.88 (m, 3H, C*H*$_2$-PPh_2/Si-^{i}PrC*H*), 3.25 (sept, 1H, $^3J_{HH}$ = 6.5 Hz, Dipp-^{i}PrC*H*), 4.51 (sept, 1H, $^3J_{HH}$ = 6.5 Hz, Dipp-^{i}PrC*H*), 6.78 (m, 5H, Ar-C*H*), 7.13 (m, 9H, Ar-C*H*), 7.80 (m, 4H, Ar-C*H*).

^{31}P{^{1}H} NMR (C_6D_6, 162 MHz, 298 K): δ = 3.2 (s, *P*Ph_2).

^{13}C{^{1}H} NMR (C_6D_6, 101 MHz, 298 K): δ = 8.3 (d, $^1J_{CP}$ = 7.6 Hz, *C*H_2-PPh_2), 17.6 (d, Si-^{i}Pr*C*H), 19.6 and 20.3 (Si-^{i}Pr*C*H_3), 20.6 (d, Si-^{i}Pr*C*H), 21.1 and 21.2 (Si-^{i}Pr*C*H_3), 22.6 and 23.2

(Dipp-^{i}PrC*H*$_3$), 28.2 (Dipp-^{i}PrC*H*), 28.3 (Dipp-^{i}PrC*H*$_3$), 28.6 (Dipp-^{i}PrC*H*), 28.8 (Dipp-^{i}PrC*H*$_3$), 123.2, 124.3, 124.5, 127.6, 129.0, 131.4, 131.5, 131.5, 134.2, 134.3, 134.4, 134.5 and 148.7 (Ar-*C*).

^{29}Si{^{1}H} NMR (C_6D_6, 99 MHz, 298 K): δ = 9.5 (d, $^2J_{SiP}$ = 13.8 Hz, CH_2-*Si*-^{i}Pr$_2$).

MS/LIFDI-HRMS found (calcd.) m/z: 639.2507 (639.2505) for $[M]^+$.

Anal. calcd. for $C_{37}H_{48}GeNPSi$: C, 69.60%; H, 7.58%; N, 2.19%; found: C, 66.48%; H, 7.48%; N, 2.21%.

^{PhiP}DippGe{3,5-(CF$_3$)$_2$C$_6$H$_3$}, 2b. The germylene was synthesized according to the general method using **1** (1.80 g, 3.0 mmol) and a freshly prepared Et_2O solution of 3,5-$(CF_3)_2$-PhMgBr using 3,5-$(CF_3)_2$-PhBr (1.15 g, 3.9 mmol), Mg (0.14 g, 5.9 mmol) and a pinch of iodide. An off-white powder of **2b** (1.26 g, mmol, 54 %) was isolated after precipitation from a pentane solution at -32°C. Colourless crystals suitable for X-ray diffraction analysis were obtained from a concentrated pentane solution, which was stored at ambient temperature for 14 days.

^{1}H NMR (C_6D_6, 400 MHz, 298 K): δ = 0.73 (d, 3H, $^3J_{HH}$ = 6.8 Hz, Si-^{i}PrC*H*$_3$), 0.82 (m, 1H, Si-^{i}PrC*H*), 0.92 (m, 3H, $^3J_{HH}$ = 7.1 Hz, Si-^{i}PrC*H*$_3$), 1.00 (d, 3H, $^3J_{HH}$ = 6.7 Hz, Dipp-^{i}PrC*H*$_3$), 1.05 (d, 3H, $^3J_{HH}$ = 6.7 Hz, Dipp-^{i}PrC*H*$_3$), 1.26 (m, 6H, Dipp-^{i}PrC*H*$_3$/Si-^{i}PrC*H*$_3$), 1.44 (d, 3H, $^3J_{HH}$ = 7.4 Hz, Si-^{i}PrC*H*$_3$), 1.48 (d, 3H, $^3J_{HH}$ = 6.9 Hz, Dipp-^{i}PrC*H*$_3$), 1.70 (m, 3H, C*H*$_2$-PPh$_2$/Si-^{i}PrC*H*), 3.07 (sept, 1H, $^3J_{HH}$ = 6.7 Hz, Dipp-^{i}PrC*H*), 4.54 (sept, 1H, $^3J_{HH}$ = 6.7 Hz, Dipp-^{i}PrC*H*), 6.61 (m, 2H, Ar-C*H*), 6.75 (m, 2H, Ar-C*H*), 6.88 (m, 1H, Ar-C*H*), 7.12 (m, 7H, Ar-C*H*), 7.80 (m, 4H, Ar-C*H*), 7.65 (s, 1H, Ge-Ar$_{CF3}$-*H*$_{para}$), 7.71 (m, 2H, Ar-C*H*), 8.11 (s, 2H, Ge-Ar$_{CF3}$-*H*$_{ortho}$).

^{31}P{^{1}H} NMR (C_6D_6, 162 MHz, 298 K): δ = 6.7 (s, *P*Ph$_2$).

^{13}C{^{1}H} NMR (C_6D_6, 101 MHz, 298 K): δ = 7.7 (*C*H$_2$-PPh$_2$), 17.4 (d, Si-^{i}Pr*C*H), 19.1 and 19.9 (Si-^{i}Pr*C*H$_3$), 20.3 (d, Si-^{i}Pr*C*H), 20.7 and 20.9 (Si-^{i}Pr*C*H$_3$), 22.3 and 23.2 (Dipp-^{i}PrC*H*$_3$), 27.7 (Dipp-^{i}PrC*H*), 28.3 (Dipp-^{i}PrC*H*$_3$), 28.7 (Dipp-^{i}PrC*H*), 28.8 (Dipp-^{i}PrC*H*$_3$), 120.0, 123.4, 124.7, 124.8, 126.1, 128.8, 129.1, 129.2, 129.5, 129.6, 129.8, 130.0, 130.3, 130.5, 130.6, 131.9, 131.9, 134.1, 134.2, 145.3, 145.4, 146.9, 146.9, 148.4, 148.4 and 163.0 (Ar-*C*).

^{29}Si{^{1}H} NMR (C_6D_6, 99 MHz, 298 K): δ = 12.6 (d, $^2J_{SiP}$ = 13.7 Hz, CH_2-*Si*-^{i}Pr$_2$).

MS/LIFDI-HRMS found (calcd.) m/z: 775.2257 (775.2253) for $[M]^+$.

Anal. calcd. for $C_{39}H_{46}F_6GeNPSi$: C, 60.48%; H, 5.99%; N, 1.81%; found: C, 58.30%; H, 5.66%; N, 1.81%.

^{PhiP}DippGe(4-CNC$_6$H$_4$), 2c. The germylene was synthesized according to the general method using **1** (1.0 g, 1.68 mmol) and a freshly prepared THF solution of 4-CN-PhLi using 4-CN-PhBr (350 mg, 1.92 mmol) and n-BuLi (2.5 M in hexane, 1.54 mL, 1.92 mmol). Because no

precipitation of **2c** was observed after storing the crude pentane solution at -32°C overnight the solution was used without further purification assuming full conversion due to the $^{31}P\{^1H\}$ NMR.

$^{31}P\{^1H\}$ NMR (toluene, 162 MHz, 298 K): δ = 5.9 (s, *P*Ph_2).

^{PhiP}DippGe(4-MeC_6H_4), 2d. The germylene was synthesized according to the general method using **1** (250 mg, 0.84 mmol) and a freshly prepared Et_2O solution of 4-Me-PhLi (131 mg, 1.34 mmol). Because no precipitation of **2d** was observed after storing the crude pentane solution at -32°C overnight the solution was used without further purification assuming full conversion due to the $^{31}P\{^1H\}$ NMR.

$^{31}P\{^1H\}$ NMR (toluene, 162 MHz, 298 K): δ = 2.1 (s, *P*Ph_2).

^{PhiP}DippGe(4-OMeC_6H_4), 2e. The germylene was synthesized according to the general method using **1** (500 mg, 0.84 mmol) and a freshly prepared Et_2O solution of 4-OMe-PhLi (153 mg, 1.34 mmol). Because no precipitation of **2e** was observed after storing the crude pentane solution at -32°C overnight the solution was used without further purification assuming full conversion due to the $^{31}P\{^1H\}$ NMR.

$^{31}P\{^1H\}$ NMR (toluene, 162 MHz, 298 K): δ = 1.4 (s, *P*Ph_2).

^{PhiP}DippGe(4-N$Me_2C_6H_4$), 2f. The germylene was synthesized according to the general method using ^{PhiP}DippGeCl (250 mg, 0.42 mmol) and a freshly prepared Et_2O solution of 4-NMe_2-PhLi (85 mg, 0.67 mmol). Because no precipitation of **2f** was observed after storing the crude pentane solution at -32°C overnight the solution was used without further purification assuming full conversion due to the $^{31}P\{^1H\}$ NMR.

$^{31}P\{^1H\}$ NMR (C_6D_6, 162 MHz, 298 K): δ = 0.3 (s, *P*Ph_2).

^{PhiP}DippGe(NMe_2), 2g. The germylene was synthesized according to the general method using **1** (250 mg, 0.42 mmol) and a freshly prepared solution of NMe_2Li using NHMe2 (1M in THF, 0.42 mL, 0.42 mmol) and n-BuLi (2.5M in hexane, 0.17 ml, 0.42 mmol) in Et_2O. Because no precipitation of **2g** was observed after storing the crude pentane solution at -32°C overnight the solution was used without further purification assuming full conversion due to the $^{31}P\{^1H\}$ NMR.

$^{31}P\{^1H\}$ NMR (toluene, 162 MHz, 298 K): δ = -24.4 (s, *P*Ph_2).

General Method for preparation of 4 [{^{PhiP}DippGe(R)}·Ni(IPr)]:

A solid mixture of $Ni(COD)_2$ and IPr was mixed with toluene at ambient temperature and stirred for 2 h. The resulting orange solution was cooled to -78°C and a toluene solution of **2** was added dropwise. Afterwards the mixture was allowed to warm to ambient temperature and stirred for 3 h. The mixture was filtered, and all volatiles removed *in vacuo*. The residue was extracted with pentane and the solution stored at -32°C for 16 h resulting in the formation of a crystalline solid of **4**.

[{^{PhiP}DippGe(C_6H_5)}·Ni(IPr)], 4a. The complex was synthesized according to the general method using **2a** (507 mg, 0.79 mmol), $Ni(COD)_2$ (218 mg, 0.79 mmol) and IPr (309 mg, 0.79 mmol). The resulting deep red pentane solution was stored at -32°C for 16 h yielding green crystals of **4a** (510 mg, 0.47mmol, 59%) suitable for X-Ray diffraction analysis.

^{1}H NMR (C_6D_6, 400 MHz, 298 K): δ = -0.54 (m, 3H, Si-^{i}PrC*H*$_3$), 1.01 (m, 37H, Si-^{i}PrC*H*/Si-^{i}PrC*H*$_3$/Dipp-^{i}PrC*H*$_3$), 1.22 (m, 3H, Dipp-^{i}PrC*H*$_3$), 1.47 (m, 6H, Dipp-^{i}PrC*H*$_3$), 1.89 (m, 2H, C*H*$_2$-PPh_2), 2.22 (m, 1H, Si-^{i}PrC*H*$_3$), 2.78 (m, 1H, Dipp-^{i}PrC*H*), 3.15 (m, 2H, Dipp-^{i}PrC*H*), 3.38 (m, 2H, Dipp-^{i}PrC*H*), 4.23 (m, 1H, Dipp-^{i}PrC*H*), 6.54 (d, 2H, $^3J_{HH}$ = 6.9 Hz, Ar-C*H*), 6.68 (s, 2H, N-C*H*=C*H*-N), 6.89 (m, 6H, Ar-C*H*), 7.09 (m, 6H, Ar-C*H*), 7.23 (m, 4H, Ar-C*H*), 7.42 (m, 4H, Ar-C*H*), 7.89 (m, 2H, Ar-C*H*).

^{31}P{^{1}H} NMR (C_6D_6, 162 MHz, 298 K): δ = 8.7 (s, *P*Ph_2).

^{13}C{^{1}H} NMR (C_6D_6, 101 MHz, 298 K): δ = 10.3 (d, $^1J_{CP}$ = 5.5 Hz *C*H_2-PPh_2), 14.8 (Si-^{i}Pr*C*H), 19.0 (Si-^{i}Pr-*C*H_3), 20.1 (Si-^{i}Pr*C*H), 20.4, 20.6 and 21.3 (Si-^{i}Pr-*C*H_3), 22.3, 22.6, 23.1, 23.2, 25.1 and 26.3 (Dipp-^{i}Pr-*C*H_3), 27.9, 28.2, 28.6 and 28.9 (Dipp-^{i}Pr*C*H), 123.0 and 124.1 (Ar-*C*), 124.2 (N-*C*H=*C*H-N), 124.7, 124.8, 125.3, 126.7, 127.3, 127.6, 127.7, 129.4, 131.9, 132.1, 133.4, 133.6, 134.9, 138.6, 141.6, 142.0, 142.8, 144.4, 145.1, 146.9, 147.0, 147.1, 156.6 and 156.7 (Ar-*C*), 203.6 (d, $^2J_{CP}$ = 18.3 Hz, ^{Carbene}*C*-Ni-P).

^{29}Si{^{1}H} NMR (C_6D_6, 99 MHz, 298 K): δ = 3.7 (d, $^2J_{SiP}$ = 10.8 Hz, CH_2-*Si*-^{i}Pr$_2$).

MS/LIFDI-HRMS found (calcd.) m/z: 1085.4713 (1085.4737) for $[M]^+$.

λ_{max}, nm (*ε*, $Lcm^{-1}mol^{-1}$): 752 (2710), 485 (6030), 388 (8600).

Anal. calcd. for $C_{64}H_{84}GeN_3NiPSi$: C, 70.80%; H, 7.80%; N, 3.87%; found: C, 70.58%; H, 7.93%; N, 4.03%.

[{^{PhiP}DippGe(3,5-(CF_3)$_2$$C_6H_3$)}·Ni(IPr)], 4b. The complex was synthesized according to the general method using **2b** (564 mg, 0.73 mmol), $Ni(COD)_2$ (200 mg, 0.73 mmol) and IPr (283 mg, 0.73 mmol). The resulting deep red pentane solution was stored at -32°C for 16 h yielding green crystals of **4b** (471 mg, 0.39 mmol, 53%) suitable for X-Ray diffraction analysis.

^{1}H NMR (C_6D_6, 400 MHz, 298 K): δ = -0.63 (m, 3H, Si-^{i}PrC*H*$_3$), 0.97 (m, 37H, Si-^{i}PrC*H*/Si-^{i}PrC*H*$_3$/Dipp-^{i}PrC*H*$_3$), 1.14 (m, 3H, Dipp-^{i}PrC*H*$_3$), 1.48 (m, 6H, Dipp-^{i}PrC*H*$_3$), 1.64 (m, 1H, C*H*$_2$-PPh$_2$), 1.91 (m, 1H, C*H*$_2$-PPh$_2$), 2.07 (m, 1H, Si-^{i}PrC*H*$_3$), 2.95 (m, 1H, Dipp-^{i}PrC*H*), 3.16 (m, 4H, Dipp-^{i}PrC*H*), 4.12 (m, 1H, Dipp-^{i}PrC*H*), 6.64 (m, 3H, Ar-C*H*/N-C*H*=C*H*-N), 7.05 (m, 7H, Ar-C*H*), 7.21 (m, 7H, Ar-C*H*), 7.36 (m, 2H, Ar-C*H*), 7.47 (m, 2H, Ar-C*H*), 7.69 (m, 3H, Ar-C*H*).

^{31}P{^{1}H} NMR (C_6D_6, 162 MHz, 298 K): δ = 11.1 (s, *P*Ph$_2$).

^{13}C{^{1}H} NMR (C_6D_6, 101 MHz, 298 K): δ = 10.1 (d, $^1J_{CP}$ = 10.9 Hz *C*H$_2$-PPh$_2$), 14.6 (Si-^{i}Pr*C*H), 19.0 (Si-^{i}Pr-*C*H$_3$), 20.1 (Si-^{i}Pr*C*H), 20.3, 20.7 and 21.3 (Si-^{i}Pr-*C*H$_3$)22.5, 22.9, 23.3, 25.4, 26.1 and 26.2 (Dipp-^{i}Pr-*C*H$_3$), 27.3, 28.1, 28.5 and 28.8 (Dipp-^{i}Pr*C*H), 120.4, 123.3 and 123.5 (Ar-*C*), 124.6 (N-*C*H=*C*H-N), 124.9, 125.0, 126.0, 128.9, 129.2, 130.3, 132.1, 132.2, 132.5, 132.6, 133.4, 137.8, 141.8, 144.1, 144.4, 145.7, 146.6, 146.9, 160.6 and 160.7 (Ar-*C*), 201.2 (d, $^2J_{CP}$ = 17.8 Hz, ^{Carbene}*C*-Ni-P).

^{29}Si{^{1}H} NMR (C_6D_6, 99 MHz, 298 K): δ = 5.3 (d, $^2J_{SiP}$ = 10.2 Hz, CH$_2$-*Si*-^{i}Pr$_2$).

MS/LIFDI-HRMS found (calcd.) m/z: 1221.4416 (1221.4485) for $[M]^+$.

λ_{max}, nm (*ε*, Lcm^{-1}mol^{-1}): 770 (2630), 485 (5980), 390 (8470), 326 (9320).

Anal. calcd. for $C_{66}H_{82}F_6GeN_3NiPSi$: C, 64.88%; H, 6.77%; N, 3.44%; found: C, 62.43%; H, 6.49%; N, 3.35%.

[{^{PhiP}DippGe(4-CNC$_6$H$_4$)}·Ni(IPr)], 4c. The complex was synthesized according to the general method using Ni(COD)$_2$ (461 mg, 1.68 mmol), IPr (651 mg, 1.68 mmol) and freshly prepared solution of **2c** from **1** (1.0 g, 1.68 mmol). After filtering and concentrating the resulting deep purple reaction solution to 5 mL, purple crystalline solid started to precipitate. After addition of 10 mL pentane the mixture was stored at -32°C for 16 h yielding purple crystalline solid of **4c** (1.08 g, 0.97 mmol, 58%). Deep purple crystals suitable for X-Ray diffraction analysis were grown from a concentrated Et$_2$O solution, which was stored at ambient temperature for two days.

^{1}H NMR (THF-d$_8$, 400 MHz, 298 K): δ = -0.97 (d, 3H, $^3J_{HH}$ = 5.3 Hz, Si-^{i}PrC*H*$_3$), 0.73 (m, 16H, Si-^{i}PrC*H*/Si-^{i}PrC*H*$_3$/Dipp-^{i}PrC*H*$_3$), 1.06 (m, 27H, Si-^{i}PrC*H*/Si-^{i}PrC*H*$_3$/Dipp-^{i}PrC*H*$_3$), 1.24 (d, 3H, $^3J_{HH}$ = 5.3 Hz, Dipp-^{i}PrC*H*$_3$), 1.65 (m, 1H, C*H*$_2$-PPh$_2$), 1.92 (m, 2H, Si-^{i}PrC*H*$_3$/C*H*$_2$-PPh$_2$), 2.70 (m, 1H, Dipp-^{i}PrC*H*), 3.01 (m, 2H, Dipp-^{i}PrC*H*), 3.26 (m, 2H, Dipp-^{i}PrC*H*), 3.94 (m, 1H, Dipp-^{i}PrC*H*), 6.29 (d, $^3J_{HH}$ = 8.0 Hz, Ge-Ph*H*-CN), 6.60 (d, 1H, $^3J_{HH}$ = 6.1 Hz, N-C*H*=C*H*-N), 6.86 (m, 3H, Ge-Ph*H*-CN/ N-C*H*=C*H*-N), 6.98 (m, 4H, Ar-C*H*), 7.19 (m, 3H, Ar-C*H*), 7.42 (m, 8H, Ar-C*H*), 7.63 (m, 2H, Ar-C*H*/N-C*H*=C*H*-N), 7.80 (m, 3H, Ar-C*H*).

^{31}P{^{1}H} NMR (THF-d$_8$, 162 MHz, 298 K): δ = 12.8 (s, *P*Ph$_2$).

$^{13}C\{^1H\}$ NMR (THF-d_8, 101 MHz, 298 K): δ = 10.3 (d, $^1J_{CP}$ = 11.5 Hz *C*H_2-PPh_2), 15.4 (Si-^{i}Pr*C*H), 19.2 (Si-^{i}Pr-*C*H_3), 20.6 (Si-^{i}Pr*C*H), 21.6, 22.7 and 22.9 (Si-^{i}Pr-*C*H_3), 23.3, 23.5, 26. and 26.6 (Dipp-^{i}Pr-*C*H_3), 28.1, 28.5, 29.4 and 29.6 (Dipp-^{i}Pr*C*H), 110.6 (Ge-Ph-*C*N), 120.4 and 123.4 (Ar-*C*), 124.4 (N-*C*H=*C*H-N), 125.0, 125.6, 126.0, 128.3, 128.4, 129.1, 129.2, 129.3, 129.7, 130.3, 132.6, 132.8, 133.8, 133.9, 135.9, 139.0, 145.0, 145.6, 147.3, 164.9 and 165.0 (Ar-*C*), 201.8 (d, $^2J_{CP}$ = 18.5 Hz, ^{Carbene}*C*-Ni-P).

$^{29}Si\{^1H\}$ NMR (THF-d_8, 99 MHz, 298 K): δ = 3.9 (d, $^2J_{SiP}$ = 10.2 Hz, CH_2-*Si*-^{i}Pr_2).

MS/LIFDI-HRMS found (calcd.) m/z: 1110.4683 (1110.4690) for $[M]^+$.

λ_{max}, nm (*ε*, $Lcm^{-1}mol^{-1}$): 799 (5030), 511 (11080), 396 (15110), 327 (16850).

Anal. calcd. for $C_{65}H_{83}GeN_4NiPSi$: C, 70.28%; H, 7.53%; N, 5.04%; found: C, 70.21%; H, 7.41%; N, 4.77%.

[{^{PhiP}DippGe(4-MeC_6H_4)}·Ni(IPr)], 4d. The complex was synthesized according to the general method using Ni(COD)$_2$ (115 mg, 0.42 mmol), IPr (163 mg, 0.42 mmol) and freshly prepared solution of **2d** from **1** (250 mg, 0.42 mmol). The resulting deep red pentane solution was stored at -32°C for 16 h yielding a red crystalline solid of **4d** (227 mg, 0.21 mmol, 49%). Green crystals suitable for X-Ray diffraction analysis were grown from a concentrated Et_2O solution, which was stored at -32°C temperature for two days.

^1H NMR (C_6D_6, 400 MHz, 298 K): δ = -0.48 (d, 3H, $^3J_{HH}$ = 5.8 Hz, Si-^{i}PrC*H*$_3$), 1.06 (m, 40H, Si-^{i}PrC*H*/Si-^{i}PrC*H*$_3$/Dipp-^{i}PrC*H*$_3$), 1.48 (d, 6H, $^3J_{HH}$ = 6.0 Hz, Dipp-^{i}PrC*H*$_3$), 1.88 (m, 2H, C*H*$_2$-PPh_2), 2.02 (s, 3H, Ge-Ph-C*H*$_3$), 2.26 (m, 1H, Si-^{i}PrC*H*$_3$), 2.78 (m, 1H, Dipp-^{i}PrC*H*), 3.17 (m, 2H, Dipp-^{i}PrC*H*), 3.40 (m, 2H, Dipp-^{i}PrC*H*), 4.23 (m, 1H, Dipp-^{i}PrC*H*), 6.47 (d, 2H, $^3J_{HH}$ = 7.7 Hz, Ge-Ph*H*-CH_3), 6.69 (s, 2H, N-C*H*=C*H*-N), 6.77 (d, 2H, $^3J_{HH}$ = 7.7 Hz, Ge-Ph*H*-CH_3), 6.91 (m, 4H, Ar-C*H*), 7.11 (m, 4H, Ar-C*H*), 7.23 (m, 5H, Ar-C*H*), 7.44 (m, 4H, Ar-C*H*), 7.90 (m, 2H, Ar-C*H*).

$^{31}P\{^1H\}$ NMR (C_6D_6, 162 MHz, 298 K): δ = 8.1 (s, *P*Ph_2).

$^{13}C\{^1H\}$ NMR (C_6D_6, 101 MHz, 298 K): δ = 10.6 (d, $^1J_{CP}$ = 9.7 Hz *C*H_2-PPh_2), 14.86 (Si-^{i}Pr*C*H), 19.0 (Si-^{i}Pr-*C*H_3), 20.2 (Si-^{i}Pr*C*H), 20.4, 20.6 and 21.4 (Si-^{i}Pr*C*H_3), 21.7 (Ge-Ph-*C*H_3), 22.4, 22.6, 23.1, 23.3, 25.0 and 26.3 (Dipp^{i}Pr-*C*H_3), 27.9, 28.2, 28.6 and 28.9 (Dipp-^{i}Pr*C*H), 123.0 and 124.0 (Ar-*C*), 124.2 (N-*C*H=*C*H-N), 124.7, 124.9, 125.4, 127.5, 127.6, 127.6, 129.4, 131.9 132.1, 133.5, 133.7, 135.1, 136.6, 138.4, 144.4, 145.2, 147.0, 147.2, 147.3, 153.4 and 153.5 (Ar-*C*), 203.9 (d, $^2J_{CP}$ = 18.1 Hz, ^{Carbene}*C*-Ni-P).

$^{29}Si\{^1H\}$ NMR (C_6D_6, 99 MHz, 298 K): δ = 3.6 (d, $^2J_{SiP}$ = 10.7 Hz, CH_2-*Si*-^{i}Pr_2).

MS/LIFDI-HRMS found (calcd.) m/z: 1099.4945 (1099.4894) for $[M]^+$.

λ_{max}, nm (*ε*, $Lcm^{-1}mol^{-1}$): 748 (2760), 487 (6170), 387 (8590).

Anal. calcd. for $C_{65}H_{86}GeN_3NiPSi$: C, 70.99%; H, 7.88%; N, 3.82%; found: C, 71.77%; H, 8.16%; N, 3.55%.

[{^{PhiP}DippGe(4-OMeC$_6$H$_4$)}·Ni(IPr)], 4e. The complex was synthesized according to the general method using $Ni(COD)_2$ (230 mg, 0.84 mmol), IPr (307 mg, 0.84 mmol) and freshly prepared solution of **2e** from **1** (500 mg, 0.84 mmol). The resulting deep red pentane solution was stored at -32°C for 16 h yielding a red crystalline solid of **4e** (433 mg, 0.39 mmol, 46%). Green crystals suitable for X-Ray diffraction analysis were grown from a concentrated Et_2O solution, which was stored at -32°C temperature for two days.

^{1}H NMR (C_6D_6, 400 MHz, 298 K): δ = -0.44 (d, 3H, $^3J_{HH}$ = 6.2 Hz, Si-^{i}PrC*H$_3$*), 0.91 (m, 12H, Si-^{i}PrC*H$_3$*/Dipp-^{i}PrC*H$_3$*), 1.07 (m, 25H, Si-^{i}PrC*H*/Si-^{i}PrC*H$_3$*/Dipp-^{i}PrC*H$_3$*), 1.23 (m, 3H, Si-^{i}PrC*H$_3$*), 1.48 (d, 6H, $^3J_{HH}$ = 5.8 Hz, Dipp-^{i}PrC*H$_3$*), 1.90 (m, 2H, C*H$_2$*-PPh$_2$), 2.29 (sept, 1H, $^3J_{HH}$ = 6.3 Hz, Si-^{i}PrC*H$_3$*), 2.75 (sept, 1H, $^3J_{HH}$ = 6.9 Hz, Dipp-^{i}PrC*H*), 3.14 (sept, 2H, $^3J_{HH}$ = 6.4 Hz, Dipp-^{i}PrC*H*), 3.22 (s, 3H, Ge-Ph-OC*H$_3$*), 3.42 (m, 2H, Dipp-^{i}PrC*H*), 4.25 (sept, 1H, $^3J_{HH}$ = 6.7 Hz, Dipp-^{i}PrC*H*), 6.48 (d, 2H, $^3J_{HH}$ = 8.5 Hz, Ge-Ph*H*-OCH$_3$), 6.57 (d, 2H, $^3J_{HH}$ = 8.5 Hz, Ge-Ph*H*-OCH$_3$), 6.68 (s, 2H, N-C*H*=C*H*-N), 6.91 (m, 4H, Ar-C*H*), 7.10 (m, 4H, Ar-C*H*), 7.24 (m, 5H, Ar-C*H*), 7.39 (m, 2H, Ar-C*H*), 7.48 (m, 2H, Ar-C*H*), 7.91 (m, 2H, Ar-C*H*).

^{31}P{^{1}H} NMR (C_6D_6, 162 MHz, 298 K): δ = 7.7 (s, *P*Ph$_2$).

^{13}C{^{1}H} NMR (C_6D_6, 101 MHz, 298 K): δ = 10.7 (d, $^1J_{CP}$ = 9.5 Hz *C*H$_2$-PPh$_2$), 14.9 (Si-^{i}Pr*C*H), 19.0 (Si^{i}Pr-*C*H$_3$), 20.1 (Si-^{i}Pr*C*H), 20.4, 20.6 and 21.4 (Si^{i}Pr*C*H$_3$), 22.5, 22.5, 23.2, 23.5, 24.9 and 26.2 (Dipp^{i}Pr-*C*H$_3$), 28.0, 28.1, 28.6 and 28.8 (Dipp-^{i}Pr*C*H), 54.3 (Ge-Ph-O*C*H$_3$), 112.4, 123.0 and 124.0 (Ar-*C*), 124.1 (N-*C*H=*C*H-N), 124.7, 124.8, 125.4, 127.5, 127.6, 129.4, 131.9, 132.1, 133.5, 133.7, 136.6, 138.5, 144.5, 145.3, 146.9, 147.3, 148.2, 148.3 and 159.6 (Ar-*C*), 204.0 (d, $^2J_{CP}$ = 18.3 Hz, ^{Carbene}*C*-Ni-P).

^{29}Si{^{1}H} NMR (C_6D_6, 99 MHz, 298 K): δ = 3.5 (d, $^2J_{SiP}$ = 10.5 Hz, CH$_2$-*Si*-^{i}Pr$_2$).

MS/LIFDI-HRMS found (calcd.) m/z: 1115.4914 (1115.4843) for $[M]^+$.

λ$_{max}$, nm (*ε*, Lcm^{-1}mol^{-1}): 747 (2840), 483 (6370), 388 (8630).

Anal. calcd. for $C_{65}H_{86}GeN_3NiOPSi$: C, 69.97%; H, 7.77%; N, 3.77%; found: C, 69.39%; H, 8.17%; N, 3.53%.

[{^{PhiP}DippGe(4-NMe$_2$C$_6$H$_4$)}·Ni(IPr)], 4f. The complex was synthesized according to the general method using $Ni(COD)_2$ (115 mg, 0.42 mmol), IPr (163 mg, 0.42 mmol) and freshly prepared solution of **2f** from **1** (250 mg, 0.42 mmol). The resulting deep red pentane solution was stored at -32°C for 16 h yielding a red crystalline solid of **4f** (226 mg, 0.20 mmol, 48%).

Green crystals suitable for X-Ray diffraction analysis were grown from a concentrated Et_2O solution, which was stored at -32°C temperature for two days.

^{1}H NMR (C_6D_6, 400 MHz, 298 K): δ = -0.33 (d, 3H, $^3J_{HH}$ = 6.8 Hz, Si-^{i}PrC*H*$_3$), 1.09 (m, 40H, Si-^{i}PrC*H*/Si-^{i}PrC*H*$_3$/Dipp-^{i}PrC*H*$_3$), 1.47 (m, 6H, Dipp-^{i}PrC*H*$_3$), 1.93 (m, 2H, C*H*$_2$-PPh$_2$), 2.38 (m, 1H, Si-^{i}PrC*H*$_3$), 2.48 (s, 6H, Ge-Ph-N(C*H*$_3$)$_2$), 2.72 (m, 1H, Dipp-^{i}PrC*H*), 3.23 (m, 2H, Dipp-^{i}PrC*H*), 3.48 (m, 2H, Dipp-^{i}PrC*H*), 4.26 (m, 1H, Dipp-^{i}PrC*H*), 6.33 (d, 2H, $^3J_{HH}$ = 8.4 Hz, Ge-Ph*H*-N(CH$_3$)$_2$), 6.46 (d, 2H, $^3J_{HH}$ = 8.4 Hz, Ge-Ph*H*-N(CH$_3$)$_2$), 6.71 (s, 2H, N-C*H*=C*H*-N), 6.93 (m, 4H, Ar-C*H*), 7.08 (m, 4H, Ar-C*H*), 7.27 (m, 5H, Ar-C*H*), 7.49 (m, 4H, Ar-C*H*), 7.93 (m, 2H, Ar-C*H*).

^{31}P{^{1}H} NMR (C_6D_6, 162 MHz, 298 K): δ = 6.5 (s, *P*Ph$_2$).

^{13}C{^{1}H} NMR (C_6D_6, 101 MHz, 298 K): δ = 10.3 (d, $^1J_{CP}$ = 8.7 Hz *C*H$_2$-PPh$_2$), 14.9 (Si-^{i}Pr*C*H), 19.0 (Si--^{i}Pr-*C*H$_3$), 20.2 (Si-^{i}Pr*C*H), 20.4, 20.7 and 21.4 (Si-^{i}Pr*C*H$_3$), 22.5, 22.6, 23.3, 23.7, 24.9 and 26.2 (Dipp-^{i}Pr-*C*H$_3$), 28.2, 28.6 and 28.8 (Dipp-^{i}Pr*C*H), 39.8 (Ge-Ph-N(*C*H$_3$)$_2$), 110.9, 123.0 and 123.9 (Ar-*C*), 124.1 (N-*C*H=*C*H-N), 124.6, 124.8, 125.3, 127.5, 127.6, 127.6, 129.2, 131.9, 132.1, 133.7, 133.9, 136.3, 138.7, 142.4, 142.7, 143.6, 144.0, 144.1, 144.6, 145.3, 147.1, 147.6 and 150.1 (Ar-*C*), 204.7 (d, $^2J_{CP}$ = 18.5 Hz, ^{Carbene}*C*-Ni-P).

^{29}Si{^{1}H} NMR (C_6D_6, 99 MHz, 298 K): δ = 3.2 (d, $^2J_{SiP}$ = 10.7 Hz, CH$_2$-*Si*-^{i}Pr$_2$).

MS/LIFDI-HRMS found (calcd.) m/z: 1128.5175 (1128.5159) for $[M]^+$.

λ_{max}, nm (*ε*, Lcm^{-1}mol^{-1}): 741 (2500), 484 (5990), 337 (15680).

Anal. calcd. for $C_{66}H_{89}GeN_4NiPSi$: C, 70.22%; H, 7.95%; N, 4.96%; found: C, 68.40%; H, 8.02%; N, 4.68%.

[[^{PhiP}DippGe(NMe$_2$)}·Ni(IPr)], 4g. The complex was synthesized according to the general method using Ni(COD)$_2$ (115 mg, 0.42 mmol), IPr (163 mg, 0.42 mmol) and freshly prepared solution of **2g** from **1** (250 mg, 0.42 mmol). The resulting deep green pentane solution was stored at -32°C for 16 h yielding a green crystalline solid of **4g** (117 mg, 0.11 mmol, 27%). Red crystals suitable for X-Ray diffraction analysis were grown from a concentrated Et_2O solution, which was stored at -32°C temperature for two days.

^{1}H NMR (C_6D_6, 400 MHz, 298 K): δ = 0.32 (m, 3H, Si-^{i}PrC*H*$_3$), 0.81 (m, 6H, Si-^{i}PrC*H*$_3$/Dipp-^{i}PrC*H*$_3$), 1.09 (m, 34H, Si-^{i}PrC*H*/Si-^{i}PrC*H*$_3$/Dipp-^{i}PrC*H*$_3$), 1.37 (m, 6H, Dipp-^{i}PrC*H*$_3$), 1.87 (m, 1H, C*H*$_2$-PPh$_2$), 2.01 (overlapping singlets, 6H, Ge-N(C*H*$_3$)$_3$), 2.13 (m, 2H, C*H*$_2$-PPh$_2$/Si-^{i}PrC*H*$_3$), 2.75 (m, 1H, Dipp-^{i}PrC*H*), 3.15 (m, 2H, Dipp-^{i}PrC*H*), 3.52 (m, 2H, Dipp-^{i}PrC*H*), 4.06 (m, 1H, Dipp-^{i}PrC*H*), 6.65 (s, 2H, N-C*H*=C*H*-N), 7.04 (m, 13H, Ar-C*H*), 7.27 (m, 2H, Ar-C*H*), 7.53 (m, 2H, Ar-C*H*), 7.92 (m, 2H, Ar-C*H*).

^{31}P{^{1}H} NMR (C_6D_6, 162 MHz, 298 K): δ = 1.5 (s, *P*Ph$_2$).

$^{13}C\{^1H\}$ NMR (C_6D_6, 101 MHz, 298 K): δ = 13.6 (d, $^1J_{CP}$ = 6.5 Hz *C*H_2-PPh_2), 14.6 and 18.9 (Si-^{i}Pr-*C*H), 20.1, 20.2, 20.5 and 21.4 (Si-^{i}Pr*C*H_3), 22.5, 23.1, 23.6, 24.0, 24.2 and 26.0 (Dipp-^{i}Pr-*C*H_3), 28.0 and 28.6 (Dipp-^{i}Pr*C*H), 43.5 (Ge-N(*C*H_3)$_2$), 123.3 and 123.8 (Ar-*C*), 124.1 (N-*C*H=*C*H-N), 124.5, 124.6, 124.7, 124.8, 124.9, 129.2, 131.8, 131.9, 134.2, 134.4, 139.1, 144.8, 145.6 and 146.8 (Ar-*C*), 205.4 (d, $^2J_{CP}$ = 22.8 Hz, ^{Carbene}*C*-Ni-P).

$^{29}Si\{^1H\}$ NMR (C_6D_6, 99 MHz, 298 K): δ = 3.7 (d, $^2J_{SiP}$ = 12.0 Hz, CH_2-*Si*-^{i}Pr$_2$).

MS/LIFDI-HRMS found (calcd.) m/z: 1052.4789 (1052.4846) for $[M]^+$.

λ_{max}, nm (*ε*, $Lcm^{-1}mol^{-1}$): 623 (2830), 395 (10290).

Anal. calcd. for $C_{60}H_{85}GeN_4NiPSi$: C, 68.45%; H, 8.14%; N, 5.32%; found: C, 67.14%; H, 8.14%; N, 4.97%.

[{^{PhiP}DippGe(C_6H_5)(H)}Ni(H)·(IPr)], 5a. A deep red Et_2O solution of **4a** (100 mg, 0.092 mmol) was subjected to 1.5 bar H_2 leading to slight decolorization and was stored at ambient temperature for 24 h, resulting in yellow crystals of **5a** (89 mg, 0.082 mmol, 89%) suitable for X-Ray diffraction analysis. NMR data of the equilibrium between **4a** and **5a** were obtained by subjecting **4a** to an ambient pressure of H_2 in a Jay-Young NMR tube.

^1H NMR (C_6D_6, 400 MHz, 333 K): δ = -1.98 (b, 2H, Ge-*H*/Ni-*H*), 0.65 (d, 6H, $^3J_{HH}$ = 5.6 Hz, Si-^{i}Pr-C*H*$_3$), 0.88 (m, 12H, ^{i}Pr-C*H*$_3$), 0.89 (m, 18H, ^{i}Pr-C*H*$_3$), 1.07 (d, 6H, $^3J_{HH}$ = 6.7 Hz, Dipp-^{i}Pr-C*H*$_3$) 1.19 (d, 6H, $^3J_{HH}$ = 6.7 Hz, -Dipp-^{i}Pr-C*H*$_3$), 1.29 (m, 2H, Si-^{i}Pr-C*H*), 1.85 (d, 2H, $^2J_{HP}$ = 12.0 Hz, C*H*$_2$-PPh_2), 3.13 (m, 4H, Dipp-^{i}PrC*H*), 3.31 (m, 2H, Dipp-^{i}PrC*H*), 6.72 (s, 2H, N-C*H*=C*H*-N), 7.00 (m, 12H, Ar-C*H*), 7.12 (m, 4H, Ar-C*H*), 7.19 (m, 2H, Ar-C*H*), 7.29 (m, 2H, Ar-C*H*), 7.65 (m, 4H, Ar-C*H*).

$^{31}P\{^1H\}$ NMR (C_6D_6, 162 MHz, 298 K): δ = 9.0 (s, *P*Ph_2).

IR, *ν*/cm^{-1} (ATR): 1949 (*Ge-H*) and 1893 (*Ni-H*).

[{^{PhiP}DippGe(C_6H_5)(D)}Ni(D)·(IPr)], 5a-D_2. A deep red Et_2O solution of **4a** (100 mg, 0.092 mmol) was subjected to 1.5 bar D_2 leading to slight decolorization and was stored at ambient temperature for 24 h, resulting in a yellow crystalline solid of **5a-D_2** (86 mg, 0.082 mmol, 86%). NMR data of the equilibrium between **4a** and **5a-D_2** were obtained by subjecting **4a** to an ambient pressure of H_2 in a Jay-Young NMR tube.

^1H NMR (toluene-d_8, 400 MHz, 333 K): δ = 0.58 (d, 6H, $^3J_{HH}$ = 5.6 Hz, Si-^{i}Pr-C*H*$_3$), 0.85 (m, 12H, ^{i}Pr-C*H*$_3$), 0.93 (m, 18H, ^{i}Pr-C*H*$_3$), 1.05 (d, 6H, $^3J_{HH}$ = 6.7 Hz, Dipp-^{i}Pr-C*H*$_3$) 1.12 (d, 6H, $^3J_{HH}$ = 6.7 Hz, -Dipp-^{i}Pr-C*H*$_3$), 1.24 (m, 2H, Si-^{i}Pr-C*H*), 1.80 (d, 2H, $^2J_{HP}$ = 12.0 Hz, C*H*$_2$-PPh_2), 3.09 (m, 4H, Dipp-^{i}PrC*H*), 3.24 (m, 2H, Dipp-^{i}PrC*H*), 6.72 (s, 2H, N-C*H*=C*H*-N), 6.95 (m, 12H, Ar-C*H*), 7.09 (D, 6H, $^3J_{HH}$ = 7.5 Hz; Ar-C*H*), 7.27 (m, 2H, Ar-C*H*), 7.61(m, 4H, Ar-C*H*).

$^{31}P\{^1H\}$ NMR (C_6D_6, 162 MHz, 298 K): δ = 9.1 (s, *P*Ph_2).

[^{PhiP}DippGe{3,5-$(CF_3)_2C_6H_3$}(H)}Ni(H)·(IPr)], 5b. A deep red pentane solution of **4b** (163 mg, 0.42 mmol) was subjected to 1.5 bar H_2 leading to a complete light-yellow solution and was stored for a prolonged time but did not result in any precipitation of **5b**. NMR data of the equilibrium between **4b** and **5b** were obtained by subjecting **4b** to an ambient pressure of H_2 in a Jay-Young NMR tube.

^1H NMR (toluene-d_8, 400 MHz, 333 K): δ = -2.58 (b, 2H, Ge-*H*/Ni-*H*), 0.57 (m, 6H, Si-^{i}Pr-C*H*$_3$), 0.75 (m, 15H, ^{i}Pr-C*H*$_3$), 0.86 (m, 20H, Si-^{i}Pr-C*H*/^{i}Pr-C*H*$_3$), 1.08 (d, 6H, $^3J_{HH}$ = 6.6 Hz, Dipp-^{i}Pr-C*H*$_3$), 1.73 (d, 2H, $^2J_{HP}$ = 13.2 Hz, C*H*$_2$-PPh_2), 2.92 (sept, 4H, $^3J_{HH}$ = 6.7 Hz, Dipp-^{i}PrC*H*), 3.21 (m, 2H, Dipp-^{i}PrC*H*), 6.67 (s, 2H, N-C*H*=C*H*-N), 6.85 (m, 2H, Ar-C*H*), 7.00 (m, 10H, Ar-C*H*), 7.23 (m, 3H, Ar-C*H*), 7.56 (m, 4H, Ar-C*H*), 7.70 (s, 1H, 3,5-$(CF_3)_2$-Ph*H*$_p$-Ge), 7.80 (s, 2H, 3,5-$(CF_3)_2$-Ph(*H*$_o$)$_2$-Ge).

$^{31}P\{^1H\}$ NMR (C_6D_6, 162 MHz, 298 K): δ = 6.7 (s, *P*Ph_2).

[{^{PhiP}DippGe(4-CNC_6H_4)(H)}Ni(H)·(IPr)], 5c. A deep purple Et_2O solution of **4c** (150 mg, 0.14 mmol) was subjected to 1.5 bar H_2 leading to a red solution and was stored at ambient temperature for 24 h, resulting in red crystals of **5c** (132 mg, 0.12 mmol, 88%) suitable for X-Ray diffraction analysis. NMR data of the equilibrium between **4c** and **5c** were obtained by subjecting **4c** to an ambient pressure of H_2 in a Jay-Young NMR tube.

^1H NMR (C_6D_6, 400 MHz, 333 K): δ = -2.33 (b, 2H, Ge-*H*/Ni-*H*), 0.58 (m, 6H, Si-^{i}Pr-C*H*$_3$), 0.88 (m, 32H, Si-^{i}Pr-C*H*/^{i}Pr-C*H*$_3$), 1.02 (d, 6H, $^3J_{HH}$ = 6.2 Hz, Dipp-^{i}Pr-C*H*$_3$), 1.13 (d, 6H, $^3J_{HH}$ = 6.7 Hz, Dipp-^{i}Pr-C*H*$_3$) 1.79 (d, 2H, $^2J_{HP}$ = 11.9 Hz, C*H*$_2$-PPh_2), 3.01 (m, 4H, Dipp-^{i}PrC*H*), 3.17 (m, 2H, Dipp-^{i}PrC*H*), 6.69 (s, 2H, N-C*H*=C*H*-N), 7.00 (m, 17H, Ar-C*H*), 7.25 (m, 2H, Ar-C*H*), 7.58 (m, 4H, Ar-C*H*).

$^{31}P\{^1H\}$ NMR (C_6D_6, 162 MHz, 298 K): δ = 8.0 (s, *P*Ph_2).

IR, *v*/cm^{-1} (ATR): 2227 (Ph-*C*≡*N*), 1934 (*Ge*-*H*) and 1885 (*Ni*-*H*).

[{^{PhiP}DippGe(4-Me-C_6H_4)(H)}Ni(H)·(IPr)], 5d. A deep red Et_2O solution of **4d** (150 mg, 0.14 mmol) was subjected to 1.5 bar H_2 leading to a red solution and was stored at ambient temperature for 24 h, resulting in yellow crystalline solid of **5d** (121 mg, 0.11 mmol, 80%). NMR data of the equilibrium between **4d** and **5d** were obtained by subjecting **4d** to an ambient pressure of H_2 in a Jay-Young NMR tube.

^1H NMR (C_6D_6, 400 MHz, 333 K): δ = -1.97 (b, 2H, Ge-*H*/Ni-*H*), 0.68 (d, 6H, $^3J_{HH}$ = 5.3 Hz, Si-^{i}Pr-C*H*$_3$), 0.89 (m, 6H, $^3J_{HH}$ = 7.5 Hz, Dipp-^{i}Pr-C*H*$_3$), 0.98 (m, 24, ^{i}Pr-C*H*$_3$), 1.07 (d, 6H, $^3J_{HH}$

= 6.7 Hz, Dipp-^{i}Pr-C*H*$_3$), 1.20 (d, 6H, $^3J_{HH}$ = 6.8 Hz, Dipp-^{i}Pr-C*H*$_3$), 1.30 (m, 2H, Si-^{i}PrC*H*), 1.85 (d, 2H, $^2J_{HP}$ = 12.0 Hz, C*H*$_2$-PPh$_2$), 2.17 (s, 3H, Ge-Ph-C*H*$_3$), 3.15 (m, 4H, Dipp-^{i}PrC*H*), 3.33 (m, 2H, Dipp-^{i}PrC*H*), 6.73 (s, 2H, N-C*H*=C*H*-N), 7.06 (m, 15H, Ar-C*H*), 7.29 (m, 4H, Ar-C*H*), 7.66 (m, 4H, Ar-C*H*).

^{31}P{^{1}H} NMR (C_6D_6, 162 MHz, 298 K): δ = 9.0 (s, *P*Ph$_2$).

IR, *v*/cm^{-1} (ATR): 1940 (*Ge-H*) and 1879 (*Ni-H*).

[{^{PhiP}DippGe(4-OMe-C$_6$H$_4$)(H)}Ni(H)·(IPr)], 5e. A deep red Et_2O solution of **4e** (100 mg, 0.089 mmol) was subjected to 1.5 bar H_2 leading to a red solution and was stored at -32°C for 24 h, resulting in yellow crystalline solid of **5e** (23 mg, 0.021 mmol, 23%). NMR data of the equilibrium between **4e** and **5e** were obtained by subjecting **4e** to an ambient pressure of H_2 in a Jay-Young NMR tube.

^{1}H NMR (toluene-d$_8$, 400 MHz, 333 K): δ = -2.02 (b, 2H, Ge-*H*/Ni-*H*), 0.62 (m, 6H, Si-^{i}Pr-C*H*$_3$), 0.84 (m, 6H, $^3J_{HH}$ = 7.5 Hz, Dipp-^{i}Pr-C*H*$_3$), 0.95 (m, 24, ^{i}Pr-C*H*$_3$), 1.06 (d, 6H, $^3J_{HH}$ = 6.6 Hz, Dipp-^{i}Pr-C*H*$_3$), 1.14 (d, 6H, $^3J_{HH}$ = 6.7 Hz, Dipp-^{i}Pr-C*H*$_3$), 1.26 (m, 2H, Si-^{i}PrC*H*), 1.80 (d, 2H, $^2J_{HP}$ = 12.0 Hz, C*H*$_2$-PPh$_2$), 3.11 (m, 4H, Dipp-^{i}PrC*H*), 3.25 (m, 2H, Dipp-^{i}PrC*H*), 3.38 (s, 3H, Ge-Ph-OC*H*$_3$), 6.54 (d, $^3J_{HH}$ = 8.0 Hz, Ge-Ph*H*-OCH$_3$), 6.73 (s, 2H, N-C*H*=C*H*-N), 6.97 (m, 11H, Ar-C*H*), 7.10 (m, 4H, Ar-C*H*), 7.22 (d, $^3J_{HH}$ = 7.7 Hz, Ge-Ph*H*-OCH$_3$), 7.63 (m, 4H, Ar-C*H*).

^{31}P{^{1}H} NMR (C_6D_6, 162 MHz, 298 K): δ = 9.2 (s, *P*Ph$_2$).

IR, *v*/cm^{-1} (ATR): 1936 (*Ge-H*) and 1881 (*Ni-H*).

[{^{PhiP}DippGe(4-NMe$_2$-C$_6$H$_4$)(H)}Ni(H)·(IPr)], 5f. A deep red Et_2O solution of **4f** (100 mg, 0.089 mmol) was subjected to 1.5 bar H_2 leading to a red solution and was stored at -32°C for 24 h, resulting in yellow crystalline solid of **5f** (23 mg, 0.021 mmol, 23%). NMR data of the equilibrium between **4f** and **5f** were obtained by subjecting **4f** to an ambient pressure of H_2 in a Jay-Young NMR tube.

^{1}H NMR (tol-d8, 400 MHz, 333.15 K): δ = -1.94 (b, 2H, Ge-*H*/Ni-*H*), 0.65 (d, 6H, $^3J_{HH}$ = 5.6 Hz, C*H*$_3$), 1.82 (d, 2H, $^2J_{HP}$ = 12.0 Hz, C*H*$_2$-PPh$_2$), 2.50 (s, 6H, Ge-N(C*H*$_3$)$_2$), 3.13 (m, 4H, Dipp-^{i}PrCH), 3.31 (m, 2H, Dipp-^{i}PrCH), 6.22 (d, $^3J_{HH}$ = 8.4 Hz, Ge-Ph*H*-NMe$_2$), 6.36 (d, $^3J_{HH}$ = 8.6 Hz, Ge-Ph*H*-NMe$_2$), 6.73 (s, 2H, N-C*H*=C*H*-N), 6.94 (m, 5H, Ar-C*H*), 7.12 (m, 4H, Ar-C*H*), 7.26 (m, 4H, Ar-C*H*), 7.42 (m, 2H, Ar-C*H*), 7.64 (m, 4H, Ar-C*H*).

In the region between 1.3 and 0.7 ppm CH_3 and CH signals of **4f** and **5f** overlap so that they can't be distinguished between.

^{31}P{^{1}H} NMR (C_6D_6, 162 MHz, 298 K): δ = 9.3 (s, *P*Ph$_2$).

IR, *v*/cm^{-1} (ATR): 1940 (*Ge-H*) and 1883 (*Ni-H*).

Hammet plot

The equilibrium constant was calculated for the H_2 activation with **4a-f** at 26°C via 1H NMR integrating each a signal of **4a-f** and **5a-f** determining the ratio. The H_2 concentration in solution was calculated by integrating the H2 signal and taking the absolute concentration of **4a-f** and **5a-f** into account. Log($K_{eq(R)}/K_{eq(Ph)}$) was plotted against the respective Hammet parameters of the aryl substituents.[9]

Ni^0 Complex (R)	***K_{eq} at 299.15 K [$Lmol^{-1}$]***	**Log(K_{eq4}/K_{eq4a})**	***Hammet parameter σ***
4a (C_6H_5)	1761	0	0
4b (3,5 (CF_3)$_2$-C_6H_3)	10307	0.767	0.86
4c (4-CN-C_6H_4)	5089	0.461	0.66
4d (4-Me-C_6H_4)	1504	-0.069	-0.17
4e (4-OMe-C_6H_4)	867	-0.308	-0.27
4f (4-NMe_2-C_6H_4)	449	-0.594	-0.83

Determination of kinetic parameters for H_2 equilibrium

The equilibrium constant was calculated for the H_2 activation with **4a-f** between 20 and 32°C via ^1H NMR integrating each a signal of **4a-f** and **5a-f** determining the ratio. The H_2 concentration in solution was calculated by integrating the H_2 signal and taking the absolute concentration of **4a-f** and **5a-f** into account. For each compound $Ln(K_{eq})$ was plotted against T^{-1}. From the slope ΔH_R can be calculated, while ΔS_R can be determined via the x-intercept. The same was also done for the D_2 activation of **4a**. Comparing the K_{eq} values to the H_2 activation could be used to obtain the kinetic isotope effect (KIE).

4a (C_6H_5) +H_2/+D_2

T [K]	*K_{eq} with H_2*	*K_{eq} with D_2*	*KIE*
295.15	2202	2723	0.81
297.15	1979	2348	0.84
299.15	1761	2129	0.83
301.15	1589	1923	0.83
303.15	1398	1726	0.81
305.15	1343	1586	0.85

4a (C_6H_5)+H_2

T [K]	T^{-1}	$\ln(K_{eq})$
295.15	0.00339	7.697
297.15	0.00337	7.591
299.15	0.00334	7.474
301.15	0.00332	7.371
303.15	0.00330	7.243
305.15	0.00328	7.203

➔ Linear fitting resulting in: y = 4661.57(±240.10)-8.10(±0.80); R^2 = 0.987

➔ ΔH_R = -38.76±2.00 kJmol^{-1}; ΔS_R = -67.37±6.65 Jmol^{-1}K^{-1}

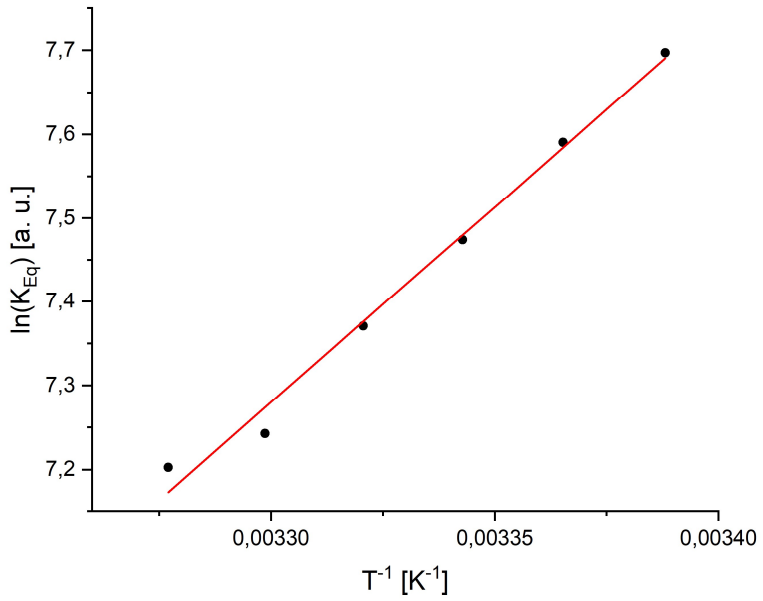

Figure 8.9 Plot of $\ln(K_{eq})$ vs T^{-1} for **4a** with H_2.

4a (C_6H_5)+D_2

T [K]	*T^{-1}*	$ln(K_{eq})$
295.15	0.00339	7.910
297.15	0.00337	7.761
299.15	0.00334	7.663
301.15	0.00332	7.562
303.15	0.00330	7.454
305.15	0.00328	7.370

➔ Linear fitting resulting in: y = 4799.06(±173.72)-8.37(±0.58); R^2 = 0.993

➔ ΔH_R = -39.90±1.44 kJmol^{-1}; ΔS_R = -69.60±4.81 Jmol^{-1}K^{-1}

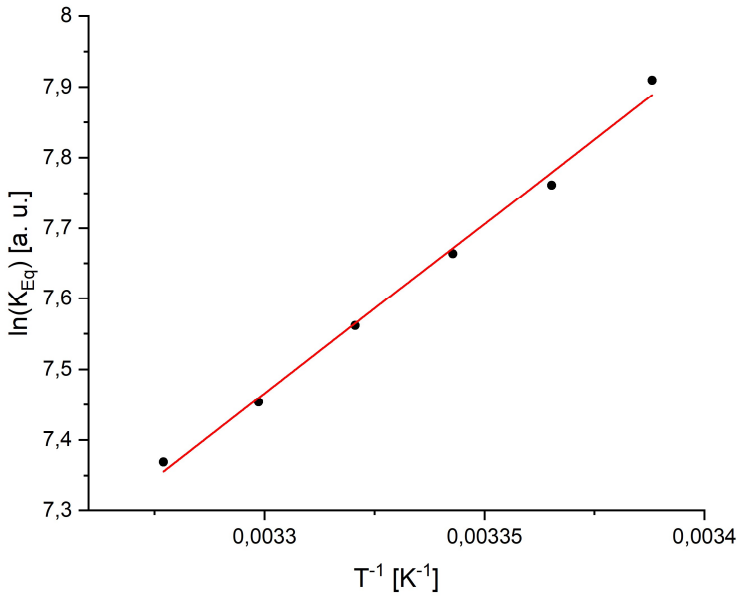

Figure 8.10 Plot of $ln(K_{eq})$ vs T^{-1} for **4a** with D_2.

4b (3,5-$(CF_3)_2C_6H_3$)+H_2

T [K]	T^{-1}	$\ln(K_{eq})$
295.15	0.00339	9.431
297.15	0.00337	9.343
299.15	0.00334	9.241
301.15	0.00332	9.104
303.15	0.00330	8.979
305.15	0.00328	8.878

➔ Linear fitting resulting in: y = 5134.97(±182.60)-7.95(±0.61); R^2 = 0.994

➔ ΔH_R = -42.69±1.52 kJmol^{-1}; ΔS_R = -66.08±5.06 Jmol^{-1}K^{-1}

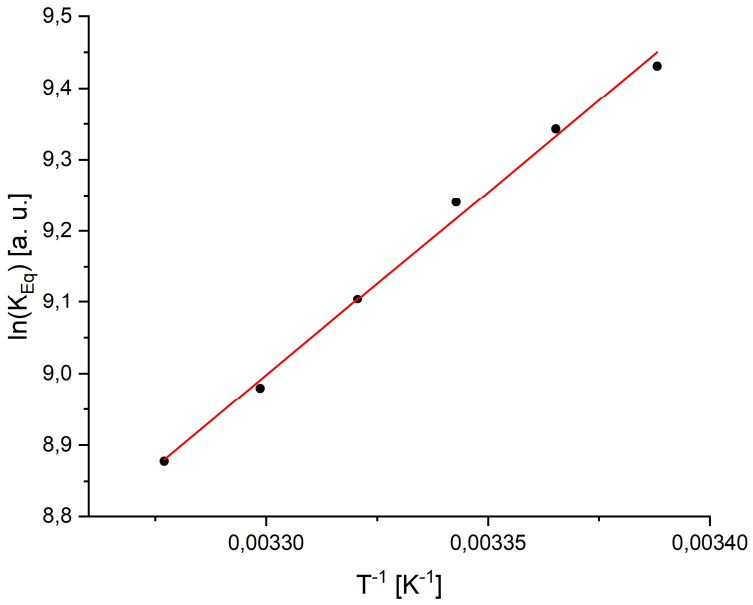

Figure 8.11 Plot of $\ln(K_{eq})$ vs T^{-1} for **4b** with H_2.

4c (4-CNC$_6$H$_4$)+H$_2$

T [K]	*T^{-1}*	ln(K$_{eq}$)
295.15	0.00339	8.754
297.15	0.00337	8.632
299.15	0.00334	8.535
301.15	0.00332	8.382
303.15	0.00330	8.285
305.15	0.00328	8.163

➔ Linear fitting resulting in: y = 5339.12(±136.85)-9.33(±0.46); R^2 = 0.997

➔ ΔH_R = -44.39±1.14 kJmol^{-1}; ΔS_R = -77.59±3.79 Jmol^{-1}K^{-1}

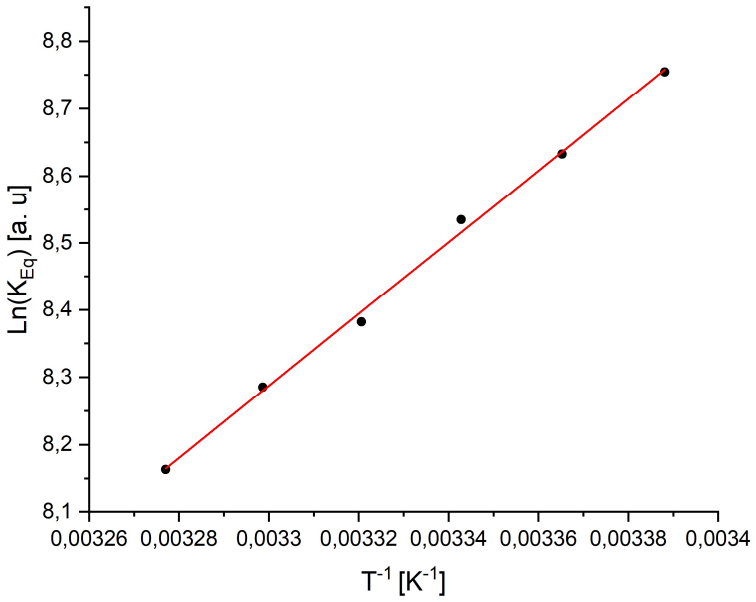

Figure 8.12 Plot of ln(K$_{eq}$) vs T^{-1} for **4c** with H$_2$.

4d (4-MeC$_6$H$_4$)+H$_2$

T [K]	*T^{-1}*	ln(K$_{eq}$)
293.15	0.00341	7.615
295.15	0.00339	7.491
297.15	0.00337	7.400
299.15	0.00334	7.316
301.15	0.00332	7.200
303.15	0.00330	7.098

➔ Linear fitting resulting in: y = 4492.09(±114.82)-7.72(±0.39); R^2 = 0.997

➔ ΔH_R = -37.35±0.95 kJmol^{-1}; ΔS_R = -64.15±3.20 Jmol^{-1}K^{-1}

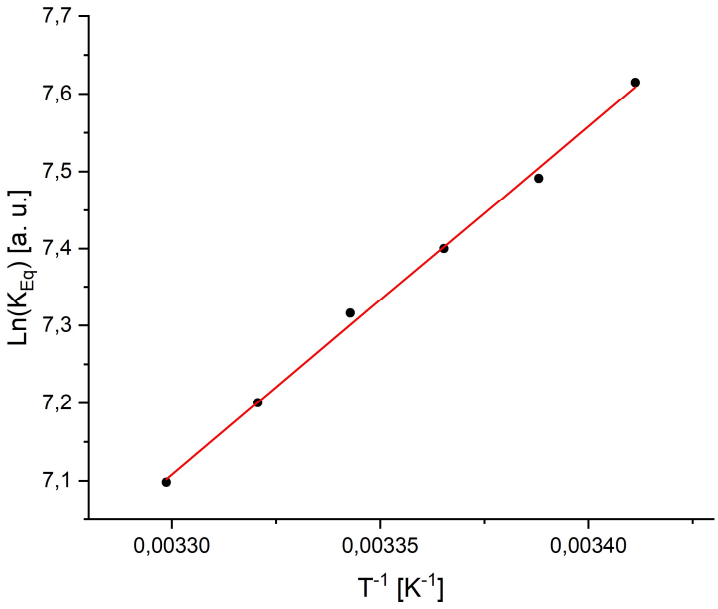

Figure 8.13 Plot of ln(K$_{eq}$) vs T^{-1} for **4d** with H_2.

4e (4-OMeC$_6$H$_4$)+H$_2$

T [K]	*T^{-1}*	ln(K$_{eq}$)
295.15	0.00339	7.000
297.15	0.00337	6.854
299.15	0.00334	6.765
301.15	0.00332	6.703
303.15	0.00330	6.626
305.15	0.00328	6.500

➔ Linear fitting resulting in: y = 4180.50(±268.02)-7.19(±0.89); R^2 = 0.980

➔ ΔH_R = -34.76±2.23 kJmol^{-1}; ΔS_R = -59.76±7.42 Jmol^{-1}K^{-1}

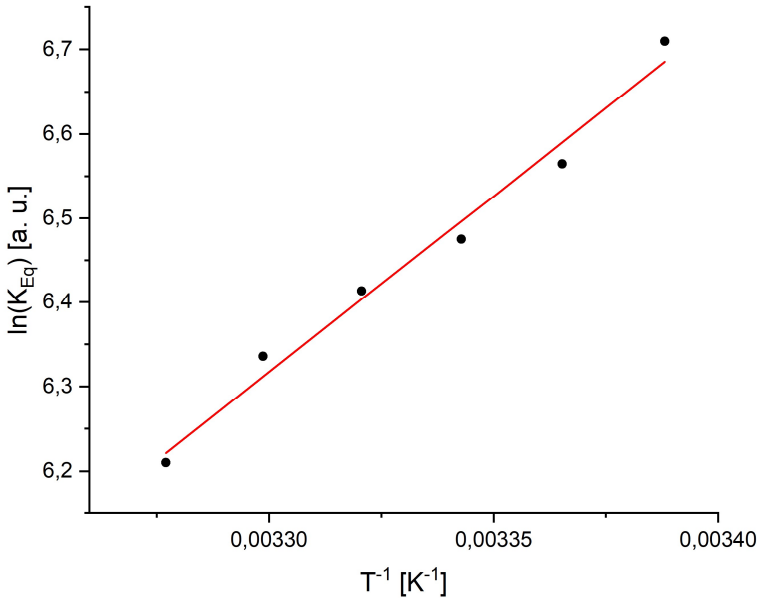

Figure 8.14 Plot of ln(K$_{eq}$) vs T^{-1} for **4e** with H$_2$.

4f (4-OMeC$_6$H$_4$)+H$_2$

T [K]	*T^{-1}*	ln(K$_{eq}$)
295.15	0.00339	6.309
297.15	0.00337	6.185
299.15	0.00334	6.108
301.15	0.00332	6.021
303.15	0.00330	5.949
305.15	0.00328	5.849

➔ Linear fitting resulting in: y = 3980.53(±144.10)-7.19(±0.48); R^2 = 0.993

➔ ΔH_R = -33.10±1.20 kJmol^{-1}; ΔS_R = -59.81±3.99 Jmol^{-1}K^{-1}

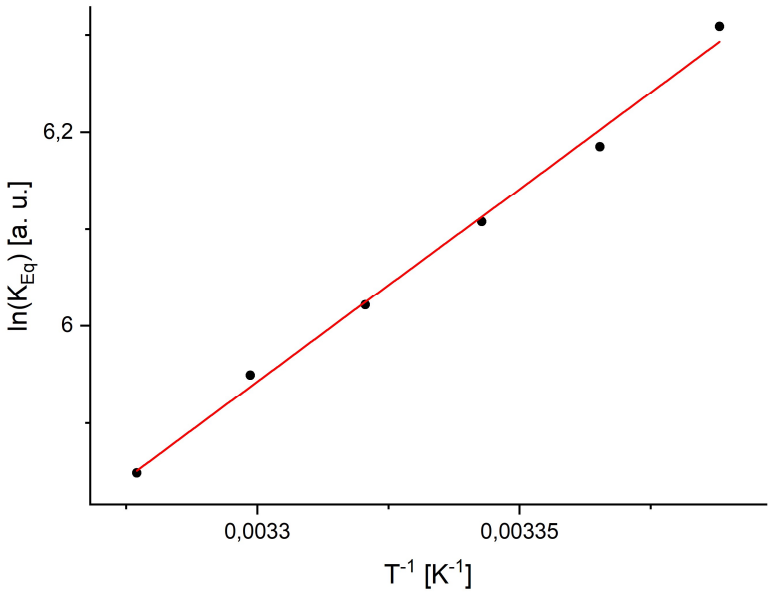

Figure 8.15 Plot of ln(K$_{eq}$) vs T^{-1} for **4f** with H$_2$.

General Method for catalytic dehydrocoupling of $PhSiH_3$ with [^{PhiP}DippGe(X)·Ni(IPr)] complexes:

0.5 mL of a C_6D_6 with **4a-f** (1.62 mM) was filled in a 15 mL Schlenk flask. Afterwards $PhSiH_3$ (20 yL, 0.16 mM) was added, and the flask stirred at 7000 rpm for 3 h while being open to the Schlenk line with a slight overpressure of 0.05 bar. Then mesitylene (11.2 yL, 0.08 mmol) was added as an internal standard and the consumption of $PhSiH_3$ was checked via ^{1}H-NMR. All measurements were performed in triplicate.

Method for Polymer synthesis via dehydrocoupling of $PhSiH_3$ with 4a:

4a was dissolved in 2.5 mL of C_6D_6 in a 250 mL Schlenk flask. Afterwards PhSiH3 (400 yL, mM) was added and the flask stirred 144 h, while being open to the Schlenk line with a slight overpressure of 0.05 bar. Afterwards all volatiles were removed in vacuo and the residue was dissolved in Et_2O. The solution was filtered through celite and after removing a volatiles in vacuo an off-white powder was obtained. The powder was analysed via GPC and ^{1}H NMR measurements.

X-ray crystallographic details

Single crystals of **2b**, **4a**, **4b**, **4c**, **4d**, **4e**, **4f**, **4g**, **5a** and **5c** suitable for X-ray structural analysis were mounted in perfluoroalkyl ether oil on a nylon loop and positioned in a 150 K cold N_2 gas stream. Data collection was performed with a STOE StadiVari diffractometer (MoKα radiation) equipped with a DECTRIS PILATUS 300K detector. Structures were solved by Direct Methods (SHELXS-97) and refined by full-matrix least-squares calculations against F^2 (SHELXL-2018).[61] The positions of the hydrogen atoms were calculated and refined using a riding model. All non-hydrogen atoms were treated with anisotropic displacement parameters. Crystal data, details of data collections, and refinements for all structures can be found in their CIF files, which will be available free of charge *via* www.ccdc.cam.ac.uk/data_request/cif once the project will be accepted for publication, and are summarised in Tables 9.5 – 9.7.

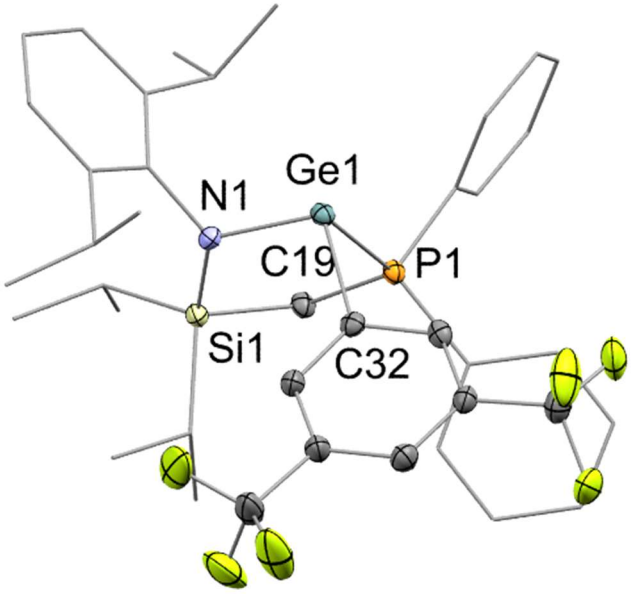

Figure 8.16 The molecular structure of **2b** with hydrogen atoms omitted and thermal ellipsoids at 25% probability. Selected distances and [Å] for **2b**: Ge1-P1 2.464(1), Ge1-N1 1.940(2), Ge1-C32 2.026(3).

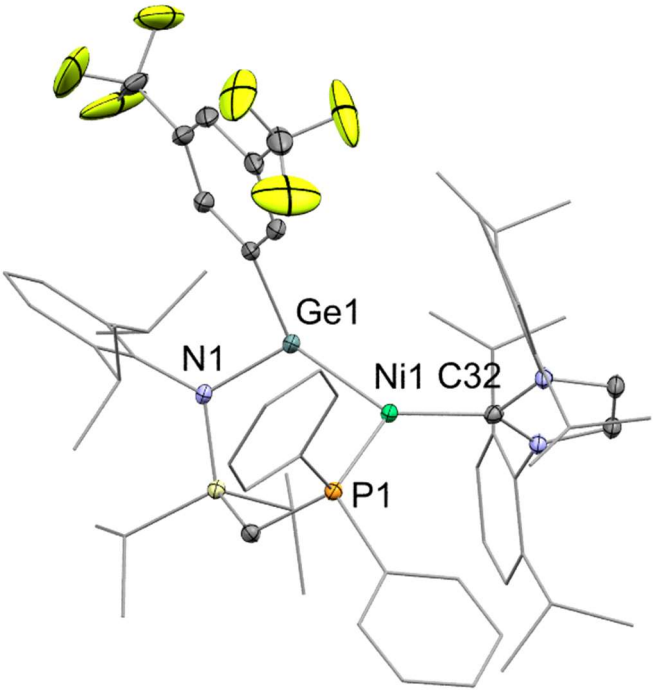

Figure 8.17 The molecular structure of **4b** with hydrogen atoms omitted and thermal ellipsoids at 25% probability. Selected distances and [Å] and angles [°] for **4b**: Ni1-Ge1 2.209(1), Ge1-N1 1.902(4), Ni1-C32 1.936(6),Ge1-Ni1-C32 138.6(2), C32-Ni1-P1 125.5(2), P1-Ni1-Ge1 95.79(5).

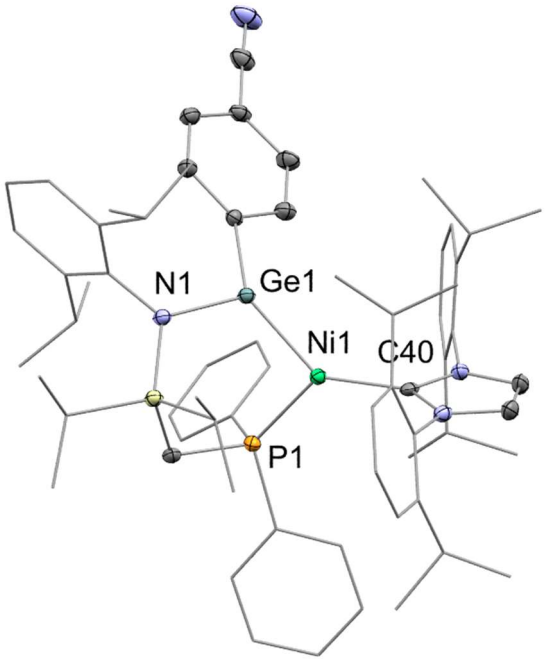

Figure 8.18 The molecular structure of **4c** with hydrogen atoms omitted and thermal ellipsoids at 25% probability. Selected distances and [Å] and angles [°] for **4c**: Ni1-Ge1 2.2216(8), Ge1-N1 1.890(3), Ni1-C40 1.927(4),Ge1-Ni1-C40 136.8(1), C40-Ni1-P1 127.3(1), P1-Ni1-Ge1 95.67(4).

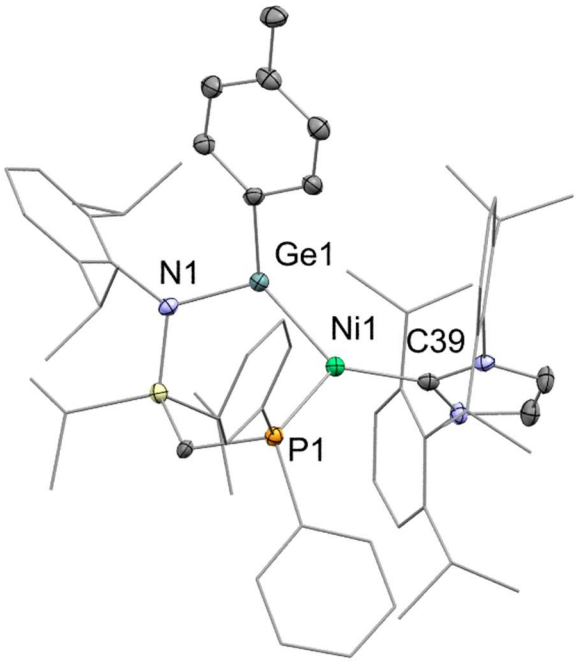

Figure 8.19 The molecular structure of **4d** with hydrogen atoms omitted and thermal ellipsoids at 25% probability. Selected distances and [Å] and angles [°] for **4d**: Ni1-Ge1 2.231(1), Ge1-N1 1.897(4), Ni1-C39 1.907(6),Ge1-Ni1-C39 138.1(2), C39-Ni1-P1 124.3(2), P1-Ni1-Ge1 97.35(75).

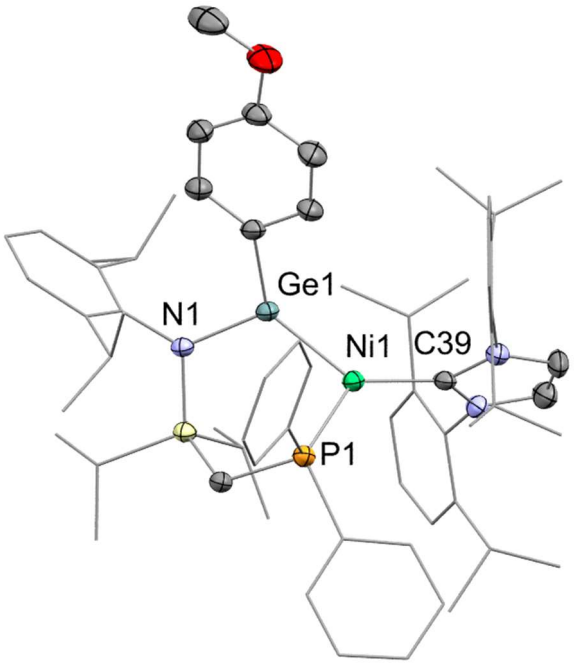

Figure 8.20 The molecular structure of **4e** with hydrogen atoms omitted and thermal ellipsoids at 25% probability. Selected distances and [Å] and angles [°] for **4e**: Ni1-Ge1 2.2203(8), Ge1-N1 1.885(3), Ni1-C39 1.904(5),Ge1-Ni1-C39 137.1(1), C39-Ni1-P1 126.8(1), P1-Ni1-Ge1 95.89(4).

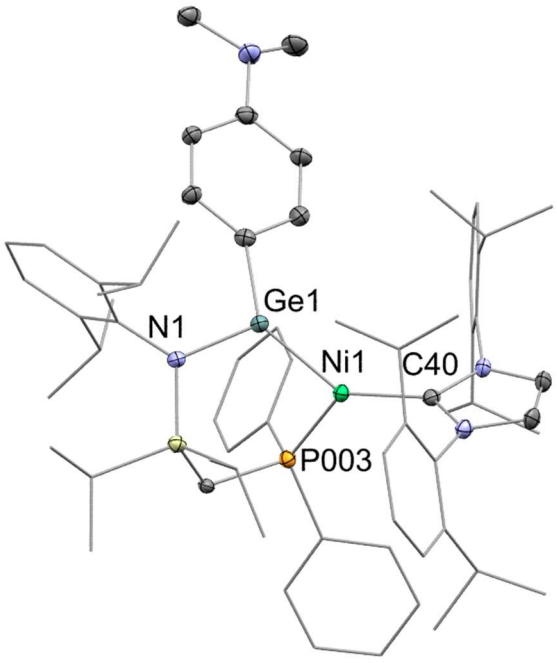

Figure 8.21 The molecular structure of **4f** with hydrogen atoms omitted and thermal ellipsoids at 25% probability. Selected distances and [Å] and angles [°] for **4f**: Ni1-Ge1 2.2176(9), Ge1-N1 1.893(4), Ni1-C40 1.901(5),Ge1-Ni1-C40 136.6(1), C40-Ni1-P003 127.3(1), P003-Ni1-Ge1 95.89(5).

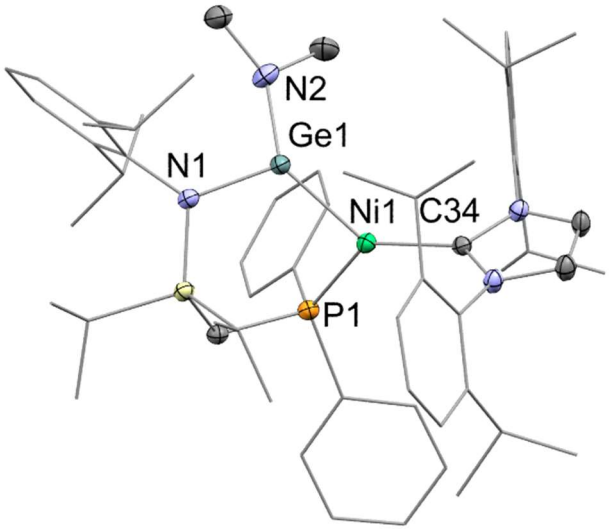

Figure 8.22 The molecular structure of **4g** with hydrogen atoms omitted and thermal ellipsoids at 25% probability. Selected distances and [Å] and angles [°] for **4g**: Ni1-Ge1 2.2162(9), Ge1-N1 1.892(2), Ge1-N2 1.848(4), Ni1-C34 1.914(3),Ge1-Ni1-C34 131.6(1), C34-Ni1-P1 132.4(1), P1-Ni1-Ge1 95.93(3).

Table 8.5 Crystallographic details for **2b**, **4a**, **4b**, and **4c**.

	2b	**4a**	**4b**	**4c**
empirical form.	$C_{39}H_{46}F_6GeNPSi$	$C_{67}H_{91}GeN_3NiPSi$	$C_{70}H_{82}F_6GeN_3NiPSi$	$C_{65}H_{83}GeN_4NiPSi \cdot 0.5(Et_2O$, hexane)
formula wt	774.42	1128.78	1269.74	1190.85
crystal syst.	triclinic	triclinic	monoclinic	monoclinic
space group	*P-1*	*P-1*	$P2_1/c$	$P2_1/n$
a (Å)	12.310(3)	12.650(3)	14.330(3)	13.882(3)
b (Å)	14.320(3)	13.610(3)	20.120(4)	22.527(5)
c (Å)	22.750(5)	19.970(4)	23.510(5)	21.112(4)
α (deg.)	97.70(3)	79.10(3)	90	90
β (δεγ)	95.30(3)	74.20(3)	97.60(3)	99.59(3)
γ (deg.)	96.20(3)	71.00(3)	90	90
vol ($Å^3$)	3927.6(14)	3108.9(13)	6719(2)	6510(2)
Z	4	2	4	4
ρ(calc) ($g.cm^{-3}$)	1.310	1.206	1.255	1.215
μ (mm^{-1})	0.907	0.872	0.827	0.837
F(000)	1608	1206	2664	2544
T (K)	150(2)	150(2)	150(2)	150(2)
reflns collect.	53284	38461	40322	89512
unique reflns	15417	12208	13162	12785
R_{int}	0.0395	0.1820	0.0466	0.1085
R1 [$I>2\sigma(I)$]	0.0416	0.0912	0.0752	0.0517
*w*R2 (all data)	0.0933	0.2591	0.2401	0.1263
CCDC No.	X	X	X	X

Table 8.6 Crystallographic details for **4d**, **4e**, and **4f**.

	4d	**4e**	**4f**
empirical form.	$C_{65}H_{86}GeN_3NiPSi$	$C_{65}H_{86}GeN_3NiOPSi$	$C_{66}H_{89}GeN_4NiPSi$
formula wt	1099.72	1115.72	1128.77
crystal syst.	monoclinic	monoclinic	monoclinic
space group	*P2₁/n*	*P2₁/n*	*P2₁/n*
a (Å)	13.880(3)	14.060(3)	14.108(3)
b (Å)	22.720(5)	22.580(5)	22.317(5)
c (Å)	20.900(4)	21.370(4)	21.590(4)
α (deg.)	90	90	90
β (δεγ)	100.50(3)	101.00(3)	101.55(3)
γ (deg.)	90	90	90
vol ($Å^3$)	6481(2)	6660(2)	6660(2)
Z	4	4	4
ρ(calc) ($g.cm^{-3}$)	1.127	1.113	1.126
μ (mm^{-1})	0.835	0.815	0.815
F(000)	2344	2376	2408
T (K)	150(2)	150(2)	150(2)
reflns collect.	56743	45595	46377
unique reflns	12727	12976	12961
R_{int}	0.1475	0.0741	0.1015
R1 [$I>2\sigma(I)$]	0.0726	0.0624	0.0699
*w*R2 (all data)	0.1638	0.1434	0.1778
CCDC No.	X	X	X

Table 8.7 Crystallographic details for **4g**, **5a** and **5c**.

	4g	**5a**	**5c**
empirical form.	$C_{60}H_{85}GeN_4NiPSi$	$C_{64}H_{86}GeN_3NiPSi \cdot Et_2O$	$C_{68}H_{92}GeN_4NiPSi$
formula wt	1052.67	1161.83	1155.81
crystal syst.	triclinic	triclinic	monoclinic
space group	*P-1*	*P-1*	*P2₁/n*
a (Å)	12.632(3)	12.740(3)	13.953(3)
b (Å)	13.335(3)	13.890(3)	22.828(5)
c (Å)	19.285(4)	19.630(4)	20.809(4)
α (deg.)	84.11(3)	81.90(3)	90
β (δεγ)	89.52(3)	84.30(3)	100.55(3)
γ (deg.)	61.95(3)	66.30(3)	90
vol ($Å^3$)	2848.9(12)	3145.5(13)	6516(2)
Z	2	2	4
ρ(calc) ($g.cm^{-3}$)	1.227	1.227	1.178
μ (mm^{-1})	0.947	0.865	0.834
F(000)	1124	1244	2468
T (K)	150(2)	150(2)	150(2)
reflns collect.	11210	42397	47185
unique reflns	11210	12355	12764
R_{int}	0.0550	0.0766	0.0429
R1 [$I>2\sigma(I)$]	0.0476	0.0548	0.0473
*w*R2 (all data)	0.1178	0.1313	0.1210
CCDC No.	X	X	X

Computational methods

DFT calculations for the reaction mechanism discovery were performed at the B97-D3(SMD=benzene)/def2-TZVPP//B97-D3/def2-SVP level of theory.[62-64] To identify stationary points on the potential energy surface (PES), harmonic vibrational frequency calculations were conducted. Transition states, distinguished by a singular imaginary frequency, were further validated using intrinsic reaction coordinate (IRC) calculations to confirm their status as intermediates. All calculations were executed using the GAUSSIAN 16 software suite.

We performed Natural Bond Orbital (NBO) analysis with the NBO program (version 3.1) as implemented in GAUSSIAN 16 at the B97-D3/def2-TZVPP level of theory using the optimised geometry gotten from the B97-D3/def2-SVP level of theory.[65] To produce the molecular orbitals, the optimised geometries were taken from the checkpoint file produced during NBO analysis at B97-D3/def2-TZVPP level of theory. By using the formchk utility program[65] a formatted checkpoint file is generated, from this file the molecular orbitals were pre-generated and visualised using the Avogadro program (version 1.20).[66]

*Optimised Structures of **3**, **4a**,**d-g***

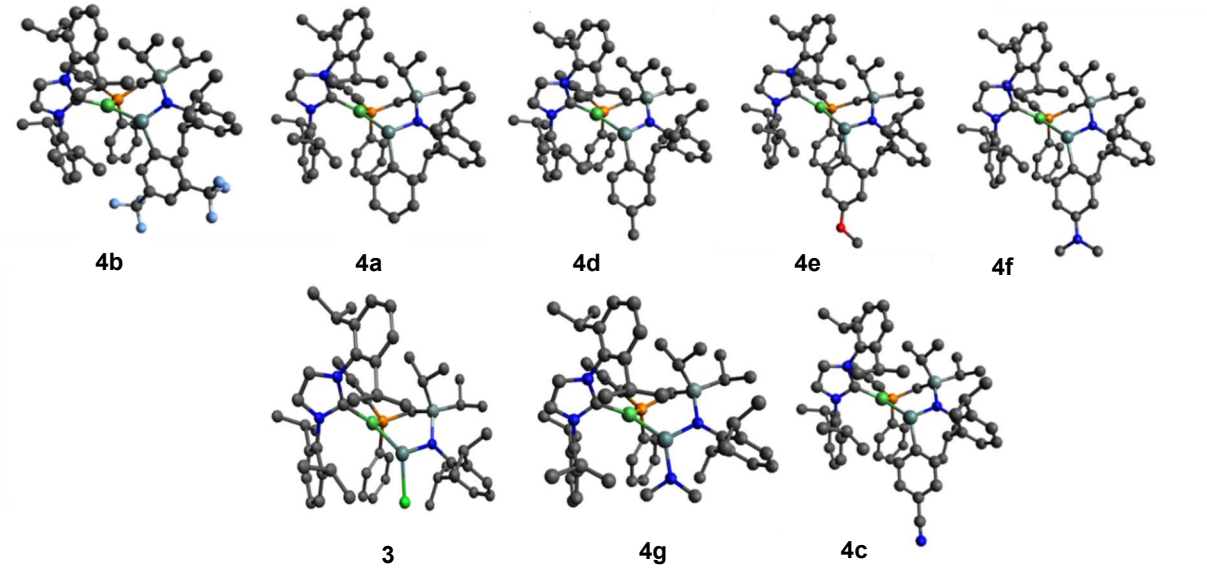

Figure 8.23 Optimised geometries for complexes **3** and **4a-g** with different substituents on Ge. Hydrogen atoms are omitted for clarity. Color code: C – gray, Ge – teal, N – blue, Ni – green, P – orange, Si – darker-teal, F – light-blue, O – red, Cl – light-green.

Table 8.8 Calculated bond length [Å], NPA, Wiberg Bond Index (WBI), and Mayer Bond Order (MBO) in the Ni-Ge moiety of **3**.

Property	**3**	
Bond length [Å]	Ni-Ge	2.232
NPA charge	Ni/Ge	-0.535/+1.110
Wiberg Bond Index	Ni-Ge	0.904
Mayer Bond Order	Ni-Ge	1.074

Table 8.9 Calculated bond length [Å], NPA, Wiberg Bond Index (WBI), and Mayer Bond Order (MBO) in the Ni-Ge moiety of **4a**.

Property	**4a**	
Bond length [Å]	Ni-Ge	2.241
NPA charge	Ni/Ge	-0.534/+1.147
Wiberg Bond Index	Ni-Ge	0.946
Mayer Bond Order	Ni-Ge	1.121

Table 8.10 Calculated bond length [Å], NPA, Wiberg Bond Index (WBI), and Mayer Bond Order (MBO) in the Ni-Ge moiety of **4b**.

Property	**4b**	
Bond length [Å]	Ni-Ge	2.243
NPA charge	Ni/Ge	-0.512/+1.116
Wiberg Bond Index	Ni-Ge	0.955
Mayer Bond Order	Ni-Ge	1.107

Table 8.11 Calculated bond length [Å], NPA, Wiberg Bond Index (WBI), and Mayer Bond Order (MBO) in the Ni-Ge moiety of **4c**.

Property	**4c**	
Bond length [Å]	Ni-Ge	2.240
NPA charge	Ni/Ge	-0.515/+1.129
Wiberg Bond Index	Ni-Ge	0.947
Mayer Bond Order	Ni-Ge	1.106

Table 8.12 Calculated bond length [Å], NPA, Wiberg Bond Index (WBI), and Mayer Bond Order (MBO) in the Ni-Ge moiety of **4d**.

Property	**4d**	
Bond length [Å]	Ni-Ge	2.242
NPA charge	Ni/Ge	-0.535/+1.150
Wiberg Bond Index	Ni-Ge	0.945
Mayer Bond Order	Ni-Ge	1.119

Table 8.13 Calculated bond length [Å], NPA, Wiberg Bond Index (WBI), and Mayer Bond Order (MBO) in the Ni-Ge moiety of **4e**.

Property	**4e**	
Bond length [Å]	Ni-Ge	2.242
NPA charge	Ni/Ge	-0.539/+1.152
Wiberg Bond Index	Ni-Ge	0.943
Mayer Bond Order	Ni-Ge	1.130

Table 8.14 Calculated bond length [Å], NPA, Wiberg Bond Index (WBI), and Mayer Bond Order (MBO) in the Ni-Ge moiety of **4f**.

Property	**4f**	
Bond length [Å]	Ni-Ge	2.243
NPA charge	Ni/Ge	-0.546/+1.160
Wiberg Bond Index	Ni-Ge	0.936
Mayer Bond Order	Ni-Ge	1.130

Table 8.15 Calculated bond length [Å], NPA, Wiberg Bond Index (WBI), and Mayer Bond Order (MBO) in the Ni-Ge moiety of **4g**.

Property	**4g**	
Bond length [Å]	Ni-Ge	2.252
NPA charge	Ni/Ge	-0.586/+1.313
Wiberg Bond Index	Ni-Ge	0.873
Mayer Bond Order	Ni-Ge	1.230

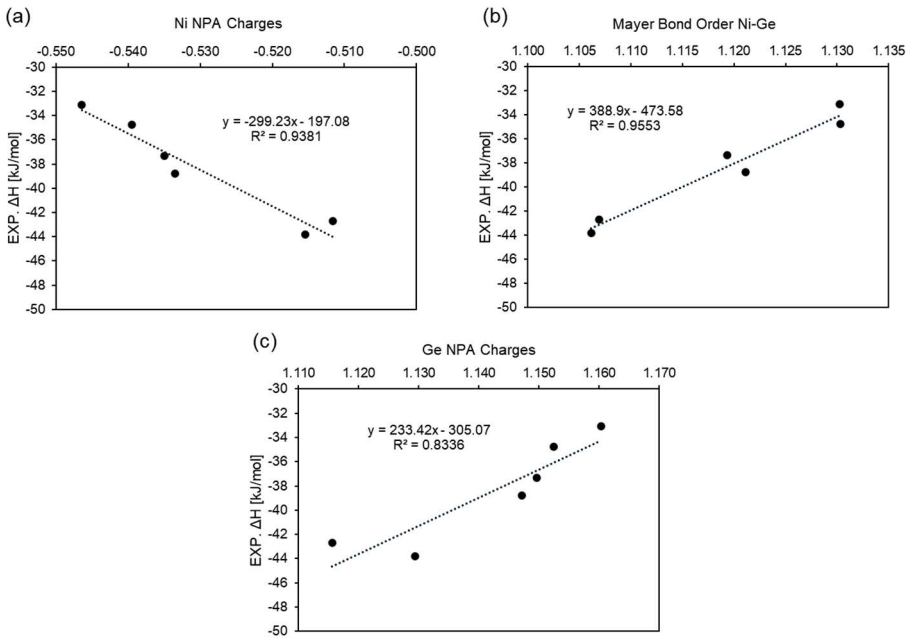

Figure 8.24 Correlation between experimentally measured ΔH and calculated a) Ni NPA charges, b) Ni-Ge Mayer Bond Order (MBO), and c) Ge NPA charges for **4a-f**.

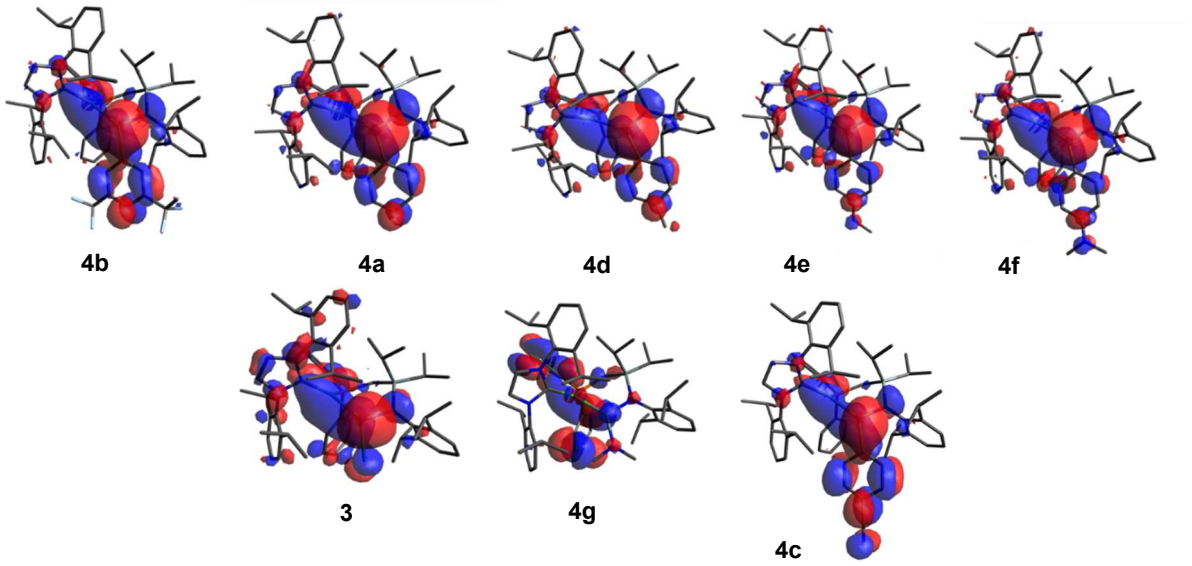

Figure 8.25 Lowest unoccupied molecular orbital (LUMO) of **3, 4a**-**g**. Orbital energies: **3**: -1.97 eV, **4a**: -1.93 eV, **4b**: -2.21 eV, **4c**: -2.35 eV, **4d**: -1.90 eV, **4e**: **-**1.85 eV, **4f**: -1.75 eV, and **4g**: -1.64 eV.

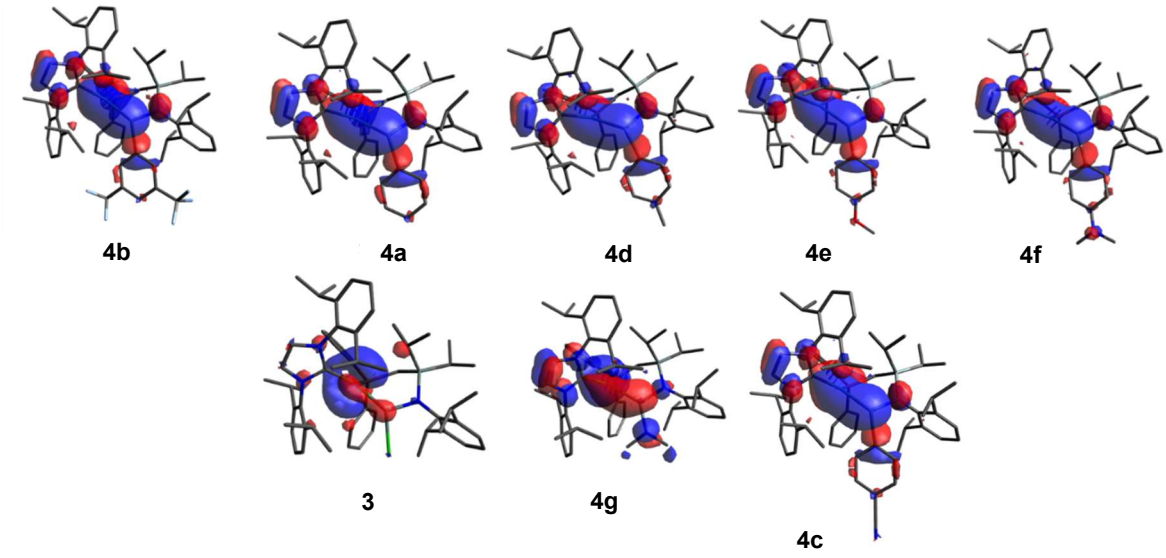

Figure 8.26 Highest occupied molecular orbital (HOMO) of **3, 4a**-**g**. Orbital energies: **3**: -3.79 eV, **4a**: -3.55 eV, **4b**: -3.76 eV, **4c**: -3.78 eV, **4d**: -3.52 eV, **4e**: **-**3.49 eV, **4f**: -3.39 eV, and **4g**: -3.44 eV.

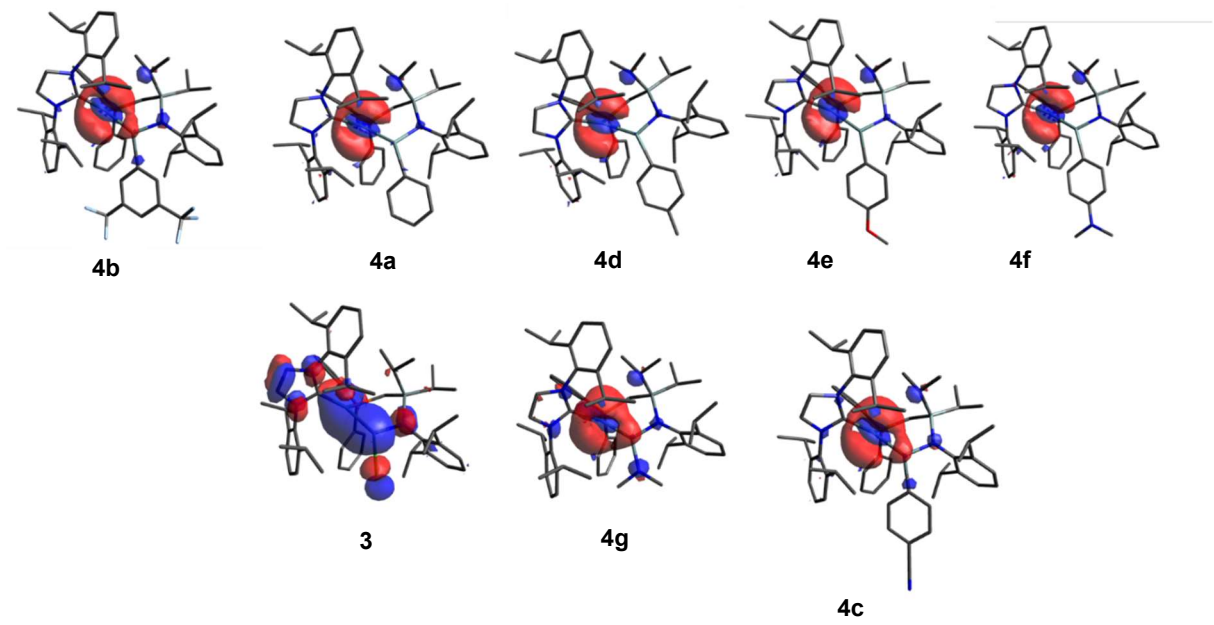

Figure 8.27 Second highest occupied molecular orbital (HOMO-1) of **3, 4a**-**g**. Orbital energies: **3**: -3.91 eV, **4a**: -3.61 eV, **4b**: -3.81 eV, **4c**: -3.84 eV, **4d**: -3.59 eV, **4e**: -3.56 eV, **4f**: -3.48 eV, and **4g**: -3.51 eV.

Table 8.16 NBO analysis of the Ni-Ge moiety of **4a**.

Alpha orbitals	Occupation	Atom	Polarisation	s-character	p-character	d-character
Bond	1.82	Ni	22.97%	34.44%	64.85%	0.71%
		Ge	77.03%	58.43%	41.34%	0.22%
Bond	1.81	Ni	83.05%	41.85%	58.05%	0.09%
		P	16.95%	34.53%	62.17%	3.29%
Bond	1.95	Ge	27.92%	35.09%	64.73%	0.17%
		C	72.08%	28.37%	71.55%	0.08%
Lone Pair	1.98	Ni	-	0.85%	0.04%	99.11%
Lone Pair	1.96	Ni	-	0.05%	0.22%	99.72%
Lone Pair	1.94	Ni	-	0.01%	0.18%	99.80%
Lone Pair	1.86	Ni	-	0.21%	0.94%	98.84%
Lone Pair	1.70	Ni	-	0.10%	3.08%	96.82%
Empty orbital	0.30	Ni	-	29.81%	67.69%	2.48%
Empty orbital	0.04	Ni	-	0.07%	99.24%	0.68%
Empty orbital	0.48	Ge	-	1.07%	98.84%	0.07%
Empty orbital	0.32	Ge	-	6.14%	93.65%	0.21%

Table 8.17 NBO analysis of the Ni-Ge moiety of **4d**.

Alpha orbitals	Occupation	Atom	Polarisation	s-character	p-character	d-character
Bond	1.82	Ni	23.02%	34.44%	64.84%	0.71%
		Ge	76.98%	58.32%	41.45%	0.23%
Bond	1.81	Ni	16.94%	34.52%	62.20%	3.27%
		P	83.06%	41.95%	57.96%	0.09%
Bond	1.95	Ge	27.93%	35.24%	64.58%	0.17%
		C	72.07%	28.49%	71.43%	0.07%
Lone Pair	1.98	Ni	-	0.85%	0.04%	99.11%
Lone Pair	1.96	Ni	-	0.06%	0.22%	99.72%
Lone Pair	1.94	Ni	-	0.01%	0.19%	99.80%
Lone Pair	1.86	Ni	-	0.21%	0.95%	98.84%
Lone Pair	1.70	Ni	-	0.09%	3.07%	96.83%
Empty orbital	0.30	Ni	-	29.82%	67.68%	2.48%
Empty orbital	0.04	Ni	-	0.07%	99.25%	0.68%
Empty orbital	0.47	Ge	-	1.08%	98.83%	0.07%
Empty orbital	0.32	Ge	-	6.09%	93.69%	0.21%

Table 8.18 NBO analysis of the Ni-Ge moiety of **4e**.

Alpha orbitals	Occupation	Atom	Polarisation	s-character	p-character	d-character
Bond	1.82	Ni	23.10%	34.45%	64.84%	0.71%
		Ge	76.90%	58.31%	41.46%	0.22%
Bond	1.82	Ni	16.94%	34.41%	62.37%	3.22%
		P	83.06%	42.05%	57.85%	0.09%
Bond	1.95	Ge	27.89%	35.29%	64.53%	0.17%
		C	72.11%	28.92%	71.00%	0.08%
Lone Pair	1.97	Ni	-	0.85%	0.04%	99.11%
Lone Pair	1.96	Ni	-	0.06%	0.23%	99.71%
Lone Pair	1.94	Ni	-	0.01%	0.18%	99.80%
Lone Pair	1.85	Ni	-	0.21%	0.97%	98.82%
Lone Pair	1.70	Ni	-	0.08%	3.03%	96.89%
Empty orbital	0.30	Ni	-	29.92%	67.55%	2.51%
Empty orbital	0.04	Ni	-	0.07%	99.23%	0.69%
Empty orbital	0.47	Ge	-	1.07%	98.85%	0.07%
Empty orbital	0.32	Ge	-	6.05%	93.73%	0.21%

Table 8.19 NBO analysis of the Ni-Ge moiety of **4f**.

Alpha orbitals	Occupation	Atom	Polarisation	s-character	p-character	d-character
Bond	1.82	Ni	23.37%	34.54%	64.73%	0.73%
		Ge	76.63%	57.96%	41.81%	0.22%
Bond	1.82	Ni	16.93%	34.21%	62.64%	3.14%
		P	83.07%	42.25%	57.65%	0.09%
Bond	1.95	Ge	28.04%	35.74%	64.09%	0.17%
		C	71.96%	29.03%	70.89%	0.08%
Lone Pair	1.97	Ni	-	0.85%	0.04%	99.11%
Lone Pair	1.96	Ni	-	0.07%	0.24%	99.70%
Lone Pair	1.94	Ni	-	0.01%	0.19%	99.80%
Lone Pair	1.85	Ni	-	0.21%	0.99%	98.79%
Lone Pair	1.71	Ni	-	0.07%	2.98%	96.96%
Empty orbital	0.30	Ni	-	30.04%	67.41%	2.53%
Empty orbital	0.04	Ni	-	0.07%	99.23%	0.70%
Empty orbital	0.47	Ge	-	1.10%	98.82%	0.06%
Empty orbital	0.31	Ge	-	5.93%	93.86%	0.21%

Table 8.20 NBO analysis of the Ni-Ge moiety of **3**.

Alpha orbitals	Occupation	Atom	Polarisation	s-character	p-character	d-character
Bond	1.93	Ni	17.88%	29.93%	69.59%	0.47%
		Ge	82.87%	41.24%	58.65%	0.10%
Bond	1.81	Ni	17.13%	38.55%	57.82%	3.62%
		P	83.24%	42.83%	57.08%	0.08%
Lone Pair	1.98	Ni	-	0.79%	0.03%	99.18%
Lone Pair	1.95	Ni	-	0.01%	0.23%	99.76%
Lone Pair	1.94	Ni	-	0.01%	0.25%	99.74%
Lone Pair	1.87	Ni	-	0.61%	0.88%	98.51%
Lone Pair	1.72	Ni	-	0.32%	2.77%	96.90%
Empty orbital	0.30	Ni	-	29.82%	67.47%	2.69%
Empty orbital	0.04	Ni	-	0.11%	99.14%	0.75%
Empty orbital	0.51	Ge	-	0.06%	99.78%	0.13%
Empty orbital	0.45	Ge		10.59%	89.14%	0.21%
Empty orbital	0.32	Ge	-	2.47%	97.24%	0.27%

Table 8.21 NBO analysis of the Ni-Ge moiety of **4g**.

Alpha orbitals	Occupation	Atom	Polarisation	s-character	p-character	d-character
Bond	1.89	Ni	21.19%	32.58%	66.80%	0.61%
		Ge	78.81%	82.18%	17.69%	0.13%
Bond	1.84	Ni	16.76%	35.20%	61.99%	2.80%
		P	83.24%	42.83%	57.08%	0.08%
Lone Pair	1.97	Ni	-	0.86%	0.03%	99.11%
Lone Pair	1.95	Ni	-	0.03%	0.22%	99.75%
Lone Pair	1.94	Ni	-	0.00%	0.24%	99.76%
Lone Pair	1.85	Ni	-	0.50%	1.28%	98.21%
Lone Pair	1.75	Ni	-	0.07%	2.41%	97.52%
Empty orbital	0.31	Ni	-	30.77%	66.34%	2.87%
Empty orbital	0.04	Ni	-	0.05%	99.21%	0.75%
Empty orbital	0.49	Ge	-	0.02%	99.82%	0.13%
Empty orbital	0.40	Ge		18.81%	81.08%	0.11%
Empty orbital	0.27	Ge	-	0.04%	99.64%	0.30%

References

1 A. Schulz, T. L. Kalkuhl, P. M. Keil, T. J. Hadlington, *Angew. Chem. Int. Ed.* **2023**, *62*, e202305996.
2 G. J. Kubas, *Acc. Chem. Res.* **1988**, *21*, 120–128.
3 R. H. Crabtree, *Acc. Chem. Res.* **1990**, *23*, 95–101.
4 P. G. Jessop, R. H. Morris, *Coord. Chem. Rev.* **1992**, *121*, 155–284.
5 M. Peruzzini, R. Poli, *Recent advances in hydride chemistry*, 1st ed., Elsevier Science Ltd. Amsterdam, Amsterdam, **2001**.
6 G. S. McGrady, G. Guilera, *Chem. Soc. Rev.* **2003**, *32*, 383–392.
7 D. M. Heinekey, A. Lledós, J. M. Lluch, *Chem. Soc. Rev.* **2004**, *33*, 175–182.
8 R. L. Sweany, *J. Am. Chem. Soc.* **2002**, *124*, 3799–3800.
9 R. Ramachandran, R. K. Menon, *Int. J. Hydrog. Energy* **1998**, *23*, 593–598.
10 J. A. Okolie, B. R. Patra, A. Mukherjee, S. Nanda, A. K. Dalai, J. A. Kozinski, *Int. J. Hydrog. Energy* **2021**, *46*, 8885–8905.
11 T. Yu, J. Jiao, P. Song, W. Nie, C. Yi, Q. Zhang, P. Li, *ChemSusChem* **2020**, *13*, 2876–2893.
12 M. P. Suh, H. J. Park, T. K. Prasad, D.-W. Lim, *Chem. Rev.* **2012**, *112*, 782–835.
13 F. Crotogino, in *Storing Energy*, 2nd ed., Elsevier, **2022**, pp. 613–632.
14 R. Tarkowski, B. Uliasz-Misiak, *Renew. Sustain. Energy Rev.* **2022**, *162*, 112451.
15 S. M. Jafari Raad, Y. Leonenko, H. Hassanzadeh, *Renew. Sustain. Energy Rev.* **2022**, *168*, 112846.
16 P. J. Brothers, in *Prog. Inorg. Chem.*, **1981**, pp. 1–61.
17 Y. Kan, Q. Zhang, in *Nanostructured Materials for Next-Generation Energy Storage and Conversion: Hydrogen Production, Storage, and Utilization*, Springer Berlin Heidelberg, Berlin, Heidelberg, **2017**, pp. 43–84.
18 G. C. Welch, R. R. S. Juan, J. D. Masuda, D. W. Stephan, *Science* **2006**, *314*, 1124–1126.
19 D. W. Stephan, G. Erker, *Angew. Chem. Int. Ed.* **2010**, *49*, 46–76.
20 C. Weetman, in *Encyclopedia of Inorganic and Bioinorganic Chemistry*, **2021**, pp. 1–27.
21 G. D. Frey, V. Lavallo, B. Donnadieu, W. W. Schoeller, G. Bertrand, *Science* **2007**, *316*, 439–441.
22 Y. Peng, J.-D. Guo, B. D. Ellis, Z. Zhu, J. C. Fettinger, S. Nagase, P. P. Power, *J. Am. Chem. Soc.* **2009**, *131*, 16272–16282.
23 Z. Zhu, X. Wang, Y. Peng, H. Lei, J. C. Fettinger, E. Rivard, P. P. Power, *Angew. Chem. Int. Ed.* **2009**, *48*, 2031–2034.
24 M. R. Elsby, R. T. Baker, *Chem. Soc. Rev.* **2020**, *49*, 8933–8987.
25 J. R. Khusnutdinova, D. Milstein, *Angew. Chem. Int. Ed.* **2015**, *54*, 12236–12273.
26 J. F. Sonnenberg, A. J. Lough, R. H. Morris, *Organometallics* **2014**, *33*, 6452–6465.
27 J. F. Sonnenberg, K. Y. Wan, P. E. Sues, R. H. Morris, *ACS Catal.* **2016**, *7*, 316–326.
28 G. Zhang, B. L. Scott, S. K. Hanson, *Angew. Chem. Int. Ed.* **2012**, *51*, 12102–12106.
29 S. Elangovan, C. Topf, S. Fischer, H. Jiao, A. Spannenberg, W. Baumann, R. Ludwig, K. Junge, M. Beller, *J. Am. Chem. Soc.* **2016**, *138*, 8809–8814.
30 Y. Li, C. Hou, J. Jiang, Z. Zhang, C. Zhao, A. J. Page, Z. Ke, *ACS Catal.* **2016**, *6*, 1655–1662.
31 R. J. Somerville, J. Campos, *Eur. J. Inorg. Chem.* **2021**, *2021*, 3488–3498.
32 K. E. Litz, K. Henderson, R. W. Gourley, M. M. B. Holl, *Organometallics* **1995**, *14*, 5008–5010.
33 T. J. Hadlington, T. Szilvasi, M. Driess, *J. Am. Chem. Soc.* **2019**, *141*, 3304–3314.
34 M. Frutos, N. Parvin, A. Baceiredo, D. Madec, N. Saffon-Merceron, V. Branchadell, T. Kato, *Angew. Chem. Int. Ed.* **2022**, *61*, e202201932.
35 S. Takahashi, M. Frutos, A. Baceiredo, D. Madec, N. Saffon-Merceron, V. Branchadell, T. Kato, *Angew. Chem. Int. Ed.* **2022**, *61*, e202208202.

36 M. Auer, J. Bolten, K. Eichele, H. Schubert, C. P. Sindlinger, L. Wesemann, *Chem. Sci.* **2023**, *14*, 514–524.
37 T. Watanabe, Y. Miyazaki, K. Inomata, H. Tobita, H. Hashimoto, *Organometallics* **2023**, *42*, 846–858.
38 Y. Wang, A. Kostenko, S. Yao, M. Driess, *J. Am. Chem. Soc.* **2017**, *139*, 13499–13506.
39 P. M. Keil, A. Soyemi, K. Weisser, T. Szilvási, C. Limberg, T. J. Hadlington, *Angew. Chem. Int. Ed.* **2023**, *62*, e202218141.
40 P. M. Keil, T. Szilvási, T. J. Hadlington, *Chem. Sci.* **2021**, *12*, 5582–5590.
41 P. M. Keil, T. J. Hadlington, *Angew. Chem. Int. Ed.* **2022**, *61*, e202114143.
42 V. Y. Lee, K. McNeice, Y. Ito, A. Sekiguchi, *Chem. Commun.* **2011**, *47*, 3272–3274.
43 T. J. Hadlington, C. Jones, *Chem Commun (Camb)* **2014**, *50*, 2321-2323.
44 M. M. Juckel, J. Hicks, D. Jiang, L. Zhao, G. Frenking, C. Jones, *Chem. Commun.* **2017**, *53*, 12692–12695.
45 D. Munz, *Organometallics* **2018**, *37*, 275–289.
46 W. Ando, H. Itoh, T. Tsumuraya, *Organometallics* **1989**, *8*, 2759–2766.
47 T. Y. Lai, J.-D. Guo, J. C. Fettinger, S. Nagase, P. P. Power, *Chem. Commun.* **2019**, *55*, 405–407.
48 T. P. Dhungana, H. Hashimoto, H. Tobita, *Dalton Trans.* **2017**, *46*, 8167–8179.
49 D. Schmidt, T. Zell, T. Schaub, U. Radius, *Dalton Trans.* **2014**, *43*, 10816–10827.
50 C. Hansch, A. Leo, R. W. Taft, *Chem. Rev.* **1991**, *91*, 165–195.
51 B. R. Bender, G. J. Kubas, L. H. Jones, B. I. Swanson, J. Eckert, K. B. Capps, C. D. Hoff, *J. Am. Chem. Soc.* **1997**, *119*, 9179–9190.
52 F.-G. Fontaine, D. Zargarian, *Organometallics* **2002**, *21*, 401–408.
53 M. Tanabe, A. Takahashi, T. Fukuta, K. Osakada, *Organometallics* **2013**, *32*, 1037-1043.
54 A. Feigl, I. Chiorescu, K. Deller, S. U. H. Heidsieck, M. R. Buchner, V. Karttunen, A. Bockholt, A. Genest, N. Rösch, B. Rieger, *Chemistry – A European Journal* **2013**, *19*, 12526-12536.
55 J. C. DeMott, N. Bhuvanesh, O. V. Ozerov, *Chem. Sci.* **2013**, *4*, 642–649.
56 S. Harder, J. Boersma, L. Brandsma, J. A. Kanters, A. J. M. Duisenberg, J. H. Van Lenthe, *Organometallics* **1990**, *9*, 511–516.
57 S. Hünig, H. Schweeberg, H. Schwarz, *Justus Liebigs Ann. Chem.* **1954**, *587*, 132–145.
58 A. J. Sicard, R. T. Baker, *Org. Process Res. Dev.* **2020**, *24*, 2950–2952.
59 B.-C. Liu, N. Ge, Y.-Q. Zhai, T. Zhang, Y.-S. Ding, Y.-Z. Zheng, *Chem. Commun.* **2019**, *55*, 9355–9358.
60 M. Muhr, P. Heiß, M. Schütz, R. Bühler, C. Gemel, M. H. Linden, H. B. Linden, R. A. Fischer, *Dalton Trans.* **2021**, *50*, 9031–9036.
61 G. Sheldrick, *Acta Crystallogr. C* **2015**, *71*, 3–8.
62 S. Grimme, *J. Comput. Chem.* **2006**, *27*, 1787-1799.
63 A. V. Marenich, C. J. Cramer, D. G. Truhlar, *The Journal of Physical Chemistry B* **2009**, *113*, 6378-6396.
64 F. Weigend, R. Ahlrichs, *Physical Chemistry Chemical Physics* **2005**, *7*, 3297-3305.
65 M. J. Frisch, G. W. Trucks, H. B. Schlegel, G. E. Scuseria, M. A. Robb, J. R. Cheeseman, G. Scalmani, V. Barone, G. A. Petersson, H. Nakatsuji, X. Li, M. Caricato, A. V. Marenich, J. Bloino, B. G. Janesko, R. Gomperts, B. Mennucci, H. P. Hratchian, J. V. Ortiz, A. F. Izmaylov, J. L. Sonnenberg, Williams, F. Ding, F. Lipparini, F. Egidi, J. Goings, B. Peng, A. Petrone, T. Henderson, D. Ranasinghe, V. G. Zakrzewski, J. Gao, N. Rega, G. Zheng, W. Liang, M. Hada, M. Ehara, K. Toyota, R. Fukuda, J. Hasegawa, M. Ishida, T. Nakajima, Y. Honda, O. Kitao, H. Nakai, T. Vreven, K. Throssell, J. A. Montgomery Jr., J. E. Peralta, F. Ogliaro, M. J. Bearpark, J. J. Heyd, E. N. Brothers, K. N. Kudin, V. N. Staroverov, T. A. Keith, R. Kobayashi, J. Normand, K. Raghavachari, A. P. Rendell, J. C. Burant, S. S. Iyengar, J. Tomasi, M. Cossi, J. M. Millam, M. Klene,

C. Adamo, R. Cammi, J. W. Ochterski, R. L. Martin, K. Morokuma, O. Farkas, J. B. Foresman, D. J. Fox, Wallingford, CT, **2016**.

66 M. D. Hanwell, D. E. Curtis, D. C. Lonie, T. Vandermeersch, E. Zurek, G. R. Hutchison, *Journal of Cheminformatics* **2012**, *4*, 17.

Chapter 9

Conclusion and Outlook

In this thesis, the bidentate ligand scaffold ^{PhR}Dipp (^{PhR}Dipp = [{$Ph_2PCH_2Si(R)_2$}(Dipp)N]$^-$; R = Ph, *i*Pr; Dipp = 2,6-*i*$Pr_2C_6H_3$) has been introduced and developed, to obtain corresponding phosphine-stabilised heavier tetrylenes, which were successfully utilised as Lewis acidic non-innocent bidentate ligands in TM^0 complexes. These compound classes were employed both in ligand-centred bond activation, as well as in metal-ligand cooperative (MLC) activation of catalytically relevant substrates, and further in efficient catalytic protocols.

We were able to access an array of different heavier tetrylene ligands with this scaffold, by altering the initial tetrylene-chloride ligands, ^{PhR}DippECl (E = Ge, Sn; Chapter 3), making *i.e.* cationic tetrylenes, [^{PhiP}DippE]$^+$, with [$BAr^F{}_4$]$^-$ ([$BAr^F{}_4$]$^-$ = [{3,5-$(CF_3)_2C_6H_3$}$_4$B]$^-$) as counter anion (Chapter 4 and 6), or (aryl)tetrylenes, [^{PhiP}DippE(Ar)], *via* simple salt metathesis of the chloride ligand in (chloro)-germylenes and -stannylenes (Chapter 9). Combining these tetrylene ligands either with Ni^0 sources (*e.g.* $Ni(COD)_2$ with PPh_3/IPr; COD = 1,5-cyclooctadiene; IPr = [{HC(Dipp)N}$_2$C:]; Chapter 3, 4, and 8), or the Fe^0 precursor [(η^2-tmvs)$_2$Fe(IPr)] (tmvs = $SiMe_3C_2H_3$; Chapter 7), led to a variety of TM^0 complexes, with a broad spectrum of electronic and structural properties (Figure 9.1).

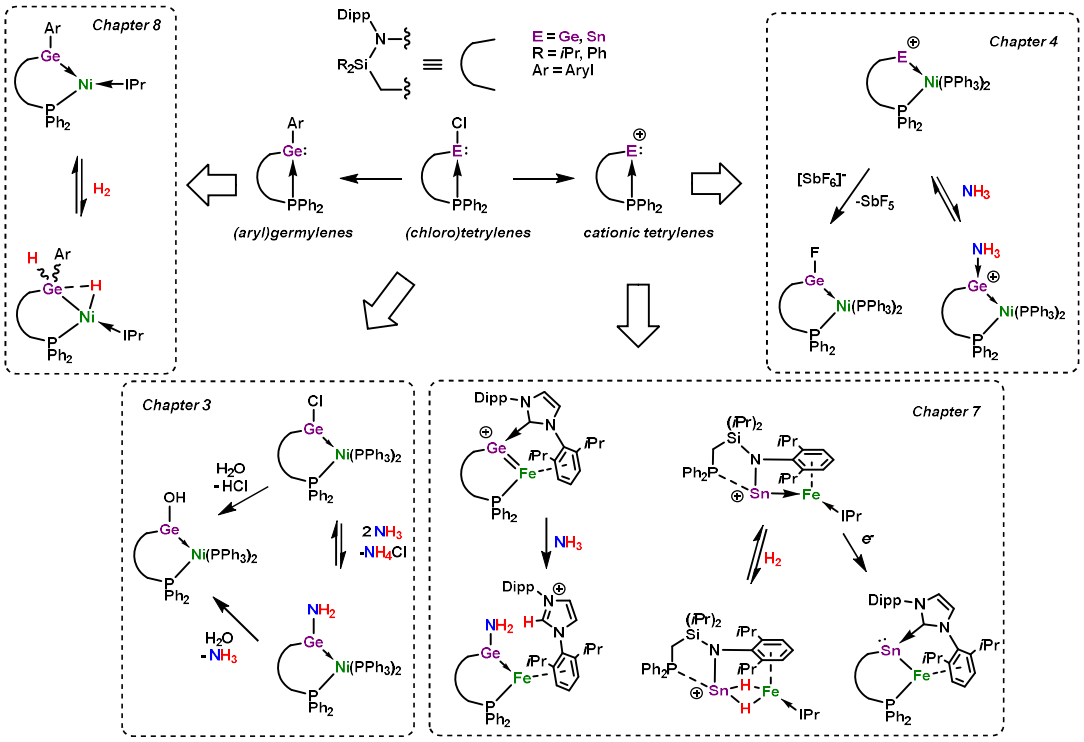

Figure 9.1 Key E^{II}-TM^0 (E = Ge, Sn; TM = Ni, Fe) complexes and corresponding reactivities presented within this thesis. For all cationic complexes the counter anion is [$BAr^F{}_4$]$^-$ = [{3,5-$(CF_3)_2C_6H_3$}$_4$B]$^-$, which is omitted in this figure.

The work described in this thesis confirms our hypothesis, that the developed bidentate ligand structure allows the tetrel element to retain Lewis acidic properties. This even leads to Lewis super acidic character of the tetrylene for the cationic tetryliumylidene-nickel(0) complexes, $[\{^{PhiP}DippE\}\cdot Ni(PPh_3)_2]^+$, as demonstrated by fluoride abstraction from $[SbF_6]^-$ by the tetrel element. By comparison to the corresponding monodentate tetryliumylidenes, employed in the related Ni^0 complexes, $[^{SiiP}DippE\cdot Ni(PPh_3)_3]^+$ ($^{SiiP}Dipp$ = $[(iPr_3Si(Dipp)N]^-$), we could show that the bidentate ligand structure is key for enforcing a bent $^{PhR}Dipp$-E-Ni angle, which minimises π-back-donation from the Ni^0 centre to the tetrel element, and hence leads to the observed high Lewis acidity of the tetrylene (Chapter 5).

The different isolated complexes displayed reactivity for the activation of several small molecules such as ammonia, H_2, and water, while the electronic properties of the respective complexes influenced the type of activation that occurred. In these systems a reactive TM centre seems to be important to achieve MLC. This is clearly shown with the $[Ni(PPh_3)_2]$ complexes, where the Ni^0 centre is electronically saturated, and exclusively tetryl-centred reactivity or coordination was found (Chapter 3 and 4). When a low-coordinate TM centre was utilised, by introducing the $[TM^0(IPr)]$ moiety, we were able to observe targeted MLC, exemplified by reversible H_2 activation at the tetrylene-TM interface (Chapter 7 and 8). In general, this ligand scaffold seems to favour reversible activation of substrates, since this was observed in most of the cases. This is an important feature for potential catalytic applications, which are the ultimate target with these systems. We could already show that these tetrylene-TM complexes can in general be used in catalysis, being capable of the catalytic hydrosilylation of alkenes and alkynes (Chapter 4), and the catalytic dative coupling of $PhSiH_3$ (Chapter 8).

Furthermore, we also obtained the rare Sn^{II}-Fe^{-I} complex $[^{PhiP}Dipp(IPr)SnFe]$, making it the first reported covalently bound Fe^{-I} compound. This is presumably stabilised by the chelating P-arm of the ligand, which essentially bridges the Sn and Fe centres. Since the reactivity of such systems is essentially unknown, further studies on this or related complexes are also intriguing, as cooperative activation and/or catalysis could be possible.

Benefits of the here used tetrylene ligands are, that they are readily accessible and easily modified at the P, Si and N positions, but also directly at the tetrylene position. In Chapter 8 we could demonstrate that varying arene residues at the tetrel element strongly affect the electronic situation of the ligand and thus the ensuing $[Ni^0(IPr)]$ complexes, influencing the enabled cooperative H_2 activation and catalytic activity for dehydrogenative coupling of $PhSiH_3$. Since this simple change has such a big impact on the reactivity of the Ni^0 complexes, further modifications of the tetrylene ligands or employment of different combinations of TM centre and ancillary ligand(s) might lead to cooperative activation of more challenging substrates, or even catalysis, such as the hydroamination with ammonia.

This work has introduced the phosphine-stabilised heavier tetrylenes as single-centre ambiphilic ligands and shown their ability to retain Lewis acidic character, while coordinating to a TM centre, allowing for non-innocent behaviour of the tetrel element and thus MLC activation of H_2. The knowledge gained in this thesis, lays the foundation for further developments of the presented highly modifiable ligand and corresponding heavier tetrylene-TM complexes, to achieve cooperative activation of further catalytically relevant substrates, and catalytic applications.

Appendix

Reprint Permissions

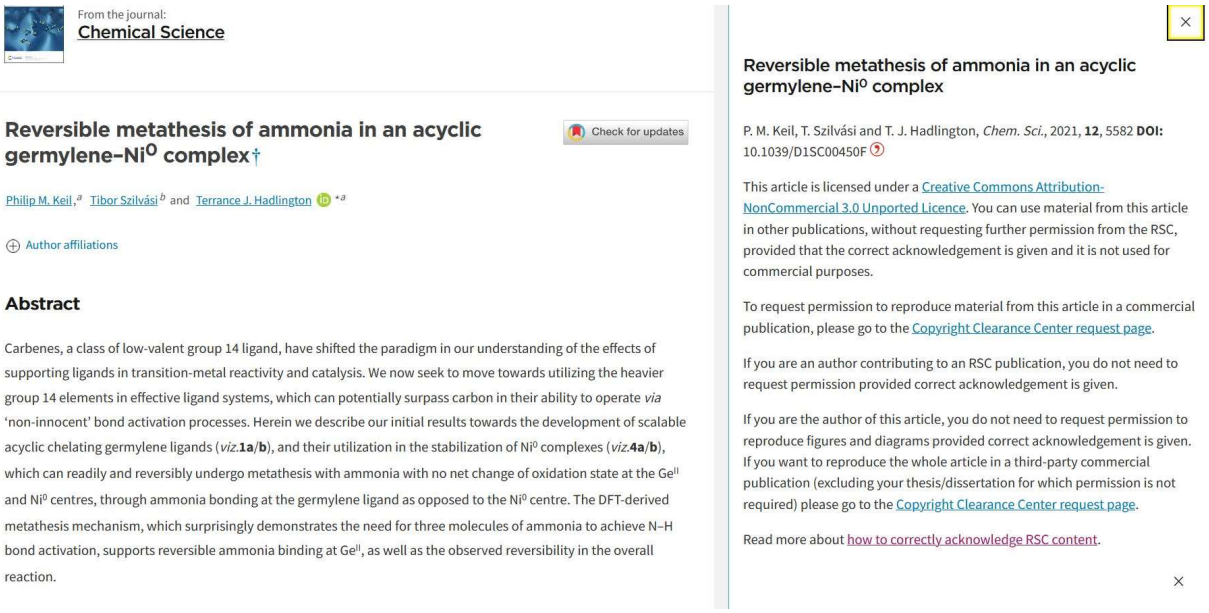

From the journal:
Chemical Science

Reversible metathesis of ammonia in an acyclic germylene–Ni^0 complex†

Check for updates

Philip M. Keil,[a] Tibor Szilvási[b] and Terrance J. Hadlington[*a]

Author affiliations

Abstract

Carbenes, a class of low-valent group 14 ligand, have shifted the paradigm in our understanding of the effects of supporting ligands in transition-metal reactivity and catalysis. We now seek to move towards utilizing the heavier group 14 elements in effective ligand systems, which can potentially surpass carbon in their ability to operate *via* 'non-innocent' bond activation processes. Herein we describe our initial results towards the development of scalable acyclic chelating germylene ligands (*viz.***1a**/**b**), and their utilization in the stabilization of Ni^0 complexes (*viz.***4a**/**b**), which can readily and reversibly undergo metathesis with ammonia with no net change of oxidation state at the Ge^{II} and Ni^0 centres, through ammonia bonding at the germylene ligand as opposed to the Ni^0 centre. The DFT-derived metathesis mechanism, which surprisingly demonstrates the need for three molecules of ammonia to achieve N–H bond activation, supports reversible ammonia binding at Ge^{II}, as well as the observed reversibility in the overall reaction.

Reversible metathesis of ammonia in an acyclic germylene–Ni^0 complex

P. M. Keil, T. Szilvási and T. J. Hadlington, *Chem. Sci.*, 2021, **12**, 5582 **DOI:** 10.1039/D1SC00450F

This article is licensed under a Creative Commons Attribution-NonCommercial 3.0 Unported Licence. You can use material from this article in other publications, without requesting further permission from the RSC, provided that the correct acknowledgement is given and it is not used for commercial purposes.

To request permission to reproduce material from this article in a commercial publication, please go to the Copyright Clearance Center request page.

If you are an author contributing to an RSC publication, you do not need to request permission provided correct acknowledgement is given.

If you are the author of this article, you do not need to request permission to reproduce figures and diagrams provided correct acknowledgement is given. If you want to reproduce the whole article in a third-party commercial publication (excluding your thesis/dissertation for which permission is not required) please go to the Copyright Clearance Center request page.

Read more about how to correctly acknowledge RSC content.

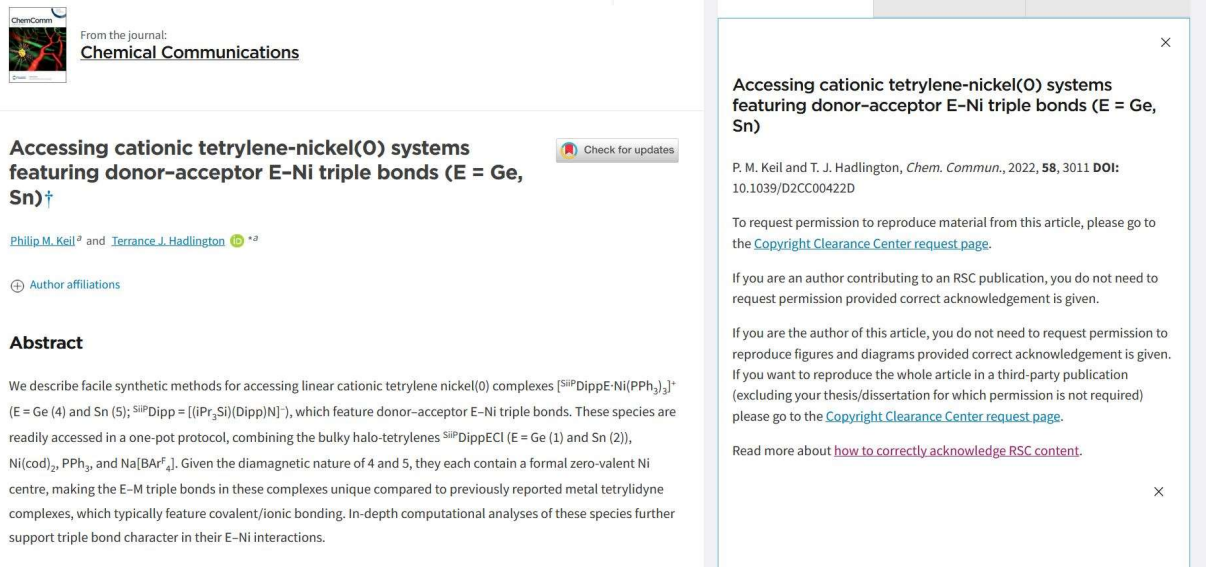

From the journal:
Chemical Communications

Accessing cationic tetrylene-nickel(0) systems featuring donor–acceptor E–Ni triple bonds (E = Ge, Sn)†

Check for updates

Philip M. Keil[a] and Terrance J. Hadlington[*a]

Author affiliations

Abstract

We describe facile synthetic methods for accessing linear cationic tetrylene nickel(0) complexes $[^{SiiP}DippE{\cdot}Ni(PPh_3)_3]^+$ (E = Ge (4) and Sn (5); $^{SiiP}Dipp = [(iPr_3Si)(Dipp)N]^-$), which feature donor–acceptor E–Ni triple bonds. These species are readily accessed in a one-pot protocol, combining the bulky halo-tetrylenes $^{SiiP}DippECl$ (E = Ge (1) and Sn (2)), $Ni(cod)_2$, PPh_3, and $Na[BAr^F{}_4]$. Given the diamagnetic nature of 4 and 5, they each contain a formal zero-valent Ni centre, making the E–M triple bonds in these complexes unique compared to previously reported metal tetrylidyne complexes, which typically feature covalent/ionic bonding. In-depth computational analyses of these species further support triple bond character in their E–Ni interactions.

Accessing cationic tetrylene-nickel(0) systems featuring donor–acceptor E–Ni triple bonds (E = Ge, Sn)

P. M. Keil and T. J. Hadlington, *Chem. Commun.*, 2022, **58**, 3011 **DOI:** 10.1039/D2CC00422D

To request permission to reproduce material from this article, please go to the Copyright Clearance Center request page.

If you are an author contributing to an RSC publication, you do not need to request permission provided correct acknowledgement is given.

If you are the author of this article, you do not need to request permission to reproduce figures and diagrams provided correct acknowledgement is given. If you want to reproduce the whole article in a third-party publication (excluding your thesis/dissertation for which permission is not required) please go to the Copyright Clearance Center request page.

Read more about how to correctly acknowledge RSC content.

JOHN WILEY AND SONS LICENSE
TERMS AND CONDITIONS

Aug 15, 2023

This Agreement between Technical University Munich -- Philip Keil ("You") and John Wiley and Sons ("John Wiley and Sons") consists of your license details and the terms and conditions provided by John Wiley and Sons and Copyright Clearance Center.

License Number	5610190507144
License date	Aug 15, 2023
Licensed Content Publisher	John Wiley and Sons
Licensed Content Publication	Angewandte Chemie International Edition
Licensed Content Title	Geometrically Constrained Cationic Low-Coordinate Tetrylenes: Highly Lewis Acidic σ-Donor Ligands in Catalytic Systems
Licensed Content Author	Terrance J. Hadlington, Philip M. Keil
Licensed Content Date	Jan 11, 2022
Licensed Content Volume	61
Licensed Content Issue	8
Licensed Content Pages	8
Type of use	Dissertation/Thesis

Requestor type	Author of this Wiley article
Format	Print and electronic
Portion	Full article
Will you be translating?	No
Title	Single Center Ambiphile Ligands towards the Hydroamination of unsaturated organic substrates
Institution name	Technical University Munich
Expected presentation date	Oct 2023
Requestor Location	Technical University Munich Aehrenweg 10 Neufahrn, 85375 Germany Attn: Technical University Munich
Publisher Tax ID	EU826007151
Total	0.00 EUR

Terms and Conditions

TERMS AND CONDITIONS

This copyrighted material is owned by or exclusively licensed to John Wiley & Sons, Inc. or one of its group companies (each a"Wiley Company") or handled on behalf of a society with which a Wiley Company has exclusive publishing rights in relation to a particular work (collectively "WILEY"). By clicking "accept" in connection with completing this licensing transaction, you agree that the following terms and conditions apply to this transaction (along with the billing and payment terms and conditions established by the Copyright Clearance Center Inc., ("CCC's Billing and Payment terms and conditions"), at the time that you opened your RightsLink account (these are available at any time at http://myaccount.copyright.com).

JOHN WILEY AND SONS LICENSE
TERMS AND CONDITIONS

Aug 15, 2023

This Agreement between Technical University Munich -- Philip Keil ("You") and John Wiley and Sons ("John Wiley and Sons") consists of your license details and the terms and conditions provided by John Wiley and Sons and Copyright Clearance Center.

License Number	5610200139996
License date	Aug 15, 2023
Licensed Content Publisher	John Wiley and Sons
Licensed Content Publication	ZEITSCHRIFT FüR ANORGANISCHE UND ALLGEMEINE CHEMIE
Licensed Content Title	Protonation of Hydrido-Tetrylenes: H2 Elimination vs. Tetrylium Cation Formation
Licensed Content Author	Philip M. Keil, Terrance J. Hadlington
Licensed Content Date	May 27, 2022
Licensed Content Volume	648
Licensed Content Issue	19
Licensed Content Pages	8
Type of use	Dissertation/Thesis
Requestor type	Author of this Wiley article

Format	Print and electronic
Portion	Full article
Will you be translating?	No
Title	Single Center Ambiphile Ligands towards the Hydroamination of unsaturated organic substrates
Institution name	Technical University Munich
Expected presentation date	Oct 2023
Requestor Location	Technical University Munich Aehrenweg 10 Neufahrn, 85375 Germany Attn: Technical University Munich
Publisher Tax ID	EU826007151
Total	0.00 EUR

Terms and Conditions

TERMS AND CONDITIONS

This copyrighted material is owned by or exclusively licensed to John Wiley & Sons, Inc. or one of its group companies (each a"Wiley Company") or handled on behalf of a society with which a Wiley Company has exclusive publishing rights in relation to a particular work (collectively "WILEY"). By clicking "accept" in connection with completing this licensing transaction, you agree that the following terms and conditions apply to this transaction (along with the billing and payment terms and conditions established by the Copyright Clearance Center Inc., ("CCC's Billing and Payment terms and conditions"), at the time that you opened your RightsLink account (these are available at any time at http://myaccount.copyright.com).

Terms and Conditions

- The materials you have requested permission to reproduce or reuse (the "Wiley Materials") are protected by copyright.

JOHN WILEY AND SONS LICENSE
TERMS AND CONDITIONS

Aug 15, 2023

This Agreement between Technical University Munich -- Philip Keil ("You") and John Wiley and Sons ("John Wiley and Sons") consists of your license details and the terms and conditions provided by John Wiley and Sons and Copyright Clearance Center.

License Number	5610200607216
License date	Aug 15, 2023
Licensed Content Publisher	John Wiley and Sons
Licensed Content Publication	Angewandte Chemie International Edition
Licensed Content Title	Cationic Tetrylene-Iron(0) Complexes: Access Points for Cooperative, Reversible Bond Activation and Open-Shell Iron(−I) Ferrato-Tetrylenes**
Licensed Content Author	Philip M. Keil, Ademola Soyemi, Kilian Weisser, et al
Licensed Content Date	Mar 22, 2023
Licensed Content Volume	62
Licensed Content Issue	19
Licensed Content Pages	11

Type of use	Dissertation/Thesis
Requestor type	Author of this Wiley article
Format	Print and electronic
Portion	Full article
Will you be translating?	No
Title	Single Center Ambiphile Ligands towards the Hydroamination of unsaturated organic substrates
Institution name	Technical University Munich
Expected presentation date	Oct 2023
Requestor Location	Technical University Munich Aehrenweg 10 Neufahrn, 85375 Germany Attn: Technical University Munich
Publisher Tax ID	EU826007151
Total	0.00 EUR

Terms and Conditions

TERMS AND CONDITIONS

This copyrighted material is owned by or exclusively licensed to John Wiley & Sons, Inc. or one of its group companies (each a"Wiley Company") or handled on behalf of a society with which a Wiley Company has exclusive publishing rights in relation to a particular work (collectively "WILEY"). By clicking "accept" in connection with completing this licensing transaction, you agree that the following terms and conditions apply to this transaction (along with the billing and payment terms and conditions established by the Copyright Clearance Center Inc., ("CCC's Billing and Payment terms and conditions"), at the time that you opened your RightsLink account (these are available at any time at